

**STUDIES ON STABILITY
ASSESSMENT OF LARGE CAVERNS
IN HIMALAYAN REGION**

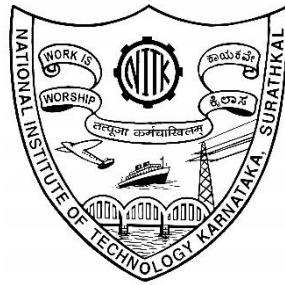
Thesis

Submitted in partial fulfillment of the requirements for the
degree of

DOCTOR OF PHILOSOPHY

by

SRIPAD RAMACHANDRA NAIK



DEPARTMENT OF MINING ENGINEERING
NATIONAL INSTITUTE OF TECHNOLOGY KARNATAKA,
SURATHKAL, MANGALORE – 575025

NOVEMBER, 2017

DECLARATION

I hereby declare that the Research Thesis entitled “**Studies on Stability Assessment of Large Caverns in Himalayan Region**” which is being submitted to the **National Institute of Technology Karnataka, Surathkal** in partial fulfillment of the requirements for the award of the Degree of **Doctor of Philosophy in Mining Engineering** is *a bonafide report of the research work carried out by me.* The material contained in this Research Thesis has not been submitted to any University or Institution for the award of any degree.

SRIPAD RAMACHANDRA NAIK

Register No. -090700MN09P02

Department of Mining Engineering

Place: NITK-Surathkal

Date: 06/11/2017

CERTIFICATE

This is to *certify* that the Research Thesis entitled “**Studies on Stability Assessment of Large Caverns in Himalayan Region**” submitted by **Sripad Ramachandra Naik** (Register Number: **090700MN09P02**) as the record of the research work carried out by him, is *accepted as the Research Thesis submission* in partial fulfilment of the requirements for the award of degree of **Doctor of Philosophy**.

Prof. V.R. Sastry

Department of Mining Engineering,
(Research Supervisor)

Chairman – DRPC
Department of Mining Engineering

Dedicated to
MY BELOVED PARENTS

Smt. Susheela

and

Sri. Ramachandra K Naik

ACKNOWLEDGEMENT

First of all, I am extremely grateful to my research supervisor, Prof. V. R. Sastry, Department of Mining Engineering, NITK, Surathkal for his excellent guidance, continuous support and inspiration throughout this research work. His deep insights helped me at various stages of my research and I remain indebted for his invaluable support at all time.

I express my sincere gratitude to RPAC members, Prof. A. Vittal Hegde, Department of Applied Mechanics and Prof. K. Narayana Prabhu, Department of Metallurgy for their critical assessment and very valuable suggestions during the progress of my research.

I am thankful to Prof. V R Sastry, Head, Department of Mining Engineering and Chairman DRPC, Prof. M Govinda Raj, Dr. M Aruna, Dr. Harsha Vardhan, former Heads of the Department of Mining Engineering, for their continuous support and encouragement during my research work.

My thanks are due to all professors at Department of Mining Engineering for offering very innovative subjects during the course work and I also thank other supporting staff for their timely help and support. I thank Mr. Raghu Chandra, Mr. Nagesha and other research scholars for their support.

I am extremely grateful to my institute, National Institute of Rock Mechanics (NIRM), Bengaluru for allowing me to take up this research work and permit me to use all the resources at the institute during my research work. I am thankful to Shri. C Sivakumar Director (Additional Charge), NIRM for his persistent encouragement and support for my PhD work. I also fondly remember the encouragement and support received from my former Directors, Dr.V Venkateswarlu, Dr. P.C. Nawani and Prof. R. N. Gupta and I am grateful to them.

I would like to place my sincere appreciation on record to the management of Tala Project, Bhutan for providing all logistic supports and help during the research work in the field. I am thankful to my colleague Mr. K. Sudhakar for his untiring efforts in

assisting me during the field investigations. I am also thankful to my other colleagues Mr. Aditya Mishra, Mr. Vijay Sekar and Dr. Rabi Bhusan for their help during numerical modelling studies and analysis of the data. I also appreciate the encouragement and support received from all my colleagues at NIRM.

My special appreciation is to my wife Padmavati and my little daughter Tanushri for their unconditional support and affection during my research work. I am also indebted to my parents Smt. Susheela and Sri. Ramachandra K Naik for their constant support. I also appreciate the encouragement received from my brother, sister and my in-laws.

Finally, I am thankful to everyone who helped me directly or indirectly during my research.

Sripad Ramachandra Naik

Place: NITK

Date: 06/11/2017

ABSTRACT

“Studies on Stability Assessment of Large Caverns in Himalayan Region” is a research study carried out to understand the behavior of large caverns in Himalayas, where rock mass is generally unfavorable for tunneling. Caverns at Tala hydroelectric project, Bhutan, situated in lower Himalayas were chosen for the study. The prime objective was to study the rock mass behavior at various stages of excavation of large caverns. Field studies were carried out to measure various parameters like, displacement, wall convergence, load on the rock bolts, load on steel ribs and strains in the rock bolt using magnetic ring multipoint borehole extensometers(MRMPBX), total station, reflective targets, load cells and instrumented bolts. 3D numerical modelling studies were carried out using continuum (FLAC-3D).

Analysis of MRMPBX data in the crown of powerhouse cavern indicated significant influence of side slashing in the crown (accounted for 71-88% of total displacement) on the stability of the crown and super incumbent rock mass. There was clear indication of joint separation taking place even upto 10m above the crown, indicating the requirement of long rock bolts of minimum 12m length. Strains calculated in the crown at some places were more than 1%. Steel ribs installed in the crown also recorded more than 100t load. Benches within one time the width of cavern had maximum influence on the rate of load increase on the steel ribs.

Upstream and downstream wall of powerhouse cavern converged by more than 200-300mm in unit bay area and 135mm in service bay area. Calculated strains during the monitoring period were 0.92 to 1.74% in the unit bay area and upto 0.66% in the service bay area. Analysis of convergence data indicated that about 88% of convergence took place during excavation of caverns and about 12% was recorded during post excavation period. Average convergence rate during excavation of benches varied from 0.56mm/day to 0.67mm/day, whereas convergence rates during other miscellaneous excavations varied from 0.38 to 0.49mm/day. During the post excavation monitoring done for 3 years, convergence of 16-50mm was observed with average convergence rate of 0.021mm/day to 0.063mm/day. Predicted convergence from 3D continuum model compared well with the field monitored values within 15% at most of the places.

3D modelling results indicated maximum strain of 3.34% on the upstream wall and 3.35% on downstream wall for the entire excavation period. On the upstream wall, strains of more than 2% were observed in unit bay area. In the service bay area, strains were restricted upto 2%. On downstream wall maximum strain was observed near the bus ducts. Higher strains were concentrated near the crown of bus ducts. On downstream wall, strains of less than 2% were observed in service bay area. In transformer hall also similar behaviour was observed. Results clearly indicated that when the height of excavation increases (w/h ratio decreases), unit bay area experiences higher strain.

Rock bolts in the walls of powerhouse cavern recorded load upto 45t. Bolts on the upstream wall experienced loads of higher magnitude compared to the bolts on downstream wall. During post excavation, load on the bolts on downstream wall was greater (average 21.4%) than the load on bolts on upstream wall (average 8.7%).

3D modelling results showed higher displacements concentrated near the intersection of floor of the cross tunnels and downstream wall of the powerhouse cavern. In general, there was increase in principal stresses in the crown and reduction in principal stresses in the walls of cavern, which corroborates with high values of convergence recordings in the walls. Tensile stresses were observed in the rock mass, particularly in the floor of powerhouse cavern due to floor heave.

Analysis of stress concentration factors in the pillar between powerhouse and transformer hall indicated factors due to maximum and intermediate principal stresses were almost equal (varied from 1.20 to 1.58). Normal stresses had higher influence on the stress concentration factors in the pillar. Stress concentration factors near the floor of transformer hall upstream wall was maximum and stress relaxation was to a lesser extent compared to other locations.

Strength of the rock mass was estimated using 3D Hoek and Brown failure criterion. Caverns are found to be stable as the strength to stress ratio in the surrounding rock mass was greater than two except for few patches near the walls of the cavern. Tensile failures were noticed in the corners and at the floor of the powerhouse cavern. Monitoring in the cross tunnels indicated development of load in the range of 100-110t in the steel ribs and >35t load on the rock bolts.

Changing the orientation of the cavern with respect to the maximum principal stress direction had maximum effect on the upstream wall of the powerhouse cavern with an increase of maximum displacement by 28.7% at an angle of 90°. Study also showed that maximum stress concentration factor in the pillar due to vertical stress does not change significantly with cavern orientation except in the pillar near the end walls.

When the cavern is oriented parallel to maximum principal stress, maximum stress concentration factors due to vertical stress were the highest on the upstream wall of powerhouse. But at an angle of 90°, confinement provided by horizontal stresses decreased, that could cause instability problems in the wall. Confinement levels provided by horizontal stresses were greater on downstream wall of transformer hall than on the upstream wall of powerhouse cavern.

Sensitivity analysis results clearly indicated that friction angle was the most sensitive parameter among the all considered parameters. Predicted convergence increased by an average of 76.2% when the friction angle was reduced by 20%, and decreased convergence by 33.9% when friction angle was increased by 20%. Thus, the friction angle has very considerable influence on the convergence in the model. Cohesion, elastic modulus and Poisson's ratio were less sensitive in that order.

In this research study, integrated approach involving field investigations during the excavation and post excavation period and 3D modelling followed by correlation between the results. Both the stages of investigations could explain the behaviour of the cavern and surrounding rock mass in a comprehensive manner under a Himalayan geological setup.

Key words: Caverns, Convergence, Displacement, Instrumentation, Monitoring, Principal Stress, Normal Stress, Strain, Numerical Modelling, Strength to Stress Ratio, Instrumented Bolt.

CONTENTS

CHAPTER 1	INTRODUCTION	1
1.1	HYDROPOWER	2
1.1.1	Hydropower Development in Himalayas	3
1.2	GEOLOGICAL CHALLENGES IN TUNNELING IN HIMALAYAS	5
1.3	STATEMENT OF THE PROBLEM	8
1.5	ORGANIZATION OF THE THESIS	10
CHAPTER 2	LITERATURE REVIEW	11
2.1	CAVERNS	11
2.1.1	Choice of Cavern Shapes	12
2.1.2	Cavern Orientation and Location	13
2.1.3	Cavern Layout	17
2.1.4	Spacing between Caverns	18
2.2	MAJOR UNDERGROUND CAVERNS IN INDIA	20
2.3	ROCK ENGINEERING TOOLS FOR STABILITY EVALUATIONS OF CAVERNS	26
2.3.1	Empirical Methods	27
2.3.2	Analytical and Numerical Methods	36
2.4	SUPPORT SYSTEM	42
2.4.1	Spot Bolting	42
2.4.2	Systematic Bolting	42
2.4.3	Design of shotcrete and fibrecrete support	44
2.4.4	Design of cast concrete support	45
2.5	STRESSES AROUND UNDERGROUND CAVERNS NEAR TOE OF SLOPES	45
2.6	CRITICAL STRAIN OF ROCK MASS	46
2.7	RESEARCH IN CAVERN STABILITY AND RELATED ISSUES	48
2.7.1	3D Physical Modelling Studies	48
2.7.2	Borehole TV Camera	49
2.7.3	Numerical Modelling Studies	50

2.8	INDIAN RESEARCH EXPERIENCES IN CAVERN RELATED STUDIES	56
CHAPTER 3	INVESTIGATIONS	60
3.1	FIELD INVESTIGATIONS	60
3.1.1	Description of the Site	60
3.1.2	Investigations in Powerhouse Complex	64
3.1.2.1	Laboratory testing and estimation of rock mass parameters	67
3.1.2.2	Geology of powerhouse complex	68
3.1.2.3	In-situ stress	70
3.1.2.4	Excavation at powerhouse cavern	70
3.1.2.5	Excavation of transformer hall	73
3.1.2.6	Excavation of bus ducts	74
3.1.3	Field Instrumentation	75
3.1.4	Instrumentation and Installation	80
3.2	NUMERICAL MODELLING	88
3.2.1	3D Discontinuum Model using 3DEC	88
3.2.2	3D Continuum Model using FLAC-3D	94
3.2.3	Basis of Analysis	101
3.2.4	Parametric Study	102
3.2.5	Sensitivity Analysis	106
CHAPTER 4	RESULTS AND DISCUSSION	107
4.1	POWERHOUSE CAVERN	107
4.1.1	Movement at the Center of Crown	107
4.1.2	Movement in the Widened part of Crown	113
4.1.3	Load on Rock Bolts in the Crown	121
4.1.4	Load on the Steel Ribs in the Crown	124
4.1.5	Movement in the Side Walls	137
4.1.6	Load on Rock Bolts in the Walls	158
4.1.7	Instrumented Bolt Observations	173

4.1.8	Pore Water Pressure Observations at Powerhouse Cavern	179
4.2	TRANSFORMER HALL CAVERN	180
4.2.1	Load on the Steel Ribs in the Crown	180
4.2.2	Load on Rock Bolts in the Walls	182
4.2.3	Movements in the Side Walls	186
4.3	CROSS TUNNELS IN POWERHOUSE COMPLEX	189
4.4	NUMERICAL MODELLING	194
4.4.1	Displacement Distribution around the Caverns	194
4.4.2	Comparison of Measured and Model Convergence	200
4.4.3	Stress Distribution	202
4.4.4	Strain on the Walls of Caverns	214
4.4.5	Strength to Stress Ratio	216
4.4.6	Effect of Cavern Orientation on Stability	219
4.4.7	Sensitivity Analysis	225
CHAPTER 5	CONCLUSIONS	229
REFERENCES		233
APPENDIX 1		244
APPENDIX 2		247
APPENDIX 3		274
APPENDIX 4		285
APPENDIX 5		291
LIST OF PUBLICATIONS		303
CURRICULUM VITAE		304

LIST OF FIGURES

Fig. No.	Title	Page No.
1.1	Per-capita energy consumption in India and selected regions (Anon, 2015)	2
1.2	Total energy consumption in India	2
1.3	Installed capacity of electricity generation in India	3
1.4	Map showing the Himalayan region	6
2.1	Different geometrical shapes of caverns	12
2.2	Conventional arched roof cavern vs elliptical cavern	13
2.3	Powerhouse cavern of Nathpa Jhakri hydro electric project, Himachal Pradesh	21
2.4	Powerhouse and transformer hall caverns of Tapovan Vishnugad hydroelectric project, Uttarakhand	24
2.5	Principle relationships between ground behaviour and rock engineering and design	26
2.6	Simplified diagram for selection of design methodology	27
2.7	Updated Q chart	29
2.8	Quantification of GSI by joint condition and RQD	35
2.9	Limitations on the use of GSI	35
2.10	Classification of modelling problems	38
2.11	Continuum and discontinuum models	39
2.12	a. Distribution of principal stresses in a gravitationally loaded slope b. Zones of overstress and failure surrounding an underground cavern at different distances from the toe of the slope	46
2.13	Hazard warning levels for assessing the stability of tunnels	47
3.1	Location of Chhukha Dzongkagh	61
3.2	Location of dam site, Tala Hydroelectric Project, Bhutan	62
3.3	Location of power house site, Tala Hydroelectric Project, Bhutan	62
3.4	Layout of Tala Hydroelectric Project, Bhutan	63
3.5	Details of caverns and connecting tunnels at powerhouse complex of Tala Hydroelectric Project, Bhutan	63
3.6	Cross section of powerhouse complex, Tala Hydroelectric Project	65
3.7	Pole projection of joint sets of powerhouse cavern for kinematic analysis	69
3.8	Sequence and period of excavation at powerhouse cavern	72
3.9	Powerhouse cavern after complete excavation, Tala Hydroelectric Project	73

3.10	Sequence and period of excavation at transformer hall cavern	74
3.11	Section of the powerhouse cavern showing location of instruments	75
3.12	Section of the transformer hall cavern showing location of instruments	75
3.13	Longitudinal section of the powerhouse cavern showing location of instruments on upstream wall	76
3.14	Longitudinal section of the powerhouse cavern showing location of instruments on downstream wall	76
3.15	Section of bus ducts showing the location of instruments	77
3.16	MRMPBX with the readout unit	81
3.17	Schematic diagram of anchor load cell with rock bolt	82
3.18	Anchor load cell with readout unit	83
3.19	Anchor load cell installed on rock bolt at powerhouse cavern	83
3.20	Load cell on the steel rib at crown of powerhouse	84
3.21	Monitoring of load cells at walls of the cavern	84
3.22	Total station TDA 5005 with reflective targets	85
3.23	Measuring the convergence using Total Station TDA 5005	85
3.24	Vibrating wire piezometer	86
3.25	Monitoring of piezometers at walls of the cavern	87
3.26	Vibrating wire instrumented bolt	87
3.27	Perspective view of powerhouse complex, Tala Hydroelectric Project	89
3.28	Excavation sequence adopted in the 3D Model	92
3.29	Boundary conditions in the 3D model	93
3.30	3D continuum model of Tala powerhouse complex	95
3.31	Perspective view of powerhouse complex, Tala Hydroelectric Project (view-1)	95
3.32	Perspective view of powerhouse complex, Tala Hydroelectric Project (view-2)	96
3.33	Typical displacement contours after complete extraction of caverns and tunnels	98
3.34	Typical displacement vector after complete extraction of caverns and tunnels	99
3.35	Typical stress tensor plot after complete extraction of caverns and tunnels	99
3.36	Typical minimum principal stress plot after complete extraction of caverns and tunnels	100
3.37	Typical maximum principal stress plot after complete extraction of caverns and tunnels	100

3.38	Typical intermediate principal stress plot after complete extraction of caverns and tunnels	101
3.39	Orientation of caverns with direction of maximum principal stress	102
4.1	Displacement at the center of crown of powerhouse cavern at RD-15	107
4.2	Displacement at the center of crown of powerhouse cavern at RD-80	109
4.3	Displacement at the center of crown of powerhouse cavern at RD-130	111
4.4	Displacement at the center of crown of powerhouse cavern at RD-150	112
4.5	Displacement at the downstream side of crown of powerhouse cavern at RD-15	114
4.6	Displacement at the upstream side of crown of powerhouse cavern at RD-15	115
4.7	Displacement at the upstream side of crown of powerhouse cavern at RD-80	116
4.8	Displacement at the upstream side of crown of powerhouse cavern at RD-130	118
4.9	Roof collapse at powerhouse cavern	119
4.10	Strain in crown of powerhouse cavern vis a vis warning levels	120
4.11	Axial load on rock bolts in the crown of powerhouse cavern	121
4.12	Axial load on steel ribs on upstream side in the crown of powerhouse cavern	129
4.13	Axial load on steel ribs on downstream side in the crown of powerhouse cavern	130
4.14	Axial load on steel ribs on upstream side during benching (B1-B11) in the crown of powerhouse cavern	130
4.15	Axial load on steel ribs on downstream side during benching (B1-B11) in the crown of powerhouse cavern	131
4.16	Rate of loading on steel ribs on upstream side during benching	131
4.17	Rate of loading on steel ribs on downstream side during benching	132
4.18	Cumulative convergence of walls at powerhouse cavern at EL-525	137
4.19	Cumulative convergence of walls at powerhouse cavern at EL-520	141
4.20	Cumulative convergence of walls at powerhouse cavern at EL-515	146
4.21	Cumulative convergence of walls at powerhouse cavern at EL-506	149
4.22	Cumulative convergence of walls at powerhouse cavern at EL-525 during excavation of main benches	152
4.23	Cumulative convergence of walls at powerhouse cavern at EL-520 during excavation of main benches	153
4.24	Cumulative convergence of walls at powerhouse cavern at EL-515 during excavation of main benches	153
4.25	Convergence rate of walls at powerhouse cavern at EL-525	154

4.26	Convergence rate of walls at powerhouse cavern at EL-520	154
4.27	Convergence rate of walls at powerhouse cavern at EL-515	155
4.28	Convergence rate of walls at powerhouse cavern at EL-506	155
4.29	Axial load on rock bolts at EL-529 on walls of powerhouse cavern	159
4.30	Axial load on rock bolts at EL-529 on walls of powerhouse cavern during excavation of main benches	160
4.31	Axial load on rock bolts at EL-525 on upstream wall of powerhouse cavern	161
4.32	Axial load on rock bolts at EL-525 on upstream wall of powerhouse cavern during excavation of main benches	161
4.33	Axial load on rock bolts at EL-525 on downstream wall of powerhouse cavern	162
4.34	Axial load on rock bolts at EL-525 on downstream wall of powerhouse cavern during excavation of main benches	162
4.35	Axial load on rock bolts at EL-520 on upstream wall of powerhouse cavern	163
4.36	Axial load on rock bolts at EL-520 on upstream wall of powerhouse cavern during excavation of main benches	164
4.37	Axial load on rock bolts at EL-520 on downstream wall of powerhouse cavern	164
4.38	Axial load on rock bolts at EL-520 on downstream wall of powerhouse cavern during excavation of main benches	165
4.39	Axial load on rock bolts at EL-515 on upstream wall of powerhouse cavern	166
4.40	Axial load on rock bolts at EL-515 on upstream wall of powerhouse cavern during excavation of main benches	166
4.41	Axial load on rock bolts at EL-515 on downstream wall of powerhouse cavern	167
4.42	Axial load on rock bolts at EL-515 on downstream wall of powerhouse cavern during excavation of main benches	167
4.43	Axial load on rock bolts at EL-506 on upstream wall of powerhouse cavern	168
4.44	Axial load on rock bolts at EL-506 on upstream wall of powerhouse cavern during excavation of main benches	169
4.45	Axial load on rock bolts at EL-506 on downstream wall of powerhouse cavern	169
4.46	Axial load on rock bolts at EL-506 on downstream wall of powerhouse cavern during excavation of main benches	170
4.47	Change in micro strain in instrumented bolt at RD 65, EL 506 at downstream wall of powerhouse cavern	174
4.48	Change in micro strain in instrumented bolt at RD 110, EL 506 at downstream wall of powerhouse cavern	175
4.49	Change in micro strain in instrumented bolt at RD 150, EL 506 at downstream wall of powerhouse cavern	175

4.50	Change in micro strain in instrumented bolt at RD 65, EL 506 at upstream wall of powerhouse cavern	176
4.51	Change in micro strain in instrumented bolt at RD 110, EL 506 at upstream wall of powerhouse cavern	176
4.52	Change in micro strain in instrumented bolt at RD 150, EL 506 at upstream wall of powerhouse cavern	177
4.53	Change in micro strain in instrumented bolt at RD 140, EL 515 at upstream wall of powerhouse cavern	178
4.54	Change in micro strain in instrumented bolt at RD 150, EL 515 at upstream wall of powerhouse cavern	178
4.55	Axial load on steel ribs on upstream side in the crown of transformer hall cavern	180
4.56	Axial load on steel ribs on downstream side in the crown of transformer hall cavern	181
4.57	Axial load on rock bolts at EL-532 on upstream and downstream wall of powerhouse cavern	183
4.58	Axial load on rock bolts at EL-525 on upstream and downstream wall of powerhouse cavern	184
4.59	Axial load on rock bolts at EL-520 on upstream and downstream wall of powerhouse cavern	184
4.60	Cumulative convergence of walls at transformer hall cavern at EL-531	186
4.61	Cumulative convergence of walls at transformer hall cavern at EL-525	187
4.62	Cumulative convergence of walls at transformer hall cavern at EL-520	187
4.63	Convergence rate of walls at transformer hall cavern	189
4.64	Axial load on steel ribs in bus ducts and passage tunnels	190
4.65	Axial load on rock bolts in bus ducts and passage tunnels	191
4.66	Axial load on steel ribs in pressure shaft manifolds tunnels	192
4.67	Axial load on rock bolts in pressure shaft manifolds tunnels	192
4.68	Tension cracks on walls of bus ducts	193
4.69	Horizontal displacement contours after excavation of bench-4 and bench-5	195
4.70	Displacement contours at RD-15, powerhouse cavern	196
4.71	Displacement contours at RD-65, powerhouse cavern	197
4.72	Displacement contours at RD-110, powerhouse cavern	197
4.73	Displacement contours at RD-150, powerhouse cavern	198
4.74	Displacement contours at EL-525, powerhouse cavern	198
4.75	Displacement contours at EL-520, powerhouse cavern	199
4.76	Displacement contours at EL-515, powerhouse cavern	199
4.77	Comparison of measured and model convergence at EL-525	200

4.78	Comparison of measured and model convergence at EL-520	201
4.79	Comparison of measured and model convergence at EL-515	202
4.80	Principal stress contours around the caverns at RD-15	203
4.81	Principal stress contours around the caverns at RD-65	204
4.82	Principal stress contours around the caverns at RD-110	205
4.83	Principal stress contours around the caverns at RD-150	206
4.84	Distribution of stress concentration factors in cross sections at EL-525	208
4.85	Distribution of stress concentration factors in cross sections at EL-520	209
4.86	Distribution of stress concentration factors in cross sections at EL-515	210
4.87	Strain distribution on upstream wall of powerhouse cavern	214
4.88	Strain distribution on downstream wall of powerhouse cavern	215
4.89	Strain distribution on upstream wall of transformer hall cavern	216
4.90	Strain distribution on downstream wall of transformer hall cavern	216
4.91	Strength to stress ratio at RD-15, powerhouse cavern	217
4.92	Strength to stress ratio at RD-65, powerhouse cavern	217
4.93	Strength to stress ratio at RD-110, powerhouse cavern	218
4.94	Strength to stress ratio at RD-150, powerhouse cavern	218
4.95	Variation of displacement with cavern configuration	219
4.96	Variation of maximum stress ratio in the pillar due to vertical stress with cavern configuration	220
4.97	Variation of maximum stress ratio in the pillar due to σ_{xx} with cavern configuration	220
4.98	Variation of maximum stress ratio in the pillar due to σ_{yy} with cavern configuration	221
4.99	Variation of maximum stress ratio in the upstream wall of powerhouse due to vertical stress (σ_{zz})with cavern configuration	222
4.100	Variation of maximum stress ratio in the upstream wall of powerhouse due to σ_{xx} stress with cavern configuration	222
4.101	Variation of maximum stress ratio in the upstream wall of powerhouse due to σ_{yy} stress	223
4.102	Variation maximum stress ratio in the downstream wall of transformer hall due to vertical stress (σ_{zz})	224
4.103	Variation maximum stress ratio in the downstream wall of transformer hall due to σ_{xx} stress	224
4.104	Variation maximum stress ratio in the downstream wall of transformer hall due to σ_{yy} stress	225
4.105	Tornado diagram of sensitivity analysis at RD-65, EL-525	227

4.106 Tornado diagram of sensitivity analysis at RD-110, EL-525	227
4.107 Tornado diagram of sensitivity analysis at RD-150, EL-525	228

LIST OF TABLES

Table No.	Title	Page No.
2.1	Major underground caverns in hydroelectric projects in India	25
2.2	Excavation Support Ratio (ESR) values for use in Q	30
2.3	Relationship between Q and deformation (Δ)	31
2.4	Guidelines for excavation and support of 10 m span rock tunnels in accordance with the RMR system	33
2.5	Empirical formulae, estimating length of rock bolts as a function of cavern span/height	44
2.6	Empirical formulae for determining spacing between rock bolts	44
3.1	Summary of laboratory test results	68
3.2	Major discontinuities in powerhouse cavern	69
3.3	Estimated rock mass parameters in powerhouse complex	89
3.4	Joint Properties in 3DEC Model	90
3.5	Rock Bolt Properties used in 3DEC (Local reinforcement axial command)	91
3.6	Shotcrete Properties used in 3DEC (liner command)	91
3.7	Steel Ribs Properties used in 3DEC (beam command)	91
3.8	Rock Bolt Properties used in FLAC-3D (Cable elements)	96
3.9	Shotcrete Properties used in FLAC-3D (Liner elements)	96
3.10	Steel Ribs Properties used in FLAC-3D (beam command)	97
3.11	Details of applied stresses for $\phi=0$	103
3.12	Details of applied stresses for $\phi = 15^\circ$ and 105°	103
3.13	Details of applied stresses for $\phi = 30^\circ$ and 120°	104
3.14	Details of applied stresses for $\phi = 45^\circ$ and 135°	104
3.15	Details of applied stresses for $\phi = 60^\circ$ and 150°	105
3.16	Details of applied stresses for $\phi = 75^\circ$ and 165°	105
3.17	Details of applied stresses for $\phi = 90^\circ$	106

4.1	MRMPBX readings at RD-15m center of crown	108
4.2	MRMPBX readings at RD-80m center of crown	110
4.3	MRMPBX readings at RD-130m center of crown	111
4.4	MRMPBX readings at RD-150m center of crown	113
4.5	MRMPBX readings at RD-15m left side of crown	114
4.6	MRMPBX readings at RD-15m right side of crown	115
4.7	MRMPBX readings at RD-80m right side of crown	117
4.8	MRMPBX readings at RD-130m right side of crown	118
4.9	Critical strain at powerhouse cavern	120
4.10	Load cell observations on rock bolts at crown of powerhouse cavern	122
4.11	Load cell readings on steel ribs on upstream side at powerhouse cavern	124
4.12	Load cell readings on steel ribs on downstream side at powerhouse cavern	126
4.13	Summary of change in load in steel ribs during each benching at powerhouse cavern	133
4.14	Convergence data of upstream and downstream wall of powerhouse cavern at EL-525	138
4.15	Convergence data of upstream and downstream wall of powerhouse cavern at EL-520	142
4.16	Convergence data of upstream and downstream wall of powerhouse cavern at EL-515	146
4.17	Convergence data of upstream and downstream wall of powerhouse cavern at EL-506	149
4.18	Details of convergence observations at powerhouse cavern during excavation of main benches	152
4.19	Summary of convergence observations at powerhouse cavern	156
4.20	Details of cumulative convergence measurements at powerhouse cavern	157
4.21	Summary of load on rock bolts on the walls of powerhouse cavern	171

4.22	Summary of strain changes in instrumented rock bolts	179
4.23	Details of load changes in ribs in the crown of Transformer Hall	181
4.24	Details of load changes in rock bolts in the walls of Transformer Hall	185
4.25	Details of convergence measurements at transformer hall cavern	188
4.26	Comparison of model and measured convergence between excavation of bench-4 (B-4) and bench-5 (B-5)	196
4.27	Comparison of convergence measurements with model results at powerhouse cavern	200
4.28	Results of sensitivity analysis	226

NOMENCLATURE

Abbreviations

3DEC	: Three Dimensional Distinct Element Code
FLAC-3D	: Fast Lagrangian Analysis of Continua in 3 Dimensions
GSI	: Geological Strength Index
MRMPBX	: Magnetic Ring Multi Point Borehole Extensometer
Q	: Q Rock Mass Classification Index
RMR	: Rock Mass Rating
SFRS	: Steel Fibre Reinforced Concrete
σ_1	: Maximum Principal Stress
σ_2	: Intermediate Principal Stress
σ_3	: Minimum Principal Stress
σ_{xx}	: Normal stress in X Direction
σ_{yy}	: Normal Stress in Y Direction
σ_{zz}	: Normal Stress in Z Diirection
σ_i	: In-situ Stress

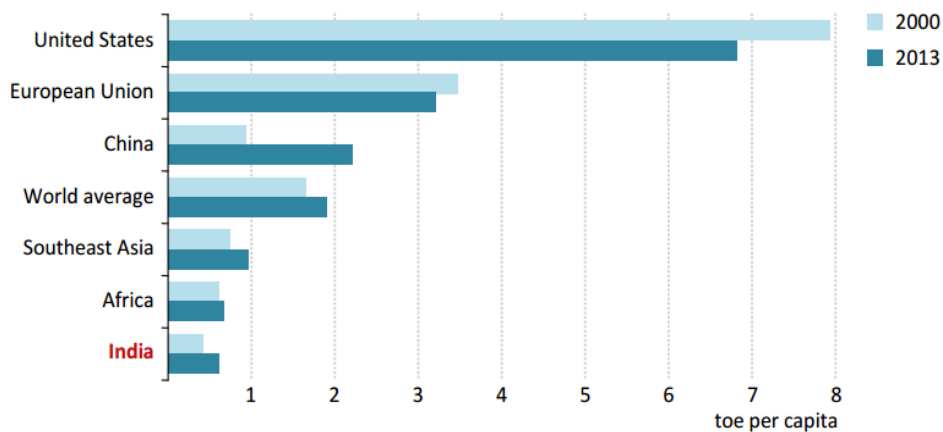
INTRODUCTION

India, home to 18% of the world's population, uses only 6% of the world's primary energy. India has been responsible for almost 10% of the increase in global energy demand since 2000. Its energy demand in this period has almost doubled, pushing the country's share in global demand upto 6% in 2015 from 4.4% at the beginning of the century. However, on a per-capita basis, energy demand in India remains only around one third of the world average, slightly lower than the average for the African continent (Fig. 1.1). Per-capita electricity consumption in India has been continuously increasing over the years. From 734kWh in 2008-09, the per capita consumption has reached 1075kWh in 2015-16, an increase of 46% in 8 years. The per capita consumption has been increasing at an average of 6% every year. India is one of the fastest growing economies in the world. India's economy, already the world's third-largest, is growing rapidly with an impressive economic growth of over 7% per annum.

India's energy consumption has been growing rapidly in the last decade. It stands third with total energy consumption of 882Mtoe after China (3101Mtoe) and United States (2196Mtoe) for the year 2015. Total energy consumption is growing at an average rate of 4.7% per year for 2000-2015 period as shown in Fig. 1.2 (Anon, 2016).

India is committed to produce low-carbon sources of energy, particularly led by renewable energy sources like solar, hydro power and wind power. India's contribution is likely to be the highest in projected rise in global energy demand, around one quarter of the total. However, energy demand per capita in 2040 will be still 40% below the world average. With energy use declining in many developed countries and China entering a much less energy intensive phase in its development, India emerges as a major driving force in global trends, with all modern fuels and technologies playing a part (Anon, 2015).

Coal still dominates the energy demand in India. In 2013, it constituted 44% of total and renewable energy including hydropower, which is just at 2%. Renewable energy in India is mainly through solar, wind and hydropower.



Note: toe = tonnes of oil equivalent.

Fig. 1.1 Per-capita energy consumption in India and selected regions (Anon, 2015)

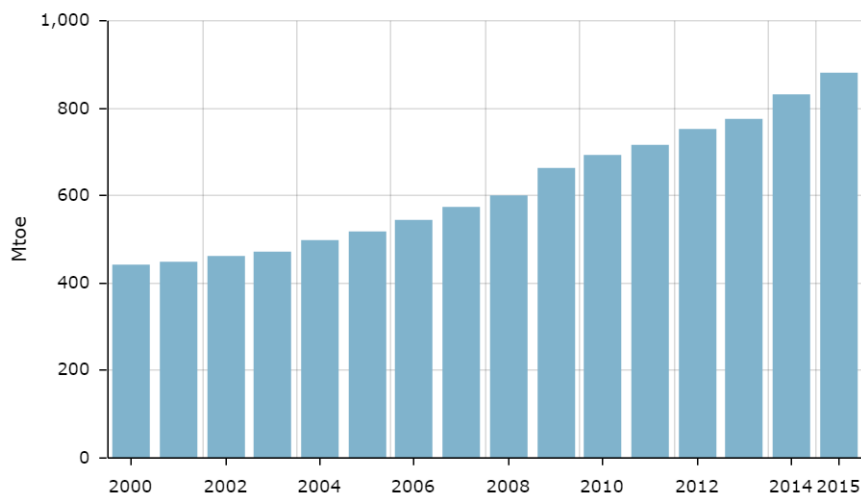


Fig. 1.2 Total energy consumption in India (Anon, 2016)

1.1 HYDROPOWER

Hydropower potential of India is about 1,48,701MW at 60% load factor, one of the largest in the world. India is 7th largest producer of hydroelectric power. Present installed capacity of electricity generation is 303.12GW of which only 15.55% (47.12GW) comes from hydropower. Although capacity has steadily increased, the contribution of hydropower to Indian power generation has been on a declining trend in recent decades, from close to 40% in 1980 to 15.5% in 2016. In India, less than 25MW capacity power plant is termed as small hydro and is classified under renewable energy source along with solar power, bio-power and wind energy and constitutes 9%

of hydropower in the country. Present capacity of 47GW represents a little under a third of the assessed hydro resource and much of the remaining potential is in the north and northeast regions (in the Himalayas). A further 14GW are under construction, although some of these plants have been delayed by technical or environmental problems and public opposition. If developed prudently, hydropower can bring multiple benefits as a flexible source of clean electricity. Fig. 1.3 shows distribution of electricity generation from different sources as on June 2016 (Anon, 2016a, 2016b).

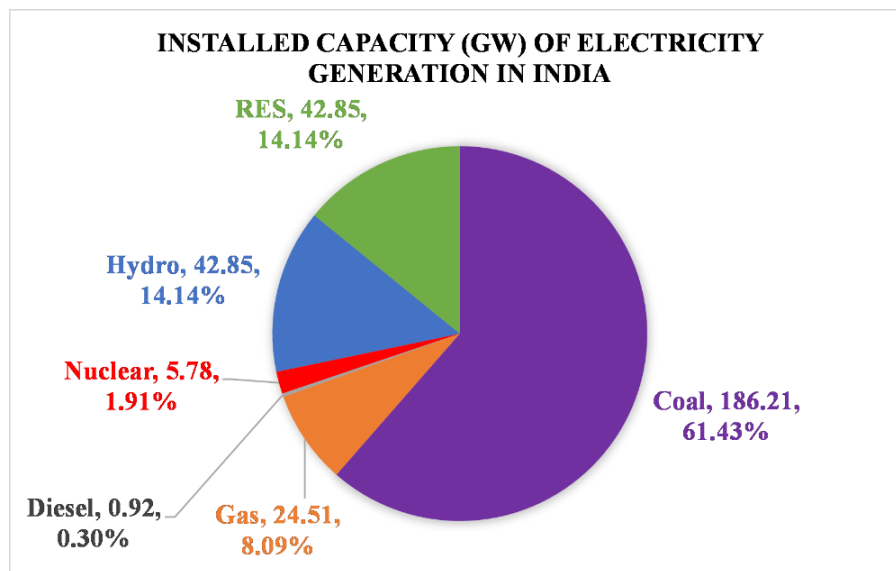


Fig. 1.3 Installed capacity of electricity generation in India (Anon, 2016b)

1.1.1 Hydropower development in Himalayas

Himalayan region offers potential for large hydro projects with water head in excess of 500m available due to the topography and geological setup of the area. Due to high risks of landslides and slope failures, the preferred method of locating the hydropower plant has been in underground caverns. Higher capacity power plants need more space to house the equipment and other facilities for power generation and this calls for creation of large underground caverns.

There are issues specific to hydropower, notably the high levels of sediment in the rivers coming down from the Himalayan mountains, which can reduce reservoir storage capacity and, if not removed, cause heavy damage to turbine blades and other steel structures in a hydropower plant. Projects are delayed beyond their schedules due to unexpected geological surprises and ground control problems.

Another avenue for India to benefit from hydropower is through co-operation with neighbouring countries. India has assisted Bhutan in developing 1.5GW of hydropower with three projects. Ten more hydro projects are in various stages of construction or preparation. Recently, India has approved projects with a combined capacity of 1.8GW with Nepal.

Currently, northern Indian states contribute 43% (18.31GW) of total installed hydro power capacity. Himalayan states of Himachal Pradesh (8%), Jammu and Kashmir (5%) and Uttarakhand (6%) constitute 19% of total hydropower in the country. Himachal Pradesh currently has two major power plants, Nathpa Jhakri hydro power plant (1500MW) and Karcham Wangtoo hydro power plant (1000MW) on river Sutlej. Both these power plants are located in large underground caverns. Other notable hydro power plants with underground caverns in Himachal Pradesh are Chamera-I (540MW), Parbati Stage III (520MW), Chamera-II (300MW), Baspa-II (300MW), Chamera-III (231MW) and Larji (126MW). In Uttarakhand, Tehri hydro power plant (1000MW) is in operation and other project with pumped storage scheme (1000MW) is under construction and both have large underground caverns. Other notable power plants which are situated in underground caverns are Tapovan Vishnugad (520MW), Vishnuprayag (400MW) and Chibro (240MW). In Jammu and Kashmir, Uri (480MW) and Baglihar Stage-1 (450MW) are located in underground caverns.

North eastern states and Sikkim also come under Himalayan region and have huge potential for development of hydro power. Estimated hydro potential in north eastern states and Sikkim is 62,604MW with many large hydropower projects identified in Brahmaputra and Teesta river basins. Currently, only 1,242MW of electricity is being generated in north eastern states and 16 hydropower projects totalling 5,576MW are under construction. In Sikkim, Teesta-V (510MW) power plant is in operation and other two, Teesta-III (1200MW) and Teesta-VI (500MW) are under construction and all of them are located in underground caverns.

Hydropower development in Bhutan

Bhutan currently produces 1,606MW of hydropower, which is about 6% of the estimated 24,000MW hydropower potential. By 2018, it is expected to reach 3,446MW. In the absence of oil and very minimum coal reserves, major thrust is on hydropower

and hydropower export (75% of total production) to India provide more than 40% of its revenue and constitutes 25% of its GDP. Major hydropower projects with large underground caverns, Tala hydroelectric project (1,020MW), Chukha (336MW) and Dagachhu (126MW) are in operation. Other major hydroelectric projects with large underground caverns, under construction are Punatsangchhu-I hydroelectric project (1,200MW), Punatsangchhu-II hydroelectric project (1,020MW) and Mangdechhu hydroelectric project (720MW) (Anon, 2015a, Anon, 2015b).

Hydropower development in Nepal

Nepal has an estimated potential of 83,000MW, of which 40,000MW is considered to be economical and technically viable. However, development of hydropower in Nepal has been sluggish and so far been able to develop only 680MW. Major hydroelectric projects in Nepal are Kali Gandaki (144MW), Middle Marsyangdi (70MW), Marshyangdi (69MW) and Kulekhani-I (60MW). However, many large hydroelectric projects are in planning stage and expected to come up in the near future (Sharma and Awal, 2013, Anon, 2016c).

1.2 GEOLOGICAL CHALLENGES IN TUNNELING IN HIMALAYAS

The Himalaya is the youngest mountain chain on the planet and is believed to be still evolving and has not yet stabilised geologically and geomorphologically. Indian Himalaya covers a stretch of over 2,500km and breadth of 250-300km from Jammu and Kashmir in the west to Arunachal Pradesh in the east. An area of about 5,33,604km² lies between 21° 57' - 37° 5' N latitudes and 72° 40' - 97° 25' E longitudes (Nandy et al., 2006). Fig. 1.4 shows Himalayan region in India. Physically Himalayas are divided into three parts separated by major geological fault lines as follows:

- Greater Himalaya (Himadri)
- Lesser Himalaya (Himanchal)
- Sub Himalayan Foothills (Siwaliks)

Himalayan region as a whole is affected by a constant tectonic uplifting as well as down cutting effects by several river systems. Himalayan topography typically consists of high hills and deep valleys with high gradients. Highly complex geological conditions exist due to active tectonics and structural discontinuities. Rock mass is subjected to varying in-situ stresses.

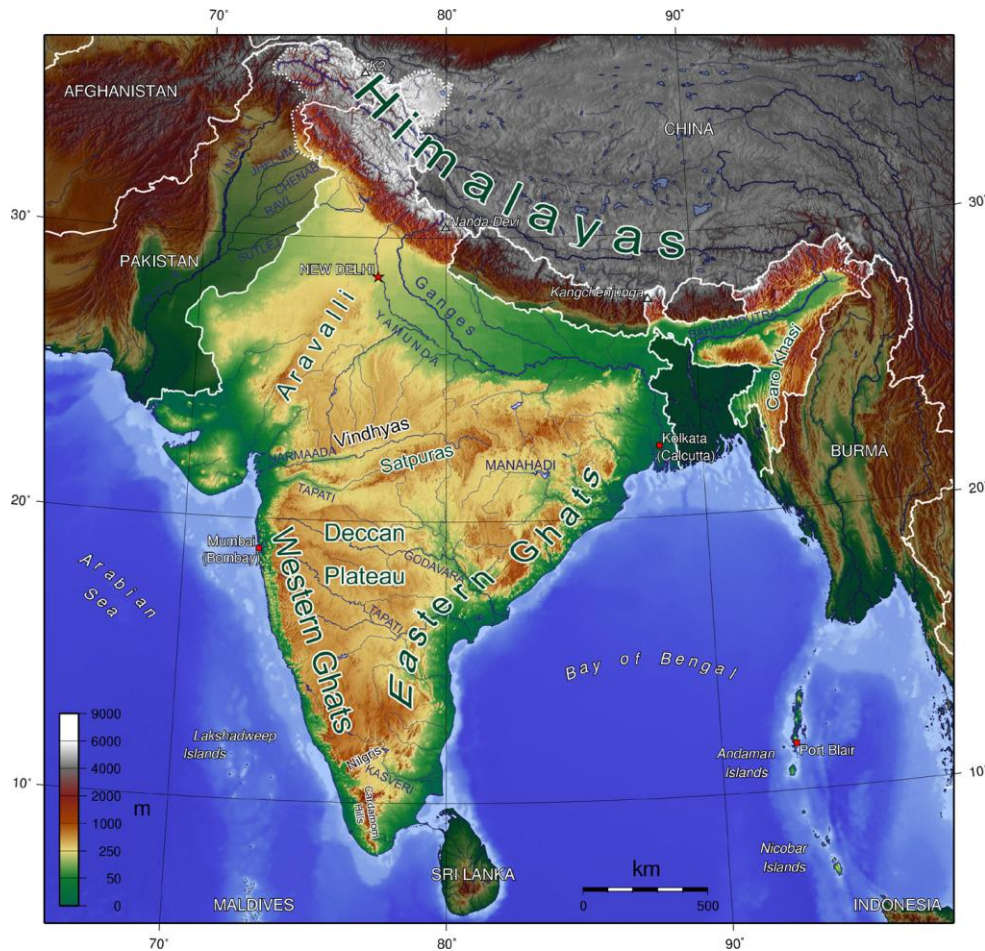


Fig. 1.4 Map showing the Himalayan region (Anon, 2008)

In addition, the compressional tectonic stress regime in the Himalaya has resulted in intense deformation of the rock mass, making it highly folded, faulted, sheared, fractured and deeply weathered. This complex geological setting has caused considerable stability problems and is a great challenge for successful tunnelling. Sharma and Tiwari (2012) discussed geological problems associated with tunnelling in Himalayas and were of the opinion that in tectonically active young mountains like the Himalayas, the rocks found during tunnelling are relatively incompetent and affected by a number of folds, faults and thrusts of various magnitudes and at many places are heavily charged with underground water. The most commonly encountered geological problems during tunnelling for hydroelectric projects in the Himalayan region are fault/thrust/shear zones, running ground conditions, squeezing, heaving and swelling, rock bursting, ground water inflow, wedge/block failures, hot temperature conditions, and gases in rock etc. Panthi (2007) summarised the factors adding to geological complexity in Himalayas as follows:

- Weak rock mass quality
- High degree of weathering and fracturing
- Rock stresses
- Ground water effect

Bedding and foliation that exist in the sedimentary and metamorphic rocks of Himalaya have made them highly directional affecting strength (strength anisotropy) and deformability of rock mass. This directional behaviour reduces the self-supporting capacity of the rock mass. Another major feature of the highly deformed rock mass of the Himalaya is frequent intercalation between different rocks and shear bands. On many occasions, thin bands of very weak and highly deformed rocks such as slate, phyllite, schists and sheared mylonites are intercalated within the bands of relatively strong and brittle rocks such as gneiss, quartzite and dolomite. These small bands of weak rock mass are squeezed and highly sheared within the stronger layers of rock mass. Being weaker in their mechanical characteristics and highly schistose, these shear bands lack sufficient bonding/friction and reduce self-supporting capability.

High degree of fracturing and weathering results in immediate tunnel collapse due to very low cohesion and friction. Fracturing in the rock mass results in many open channels facilitating the water inflow into the tunnels.

The third major stability problem faced during tunneling in the Himalaya is stress anisotropy. Due to topographic reasons, most of the tunnel projects are constructed in the Siwaliks and lesser Himalayan zones, where highly deformed rocks such as shale, mudstone, siltstone, slate, phyllite, schist, schistose gneiss and highly sheared fault gouge and mylonites are present. In general, highly deformed rock mass has very weak rock mass strength, and tunnelling through such rock mass may cause severe squeezing as soon as the overburden stress exceeds the rock mass strength. Severe squeezing has been observed even with relatively low overburden, where tunnels pass through highly sheared fault zones with extremely poor rock mass (Panthi and Nilsen, 2007).

The fault zones, sheared zones, fractured and weathered rock mass of the Himalaya are highly permeable and water bearing. Tunnelling through such permeable zones always poses great difficulties and considerable challenges. The severity of the problems caused by water inflow and leakage are huge in the Himalayas.

1.3 STATEMENT OF THE PROBLEM

In many cases, underground caverns are constructed in adverse geology, and in some cases, exist in close proximity to major geological structures like Main Central Thrust (MCT) and Main Boundary Thrust (MBT) etc. Construction of major underground caverns under such conditions poses difficulties, with respect to stability, as proper choice of support becomes a complex issue. Generally, the choice of supports under such conditions is mainly done using the rock mass classification systems such as “Q”, “RMR” or “GSI”. There are many disadvantages of using these systems and in many cases, it gives a qualitative description of the support system. Improper choice of the support system may lead to the failure of support and in turn may lead to failure of the structure. There are many cases where in, the designed supports have failed to provide adequate resistance causing grave consequences by jeopardising the stability of the caverns.

Every underground excavation project in Himalaya starts with lot of uncertainties as adequate pre-construction stage investigations are not carried out as they are difficult to carry out or quite expensive and time taking. Some of the ground control issues faced while constructing large caverns are as follows:

- Structurally controlled failures at shallow depths, if in-situ stresses are not adequate and supports are not put on time, any opening up of joints can trigger roof fall or wedge failures, particularly in the roof of cavern.
- Sudden geological surprises like shear zone, fractured zone. If preparedness to deal with such situations is not there, it can hamper the progress. Also, if not dealt with proper treatment, may influence the stability of the cavern, with further excavation.
- Sudden in-rush of water can create serious strata control problems. If correct assessment of its source and method to deal with are not done, it can halt the progress of the cavern/tunnels for years. There was one such case in Himalaya where sudden in-rush of water halted the tunnel boring machine (TBM) for many years.
- High wall displacements or convergence of walls far more than the design limits may affect installation and maintenance of utilities.

- Failure of rock bolts and shooting out of rock bolts in high stress regime were observed in many caverns in Himalayas and could be major strata control problem.
- Floor heave is likely and was reported from many caverns. If sufficient time is not allowed after complete excavation or if floor is not reinforced, it can hamper the progress and affect turbine foundation and alignment.
- Time dependent deformations can affect the working powerhouses.

Proper design and construction of the cavern is only possible, if the response of the surrounding rock mass is correctly understood during various stages of cavern excavation. A research study was taken up to assess stability of large caverns at various phases of excavation with a view to understand the rock mass behaviour. Study was continued during post excavation period to observe rock mass response after complete excavation.

In this study, an underground cavern site in lower Himalayas was selected at Tala Hydroelectric Project, Bhutan. At this site, two large caverns were excavated and behaviour of surrounding rock mass and the installed support during construction of the caverns was studied by monitoring the displacement of crown, side walls of the cavern and the load developed in rock bolts. The following stability issues were observed during the construction of caverns:

- Failure of the crown of powerhouse cavern.
- Large number of rock bolt failures in the side walls.
- Large displacement/convergence of side walls during construction and post construction.
- Recording of large load on steel ribs and appearance of tension cracks in cross tunnels.

In the caverns so far constructed in Himalayas, limited monitoring was done using geotechnical instruments during construction and there was no continuity of monitoring of same instruments during post excavation period. In this research study, an attempt is made to understand rock mass response at every stage of excavation by capturing them through instruments and simulate the same response in 3D numerical models. Study was carried out in following phases:

- Field investigations that included collection of rock samples for laboratory testing, rock mass characterisation and installation and monitoring of instruments at various stages of construction.
- Numerical modelling that included creation of 3D continuum and discontinuum models and calibration of the model with field measurements, assessment of stability of the cavern through model results.

A calibrated model could give insight into areas not covered by instruments and influence of other parameters on cavern stability, which are not measured in the field. Behaviour of the cavern was simulated using both continuum and discontinuum 3D numerical models.

Stability of the cavern was assessed based on combined approach utilising, calculation of strength to stress ratio, strain on the walls, field measurements and physical observations. Cavern orientation with principal stress direction is an important parameter that governs the stability of cavern. Parametric study was done using the calibrated model for different orientation of the cavern. Stress distributions in the pillar and side abutments were studied. Sensitivity analysis was carried out to identify the most sensitive parameter among the parameters used in 3D numerical modelling.

1.4 ORGANISATION OF THE THESIS

This thesis is divided into chapters for disseminating relevant information. Chapter -1, briefly introduces the research topic giving the background information. Available literature and latest developments in this area of research are briefly outlined in Chapter-2. Investigations carried out during this research study (both field investigations and numerical modelling studies) are explained in Chapter-3. Results of instrumentation from field investigation and 3D numerical modelling results are analysed and presented in Chapter-4. Conclusions drawn from the research study and suggestions for future research are presented in Chapter-5. Research findings from other researchers and other relevant references are listed out in Reference section. Details of field data and other supplementary information are appended at the end of the thesis.

LITERATURE REVIEW

Stability of large underground caverns revolves around interaction of surrounding rock mass with the cavern and its support elements. There are two factors, fixed one like geological setup, in-situ state of stress and variable factors like shape and size of cavern, orientation of cavern, existence of other caverns in the vicinity, method of excavation and finally support elements provided to aid its interaction with the surrounding rock mass, that determine the stability of the cavern. Interaction of cavern in Himalayas is more complex due to variable geological setup and in-situ stress regime. Many researchers have contributed to understanding the mechanics involved and in-turn facilitated in improving the stability so that the very purpose of the cavern is justified both technically and economically. Some of the important research leading us to present status of understanding of caverns is presented below.

2.1 CAVERNS

An underground opening having a cross sectional area of 120m² or more and an axial dimension of not exceeding 15 times the lateral dimension is classified as a “Cavern” (Sinha, 1989). Caverns are constructed to cater facilities such as underground powerhouses, pumped storage units, storage of food, drinking water, oil and other liquid hydrocarbons, pressurised gas and air, industrial waste, subway stations, sewage treatment plants, parking garages, swimming pools, shelters, testing facilities, military facilities and for recreational uses. Broch (2016) reviewed extensive use of rock caverns in Norway.

Traditionally, roof of the cavern is a circular arch, but could be changed to multi-radial or elliptical to suit the host geology. Trapezoidal roof with side haunches limiting the length of flat spans of the roof were used for the caverns at Drakensburg (South Africa), and Poatina (Tasmania, Australia). The sides of cavern could remain straight or curved. The invert of the cavern could be straight or remain curved. In South Korea, mushroom and egg shaped caverns have been constructed. Numerical analysis by Lee et al. (2003) showed that egg shaped cross section provides many advantages in structural stability. Some of the shapes of the cavern generally used are shown in Fig. 2.1.

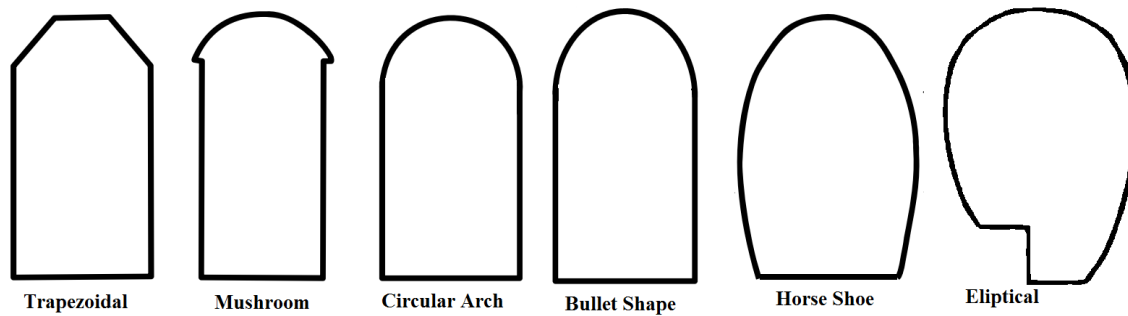


Fig. 2.1 Different geometrical shapes of caverns (Saurer et al., 2013)

2.1.1 Choice of Cavern Shapes

Conventional shape chosen for an underground powerhouse cavern in competent rock mass is circular arch. Arched roof provides stability in the rock mass above the cavern roof with uniform stress distribution and also provides convenient headroom for an overhead crane and ventilation ducts. Also, sidewalls are simple to excavate by vertical drill-and-blast benching and provide straight walls for crane column location and utilization of space to the maximum extent possible. However, problem with this cavern shape when used in weak rock masses, particularly with high horizontal in-situ stresses, is that tall straight sidewalls tend to deflect inwards and tensile failure is induced as shown in Fig. 2.2 (Hoek, 2000). Stabilisation of the rock mass surrounding this cavern requires significant reinforcement in the form of grouted cables or rock bolts. Under such condition, use of elliptical shape is a practical choice, which can reduce the failure zones substantially and the support requirement.

Elliptical shape has been used in Waldeck II cavern in Germany and Singkarak cavern in Indonesia (Lottes, 1972). Although, elliptical shape is better from geotechnical point of view, it has some practical disadvantages. Cavern shape is such that the construction has to be more carefully executed than the conventional straight-walled cavern and items such as the cranes and services have to be designed to fit into the cavern shape. These differences can create significant problems where the skill of workforce is limited.

Each scheme should be investigated on its own merits, taking into account construction problems as well as geotechnical factors. In some cases, the use of an elliptical cavern

shape may be justified but, in general, the conventional cavern shapes with circular arch or mushroom shaped arch may be suitable except for very weak rock masses.

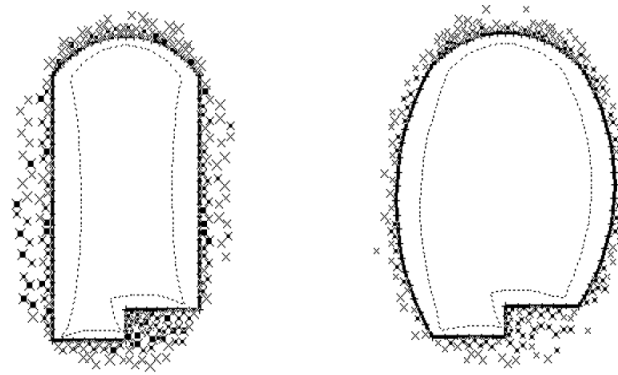


Fig. 2.2 Conventional arched roof cavern vs elliptical cavern (Hoek, 2000)

2.1.2 Cavern Orientation and Location

Optimum orientation for a cavern is the direction which utilizes the rock arching action to the maximum extent. This is normally achieved by aligning the cavern in a direction normal to the strike direction. However, orientation of geological discontinuities such as joints, slip planes and seams and identification of favorable and unfavorable joint sets is equally important while deciding the orientation of cavern. Indian standard, IS 9120-1979 states that a machine hall cavity may be aligned on the basis of an optimum compromise between the direction of the ruling strike and the direction of such features so as to ensure that inferior rock formation is confined to the shortest dimension of the cavity.

There are many constraints in selecting the cavern location. Some of the main constraints are location of portals, access tunnels, size and operation of the cavern facility, utilization of maximum water head in case of hydro projects (Anon,1992). Within such constraints the cavern location should be optimized with respect to the topography and geology. Some important factors in this optimization are:

- a. Adequacy of rock cover.
- b. Avoidance of weakness zones or the crossing of them in the shortest possible duration.
- c. Avoidance of adverse orientation relative to major joint sets.

- d. Sufficient depth below the groundwater table.
- e. Avoidance of rock with abnormally low stresses, giving reduced confinement.
- f. Avoidance of rock with very high stresses.

Minimum rock cover

Minimum rock cover is the most important parameter for shallow caverns. Minimum rock cover should be able to give adequate normal stresses on joints such that joints don't open up and aid natural arch and self-supporting as far as possible. Minimum rock cover required can be a major constraint on cavern location and is determined from an assessment of many factors, which may include:

- Quality of the geological information.
- Rock properties.
- Thickness of superficial deposits.
- Depth of weathering.
- Cavern span.
- Cost implications.

As a general rule, the minimum cover of strong rock should be at least equal to half the cavern span. However, many large span tunnels and caverns have been constructed with rock cover of one fourth of the cavern or tunnel span. In the Valerenga road tunnel in Oslo, Norway, rock cover down to 3.5m was adopted for a span of 12.6m (Anon, 1992). A minimum rock cover in weak rock above the crown of large caverns should be preferably three times the width of cavern.

In general, reduced rock cover increases the cost of geotechnical investigations and rock support requirement and this cost is offset by advantages in adopting reduced cover. Reduced rock cover is normally limited to small areas, such as the section of cavern closest to the portal. Design of such low cover is only acceptable where the fresh rock surface is competent and fully understood with detailed site investigations.

Jointing

Stability of the cavern and the amount of overbreak is influenced by orientation of joints with respect to the axis of the excavation. Properties of the in-situ rock mass are largely governed by the properties of joints and discontinuities. This is the case, even for strong and hard rocks. Joints transfer compressive and shear forces, but not tensile forces. Two main methods of rock mass classification, Q-system (Barton, 1974) and RMR (Bieniawski, 1989) take into account the influence of joint orientation on rock classification and support requirements. If the angle between the excavation axis and the strike of a major joint set is small, say less than 30° , the amount of overbreak is likely to increase. Joint characteristics can have major influence on the orientation of caverns. For caverns with long and high walls, it is important to have an angle of at least 25° to the strike of steeply dipping discontinuities.

It is necessary to carry out a detailed survey of the bedding or foliation and the jointing of the rock mass so that optimization of the direction of the excavation axis with respect to joint orientation could be done. For openings situated at shallow or intermediate depths, the longitudinal axis of the cavern is ideally oriented along the bisection line of the largest intersection angle of the strike of the two dominant sets of discontinuities (joints, bedding or foliation). Close alignment with any further joint sets may be avoided, so as to reduce the extent of potentially unstable rock (Jack and Parry, 2015).

Weakness zones

Weakness zones are defined as zones that are weaker than the surrounding rock mass. Thickness of a weakness zone can range from a few centimeters to several hundred meters. Weakness zones may be in the form of weak rocks, faults, shear zones, heavily fissured zones, hydrothermally altered rocks and deeply weathered zones. Cost of cavern construction can be strongly influenced by the presence and nature of the weakness zones encountered and the mode of treatment. Many major problems in underground construction are related to such zones and the cost implications can be considerable. These problems commonly result in poor stability of unsupported rock and heavy inflows of water from fissured zones. It is, therefore, important that weakness zones are identified and, if possible,

avoided. If the space between faults, gouges, crushed zones or weathered seams is too small for the cavern space, the different zones have to be evaluated and a location is chosen that gives the minimum excavation in these difficult materials. Alternatively, a different cavern geometry that fits between the weakness zones may be considered. Consideration should be given to the orientation of the weakness zones in the rock mass, as steeply dipping features can have a major influence on the stability of walls, while flat lying ones can be a threat to roof stability. Although, it may not be possible to completely avoid weakness zones, their influence on the cavern stability can be minimized by identifying them in advance and with proper treatment.

In-situ stress condition

In-situ stresses in rock mass can have one or more origins. Gravitationally induced stresses and tectonic stresses are often the major components, but residual stresses, the locked in stresses resulting from the stress history of the rock, can be significant. Rock stresses are also influenced by structural heterogeneities, such as major weakness zones, where highly anisotropic stress conditions can occur. Grov and Lu (2015) discussed importance of in-situ stresses in design and building of rock caverns and requirement of sufficient in-situ horizontal stress for maintaining large span.

In-situ stresses and redistribution of stresses with cavern excavation greatly influence the stability of cavern. Orientation of cavern axis with the direction of principal stress can greatly influence the behavior of cavern. Generally, it is considered to have cavern axis parallel to major principal stress direction in order to minimize the ground control problems. It is also important to have required confining stress to achieve higher rock mass strength. In specific cases, increased stresses in the rock mass give rise to greater frictional forces on joints and thus greater rock mass strength.

Stresses in hard rocks are normally anisotropic. Degree of anisotropy can influence cavern stability and therefore optimal shape is very important in this case. Anisotropic and high stresses and accompanying stability problems can be associated with caverns constructed in high valley sides. Investigations for caverns in such locations must, therefore, establish if these conditions exist and appropriate designs are adopted. High tectonic and residual

stresses could have an influence on the location and shape of shallow caverns. According to Edvardsson and Broch (2002), in areas with high anisotropic stresses, the longer axis of the caverns should be oriented at an angle of 15° - 25° to the horizontal projection of the major principal stress to obtain the most stable situation regarding stress-induced instability.

Groundwater

Location of the water table and possibility of water flow through the joint network is an important factor while deciding the elevation of underground cavern. Some schemes require a constant seepage towards the caverns and for some uses, such as oil products storage and gas storage, the groundwater pressure is used to confine the oil or gas and is thus a prerequisite for successful implementation. For such cases, the groundwater pressure has to be maintained with water curtains. For other applications, the location of the groundwater is less important, and some caverns should ideally be placed above the groundwater surface to obtain as dry a cavern as possible. When the caverns are located in close proximity to shear zones or faults, water inflow may considerably alter the stability of caverns.

2.1.3 Cavern Layout

Design of cavern geometry and layout of a system of caverns is generally based on objective of the cavern, various essential components in the system, their orientation and dimensions and importantly, cost of excavation and support and cost of maintenance during the service life. Ultimate aim is to create cavern space with least cost with maximum utilization of space and without compromising the safety. Main parameters defining cavern layout and geometry are the cavern size and shape and the spacing between caverns. In case of landslide prone areas, powerhouse should be deeper in the hill for protection from landslides. In case of large span, low gripping tension allows potential wedges to slide and destabilizes the excavation. Increasing span allows larger blocks to be relieved. Stability problems in caverns in general increase with increasing span. It is often preferable to meet the need for increased volumes by extending the opening along its length axis rather than increasing the span (Nilsen and Thidemann, 1993). The cavern should be placed deep

enough to give the normal stresses on joints and fissures, which are necessary for a self-supporting roof. It is also important to leave a reasonable layer of unweathered rock above the cavern. For more deep-seated caverns, it is important that the stresses don't exceed a level which can cause overstressed rock and stress-induced stability problems. Weakness zones and heavy jointing should also be avoided. Mapping and evaluation of jointing and weakness zones are important pre-construction phase investigations (Edvardsson and Broch, 2002).

In general, layout of the main caverns is given preference over the layout of other tunnels like, bus ducts, draft tubes, penstocks, tail race tunnels and other cross tunnels. Caverns and their spacing are favorably designed with respect to in-situ stresses and geological features compared to other associated tunnels as the size of other tunnels in the layout are small compared to the main caverns and can be managed even if they are oriented adversely. It is important to strike a balance between various issues involved in interaction of interconnecting tunnels with main caverns so as to produce economically viable and stable cavern layout.

2.1.4 Spacing between Caverns

Spacing between two caverns results in the formation of pillar, whose dimension is determined by other cross tunnels connecting the cavern. Width of pillars depends mainly on the rock quality, orientation of the discontinuities, cavern spans and heights and any openings formed in the pillars. In-situ stresses can also affect pillar widths, especially for caverns at depth. Pillar widths are normally equal to between half and the full cavern span or height, whichever is the greater (Anon, 1992). At the preliminary planning stage pillar widths should be conservative. As planning progresses on the basis of improved geological data, narrower pillars may be considered. As per Hoek (2007), pillar width should be preferably equal to one-half of the sum of widths of both the caverns or maximum height of adjoining openings, whichever is higher, depending on the general quality of rock masses.

Pillar dimension is an important parameter when multiple caverns are planned in close proximity. Estimates of acceptable pillar width can be made on the basis of assuming

kinematically possible sliding in unfavorable joints and calculating the factors of safety. Other approach is to calculate the pillar strength and pillar stress using various empirical formulae and calculate the factor of safety. Estimates of vertical stresses and joint shear strengths in the pillar are required for this type of analysis.

Zhao and Ma (2009) studied the influence of cavern spacing on the stability of adjacent caverns. Study was done for three different strengths of surrounding rock mass (soft rock ($E=18\text{GPa}$), medium hard rock ($E=40\text{GPa}$) and hard rock ($E=88\text{GPa}$)). One model included two caverns and the other model included three caverns. Numerical analysis was done under gravity loading and gravity plus earthquake loading. Damaged plasticity model with a non-associated potential flow was adopted for the surrounding rocks to study the effect of earthquake loading. Their results indicated that in the case of soft rock, if the spacing is less than typical length of one cavern (taken as largest width of a cavern in the group), the static and dynamic responses of adjacent caverns are significantly affected by their spacing. The damage and the distribution of tensile stress surrounding the caverns are extensive. Once the spacing approaches or exceeds twice the cavern length, the damage and the distribution of tensile stress of caverns keep unchanged, and the effect of nearby caverns disappears. Regardless of the strength of the rocks that the caverns are located in, once the cavern spacing is less than one cavern length (minimum length out of all caverns), the stability of adjacent caverns is severely affected by the cavern spacing. The damage and tensile stress areas of adjacent caverns are quite significant. The stiffer the rocks are, the smaller is the critical cavern spacing. The corresponding critical cavern spacing for the adjacent caverns located in soft rock, medium hard rock and hard rock is twice, less than twice, and one time the cavern characteristic length, respectively. Once the cavern spacing exceeds the critical cavern spacing, the static and dynamic damage and the distributed area of tensile stress will hardly develop any further and the cavern spacing will have insignificant influence on the stability of adjacent caverns. In some situations, as the rock strength decreases, the damage becomes more severe and the area of tensile stress becomes more extensive. The critical distance of cavern spacing decreases as the strength of the surrounding rocks increases. Abolfazal and Hossein (2014) determined the rock pillar

between two adjacent caverns in Iran based on ratio of elasto-plastic and elastic displacement and the plastic zone determined by numerical modelling.

2.2 MAJOR UNDERGROUND CAVERNS IN INDIA

Brief information about major hydroelectric projects with underground caverns in India are given here. Some of major underground hydroelectric projects with underground caverns are:

1. Nathpa Jhakri hydroelectric project (1500MW)
2. Sardar Sarovar hydroelectric project (1200MW)
3. Teesta III hydroelectric project (1200MW)
4. Karcham Wangtoo hydroelectric project (1000MW)
5. Tehri hydroelectric project (1000MW)
6. Koyna IV hydroelectric project (1000MW)
7. Srisaillam hydroelectric project (LBPH 900MW)
8. Tapovan Vishnugad hydroelectric Project (520MW)

1. Nathpa Jhakri hydroelectric project (1500MW)

Nathpa Jhakri hydroelectric power project is the largest hydroelectric project in India with installed capacity of 1500MW (Fig. 2.3) It is a run of the river scheme project on river Sutlej situated in Kinnur district of Himachal Pradesh. The salient features are:

- 62.50m high concrete dam.
- Underground desilting complex, comprising four chambers, each 525m long, 16.31m wide and 27.5m deep, which is one of the largest underground complexes for the generation of hydro power in the world.
- 10.15m diameter and 27.394km long head race tunnel, which is one of the longest hydro power tunnels in the world, terminating in a 21.60m/10.20m diameter and 301m deep surge shaft.

- Underground power house with a cavern size of 222m x 20m x 49m having six Francis turbine units of 250MW each, to utilize a design discharge of 405cumecs and a design head of 428m.



Fig. 2.3 Powerhouse cavern of Nathpa Jhakri hydro electric project, Himachal Pradesh (Hoek, 2000)

2. Sardar Sarovar hydroelectric project (1200MW)

Sardar Sarovar project, on the right bank of river Narmada, has two powerhouses, the river bed powerhouse and canal head powerhouse with installed capacity of 1200MW and 250MW respectively. The river bed powerhouse is an underground powerhouse. Underground powerhouse complex consists of powerhouse of 23m wide, 57m high and 210m long. There are six pressure shafts of 9m diameter for intake of water from the reservoir to the powerhouse and six draft tubes of 16m wide double D shaped for drawing out water to collection pool. On the downstream side, there are three D-shaped bus galleries of 12m wide and 7.5m high connected to bus shafts. There are a few interconnecting tunnels and access tunnels, which are close to the powerhouse.

3. Teesta III hydroelectric project (1200MW)

Teesta Stage III is one of the largest hydropower plants in India under construction, with a head of 800m. It is located in the north eastern state of Sikkim. The project comprises of 60m high concrete face rock fill dam (CFRD), with the two bays of chute spillway on the left bank, two desilting chambers of size 320m (l) x 17m (w) x 23m (h) and about 13.8km long 7.5m diameter head race tunnel to carry water to the underground powerhouse (214.3m x 21.3m x 44.8m) to feed six units of vertical pelton turbines.

4. Karcham Wangtoo hydroelectric project (1000MW)

Karcham Wangtoo hydroelectric project is a run-of-the-river hydroelectric power station on the Sutlej river in Kinnaur district of Himachal Pradesh. Presently it is the largest hydroelectric project in the private sector in India. There is a concrete gravity dam of 43m high above the river bed. The dam is having six sluice spillway bays of size 9m (width) x 9m (height). Other main components are a 10.48m diameter, 17.2km long headrace tunnel; 4.75m diameter four pressure shafts; an underground powerhouse (187m x 21.6m x 52m) and transformer hall (116.5m x 15m x 24.2m) with 4 x 250MW installed capacity and 909m long and 10.48m diameter tailrace tunnel.

5. Tehri hydroelectric project (2400MW)

Tehri hydro power complex (2400MW), comprises of the following components:

- Tehri dam and hydro power plant (HPP) (1000MW)
- Koteshwar hydro electric project (400MW)
- Tehri pumped storage plant (PSP) (1000MW)

The 1000MW Tehri dam and hydro power plant is under operation and other two components are under construction. The 1000MW Tehri HPP comprises a 260.5m high Tehri dam, which is the highest earth and rockfill dam in the Asian region, two numbers of head race tunnels, an underground hydro powerhouse complex with machine hall (197m x 22m x 47.2m) and transformer hall (161m x 18.5m x 29m) having four conventional turbine/generator sets of 250MW each. Spillway system comprises chute spillway, two gated shaft spillways and two ungated shaft spillways.

6. Koyna IV hydroelectric project (1000MW)

Koyna dam is a rubble concrete dam constructed across river Koyna, a tributary of Krishna basin in Satara district, Maharashtra, The dam is founded on basalt rock. Koyna is one of the major hydroelectric projects in the country and impound (initially 2797.4Mcu.m) water to generate 1920MW power in four stages. Dam is 103.2m high above the deepest foundation and its total length is 807.22m. There are in all 53 monoliths of which six end monoliths are constructed in masonry and the rest in rubble concrete. Spillway is centrally located and extends from monolith no 18 to 24 over a length of 88.70m.

Koyna stage IV (100MW) has many underground components, as given below:

- Underground machine hall (145m x 20m x 50m)
- Transformer hall (173m x 20/18m)
- Head race tunnel (7m x 9.5m and 4.22km long)
- Tail race tunnel (10m x 10m D shaped 1.94km long)

7. Srisaillam hydroelectric project (LBPH 900MW and RBPH 770MW)

Srisaillam dam is constructed across the Krishna river at Srisaillam in Kurnool district of Andhra Pradesh and is the 2nd largest capacity hydroelectric project in the country. Dam was constructed in a deep gorge in the Nallamala hills, 300m above sea level. It is 512m long, 240.79m high and has 12 radial crest gates. It has a huge reservoir of 800sq.km. The left bank hydroelectric power station generates 6 x 150MW of power and right bank generates 7 × 110MW of power.

Underground hydropower complex of the Srisaillam left bank project consists of three large caverns, powerhouse (236.2m x 25.7m x 52.4m), transformer hall (176m x 16.2m x 26.5m) and surge chamber (181.6m x 18m/24m x 74.5m). There are six pressure shafts joining the powerhouse on the upstream side and six bus ducts joining the powerhouse and the transformer hall caverns. There are six draft tubes between powerhouse and the surge chambers.

8. Tapovan Vishnugad hydroelectric project (520MW)

Tapovan Vishnugad Hydroelectric Project (4 x 130MW) is a run-of-the-river scheme being executed by NTPC Ltd. in the state of Uttarakhand. It is a project on river Dhauliganga, a tributary of Alakananda. Powerhouse complex is located on the left bank of Alakananda near Joshimath. The scheme involves construction of 70m long barrage, 12km long head race tunnel (HRT) and powerhouse of 520MW installed capacity along with other appurtenant structures.

Underground powerhouse complex consists of underground excavations, powerhouse (158.5 x 22.3 x 48.6), transformer hall (147.75m x 18.3m x 27.8m) and bus ducts (2 nos. of 12m x 8m D shaped tunnels). Underground caverns of Tapovan Vishnugad project is shown in Fig. 2.4.



Fig. 2.4 Powerhouse and transformer hall caverns of Tapovan Vishnugad hydroelectric project, Uttarakhand (NTPC Ltd.)

Some of the large hydroelectric power plants, where underground caverns (powerhouse (PH), transformer hall (TH) and surge chamber (SC) exist are listed in Table 2.1.

Table 2.1 Major underground caverns in hydroelectric projects in India

Name of Project	State	Capacity (MW)	Size of Cavern [L (m) x W(m) x H(m)]	Status
Nathpa Jhakri	Himachal Pradesh	1500	PH 222 x 20 x 49 TH 196 x 17.5 x 27.4	Completed
Sardar Sarovar	Gujarat	1450	PH 210 x 23 x 57	Completed
Teesta III	Sikkim	1200	PH 214.3 x 21.3 x 44.8	Under Construction
Koyna Stage IV	Maharashtra	1000	PH 145 x 20 x 50	Completed
Tehri Stage I	Uttarakhand	1000	PH 197 x 22 x 47.2	Completed
Tehri PSP	Uttarakhand	1000	PH 202.9 x 26.2 x 58.6	Under Construction
Karcham Wangtoo	Himachal Pradesh	1000	PH 187 x 21.6 x 52 TH 116.5 x 15 x 24.2	Completed
Srisaillam Left Bank	Telangana	900	PH 236 x 25 x 53 TH 176 x 17 x 26 SC 181 x 21.5 x 76	Completed
Idduki	Kerala	780	141.1 x 19.8 x 34.6	Completed
Chamera-I	Himachal Pradesh	540	PH 112 x 24 x 37	Completed
Tapovan Vishnugad	Uttarakhand	520	158.5 x 22.3 x 48.6	Under Construction
Parbati Stage III	Himachal Pradesh	520	PH 122 x 22 x 41.7 TH 98.2 x 15.5 x 25.2	Completed
Teesta V	Sikkim	510	PH 117.5 x 22 x 47 TH 100.5 x 14 x 15	Completed
Teesta VI	Sikkim	500	140 x 19.52 x 49.65	Under Construction
Uri	Jammu and Kashmir	480	PH 122 x 22 x 38 TH 127 x 17 x 24	Completed
Baglihar Stage-1	Jammu and Kashmir	450	PH 121 x 24 x 50 TH 112 x 15 x 24.5	Completed
Vishnuprayag	Uttarakhand	400	PH 122x 8.50 x 38.10 TH 103 x 14 x 21.50	Completed
Chamera-II	Himachal Pradesh	300	PH 100 x 22 x 40 TH 88 x 14m x 13	Completed
Baspa-II	Himachal Pradesh	300	PH 92 x 18 x 39 TH 75 x 13 x 20	Completed
Ghatghar	Maharashtra	250	PH 123 x 23.4 x 46.80 TH 81.35 x 20 x 26	Completed
Chibro	Uttarakhand	240	PH 113 x 18.2 x 32.5	Completed
Chamera-III	Himachal Pradesh	231	PH 100 x 18.6 x 42	Completed
Pykara	Tamilnadu	150	PH 78 x 20 x 36 TH 56 x 12 x 13	Completed
Larji	Himachal Pradesh	126	PH 109 x 20 x 42 TH 50 x 15 x 19	Completed

2.3 ROCK ENGINEERING TOOLS FOR STABILITY EVALUATIONS OF CAVERNS

Response of surrounding rock mass when the cavern is excavated needs to be quantified to assess the stability of cavern. Assessment of stability condition of a cavern requires integration of geological, geotechnical, in-situ stress and hydrological parameters. Various rock engineering tools are available to assess the ground behavior with a view to optimize the cavern design parameters. Stille and Palmstrom (2003) presented principal relationships between ground behavior and rock engineering and design tools. Although, it is applicable in general to any underground excavation, it is relevant for cavern excavation and is presented in Fig. 2.5.

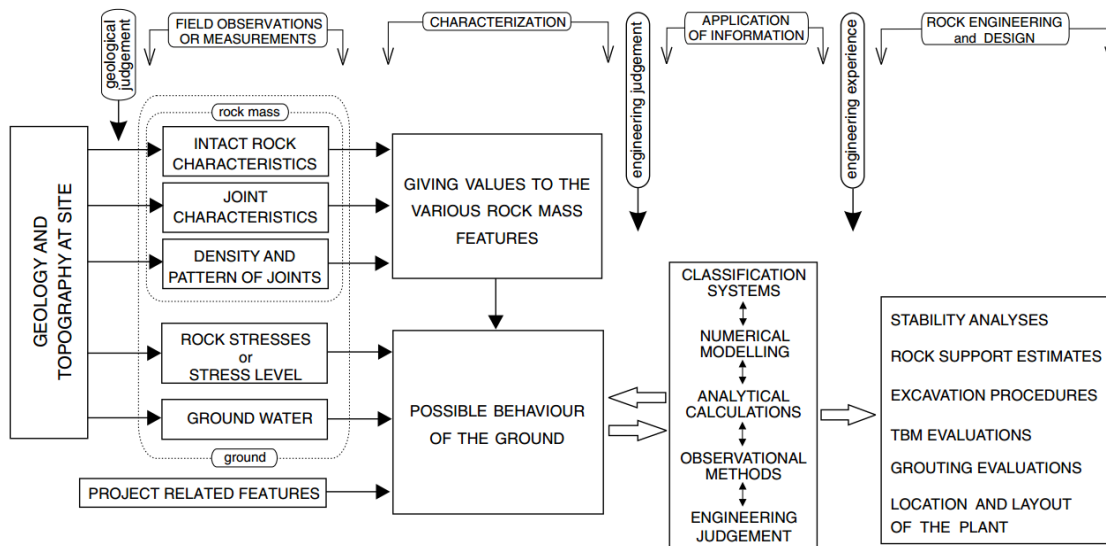


Fig. 2.5 Principle relationships between ground behaviour and rock engineering and design (Stille and Palmstrom, 2003)

As per Bieniawski (1984) “Provision of reliable input data for engineering design of structures in rock is one of the most difficult tasks facing engineering geologists and design engineers.”. Under such condition, frequently, the design of tunnels and caverns is based on observations, experience and personal judgement, where empirical design methods such as rock engineering classification systems play an important role. Palmstrom and Stille (2007) discussed the current rock engineering tools in the following headings:

- Empirical methods (rock engineering classification systems)

- Analytical and numerical methods

Palmstrom and Stille (2007) presented simplified diagram for selection of design methodology based on the behaviour (instability) of rock excavations as given in Fig. 2.6.

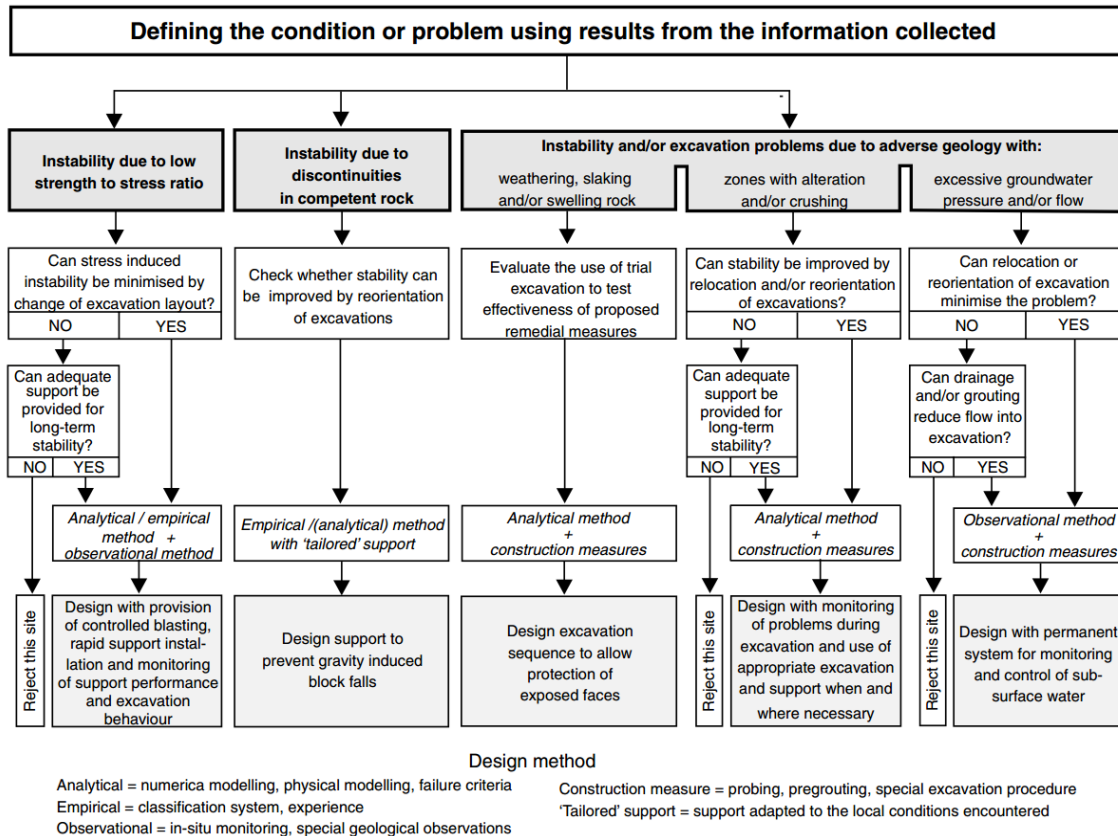


Fig. 2.6 Simplified diagram for selection of design methodology (Palmstrom and Stille, 2007)

2.3.1 Empirical Methods

Rock mass classification systems have been in use for more than 40 years. Some of the classification systems developed are aimed to characterize the rock mass or to give design inputs. Some of the popular systems are Rock Mass Rating (Bieniawski, 1976, 1989), Q (Barton et al. 1974, 2014), Geological Strength Index (Hoek, 1994), and Rock Mass Index, (Palmstrom, 1995).

Detailed description of these methods was given by Hoek, (1999), Hudson and Harrison (1997). Milne et al. (1998) lists the aim of rock mass classification systems as:

- To identify zones of material of similar geo-mechanical characteristics.
- To provide an indication of predicted stability for excavations of a given size.
- To aid in the selection of an appropriate support strategy.
- To provide an indication of in-situ rock mass strength, modulus of deformability, etc.

Use of rock mass classification system is wide spread and generally preliminary design of rock support is usually made on the basis of guidelines listed in popular rock mass classification systems such as Q-system or the RMR in the absence of any specific guidelines for caverns. These methods allow the suitable type of support to be determined for various rock classes that have been identified during cavern excavation. These methods may also be used for the final design, which necessarily involve their use during construction. Both methods may be used in parallel for complex and difficult ground conditions and the results compared. Rock bolt lengths are estimated on an empirical basis taking into account block size in the case of spot bolting, and cavern span in the case of systematic bolting. Only recent updates in popular methods like RMR, Q and GSI are discussed below.

Q-system for rock mass classification and support estimation

The Q-system was developed by Barton et al. (1974) at NGI (Norwegian Geotechnical Institute) after analyzing 212 tunnel case studies. In 1993, Q system was updated with analysis of additional 1050 additional tunnel case records (Grimstad and Barton, 1993). It was further modified in 2007 with 800 additional case histories (Grimstad, 2007). The method is empirical and is based on the Rock Quality Designation, RQD (Deere, 1963), and five additional parameters, number of joint sets, joint roughness and alteration (infilling), amount of water and various adverse features associated with loosening, high stress, squeezing and swelling. The Q-system also takes account of the intended use of the excavated space. Latest updated chart of Q with suggested support measure is shown in Fig. 2.7. The Q-value is expressed by the formula:

$$Q = \frac{RQD}{J_n} \times \frac{J_r}{J_a} \times \frac{J_w}{SRF} \quad (2.1)$$

where,

RQD = Rock Quality Designation

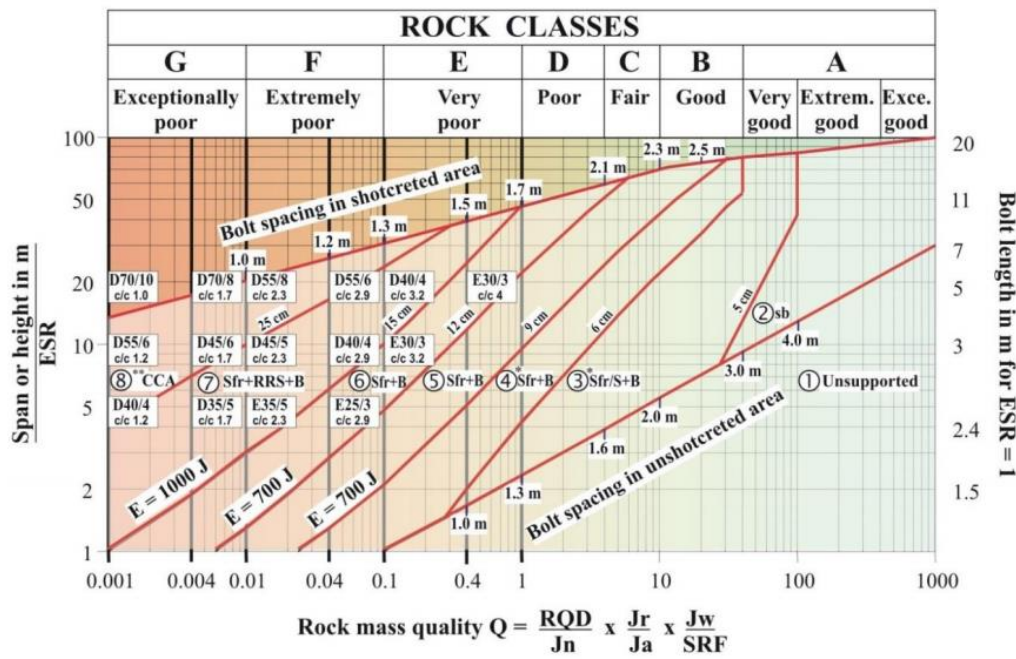
J_n = Number of joint sets

J_r = Joint roughness parameter

J_a = Joint alteration or filling parameter

J_w = Water pressure or leakage parameter

SRF = Stress reduction factor



REINFORCEMENT CATEGORIES

- 1) Unsupported
- 2) Spot bolting, sb
- 3) Systematic bolting, and unreinforced or fibre reinforced shotcrete, 5-6 cm), Sfr/B+S
- 4) Fibre reinforced shotcrete and bolting, 6-9 cm, Sfr+B
- 5) Fibre reinforced shotcrete and bolting, 9-12 cm, Sfr (E700) +B
- 6) Fibre reinforced shotcrete and bolting, 12-15 cm, Sfr (E700) +B
- 7) Fibre reinforced shotcrete > 15 cm + reinforced ribs of shotcrete and bolting, Sfr (E1000) +RRS+B
- 8) Cast concrete lining, CCA or Sfr (E1000) +RRS+B

The bolts are 20 or 25 mm in diameter

E) Energy absorption in fibre reinforced shotcrete at 25 mm bending during plate testing

$\left[\begin{array}{l} D45/6 \\ \text{c/c } 1.7 \end{array} \right]$ = RRS with totally 6 reinforcement bars in double layer in 45 cm thick ribs with centre to centre (c/c) spacing 1.7 m. Each box corresponds to Q-values on the left hand side of the box

*) Up to 10 cm in large spans

**) Or Sfr+RRS+B

Fig. 2.7 Updated Q chart (Barton and Grimstad, 2014)

The numerical value of Q ranges from 0.001 for exceptionally poor quality squeezing ground upto 1000 for exceptionally good quality rock, which is practically unjointed. The six parameters, each of which has an importance rating and can be estimated from site investigation results and verified during excavation. In combination they represent:

- a. Block size by the quotient RQD/J_n .
- b. Inter-block shear strength by the quotient J_r/J_a .
- c. Active stress by the quotient J_w/SRF .

The equivalent span or height in Fig. 2.7 is found by dividing the actual excavation dimension by a factor, the Excavation Support Ratio (ESR value), representing the safety requirement for the use of the space. Developers of Q system have been updating the ESR values keeping in view of the demand for greater safety of the tunnels. The updated ESR values for different applications are given in Table 2.2.

Table 2.2 Excavation Support Ratio (ESR) values for use in Q (Barton and Grimstad, 1994, 2014)

	Type of Excavation	ESR (1994)	ESR (2014)
A	Temporary mine openings, etc.	ca. 2-5	ca. 2 -5 (No Change)
B	Permanent mine openings, water tunnels for hydropower (exclude high pressure penstocks), pilot tunnels, drifts and headings for large openings, surge chambers	1.6 – 2.0	1.6 – 2.0 (No Change)
C	Storage caverns, water treatment plants, minor road and railway tunnels, access tunnels	1.2 – 1.3	0.9 to 1.1 Storage Caverns 1.2 – 1.3
D	Power stations, major road and railway tunnels, civil defence chambers, portals, intersections	0.9 – 1.1	Major road and railway tunnels 0.5 to 0.8
E	Underground nuclear power stations, railway stations, sports and public facilities, factories, major gas pipeline tunnels	0.5 – 0.8	0.5 – 0.8

For underground power stations (caverns) ESR generally used is 1.0. The support derived from chart depicted in Fig. 2.7 is the permanent roof support. Evaluation of permanent wall support by this method requires a modification of the Q-value as shown below:

Q-value for roof (Q_r)

> 10

0.1 < to < 10

< 0.1

Q-value for wall (Q_{wall})5.0 x Q_r,2.5 x Q_r,1.0 x Q_r.

In order to calculate the Q-value for tunnel or cavern intersections, a joint set number value of **3 x J**, is normally used.

The use of the Q-system requires detailed engineering geological mapping and analysis of all the geological features encountered. The rock support evaluated from the Q-value and the corresponding tables give only probable amounts and support types to be used. During construction of the underground opening, the rock support types and quantities should be adopted to the observed rock conditions. The heterogeneous nature of rock masses precludes the design of definitive, cost-effective support systems prior to excavation. To simplify the classification of the rock mass quality and the rock support evaluation, it is common practice to divide the Q-value range into classes as indicated in Fig. 2.7.

Barton et al. (1994) found simple relationship between Q and observed deformation data from various tunnels. They found good agreement with measurement at Nathpa Jhakri powerhouse and Gjøvik Olympic cavern in Norway as illustrated in Table 2.3.

Table 2.3 Relationship between Q and deformation (Δ) (Barton et al., 1994)

$\Delta = \frac{\text{SPAN}}{Q}$	$\Delta_v = \frac{\text{SPAN}}{100Q} \sqrt{\frac{\sigma_v}{\sigma_c}}$	$\Delta_h = \frac{\text{HEIGHT}}{100Q} \sqrt{\frac{\sigma_h}{\sigma_c}}$	$k_o = \left(\frac{\text{SPAN}}{\text{HEIGHT}} \right)^2 \left(\frac{\Delta_h}{\Delta_v} \right)^2$
Nathpa Jakri power station cavern		Gjøvik Olympic cavern	
$\Delta_v = \frac{20,000}{100 \times 3} \times (6/35)^{1/2} = 28 \text{ mm}$ $\Delta_h = \frac{50,000}{100 \times 3} \times (4/35)^{1/2} = 56 \text{ mm}$ (SPAN = 20m, HEIGHT = 50m, Q = 3, $\sigma_v=4 \text{ MPa}$, $\sigma_h = 6 \text{ MPa}$, $\sigma_c = 35 \text{ MPa}$). (In the middle of the range of MPBX measurements for the arch and walls).		$\Delta_v = \frac{60,000}{100 \times 10} \times (1/75)^{1/2} = 6.9 \text{ mm}$ (SPAN = 60m, $Q_{\text{mean}} = 10$, $\sigma_v = 1 \text{ MPa}$ at 40 m depth, $\sigma_c = 75 \text{ MPa}$) (Almost identical to that measured with nine MPBX, and almost identical to UDEC-BB modelling results).	

Equations for estimating the deformation modulus for the rock mass (E_{mass}) relating it with Q and P wave velocity (V_p in km/s) suggested by Barton and Grimstad (2014) are given below:

$$E_{mass} = 10 \left\{ \frac{\sigma_c}{100} Q \right\}^{1/3} \quad (2.2)$$

$$E_{mass} = 10^{(V_P - 0.5)/3} \quad (2.3)$$

RMR classification

The RMR method of rock mass classification also called ‘Geomechanics Classification’ was developed by Bieniawski (1976) and he has revised the system over the years with inclusion of more case histories (Bieniawski, 1989). Following six parameters are used to classify a rock mass using the RMR system:

1. Uniaxial compressive strength of intact rock.
2. Rock quality designation, RQD.
3. Spacing of discontinuities including joints, faults, bedding planes, etc.
4. Condition of the discontinuities including aperture, continuity, roughness, wall condition and infilling.
5. Groundwater conditions where the effects of water on rock mass strength are taken into account.
6. Orientation of discontinuities.

In this system, the rock mass is divided into a number of structural regions and each region is classified separately. Boundaries of the structural regions usually coincide with a major structural feature such as a fault or with a change in rock type. In some cases, significant changes in discontinuity spacing or characteristics, within the same rock type, may necessitate the division of the rock mass into a number of small structural regions. Accordingly, rock mass is classified into five classes and support recommendations given by RMR system are given in Table 2.4.

Bieniawski (1976) showed that the relationship between RMR and the equivalent Q-values described by the equation:

$$\text{RMR} = 9 \log_e Q + 44 \quad (2.4)$$

Barton (1995) related RMR and Q as :

$$\text{RMR} = 15 \log Q + 50 \quad (2.5)$$

Table 2.4 Guidelines for excavation and support of 10 m span rock tunnels in accordance with the RMR system (Bieniawski 1989)

Rock Mass Class	Excavation	Rock Bolts (20mm diameter, Fully Grouted)	Shotcrete	Steel Sets
I – Very good rock RMR: 81 - 100	Full Face 3m advance	Generally no support required except spot bolting		
II – Good rock RMR: 61 – 80	Full Face 1 – 1.5m advance. Complete support 20m from face.	Locally, bolts in crown 3m long, spaced 2.5m with occasional wire mesh.	50mm in crown where required.	None.
III – Fair rock RMR: 41 – 60	Top Heading and Bench 1.5 – 3m advance in top heading Commence support in each blast. Complete support 10m from face.	Systematic bolts 4m long, spaced 1.5 – 2m in crown and walls with wire mesh in crown.	50-100mm in crown and 30mm in sides.	None.
IV – Poor rock RMR: 21 – 40	Top Heading and Bench 2.3 – 1.5m advance in top heading. Install support concurrently with excavation, 10m from face.	Systematic bolts 4-5m long, spaced 1.0 – 1.5m in crown and walls with wire mesh.	100-150mm in crown and 100mm in sides.	Light to medium ribs spaced 1.5m where required.
V - Very poor rock RMR: < 20	Multiple drifts 0.5 – 1.5m advance in top heading. Install support concurrently with excavation. Shotcrete as soon as possible after blasting.	Systematic bolts 5-6m long, spaced 1.0 – 1.5m in crown and walls with wire mesh. Bolt invert	150-200mm in crown and 150mm in sides, and 50mm on face	Medium to heavy ribs spaced 0.75m with steel lagging and forepoling if required. Close invert.

Geological Strength Index (GSI)

Since both RMR and Q classifications include RQD and in most of the weak rock masses, RQD is essentially zero or meaningless, an alternative classification system was developed by Hoek (1994). This system does not include RQD and places greater emphasis on basic geological observations of rock-mass characteristics, reflecting the material, its structure and its geological history and developed specifically for the estimation of rock mass properties rather than for tunnel reinforcement and support. GSI is closely associated with Hoek and Brown failure criteria. This system was initially developed for hard rock tunneling and later included poor quality rock masses and heterogeneous rock masses (Hoek, 1998, Marinos and Hoek, 2000, 2001). Charts for selecting GSI and its applications and limitations were well described by Marinos et al. (2000, 2007). GSI estimation from the given chart is purely qualitative and Hoek et al. (2013) proposed quantification of the GSI chart on the basis of two well established parameters, joint condition (Jcond89) rating defined by Bieniawski (1989) and the RQD defined by Deere (1963). Updated chart of GSI with these two parameter is shown in Fig. 2.8.

A fundamental assumption of the Hoek-Brown criterion for the estimation of the mechanical properties of rock masses is that the deformation and the peak strength are controlled by sliding and rotation of intact blocks of rock defined by intersecting discontinuity systems. It is assumed that there are several discontinuity sets and that they are sufficiently closely spaced, relative to the size of the structure under consideration, that the rock mass can be considered homogeneous and isotropic. These concepts are illustrated diagrammatically in Fig. 2.9.

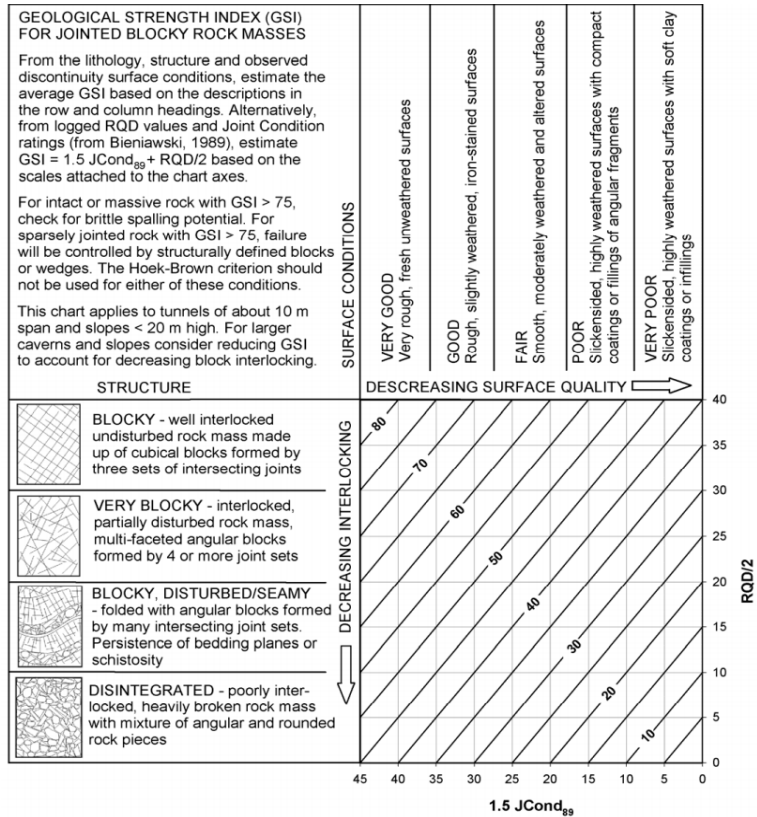


Fig. 2.8 Quantification of GSI by joint condition and RQD (Hoek et al., 2013)

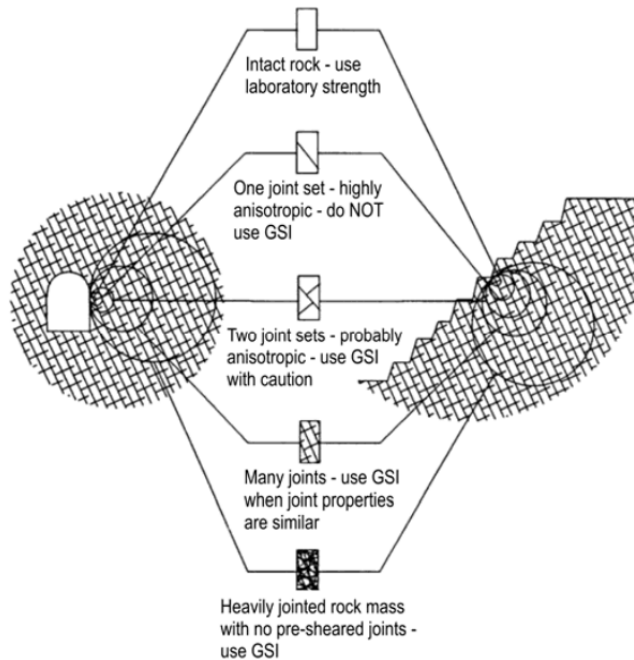


Fig. 2.9 Limitations on the use of GSI

2.3.2 Analytical and Numerical Methods

Analytical and numerical methods in cavern engineering can be divided into the following classes:

- a. Limit equilibrium methods for discrete blocks and wedges.
- b. Statistical-analytical methods, e.g. key block analysis.
- c. Numerical continuum methods, e.g. finite element methods and boundary element methods.
- d. Numerical discontinuum methods (distinct element methods).

For an analysis to be useful, it should address the factors that are important for cavern design. For example, the design of caverns planned at modest depths in hard rock is normally governed by the weakness zones and a series of intersecting joints, and not by in-situ or induced stresses and intact rock strength. Simple stability analysis of problematic areas using limit equilibrium methods are therefore, often used to supplement the support design given by the rock mass classification systems.

Sliding blocks and wedges

There are many published methods for determining the stability of blocks and wedges in excavated rock surfaces and the support required to achieve stability. These methods are based on limit equilibrium analysis. Hoek and Brown (1980) presented such methods. Similar analyses may be made to check pillar widths and their support requirements.

Key block analysis

Key block analysis may be used to determine which blocks in a cavern roof or walls control stability. Securing these key blocks will ensure overall stability. The analyses may be used to predict the likely location and appearance of key blocks using statistical joint data or joint maps taken from excavations when specific key blocks can be identified. The first mentioned use is an aid to recognizing the key blocks as such from the joint pattern observed. The ultimate purpose is to apply support where required and in the most cost-efficient way. The method is described in detail by Goodman and Shi (1985).

Numerical models

Numerical models are useful to evaluate qualitatively and quantitatively the effects of geology on the design. These methods can be used both in a forward analysis where, for given geometry and properties, results are obtained (for example stresses and displacements), or on a backward analysis where, given results or measurements, rock mass properties or rock mass behavior are approximated.

The interest of the design engineer is to assess the stability condition of the tunnel or cavern when no support is installed and when suitable support system is installed. Such assessment requires understanding the rock mass in terms of geological, geotechnical, in-situ stress and hydrological parameters. Further, the fundamental components of rock mass behavior needs to be accounted for using appropriate methods for the analysis of stresses and displacements in the rock mass around the tunnel and the associated structural components.

A number of methods of stress analysis are available from the closed form solutions to numerical models. Numerical modeling is a stress analysis technique, which uses the power of modern computers, numerical analysis technique and the principle of mechanics. With the rapid advancements in computer technology, numerical methods provide extremely powerful tools for analysis and design of engineering systems with complex factors that was not possible or very difficult with the use of the conventional methods, often based on closed form analytical solutions.

Rock mechanics problems of practical concern may not be solved analytically as the rock mass is inhomogeneous and the constitutive relations for the rock mass are non-linear and mathematical formulation of the problem is difficult. In such cases, approximate solutions may be found by computer-based numerical methods. In recent years, the development in the area of computational methods, numerical methods and rock mechanics has evolved many tools, which the rock mechanics engineer can use for the analysis.

Starfield and Cundall (1988) proposed a methodology for modelling rock mechanics problems and reference to this paper may be made for guidance and necessary cautions. Hoek et al. (1991) provided similar guidance with an overview on the use of various numerical modelling methods. Holling (1978) classified numerical modelling problems

into four regions according to the data available and the understanding of the problem as depicted in Fig. 2.10 (Holling, 1978; Hadjigeorgiou, 2012).

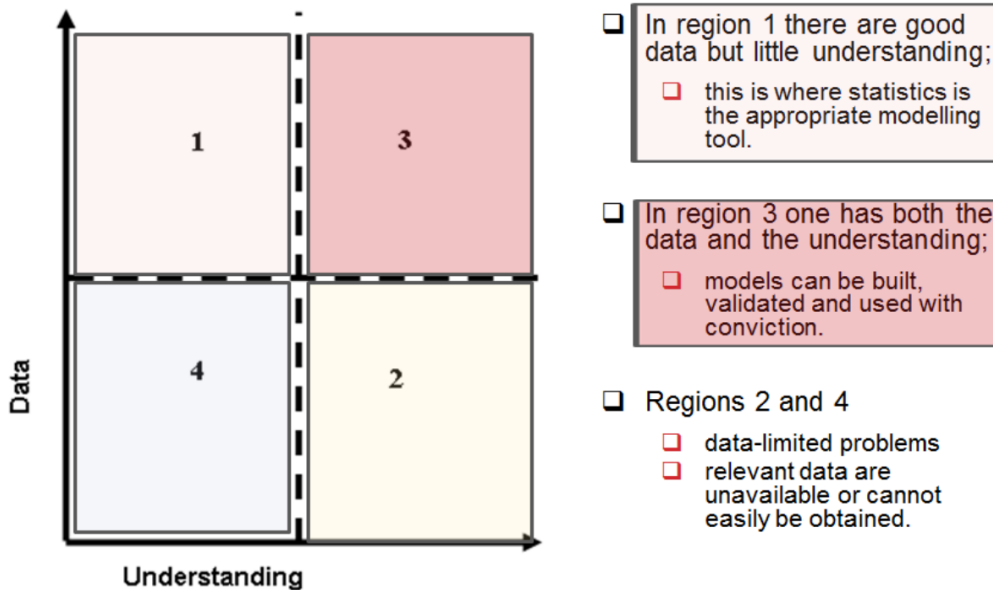


Fig. 2.10 Classification of modelling problems

In region 1, there is good data but poor understanding, and in region 3, there is both good understanding and good data. Regions 2 and 4 represent problems, where data is limited or cannot easily be obtained. Most problems in rock mechanics fall into this group of data-limited problems, whereas problems in structural engineering fall largely into region 3. Attempts have been made to collect sufficient data to move rock mechanics problems into region 3. This may, however, lead to more complex models and increasingly expensive ground investigations without significant improvements in understanding and design. Closed-form solutions that indicate the relations between stress and displacement around underground openings are available for simple excavation shapes in homogeneous ground conditions. These solutions have considerable value in providing a conceptual understanding of rock mass behavior and in testing numerical models.

Numerical models may be classed either as the continuum type or the discontinuum (Jing and Hudson, 2002; Jing, 2003). Continuum methods may include the discontinuities in the medium, if present, explicitly or implicitly, while in discontinuum methods discontinuities are incorporated explicitly. The need to use, for a particular problem, continuum or discontinuum methods depend on the size or scale of the discontinuities with respect to the size or scale of the problem that needs to be solved. There are no universal quantitative guidelines available to determine when one method should be used instead of the other one (Bobet et al., 2009). Brady (1987) provided some qualitative guidance in this respect is shown in Fig. 2.11.

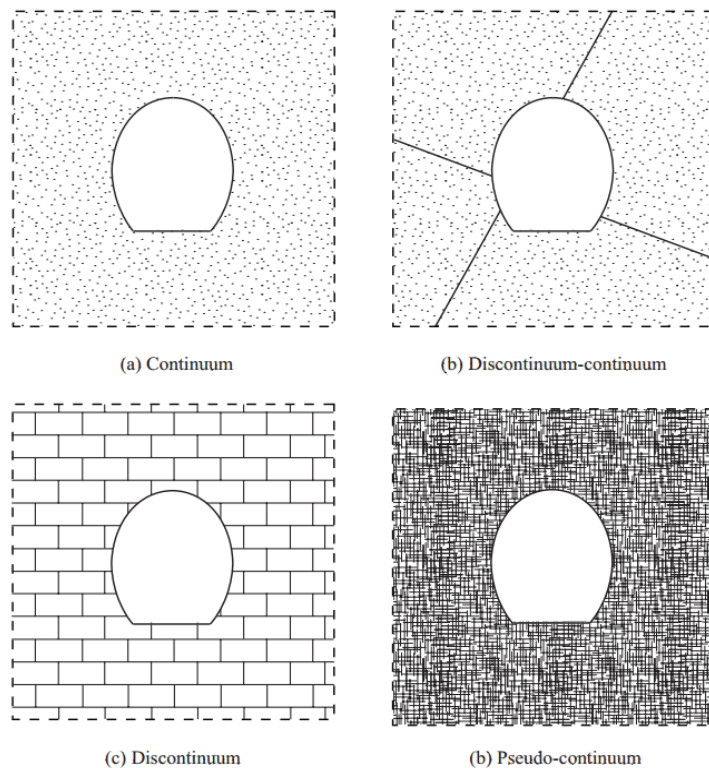


Fig. 2.11 Continuum and discontinuum models (Brady, 1987)

For example, Fig. 2.11a illustrates an opening in a medium without discontinuities. In this case, the displacement field is continuous and thus continuum numerical methods are appropriate. Fig. 2.11b shows a tunnel excavated in a medium with a small number of discontinuities that divide the medium into a small number of continuous regions. The displacement field will be continuous inside each region, but may be discontinuous across

the regions. If a continuum model is used, the model should be able to consider the specific discontinuities. The medium depicted in Fig. 2.11c is determined by a number of discontinuities with spacing and continuity such that the blocks defined are within the scale of the opening. In this case, displacements are determined by the slip along the discontinuities and rotation of the blocks. Thus a discontinuum numerical method is more appropriate. If the medium is heavily jointed such that the blocks defined by the discontinuities have a size much smaller than the opening, a pseudo-continuous displacement field is produced and the use of a continuum model (equivalent continuum) seems reasonable.

For continuum models based on the boundary element method, the free surfaces are divided into elements and the interior of the rock mass is treated as an infinite continuum. The stresses and strains applied to an element have a calculable effect on the other surface elements and throughout the medium. Thus changes at one surface element will affect all other elements. The method has the advantage that only the boundaries have to be divided into elements, and the far-field stresses are not influenced by the creation of an excavation. Although joints can be modelled by means of the displacement discontinuity approach, the boundary element method is not suitable for problems requiring explicit consideration of several joints or the sophisticated modelling of joint behavior. Also, in general, the method is not capable of incorporating variable material properties or modelling interaction between rock and support. Other numerical methods are more suitable for problems involving these considerations.

Continuum models based on finite element and finite difference methods relate the conditions at nodal points to the state within the elements. The physical problem is modelled numerically by discretizing the problem region. These methods have the advantage of being able to handle material heterogeneity and non-linearity, but they handle infinite boundaries poorly. Joints can be represented explicitly by means of specific joint elements, but generally in limited numbers.

The discrete element method considers blocky materials as a discontinuum and is well suited to modelling these highly non-linear problems. In this approach, the jointed rock

mass is represented by a series of blocks, each of which is considered a unique free body and can be discretized into deformable zones. The blocks can rotate, separate and slide according to Newton's second law of motion. The method has been until now primarily a research tool, but recently some understanding has been gained of where, how and when the method may best be applied.

Hybrid approaches to modelling can be used advantageously, whereby the desirable elements of each approach are retained and the undesirable aspects suppressed. Thus, the far-field behavior of material in a finite element analysis may be modelled by linking the outer elements to a boundary element system, which models the effect of infinite boundaries well. Following is a list of the numerical modelling codes most referenced in the literature:

- Finite Difference Method (FDM)
 - FLAC and FLAC3D (Itasca Consulting Group, Inc.)
- Finite Element Method (FEM)
 - ABAQUS (Hibbit, Karlson, and Sorensen, Inc.)
 - PENTAGON-2D and 3D (Emerald Soft)
 - PHASE2 (Rocscience)
 - PLAXIS (Plaxis BV)
- Boundary Element Method (BEM)
 - BEFE (coupled BEM-FEM), (Computer Software and Services) CSS
 - EXAMINE2D and EXAMINE3D (Rocscience)
- Distinct Element Method (DEM)
 - UDEC, 3DEC (Itasca Consulting Group, Inc.)
 - EDEM (DEM Solutions)
 - LDEC (licensed by Lawrence Livermore National Laboratory)
- Bonded Particle Method (BPM)
 - PFC2D and PFC3D (Itasca Consulting Group Inc.)

All codes are based on the principles of mechanics and they rigorously solve (in the context of numerical solutions) equilibrium equations, boundary conditions, strain compatibility, and the constitutive material model.

2.4 SUPPORT SYSTEM

In hard rock tunneling and cavern construction, the term 'bolt' normally refers both to tensioned bolts and fully grouted untensioned bolts, as the mode of action is dominantly in tension in both cases.

2.4.1 Spot Bolting

Design of spot bolting is done as excavation proceeds and is actually part of the construction process. Spot bolting is used to secure individual blocks of rock. The size of the block can be estimated from observation of the joints that define the block. The bolt should be long enough to obtain adequate anchorage in stable rock beyond the block. Block sizes are estimated from joint directions and spacing relative to the excavation.

Length of bolt should be 1 - 2m beyond the block, and preferably not less than 1.5m. Spot bolting at the excavation face is determined on the basis of experience as the time available precludes analysis. Some bolts are pre-tensioned to activate the anchorage and ensure that these are effective. It is good practice to assume that only half of the bolts will be effective, so the number of bolts is doubled, thus giving an added factor of safety over and above the factor of safety given by consideration of the ultimate load capacity of each bolt (Anon, 1992).

The number of bolts can be reduced with pre-tensioned bolts depending on the installation procedure and quality, as pre-tensioning gives assurance that they are carrying load. The extent to which joint shear strength can be taken into account varies with circumstances. For smaller blocks, joint shear strength is commonly ignored.

2.4.2 Systematic Bolting

Systematic bolting is used to achieve a general increase in stability. The bolts are normally installed in a pattern. The block size is the principal factor in determining bolt spacing and

cavern span dominates the determination of bolt length. Bolting is frequently done in conjunction with shotcrete or fibrecrete, and can be installed after its application.

Rock bolt spacing is conveniently estimated using Q-system or RMR classifications. Details of recommended support measures were adequately described by Barton et al. (1974), Bieniawski (1976, 1989) and Hoek and Brown (1980). Bolt spacing of 1 - 3m are indicated for most situations depending on the calculated rock quality. Bieniawski (1976) gave rock bolt spacing of 2.5m for RMR values of 61 to 80, 1.5m to 2m for RMR values of 41 to 60 and 1m to 1.5m spacing for RMR of < 41. No bolting is indicated for RMR value of > 80. Bolt spacing of less than 1m is not normally considered practicable and alternatives such as straps, shotcrete and fibrecrete may be considered in conjunction with bolting.

There are several means of estimating bolt lengths in common use. Schach et al. (1979) developed a formula giving bolt lengths in meters in accordance with common practice:

$$L = 1.40 + 0.184 B \quad (2.6)$$

where,

L = Bolt length, m

B = Cavern span, m

In any case the length should not be less than that required for spot bolting. Shorter bolts may be used towards the cavern walls, but should not be less than 2m. In some cases, it may be cost-effective to use two lengths of bolt alternately. Rock bolts placed systematically are in general located normal to the theoretical excavation line. Occasionally, a case may be made for angling the holes to take into account the joint directions, but the designer must take into account the added complication in installation and control.

Other empirical relationships defining the length and spacing of rock bolts are given in Tables 2.5 and 2.6 respectively.

Table 2.5 Empirical formulae, estimating length of rock bolts as a function of cavern span/height

Bolt Length (m)	Reference	Comment
$L= 0.3 \times S$	Farmer and Shelton (1980)	Span > 15m alternate with secondary bolting
$L=0.3 \times Sp$	Farmer and Shelton (1980)	Secondary bolting
$L= 0.67 \times S^{0.67}$	Lang and Bischoff (1984)	
$L= 2+ 0.15 \times S$	Hoek (2000)	Suited for weaker rock masses (roof)
$L= 2 +0.15 \times H$	Hoek (2000)	Suited for weaker rock masses (walls)
$L=1.40 + 0.184 \times S$	Myrvang (2001)	Norwegian Approach
L = Bolt length, S = Span, H = Height, Sp = Spacing of primary bolting		

Table 2.6 Empirical formulae for determining spacing between rock bolts

Spacing	Reference	Comment
$Spacing = \sqrt{T/P}$	Hoek (2000)	T= Working load of bolt or cable P= Support pressure
$Spacing = 0.5 \times L$	Farmer and Shelton (1980)	Primary Bolting
$Spacing = 0.5 \times L$ (Secondary)	Farmer and Shelton (1980)	Secondary bolting
$Spacing = 0.5 \times L$	Myrvang (2001)	Applicable to jointed rock mass
L = Bolt length		

2.4.3 Design of shotcrete and fibrecrete support

Both the Q-system and RMR method indicate the thickness of shotcrete support required for various rock qualities. With the development of the support method, fibrecrete technology has advanced significantly and has largely replaced mesh reinforced shotcrete. The support guidelines given by Barton et al. (1994) include a recommendation for very large thicknesses of shotcrete for some situations. This advice should be treated with caution as little advantage can be obtained by applying more than 200mm of shotcrete, when this is combined with rock bolting. This is particularly the case when the shotcrete contains steel fibre as reinforcement. However, thick layers of shotcrete may be applied occasionally to small areas of particularly poor rock.

As a general rule, systematic bolting with fibrecrete should be used for permanent support of roof of caverns that will be occupied most of the time or caverns that contain important processes or machinery. Shotcrete and fibrecrete support have a better effect if they act in unison with the rock bolts. The bolt heads should either be incorporated in the sprayed concrete or the bolts may be installed with bearing plates after spraying. In some situations the heads of the bolts may be protected prior to spraying concrete, and bearing plates and nuts installed afterwards. Plates installed after placing the shotcrete or fibrecrete support may require further sprayed concrete for corrosion protection.

2.4.4 Design of cast concrete support

Cast concrete support is not a realistic means of achieving general stability in cavern excavations, although it can be applied to limited areas of instability such as weakness zones. Stability of the rock mass is achieved primarily with rock bolts and sprayed concrete. A requirement for concrete lining is for reasons other than achieving primary rock stability and is subject to design on the basis of parameters other than those of rock mechanics. Operators may in some instances require an arched cast concrete roof as insurance against the fall of rock or loosened shotcrete.

2.5 STRESSES AROUND UNDERGROUND CAVERNS NEAR TOE OF SLOPES

Many hydroelectric projects, particularly in hilly terrains (like in Himalayas) are located at the toe of the hill or very close to the toe. In such cases, in-situ stresses vary abruptly depending upon the topography. Hoek and Moy (1993) discussed in detail about the distribution of in-situ stresses and factors that decide the location of underground caverns. Fig. 2.12a shows the maximum and minimum principal stresses in a gravitationally loaded slope with a far field horizontal to vertical in-situ stress ratio of 3:1. The in-situ stresses, particularly the minimum principal stress σ_3 , are significantly altered in the vicinity of the slope face as compared to the far field stresses. These local changes in the in-situ stress field influence the stresses induced in the rock mass surrounding an underground cavern located near the toe of slope.

Hoek and Moy (1993) also analyzed location of underground cavern at different distances from the toe of the slope using boundary element method. Contours showing zones in

which tensile and shear strength exceeded are shown in Fig. 2.12b. Failure trajectories in these overstressed zones indicate the direction in which failure of the rock would propagate, assuming the rock mass to be homogeneous.

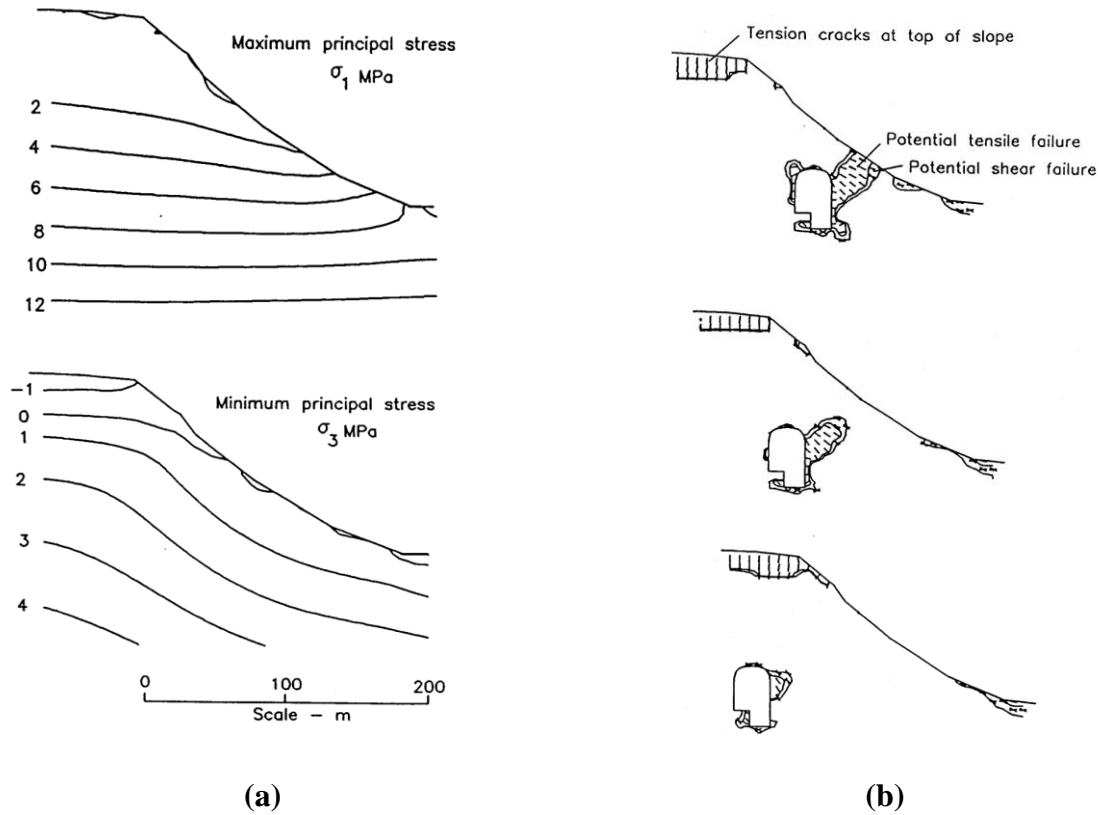


**Fig. 2.12 a. Distribution of principal stresses in a gravitationally loaded slope
b. Zones of overstress and failure surrounding an underground cavern at different distances from the toe of the slope (Hoek and Moy, 1993)**

2.6 CRITICAL STRAIN OF ROCK MASS

According to Sakurai (1997), critical strain is a better measure of failure. The critical strain (mass) is defined as a ratio between UCS (qc_{mass}) and the modulus of deformation (Ed) of rock mass. He found that critical strain is nearly independent of joints, water content and temperature. Hence, equation for ϵ_{mass} is given as follows:

$$\epsilon_{mass} = \epsilon_r \left[\frac{E_r}{E_d} \right]^{0.3} \left[\frac{d}{S_{rock}} \right]^{0.2} \quad (2.7)$$

$$\geq \epsilon_\theta = u_a/a$$

where,

$\epsilon_r = q_c/E_r$ = Critical strain of rock material (obtained from tests in the laboratory)

ϵ_c = Tangential strain around opening

(observed deflection of crown in downward direction/radius of tunnel)

= u_a/a (Fig. 2.13)

S_{rock} = Average spacing of joints and

q_c = UCS of rock material for core of diameter, d .

Experience in Japan is that there were not many construction problems in tunnels where $\epsilon_\theta < \epsilon_{mass}$ or ϵ_r . It can be noted that critical strain appears to be somewhat size dependent according to equation 2.7. There is a lot of difference in predictions and actual observations in the tunnels. One has to give more attention to the joints. It is easier to observe strains than stresses in the rock mass. Sakurai (1997) classified the hazard warning level into three stages in relation to the degree of stability as shown in Fig. 2.13.

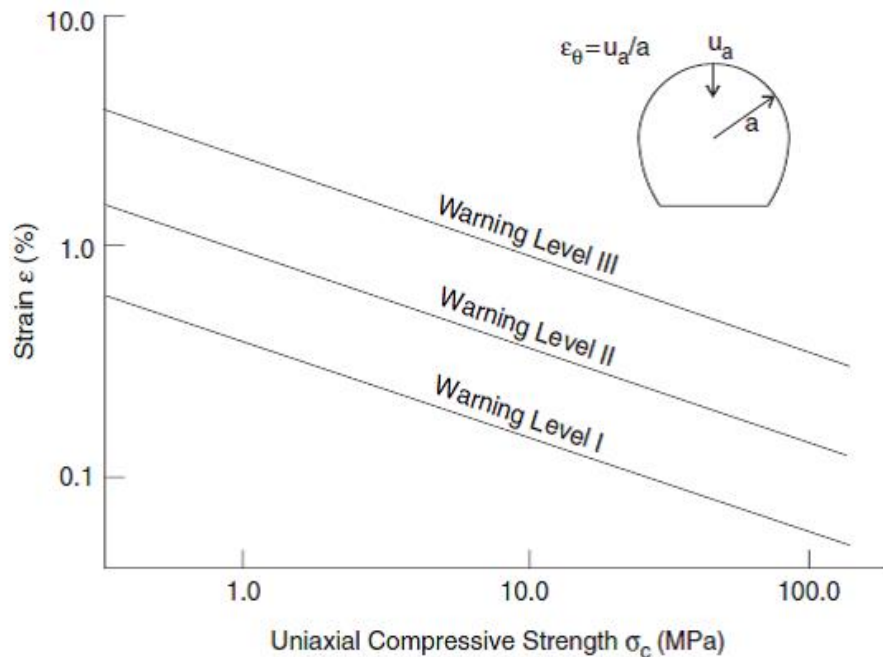


Fig. 2.13 Hazard warning levels for assessing the stability of tunnels (Sakurai, 1997)

He observed that where strains in the crown ($\epsilon_{\theta} = ua/a$) are less than the warning level I, there were no problems in the tunnels. Whereas, tunneling problems were encountered where strains approached warning level III. Swarup et al. (2000) have confirmed these observations in 19 tunnels in weak rocks in the Himalayas.

2.7 RESEARCH IN CAVERN STABILITY AND RELATED ISSUES

2.7.1 3D Physical Modelling Studies

In 1980's physical modelling was one of the main methods to identify the geotechnical problems. However, rapid developments in computational power and numerical methods, numerical modelling has become the preferred choice. Complexity and uncertainty of geological conditions and complex geotechnical issues have posed greater challenge to numerical modelling. Over a period of time, again significance of physical modelling has caught the attention of the researchers. Attempts are made to combine the advantages of both the models. Li et al. (2005) created a 3-D geo-mechanical model of the underground caverns of the Xiluodu hydropower station, China, combining the advantages some of the primary principles of the numerical method with the physical model process. Considering that the boundary condition has a great effect on the stress distribution, a larger test model was set up. The numerical discrete principle was also used to simulate an initial geo-stress field. As per the basic principle of cavern excavation that loading comes first, followed by excavation, a new technique, in which a high fidelity simulation of the excavation process and a very difficult cavern excavation were successfully achieved. The new method produced test results more satisfactorily, and this simulation was an obvious improvement of existing techniques. The results of the tests were compared with FLAC-3D model results. The displacement distribution form and global trend were the same in the data from both techniques, with a slight difference in the displacement values. The horizontal displacement results from the two methods were quite similar, but the vertical displacement in the numerical model was a little less than that of the physical model, which may be due to the fact that the numerical analysis did not simulate the joints and beddings as much as the physical model, and can not completely simulate the boundary conditions of the model.

Comparison of the two methods showed that the effect of the physical model test was satisfactory, and that some geological weak structures are difficult to simulate numerically. Both numerical simulations and physical model tests have their own advantages, and combining the advantages of the two methods enabled to overcome many difficult problems. For some moderate and small-scaled projects, numerical simulation can generally solve problems sufficiently. But for large or huge scaled underground projects, physical model testing is also a competitive method. To further the development of physical model tests, it is important to introduce more new and advanced technologies to be used in 3-D model tests.

Zhang et al. (2016) investigated the stability of an underground cavern group on the basis of large-scale 3D geomechanical model tests and numerical simulations. Multiple measurement techniques were developed to measure the convergence in the cavern, displacements at key points in the side walls and the damage pattern during the excavation process. The digital photogrammetric technique and fibre Bragg grating (FBG) based displacement sensing bars were applied to measure displacements in the surrounding rock mass. Mini multi-point extensometers with high-precision grating scales are developed as transducers for displacement monitoring. Results were compared with numerical modelling results of a nodal-based discontinuous deformation analysis method.

2.7.2 Borehole TV Camera

Yoshida et al. (2004) carried out borehole TV investigations to observe the behaviour of discontinuities during the construction of two large underground caverns in Japan. One was Okawachi power station with highly jointed rock mass and other one was Okutataragi power station with less jointed rock mass. Boreholes were drilled into the side walls of the cavern from a tunnel and behaviour of the discontinuities were measured before and after the excavation of the cavern.

Hibino and Motojima (1995) discussed the results obtained from in-situ measurements of rock behaviour at 16 caverns at underground power plants at Japan. These measurements were done using borehole camera, extensometers, convergence measurements etc. They

concluded that rock mass deformation mainly consists of ‘opening displacement’ (joint opening etc.) and ‘strain displacement’.

Maejima et al. (2003) characterised the behaviour of joints based on borehole camera investigation and finite element modelling based on micromechanics based continuum model (MBC Model). Borehole camera investigations showed that joint opening was taking place near to the walls of the cavern and displacements due to joint opening were more prominent than the displacement due to the strain in the rock. Joint data from these studies were incorporated in MBC model and good correlation was observed between results of MBC model and extensometer data.

2.7.3 Numerical Modelling Studies

The 62m span Olympic Ice Hockey Cavern was constructed in Gjøvik, Norway in 1991 with a cavern rock over of 25-50m only. Barton et al. (1994) predicted and measured the performance of the cavern using various tools like, rock stress measurements, cross hole seismic tomography, geotechnical core logging, Q-System of classification and modelled the cavern using UDEC-BB 2D numerical model. This model utilised the Barton-Bandis Joint model (Barton and Bandis, 1990) and predicted displacement of 4-8mm, which compared well with MPBX observation of 7-8mm.

Yoshida and Horri (1995, 2004) developed constitutive model of a rock mass containing multiple joint sets formulated on the basis of micromechanics, and implemented the same in finite-element analysis code to analyze rock structures under arbitrary loading and boundary conditions. This method enabled them to understand the behavior of a jointed rock mass, but also the deformation of joints during excavation of a large-scale cavern. This method was tested at Shiobara power station cavern in Japan and they found the results of models were in good agreement with the measured data. During the study it was noted that largest value of displacement is located at around the middle of the cavern, and displacement on the penstock side is much larger than on the tail race side and was according to the joint distributions in the rock mass. It was concluded that in a jointed rock mass, joint deformation is responsible for a large portion of the displacement.

Yoshida et al. (1995) formulated a micromechanics based continuum model for jointed rock mass. This MBC (micromechanics-based continuum) model reflects the effect of density, orientation and connectivity of joints as well as the property of joints. The constitutive equation is implemented into the FEM code for the analysis of problems with arbitrary geometry and boundary conditions. This method was applied to model a trial excavation of the reduced-scale cavern preceding the construction of the Kazunnogawa power station in Japan and found good agreement with the field results.

Zhu et al. (2008) analysed several caverns setup in China with 3 parallel caverns using FLAC-3D and formulated a method to study the safety of the underground caverns. An equation considering four basic factors were fitted for prediction of displacement at the key point on the high sidewalls of the powerhouse, on the basis of a large number of numerical simulations. The basic factors included rock deformation modulus, overburden depth of caverns, height of the powerhouse and the lateral pressure coefficient of the initial stress. Following equation was proposed for predicting the elasto-plastic displacement (U_{ep}) at the key point on the high sidewall of the powerhouse:

$$U_{ep} = h[a(1000 k \gamma H/E)^2 + b (1000 k \gamma H /E) + c] \times 10^{-3} \quad (2.8)$$

where,

h = Height of powerhouse, m

k = Lateral pressure (geo-stress) coefficient

γ = Bulk density of rock, kN/m^3

H = Lower overburden depth of the powerhouse (calculated from the cavern floor to ground surface), m

E = Deformation modulus of rock, Pa

a , b , and c are regression coefficients related to geometric structure and characteristics of the caverns

Zhu et al. (2010) modified equation 2.8 to include the ratio of the height of the powerhouse (h) to the net spacing (B) between the powerhouse and the transformer house. After a large

number of calculations for different schemes of cavern layout with different spacing, following displacement prediction equation was proposed:

$$U_{ep} = h[a(1000 k\gamma H/E)^2 + b(1000 k\gamma H/E) + c(B/H) + d] \times 10^{-3} \quad (2.9)$$

where,

B = Spacing between powerhouse and transformer hall cavern, m

Equation 2.9 was applied to predict the displacements at key points on the sidewalls for caverns of nine projects. Computation results were compared with numerical modelling or back-analysis results and the errors were less than 15%. A stability evaluation criteria of the surrounding rock mass based on the ratio (Θ) between the elasto-plastic (U_{ep}) and elastic displacement (U_e) to evaluate the extent of stability deterioration of surrounding rock was proposed and critical displacement ratio (Θ_c) equation was given as:

$$\Theta_c = 0.001403H - 0.01138E + 1.214375 \quad (2.10)$$

where,

H = Overburden depth, m

E = Rock mass modulus, GPa

Lee and Song (2003) highlighted the geotechnical work carried out in South Korea, particularly in mushroom and egg shaped caverns. Two-dimensional numerical analysis was carried out to determine the stability of the underground powerhouse cavern. The analysis used a coupled method that combines both the boundary element and finite element methods. In addition, a three-dimensional finite element method for continuum was used to examine effect of the discontinuities around the powerhouse cavern on the stress distribution. Their analysis concluded that an egg-shaped cross-section provides many advantages in structural stability.

Lee et al. (1995) investigated the effect of excavation-support sequences on the behaviour of underground crude oil storage caverns in a jointed rock mass using visco-plastic finite element model. They used back analysis based on the inverse method to evaluate the deformation modulus and the initial in-situ stress around caverns.

Lim and Kim (2003) carried out a comparative study on the stability analysis methods for underground pumped powerhouse cavern. For the stability analysis of the five underground powerhouses, finite element method was used. Visco-elastic finite element method with creep coefficient was used for stability analysis of Samrangjin pumped powerhouse cavern. Park et al. (2003) studied the stability of the cavern excavated in highly stress region (with high horizontal stress, where K_0 value was close to 3) using FLAC 2D Model. Results showed that stress exerted in the shotcrete at crown exceeds allowable value when 3rd bench (the lowest bench) is excavated for rock mass classes IV and V, and found tensile failure of shotcrete near the boundaries between benches for all classes of rock mass.

Lee et al. (2009) used a non-linear, three-dimensional finite element model to simulate the excavation of Baishan hydropower station in China. Drucker-Prager elastic-perfectly plastic material model was used for the simulation of rock mass, faults and the supporting structures. Material non-linearity was dealt with using an incremental technique. Displacement of the cavern wall was measured using three point rod extensometers. Field measurement results showed that the surrounding rock of cavern was stable with rock bolts and shotcrete as main supporting elements. Maximum deformation of cavern surface was less than 6mm and there was no further displacement after the cavern excavation was completed.

Ghorbani and Sharifzadeh (2009) assessed the long term stability of powerhouse cavern of Siah Bisheh pumped storage scheme in Iran under saturated condition using discontinuum modelling 3DEC. In this study, they used displacement measured from MPBX to carry out back analysis using univariate optimization algorithm. Their results showed increase in uplift pressures in discontinuities and local failures around the powerhouse after impounding of dam. Construction of a cut off curtain around the cavern was recommended. Same powerhouse was also modelled by Moosavi and Fattahpour (2009) using 3D finite difference models. Due to the closely spaced bedded sedimentary rocks (mostly quartzitic sandstones and reddish-brown and blackish siltstone of shaly appearance with low RQD index) around the cavern, the transversely isotropic elastic model was chosen to simulate the powerhouse cavern and related excavations. In addition, sheared and altered zones also

crossed the cavern axis. The results obtained from installed extensometers in sidewalls of powerhouse cavern showed good agreement with the displacements obtained from numerical modelling results. Safety factor for rock mass surrounding the caverns was determined using the induced stresses using Hoek and Brown Failure criteria. Results obtained from evaluation of safety factor showed some unstable zones around the cavern due to the existence of main sheared zone. Model results also showed an unstable zone between transformer and powerhouse caverns.

Wang and Zhu (2006) did bolting pattern optimisation for Yantan underground powerhouse in China using FLAC and FLAC-3D. Zhu and Chen (2009) studied the wall rock stability of the powerhouse of second extension project of Yantan using FLAC-3D and identified the zones of stress concentration and failure zones, and found that the cavern as a whole was stable.

Saran and Broch (2008) studied the stability of underground powerhouse cavern, transformer hall cavern, draft tube gate cavern, six bus tunnels and six draft tube tunnels of Xiaolangdi multi-purpose project in China using FLAC-3D. Both elastic and elasto-plastic analysis were carried out and following conclusions were made:

- Deformations of the powerhouse walls were much higher than that at the crown (H/W ratio is 2.34).
- Deformations of the transformer hall walls were almost same in both crown and side walls (H/W ratio is 1.19).
- Destressing of the rock mass was observed on downstream wall of the powerhouse extending upto 10 - 12m.
- After the excavation of bus tunnels and draft tubes, destressed zone increased on the downstream wall of powerhouse and destressed zone on upstream wall remained same.

Zhu and Zhu (2013) used discontinuum software 3DEC to analyse stability of the crown of cavern at Baihetan hydropower project, China. They studied stress induced failure of the crown due to stress localisation effect due to nearby shear zone. They also identified the

potential wedges formed by discontinuities and designed the support system based on results of the model.

Moghadam et al. (2013) studied the time dependent behaviour of underground caverns excavated in rock salt considering creep, dilatancy and failure. An elasto-visco-plastic constitutive model was utilized to describe dilatancy, short term failure as well as long term failure during transient and steady state creep of rock salt. Constitutive model was employed in a finite element code to simulate the stress variation and ground movement during creep of rock salt around the cavern within the framework of large deformations.

Xu et al. (2015) modelled the behaviour of rock mass containing an interlayer shear weakness zone in an underground cavern site. They used 3D continuum model with an equivalent continuum approach, including a rock-soil composite material model, and found it suitable for describing the behaviour of rock mass containing discontinuities.

Zhang et al. (2016) analysed the stability of the blocks formed by joints using 3DEC during the construction of Shenzhen pumped storage caverns in China. Joints mapped during pilot tunnel excavation were updated in the model after each excavation step and potentially unstable blocks in the next excavation step were identified and designed the support requirement accordingly.

Wu et al. (2016) conducted extensive rock mechanics investigations in the underground caverns of Jinping hydropower station in China. They studied the deformation and failure characteristics of the surrounding rock mass and stress characteristics of anchorage structures during the construction of the cavern. Layered rock mass composite model, LRCM was used to study the rock mass behaviour and response of support system. Model was able to consider the failure patterns of rock mass and joint planes to describe the anisotropic features of deformation and strength variations in the rock mass, and to simulate the progressive failure of rock mass induced by deformation.

Ma et al. (2016) conducted stability analysis of oil storage caverns by integrating numerical modelling and micro seismic monitoring. A numerical method called Continuous–Discontinuous Element Method (CDEM) was applied to simulate micro-cracks under excavation-induced unloading conditions. Microseismic (MS) monitoring system was

employed to monitor real time MS events during construction of storage caverns. Numerical results were validated using the monitoring data from the MS monitoring system. They found that the integrated method was useful in capturing micro cracks in underground storage caverns.

Xiao et al. (2016) studied stress-structure controlled collapse of surrounding rock mass during the construction of Baihetan hydropower station, China. An in-situ experiment involving microseismic monitoring was carried out in the powerhouse cavern and consistent set of results were obtained. They concluded that tensile fracturing is the rock mass fracturing mechanism that is most active during the process of evolution of stress structure controlled collapse.

2.8 INDIAN RESEARCH EXPERIENCES IN CAVERN RELATED STUDIES

In depth investigative and performance monitoring studies were carried out during the construction of Nathpa Jhkari Power Project in Himachal Pradesh, India. Underground powerhouse cavern [20m (W) x 49m (H) x 216m (L)] was investigated by Bhasin et al. (1996) using updated Q System (empirical) and analysed with 2D discontinuum model, UDEC-BB (which incorporates Barton-Bandis non-linear joint behaviour model). Model results were compared with the multi-point borehole extensometer results obtained during the instrumentation studies at the cavern. The results of deformation measurements indicated that the displacements in the periphery of the arch and in the deeper sections of the rock mass are similar to those predicted through the empirical and numerical approaches.

Dasgupta et al. (1995a, 1995b) used 3D discontinuum models using 3DEC to investigate the distress condition at the powerhouse of Sardar Sarovar project after cracks appeared on the walls of the cavern and inside the bus ducts. Horizontal major principal stress along the longitudinal axis of the cavern was found to be 3 times the vertical stress and intermediate principal stress across the cavern was 1.4 times the vertical stress. Narrow shear zones were explicitly modelled in 3DEC. Movement of the wedge was analysed and cable bolts were recommended as additional supports.

Dasgupta et al. (1999) used numerical modelling and instrumentation data as the basis for design of powerhouse cavern at Tehri hydroelectric project, Uttarakhand. A combination of two and three dimensional modeling was used in order to arrive at an effective and optimized support design. A two-dimensional analysis using FLAC was carried out to design a pattern of rock bolt support system and shear zones and major shear planes were modelled using 3DEC to advice on additional support.

Varadarajan et al. (2001) carried out finite element analysis of powerhouse cavern of Nathpa Jhakri project using computer code DSC-SST-2D developed by Desai (1997) with the constitutive model based on DSC. The procedure proposed by Ramamurthy (1993, 2001) to determine the strength and the Young's modulus of the jointed rock mass from the intact rock properties was suitably adopted to determine the material parameters for the constitutive model. They observed higher movements of the wall around mid-height of the cavern wall.

Finite element analysis of underground caverns of Koyna hydroelectric project was carried out by Dhawan et al. (2002). Four caverns, Machine hall [20.6m (W) x 50.14m (H) x 145m (L)], Valve house [(7m (W) x 13.15m (H) x 145m (L)], Transformer hall [20m (W) x 23.5m (H) x 173m (L)] and Collection gallery [10.8m (W) x 10.6m (H) x 173m (L)] at a depth of 160m were analysed. These caverns are located in amygdaloidal basalt comprising of horizontal and vertical brecciated rock horizons, at several locations. Finite element software Solvia 90, developed by Solvia Engineering AB, Sweden, was used for the analysis. Drucker-Prager failure criteria was adopted as the failure criteria in the model. They found that 3D elasto-plastic FEM analysis results closely matched with the field deformation observations for the nonhomogeneous rock mass with weak zones compared to the 2D modelling results. It was also observed that in multi-stage excavation, stresses at the end of a partial stage are higher than those occurring at the end of the complete excavation.

Sitharam and Lata (2002) used equivalent continuum method in FLAC and FLAC3D and analysed the powerhouse cavern of Nathpa Jhakri Project and found good agreement with the measured instrumentation data.

Samadhiya et al. (2004) developed an approach for analysis of caverns in jointed rock mass and shear zone and applied the method for the analysis of cavern at Sardar Sarovar Project, Gujarat. Shear zones were modelled using ASARM (Analysis of Stresses in Anisotropic Rock Masses). Elastic constitutive equations based on equivalent material approach were used to simulate the overall behaviour of the jointed rock mass. They found that stress concentration at the crown is much higher than in the sidewalls. Displacement in the sidewalls was much higher than the displacement at the crown.

Nair and Sripad (2012) studied the behaviour of powerhouse and transformer hall cavern of Tapovan Vishnugad hydroelectric project in Uttarakhand. They used 3D discontinuum modelling with 3DEC and the effect of a shear zone and biotite band behaviour on the stability of the cavern was studied. They recommended to install cable bolts in the pillar between the bus ducts.

Bhandari et al. (2016) carried out 3D analysis of two caverns, eight tunnels, and four shafts with different dimensions using FLAC-3D. Isotropic behaviour of relatively weak rock mass was modelled using Mohr-Coulomb model and anisotropic behaviour of schistose rock mass characterised by discontinuities was modelled using ubiquitous joint model. Trend of displacement with progress of excavation was also studied to establish the stability of caverns.

Various research studies related to cavern were briefly reviewed and presented. Review covered recent development in rock mass classification, major underground caverns in India, numerical modelling and other studies and research related to Indian caverns. It was found that detailed instrumentation to study the behaviour of caverns has not been carried out, particularly in the caverns in Himalayas. Stress distribution in the pillar between two caverns and effect of intermediate principal stresses has not been dealt with in detail. Instrumentation done during the construction of the cavern, in all cases was limited and was not continued during post excavation period. Orientation of the cavern with respect to principal stresses was also not covered in detail. Considering the lacunae in the so far available studies, an attempt is made in this research study to look into the following aspects:

- Study the behaviour of cavern during entire cycle of excavation and continue the monitoring during post excavation period.
- Study the effect of intermediate principal stress on stress distribution in pillar and abutment.
- Effect of orientation of the cavern on stress and displacement.

INVESTIGATIONS

The purpose of research study is to assess the behaviour of caverns and the surrounding rock mass in Himalayas.

Investigations were carried out with the following objectives:

- To study the deformational behaviour of crown of the cavern.
- To study the behaviour of side walls of the cavern.
- To study the effectiveness of rock bolts.
- To assess the influence of excavation of main cavern on the cross tunnels.
- To simulate the behaviour of the cavern in jointed rock mass using 3D Distinct Element Modelling and 3D Continuum Modelling, and compare the results with field observations.

The study was carried out in two phases:

1. Field Investigations
2. Numerical Modelling

3.1 FIELD INVESTIGATIONS

For this study, two large underground caverns at Tala Hydroelectric Project, Bhutan, situated in lower Himalayas were chosen. Field investigations were conducted in powerhouse cavern, transformer hall cavern and interconnecting tunnels from the beginning of the excavation. Information about geology of the area and the details of in-situ stresses were generated at the beginning of the excavation.

Following field investigations were conducted to generate geotechnical parameters:

- Collection of rock samples for determining physico-mechanical properties in the laboratory, as per ISRM standards.
- Monitoring the behaviour of surrounding rock mass using geotechnical instruments during each stage of excavation.

3.1.1 Description of the Site

There are many large underground caverns in Himalayas under construction. In order to study the stability issues of large caverns, a detailed field instrumentation programme was taken up at two caverns in Himalayas. Instrumentation studies were carried out at

caverns of Powerhouse complex of Tala Hydroelectric Project, Bhutan. Tala Hydroelectric Project is of 1020 MW capacity run of the river scheme in Bhutan on river Wangchu in Chukha Dzongkagh of Western Bhutan, immediately downstream of Chukha Hydroelectric Project (Fig.3.1).



Fig. 3.1 Location of Chukha Dzongkagh (CartoGIS, College of Asia and the Pacific, The Australian National University)

This project utilizes 861.5m of head available from Chukha downstream to Tala powerhouse. Main components of the project consist of a 92m high and 130m long concrete gravity dam located at Wangkha, about 3km downstream of Chukha powerhouse, an underground desilting complex comprising of three chambers (three intakes, each of 250m long, 13.9m wide and 18.5m high), 23km long and 6.8m diameter modified horse shoe shaped head race tunnel (with 5 adits) terminating in a 178m deep restricted orifice type surge shaft with a diameter of 15m/12m, two pressure shafts of 1.1km long and 4m diameter each and an underground powerhouse with powerhouse cavern of 206.4m x 20.4m x 44.5m dimension to house six generating units, each of 175MW, located on right bank of Wangchu river. Transformers and switchgears are also located in an underground cavern of 191m x 16m x 24.5m dimension, 40m downstream of powerhouse cavern. Water is taken back to river through a 7.75m

diameter horseshoe shaped, 3.1km long tail race tunnel. Location of dam site and powerhouse complex are shown in Figs. 3.2 and 3.3 respectively.

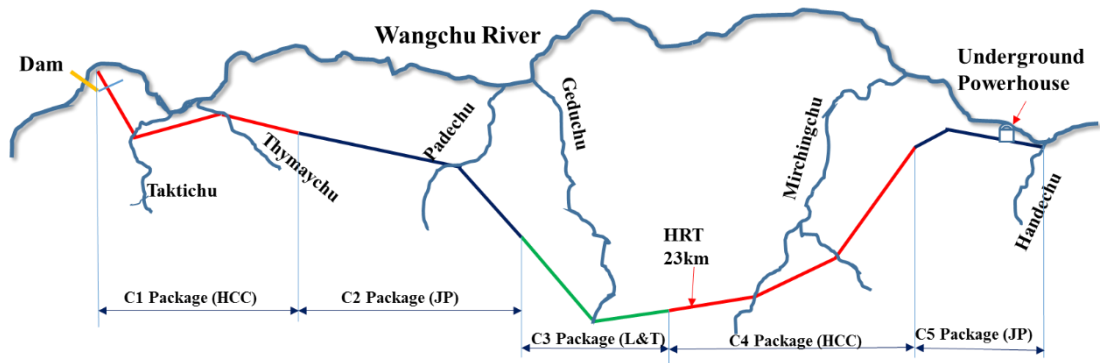


Fig. 3.2 Location of dam site, Tala Hydroelectric Project, Bhutan



Fig. 3.3 Location of powerhouse site, Tala Hydroelectric Project, Bhutan

The project is divided into five packages for effectively distributing the construction activities. Outline of the five packages (C1 to C5) is shown in Fig. 3.4. Plan depicting the caverns and tunnels in the powerhouse area is shown in Fig. 3.5.



Key Plan (not to scale)

Fig. 3.4 Layout of Tala Hydroelectric Project, Bhutan

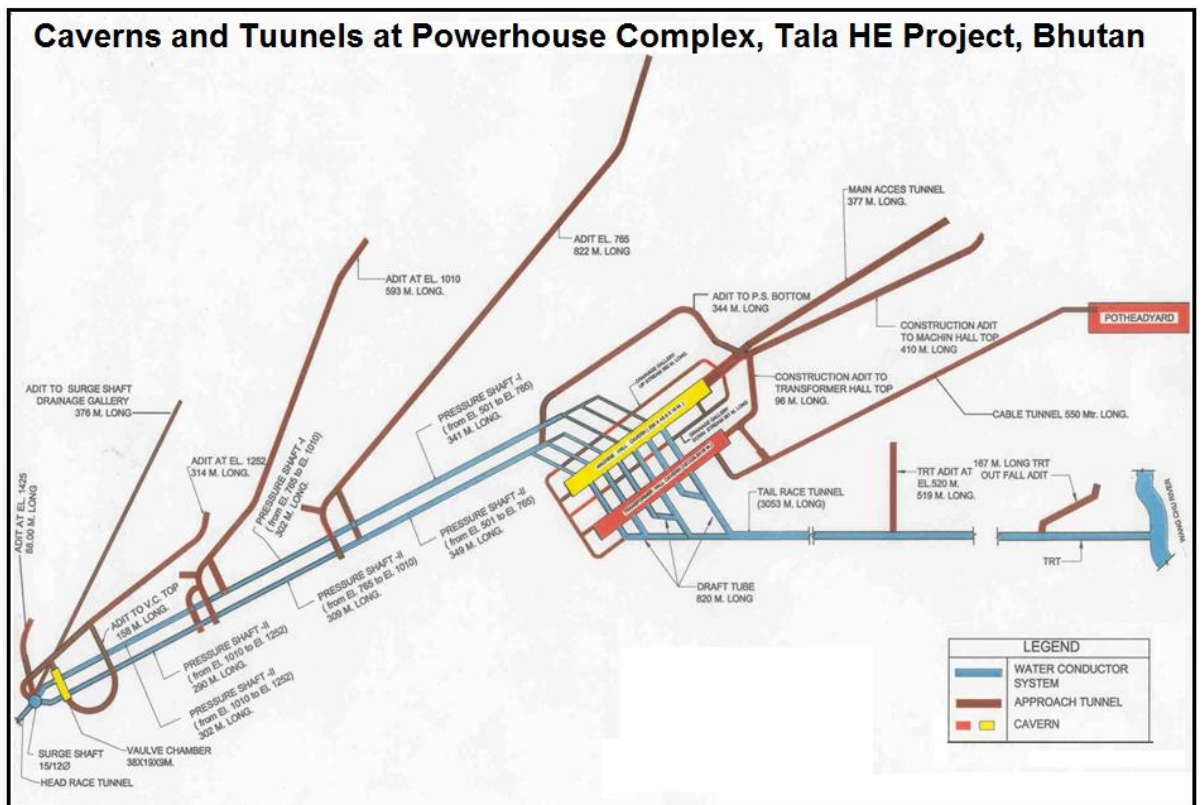


Fig. 3.5 Details of caverns and connecting tunnels at powerhouse complex of Tala Hydroelectric Project, Bhutan

3.1.2 Investigations in Powerhouse Complex

Powerhouse complex consists of powerhouse cavern, transformer hall cavern, bus ducts, pressure shaft manifolds, TRT manifolds, drainage galleries and other connecting tunnels. Salient features of powerhouse complex are as follows:

Powerhouse Cavern

a. Length	:	206.4m
b. Width	:	20.4m
c. Height	:	44.5m
d. Crown Elevation	:	538m
e. Springing Level EL	:	533m
f. Service Bay EL	:	514.5m

Transformer Hall Cavern

a. Length	:	191m
b. Width	:	16m
c. Height	:	24.5m
d. Crown Elevation	:	539m
e. Floor EL	:	514.5m

Bus Ducts and other Tunnels

a. Bus Ducts	:	10m x 8.5m D shaped tunnel 3 nos.
b. Passage Tunnels	:	2 nos.
c. Pressure Shaft Manifolds	:	6 nos.
d. TRT Manifolds	:	6 nos.

Powerhouse and transformer hall caverns are separated by a pillar of 40m thickness. Cross section of the powerhouse complex showing the dimensions of various components are shown in Fig. 3.6.

Vertical positions in the cavern are denoted by actual elevation (EL) and the horizontal positions along the length of cavern are denoted by reduced distance (RD). RD-0 refers to starting point of the corresponding cavern. RD-0 in transformer hall corresponds to RD-15.4 in powerhouse cavern as the end point of both the caverns (RD-206 of powerhouse and RD-191 of transformer hall) are aligned.

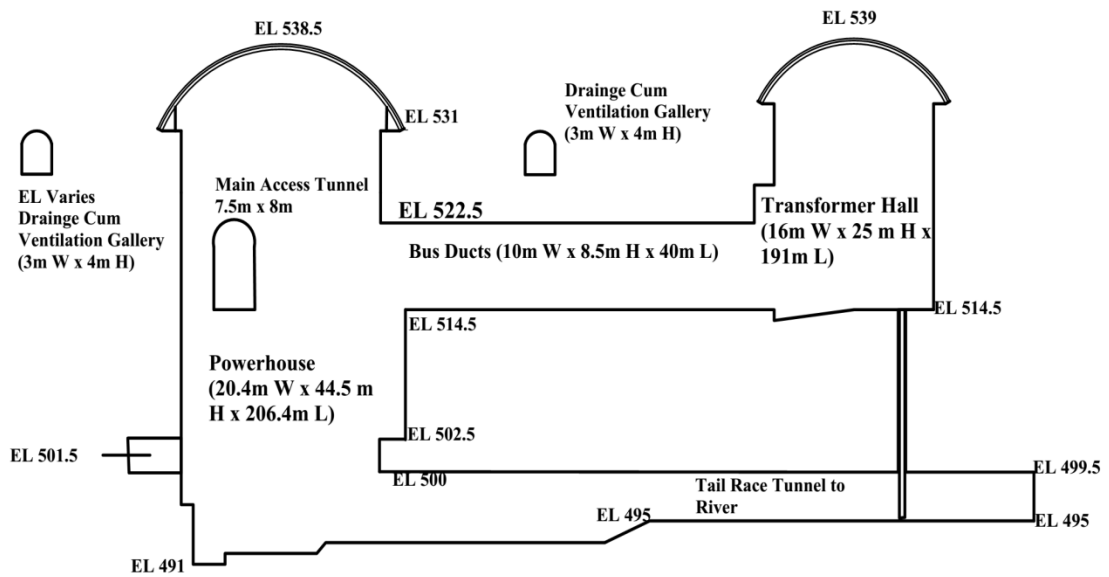


Fig. 3.6 Cross section of powerhouse complex, Tala Hydroelectric Project

Monitoring was carried out using various instruments in powerhouse cavern, transformer hall cavern in the following stages:

1. **Measurement of axial load on the rock bolts in the crown:** Axial loads on the rock bolts in the crown were monitored using Vibrating Wire Load Cells. Vibrating wire load cells of 40t capacity were installed at RD-15, RD-80, RD-130 and RD-150 of powerhouse cavern and RD-14, RD-59, RD-114 and RD-156 of transformer hall cavern. Load cell data collected was used for assessing adequate capacity of rock bolts in the crown and the behaviour of rock bolts with the excavation of crown.
2. **Measurement of displacements at various horizons in the crown of cavern:** In the crown of powerhouse cavern, Magnetic Ring Multi Point Borehole Extensometers (MRMPBX) of 20m length were installed at RD-15, RD-80, RD-130 and RD-150 of powerhouse cavern, and RD-14, RD-59, RD-114 and RD-156 of transformer hall cavern. Displacement data collected at various horizons in the crown was used to assess the joint opening and the overall bolt length required.
3. **Measurement of axial load in steel ribs in the crown:** Steel ribs of ISMB:350mm x 140mm sections were used in powerhouse cavern and ISMB: 300mm x 140mm section were used in transformer hall as final support in the crown. Axial load on the ribs was monitored using the solid load cells of 100t

capacity at EL-533. Load cells were used at six sections in powerhouse cavern, and at each section one load cell was installed on downstream side and one on upstream side. Load cell data was used to ascertain the efficacy of steel rib supports in the crown.

4. **Measurement of pore water pressure in the crown:** Pore water pressure in the surrounding rock mass was monitored using Vibrating Wire Piezometers of 7.0MPa capacity. Piezometers were installed at RD-15, RD-80, RD-130 and RD-150 of powerhouse cavern. Piezometer data was utilised for assessing build-up of water pressure in the crown area.
5. **Measurement of load on rock bolts in the side walls:** Development of load on 12m long Dywidag rock bolts in the side walls of powerhouse cavern and 8m long Dywidag rock bolts in side walls of transformer hall was measured using Vibrating Wire Anchor Load Cells. Load cell data was used to assess the efficacy of Dywidag rock bolts and to decide the adequacy of support requirements in side walls. Load cells were installed on the rock bolts at EL-525, EL-520, EL-515 and EL-506 at RD-15, RD-65, RD-110 and RD-150 in the powerhouse cavern on both upstream and downstream walls. In transformer hall cavern, the load cells were installed at RD-14, RD-60, RD-114 and RD-156 at EL-532, EL-525, and EL-520 on both walls. Load cell data was recorded with the progress of benching in the cavern.
6. **Measurement of convergence of side walls:** Convergence in the side walls of cavern was monitored using reflective targets with Total Station. Total Station, Leica TDA 5005, with angular accuracy of 0.5s was used for this purpose. Cumulative convergence was measured with the progress of cavern benches. Convergence was measured at RD-15, RD-65, RD-110 and RD-150 at elevations of EL-525, EL-520, EL-515 and EL-506 in powerhouse cavern and RD-60 at EL-531, RD-14, RD-60, RD-114 and RD-155 at EL-525 and EL-520 of transformer hall cavern. Convergence measurement was continued with benching in the cavern, and data was used for assessing the stability of cavern and calculating the strain values.
7. **Measurement of strain along the length of rock bolts:** Strains developing in the rock bolt along the length were measured using Rock Bolt Stress Meter,

also known as instrumented bolt. Instrumented bolts were installed at EL-506 on both upstream and downstream wall at RD-65, RD-110, RD-150 and at EL-515 (RD-140 and RD-150) of powerhouse cavern. Data from instrumented bolts was used to assess the distribution of strains along the length of rock bolts.

8. **Measurement of pore water pressure inside walls:** Pore water pressure in the surrounding rock mass was monitored using Vibrating Wire Piezometers of 7.0MPa capacity. Piezometers were installed at EL-525, EL-520, EL-515 and EL-506 at RD-15, RD-65, RD-110 and RD-150 in the powerhouse cavern on both upstream and downstream walls.

3.1.2.1 Laboratory testing and estimation of rock mass parameters

Laboratory testing was carried out by National Institute of Rock Mechanics (NIRM), Bengaluru, where the author is employed. Author was also part of the team and selected the samples from the field and the testing was carried out in his presence. Estimation of the rock mass properties was entirely done by the author.

Rock blocks of phyllitic quartzites and quartzites containing fractures and foliation planes were collected from the pilot tunnel of the powerhouse cavern. Cylindrical samples (BX and NX size) were prepared from the blocks by diamond drilling in the laboratory. Core samples were cut to the required length using rock cutting machine and the loading faces of samples were polished using an automatic surface grinder. Length to diameter ratio of 2.5 to 3.0 was maintained for all the tests. Following tests were conducted at the laboratory:

1. Uniaxial compression test.
2. Triaxial compression test.
3. Normal and shear tests on jointed rock.

Summary of the test results are shown in Table 3.1. Some of the properties could not be determined in the laboratory as sample preparation of quartzite from this site as per ISRM standard was difficult.

Table 3.1 Summary of laboratory test results

Property	Phyllitic Quartzite		Quartzite	
	Dry	Saturated	Dry	Saturated
Density, kg/m ³	2650	2650	-	-
Uniaxial Compressive Strength, MPa	63.17	51.90	-	-
Young's Modulus, GPa	18.35	12.93	70.6	61.24
Poisson's Ratio	0.35	0.36	0.18	0.19
Cohesion, MPa	18.56	15.71	-	-
Friction Angle, degrees	28.86	28.33	-	-
Hoek and Brown constant, m _i	4.18	4.49	-	-
Joint Normal Stiffness, GPa/m	10.4			
Joint Shear Stiffness, GPa/m	0.97			
Joint Cohesion, MPa	0			
Joint Friction Angle, degrees	25			

3.1.2.2 Geology of powerhouse complex

Geological investigations while excavating the caverns were done by geologists at Tala project Bhutan and author was interacting with them on daily basis. Geotechnical investigations while excavating the caverns was done by the author.

Powerhouse complex is situated in a hillock with overburden ranging from 400 - 500m. The host rock is fresh and hard, with inter banded sequence of quartzite, phyllitic quartzite and amphibolite schist partings. These rocks are highly puckered and folded into tight synform and antiform. Major discontinuity features were mapped from the exploratory drift of 2m x 2m driven in N37°W-S37°E (N143° – N323°) direction along the crown of powerhouse cavern. In addition to the foliation, five more sets of joints were identified. General foliation trend was found to vary from N65°E-S65°W to N70°W-S70°E with 35° to 60° (N25°W to N20°E) dips. Average dip of the foliation is 45.5° and dip direction N357°. Details of major discontinuities are listed in Table 3.2 (Singh et al., 2002).

Plunge/Trend of the folded axis was recorded at RD-16 (25°/270°), RD-93 (18°/056°), RD-128 (10°/090°), RD-143 (15°/130°) and at RD-183 (10°/088°). Long axis of the

powerhouse in N37°W-S37°E direction is across the strike of foliation. Due to folding, the angle between the long axis of powerhouse and strike of formation varied from 150° to 55°. Average value of foliation and five joint sets as given in Table 3.2 were used for the pole projection and kinematic analysis as shown in Fig. 3.7. In total, 10 wedges (W) have been marked and listed in Appendix-1. Kinematic analysis was done using friction angle (ϕ) of 30°.

Table 3.2 Major discontinuities in powerhouse cavern

Sl. No.	Strike	Dip	*AD	*ADD	Spacing	Continuity	Nature
Foliation (F1)	N65°E-S65°W to N70°W-S70°E	35°-60° N25°W to N20°E	45.5°	357°	10cm - 3m	5 - 12m	RU
J1	N20°W-S20°E to N15°W-S15°E	40°-80° N70°E to N75°E	60°	072°	1m - 2m	2 - 5m	RU
J2	N-S to N30°E-S30°W	25°-80° W to N60°W	52.5°	285°	5cm - 2m	2 - 10m	RU
J3	N30°E-S30°W to N20°E-S20°W	30°-50° S60°E to S70°E	40°	115°	6cm - 20cm	2m	RP
J4	N50°W-S50°E to N30°W-S30°E	60°-70° S40°W to S60°W	65°	230°	10cm - 2m	2 - 5m	SP
J5	N80°E-S80°W to N70°W-S70°E	40°-70° S10°E to S20°W	55°	185°	20cm - 2m	2 - 5m	RP

*AD – Average Dip, *ADD – Average Dip Direction, RU -Rough Undulating, RP - Rough Planar, SP - Smooth Planar

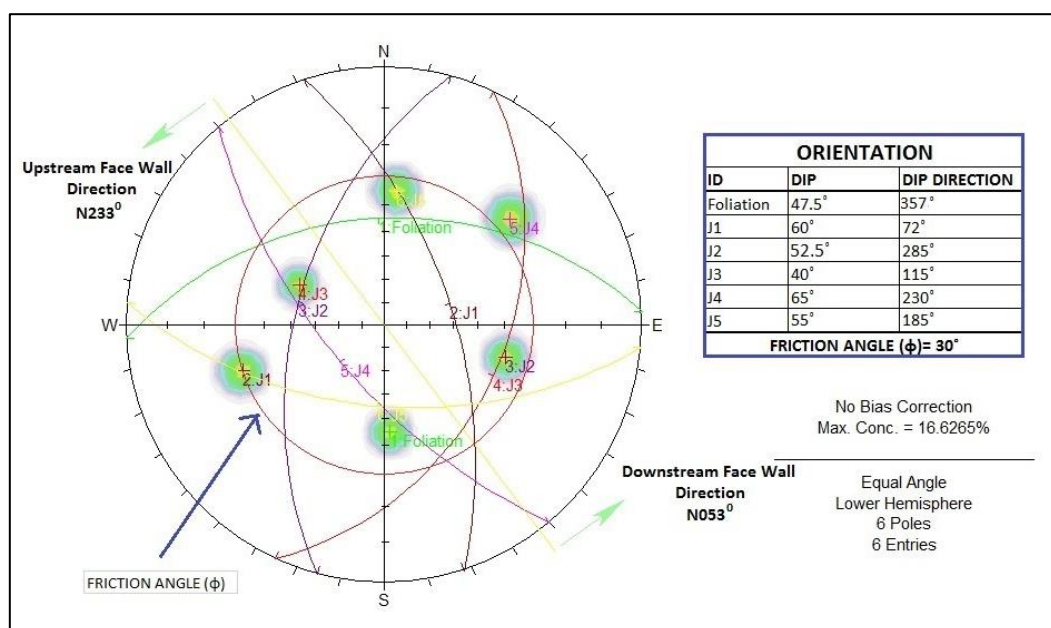


Fig. 3.7 Pole projection of joint sets of powerhouse cavern for kinematic analysis

Initially, mapping of powerhouse and transformer hall was carried out and the rock mass was found to be Fair to Good category, with 'Q' value ranging from 4.3 to 11 between RD-0 to RD-180, and around 2 between RD-180 and RD-206m. Estimated GSI values along powerhouse cavern drift were found to vary from 44 to 52, with fresh and hard quartzite and phyllitic quartzite constituting about 85-90% of the rock mass. Average GSI value of 50 was taken for further calculations.

3.1.2.3 In-situ stress

In-situ stress measurements were carried out by the team from National Institute of Rock Mechanics, Bengaluru, and the author witnessed the entire procedure at the site. Stress measurements were carried out at the powerhouse drift. The stress measurement indicated following stress regime:

Vertical stress = 10.9MPa (calculated from overburden weight)

Minimum horizontal stress = 9.5MPa (approximately normal to cavern axis)

Maximum horizontal stress = 14.2MPa (approximately parallel to cavern axis)

3.1.2.4 Excavation at powerhouse cavern

Excavation of powerhouse cavern started with 7m (W) x 7.5m (H) central gullet for the entire length of the cavern and later side slashing on either side to the full width of the cavern. The gullet was supported with 6m and 8m long rock bolts of 32mm diameter at 3m x 1.5m pattern and a layer of Steel Fibre Reinforced Shotcrete (SFRS) of 100mm.

During the crown excavation, there were roof collapses between RD-90 and RD-160. It was observed that, at most of the places, end anchors and bearing plates were intact and bolt shearing took place upto 3-4m distance into the roof and also rock mass between the bolts also failed. This indicated the separation of joints in the immediate roof (consistent with MPBX observation) and also the inadequate density of bolts. Subsequently, the crown of entire length of powerhouse cavern was supported with steel ribs of ISMB 350mm x 140mm section at 0.6m spacing, back filling with concrete and grouting.

After completion of the ribs and subsequent back filling, benching down of the powerhouse cavern started. First bench was started with excavation of central gullet of 6.5m width and 2.6m deep. The central gullet was advanced on either direction and

benches were formed on both upstream and downstream side. Benches were excavated with controlled blasting technique and by providing line drilling along the contact of wall rock. At any given time, a maximum of 9m span was exposed. The exposed wall was immediately shotcreted with 50mm thick plane shotcrete (M35 A10). On this surface, welded wire mesh of 100mm x 100mm x 5mm was fixed followed by installation of high strength Dywidag bolts of 12m long and 32mm/26.5mm diameter at 1.5m centre to centre, in a staggered manner. The Dywidag rock bolts of 26mm diameter had yield strength of 1,033MPa and tensile strength of 1,122MPa (Singh et al. 2003). The rock bolts were end anchored with resin capsules for initial 4m and rest was grouted with cement slurry. This was followed by two more layers (each 50mm) of shotcrete. Sequence of excavation of benches and the duration of excavation of each bench is shown in Fig. 3.8.

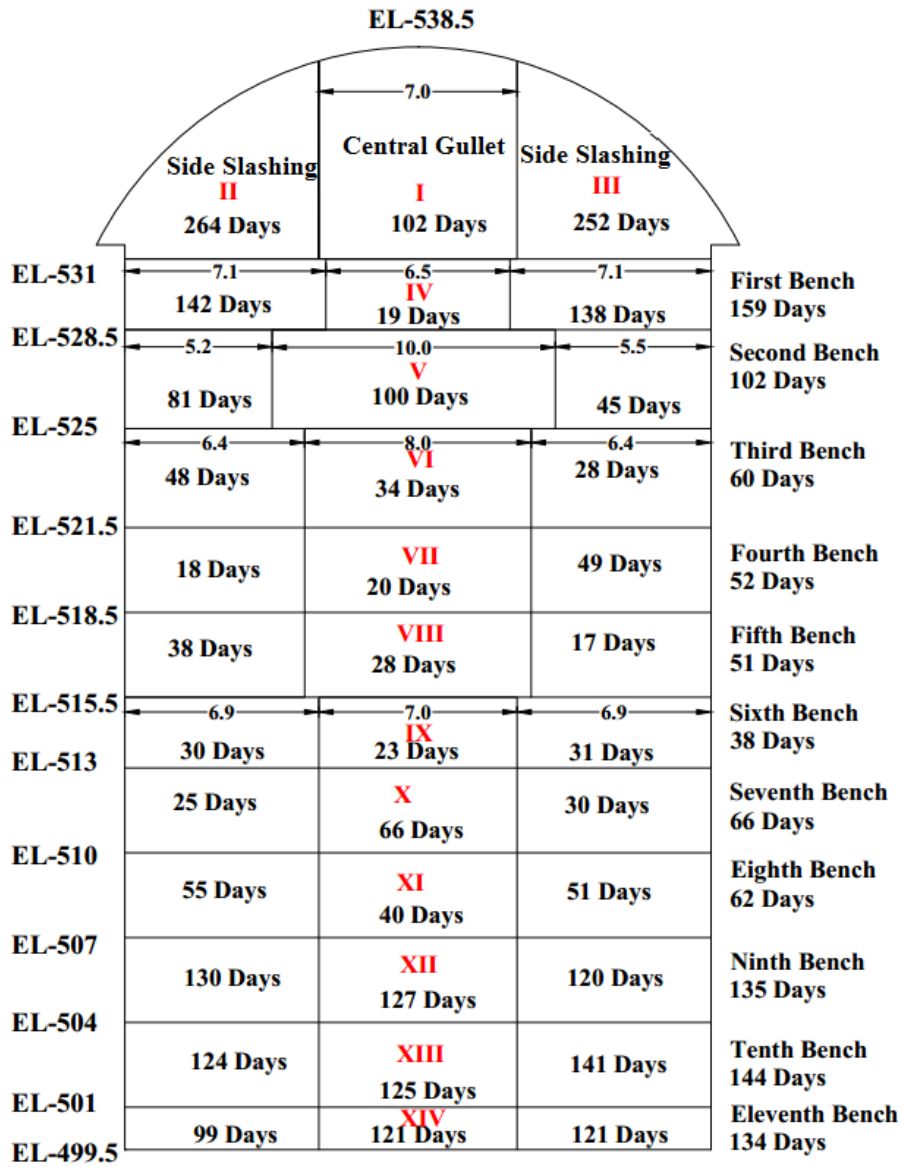


Fig. 3.8 Sequence and period of excavation at powerhouse cavern

Widths of central gullet and benches were varied to suit the geological conditions. From 6th bench and downwards, the benching was done between RD-60 and RD-206.4 only. Eleven benches were excavated upto EL-499.5. View of the powerhouse cavern after complete excavation is shown in Fig. 3.9.



Fig. 3.9 Powerhouse cavern after complete excavation, Tala Hydroelectric Project

3.1.2.5 Excavation of transformer hall

Transformer hall of 191m x 16m x 24.5m dimensions was excavated on the downstream side of powerhouse cavern in the power house complex. A rock pillar of 40m thickness was left between powerhouse and transformer hall. The EL of the crown was 539m, floor was 514.5m and springing level was at 535.5m.

Excavation of transformer hall started with excavation of the central gullet of 7.5m (W) x 7.5m (H). Central gullet was supported by SFRS and 6m long rock bolts of 32mm diameter with 1.5m x 1.5m pattern. This was followed by side slashing with SFRS of 150mm and rock bolts of 6m and 8m long, 32mm diameter at 1.25m x 1.25m pattern. Further, the entire cavern roof was supported with steel ribs of ISMB 300mm x 140mm section with back filling and contact grouting.

The benching operation in transformer hall started with the excavation of first bench from EL-533 to EL-530. The second bench was excavated from EL-530 to EL-527. The walls were supported with Dywidag bolts of 8m long and 32mm/26.5mm diameter in conjunction with wire mesh and plain shotcrete. The sequence of excavation of benches and the duration of excavation of each bench in transformer hall is shown in Fig. 3.10.

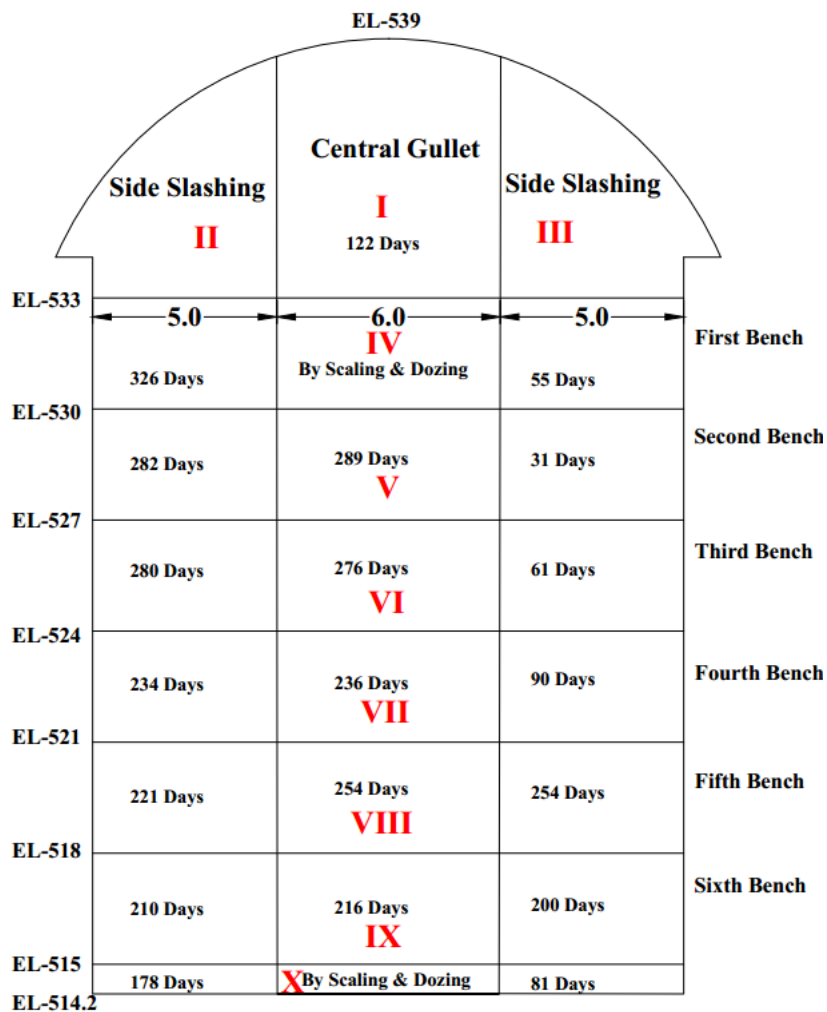


Fig. 3.10 Sequence and period of excavation at transformer hall cavern

3.1.2.6 Excavation of bus ducts

Bus ducts were excavated upto 10m initially from powerhouse side. The excavation of bus ducts which was earlier upto 10m from powerhouse side was continued from transformer hall side and excavation was completed.

3.1.3 Field Instrumentation

Various geotechnical instruments were installed by the author in powerhouse cavern, transformer hall cavern and bus ducts during various stages of construction. Section showing the location of various types of instruments is shown in Figs. 3.11 to 3.15.

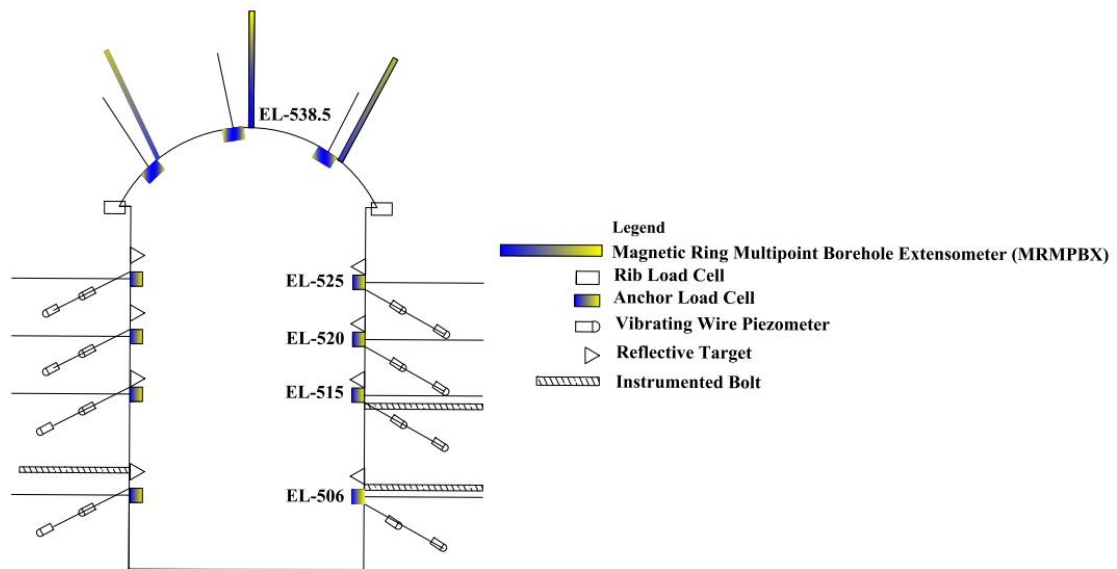


Fig. 3.11 Section of the powerhouse cavern showing location of instruments

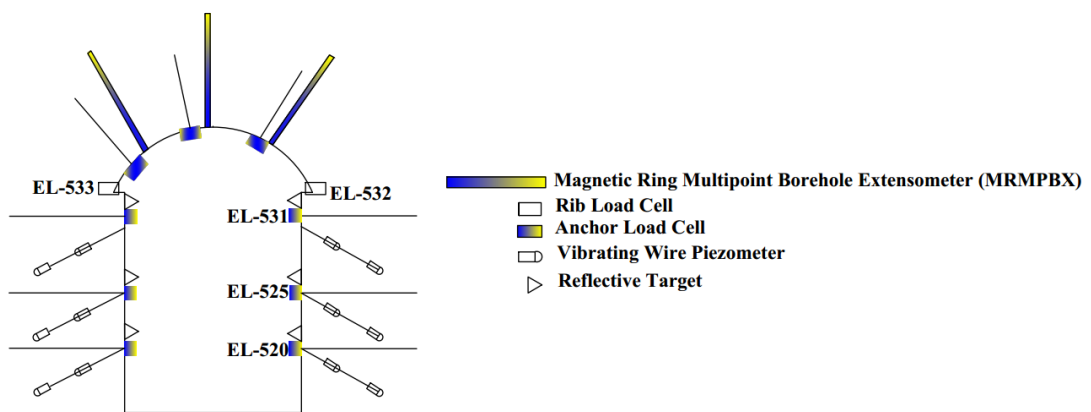


Fig. 3.12 Section of the transformer hall cavern showing location of instruments

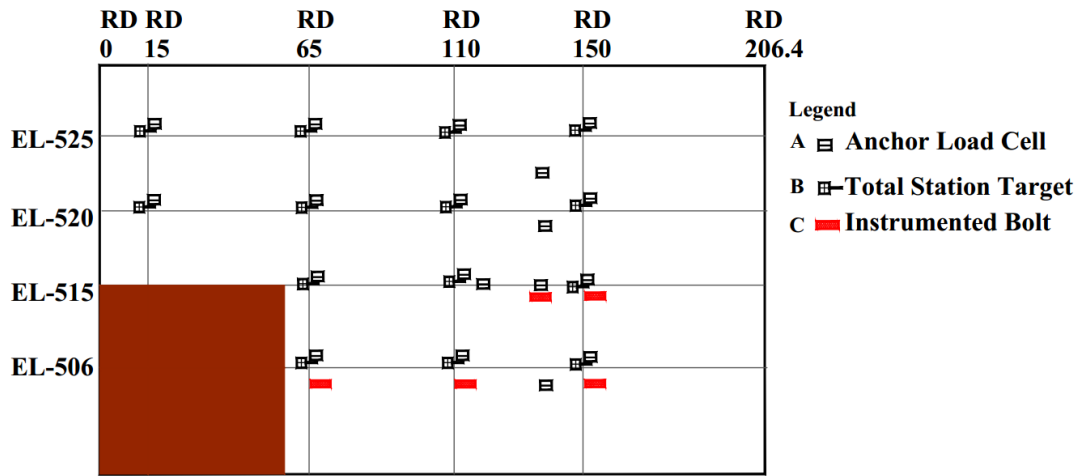


Fig. 3.13 Longitudinal section of the powerhouse cavern showing location of instruments on upstream wall

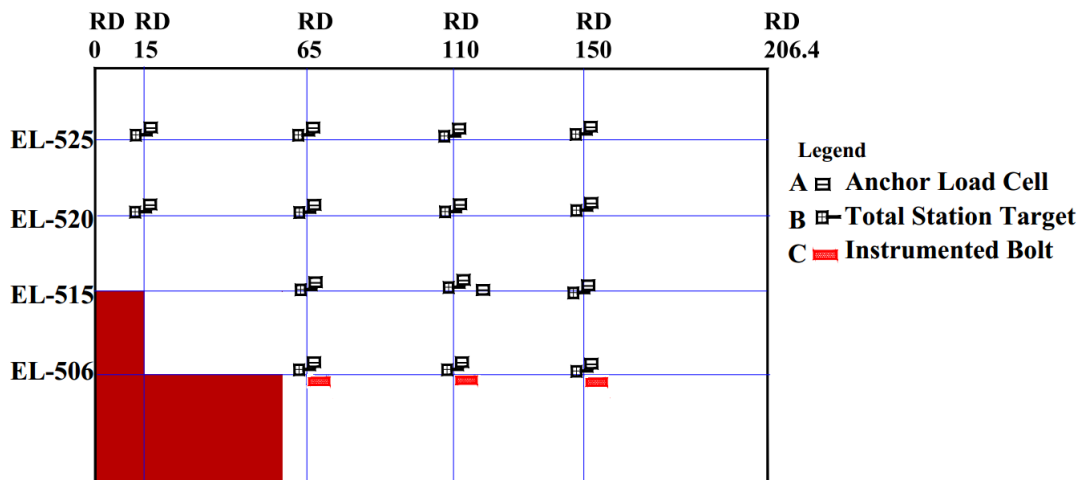


Fig. 3.14 Longitudinal section of the powerhouse cavern showing location of instruments on downstream wall

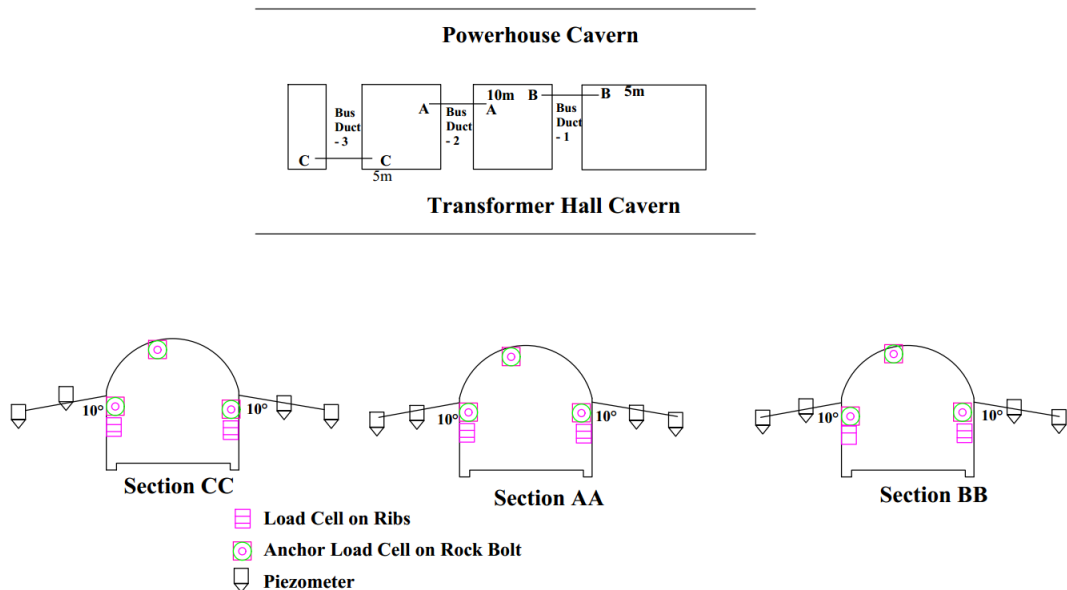


Fig. 3.15 Section of bus ducts showing the location of instruments

Monitoring details of the instruments are given below:

a. Monitoring at Powerhouse cavern

Displacement monitoring in surrounding rock mass	Crown: MRMPBX were installed in the crown at RD-15, RD-80, RD-130 and RD-150 at center, left and right side of crown. Instruments were regularly monitored till the installation of ribs in the cavern. Readings were taken manually.
Load on the rock bolts and ribs	Crown: Load cells were installed on the 8m long rock bolts at RD-15, 80, 90, 100 and 110 and were regularly monitored till the installation of the ribs in the crown. Walls: Load cells were installed at EL-525, 520, 515 and 506 at RD-15, 65, 110 and 150 on both walls and at few other selected locations. Load cells were monitored regularly. Ribs: Load Cells were put on the ribs at RD-18.5, RD-56.5, RD-126, RD-143.4 and RD-173.5 on upstream and downstream wall. Load on the ribs were regularly monitored.

Convergence of the side walls	Cumulative convergence of the side walls was monitored using reflective targets and total station. Reflective targets were installed at RD-15 at EL-525 & 520 and at RD-65, 110, and 150 at EL-525, 520, 515 and 506. Since no physical access was required for their monitoring, the convergence was monitored regularly during the entire excavation of the cavern.
Strains along the length of rock bolts	Strains along the length of rock bolts were monitored using vibrating wire instrumented bolts. Instrumented bolts were installed at EL-515 at RD-140 & 150 and at EL-506 at RD-65, 110 and 150. Strains were regularly monitored.
Pore water pressure	Pore water pressure in the surrounding rock mass was monitored with vibrating wire piezometers. Piezometers were installed at EL-525, 520, 515 and EL-506 at RD-15, 65, 110 and 150. Pore water pressure was monitored during various excavation stages.

b. Monitoring at Transformer hall cavern

Load on the rock bolts and ribs	<p>Crown: Load cells were installed on the rock bolts in the crown of the central gullet at RD-14, 60, 114 and 156.</p> <p>Ribs: Load cells were installed at RD-14, 70.6, 84.5, 113.2, 129.4 and 154.4 on both upstream and downstream side.</p> <p>Walls: At EL-532, load cells were installed at RD-13, 15, 80 and 155 on upstream side and at RD-80, 81 and 155 on downstream side. At EL-525, load cells were installed at RD-14, 60, 121 and 164 on upstream side and 113.5 and 154 on downstream wall. At EL-520, load cells were installed at RD-14, 58, 121 and 162 on</p>
---------------------------------	---

	upstream side and RD-13, 60, 114 and 162 on downstream wall. Load cells were regularly monitored.
Convergence of the side wall	Convergence of the side walls was measured using reflective targets and total station at EL-531, RD-60, EL-525 at RD-14, 60, 114 and 155, EL-520 at RD-14, 60, 121 and 155. Convergence was monitored regularly during the entire excavation of the cavern.
Pore water pressure	Piezometers were installed at EL-531 at RD-60 and RD-155 and at EL-525, at RD-60 and RD-162 on both walls of transformer hall. At each section, one piezometer was installed at a depth of 5m and one more piezometer was installed at a depth of 10m. Pore water pressure was monitored during various excavation stages.

c. Monitoring at bus ducts and connecting tunnels

Load on the rock bolts and ribs	<p>Ribs: Load cells were put on the ribs at RD-5 from powerhouse side in bus duct no.1, 10m from powerhouse side in bus duct no.2 and 5m from transformer hall side in bus duct no.3 and at RD-24.75 at passage no.1.</p> <p>Walls: Load cells were put on rock bolts at RD-5 on left wall in bus duct no.1, RD-10 left and right side crown in bus duct no.2, RD-35 at bus duct no.3 in the crown.</p>
Pore water pressure	Piezometers were installed on the side walls of bus ducts at the same sections, one at 5m depth and other at 10m depth.

3.1.4 Instrumentation and Installation

Instruments were installed and monitored by the author with the help of a colleague (both were stationed at the site) during the excavation of entire powerhouse complex. Analysis of the instrumentation data was also carried out simultaneously. Details of various monitoring instruments used in the field investigations and installation procedures are described below:

Monitoring of displacement

Multipoint borehole extensometers were used to monitor the displacements at various depths in the surrounding rock mass during various stages of excavation of the caverns. Anchors were placed at various depths at close intervals above and below the bolted horizon. The details and installation procedure are outlined below.

Multi-point borehole extensometers

There are various types of extensometers depending on different technologies. In this study, Magnetic ring multi point borehole extensometer (MRMPBX) were used.

Magnetic ring multi point borehole extensometer (MRMPBX)

MRMPBX was used to study displacement at various depths and joint separation in the roof and walls of the caverns. In this type of extensometer, anchors are magnetic rings that are placed at desired depths. Position of each anchor was measured with respect to the deepest anchor and distances obtained were used to determine the rock movement at various depths. An access pipe passes through the central hole of each anchor and is connected to the face plate anchored to the rock surface. Measurements were taken by lowering a probe through the access pipe to detect the depth of the magnetic anchor.

Installation: A NX size borehole (55mm diameter) was drilled upto a depth of 25m with Boomer machine. Borehole was flushed with compressed air and later cleaned with water to clear drill cuttings. The deepest anchor was attached to a hollow PVC pipe (access pipe) and pushed to deepest point in the borehole. Other anchors were put at required depths with the help of installation tool. Each anchor passed through the hollow pipe installed earlier and released at the required depth so that it is tightly anchored to the rock mass. Procedure was repeated till all the magnetic anchors were in place. Face plate was put at borehole collar so that hollow access pipe passed through the plate and excess length of tube was cut such that it matched with the reference

marking on the face plate. A sensor probe with graduated scale was put through the hollow PVC pipe and pushed inside by attaching additional graduated scales. Sensor probe detects each magnetic ring when it passes through the anchor with an audio and visual indicator on the readout unit. Reading of the graduated scale at that point was read against the reference mark on the face plate and exact position of anchor was noted. Procedure was repeated till all the magnetic sensors were sensed and the exact location of each anchor was noted as initial reading. Monitoring was done regularly and any relative movement between the anchors was determined by comparing the readings with the initial reading. Fig. 3.16 shows the MRMPBX with the readout unit.

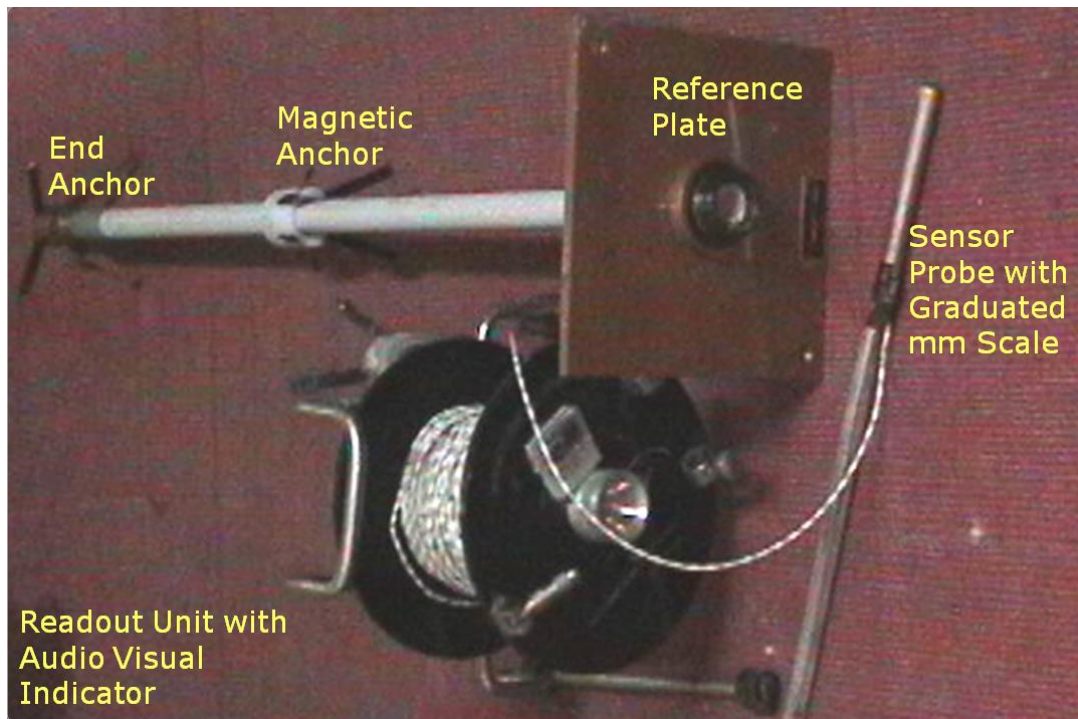


Fig. 3.16 MRMPBX with the readout unit

Measurement of load in rock bolts

Axial loads on the rock bolts were measured using anchor load cell of 50t capacity. Similarly, the axial load on the steel ribs was measured using solid load cell of 100t capacity. Both types of load cells were of vibrating wire type. Load cell was installed immediately after the rock bolt or steel ribs at the specified location was put, and was monitored regularly with the excavation of the cavern. Details of load cell and installation procedure are outlined below.

Anchor load cell

Vibrating wire anchor load cells were used for the measurement of loads in rock bolts. Anchor load cell in this investigation consisted of four vibrating wire strain gauges mounted parallel to the cell axis of symmetry and equally spaced. Each vibrating wire assembly consisted of a tensioned wire clamped at both ends. Located at the mid-section of the wire is a coil/magnet. When an electrical pulse was supplied to the coil/magnet, the wire oscillated at its natural resonant frequency. Oscillations of the wire through the magnetic field induced an alternating current in the coil, detected by a readout unit. Readout unit displayed the frequency in Hz after converting the sinusoidal alternating voltage to frequency. Each load cell came with heavy gauge multicore and PVC sheathed cable.

Load cells were installed immediately after installation of rock bolts. It was made sure that sufficient length of rock bolt was projecting outside and rock mass around the rock bolt is even. A face plate made of steel slightly bigger than the load cell cross section was put through the bolt and held against the rock. Load cell was then inserted through the bolt and reaction plate of same dimension as face plate was put on top of the load cell. Later, nut was put on top of that and tightened. After tightening, initial reading of the load cell was noted down. Subsequently, required tension was applied to the rock bolt with the help of torque meter and change in load was noted down using the read out unit. The design concept of anchor load cell is shown in Fig.3.17.

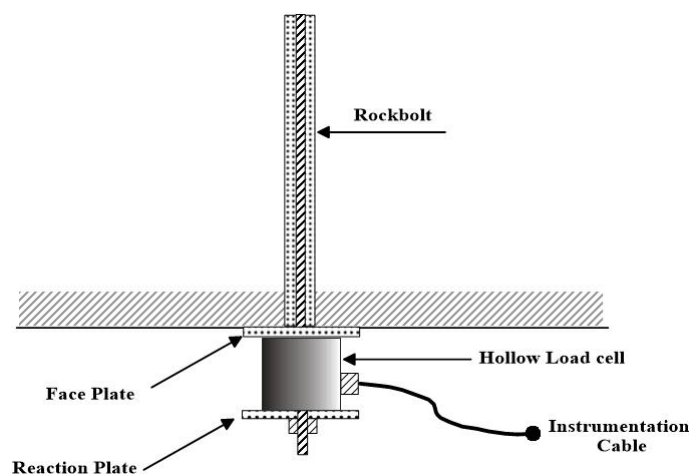


Fig. 3.17 Schematic diagram of anchor load cell with rock bolt

Fig. 3.18 shows the anchor load cell with the readout unit and the anchor load cell installed on the rock bolt at powerhouse cavern is shown in Fig. 3.19. Fig. 3.20 shows rib load cell installed at the crown of powerhouse. A typical output monitoring is shown in Fig. 3.21.



Fig. 3.18 Anchor load cell with readout unit

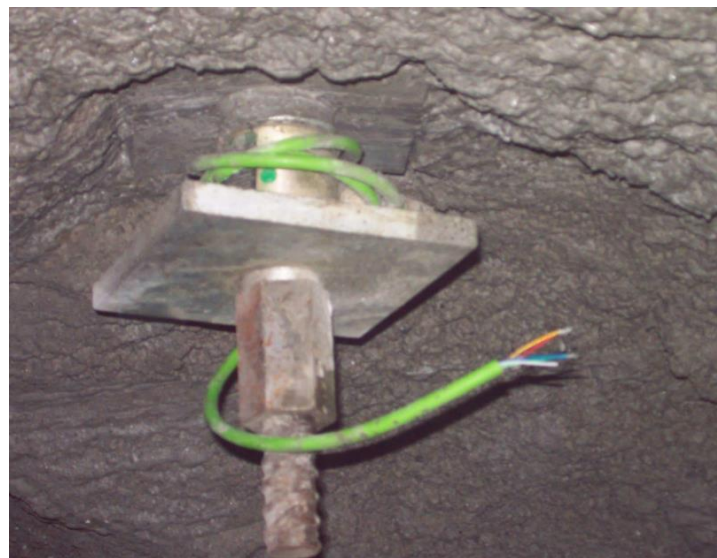


Fig. 3.19 Anchor load cell installed on rock bolt at powerhouse cavern

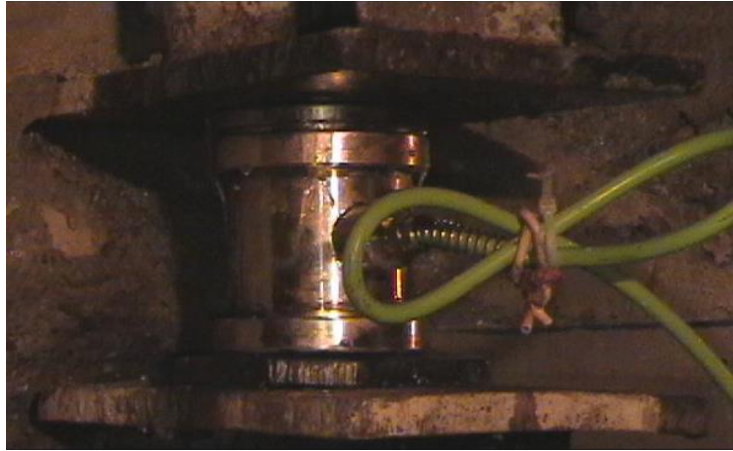


Fig. 3.20 Load cell on the steel rib at crown of powerhouse



Fig. 3.21 Monitoring of load cells at walls of the cavern

Monitoring of convergence of side walls

Convergence between main walls of the cavern was monitored using geodetic technique, with combination of reflective paper targets and total station. Convergence of the walls was measured on a regular basis during all stages of excavation of the cavern. The procedure is described below.

Reflective targets and total station

Wall convergence of the caverns was measured using reflective targets with Total Station. Total Station, Leica TDA 5005, with an angular accuracy of 0.5s was used for this purpose. Reflective targets were fixed on a plate which was held by a rod grouted

into the wall to a depth of 1m. Stations were fixed opposite to each other on upstream and downstream walls. Instrument was set on the ground and levelled and the distances between the reflective targets were measured using the total station. Cumulative convergence of the two walls was computed based on the distances between the points at different stages of excavation. Fig. 3.22 shows the Total Station TDA 5005 with the reflective targets used at the cavern. A program in the Total Station called Tie-Distance was used for measuring the convergence. Monitoring of the reflective targets using Total Station is shown in Fig. 3.23.



Fig. 3.22 Total station TDA 5005 with reflective targets

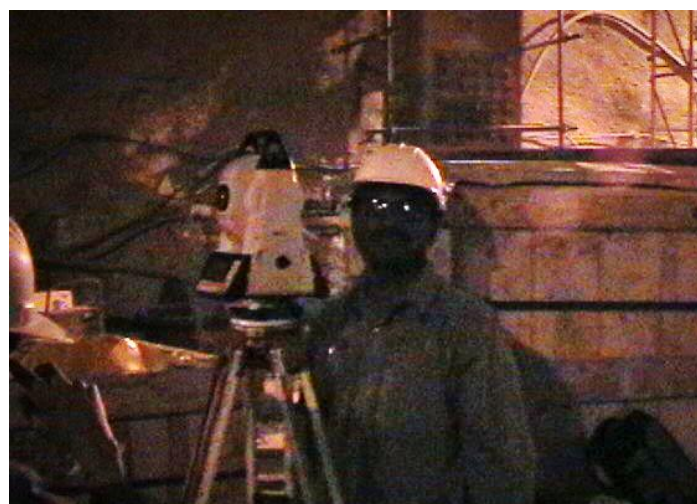


Fig. 3.23 Measuring the convergence using Total Station TDA 5005

Monitoring of pore water pressure

Pore water pressure in the rock mass was measured using vibrating wire piezometers.

Vibrating wire piezometers

Piezometer is an instrument used to measure the pore water pressure. VW piezometer converts water pressure to a frequency signal through a diaphragm, a tensioned steel wire, and an electromagnetic coil. Piezometer is designed so that a change in pressure on the diaphragm causes a change in tension of the wire. When excited by the electromagnetic coil, the wire vibrates at its natural frequency. Vibration of the wire in the proximity of coil generates a frequency signal that is transmitted to the readout device. The readout device processes the signal, applies calibration factors, and displays a reading in the required engineering unit. Fig. 3.24 shows vibrating wire piezometer and schematic diagram of installation. Monitoring of the piezometer at the powerhouse cavern is shown in Fig. 3.25.

Installation: Borehole of 38mm diameter was drilled beyond the proposed piezometer location by about 15cm and cleaned thoroughly with compressed air and water. The bottom 15cm was then filled with clean fine sand and piezometer was lowered and put in place and clean sand was placed all around it for about 15cm to form collection zone. Above this, a layer of bentonite was put followed by grouting of the entire hole. Initial reading was taken after the grout was set. Reading in frequency was converted to piezometric pressure using the formula given in the calibration sheet for each instrument.

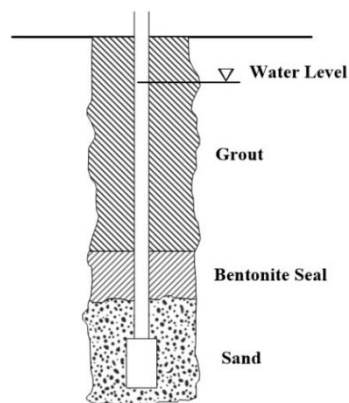


Fig. 3.24 Vibrating wire piezometer



Fig. 3.25 Monitoring of piezometers at walls of the cavern

Vibrating wire rock bolt stress meter/instrumented bolt

Vibrating wire rock bolt stress meter is an instrumented bolt which measures the strain on rock bolt, which is then converted to the stress. It consists of rock bolt anchor, sensor head and signal cable. Vibrating wire strain gauges fitted inside the rock bolt at 1m interval detects stress caused by strata movement, relaxation, etc. Vibrating wire gauges were pre-tensioned to about 2000Hz. When displacements perpendicular to the rock bolt occur, the gauges detect and output the corresponding frequency signal. Signal is transmitted to the VW readout unit. Fig. 3.26 shows the instrumented bolt.



Fig. 3.26 Vibrating wire instrumented bolt

Installation: Instrumented bolt looks like normal rock bolt and sensor head with signal cable from all the sensors are projected from one end. It was installed in the same way as normal rock bolt. Sensors at various depths along the bolt are identified by color codes and frequency was measured with the readout unit and converted to strain and stress using the formula given in the calibration sheet for each instrumented bolt.

3.2 NUMERICAL MODELLING

In this stage of the study, behaviour of the powerhouse cavern, transformer hall cavern and cross tunnels were studied at various stages of excavation and supporting using 3D numerical models. Three dimensional stress analysis of the caverns was carried out by the author using 3D Discontinuum software 3DEC (Anon, 2010) and 3D continuum software FLAC-3D (Anon, 2015).

3.2.1 3D Discontinuum Model using 3DEC

A 3D discontinuum model was constructed with the actual geometry of the powerhouse cavern, transformer hall cavern, cross tunnels (bus ducts and passages) and peripheral tunnels (penstock manifolds and tail race tunnel manifolds). Major joints crossing the powerhouse cavern at the center of the cavern were mapped and incorporated into the model. Details of joints mapped and used in the model are given in Appendix-1. Model size of 250m across the cavern axis (X-direction), 350m along the length of cavern axis (Y direction) and 200m in the vertical direction (Z-direction) was taken. In the model, 500m overburden load was applied. From the crown of the cavern 112m was modelled and the balance 388m of overburden load was applied on the top boundary of the model. Boundary in X-direction was at a distance of 12.25 times the biggest cavern width (20.4m) and in Y-direction it was at a distance of 17.15 times the cavern width. Thus boundaries were placed at sufficient distances away from the excavation in order to prevent the end constraint effect. Model was discretised into zones using 3DEC's inbuilt mesher. Zone size of 1m was chosen in the immediate wall and gradually increased outwards so that the ratio between immediate edges does not exceed 3. A typical 3D view of the model developed using 3DEC is shown in Figs. 3.27.

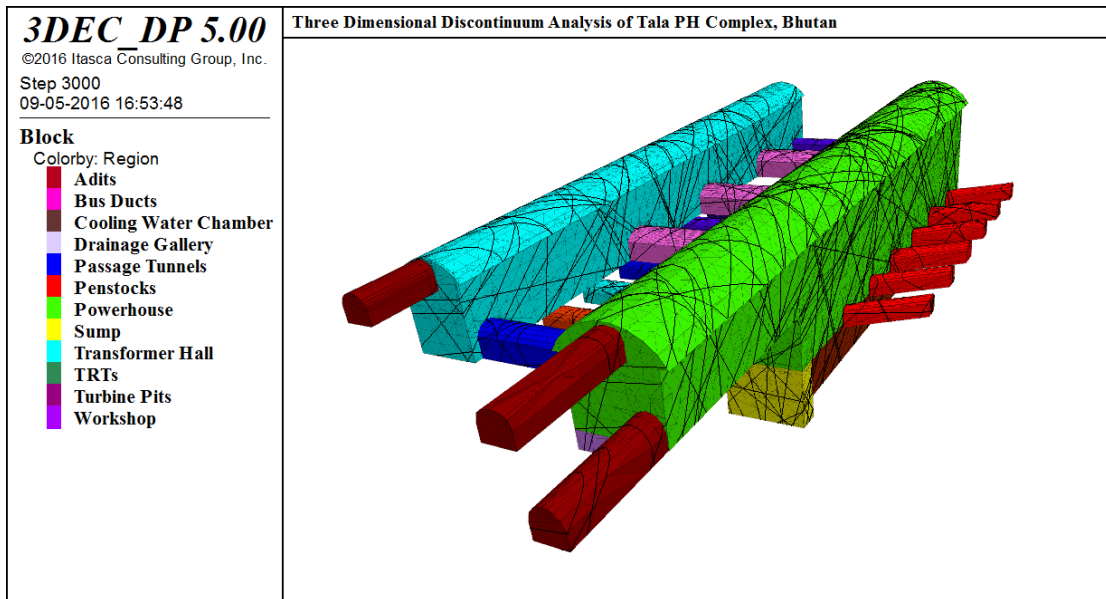


Fig. 3.27 Perspective view of powerhouse complex, Tala Hydroelectric Project

Rock mass properties for the model were estimated based on the procedure outlined by Hoek et al. (2002) and Hoek and Diederichs (2006), using the laboratory test data and the rock mass classification parameters. These rock mass parameters were further used in the 3D modelling. Estimated rock mass parameters with disturbance factor (D) of zero (undisturbed) and 0.8 (disturbed zone due to blasting) are listed in Table 3.3.

Table 3.3 Estimated rock mass parameters in powerhouse complex

Property	Depth: 500m				Unit
	Dry Condition		Saturated Condition		
	D=0	D=0.8	D=0	D=0.8	
Hoek – Brown Classification Parameters					
Uniaxial Compressive Strength (UCS)	63	63	51.9	51.9	MPa
GSI	50	50	50	50	
m_i	4.18	4.18	4.49	4.49	
E	18.35	18.35	12.93	12.93	GPa
m_b	0.701	0.213	0.753	0.229	
s	0.0039	0.0005	0.0039	0.0005	
a	0.506	0.506	0.506	0.506	
Mohr Coulomb Equivalent Parameters					
c	1.44	0.83	1.32	0.78	MPa
ϕ	30.71	21.82	29.90	21.07	degree

Rock Mass Parameters					
Rock Mass Tensile Strength	-0.35	-0.15	-0.27	-0.12	MPa
Rock Mass Strength, σ_{cm}	7.38	3.87	6.27	3.30	MPa
Elastic Modulus of Rock Mass E_{rm}	5682.94	1693.15	3971.91	1183.38	MPa
Poisson's Ratio	0.35	0.35	0.36	0.36	
Bulk Modulus, K	6314.38	1881.28	4728.46	1408.79	MPa
Shear Modulus, G	2104.79	627.09	1460.26	435.07	MPa
Density	2650	2650	2650	2650	kg/m ³

Geo-mechanical properties were assigned to major joints (fractures) in the 3DEC Model and properties assigned are listed in Table 3.4.

Table 3.4 Joint Properties in 3DEC Model

Property	Major Joints	Shear Joints
Joint Normal Stiffness	40 GPa/m	10 GPa/m
Joint Shear Stiffness	10 GPa/m	2 GPa/m
Joint Cohesion	0	0.003 MPa
Joint Friction angle	36	25
Joint Tensile Strength	0	0

Mohr Coulomb elasto-plastic model was used for simulation of excavation. Measured in-situ stresses were applied in the model and model was brought to equilibrium. Excavation in the model was done as per the actual excavation sequence followed during the excavation of the cavern. Supports were applied in the model after allowing initial deformation of 30% to occur (Hoek, 2001). Steel ribs in the crown were modelled with beam elements. Shotcrete was modelled as liner elements in 3DEC and rock bolts were modelled as reinforcing elements, which act at the intersection of joints. Properties of support elements used in the model are given in Tables 3.5 to 3.7.

Table 3.5 Rock Bolt Properties used in 3DEC (Local reinforcement *axial* command)

Property	8m long 32mm dia Bolt Fe500	12m long 32mm dia Dywidag Bolt	12m long 26.5mm dia Dywidag Bolt
Area of Bolt	8.04E-04 m ²	8.04E-04 m ²	5.51E-04 m ²
Axial Stiffness	5.33 GPa/m	5.54 GPa/m	3.67 GPa/m
½ Active Length	0.0349 m	0.0342 m	0.0317 m
Shear Stiffness	0.819 GPa/m	0.865 GPa/m	0.514
Ultimate Axial Capacity	0.362 MN	0.672 MN	0.568 MN
Ultimate Shear Capacity	0.184 MN	0.403 MN	0.341 MN

Table 3.6 Shotcrete Properties used in 3DEC (*liner* command)

Property	
Density	2400 kg/m ³
Elastic Modulus of shotcrete	21 GPa
Poisson's ratio of Shotcrete	0.2
Normal Stiffness between shotcrete and rock contact (kn)	1 GN/m
Shear Stiffness between liner and rock contact (ks)	1 GN/m
Cohesion limit for contact between rock and shotcrete	1 MPa
Friction coefficient for contact between shotcrete and rock	60 deg
Tensile limit for contact between shotcrete and rock	500 kN

Table 3.7 Steel Ribs Properties used in 3DEC (*beam* command)

Property	ISMB 350	ISMB 300
Area	66.71e-4 m ²	56.26e-4 m ²
Density	7650 kg/m ³	7650 kg/m ³
Young's Modulus	200 GPa	200 GPa
Bending inertia about local axis S1	13630.3e-8 m ⁴	8603.6e-8 m ⁴
Bending inertia about local axis S2	537.7e-8 m ⁴	453.9e-8 m ⁴
Poisson's ratio	0.3	0.3
Yield capacity in compression	1.06 MN	0.9 MN
Yield capacity in tension	1.66 MN	1.41 MN
Properties of contacts between Steel Ribs and Rock		
Cohesive shear strength	0	0
Friction angle	30 deg	30 deg
Normal Stiffness, kn	10000 MPa/m	10000 MPa/m
Shear Stiffness, ks	10000 MPa/m	10000 MPa/m
Tensile Strength	0	0

Model was again brought to equilibrium till the unbalanced forces in the model were reduced to 1E-3 of its initial value (Anon, 2010). This was followed by next excavation step and continued till all the benches and tunnels were excavated in the model. Excavation sequence followed in the model is shown in Fig. 3.28. Typical size of the model after the in-situ stresses was 1.27GB and final model size was 1.37GB. Model was run on HP Z840 Workstation (Intel Xeon CPU E5-2687W v3 @3.10GHz) running on Windows 10 with 64GB RAM. Each model run took 3 days and 8 hrs for completion.

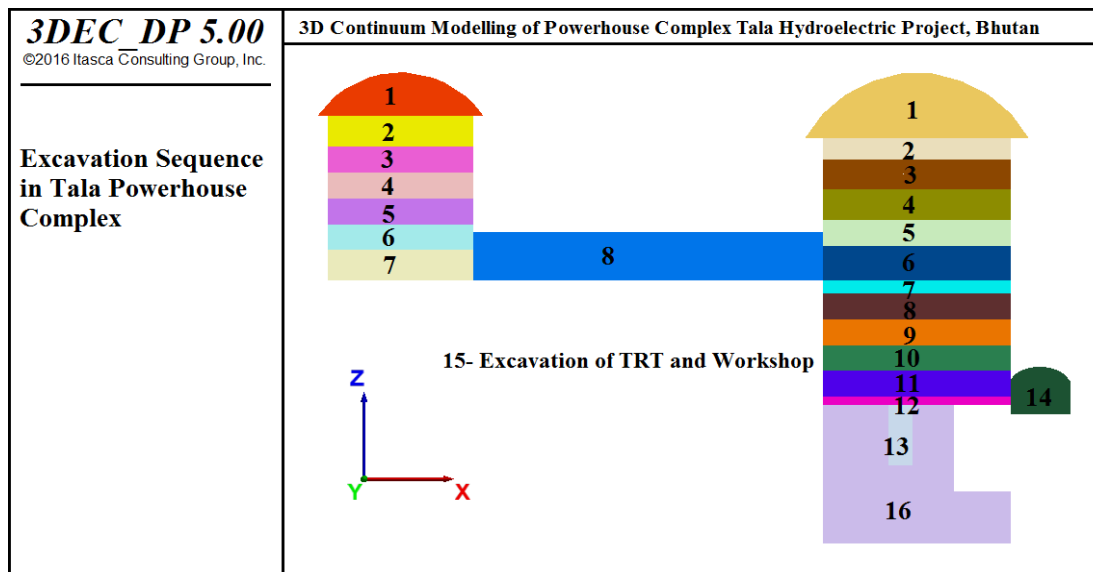


Fig. 3.28 Excavation sequence adopted in the 3D Model

Model assumptions

Following are the assumptions made in the modelling:

1. A constant depth cover of 500m was used.
2. Since in-situ stresses were determined on the assumption that vertical stress is one of the principal stresses, same assumption was followed in the model also.
3. GSI value of 50 was used and derived rock mass parameters for saturated conditions were used in the model.
4. Only major joints intersecting the powerhouse crown were explicitly modelled in 3DEC model.
5. Model was considered to be elasto-plastic with yielding of rock mass at failure.
6. Various stages of excavation were done as per the overall bench details. For example each bench is excavated at once.

7. Excavation was simultaneously done in powerhouse and transformer hall cavern.
8. Supports were installed after allowing 30% of deformation after the excavation in the model.
9. Compressive stresses are negative and tensile stresses are positive.
10. Equivalent stress of overburden load was applied on top of the model and bottom boundary was fixed and sides were given roller boundaries. Boundary conditions are shown in Fig. 3.29.

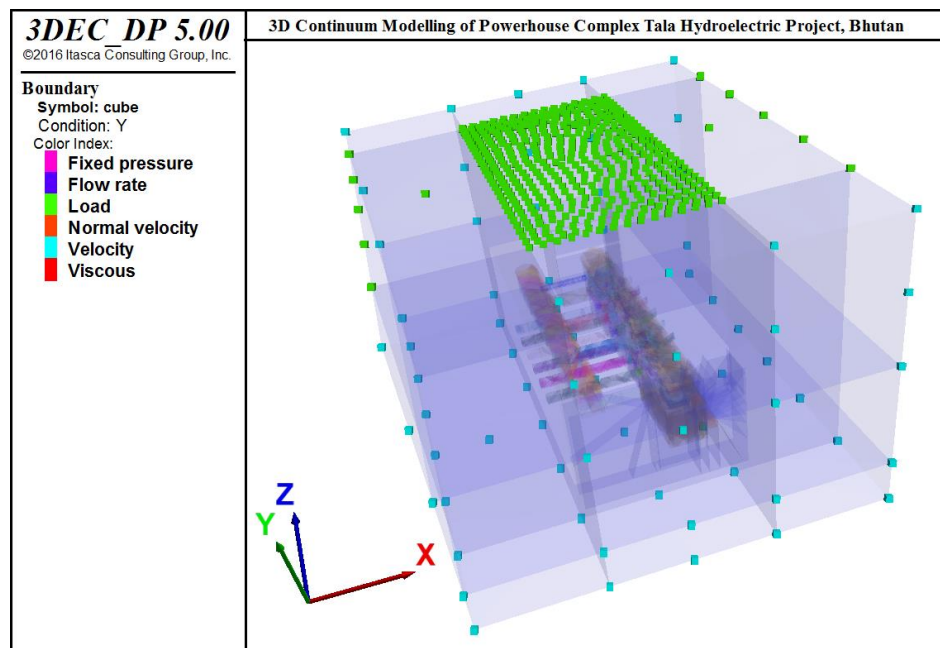


Fig. 3.29 Boundary conditions in the 3D model

Failure criteria for calculation of strength to stress ratio

The original Hoek and Brown yield criteria is an empirical criterion developed through curve-fitting of triaxial test data. However, the criterion was revised substantially based on the large scale field test on different types of rock mass. Currently, this criterion is the most widely used failure criterion for estimating the strength of jointed rock masses. In case of Himalayan region, it was observed that intermediate stresses also play an important role in influencing the stability of the underground structures. As Tala powerhouse is located in the active Himalayan tectonics, it was found necessary to consider all the three principal stresses in the analyses. Numerous extensions of modified Hoek and Brown yield criterion to 3D space have been proposed by various

researchers (Pan and Hudson, 1988; Priest and Hunt, 2005; Zhang and Zhu, 2007; Zhang, 2008; Melkounian et al., 2008). In this study, three dimensional Hoek and Brown yield criterion proposed by Melkounian et al. (2008) was used in the analysis of failure state of rock mass.

Output from the Model

3DEC has post processing terminal where all the results of the model can be accessed through an interactive terminal. Cross sections at any point can be taken in the model and the following output were available:

- Principal stress distribution (color scale)
- Normal stress contours in any plane (color scale)
- Shear stress contours in any plane (color scale)
- Stress tensor plot
- Displacement contours (Total, X-Displacement, Y-Displacement, Z-Displacement)
- Strain (color scale) (XX, YY, ZZ, XY and XZ strain)
- Displacement vector plot
- Joint normal stress, shear stress, normal displacement, shear displacement

3.2.2 3D Continuum Model using FLAC-3D

A 3D continuum model was constructed with the actual geometry of the powerhouse cavern, transformer hall cavern, cross tunnels (bus ducts and passages) and peripheral tunnels (penstock manifolds and tail race tunnel manifolds). Model sizes and boundary conditions were same as 3DEC model developed in this study. In the model, no discontinuities were modelled explicitly as the rock mass classification includes the influence of discontinuities and properties were estimated using laboratory and rock mass classification parameters. In the model, blasting zone of 2m was provided in the immediate vicinity of the excavation. Entire geometrical model was created in Rhinoceros-3D software (Anon, 2012) and model was taken to Kubrix software (Anon, 2014) for mesh generation. Mesh sizes were 1m in the blasting zone and increased gradually outwards keeping the ratio of adjacent edges of zone to less than 3. Mesh grid was imported to FLAC-3D and was available for run with all the excavation steps clearly identified as separate regions. A Typical model in FLAC-3D is shown in Fig.

3.30. Details of the caverns and tunnels modelled in FLAC-3D are shown in Figs. 3.31 and 3.32. In this case, same procedure of excavation and supporting was done as followed in the case of 3DEC model. The properties used for various support elements in FLAC-3D are listed in Tables 3.8 to 3.10

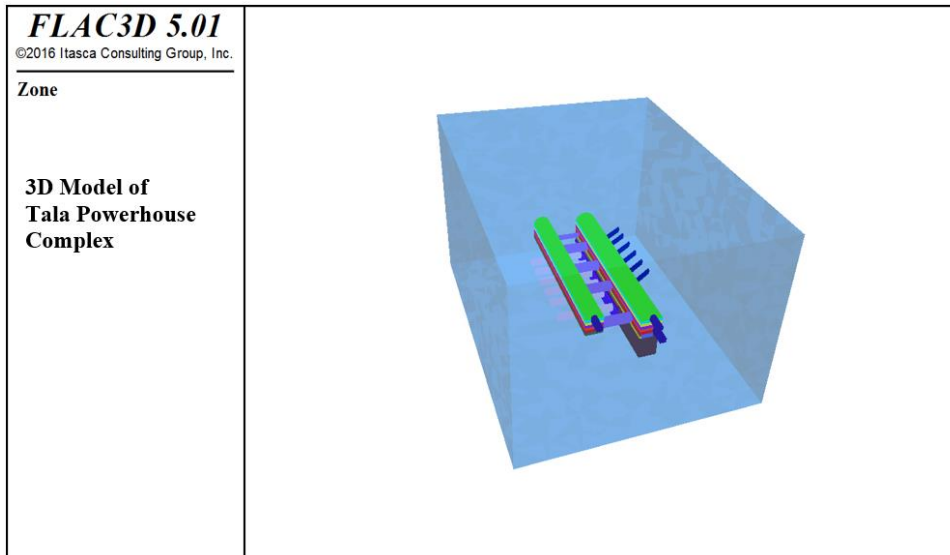


Fig. 3.30 3D continuum model of Tala powerhouse complex

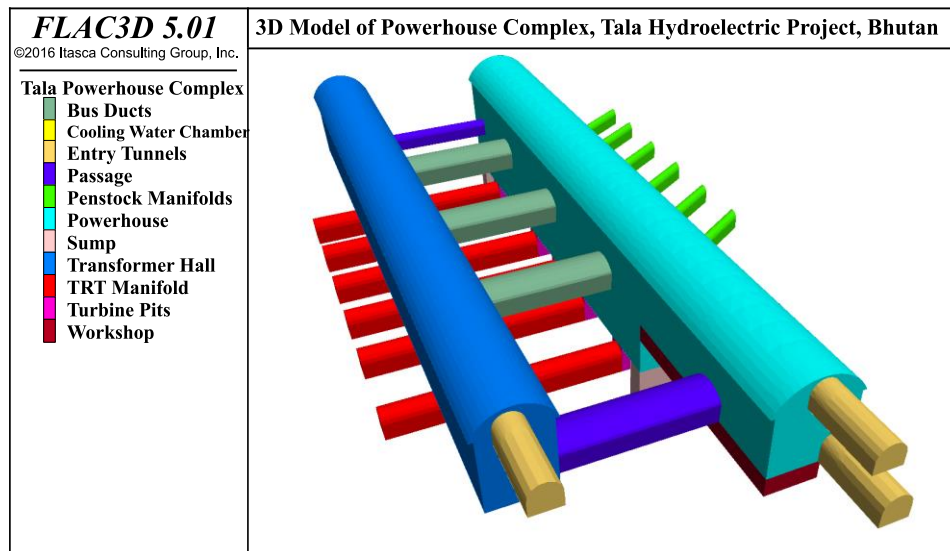


Fig. 3.31 Perspective view of powerhouse complex, Tala Hydroelectric Project (view-1)

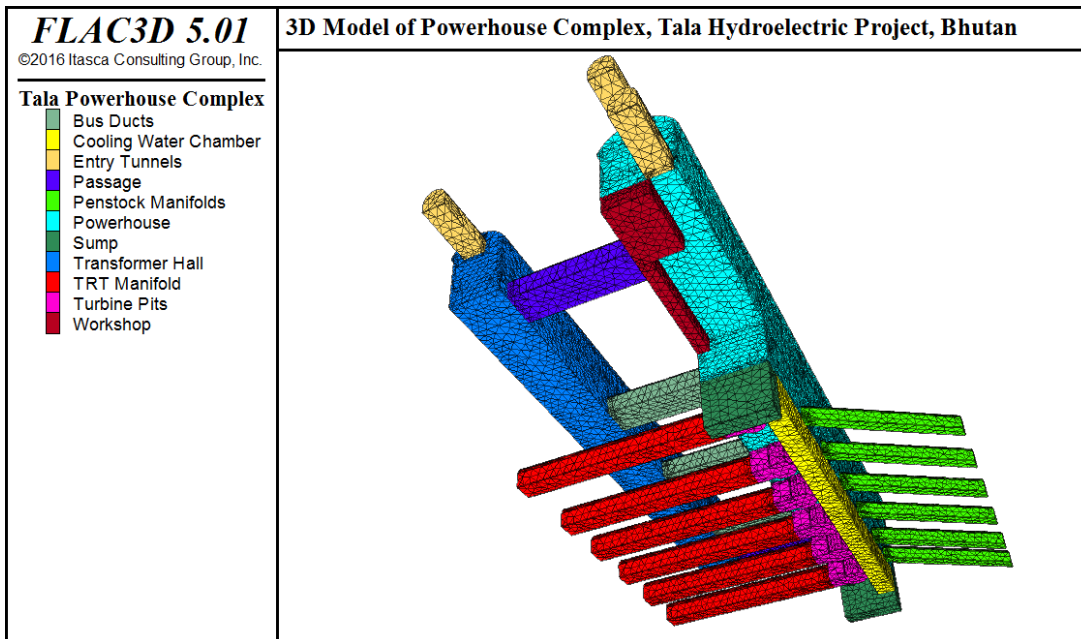


Fig. 3.32 Perspective view of powerhouse complex, Tala Hydroelectric Project (view-2)

Table 3.8 Rock Bolt Properties used in FLAC-3D (Cable elements)

	Fe500 Rock Bolts of 32mm dia 8m length	Dywidag Rock Bolts of 26.5mm dia 12m length
cross-sectional area	8.04E-04 m ²	5.51E-04 m ²
Density	7750 kg/m ³	7750 kg/m ³
Young's Modulus	200 GPa	200 GPa
grout cohesive strength	0.989 MPa	1.20 MPa
grout friction angle	20.05 deg	20.05 deg
grout stiffness	20.79 GPa	8.63 GPa
grout exposed perimeter	0.132 m	0.160 m
Tensile yield strength	0.402 MN	0.569 MN

Table 3.9 Shotcrete Properties used in FLAC-3D (Liner elements)

Density	2400 kg/m ³
Young's Modulus	21 GPa
Poisson's Ratio	0.15
Normal coupling spring tensile strength (cs-ncut)	20 MPa
Normal coupling spring stiffness (cs_nk)	5.5435E10 Pa/m
Shear coupling spring cohesion (cs_scoh)	2.5 MPa
Shear coupling spring friction angle (cs_sfrie)	40
Shear coupling spring stiffness per unit area (cs_sk)	5.54E10 Pa/m

Table 3.10 Steel Ribs Properties used in FLAC-3D (beam command)

Density	7855.8 kg/m ³
Young's modulus	200 GPa
Poisson's ratio	0.3
Cross-sectional area	0.0061833 m ²
Second moment with respect to beamSEL y-axis, I _y	1.29E-4 m ⁴
Second moment with respect to beamSEL z-axis, I _z	8.55E-6 m ⁴
Polar moment of inertia, J	1.38E-4 m ⁴

Mohr Coulomb elasto-plastic model was used for simulation of excavation. Measured in-situ stresses were applied in the model and model was brought to equilibrium. Excavation in the model was done as per the actual excavation sequence followed during the excavation of the cavern. Supports were applied in the model after allowing initial deformation of 30% to occur (Hoek, 2001). Steel ribs in the crown were modelled with beam elements, shotcrete was modelled as liner elements in FLAC-3D and rock bolts were modelled as cable elements. Model was again brought to equilibrium till the unbalanced forces in the model were reduced to 1E-3 of its initial value (Anon, 2010). This was followed by next excavation step and continued till all the benches and tunnels were excavated in the model.

In this case also, model at each stage of excavation was saved so that comparison between the excavation stages could be made or data pertaining to any individual excavation stage could be extracted during the analysis of model results.

Typical size of the model after imposing the in-situ stresses was 1.01GB and final model size was 1.28GB. Model was run on HP Z840 Workstation (Intel Xeon CPU E5-2687W v3 @3.10GHz) running on Windows 10 with 64GB RAM. Each model run took 14hrs.

Output from the model

FLAC-3D has post processing terminal where all the results of the model can be accessed through an interactive terminal. Cross sections at any point can be taken in the model and the following output were available:

- Principal stress distribution color scale
- Normal stress contours in any plane color scale
- Shear stress contours in any plane color scale
- Stress tensor plot
- Displacement contours (Total, X-Displacement, Y-Displacement, Z-Displacement)
- Strain color scale (XX, YY, ZZ, XY and XZ strain)
- Displacement vector plot
- Zone contour maps of principal stresses

Some of the typical outputs from the FLAC-3D model are presented in Figs. 3.33 to 3.38.

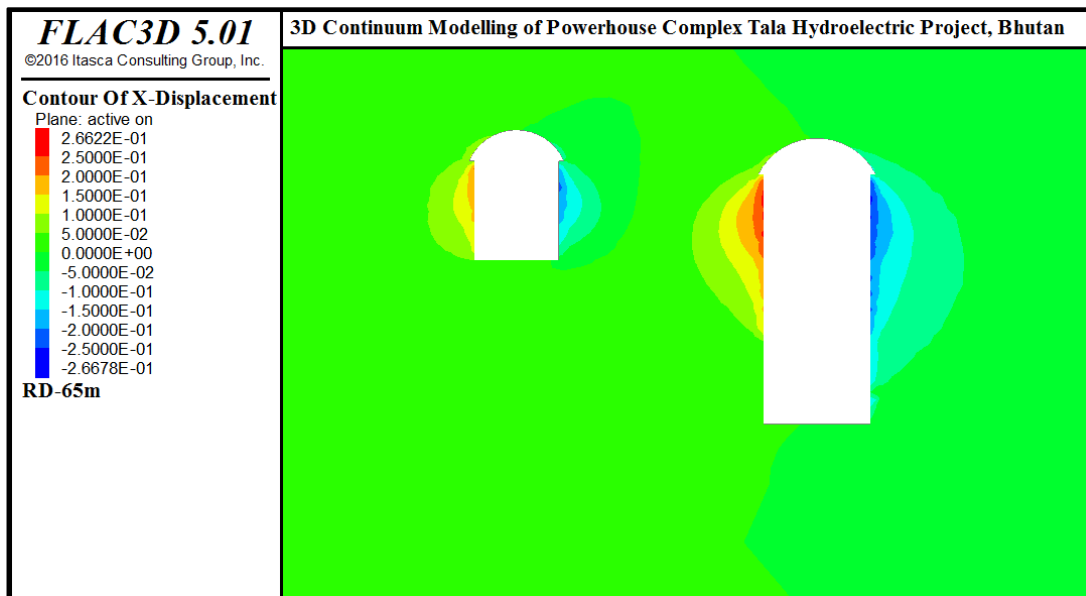


Fig. 3.33 Typical displacement contours after complete extraction of caverns and tunnels

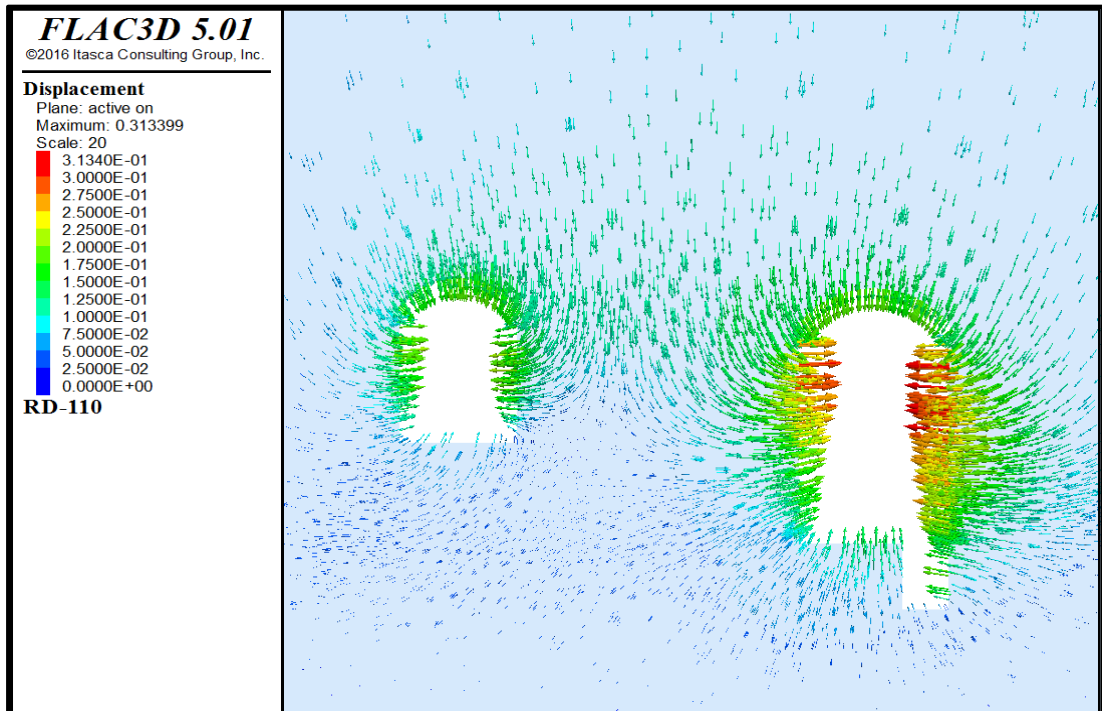


Fig. 3.34 Typical displacement vector after complete extraction of caverns and tunnels

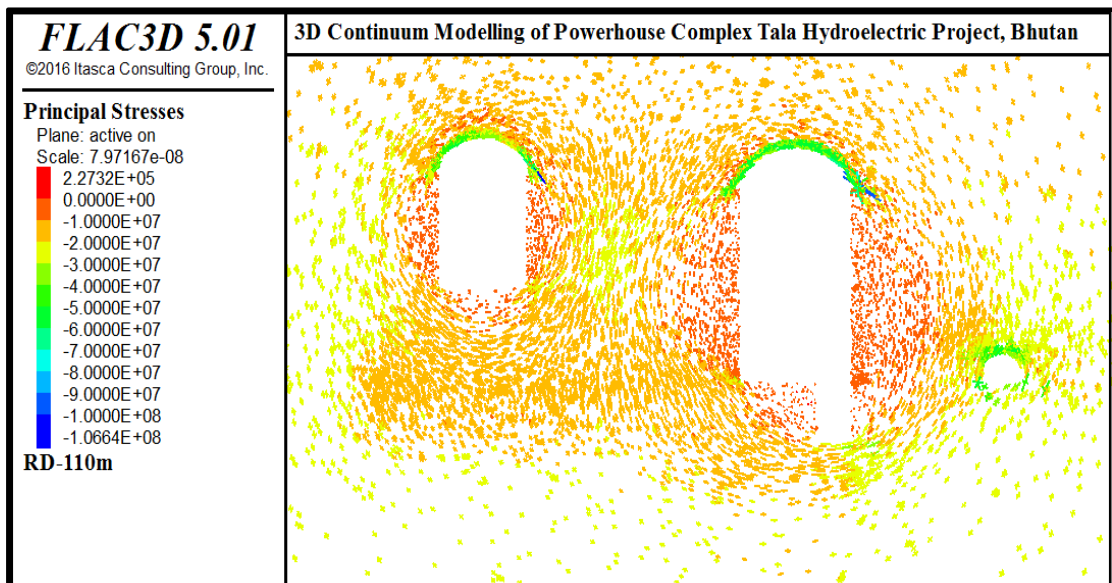


Fig 3.35 Typical stress tensor plot after complete extraction of caverns and tunnels

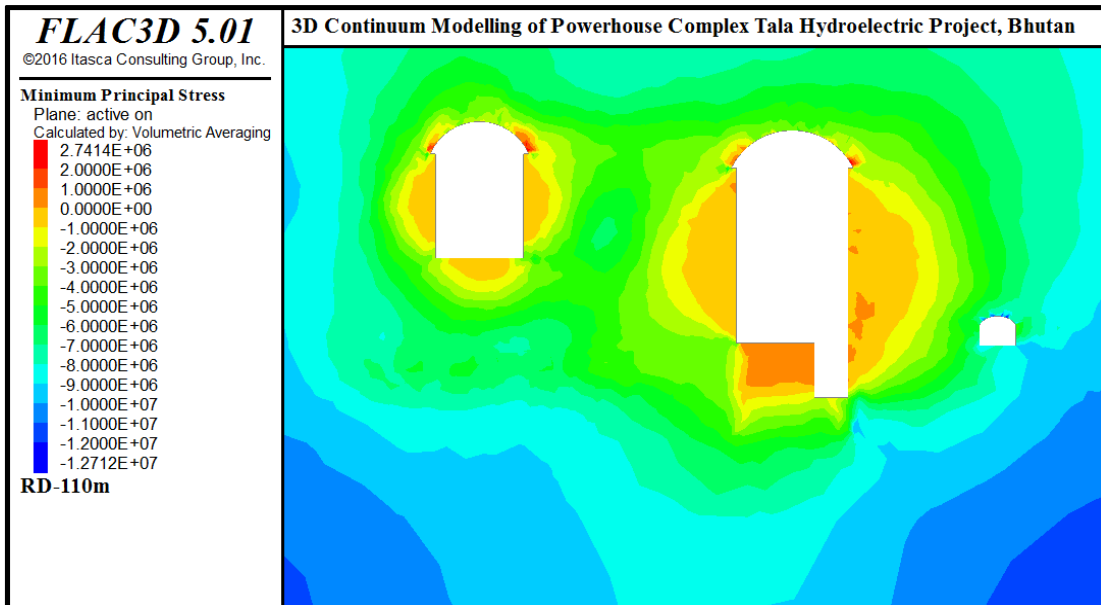


Fig 3.36 Typical minimum principal stress plot after complete extraction of caverns and tunnels

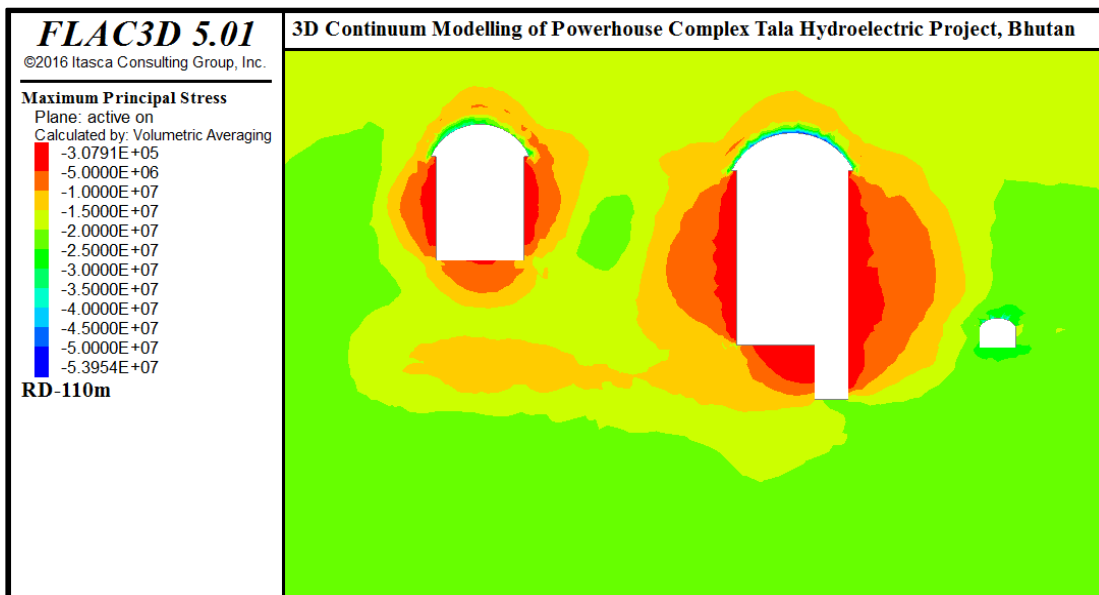


Fig. 3.37 Typical maximum principal stress plot after complete extraction of caverns and tunnels

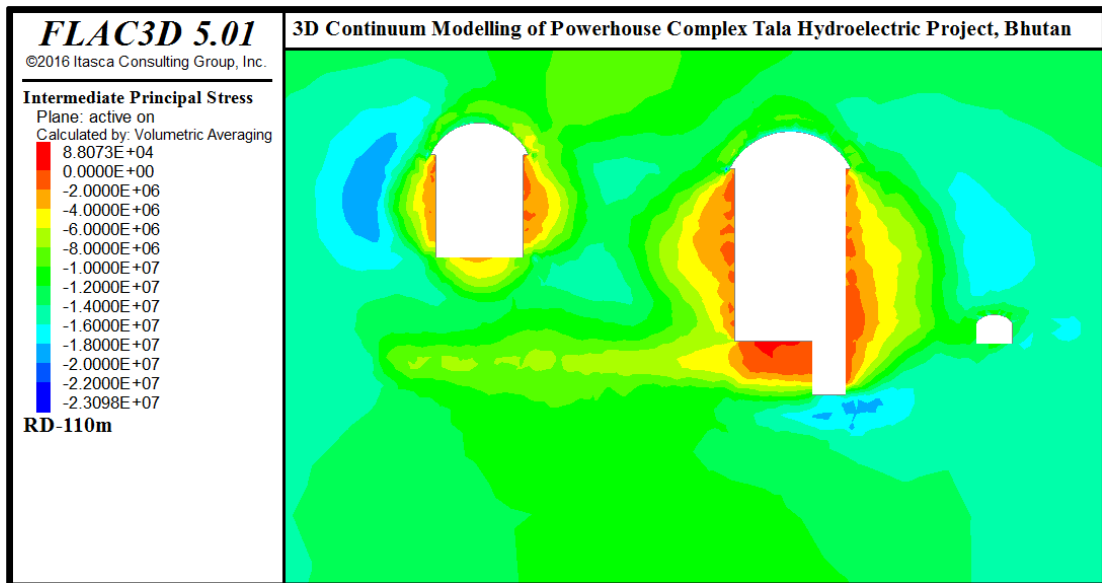


Fig. 3.38 Typical intermediate principal stress plot after complete extraction of caverns and tunnels

3.2.3 Basis of Analysis

Output from both 3DEC and FLAC-3D were available in the form of displacements (total displacement, and displacement in X, Y and Z direction) at each zone, all three principal stresses, normal stresses, shear stresses. In structural elements (bolts and shotcrete), normal and axial forces and stresses were also available. In addition, in 3DEC, normal and shear stresses in the joints, normal and shear displacements in the joints were also available. In this investigation since displacement and convergence data was mainly available, it was compared with the model results. All the output available from the model were of cumulative in nature and data pertaining to any excavation stage was extracted by the saved files of the model so that comparison could be made between successive excavation stages. Convergence stations at EL-525 were installed when the excavation of bench-4 was nearing completion. Therefore bench-4 displacements were taken as reference and cumulative convergence from the model at each stage was computed from data extracted at each excavation stage. Similarly, for EL-520 and EL-515, bench-6 and bench-7 results were taken as reference respectively. Principal stresses were used to estimate the strength of rock mass using 3D failure criteria and strength to stress ratio were plotted using FISH function in FLAC 3D. Strain in the walls of the cavern were also calculated using FISH function taking the displacement output from the model.

Stability of the caverns was assessed based on the comparison of displacement, strength to stress ratio and the strain distributions in the model coupled with physical observations in the caverns.

3.2.4 Parametric Study

Cavern orientation with respect to direction of major principal stress direction is one of the important parameters in cavern stability. Variation of stress distribution in the pillar between powerhouse and transformer hall and on the side abutments of cavern can influence the cavern behaviour and selection of appropriate supports. Parametric study was carried by varying the angle (Φ) between cavern axis and direction of major principal stress direction. Final FLAC-3D model, where there was close agreement with the measured data, was taken as the base model and alignment of the caverns were changed at an interval of 15° . Analysis was done for 12 orientations upto an angle of 165° as shown in Fig. 3.39.

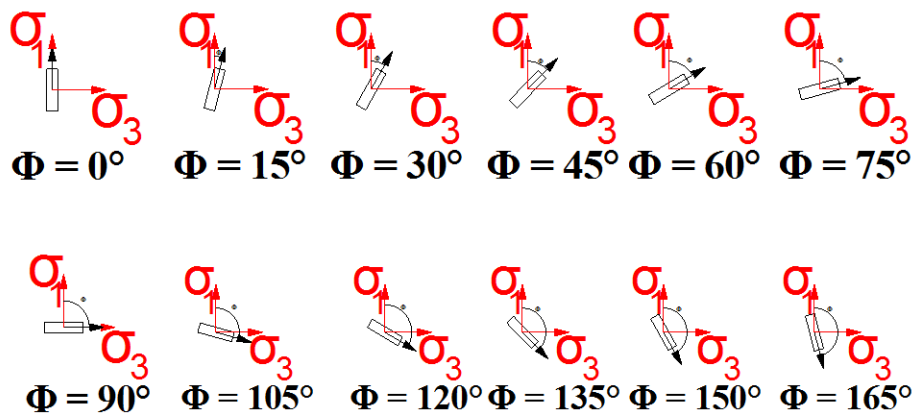


Fig. 3.39 Orientation of caverns with direction of maximum principal stress

In-situ stresses were resolved in the direction of new orientation and were applied in the model to simulate the effect of change in cavern orientation. Shear stresses were applied while investigating the effect of cavern orientation on cavern stability. Tables 3.11 to 3.17 give details of all the stresses (including the shear stresses). For orientations 15° and 105° the magnitudes of shear stress will be same but direction will be clock wise and anti-clock wise respectively. This is applicable to other directions also like 30° and 120° , 45° and 135° , 60° and 150° and 75° and 165° .

Table 3.11 Details of applied stresses for $\dot{\theta}=0$

Type of Stresses	Stresses (MPa)	Stress Values (MPa) (Compressive)			
		Constant	Gradient in X-Direction (MPa)	Gradient in Y-Direction (MPa)	Gradient in Z-Direction (MPa)
Insitu Stress Applied	Vertical Stress(σ_{zz})	25.68	0	0	0.026
	Horizontal Stress(σ_{yy})	41.10	0	0	0.041
	Horizontal Stress(σ_{xx})	22.35	0	0	0.022
	Shear Stress(σ_{xy})	0.00	0	0	0.000
Applied Stress at Top Boundary	Vertical Stress(σ_{zz})	8.78			
	Horizontal(σ_{yy})	14.45			
	Horizontal(σ_{xx})	8.05			
	Shear Stress(σ_{xy})	0.00			

Table 3.12 Details of applied stresses for $\dot{\theta} = 15^\circ$ and 105°

Type of Stresses	Stresses (MPa)	Stress Values (MPa) (Compressive)			
		Constant	Gradient in X-Direction (MPa)	Gradient in Y-Direction (MPa)	Gradient in Z-Direction (MPa)
Insitu Stress Applied	Vertical Stress(σ_{zz})	25.68	0	0	0.026
	Horizontal Stress(σ_{yy})	23.60	0	0	0.024
	Horizontal Stress(σ_{xx})	39.84	0	0	0.040
	Shear Stress(σ_{xy})	4.69	0	0	0.046
Applied Stress at Top Boundary	Vertical Stress(σ_{zz})	8.78			
	Horizontal(σ_{yy})	13.63			
	Horizontal(σ_{xx})	8.07			
	Shear Stress(σ_{xy})	1.60			

Table 3.13 Details of applied stresses for $\theta = 30^\circ$ and 120°

Type of Stresses	Stresses (MPa)	Stress Values (MPa) (Compressive)			
		Constant	Gradient in X-Direction (MPa)	Gradient in Y-Direction (MPa)	Gradient in Z-Direction (MPa)
Insitu Stress Applied	Vertical Stress(σ_{zz})	25.68	0	0	0.026
	Horizontal Stress(σ_{yy})	27.03	0	0	0.027
	Horizontal Stress(σ_{xx})	36.41	0	0	0.038
	Shear Stress(σ_{xy})	8.12	0	0	0.008
Applied Stress at Top Boundary	Vertical Stress(σ_{zz})	8.78			
	Horizontal(σ_{yy})	12.45			
	Horizontal(σ_{xx})	9.24			
	Shear Stress(σ_{xy})	2.78			

Table 3.14 Details of applied stresses for $\theta = 45^\circ$ and 135°

Type of Stresses	Stresses (MPa)	Stress Values (MPa) (Compressive)			
		Constant	Gradient in X-Direction (MPa)	Gradient in Y-Direction (MPa)	Gradient in Z-Direction (MPa)
Insitu Stress Applied	Vertical Stress(σ_{zz})	25.68	0	0	0.026
	Horizontal Stress(σ_{yy})	31.72	0	0	0.032
	Horizontal Stress(σ_{xx})	31.72	0	0	0.032
	Shear Stress(σ_{xy})	9.38	0	0	0.010
Applied Stress at Top Boundary	Vertical Stress(σ_{zz})	8.78			
	Horizontal(σ_{yy})	10.85			
	Horizontal(σ_{xx})	10.85			
	Shear Stress(σ_{xy})	3.21			

Table 3.15 Details of applied stresses for $\theta = 60^\circ$ and 150°

Type of Stresses	Stresses (MPa)	Stress Values (MPa) (Compressive)			
		Constant	Gradient in X-Direction (MPa)	Gradient in Y-Direction (MPa)	Gradient in Z-Direction (MPa)
Insitu Stress Applied	Vertical Stress(σ_{zz})	25.68	0	0	0.026
	Horizontal Stress(σ_{yy})	27.03	0	0	0.027
	Horizontal Stress(σ_{xx})	36.41	0	0	0.037
	Shear Stress(σ_{xy})	8.12	0	0	0.008
Applied Stress at Top Boundary	Vertical Stress(σ_{zz})	8.78			
	Horizontal(σ_{yy})	9.24			
	Horizontal(σ_{xx})	12.45			
	Shear Stress(σ_{xy})	2.78			

Table 3.16 Details of applied stresses for $\theta = 75^\circ$ and 165°

Type of Stresses	Stresses (MPa)	Stress Values (MPa) (Compressive)			
		Constant	Gradient in X-Direction (MPa)	Gradient in Y-Direction (MPa)	Gradient in Z-Direction (MPa)
Insitu Stress Applied	Vertical Stress(σ_{zz})	25.68	0	0	0.026
	Horizontal Stress(σ_{yy})	23.60	0	0	0.024
	Horizontal Stress(σ_{xx})	39.84	0	0	0.040
	Shear Stress(σ_{xy})	4.7	0	0	0.005
Applied Stress at Top Boundary	Vertical Stress(σ_{zz})	8.78			
	Horizontal(σ_{yy})	8.07			
	Horizontal(σ_{xx})	13.63			
	Shear Stress(σ_{xy})	1.60			

Table 3.17 Details of applied stresses for $\theta = 90^\circ$

Type of Stresses	Stresses (MPa)	Stress Values (MPa) (Compressive)			
		Constant	Gradient in X-Direction (MPa)	Gradient in Y-Direction (MPa)	Gradient in Z-Direction (MPa)
Insitu Stress Applied	Vertical Stress(σ_{zz})	25.68	0	0	0.026
	Horizontal Stress(σ_{yy})	22.35	0	0	0.022
	Horizontal Stress(σ_{xx})	41.10	0	0	0.041
	Shear Stress(σ_{xy})	0.00	0	0	0.000
Applied Stress at Top Boundary	Vertical Stress(σ_{zz})	8.78			
	Horizontal(σ_{yy})	8.05			
	Horizontal(σ_{xx})	14.45			
	Shear Stress(σ_{xy})	0.00			

A database program was created in Microsoft Access-2013 and output from each model were extracted and taken into the database for further data extraction and analysis.

3.2.5 Sensitivity Analysis

Sensitivity analysis is defined as the study of how uncertainty in the output (dependent variable) of a model can be attributed to different sources of uncertainty in the model input (independent variable). It is a technique used to determine how different values of an independent variable impact a particular dependent variable under a given set of assumptions. This technique is used within specific boundaries that depend on one or more independent variables. In this study, local sensitivity analysis approach is used. Local sensitivity analysis is a one-at-a-time (OAT) technique. OAT techniques analyze the effect of one parameter on the final output at a time, keeping the other parameters fixed.

Sensitivity of the developed 3D model to changes in cohesion, friction angle, elastic and Poisson's ratio were tested by changing each parameter value in the range of -20% to 20% at a step of 5%. Sensitivity of the model was analysed using tornado diagrams.

RESULTS AND DISCUSSION

The results from field investigations and numerical modelling are analysed and presented in this chapter.

4.1 POWERHOUSE CAVERN

4.1.1 Movement at the Center of Crown

The movement of rock mass at different horizons above crown was monitored by Multiple Ring Magnetic Point Borehole Extensometers (MRMPBX). Cumulative data of MRMPBX observations at RD-15 center of the crown are shown in Fig. 4.1. The displacements noted at surface, 0.7m, 1.5m, 2.2m, 3m, 4.3m, 5.1m, 6m, 8m, 8.7m, 9.5m, 11.5m, 14.2m, 14.7m, 18m, 20m and 25.5m depths above crown are listed in Table 4.1 and depicted in Fig. 4.1. Displacements at various anchors within first 27 days were 3mm. During this period, side slashing at this location had not started. When the side slashing started at this location, the surface displacement increased to 20mm. A displacement of 8mm was observed at 0.7m depth, 2mm at 1.5m depth, clearly indicating separation of SFRS layer from the roof. After a period of 107 days, joint separation at the bolted horizon (8m) started, which further extended upto a depth of 9.5m. At this point, minor cracks started appearing on the surface of the crown. With further side slashing and with time, separation of joints at other horizons also started, as indicated by displacement recordings shown in Fig. 4.1.

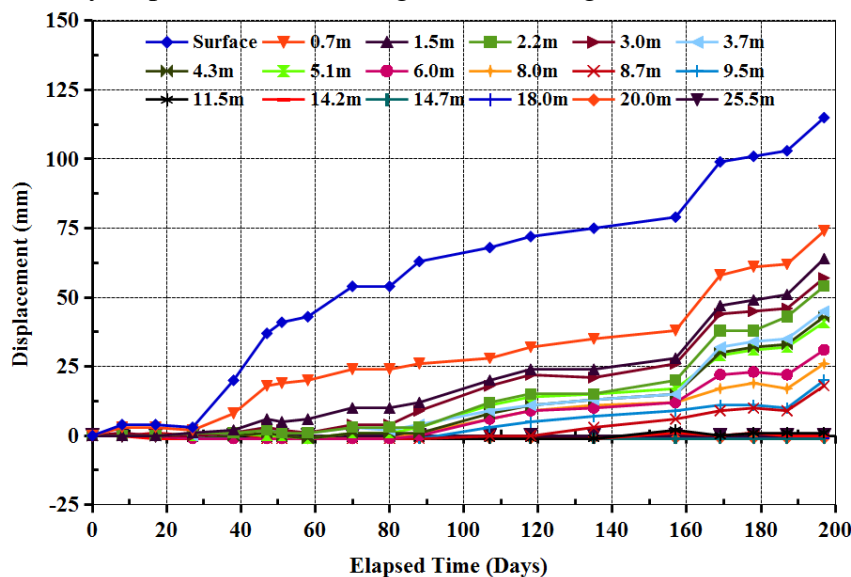


Fig. 4.1 Displacement at the center of crown of powerhouse cavern at RD-15

Table 4.1 MRMPBX readings at RD-15 center of crown

Elapsed Time (Days)	Anchor Depth (m)																	
	Surface	0.7	1.5	2.2	3.0	3.7	4.3	5.1	6.0	8.0	8.7	9.5	11.5	14.2	14.7	18.0	20.0	25.5
	Displacement (mm)																	
0	0	0	0	0	0	0	0	0	0	0	0	0	0	0	0	0	0	0
8	4	3	0	0	1	0	0	0	0	0	0	0	0	0	0	0	0	0
17	4	3	0	0	0	0	0	0	0	0	1	0	0	-1	0	0	0	0
27	3	2	1	1	0	0	0	0	-1	1	0	0	-1	-1	-1	-1	-1	0
38	20	8	2	1	1	1	0	1	-1	1	1	-1	0	-1	-1	0	-1	0
47	37	18	6	2	3	3	1	0	-1	0	-1	-1	-1	-1	-1	-1	-1	0
51	41	19	5	1	2	1	0	0	-1	-1	-1	-1	-1	-1	-1	-1	-1	0
58	43	20	6	1	1	1	-1	-1	-1	-1	-1	-1	-1	-1	-1	-1	-1	0
70	54	24	10	3	4	3	1	1	-1	-1	-1	-1	-1	-1	-1	-1	-1	0
80	54	24	10	3	4	2	1	1	-1	-1	-1	-1	-1	-1	-1	-1	-1	0
88	63	26	12	3	9	4	1	3	0	1	-1	-1	-1	-1	-1	-1	-1	0
107	68	28	20	12	18	9	8	11	6	6	0	3	-1	-1	-1	-1	-1	0
118	72	32	24	15	22	11	11	14	9	9	0	5	-1	-1	-1	-1	-1	0
135	75	35	24	15	21	13	13	15	10	11	3	7	-1	-1	-1	-1	-1	0
157	79	38	28	20	26	15	15	17	12	12	6	9	2	1	-1	-1	-1	0
169	99	58	47	38	44	32	30	29	22	17	9	11	0	0	-1	-1	-1	0
178	101	61	49	38	45	34	32	31	23	19	10	11	1	1	-1	-1	-1	0
187	103	62	51	43	46	35	33	32	22	17	9	10	1	0	-1	-1	-1	0
197	115	74	64	54	57	45	43	41	31	26	18	20	1	0	-1	-1	-1	0
	Joint Separation (mm)																	
		41	10	10	-3	12	2	2	10	5	8	-2	19	1	1	0	0	-1

After a period of 197 days, surface displacement recorded was 115mm with 20-74mm displacements recorded between 0.7m and 9.5m horizons, indicating development of cracks in the range of 2-41mm. MRMPBX observations beyond 11.5m upto a depth of 25m showed that there was no movement beyond 11.5m.

MRMPBX observations at RD-80 center of crown for different depths are shown in Fig. 4.2 and the displacement recordings are given in Table 4.2. During initial 27 days, where there was no side slashing done, surface displacement was 3-4mm and this was recorded at 0.7m depth also indicating that the SFRS had just begun to separate from the roof and there was no movement beyond that. Once the side slashing of the crown started at this location, the surface displacement (6-52mm) and displacement at 0.7m depth (5-47mm) increased. Also separation at other deeper horizons was observed with further side slashing. In this case also, joints were found separating beyond the bolted horizon of 8m. MRMPBX recordings indicated that there was no movement beyond 9.5m depth. Monitoring done for 197 days showed displacement of 52mm at surface, 47mm at 0.7m depth, and displacements in the range of 2-31mm at other deeper points. Magnitude of joint separation varied from 1-16mm at various horizons. After installation of the steel ribs in the crown, MRMPBX was extended below the ribs. Further monitoring of MRMPBX did not indicate any increase in displacement in crown.

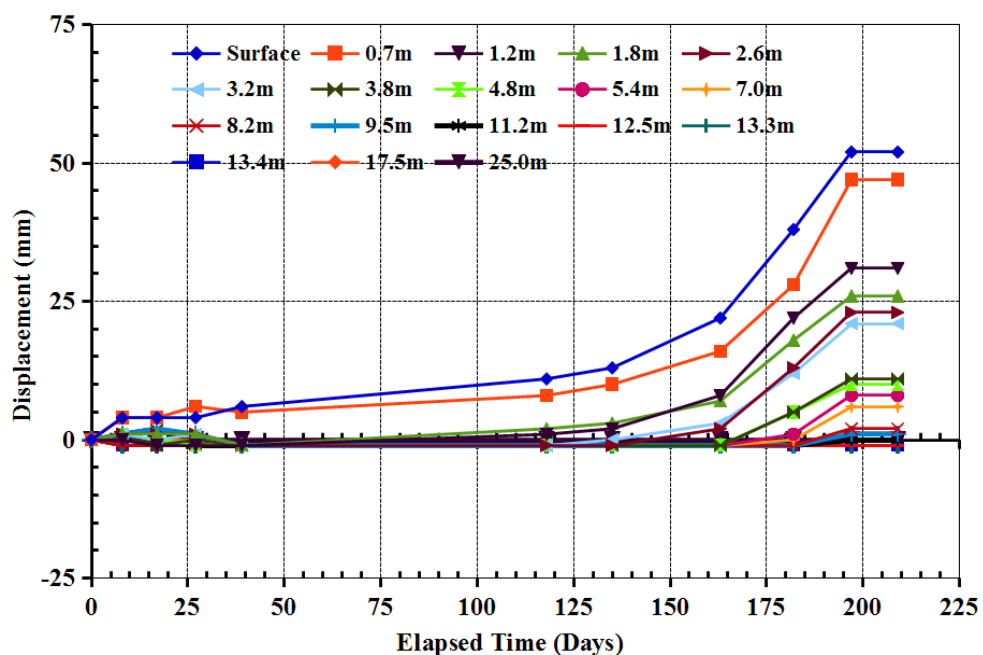


Fig. 4.2 Displacement at the center of crown of powerhouse cavern at RD-80

Table 4.2 MRMPBX readings at RD-80 center of crown

Elapsed Time (Days)	Anchor Depth (m)																	
	Surface	0.7	1.2	1.8	2.6	3.2	3.8	4.8	5.4	7.0	8.2	9.5	11.2	12.5	13.3	13.4	17.5	25.0
	Displacement (mm)																	
0	0	0	0	0	0	0	0	0	0	0	0	0	0	0	0	0	0	0
8	3	3	0	1	1	1	1	1	1	1	-1	1	1	-1	-1	-1	-1	0
17	4	4	-1	1	1	0	-1	0	-1	0	-1	1	1	-1	-1	-1	-1	0
27	4	4	-1	1	1	1	0	-1	-1	0	-1	1	-1	-1	-1	-1	-1	0
39	6	5	-1	-1	-1	-1	-1	-1	-1	-1	-1	-1	-1	-1	-1	-1	-1	0
118	11	8	1	2	-1	-1	-1	-1	-1	-1	-1	-1	-1	-1	-1	-1	-1	0
135	13	10	2	3	-1	0	-1	-1	-1	-1	-1	-1	-1	-1	-1	-1	-1	0
163	22	16	8	7	2	3	-1	-1	-1	-1	-1	-1	-1	-1	-1	-1	-1	0
182	38	28	22	18	13	12	5	5	1	0	-1	-1	-1	-1	-1	-1	-1	0
197	52	47	31	26	23	21	11	10	8	6	2	1	0	-1	-1	-1	-1	0
209	52	47	31	26	23	21	11	10	8	6	2	1	0	-1	-1	-1	-1	0
	Joint Separation (mm)																	
		5	16	5	3	2	10	1	2	2	4	1	1	1	0	0	0	-1

MRMPBX observations at center of crown at RD-130 are shown in Fig. 4.3 and the displacement recordings are given in Table 4.3.

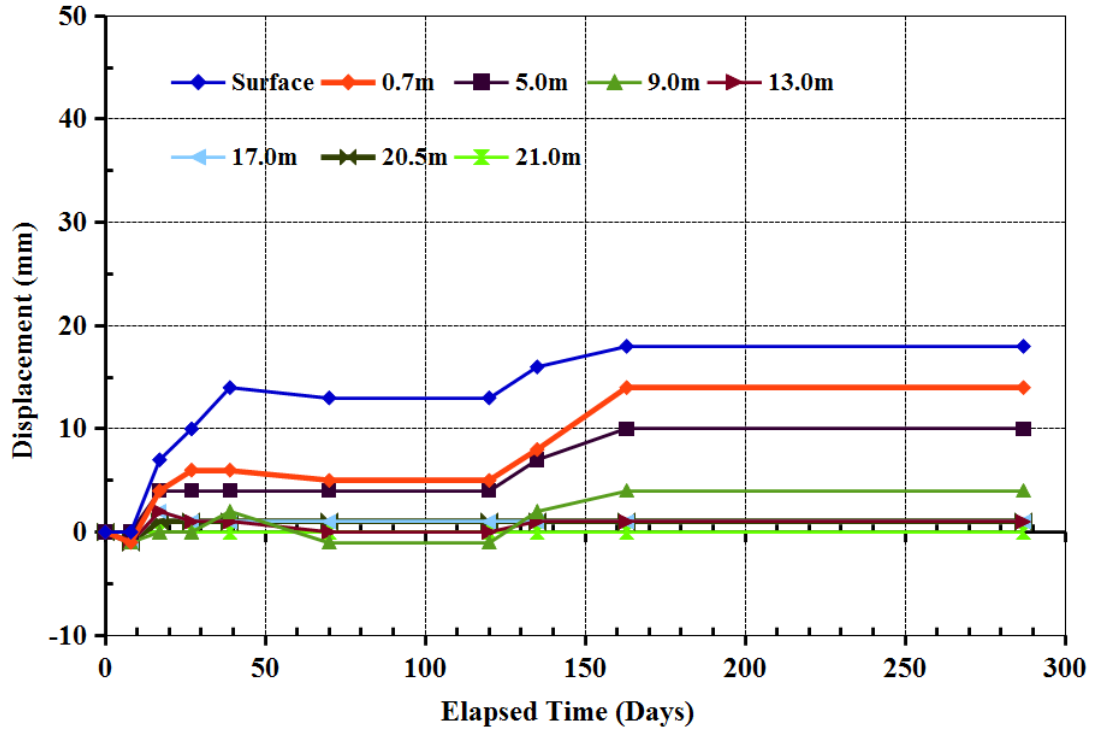


Fig. 4.3 Displacement at the center of crown of powerhouse cavern at RD-130

Table 4.3 MRMPBX readings at RD-130 center of crown

Elapsed Time (Days)	Anchor Depth (m)							
	Surface	0.7	5.0	9.0	13.0	17.0	20.5	21.0
	Displacement (mm)							
0	0	0	0	0	0	0	0	0
8	0	-1	0	-1	-1	-1	-1	0
17	7	4	4	0	2	2	1	0
27	10	6	4	0	1	1	1	0
39	14	6	4	2	1	1	1	0
70	13	5	4	-1	0	1	1	0
120	13	5	4	-1	0	1	1	0
135	16	8	7	2	1	1	1	0
163	18	14	10	4	1	1	1	0
287	18	14	10	4	1	1	1	0
	Joint separation (mm)							
		4	4	6	3	0	0	0

During initial 8 days there was no displacements at this location. With the starting of the side slashing at this location, surface displacement of 7mm was noted after 17 days and 4mm displacement at 0.7m and 5m depths. Monitoring done for 163 days before the installation of the ribs in the crown recorded 18mm of surface displacement, 10mm at 0.7m depth and 14mm at 5m depth. Displacements were observed upto 9m depth. Joint separation of 3 to 10mm was observed at various depths. MRMPBX recordings did not show any significant movement beyond 9m depth. After installation of the steel ribs in the crown, MRMPBX was extended below the ribs. Further monitoring of MRMPBX did not indicate any increase in the displacement of the crown (Fig. 4.3).

MRMPBX observations at center of crown at RD-150 are shown in Fig. 4.4 and the displacement recordings are given in Table 4.4. Installation of MRMPBX at this location was delayed due to site constraints and by the time the MRMPBX was installed, side slashing at this location was over. This MRMPBX was monitored for 163 days and surface displacement of 7mm was recorded. At 0.7m depth, 2mm displacement was recorded and beyond 0.7m, the displacements were negligible. After installation of the steel ribs in the crown, this MRMPBX could not be extended below the ribs and could not be monitored further (Fig. 4.4).

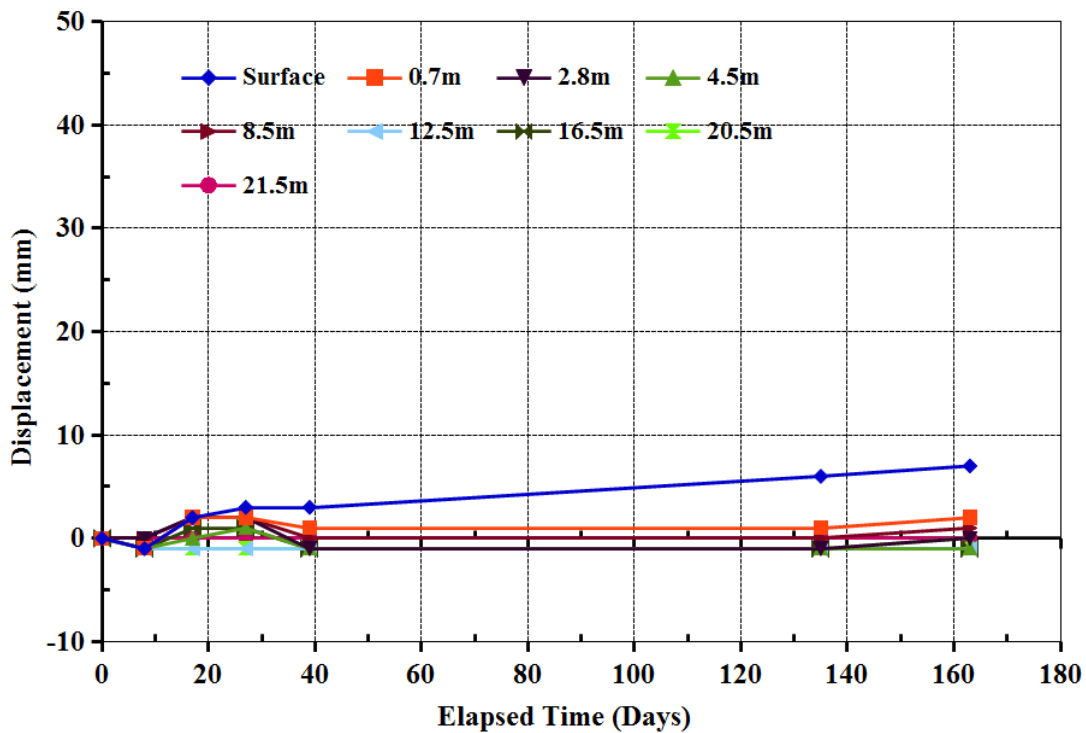


Fig. 4.4 Displacement at the center of crown of powerhouse cavern at RD-150

Table 4.4 MRMPBX readings at RD-150 center of crown

Elapsed Time (Days)	Anchor Depth (m)								
	Surface	0.7	2.8	4.5	8.5	12.5	16.5	20.5	21.5
	Displacement (mm)								
0	0	0	0	0	0	0	0	0	0
8	-1	-1	0	-1	0	-1	-1	-1	0
17	2	2	2	0	2	-1	1	-1	0
27	3	2	2	1	2	-1	1	-1	0
39	3	1	-1	-1	0	-1	-1	-1	0
135	6	1	-1	-1	0	-1	-1	-1	0
163	7	2	0	-1	1	-1	-1	0	0
	Joint Separation (mm)								
		5	2	1	-2	2	0	-1	0

MRMPBX observations at the center of the crown clearly indicated that, side slashing accounted for 71-88% of total displacement (when central gullet of 7m wide is side slashed on one side, span increased to 13.7m, and side slashing on the other side increased the span to 20.4m). In most cases, 80-100% of total joint separation took place within 10m into the crown. Joint separation within bolted horizon of 8m varied from 68-100% of total separation. Within 0.7m depth, joint separation varied from 9.6-71.4% of total separation. This clearly indicated detachment of SFRS from the roof. Bolt length of 8m was not sufficient when the side slashing of the crown was done. Displacements above the bolted horizon as a result of separation of joint was making the bolting action ineffective when the span was increasing as a result of side slashing.

4.1.2 Movement in the Widened part of Crown

After side slashing of the crown and supporting it with SFRS and rock bolts, four more extensometers were installed in the widened portion of the crown at RD-15DCR (downstream side), RD-15UCR (upstream side), RD-80UCR and RD-130UCR.

MRMPBX (installed after side slashing) observations at RD-15DCR are given in Table 4.5 and values are depicted in Fig. 4.5. In this case, displacement of 12mm was observed at a depth of 22.5m indicating that joint separation was taking place at deeper points as well. As MRMPBX at the center of crown at RD-15 indicated initiation of joint separation with side slashing, observation from this instrument further

corroborated that joint separation was extending to the side of the crown also. Rate of movement in the initial 40 days varied from 0.27-1.0mm per day (evident from steep portion of graph). Rock bolts in this case failed to arrest the movement, as joint separation in the roof had already started with side slashing. This instrument was extended below steel ribs. After supporting with the steel ribs, there was no further displacement (Fig. 4.5).

Table 4.5 MRMPBX readings at RD-15 left side of crown

Elapsed Time (Days)	Anchor Depth (m)							
	Surface	0.5	4.5	8.5	12.5	16.5	22.5	24.0
	Displacement (mm)							
0	0	0	0	0	0	0	0	0
7	7	7	8	7	7	5	5	0
29	13	12	12	12	12	10	9	0
41	24	23	16	14	11	11	10	0
54	25	25	17	14	13	12	11	0
69	30	30	21	18	13	13	12	0
76	30	30	21	18	13	13	12	0
141	31	30	21	18	13	13	12	0
178	31	30	21	18	13	13	12	0
	Joint Separation (mm)							
		1	9	3	5	0	1	12

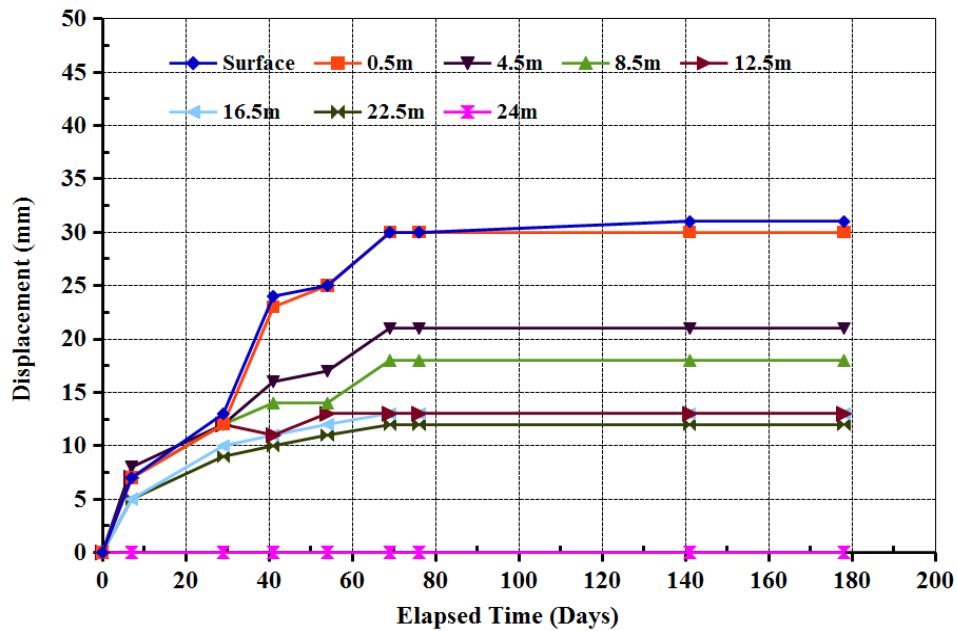


Fig. 4.5 Displacement at the downstream side of crown of powerhouse cavern at RD-15

MRMPBX (installed after side slashing) observations at RD-15UCR are shown in Fig. 4.6. Displacement recordings are given in Table 4.6. This instrument was monitored for 28 days. Surface displacement of 53mm was recorded. Also, displacement of 10mm was noticed at a depth of 16.5m, which confirmed that joint separation was taking place at deeper horizons.

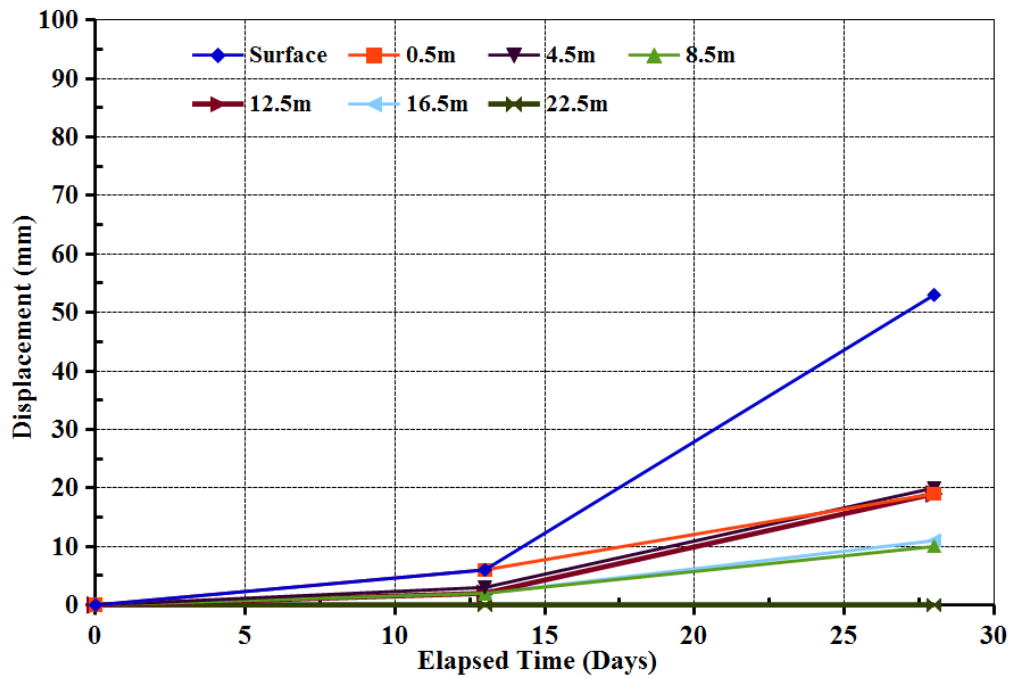


Fig. 4.6 Displacement at the upstream side of crown of powerhouse cavern at RD-15

Table 4.6 MRMPBX readings at RD-15 right side of crown

Elapsed Time (Days)	Anchor Depth (m)						
	Surface	0.5	4.5	8.5	12.5	16.5	22.5
	Displacement (mm)						
0	0	0	0	0	0	0	0
13	6	6	3	2	2	2	0
28	53	19	20	10	19	11	0
	Joint Separation (mm)						
		34	-1	10	-9	8	11

MRMPBX (installed after side slashing) observations at RD-80UCR are shown in Fig. 4.7 and displacement recordings are given in Table 4.7. There was no joint movement for initial 27 days after installation of the instrument. After a period of 139 days, there was 97mm of surface displacement. Joint separation was observed upto 6.2m depth into the crown. Joint separation was varying from 1 to 56mm. Recordings at this instrument showed that in some cases, the time period for starting of the separation of the joints is more, and over a period of time, separation starts and moves up in the crown of the powerhouse.

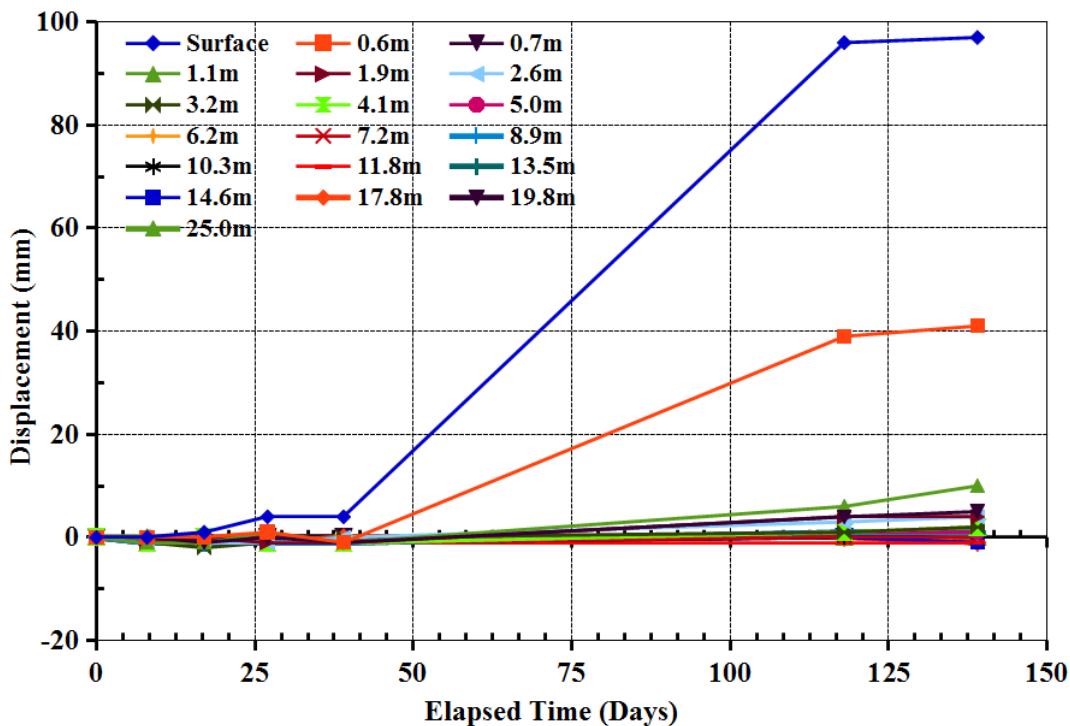


Fig. 4.7 Displacement at the upstream side of crown of powerhouse cavern at RD-80

MRMPBX (installed after side slashing) observations at RD-130UCR are shown in Fig. 4.8 and displacement recordings are given in Table 4.8. In this case also, joint separation was taking place upto a height of 7m into the crown. Surface displacement of 18mm and joint separation upto 9mm was recorded from this instrument.

Table 4.7 MRMPBX readings at RD-80 right side of crown

Elapsed Time (Days)	Anchor Depth (m)																			
	Surface	0.6	0.7	1.1	1.9	2.6	3.2	4.1	5.0	6.2	7.2	8.9	10.3	11.8	13.5	14.6	17.8	19.8	25.0	
	Displacement (mm)																			
0	0	0	0	0	0	0	0	0	0	0	0	0	0	0	0	0	0	0	0	
8	0	0	0	-1	-1	-1	-1	-1	-1	-1	-1	-1	-1	-1	-1	-1	-1	-1	-1	0
17	1	0	-1	-1	0	-1	-2	0	-1	0	-1	-1	-1	0	-1	0	-1	-1	-1	0
27	4	1	0	1	-1	-1	-1	-1	0	-1	0	-1	0	0	-1	-1	-1	-1	0	0
39	4	-1	-1	-1	-1	0	0	-1	-1	-1	-1	-1	-1	-1	-1	-1	0	0	0	0
118	96	39	4	6	4	3	1	1	1	1	0	1	0	-1	1	0	0	0	0	0
135	97	41	5	10	4	4	2	2	1	2	0	1	1	-1	1	-1	-1	-1	-1	0
	Joint Separation (mm)																			
		56	36	-5	6	0	2	0	1	-1	2	-1	0	2	-2	2	0	0	0	-1

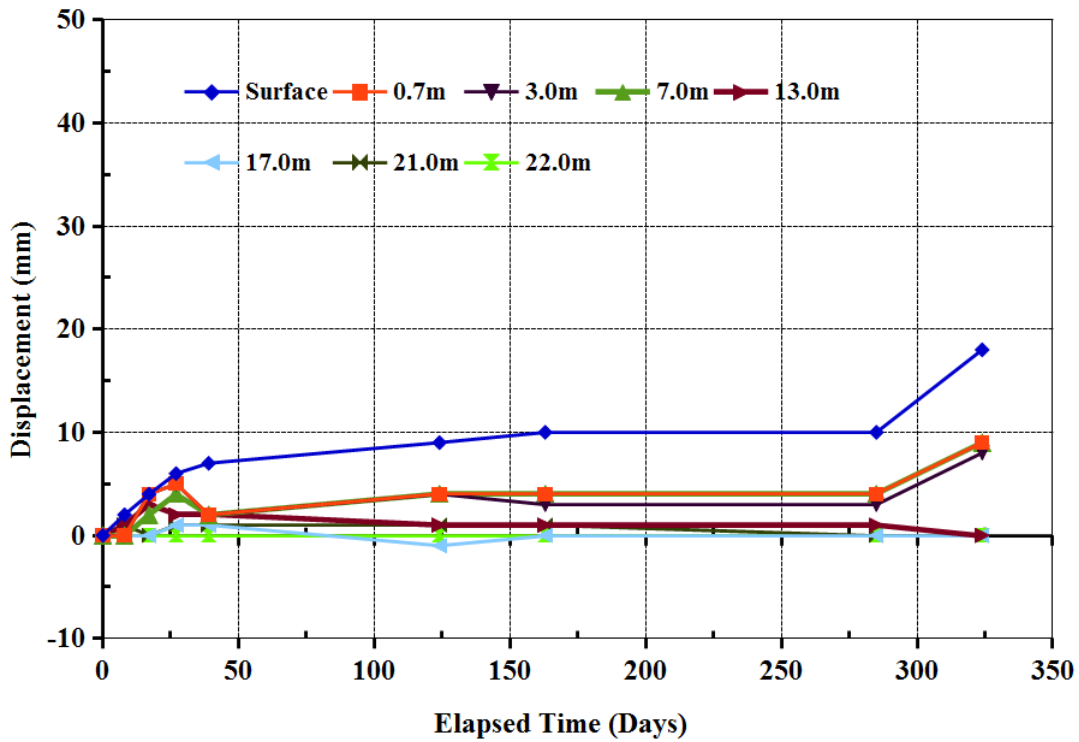


Fig. 4.8 Displacement in the upstream side of crown of powerhouse cavern at RD-130

Table 4.8 MRMPBX readings at RD-130 right side of crown

Elapsed Time (Days)	Anchor Depth (m)							
	Surface	0.7	3.0	7.0	13.0	17.0	21.0	22.0
	Displacement (mm)							
0	0	0	0	0	0	0	0	0
8	2	0	0	0	1	0	1	0
17	4	4	4	2	3	0	0	0
27	6	5	5	4	2	1	1	0
39	7	2	2	2	2	1	1	0
124	9	4	4	4	1	-1	1	0
163	10	4	3	4	1	0	1	0
285	10	4	3	4	1	0	0	0
324	18	9	8	9	0	0	0	0
	Joint Separation (mm)							
		9	1	-1	9	0	0	0

MRMPBX (installed after side slashing) observations in the widened portion of the crown indicated that joint separation that took place in the central portion of crown, extended to sides also. Joint separation started within 7 days upto 22.5m depth into the crown and accelerated between 29 to 41 days with 42-77% of total displacement. With an increase in span (20.4m), joint separation started at deeper depths in the crown. This caused roof collapses at few places. Fig. 4.9 shows one such collapse where roof came down along with rock bolts, which corroborated MRMPBX data (joint separation at deeper depths into crown).

MRMPBX recordings were used to calculate critical strain as per Sakurai et al. (1997). Strains calculated are plotted on Sakurai's warning level graphs and shown in Fig. 4.10. Uniaxial compressive strength of rock mass was taken as 6.27MPa (Table 3.3). Calculated strains are tabulated in Table 4.9. At most of the places, critical strain was lying between warning level-I and warning level-III. At RD-15, critical strain observed was 1.13% and was approaching warning level-III.



Fig. 4.9 Roof collapse at powerhouse cavern

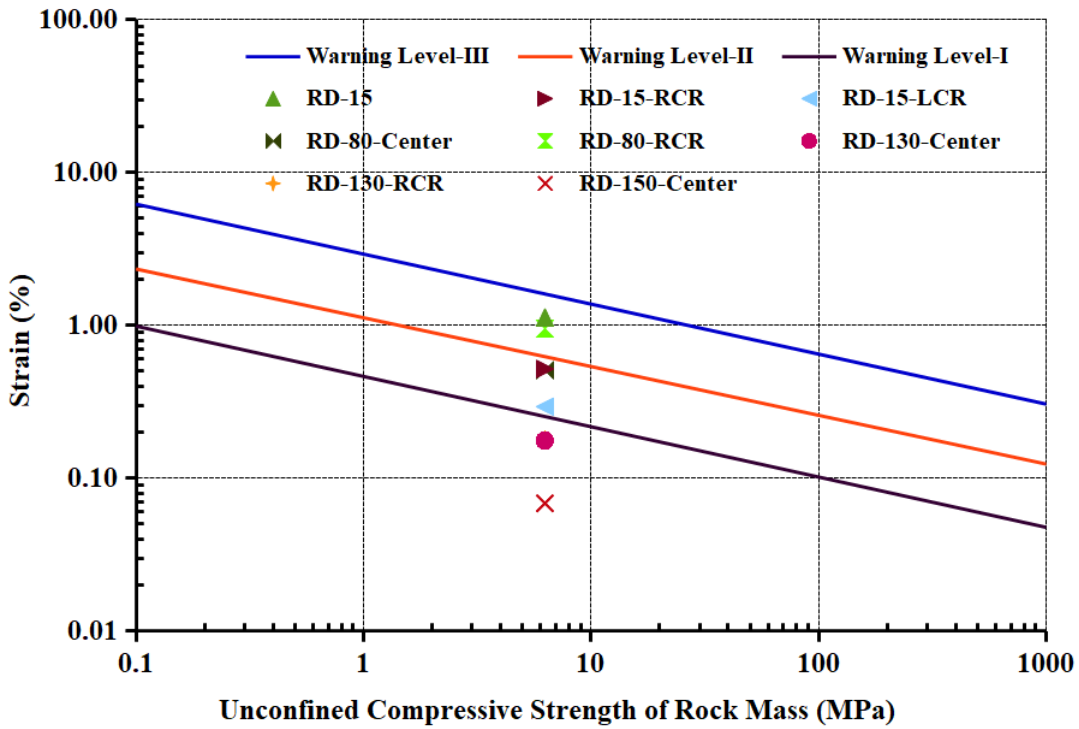


Fig. 4.10 Strain in crown of powerhouse cavern vis a vis warning levels (Sakurai, 1997)

Table 4.9 Critical strain at powerhouse cavern

Location	Maximum Observed Crown Displacement (mm)	Radius of Crown (m)	Critical Strain (%)
RD-15-Center	115	10.2	1.13
RD-15-UCR	53	10.2	0.52
RD-15-DCR	30	10.2	0.29
RD-80-Center	52	10.2	0.51
RD-80-UCR	97	10.2	0.95
RD-130-Center	18	10.2	0.18
RD-130-UCR	18	10.2	0.18
RD-150-Center	7	10.2	0.07

4.1.3 Load on Rock Bolts in the Crown

Vibrating wire anchor load cells were installed on some of the rock bolts in the crown of powerhouse cavern. Load cell observations on rock bolts is shown in Fig. 4.11 and observations are tabulated in Table 4.10.

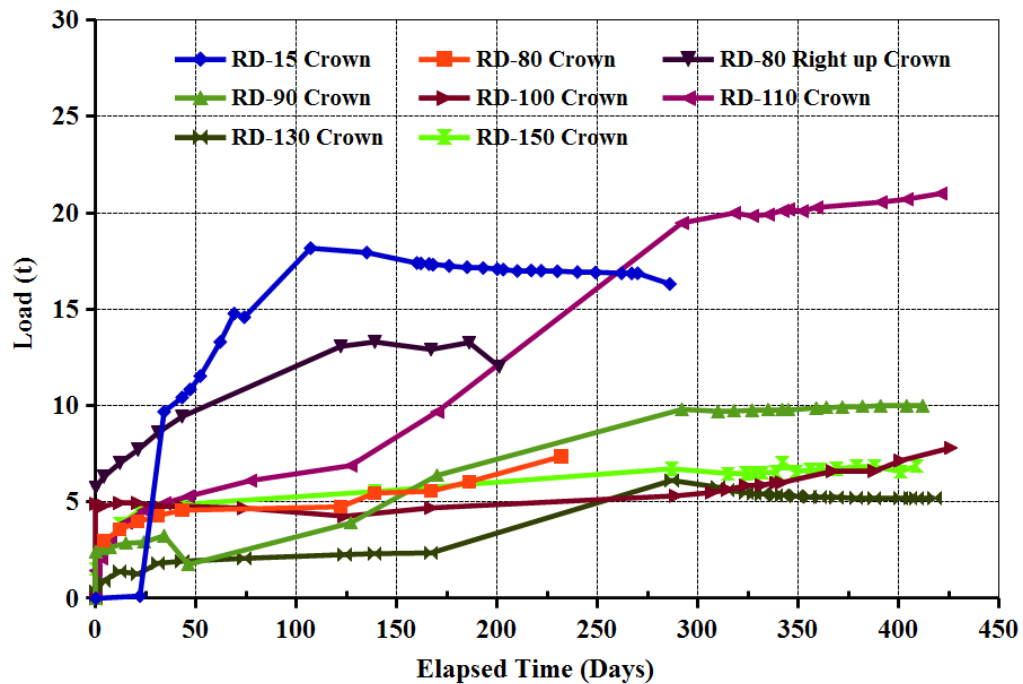


Fig. 4.11 Axial load on rock bolts in the crown of powerhouse cavern

Load cell on rock bolt at RD-15 center of crown showed maximum load of 18.17t. At that time cracks started appearing in the crown at this location and load on the rock bolts started decreasing (due to loss of tension in the bolt) and lost about 1.33t and recorded load of 16.84t. Load cell could not be monitored further due to installation of the steel ribs. Rate of increase of load varied from 0.01-0.8t/day.

Load cell at RD-80 crown was showing increasing trend and recorded maximum load of 13.57t before it was removed for steel rib placement. Rate of increase of load varied from 0.01-0.14t/day. Load cell at RD-80 upstream side of the crown also showed maximum rate of increase of 0.14t/day and recorded maximum load of 12.02t.

Load cell on rock bolt at RD-110 crown recorded maximum load of 21.01t (70% of yield load) and showed rate of increase in the range of 0.01-0.22t/day. Other load cells at RD-90, RD-100, RD-130 and RD-150 showed loads in the range of 5.20-10t and showed rate of increase in load varying from 0.01t/day to 0.04t/day.

Table 4.10 Load cell observations on rock bolts at crown of powerhouse cavern

Elapsed Time (Days)	RD-15 Crown	Elapsed Time (Days)	RD-80 Crown	Elapsed Time (Days)	RD-80 Right up Crown	Elapsed Time (Days)	RD-90 Crown	Elapsed Time (Days)	RD-100 Crown	Elapsed Time (Days)	RD-110 Crown	Elapsed Time (Days)	RD-130 Crown	Elapsed Time (Days)	RD-150 Crown
Load on Rock Bolt (t)															
0	0.00	0	2.97	0	5.77	0	0.00	0	0.00	0	0.00	0	0.00	0	0.00
22	0.12	4	3.58	4	6.31	0	2.43	0	4.91	0	1.44	0	0.36	0	1.52
34	9.69	12	3.97	12	7.03	3	2.58	4	4.80	3	2.07	4	0.92	12	3.86
43	10.43	21	4.30	21	7.71	7	2.66	12	4.95	7	2.97	12	1.39	21	4.50
47	10.84	31	4.57	31	8.59	15	2.86	21	4.95	15	3.93	21	1.27	31	4.71
52	11.54	43	4.76	43	9.44	24	2.91	31	4.80	24	4.56	31	1.83	43	4.88
62	13.31	122	5.47	122	13.08	34	3.25	43	4.78	34	4.94	43	1.93	139	5.55
69	14.78	139	5.56	139	13.31	46	1.76	74	4.69	46	5.30	74	2.08	287	6.73
74	14.59	167	6.05	167	12.92	127	3.92	124	4.26	77	6.11	124	2.27	315	6.47
106	18.17	186	7.36	186	13.28	170	6.38	167	4.70	127	6.89	139	2.32	324	6.48
134	17.94	232	13.57	201	12.02	292	9.81	289	5.32	170	9.68	167	2.36	328	6.51
160	17.40					310	9.70	307	5.50	292	19.48	287	6.12	332	6.53
162	17.38					318	9.72	315	5.65	318	19.99	310	5.77	339	6.54
166	17.35					327	9.76	324	5.86	327	19.85	315	5.62	342	7.01
168	17.31					335	9.79	332	5.88	335	19.92	324	5.48	349	6.59
176	17.25					342	9.79	339	6.00	342	20.11	328	5.44	356	6.65
185	17.18					345	9.78	342	6.01	345	20.19	332	5.41	361	6.67
193	17.14					359	9.86	367	6.61	352	20.10	339	5.36	369	6.72
200	17.08					364	9.90	388	6.61	359	20.28	342	5.36	379	6.84
203	17.06					372	9.92	401	7.15	391	20.56	349	5.31	388	6.86

Elapsed Time (Days)	RD-15 Crown	Elapsed Time (Days)	RD-80 Crown	Elapsed Time (Days)	RD-80 Right up Crown	Elapsed Time (Days)	RD-90 Crown	Elapsed Time (Days)	RD-100 Crown	Elapsed Time (Days)	RD-110 Crown	Elapsed Time (Days)	RD-130 Crown	Elapsed Time (Days)	RD-150 Crown
210	16.99					382	9.96	426	7.81	404	20.71	356	5.27	401	6.58
217	17.01					391	9.98			421	21.01	361	5.26	409	6.87
222	17.00					404	9.99					369	5.23		
230	16.98					412	10.00					379	5.22		
240	16.93											388	5.20		
249	16.91											401	5.20		
262	16.87											406	5.20		
267	16.87											409	5.20		
270	16.87											418	5.20		
286	16.31														

From Fig. 4.11 it could be noted that at RD-15 crown, load on the rock bolt was steadily increasing at a rate varying from 0.01 to 0.8t/day. After 107 days, load cell recorded maximum load of 18.17t. At this point MRMPBX at this location recorded surface displacement of 67mm (Fig. 4.1) and minor cracks started appearing on the surface. This resulted in loss of tension in the rock bolt as indicated by load cell readings. Similar observation was made at RD-80 upstream side, where load cell recorded maximum load of 13.31t after a period of 139 days and MRMPBX recorded displacement of 97mm.

During the monitoring period, load cells could measure load upto 70% of yield load on some of the bolts. Some of the load cells showed increasing trend, but monitoring could not continue as steel ribs with back fill concrete was put in the crown as final support. Wherever cracks appeared in the crown, there was loss of tension in the bolts which was evident in the load cell observations.

4.1.4 Load on the Steel Ribs in the Crown

While installing steel ribs in the crown of powerhouse cavern, load cells were installed on the ribs at EL-533 on both upstream and downstream side. Load cell recordings on upstream and downstream side are given in Tables 4.11 and 4.12 respectively. Axial load on ribs on upstream side and downstream side are shown in Figs. 4.12 and 4.13 respectively.

Table 4.11 Load cell readings on steel ribs on upstream side at powerhouse cavern

Elapsed Time (Days)	RD-18.5 U/S	Elapsed Time (Days)	RD-56.5 U/S	Elapsed Time (Days)	RD-76 U/S	Elapsed Time (Days)	RD-126 U/S	Elapsed Time (Days)	RD-143.4 U/S	Elapsed Time (Days)	RD-173.5 U/S
6	2.74	27	4.79	0	6.10	22	8.15	34	4.92	34	2.58
22	4.80	34	2.54	6	6.86	34	7.87	34	8.87	39	5.35
27	3.78	39	2.81	14	9.73	39	9.34	39	2.59	48	6.05
34	3.79	48	3.03	22	14.55	48	7.66	48	6.88	54	7.57
39	3.87	54	3.13	27	15.93	54	7.65	54	6.69	55	7.66
48	4.22	60	3.22	39	13.25	60	7.82	55	6.94	60	7.56
54	4.50	62	3.24	48	14.24	62	8.28	60	7.27	62	7.60
60	4.16	66	3.27	60	15.04	66	9.60	62	7.39	66	10.69
62	4.64	68	3.24	62	15.13	68	8.85	66	7.58	68	8.13
66	4.71	76	3.12	66	15.26	76	8.96	68	7.92	76	8.77
68	4.82	85	3.61	68	15.99	85	9.55	76	8.37	85	9.84
76	5.27	93	3.79	76	15.35	89	9.60	85	9.75	89	10.13
85	5.54	100	3.83	85	15.88	93	9.77	89	10.30	93	10.47
93	5.64	103	3.86	93	16.38	100	9.82	93	10.79	100	10.78

Elapsed Time (Days)	RD-18.5 U/S	Elapsed Time (Days)	RD-56.5 U/S	Elapsed Time (Days)	RD-76 U/S	Elapsed Time (Days)	RD-126 U/S	Elapsed Time (Days)	RD-143.4 U/S	Elapsed Time (Days)	RD-173.5 U/S
100	5.14	110	5.00	100	16.40	103	9.85	100	11.08	103	10.88
103	5.72	117	4.54	103	16.51	110	10.03	103	11.19	110	12.24
110	6.10	122	4.99	110	17.01	117	10.08	110	11.97	117	11.73
117	6.34	140	5.83	117	15.36	122	10.22	117	11.58	122	11.57
122	6.50	149	6.41	128	15.86	130	10.27	122	12.25	130	12.92
130	6.81	162	7.20	140	16.25	140	10.50	130	12.97	140	13.02
140	7.00	172	7.95	149	16.56	149	10.80	140	13.36	149	13.11
149	6.37	187	9.09	162	17.26	162	11.43	149	13.93	162	13.48
162	7.60	207	12.00	179	17.86	167	11.67	162	15.38	179	14.55
167	7.41	225	14.42	187	18.43	170	11.82	170	16.46	190	14.24
170	7.65	246	21.50	207	18.85	179	11.62	186	17.68	214	15.49
186	8.23	256	23.58	225	17.84	186	12.31	214	21.92	225	15.99
195	8.45	265	25.45	244	18.86	220	13.70	225	23.29	232	16.39
203	8.82	275	43.02	256	19.79	225	14.41	241	31.27	241	17.17
225	8.67	286	49.49	265	20.39	242	15.40	244	32.57	244	17.20
244	9.62	300	46.67	275	20.19	244	15.66	256	38.67	256	17.94
256	10.01	316	59.65	256	19.97	256	16.07	265	40.87	265	18.20
264	9.92	331	61.11	300	19.87	265	16.72	275	43.37	275	18.75
286	13.29	344	63.16	316	19.53	275	17.40	286	45.36	286	19.37
296	13.49	365	69.35	331	19.05	286	17.68	300	43.74	309	22.07
332	18.65	379	66.50	344	18.69	300	18.93	316	45.64	320	22.52
338	19.84	404	71.96	365	18.44	316	20.51	331	48.56	323	23.46
344	20.67	419	75.03	379	18.33	331	22.33	344	52.03	328	24.54
362	22.10	442	80.24	404	18.31	344	23.49	365	57.33	334	26.06
375	23.22	459	84.97	419	18.42	365	23.80	379	60.88		
386	24.32	468	86.67	442	18.75	379	23.43				
407	25.87	477	88.21	459	19.06	404	24.43				
419	26.89	488	89.56	468	19.14	419	25.05				
442	28.98	502	86.28	488	19.40	442	25.18				
456	30.39	520	94.00	502	19.86	459	25.40				
467	30.53	526	94.70	520	20.25	466	25.60				
478	30.82	529	94.76	551	22.98	477	25.77				
488	31.41	551	99.45	579	24.82	488	25.90				
497	31.68	579	104.60	610	27.26	502	26.25				
506	31.90	610	109.80	631	29.72	520	27.03				
520	32.02	631	113.00	653	34.79	551	26.07				
529	32.12	653	117.50	674	37.67	579	25.82				
585	34.37	674	118.00	703	44.16	610	26.19				
620	34.72	703	118.70	725	48.36	631	25.97				
655	32.77	725	117.70	746	51.05	653	25.63				
666	33.31	746	118.30	764	53.00	674	23.95				
709	33.81	764	113.70	781	52.91	703	22.49				
730	33.13	781	122.20	800	56.06	725	21.85				
746	34.86	800	131.50	832	59.55	746	21.58				
760	32.70	832	99.77	858	61.91	764	21.49				
926	33.20	858	101.10			781	23.97				

Elapsed Time (Days)	RD-18.5 U/S	Elapsed Time (Days)	RD-56.5 U/S	Elapsed Time (Days)	RD-76 U/S	Elapsed Time (Days)	RD-126 U/S	Elapsed Time (Days)	RD-143.4 U/S	Elapsed Time (Days)	RD-173.5 U/S
981	32.93	888	102.30			800	24.02				
1006	32.97	926	102.80			832	21.65				
1031	32.91	1006	101.30			858	21.49				
1045	32.74	1045	100.80			888	18.66				
1069	32.65	1095	101.50			926	17.54				
1095	32.97					981	16.36				
1121	32.99					1006	16.98				
1160	33.31					1101	16.43				
1186	33.37					1158	3.39				
1213	33.52					1199	3.73				
1242	33.35					1242	3.93				
1276	33.71					1276	4.35				
						1308	4.33				
						1339	4.27				
						1397	3.49				
						1435	3.34				
						1450	3.27				
						1493	3.52				
						1517	3.59				
						1544	2.11				
						1590	4.00				
						1618	3.74				
						1642	3.68				
						1674	2.86				
						1707	3.36				
						1738	2.89				

Table 4.12 Load cell readings on steel ribs on downstream side at powerhouse cavern

Elapsed Time (Days)	RD 18.5 D/S	Elapsed Time (Days)	RD 56.5 D/S	Elapsed Time (Days)	RD 76 D/S	Elapsed Time (Days)	RD 126 D/S	Elapsed Time (Days)	RD 143.4 D/S	Elapsed Time (Days)	RD 173.5 D/S
6	3.54	27	1.44	0	0.03	22	2.80	34	5.88	34	2.86
22	4.58	43	1.71	6	0.86	34	3.71	39	5.52	39	11.09
27	3.85	48	1.76	14	1.78	39	5.20	48	8.99	48	11.02
34	3.79	55	1.87	22	3.42	48	4.99	54	4.67	54	13.60
39	3.83	60	1.88	27	4.10	54	5.19	55	4.50	55	14.10
48	3.87	69	1.90	34	4.68	60	5.66	60	4.68	60	13.31
54	4.17	75	1.93	39	4.93	62	5.94	62	5.06	62	9.84
60	4.19	81	1.70	48	5.54	66	6.47	66	5.59	66	14.99
62	3.97	83	1.91	54	5.99	68	6.62	68	5.69	68	14.62
66	4.05	87	2.10	60	6.44	76	7.17	76	6.13	76	16.04

Elapsed Time (Days)	RD 18.5 D/S	Elapsed Time (Days)	RD 56.5 D/S	Elapsed Time (Days)	RD 76 D/S	Elapsed Time (Days)	RD 126 D/S	Elapsed Time (Days)	RD 143.4 D/S	Elapsed Time (Days)	RD 173.5 D/S
68	4.15	89	2.16	62	6.51	85	7.15	85	6.85	85	21.83
76	4.54	97	2.30	66	6.63	89	7.22	89	7.11	89	24.87
85	4.69	106	3.02	68	6.70	93	7.17	93	7.31	93	25.88
93	3.83	114	2.32	76	7.04	100	8.04	100	7.35	100	26.23
100	3.74	121	2.46	85	7.44	128	8.30	103	7.44	103	26.94
103	3.72	124	2.56	93	8.08	140	8.51	110	7.94	110	28.78
110	4.08	131	2.56	100	8.24	149	8.47	117	8.18	117	29.03
117	3.98	138	2.56	103	8.41	162	8.89	122	8.06	122	29.47
122	4.26	143	2.74	110	8.93	170	8.98	130	8.20	130	30.78
130	5.34	151	2.36	117	9.36	179	8.86	140	8.26	140	31.16
140	4.12	161	2.50	122	9.70	186	9.31	149	7.67	149	32.39
149	5.11	170	2.64	130	10.37	204	9.38	162	7.83	162	33.45
162	4.93	183	3.21	140	10.96	220	11.88	172	8.45	167	35.26
167	5.11	188	3.76	149	11.48	225	11.21	190	9.98	170	33.04
170	5.36	191	4.96	162	12.37	244	13.70	214	10.14	190	38.49
186	5.91	207	5.44	172	12.86	256	15.07	225	12.52	195	38.75
203	6.79	224	7.66	186	13.85	265	16.07	244	15.67	214	43.62
246	10.81	267	7.34	204	13.44	275	16.54	246	16.61	225	48.80
256	11.71	277	9.99	225	17.74	286	16.89	256	16.88	235	54.79
265	16.38	286	16.37	244	19.04	300	18.50	265	17.50	261	70.03
275	15.51	296	18.06	256	19.70	316	20.93	275	18.75	264	70.44
286	19.72	307	21.00	265	21.88	331	21.58	286	19.84	275	72.29
300	20.88	321	23.30	275	24.20	344	20.15	300	23.99	283	73.54
389	23.16	410	25.16	286	24.79	365	21.95			286	75.98
407	25.44	428	26.01	300	27.46	379	22.92			292	76.25
410	25.62	431	26.86	316	33.23	391	24.57			296	80.90
419	25.79	440	29.16	331	36.04	404	26.61			302	85.56
428	25.91	449	30.99	344	33.41	419	28.37			309	88.04
442	25.90	463	32.99	365	37.07	432	29.71			317	91.36
456	26.20	477	34.28	379	39.16	459	31.82			320	89.78
468	26.32	489	52.04	391	40.43	466	32.28			323	86.45
478	24.05	499	53.13	404	42.05	477	32.57			328	80.02
510	27.44	531	53.54	419	44.02	488	33.04			332	70.08
520	28.01	541	54.62	432	45.66	502	33.50			334	74.70
529	28.35	550	55.16	459	46.25	520	34.58			337	74.93
545	28.76	566	57.19	468	47.10	529	34.80			344	78.33
562	25.09	583	63.25	477	47.67	551	35.76			358	81.94
579	25.32	600	63.10	488	48.10	579	37.92			372	88.48

Elapsed Time (Days)	RD 18.5 D/S	Elapsed Time (Days)	RD 56.5 D/S	Elapsed Time (Days)	RD 76 D/S	Elapsed Time (Days)	RD 126 D/S	Elapsed Time (Days)	RD 143.4 D/S	Elapsed Time (Days)	RD 173.5 D/S
590	25.15	611	53.18	502	48.35	631	41.21			374	89.41
666	25.13	687	51.59	520	49.53	653	42.44			381	92.40
713	25.27	734	63.31	529	49.84	674	43.64			386	94.86
769	25.99	790	79.46	551	49.50	703	44.14			400	86.13
832	26.63	853	87.51	579	49.13	725	46.85			404	87.85
872	27.50	893	93.72	610	49.94	746	48.62			407	88.78
900	28.90	921	102.60	631	51.09	764	49.19			410	89.96
926	31.84	947	103.50	653	52.08	781	48.84			417	93.09
981	31.41	1002	103.80	674	51.40	800	44.12			424	97.03
1006	31.17	1027	104.00	703	53.53	832	43.12			435	100.20
1045	30.74	1066	103.30	725	53.23	888	44.90			436	100.50
1095	30.91	1116	95.50	746	52.55	926	45.60			440	101.10
1158	31.98	1179	85.50	764	51.79	981	45.29			445	101.60
1199	32.42	1220	85.76	781	51.90	1006	32.65			450	102.50
1242	32.62	1263	85.30	800	52.38	1045	29.56			456	114.30
1276	33.08	1297	85.37	832	47.14	1101	28.39			459	117.60
1308	33.08	1329	86.90	888	48.69	1158	28.43			462	117.40
1339	32.92	1360	88.68	926	50.18	1199	29.49			466	117.20
1397	32.66	1418	87.98	1006	50.55	1242	29.28			467	116.10
1435	32.82	1456	86.29	1045	50.65	1276	29.92			468	115.80
1450	32.79	1471	85.30	1101	51.28	1308	28.98			469	113.00
1471	33.13	1492	86.50	1158	51.54	1339	34.11			470	110.60
1493	33.21	1514	87.50	1199	51.59	1397	36.34			472	112.90
1517	33.43	1538	87.69	1242	51.65	1435	36.56			474	115.60
1544	33.95	1565	90.42	1276	51.97	1450	36.50			477	112.70
1590	34.20			1308	52.02	1471	36.66			482	119.10
1618	34.26			1339	51.95	1493	38.70			486	120.00
1642	34.28			1435	51.53	1517	39.94			491	120.40
1674	34.17			1493	51.80	1544	40.37			494	120.40
1691	34.11					1590	40.82			497	120.90
1707	33.94					1618	40.90			501	120.80
1720	33.91					1642	41.07			505	121.20
1737	33.75					1674	40.73			506	121.70
1740	33.70					1707	40.32			508	121.30
						1738	39.79			510	121.30
										515	122.00
										527	122.80
										536	123.30

Elapsed Time (Days)	RD 18.5 D/S	Elapsed Time (Days)	RD 56.5 D/S	Elapsed Time (Days)	RD 76 D/S	Elapsed Time (Days)	RD 126 D/S	Elapsed Time (Days)	RD 143.4 D/S	Elapsed Time (Days)	RD 173.5 D/S
										543	124.00
										551	124.60
										565	125.90
										579	127.00
										595	128.10
										607	128.90
										1079	132.20
										1093	132.60
										1186	135.50
										1216	136.30
										1271	136.60
										1352	135.60

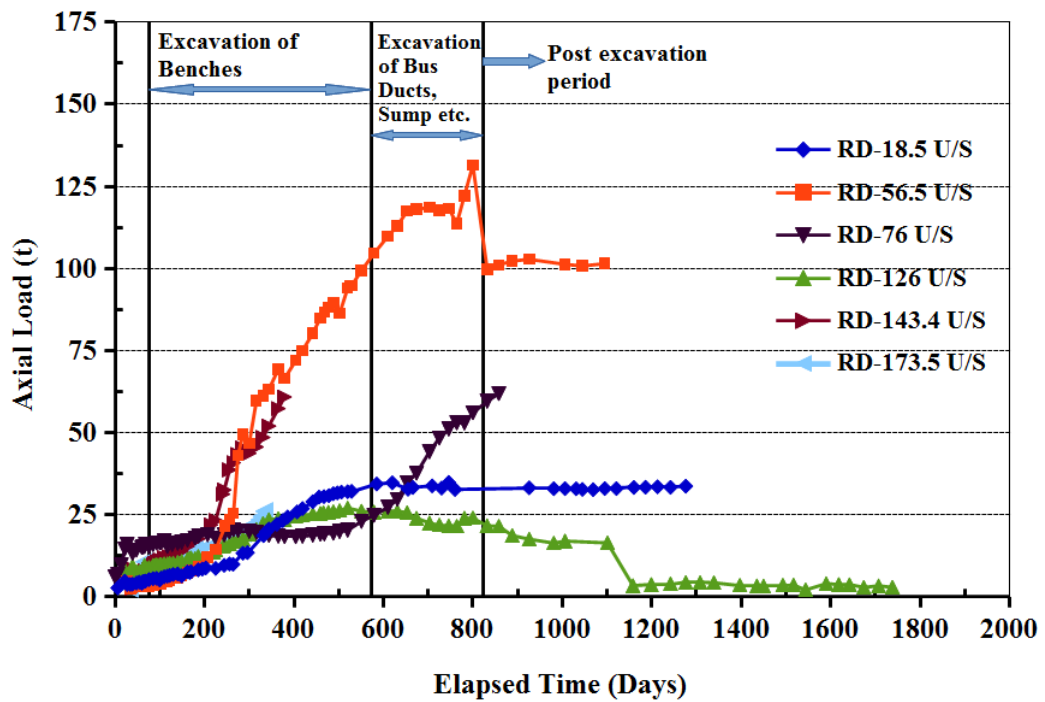


Fig. 4.12 Axial load on steel ribs on upstream side in the crown of powerhouse cavern

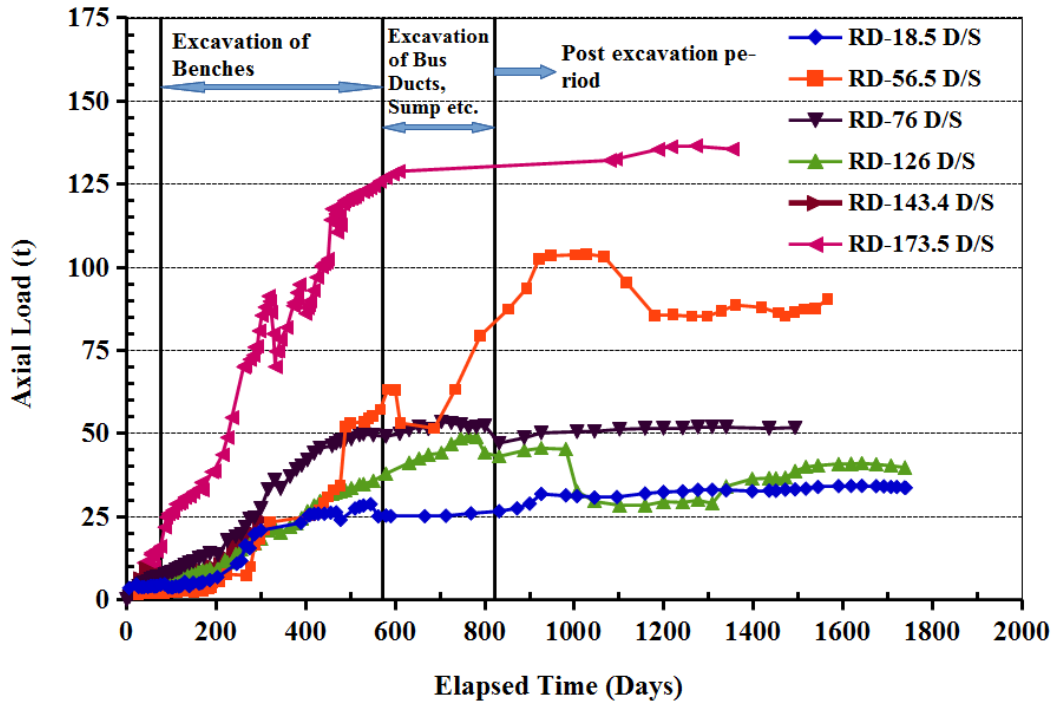


Fig. 4.13 Axial load on steel ribs on downstream side in the crown of powerhouse cavern

Figs. 4.14 and 4.15 show axial load on upstream side and downstream of the steel ribs during benching of powerhouse cavern with time period of each bench (B1-B11) marked on the graphs.

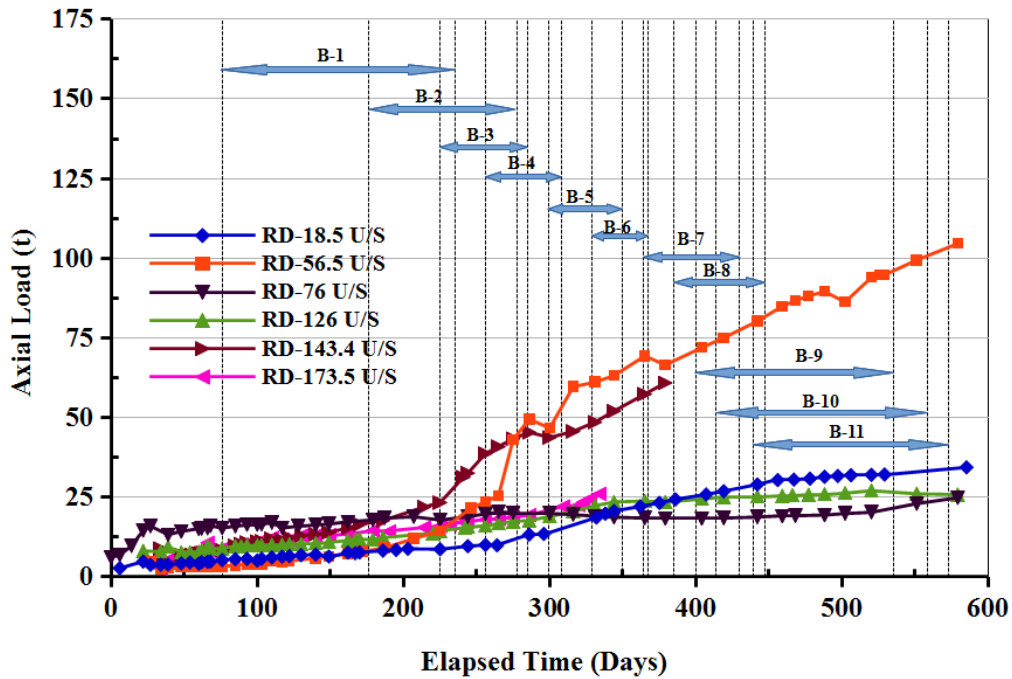


Fig. 4.14 Axial load on steel ribs on upstream side during benching (B1-B11) in the crown of powerhouse cavern

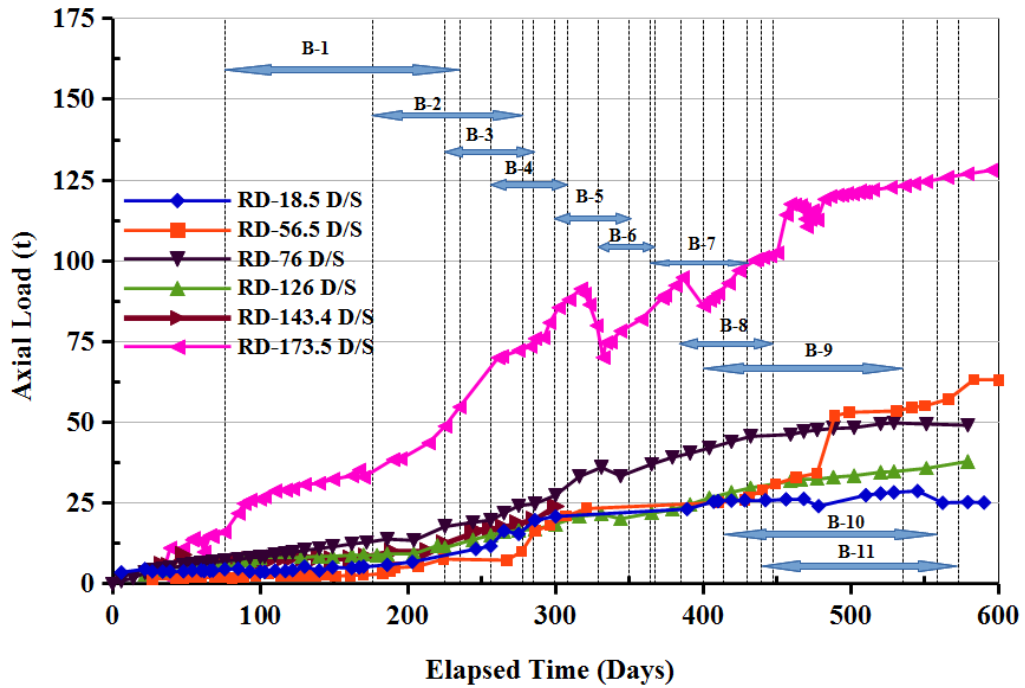


Fig. 4.15 Axial load on steel ribs on downstream side during benching (B1-B11) in the crown of powerhouse cavern

Figs. 4.16 and 4.17 show rate of loading on upstream and downstream side of steel ribs during extraction of each bench.

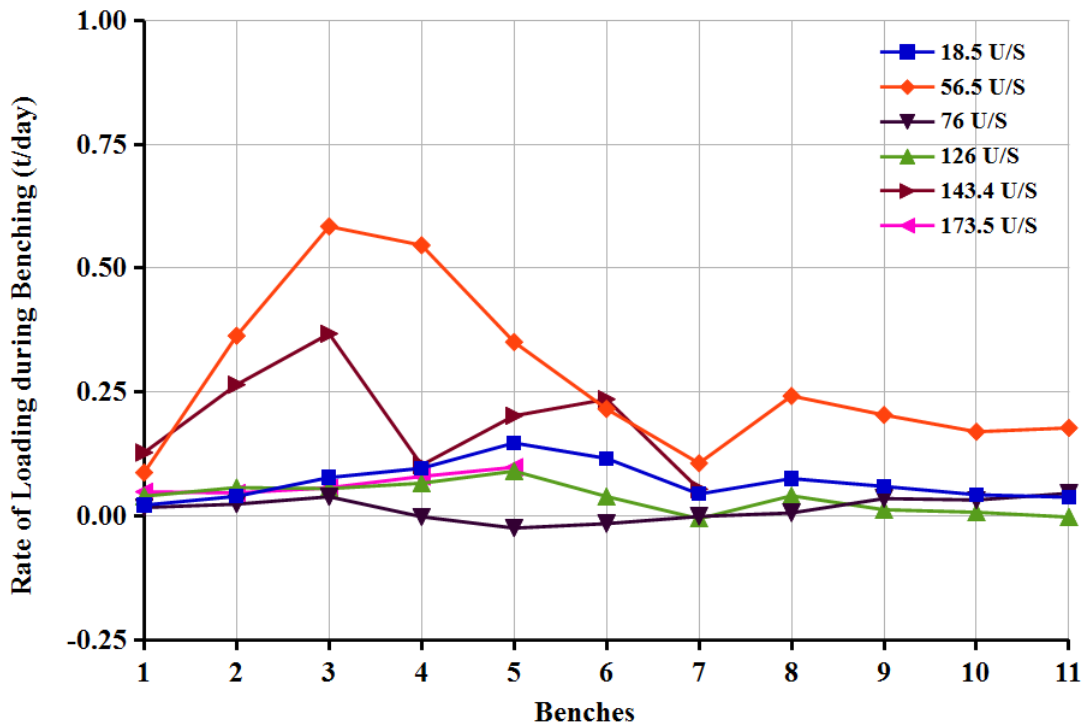


Fig. 4.16 Rate of loading on steel ribs on upstream side during benching

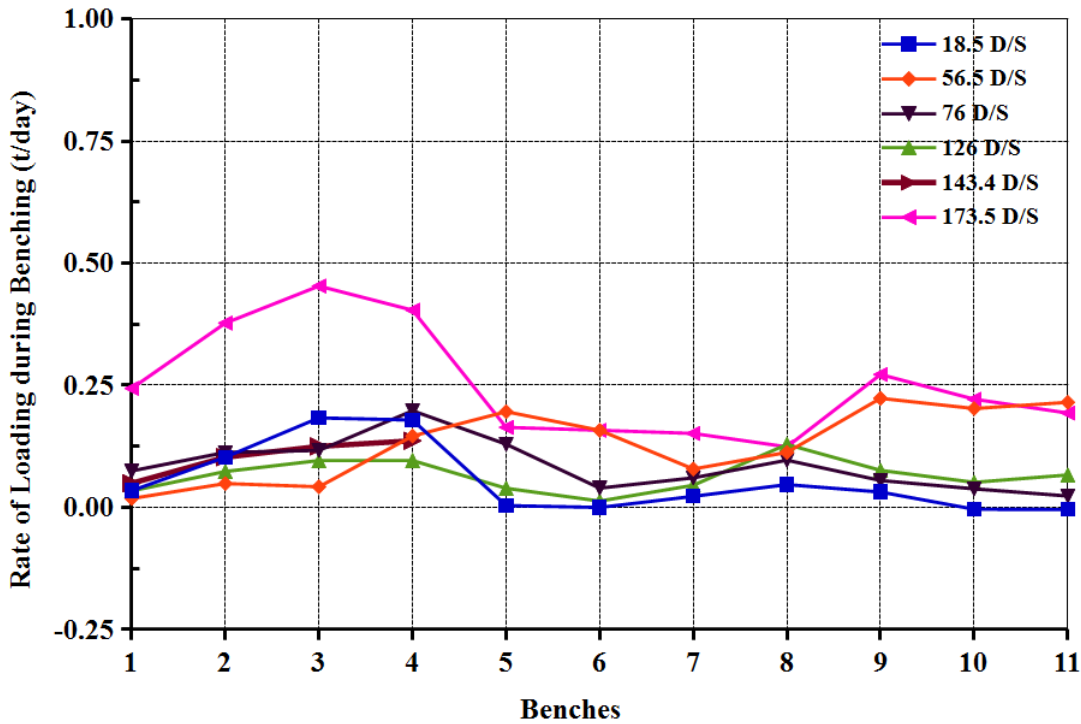


Fig. 4.17 Rate of loading on steel ribs on downstream side during benching

Summary of change in load on steel ribs during excavation of each bench is given in Table 4.13. Bench wise explanation of loading on steel ribs is described below.

Bench-1 (B-1, EL 531 to 528.5)

During excavation of first bench, maximum load recorded on upstream side was 29t at RD-143.4, with rate of loading of 0.13t/day. Loads at RD-18.5, RD-56.5, RD-76, RD-126 and RD-173.5 on upstream side were 8.67t, 17t, 18t, 15t and 16.4t, respectively. Total load increase at RD-56.5 was 13.88t with a rate of 0.09t/day (Fig. 4.16).

On downstream side, maximum load recorded was 54.78t at RD-173.5, an increase of 38.75t with 0.24t/day. At RD-76, load recorded was 19t (increase of 11.9t) with 0.07t/day (Fig. 4.17). Loads at RD-18.5, RD-56.5, RD-126 and RD-143.4 were 10t, 5t, 12.5t and 14t respectively.

Table 4.13 Summary of change in load in steel ribs during each benching at powerhouse cavern

Upstream Side													
	Change in Load(t) for Excavation of each Bench												
RD/ Bench	1	2	3	4	5	6	7	8	9	10	11	Max	Min
18.5	3.4	4	4.63	4.99	7.5	4.4	2.9	0.68	8	6.11	5.02	8	0.68
56.5	13.88	37.1	35.07	28.42	17.9	8.2	0.7	4	26.04	24.42	23.76	37.1	0.7
76	2.64	2.4	2.3	-0.11	-1.27	-0.61	-0.1	0	4.67	4.58	6.07	6.07	-1.27
126	6.3	5.8	3.29	3.42	4.6	1.48	-0.4	0.9	1.64	1.01	-0.36	6.3	-0.4
143.4	20.3	27	22.07	5.32	10.3	8.94	3.54					27	3.54
173.5	7.7	4.7	3.39	4.13	5	Could not monitor						7.7	3.39
Max	20.3	37.1	35.07	28.42	17.9	8.94	3.54	4	26.04	24.42	23.76		
Min	2.64	2.4	2.3	-0.11	-1.27	-0.61	-0.4	0	1.64	1.01	-0.36		
Downstream Side													
	Change in Load(t) for Excavation of each Bench												
RD/ Bench	1	2	3	4	5	6	7	8	9	10	11	Max	Min
18.5	5.46	10.5	11	9.3	0.2	0	1.5	2	4.76	-0.53	-0.58	11	-0.58
56.5	2.9	5	2.54	7.6	10	6	5.2	1.2	28.16	29.16	28.84	29.16	1.2
76	11.9	11.5	7	10.3	6.6	1.5	4	1.5	7.45	5.48	3.13	11.9	1.5
126	5.4	7.5	5.7	5	2	0.5	3	3	11.76	7.39	8.904	11.76	0.5
143.4	7.87	10.5	7.5	7.1	Could not monitor						10.5	7.1	
173.5	38.75	38.5	27.2	21	8.36	6	10	-4.3	38.47	31.91	25.9	38.75	-4.3
Max	38.75	38.5	27.2	21	10	6	10	3	38.47	31.91	28.84		
Min	2.9	5	2.54	5	0.2	0	1.5	-4.3	4.76	-0.53	-0.58		

Bench-2 (B-2, EL 528.5 to 525)

Excavation of second bench recorded acceleration in load on upstream side at RD-143.4 and RD-56.5. Maximum load recorded at RD-143.4 was 44t (an increase of 27t) with 0.26t/day. At RD-56.5, maximum load was 45t (an increase of 37.1t) with 0.36t/day. At other locations, rate of loading varied from 0.02 – 0.06t/day (Fig. 4.16).

On downstream side, load at RD-173.5 increased to 72.5t (an increase of 38.5t) with 0.38t/day. At RD-76, load increased to 24.5t (an increase of 11.5t) with 0.11t/day. Loads at RD-18.5, RD-56.5, RD-126 and RD-143.4 were 16t, 7.6t, 16.5t and 19t respectively with loading rates of 0.05-0.10t/day (Fig. 4.17).

Bench-3 (B-3, EL 525 to 521.5)

On upstream side, load at RD-143.4 increased to 45.37t (an increase of 22.07t) with 0.37t/day. Load at RD-56.5 increased to 49.49t (an increase of 35.07t) with 0.58t/day (Fig. 4.16). Load cells at other locations recorded loading rates between 0.04t/day and 0.08t/day.

On downstream side, load at RD-173.5 increased to a maximum of 76t (an increase of 27.20t) with 0.45t/day (Fig. 4.17). At other locations rate of loading varied from 0.04-0.18t/day.

Bench-4 (B-4, EL 521.5 to 518.5)

On upstream side, maximum load at RD-143.4 and RD-56.5 was 44t (an increase of 5.32t with 0.10t/day) and 52t (an increase of 28.42t with 0.55t/day), respectively. There was no change in load at RD-76 and other locations showed loading rates of 0.07-0.10t/day (Fig. 4.16).

On downstream side, load at RD-173.5 increased to 88t (an increase of 21t with 0.40t/day). Load at other locations increased in the range of 5-10.3t with 0.10-0.20t/day (Fig. 4.17).

Bench-5 (B-5, EL 518.5 to 515.5)

On upstream side, maximum load at RD-143.4 and RD-56.5 was 54t (an increase of 10.3t with 0.20t/day) and 64.5t (an increase of 17.9t with 0.35t/day), respectively (Fig. 4.16). Load cells at RD-18.5, RD-126 and RD-173.5 showed an increase of 4.6 to 7.5t with 0.09- 0.15t/day whereas, RD-76 recorded decrease of 1.27t.

On downstream side, load at RD-173.5 increased to 91.36t. However, total increase in load during excavation of this bench was only 8.36t. With the excavation of bus duct No.3 during the excavation of 5th bench, the load on the ribs started decreasing possibly due to the deformations in the bus duct (as the location of bus duct is just beneath it). There was a reduction of 20t (Fig. 4.15). However, towards the end, load started increasing as excavation of passage to the transformer hall and excavation of sixth bench started. Load cells at RD-56.5 and RD-76 recorded increase of 10t (0.2t/day) and 6.6t (0.13t/day).

Bench-6 (B-6, EL 515.5 to 513)

On upstream side, loads at RD-143.5 increased at 0.24t/day to 57.5t. At RD-56.5 load of 69.3t was measured at a rate of 0.22t/day. Total increase in load during excavation of 6th bench was 8.9t and 8.2t at RD-143.4 and RD-56.5 respectively. Loads at other locations showed increase of 1.48t to 4.40t during this period (Fig. 4.14).

On downstream side, load at RD-173.5 increased from 80t to 86t, an increase of 6t. Load at RD-56.5 increased from 18t to 24t at a rate of 0.16t/day. At other locations increase in load varied in the range of 0.5t to 1.5t (with rate of 0.01 to 0.04t/day) (Fig. 4.15 and 4.17)

Bench-7 (B-7, EL 513 to 510)

On upstream side, loads continued to rise at RD-143.4 and RD-56.5 during excavation of 7th bench and recorded load of 60.8t and 70t respectively (an increase of 3.54t (0.05t/day) and 7t (0.11t/day), respectively). During this period at RD-18.5, there was an increase of 2.9t (0.04t/day) (Fig. 4.14 and 4.16).

On downstream side, load at RD-173.5 increased further and recorded a load of 94t, an increase of 10t at 0.15t/day (Fig. 4.15 and 4.17). At other locations, load increased in the range of 1.5t to 5.20t (0.02 to 0.08t/day).

Bench-8 (B-8, 510 to 507)

On upstream side, RD-56.5 recorded load of 82t, an increase of 15t at 0.24t/day. At other locations, loads increased in the range of 0.35t-4.66t at 0.01t/day to 0.08t/day.

On downstream side, load at RD-173.5 increased further and recorded a load of 102.5t, an increase of 7.7t at 0.12t/day (Fig. 4.15 and 4.17). At RD-126, there was an increase of 8t (0.13t/day). At other locations, load increased in the range of 2.9t to 6.99t (0.05 to 0.11t/day).

Bench-9 (B-9, 504 to 507)

On upstream side, RD-56.5 recorded load of 99.45t, an increase of 27.49t at 0.20t/day. At other locations, loads increased in the range of 1.64t-8.00t at 0.01t/day to 0.06t/day (Fig. 4.14 and 4.16).

On downstream side, load at RD-56.5 rose to 55.16t, an increase of 30.16t at 0.22t/day. Similarly at RD-173.5, load increased further and recorded a load of 124.6t, an increase

of 36.75t at 0.27t/day (Fig. 4.15 and 4.17). At RD-126, there was an increase of 10.26t (0.08t/day). At other locations, load increased in the range of 4.26t to 7.45t (0.03 to 0.06t/day).

Bench-10 (B-10, 501 to 504)

On upstream side, RD-56.5 recorded load of 99.45t, an increase of 24.42t at 0.17t/day. At other locations, loads increased in the range of 1.01t-6.11t at 0.01t/day to 0.04t/day (Fig. 4.14 and 4.16).

On downstream side, load at RD-56.5 rose to 55.16t, an increase of 29.16t at 0.20t/day. Similarly at RD-173.5, load increased further and recorded a load of 125t, an increase of 31.91t at 0.22t/day (Fig. 4.15 and 4.17). At RD-126, there was an increase of 7.39t (0.05t/day). At other locations, load increased in the range of 5.48t to 7.39t (0.04 to 0.05t/day).

Bench-11 (B-11, 499.5 to 501)

On upstream side, RD-56.5 recorded load of 104t, an increase of 23.76t at 0.18t/day (Fig. 4.14 and 4.16). At other locations, loads increased in the range of 5.02t-6.07t at 0.04t/day to 0.05t/day.

On downstream side, load at RD-56.5 rose to 58t, an increase of 28.84t at 0.22t/day. Similarly at RD-173.5, load increased further and recorded a load of 127t, an increase of 25.90t at 0.19t/day (Fig. 4.15 and 4.17). At RD-126, there was an increase of 8.90t (0.07t/day).

Excavation of bench-3 had maximum rate of increase of load on the steel ribs in both upstream and downstream sides of crown with maximum rate of 0.56t/day and 0.45t/day, respectively. On upstream side, excavation of benches 2, 3, 4 and 5 had maximum influence on load in steel ribs at RD-56.5 and RD-143.4 with more than 0.25t/day. This influence zone comes within 1.05 times the width of the cavern. Beyond that height (i.e. excavation of 6th bench onwards, the rate of loading is less than 0.25t/day). On downstream side, excavation of bench-1 to bench-5 had maximum influence on load in steel ribs at RD-173.5 with more than 0.25t/day. In this case also, this influence zone comes within 1.05 times the width of the cavern.

Although, there was an average increase of 24.74t each at RD-56.5 upstream, during excavation of bench-9, 10 and 11, rate of loading was less as time for each benching was 136.5 days compared to average benching period of 54.83 days for benches 3 to 8. Similar behaviour was observed at RD-56.5 downstream and RD-173.5 downstream.

4.1.5 Movement in the Side Walls

Instrumentation in the walls of cavern continued with excavation of benches. Reflective targets were installed at elevations 525, 520, 515 and 506 on both walls at RD-15, RD-65, RD-110m and RD-150m. Cumulative convergence of main walls of cavern was measured using total station. Cumulative convergence observations at EL-525 are shown in Fig. 4.18 and data is listed in Table 4.14.

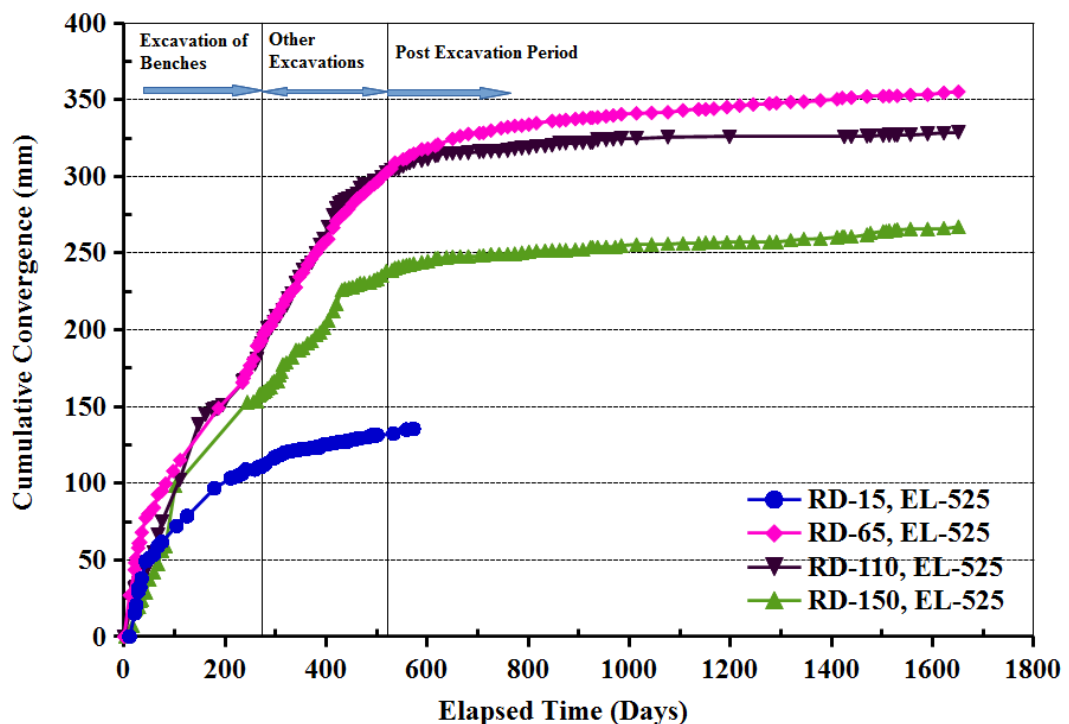


Fig. 4.18 Cumulative convergence of walls at powerhouse cavern at EL-525

At EL-525, cumulative convergence at RD-65 and RD-110 was almost similar (305mm) during the excavation of the cavern and followed same trend (Fig. 4.18). However, during post excavation period, convergence at RD-65 was higher (355.2mm) than convergence at RD-110 (328.8mm).

Table 4.14 Cumulative convergence data of upstream and downstream wall of powerhouse cavern at EL-525

Convergence of Upstream and Downstream Wall of Powerhouse Cavern (mm)							
EL-525							
Elapsed Time (Days)	RD-15	Elapsed Time (Days)	RD-65	Elapsed Time (Days)	RD-110	Elapsed Time (Days)	RD-150
0	0	0	0	0	0	0	0
21	15.10	11	26.98	17	24.6	17	7.03
24	20.55	21	43.65	21	30.61	21	17.42
28	29.45	22	48.14	22	31.59	22	18.21
29	31.58	24	51.23	24	32.46	24	18.53
32	32.26	28	57.89	29	34.78	29	19.7
35	37.88	29	60.96	32	35.5	32	23.3
43	49.15	32	61.52	35	37.16	35	24.16
50	51.10	35	67.99	43	43.44	43	28.97
59	53.35	43	77.39	48	46.56	50	36.9
67	58.87	48	80.06	59	54.88	59	41.69
75	61.73	50	80.33	67	66.63	67	47.62
104	72.16	59	84.1	75	75.18	75	56.06
125	78.57	67	92.73	110	102.3	82	59.06
179	96.73	75	94.96	147	138.1	101	98.11
211	103.2	82	99.74	161	144.8	244	152.9
214	103.6	97	108	175	147.8	256	153.1
216	103.8	111	115.1	179	148.2	263	153.4
221	104.2	187	149	183	148.5	267	157.5
227	105.2	234	165.7	187	148.9	269	158.2
234	106.2	237	168.5	195	151.1	272	158.5
241	108.8	242	172.1	235	165.9	276	159.3
259	108.8	249	176.7	237	166.9	280	160.2
266	110.4	256	180.8	259	177.7	284	161.8
272	110.8	263	189.5	263	180.9	290	162.5
280	112.5	266	189.8	269	187.4	293	165.4
296	116	269	192.8	272	190.8	297	166.6
298	117	272	192.9	276	194.4	304	166.8
304	117.8	276	197.2	280	195.3	307	170.7
311	118.6	280	199	284	200.9	311	172.5
319	120.1	284	201.2	290	201.2	314	177.4
325	120.6	287	202.3	291	201.5	321	178.5
332	121	291	202.8	297	205.1	332	182.1
340	121.6	297	208.1	301	208.6	340	186.8
347	121.8	301	208.4	307	208.9	346	186.8

Convergence of Upstream and Downstream Wall of Powerhouse Cavern (mm)							
EL-525							
Elapsed Time (Days)	RD-15	Elapsed Time (Days)	RD-65	Elapsed Time (Days)	RD-110	Elapsed Time (Days)	RD-150
354	122	307	212.2	314	212.8	354	187.8
363	122.4	314	216.2	321	215.9	363	191.1
371	123.2	321	220	325	220.1	371	192.5
380	123.4	325	222	332	223.8	380	196.3
388	123.4	332	225	340	230.1	388	198.3
395	125	340	227.7	347	234.4	395	201.5
404	125.3	347	234.5	354	239	404	206.1
414	126.3	354	237.3	363	241.6	414	212.2
420	126.4	363	242.3	371	243.8	420	216.9
426	126.7	371	246.2	380	249.5	431	225.8
431	126.9	380	250.1	388	255.4	437	226.8
437	127.2	388	253.7	395	259.2	445	227.3
444	127.3	395	256.5	404	267.1	452	227.8
452	128.4	404	259.1	414	274.3	461	229.2
461	128.9	414	266.5	420	279	467	230.3
467	129.1	420	270.8	426	281.9	475	230.5
482	129.9	426	272.9	431	283.3	486	231
490	131.1	431	274.7	437	284.9	495	232.4
495	131.2	437	276.1	444	285.6	501	233.3
501	131.2	444	278.7	452	287	510	235.3
533	132.3	452	282	461	288.8	519	238.3
559	134.9	461	285.4	467	292.6	530	238.8
573	135.3	467	286.8	475	294.3	536	240.3
		475	289	486	294.8	543	241
		486	292.5	495	296.9	552	241.7
		495	294.8	501	297	559	242.2
		501	296.4	510	299	565	242.5
		510	299.6	519	302.3	573	243.2
		519	302.4	529	304.2	589	244
		529	305	536	304.5	601	244.8
		536	309	543	304.8	616	246.5
		552	311.1	552	306.6	621	246.7
		559	311.7	559	308.4	638	247.2
		565	313.4	565	308.8	650	247.5
		573	314.7	573	309.7	665	247.7
		589	317.6	589	310.3	681	247.8
		601	318.1	601	311.3	703	248.1

Convergence of Upstream and Downstream Wall of Powerhouse Cavern (mm)							
EL-525							
Elapsed Time (Days)	RD-15	Elapsed Time (Days)	RD-65	Elapsed Time (Days)	RD-110	Elapsed Time (Days)	RD-150
		616	319.9	616	313.4	711	248.4
		621	320.8	621	313.8	726	249.2
		650	324.5	638	315	742	249.3
		665	326.3	650	315	759	249.3
		681	327.6	665	315.1	773	249.6
		703	328.2	681	315.3	787	250.2
		711	328.4	703	316	801	250.8
		726	329.9	711	316.2	816	251.3
		746	331.4	726	316.3	833	251.5
		759	332.2	742	316.4	847	251.8
		773	332.9	759	316.8	862	251.9
		787	333.1	773	317.9	874	251.9
		801	333.8	787	318.3	893	252.1
		816	334.7	801	318.6	908	252.2
		847	336.1	816	319.7	923	253.7
		862	336.3	833	319.7	927	253.7
		874	336.8	847	320.3	937	253.8
		893	337.4	862	321.6	954	253.9
		908	337.9	874	321.7	972	253.9
		923	338.2	893	321.7	984	254.9
		927	338.2	908	321.9	1014	255.5
		937	338.5	923	322.1	1044	255.7
		954	339.2	927	322.1	1076	255.9
		968	339.7	937	323.8	1106	256.2
		984	340.5	954	323.9	1137	256.4
		1014	341.1	968	324.2	1151	256.7
		1044	341.4	984	324.5	1167	256.7
		1076	341.8	1014	325	1193	256.9
		1106	343.1	1076	325.6	1218	257.1
		1137	343.7	1198	325.8	1245	257.2
		1151	343.7	1425	325.8	1277	257.2
		1167	344.1	1439	325.9	1291	257.3
		1193	345.1	1470	326.2	1319	258.2
		1218	346.1	1477	326.5	1345	259.1
		1245	346.9	1502	326.6	1378	259.3
		1277	347.4	1514	326.8	1411	260.3
		1291	347.8	1525	326.9	1421	260.5

Convergence of Upstream and Downstream Wall of Powerhouse Cavern (mm)							
EL-525							
Elapsed Time (Days)	RD-15	Elapsed Time (Days)	RD-65	Elapsed Time (Days)	RD-110	Elapsed Time (Days)	RD-150
		1319	348.5	1530	326.9	1425	260.6
		1345	348.7	1556	327.2	1439	260.7
		1378	349.5	1590	327.6	1470	262
		1411	350.3	1622	328.2	1477	263
		1421	351.1	1651	328.8	1502	264.1
		1439	351.3			1508	264.2
		1470	352.1			1514	264.6
		1502	352.3			1525	264.9
		1514	352.4			1530	265.3
		1530	352.5			1556	265.7
		1556	353.1			1590	265.7
		1590	353.3			1622	266.1
		1622	354.5			1651	267.2
		1651	355.2				

Cumulative convergence observations at EL-520 are shown in Fig. 4.19 and data is listed in Table. 4.15.

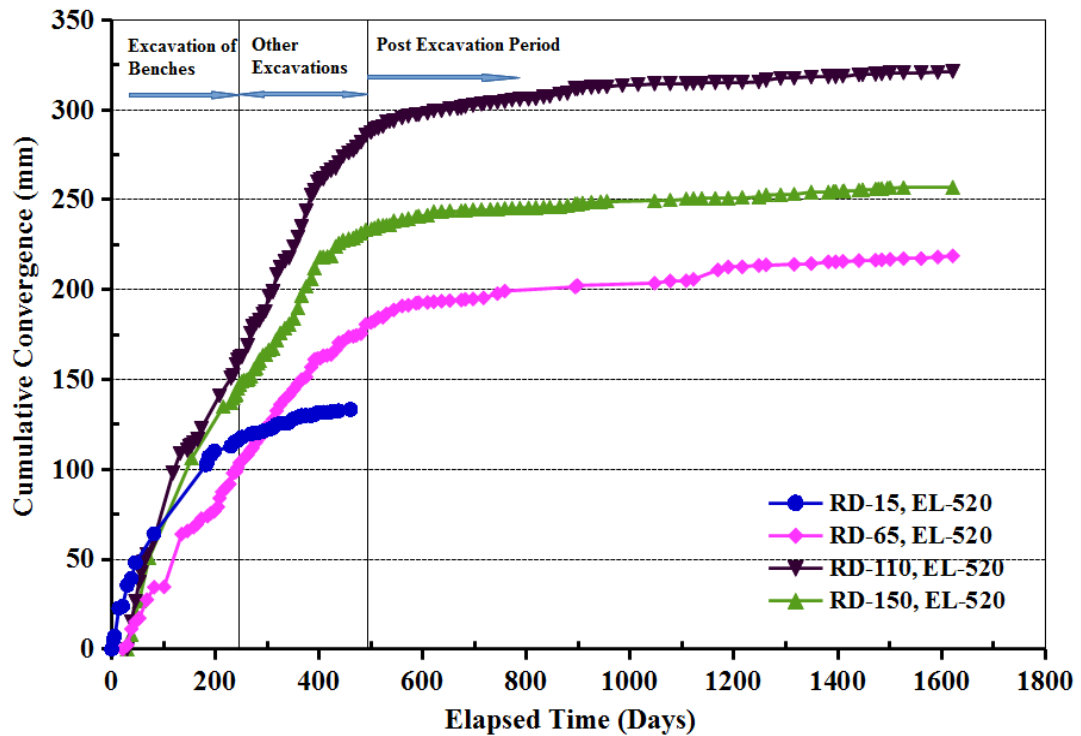


Fig. 4.19 Cumulative convergence of walls at powerhouse cavern at EL-520

At EL-520, maximum convergence was recorded at RD-110 (321.4mm) and RD-65 (218.8mm) recorded lower convergence than RD-150 (256.9mm) as shown in Fig. 4.19. Convergence at RD-15 (located at service bay area) at EL-525 (135.3mm) and EL-520 (133.3mm) showed a different trend of convergence at other points in the unit bay area.

Table 4.15 Cumulative convergence data of upstream and downstream wall of powerhouse cavern at EL-520

Convergence of Upstream and Downstream wall of Powerhouse Cavern (mm)							
Elapsed Time (Days)	RD-15	Elapsed Time (Days)	RD-65	Elapsed Time (Days)	RD-110	Elapsed Time (Days)	RD-150
EL-520							
0	0	21	0	30	0	30	0
3	5.02	30	2.179	38	15.43	38	7.884
6	7.135	38	11.23	46	26.81	46	19.56
14	22.77	46	15.34	53	37.34	53	26.81
21	23.71	53	17.25	57	42.61	72	50.62
30	35.58	68	27.54	62	48.55	154	106
38	39.29	82	34.45	68	52.87	215	134.8
46	48.05	101	34.65	81	60.49	230	136.9
82	64.23	135	64.04	118	97.87	234	139.7
182	102.5	146	65.78	132	108.9	238	140.8
185	104.5	158	67.88	146	110.6	240	141.5
187	106.9	164	69.36	150	112.5	243	144.9
192	108.1	173	72.6	154	113.1	247	147.2
198	110.1	185	74	158	115	251	148.9
230	112.8	191	75.61	166	116.5	255	149.6
237	115.1	198	76.68	173	122.8	261	149.8
243	116.1	205	79.16	208	141.1	264	150.2
251	117.8	208	83.96	230	150.7	268	151.8
269	119.7	213	87.45	234	152.5	275	155.8
275	120.2	220	89.56	240	158.5	278	156.6
282	120.3	227	91.79	243	160.6	282	159.1
290	120.8	234	97.85	247	162.4	285	160.7
296	121.7	237	98.32	251	162.6	292	163.5
303	122.1	240	98.72	262	168.7	297	164.1
311	123.1	243	101.1	268	175.8	303	166.5
318	125	247	103.7	272	179.3	311	167.4
325	125.5	251	104.9	278	181.1	317	171.9
334	125.7	255	106.1	285	182.8	318	172.1
342	126	258	107.2	292	186.2	325	175.8

Convergence of Upstream and Downstream wall of Powerhouse Cavern (mm)							
Elapsed Time (Days)	RD-15	Elapsed Time (Days)	RD-65	Elapsed Time (Days)	RD-110	Elapsed Time (Days)	RD-150
EL-520							
351	128.1	262	108.1	296	187.9	334	178.5
359	128.7	268	110.7	303	196.6	342	180.8
366	129.8	272	112	311	198.7	351	184
375	129.9	278	115	318	208.4	359	189.6
385	129.9	285	117.6	325	212.1	366	196.7
391	130.4	292	120.3	334	215.8	375	201.6
397	131.5	296	123.2	342	217.7	385	205.9
402	131.6	303	124.1	351	224	391	211.9
408	131.8	311	127.9	359	229.4	402	218.1
415	131.8	318	132.6	366	234.8	408	218.2
423	131.9	325	136.1	375	243.8	416	218.4
432	132.1	334	139.2	385	252.3	423	218.9
438	132.5	342	141.2	391	255.1	432	224
461	133.3	351	144.5	397	259.9	438	225.8
		359	147.6	402	261.3	446	227.5
		366	150	408	261.6	457	228.3
		375	151.5	415	264.8	466	228.7
		385	156.9	423	266.3	472	229.9
		391	161.2	432	267.6	481	231.4
		397	161.7	438	270.8	490	233.2
		402	161.8	446	274.2	501	233.7
		408	163.2	457	276.1	507	234.3
		415	163.4	466	277.4	514	235.6
		423	163.9	472	279.3	523	235.7
		432	166.6	481	282.1	530	235.8
		438	170.5	490	285.8	536	235.8
		446	171.1	500	287.5	544	238.3
		457	173.7	507	289.4	560	238.8
		466	174	514	289.8	572	239.5
		472	174.6	523	290.8	587	240.4
		481	175.5	530	293.4	592	240.9
		490	180.7	536	293.6	609	241.4
		500	181.7	544	293.8	621	243.4
		507	182.7	560	295.6	636	243.5
		514	184.4	572	296.5	652	243.8
		523	184.6	587	297.4	674	243.8

Convergence of Upstream and Downstream wall of Powerhouse Cavern (mm)							
Elapsed Time (Days)	RD-15	Elapsed Time (Days)	RD-65	Elapsed Time (Days)	RD-110	Elapsed Time (Days)	RD-150
EL-520							
		530	186.5	592	297.4	682	244.1
		544	188.7	609	298.2	697	244.4
		560	190.9	621	299.5	713	244.5
		572	191.3	636	299.6	730	244.6
		587	192.5	652	300.5	744	244.8
		592	192.8	667	300.8	758	245.1
		609	192.9	674	301.1	772	245.2
		621	193.2	682	301.9	787	245.4
		636	193.6	697	302.5	804	245.5
		652	193.9	713	303.2	818	245.7
		674	194.2	717	303.6	833	245.8
		682	194.6	730	303.8	845	245.9
		697	194.8	744	304.2	864	246.1
		717	195.4	758	304.5	879	246.8
		744	197.8	772	305.4	894	247.7
		758	199.2	787	305.7	898	247.7
		894	201.5	804	306	908	248.1
		898	202.3	818	306.2	925	248.5
		1047	203.6	833	307.1	943	248.8
		1077	204.8	845	307.5	955	249.1
		1108	204.9	864	308.9	1047	249.3
		1122	205.7	879	309.2	1077	249.8
		1169	211	894	311.7	1108	250.4
		1189	212.6	898	311.7	1122	250.6
		1216	212.7	908	312.2	1138	250.7
		1248	213.5	925	312.5	1164	250.7
		1262	213.8	939	312.8	1189	250.9
		1316	214.1	955	312.9	1216	251.2
		1349	214.5	985	313.6	1248	251.6
		1382	215.5	1015	314.1	1262	252.6
		1396	215.5	1047	314.5	1290	252.7
		1410	215.8	1077	314.6	1316	253.1
		1441	216.2	1108	314.6	1349	254.3
		1473	216.4	1122	314.8	1382	254.3
		1485	216.6	1138	315	1392	254.6
		1501	216.9	1164	315.1	1396	254.6

Convergence of Upstream and Downstream wall of Powerhouse Cavern (mm)							
Elapsed Time (Days)	RD-15	Elapsed Time (Days)	RD-65	Elapsed Time (Days)	RD-110	Elapsed Time (Days)	RD-150
EL-520							
		1527	217.3	1189	315.2	1410	254.8
		1561	217.3	1216	315.3	1412	254.9
		1593	218.2	1248	315.6	1441	255.2
		1622	218.8	1262	316.5	1448	255.5
				1290	317.5	1473	255.9
				1316	317.7	1479	256.1
				1349	318.3	1485	256.2
				1382	318.4	1496	256.4
				1396	318.4	1501	256.6
				1410	318.8	1527	256.7
				1441	319.5	1622	256.9
				1448	319.6		
				1473	319.8		
				1485	320.1		
				1501	320.5		
				1527	320.7		
				1561	320.7		
				1593	320.9		
				1622	321.4		

Cumulative convergence observations at EL-515 are shown in Fig. 4.20 and data is listed in Table 4.16.

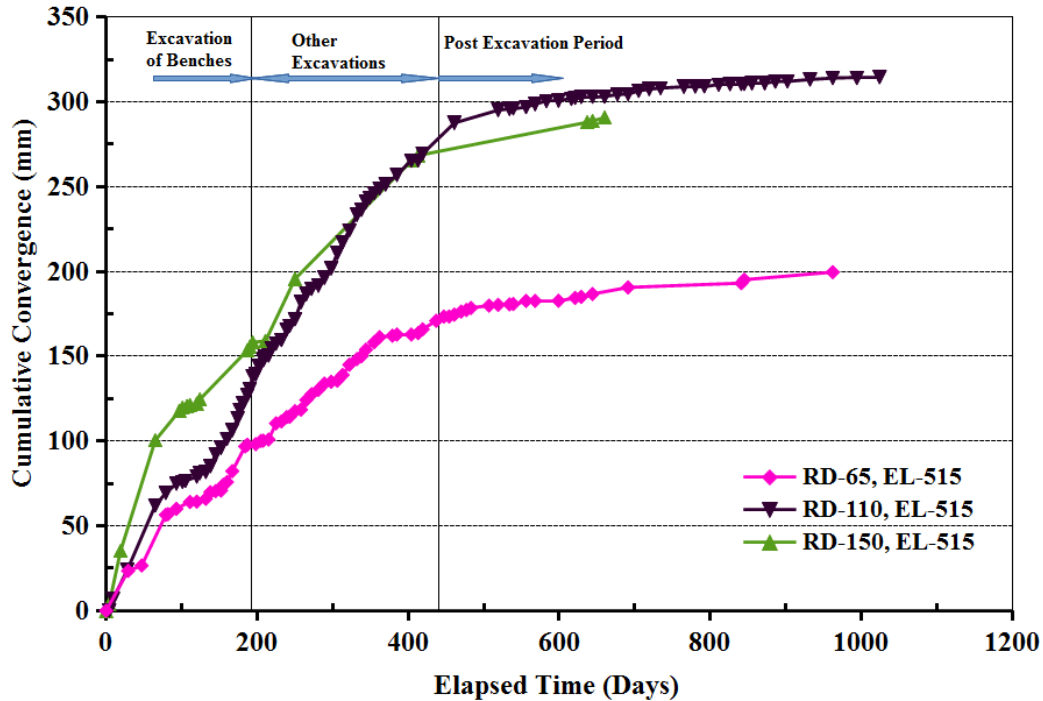


Fig. 4.20 Cumulative convergence of walls at powerhouse cavern at EL-515

At EL-515, maximum convergence was recorded at RD-110 (314.56mm), followed by RD-150 (290.78mm) and RD-65 (199.59mm) as shown in Fig. 4.20.

Table 4.16 Cumulative convergence data of upstream and downstream wall of powerhouse cavern at EL-515

Convergence of Upstream and Downstream Wall of Powerhouse Cavern (mm)					
EL-515					
Elapsed Time (Days)	RD-65	Elapsed Time (Days)	RD-110	Elapsed Time (Days)	RD-150
0	0	4	0	0	0
29	23.48	9	6.75	4	3.94
47	26.62	28	23.94	19	35.16
79	56.53	65	62.04	65	100.4
82	56.91	79	69.45	97	117.84
93	60.06	93	74.88	101	119.68
111	64.09	101	75.97	107	120.65
120	64.27	105	76.55	111	121.20
132	65.96	120	79.04	120	122.17
138	69.87	124	81.03	124	124.55
145	70.5	132	81.80	187	153.50

Convergence of Upstream and Downstream Wall of Powerhouse Cavern (mm)					
EL-515					
Elapsed Time (Days)	RD-65	Elapsed Time (Days)	RD-110	Elapsed Time (Days)	RD-150
152	70.85	138	85.17	190	155.40
155	74.18	145	92.11	194	158.24
160	75.87	152	95.95	211	159.03
167	82.28	160	101.32	250	195.62
184	96.84	167	106.45	404	265.17
187	97.83	174	113.32	413	268.37
198	98.19	177	118.44	637	288.01
205	100.14	181	122.21	637	288.01
208	100.28	187	126.93	644	288.68
215	100.93	190	130.52	660	290.78
225	110.48	194	138.32		
232	111.58	198	139.15		
239	114.15	202	144.21		
243	114.25	208	147.55		
250	117.63	209	148.5		
258	118.53	210	149.8		
265	124.23	215	150.45		
272	127.66	219	154.74		
281	130.24	225	157.48		
289	133.91	232	159.57		
298	134.96	239	165.77		
306	135.64	243	167.9		
313	138.98	250	171.84		
322	145.01	258	181.84		
332	148.29	265	186.59		
338	149.97	272	189.8		
344	153.86	281	191.63		
355	158.35	289	196.16		
362	161.31	298	201.74		
379	162.15	306	210.64		
385	162.82	313	217.17		
404	162.82	322	224.31		
419	165.89	338	236.42		
437	170.96	344	240.9		
447	173.39	349	243.54		
454	173.43	355	246.23		
461	174.52	362	248.96		

Convergence of Upstream and Downstream Wall of Powerhouse Cavern (mm)					
EL-515					
Elapsed Time (Days)	RD-65	Elapsed Time (Days)	RD-110	Elapsed Time (Days)	RD-150
470	176.36	370	251.25		
477	177.3	385	256.85		
483	178.5	404	265.3		
507	179.91	413	265.43		
519	180.3	419	269.38		
534	180.62	461	287.56		
539	180.83	519	295.1		
556	182.65	534	295.76		
568	182.68	539	296.19		
599	182.74	556	296.96		
621	184.42	568	298.62		
629	185.05	583	300.48		
644	186.72	599	300.69		
691	190.62	616	301.76		
841	193.14	621	302.36		
845	195.17	629	302.88		
962	199.59	644	303.06		
		660	303.08		
		677	304.35		
		691	304.56		
		705	306.52		
		719	307.5		
		734	308.1		
		765	308.84		
		780	309.04		
		792	309.2		
		811	310.14		
		826	310.46		
		845	310.6		
		855	310.88		
		872	310.9		
		886	311.95		
		902	312.07		
		932	313.17		
		962	314.03		
		994	314.06		
		1024	314.56		

Cumulative convergence observations at EL-506 are shown in Fig. 4.21 and data is given in Table 4.17. At EL-506, maximum convergence was recorded at RD-150 (188.20mm), followed by RD-110 (154.56mm) and RD-65 (105.91mm) as shown in Fig. 4.21.

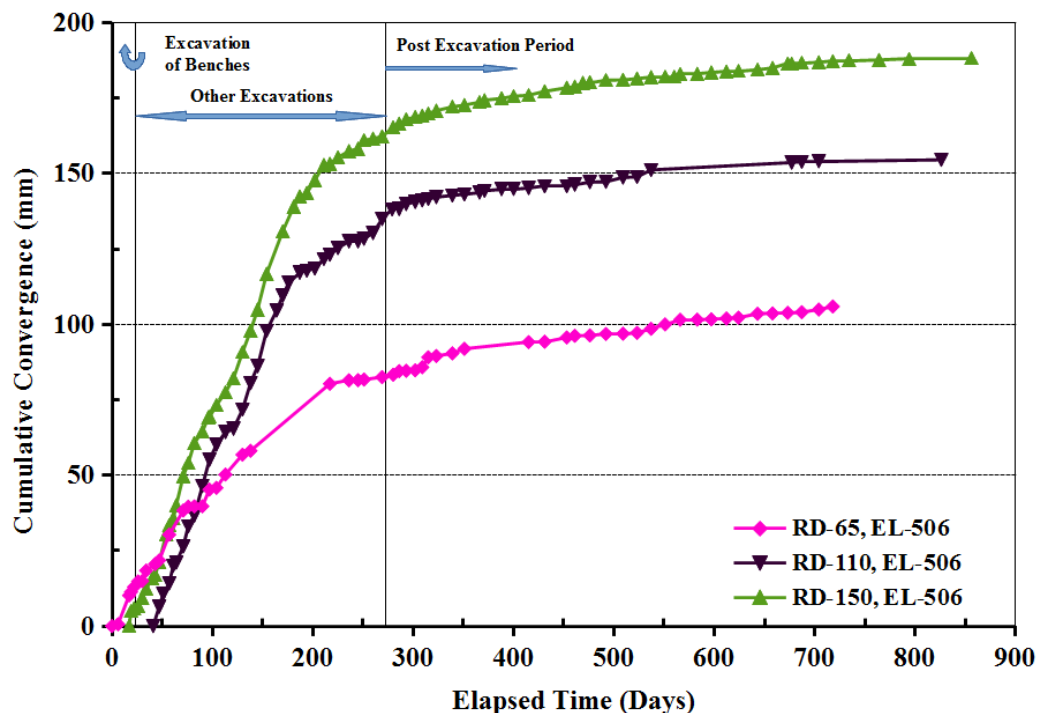


Fig. 4.21 Cumulative convergence of walls at powerhouse cavern at EL-506

Table 4.17 Cumulative convergence data of upstream and downstream wall of powerhouse cavern at EL-506

Convergence of Upstream and Downstream Wall of Powerhouse Cavern (mm)					
EL-506					
Elapsed Time (Days)	RD-65	Elapsed Time (Days)	RD-110	Elapsed Time (Days)	RD-150
0	0	41	0	17	0
6	0.61	47	6.32	19	4.94
17	10.13	51	10.62	22	5.87
19	11.28	57	14.14	26	6.6
22	12.96	61	20.04	30	9.42
26	14.79	64	21.03	34	12.38
30	14.9	71	26.38	40	15.76
34	18.39	76	33.1	43	16.8
43	20.54	82	36.58	47	21.29
47	21.75	90	46.38	54	30.51
57	30.31	97	55.05	57	33.38
71	38.28	104	60.09	61	35.62

Convergence of Upstream and Downstream Wall of Powerhouse Cavern (mm)					
EL-506					
Elapsed Time (Days)	RD-65	Elapsed Time (Days)	RD-110	Elapsed Time (Days)	RD-150
76	39.58	113	64.27	64	40.07
82	39.65	121	65.34	71	49.7
90	39.7	130	71.79	76	54
97	45.25	138	80.51	82	60.65
104	45.81	145	86.1	90	64.43
113	50.21	154	97.88	96	69.18
130	56.82	164	104.59	97	69.31
138	58.1	170	109.43	104	73.22
217	80.32	176	113.82	113	77.49
236	81.47	187	117.09	121	82.11
245	81.5	194	117.82	130	90.77
251	81.72	202	118.53	138	97.85
269	82.5	211	121.68	145	104.93
280	83.31	217	123.09	154	116.77
286	84.5	225	125.3	170	130.84
293	84.6	236	127.47	181	139.05
302	84.78	245	127.5	187	142.39
309	85.77	251	128.39	194	143.56
315	89.08	260	130.25	202	147.78
323	89.51	269	134.93	211	152.84
339	90.4	279	138.12	217	153.23
351	91.9	286	138.24	225	155.34
415	94.12	293	139.86	236	157.44
431	94.23	302	140.58	245	158.23
461	96.22	315	141.57	260	161.57
476	96.33	323	142.16	269	162.26
492	96.83	339	142.72	280	165.32
509	96.9	351	143.11	286	166.52
523	97.18	366	143.69	293	167.91
537	98.53	371	144.3	302	168.74
551	99.99	388	144.81	309	169.12
566	101.53	400	144.9	315	169.86
583	101.58	415	145.2	323	170.84
597	101.69	431	145.79	339	172.1
612	101.94	453	145.83	351	172.7
624	102.22	461	146.3	366	173.62
643	103.5	476	147.14	371	174.27

Convergence of Upstream and Downstream Wall of Powerhouse Cavern (mm)					
EL-506					
Elapsed Time (Days)	RD-65	Elapsed Time (Days)	RD-110	Elapsed Time (Days)	RD-150
658	103.63	492	147.26	388	174.91
673	103.83	509	148.68	400	175.6
687	104.02	523	148.9	415	175.95
704	104.92	537	151.2	431	177.24
718	105.91	677	153.62	453	178.45
		687	153.9	461	178.81
		704	154.08	469	180.04
		826	154.56	476	180.22
				492	180.92
				509	181.03
				523	181.45
				537	181.93
				551	182.03
				560	182.03
				566	182.92
				583	183.05
				597	183.5
				612	183.76
				624	183.95
				643	184.41
				658	184.98
				673	186.38
				677	186.38
				687	186.68
				704	186.87
				718	187.2
				734	187.5
				764	187.65
				794	187.9
				856	188.2

Effect of excavation of each bench on the wall convergence was analysed and given in Table 4.18 and presented in Figs. 4.22 to 4.24.

Table 4.18 Details of cumulative convergence observations at powerhouse cavern during excavation of main benches

RD/Bench	Convergence measured during benching (mm)								
	4	5	6	7	8	9	10	11	
EL-525									
15	0	51.1	26.6	20.1	20.0	32.7	32.8	28.8	
65	24	80.3	31.8	32.3	33.3	58.5	67.0	70.2	
110	15	46.6	31.1	58.4	52.1	71.9	72.8	64.9	
150	4	36.9	27.9	60.4	54.0	51.9	49.2	39.6	
EL-520									
15	-	23.7	39.3	30.7	24.0	52.0	46.8	41.0	
65	-	-	11.2	23.3	31.0	57.5	59.5	52.0	
110	-	-	15.4	54.6	55.2	87.1	84.7	74.0	
150	-	-	7.9	70.1	49.0	98.0	75.9	71.0	
EL-515									
65	-	-	-	27.0	40.0	56.1	70.0	63.5	
110	-	-	-	48.0	62.0	77.9	89.4	79.0	
150	-	-	-	76.0	96.0	103.0	95.0	69.0	

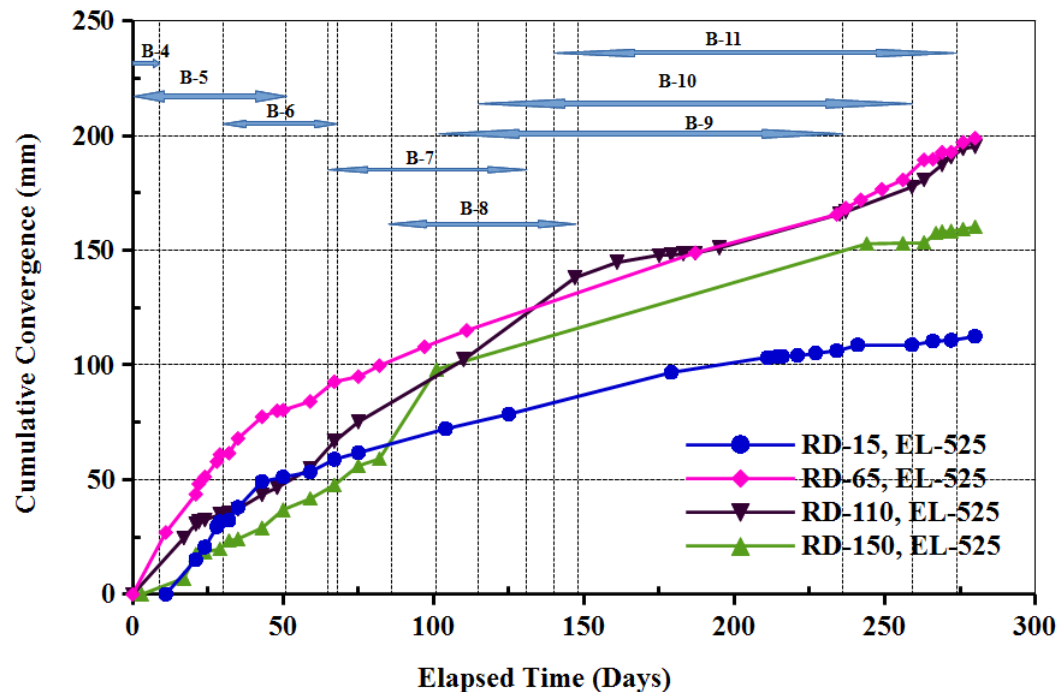


Fig. 4.22 Cumulative convergence of walls at powerhouse cavern at EL-525 during excavation of main benches

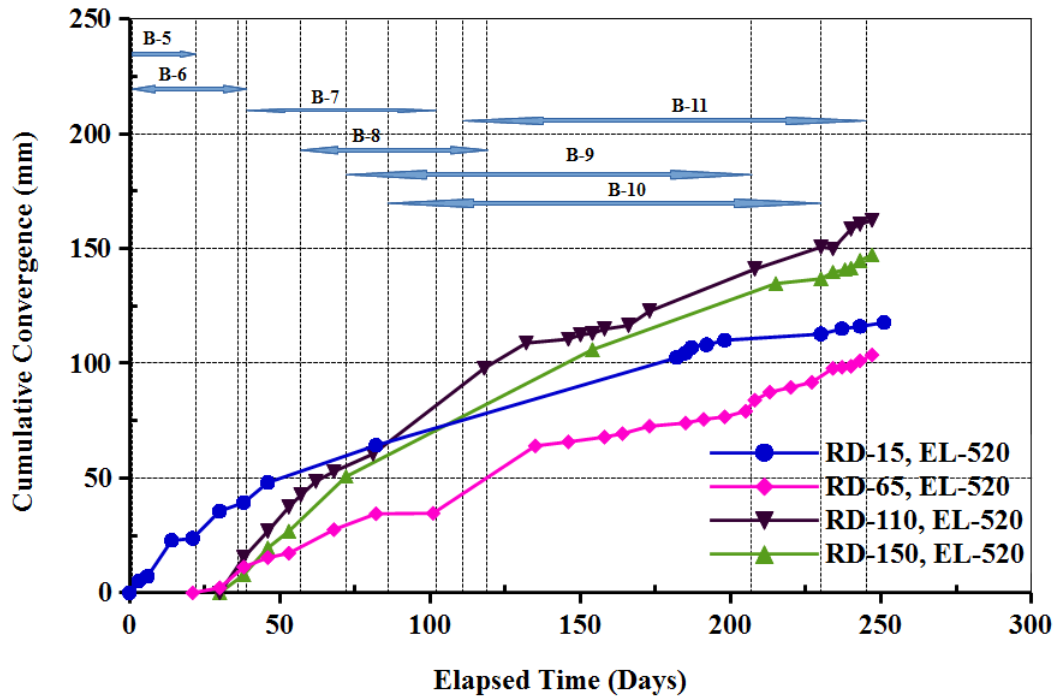


Fig. 4.23 Cumulative convergence of walls at powerhouse cavern at EL-520 during excavation of main benches

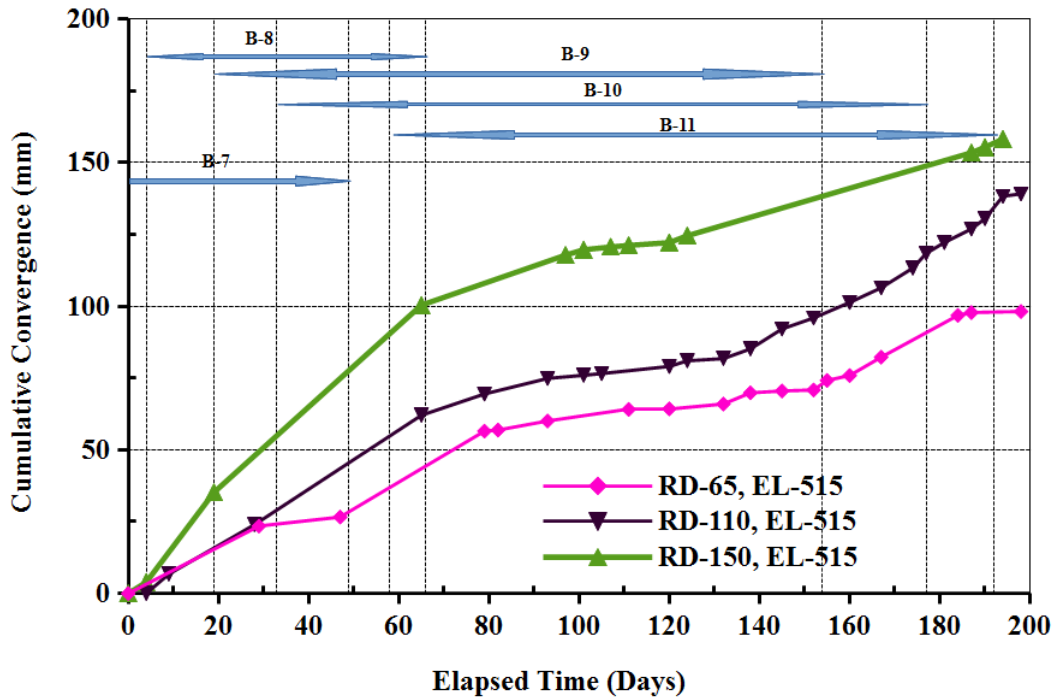


Fig. 4.24 Cumulative convergence of walls at powerhouse cavern at EL-515 during excavation of main benches

Convergence rates calculated from the measured convergence are presented in Figs. 4.25 to 4.28.

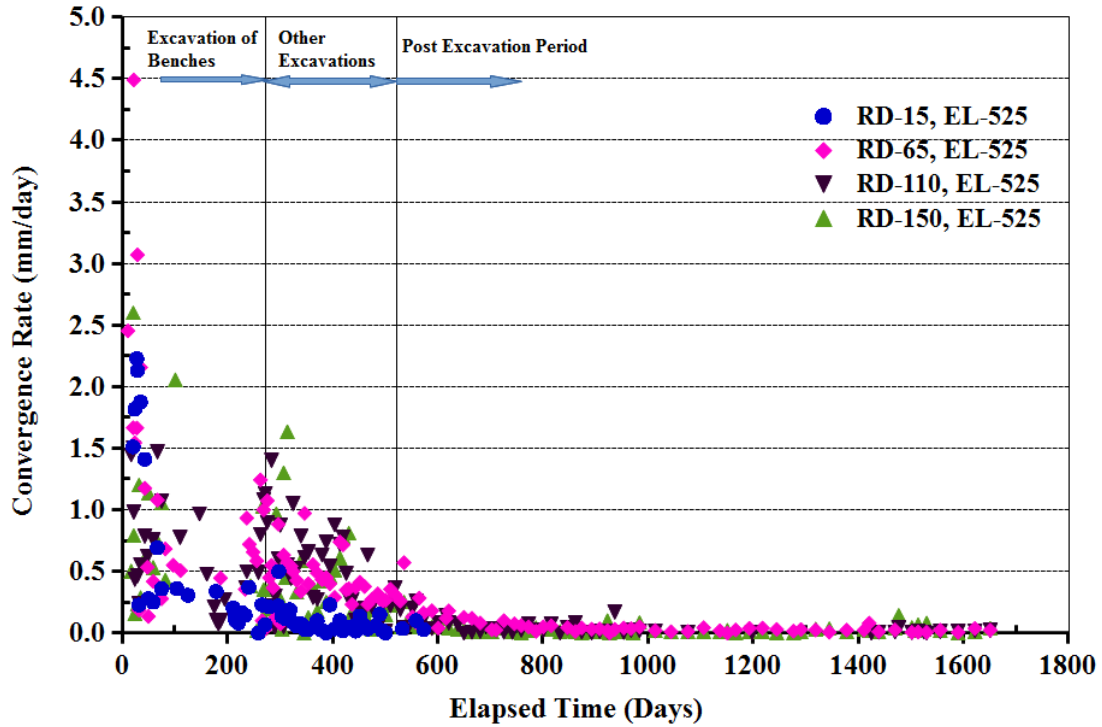


Fig. 4.25 Convergence rate of walls at powerhouse cavern at EL-525

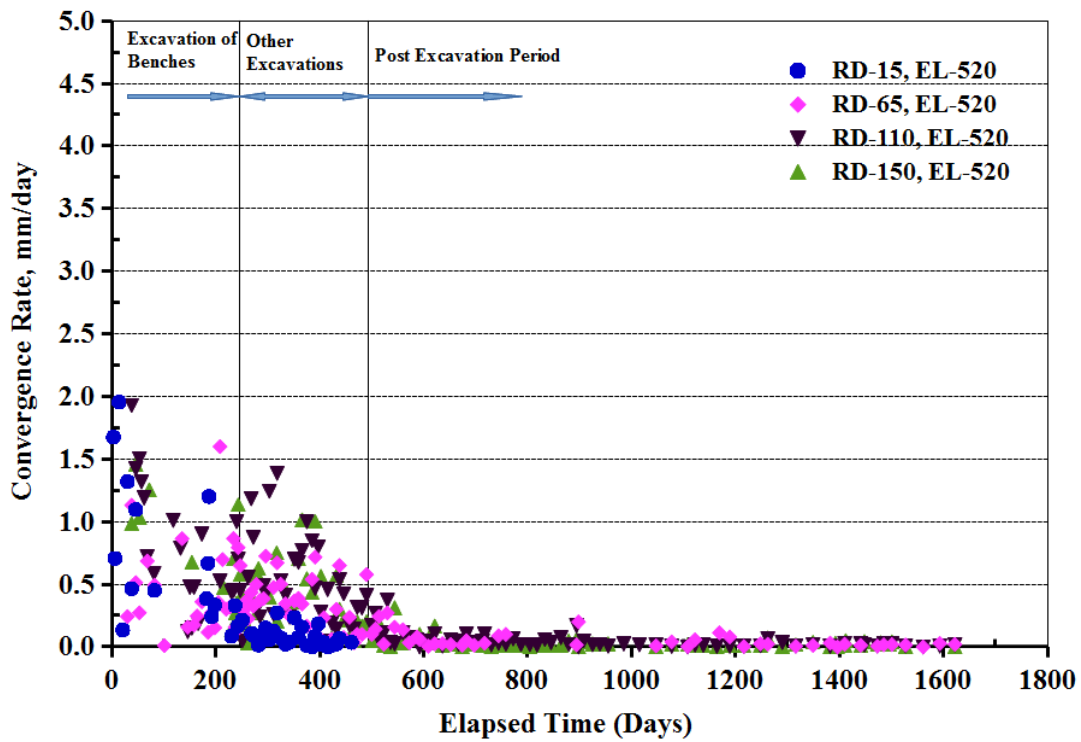


Fig. 4.26 Convergence rate of walls at powerhouse cavern at EL-520

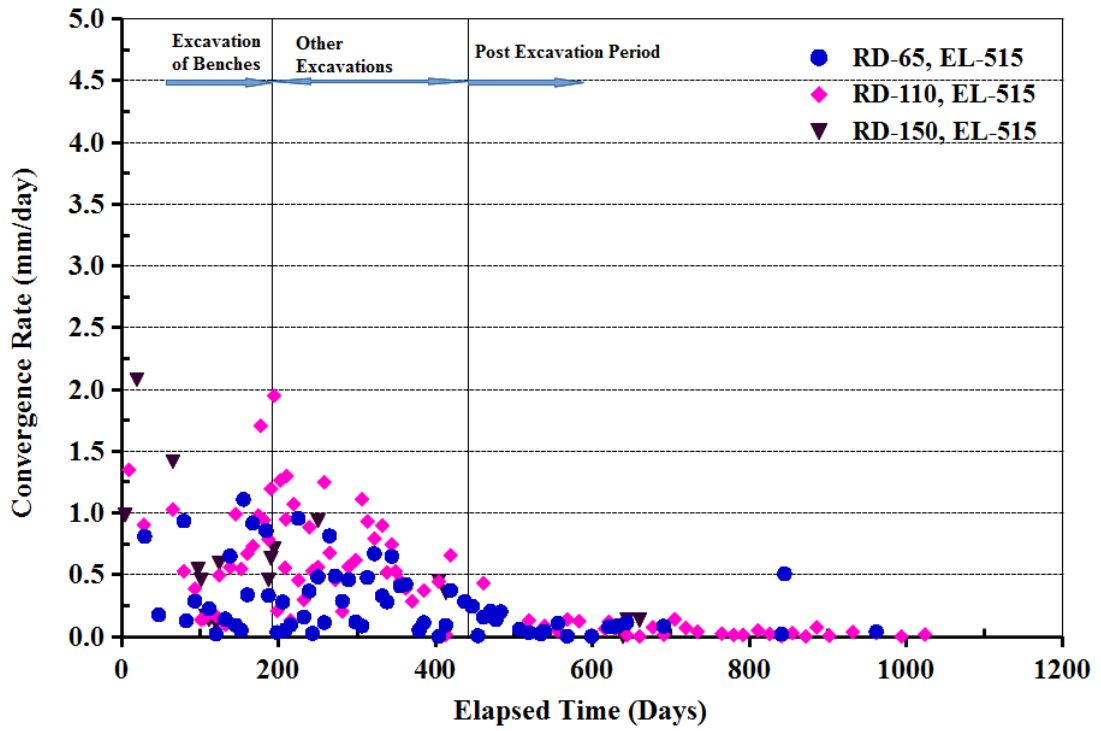


Fig. 4.27 Convergence rate of walls at powerhouse cavern at EL-515

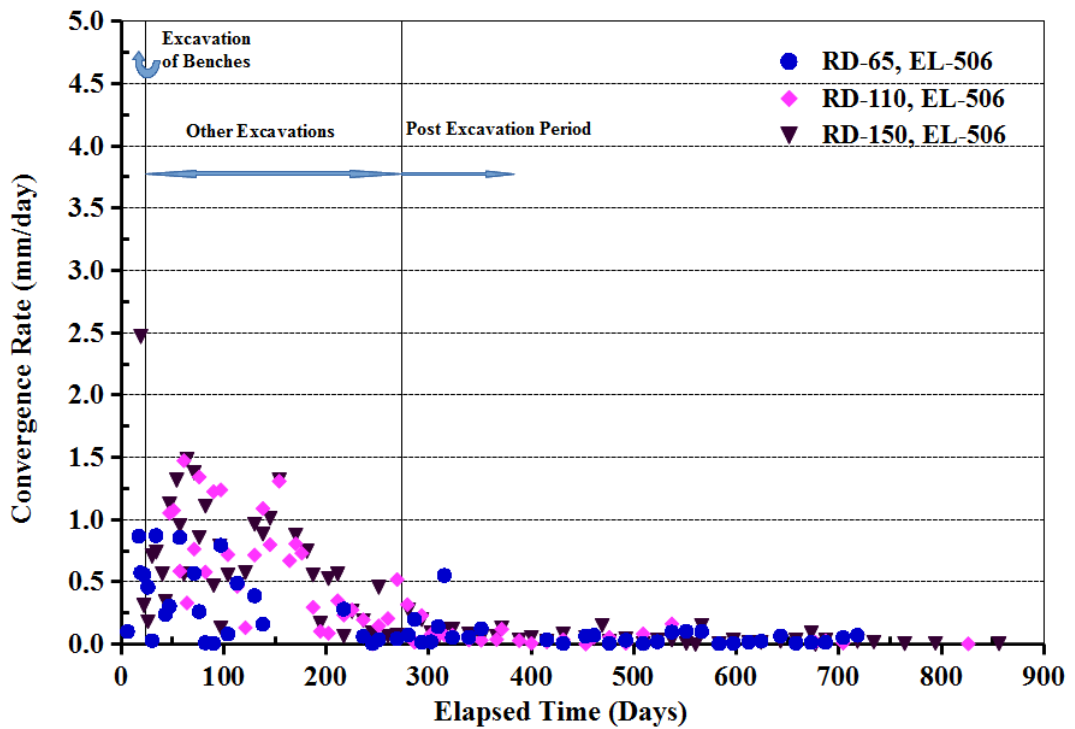


Fig. 4.28 Convergence rate of walls at powerhouse cavern at EL-506

Convergence rate during the excavation of main benches at EL-525 was very high (maximum at RD-65, 4.49mm/day and at RD-150, 2.6mm/day) as shown in Fig. 4.25, which reduced to 0.5mm/day at the end of complete excavation. At EL-520, convergence rate upto 1.95mm/day was observed as shown in Fig. 4.26 and reduced to 0.5mm/day at the end of complete excavation. At EL-515, convergence rate upto 2.08mm/day was observed as shown in Fig. 4.27. This reduced to 0.66mm/day at the end of complete excavation. At EL-506, convergence rate upto 2.47mm/day was observed as shown in Fig. 4.28 and reduced to 0.52mm/day at the end of complete excavation. Total convergence measured during a period of 4.5 years and the computed strain (taking the width of powerhouse cavern as 20.4m) are summarised in Table 4.19.

Table 4.19 Summary of convergence observations at powerhouse cavern

	EL-525		EL-520		EL-515		EL-506	
	Total Convergence (mm)	Per cent strain	Total Convergence (mm)	Per cent strain	Total Convergence (mm)	Per cent strain	Total Convergence (mm)	Per cent strain
RD-15	135.3*	0.66	133.3*	0.65	-		-	
RD-65	355.2	1.74	218.8	1.07	199.59	0.98	105.91	0.52
RD-110	328.8	1.61	321.4	1.58	314.56	1.54	154.56	0.76
RD-150	267.2	1.31	256.9	1.26	290.78	1.43	188.2	0.92
Max	355.2	1.74	321.4	1.58	314.56	1.54	188.2	0.92
Min	135.3	0.66	133.3	0.65	199.59	0.98	105.91	0.52

*could not monitor it during post excavation period and excavation was done upto EL-515m only (service bay area)

Convergence percentage and rate of change in convergence were calculated during excavation of main benches, during entire period of excavation and during post excavation period from the original data and are presented in Table 4.20.

In the service bay area (RD-15), where excavation was done upto EL-514.5m, convergence observed at EL-525 and EL-520 were 135.3mm and 133.3mm, respectively. Percentage strain calculated during the monitoring period taking width of the powerhouse cavern (20.4m) was 0.66%. Whereas in unit bay area (RD-60 to RD-206) where excavation extended till EL-499, convergence upto 355.2mm was observed with percentage strain of 1.74%. At EL-520, maximum percentage strain was 1.58% at RD-110 and at EL-515, maximum percentage strain was 1.54% at RD-110. At EL-506, the maximum percentage strain observed was 0.92% at RD-150.

Table 4.20 Details of cumulative convergence measurements at powerhouse cavern

	Total Convergence (mm)	Convergence during excavation of main benches (mm)	Convergence rate during excavation of main benches (mm/day)	Convergence after complete excavation (mm)	Convergence rate during complete excavation (mm/day)	Convergence during post excavation period (mm)	Convergence rate during post excavation Period (mm/day)
EL-525							
RD-15	135.3	110.8 (81.89%)	0.41	132.3 (97.78%)	0.25	-	-
RD-65	355.2	197.2 (55.52%)	0.71	305 (85.87%)	0.58	50.2	0.045
RD-110	328.8	194.4 (59.12%)	0.70	304.2 (92.52%)	0.58	24.6	0.022
RD-150	267.2	159.3 (59.62%)	0.58	238.8 (89.37%)	0.45	28.4	0.025
EL-520							
RD-15	133.3	116.1 (87.10%)	0.48	-	-	-	-
RD-65	218.8	103.7 (47.39%)	0.42	181.7 (83.04%)	0.36	37.1	0.033
RD-110	321.4	162.4 (50.53%)	0.66	287.5 (89.45%)	0.58	33.9	0.030
RD-150	256.9	147.2 (57.30%)	0.60	233.7 (90.97%)	0.47	23.2	0.021
EL-515							
RD-65	199.59	98.19 (49.20%)	0.50	173.39 (86.87%)	0.39	26.2	0.051
RD-110	314.56	138.32 (43.97%)	0.71	278.47 (88.53%)	0.50	36.09	0.063
RD-150	290.78	158.24 (54.42%)	0.82	268.37 (92.29%)	0.65	22.41	0.044
EL-506							
RD-65	105.91	-	-	83.31 (78.66%)	0.30	22.6	0.052
RD-110	154.56	-	-	138.12 (89.36%)	0.50	16.44	0.030
RD-150	188.20	-	-	165.32 (87.24%)	0.59	22.88	0.040

It was observed that 49-58% of total measured convergence during a period of 4.5 years occurred during the excavation of main benches, which reached to 87-89% when all excavation activity was completed in the powerhouse complex. This indicates that about 11%-13% of total observed convergence occurred during post excavation period.

Average convergence rate during excavation of benches varied from 0.56mm/day to 0.67mm/day, whereas, convergence rates during other miscellaneous excavations varied from 0.38 to 0.49mm/day. However, for entire excavation period, the average convergence rate varied from 0.25mm/day to 0.65mm/day. During the post excavation period (monitored for 3 years), convergence of 16-50mm was observed at various locations (Table 4.20). Average convergence rate during the post excavation stage varied from 0.021mm/day to 0.063mm/day.

Monitoring of cumulative convergence between upstream and downstream walls of powerhouse cavern indicated high displacement of side walls with strain varying from 0.92 to 1.74% in the unit bay area and upto 0.66% in the service bay area. Convergence data clearly indicated that in the cavern in Himalayas, where rock mass predominantly consisted of phyllites and phyllitic quartzites, rock mass continue to deform even after the completion of excavation.

4.1.6 Load on Rock Bolts in the Walls

Rock bolts (12m long Dywidag make) in upstream and downstream walls of powerhouse cavern were monitored with vibrating wire anchor load cells. Build-up of load in the rock bolt was monitored by regular recording with continuation of excavation of lower benches. Monitoring of these load cells continued during post excavation stage also. Behaviour of rock bolts at EL-529, EL-525, EL-520, EL-515 and EL-506 on upstream and downstream walls are discussed in this section. Entire load cell data in the walls of powerhouse cavern is given in Appendix-2.

EL-529: Load cell data at EL-529 (RD-123 u/s and RD-123 d/s) is shown in Fig. 4.29 and period of benching is marked in the plot and is shown in Fig. 4.30.

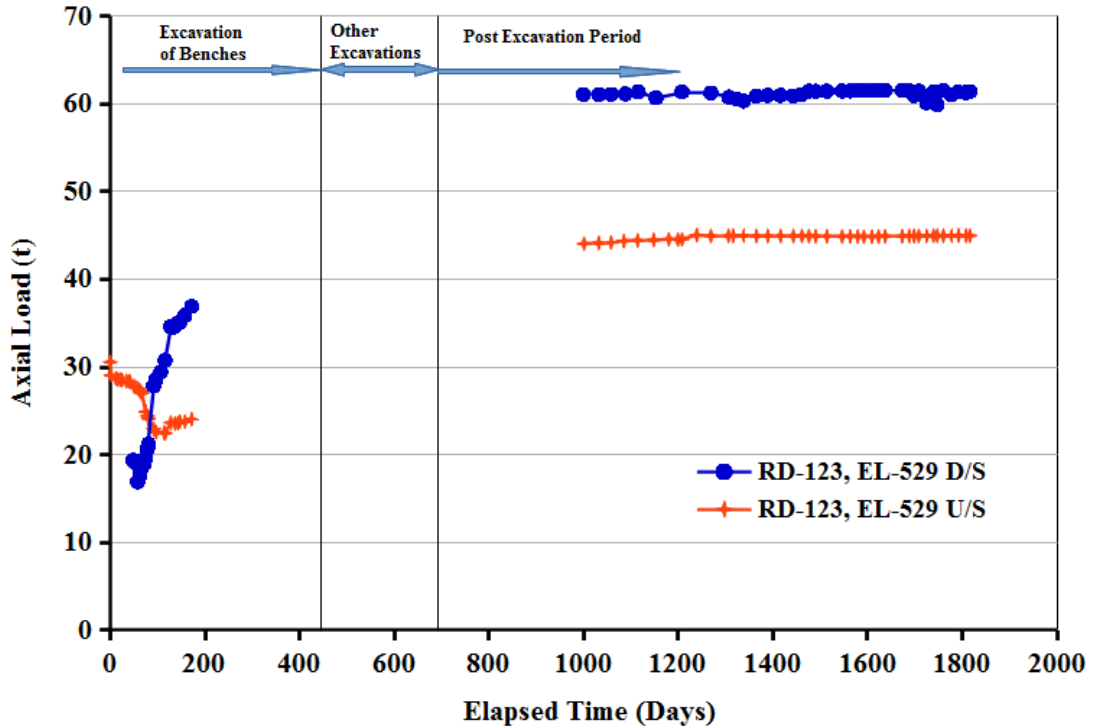


Fig. 4.29 Axial load on rock bolts at EL-529 on walls of powerhouse cavern

At RD-123 upstream, rock bolt was pre-tensioned to 30.59t. Load on the rock bolt started decreasing at a steady rate. For initial 67 days, there was a reduction in load of 3.57t. Subsequently, the load further decreased at faster rate and there was a further reduction of 4.43t during a period of another 30 days. Thus after a period of 116 days, the load on the rock bolt was 22.46t (a decrease of 8.13t). During this period, the excavation of second bench had already begun. Since, the pre-tensioning of the rock bolts was very high, the rock mass near the wall surface might have lost the capacity to transfer the load arising out of the excavation of the lower bench to rock bolt and allowing the wall deformation to take place. However, when the excavation of the 3rd bench started, the load on the rock bolts stabilized and there was marginal increase in the load on rock bolt. The load loss of 8t occurred during the excavation of 1st bench and 4t during the excavation of 2nd bench. There was an increase in load of 1.22t due to the excavation of the 3rd bench. The load increased by only 0.39t during the excavation of 4th bench.

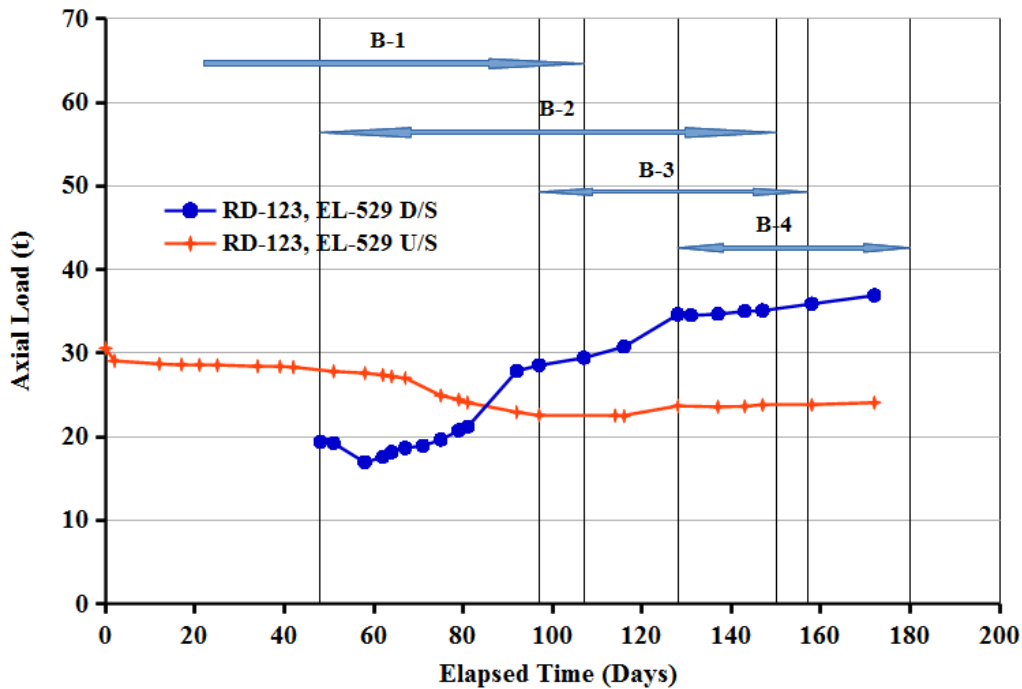


Fig. 4.30 Axial load on rock bolts at EL-529 on walls of powerhouse cavern during excavation of main benches

Load cell at RD-123 downstream side was pre-tensioned to 19.37t. It could be noted from Fig. 4.30 that there was a reduction of 2.45t during the initial 10 days. Later, the load on rock bolt started increasing. Load on rock bolt increased by 4.26t during a period of 23 days. There was an increase of 18.16t (increase from 16.93t to 35.09t) due to the excavation of 2nd bench. There was an increase of 7.36t (from 28.54t to 35.90t) load on the bolt due to the excavation of 3rd bench. The increase in load during the excavation of the 4th bench was 6.13t, which also suggested the diminishing influence of the lower benches on the rock bolt.

EL-525: Load cell data of rock bolts at EL-525 upstream wall and data during excavation of main benches are shown in Figs. 4.31 and 4.32, respectively. Load cells at RD-16.8, RD-62 and RD-106 on upstream wall at EL-525m were installed during the excavation of bench-3. Load on rock bolts at RD-16.8 and RD-62 started increasing when bench-4 excavation started. At RD-16.8, maximum increase in load was recorded during excavation of bench-4 (9.71t). At RD-62, maximum increase in load occurred during excavation of bench-5 (18.60t). At RD-106, excavation of benches had very

little effect. Rock bolt at RD-62 failed and load of 43.01t was recorded by load cell before failure.

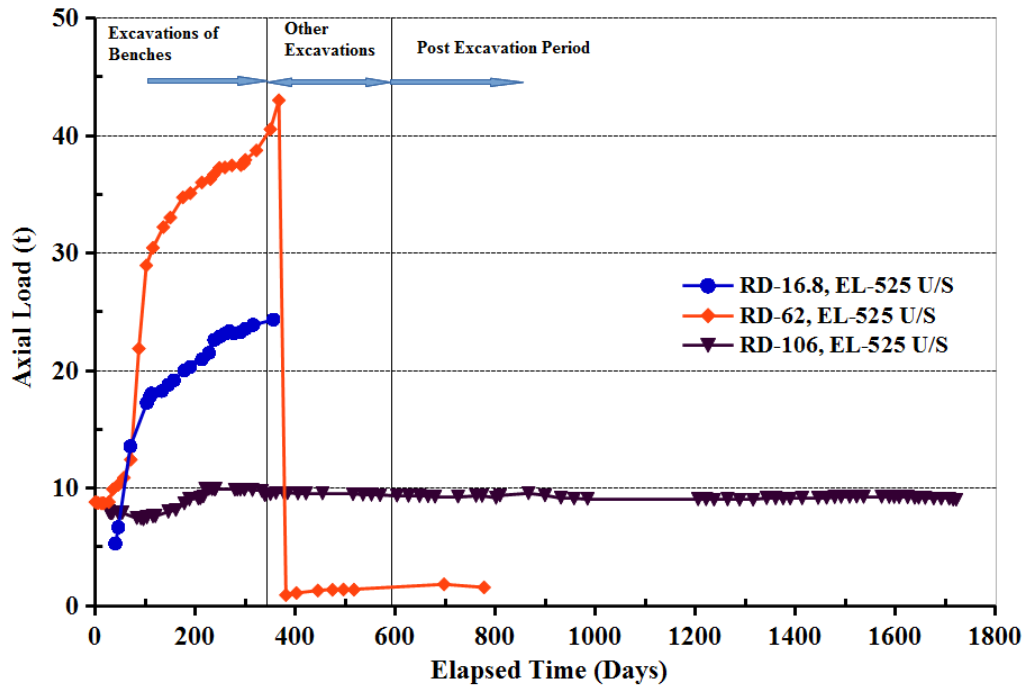


Fig. 4.31 Axial load on rock bolts at EL-525 on upstream wall of powerhouse cavern

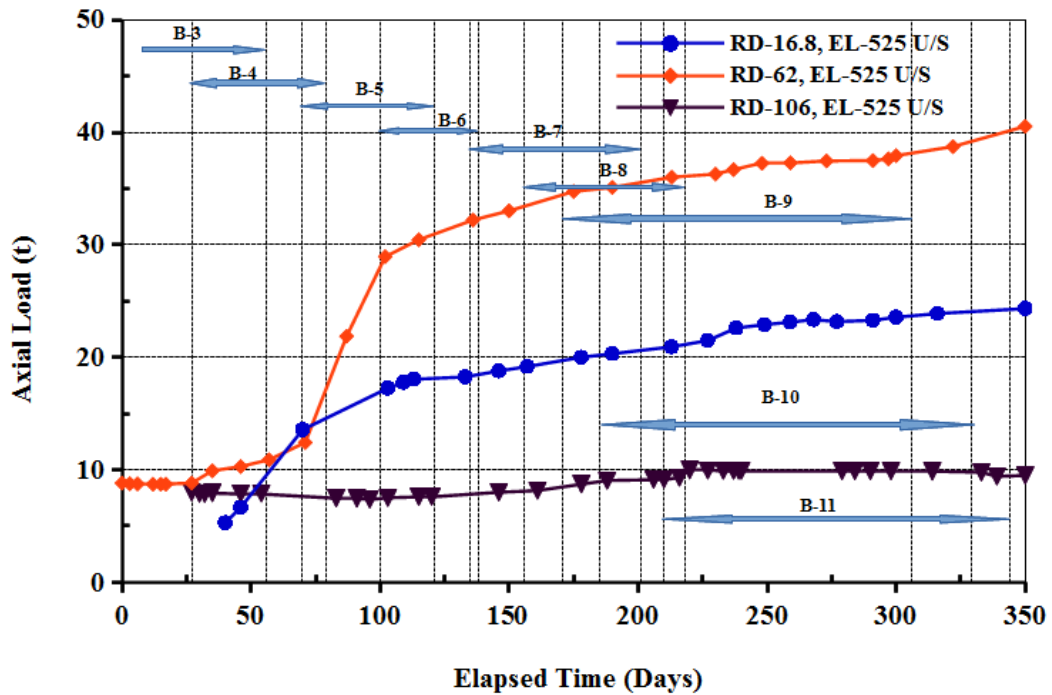


Fig. 4.32 Axial load on rock bolts at EL-525 on upstream wall of powerhouse cavern during excavation of main benches

Load cell data on rock bolts at EL-525 downstream wall and data during excavation of main benches are shown in Figs. 4.33 and 4.34, respectively.

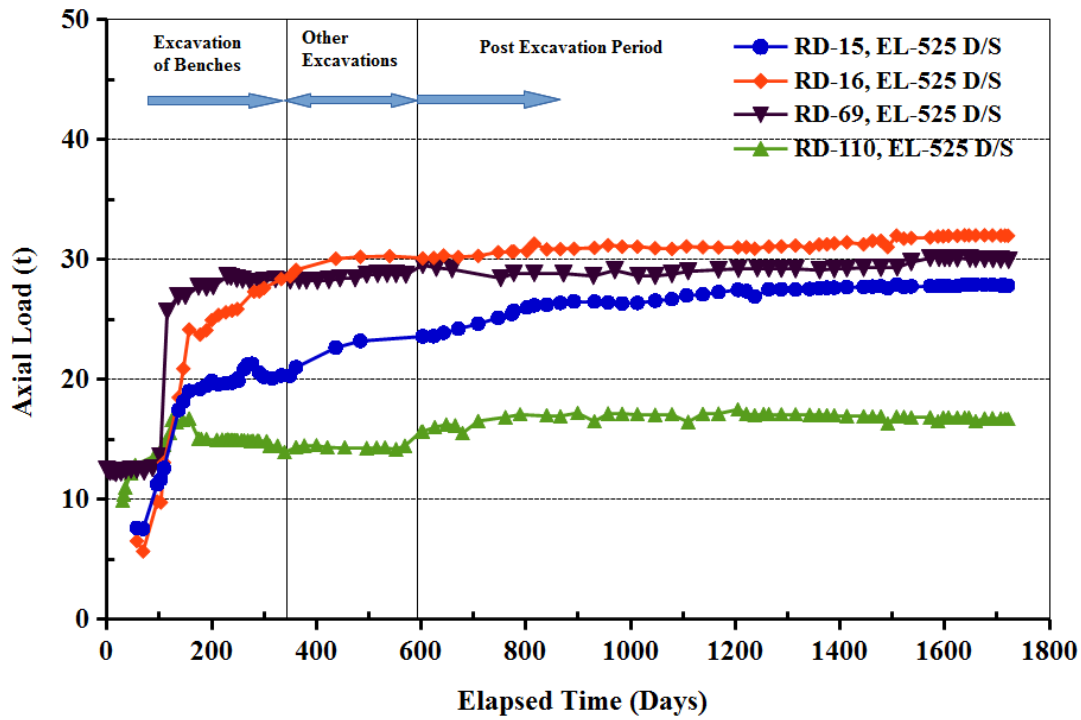


Fig. 4.33 Axial load on rock bolts at EL-525 on downstream wall of powerhouse cavern

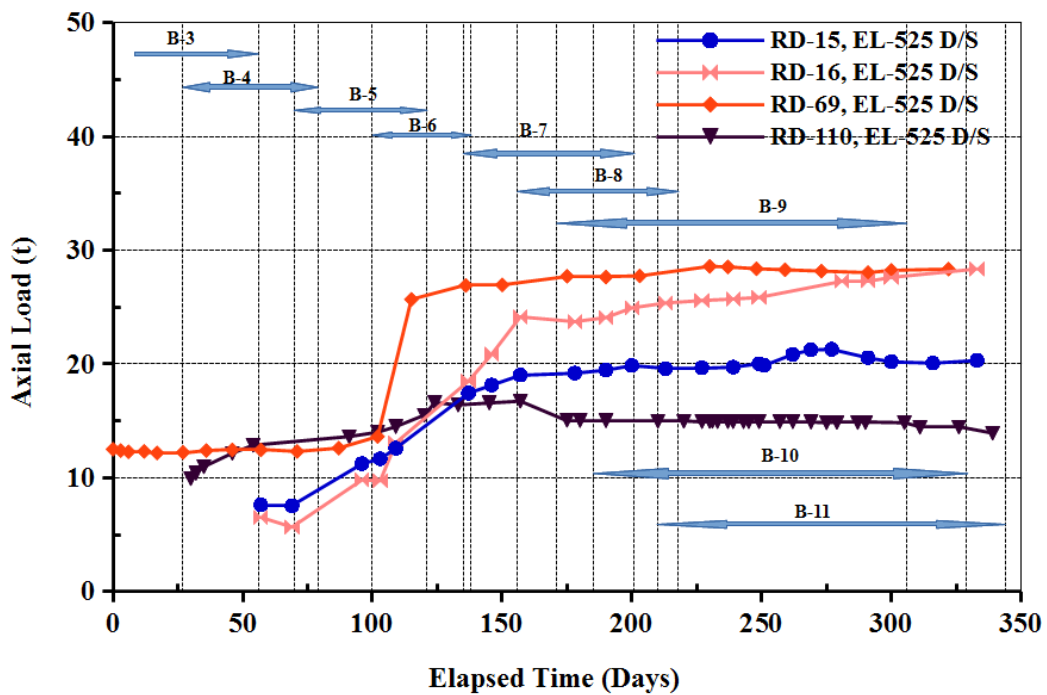


Fig. 4.34 Axial load on rock bolts at EL-525 on downstream wall of powerhouse cavern during excavation of main benches

Load cells at RD-15, RD-16, RD-69 and RD-110 on downstream wall at EL-525 were installed during excavation of bench-3 and 4. Excavation of bench-5 had maximum influence on the rock bolts at RD-15, RD-16 and RD-69, with an increase of 7.5t, 9.83t and 14.06t, respectively. Excavation of bench-4 had increased load at RD-110 by 3.57t.

EL-520: Load cell data of rock bolts at EL-520 upstream wall and data during excavation of main benches are shown in Figs. 4.35 and 4.36, respectively.

Load cells at RD-15, RD-65, RD-110 and RD-150 on upstream wall at EL-520 were installed during the excavation of bench-4. Excavation of bench-5 had maximum influence on rock bolts at RD-15, RD-65, RD-110 and RD-150 with an increase of 9.61t, 13.24t, 5.18t and 11t, respectively.

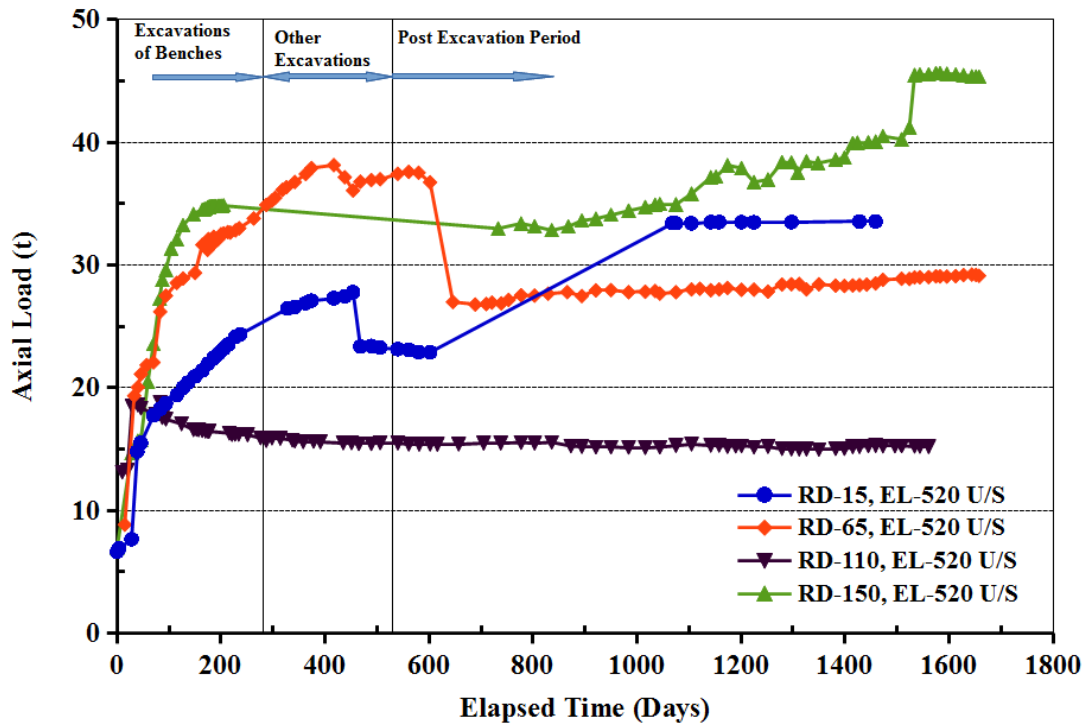


Fig. 4.35 Axial load on rock bolts at EL-520 on upstream wall of powerhouse cavern

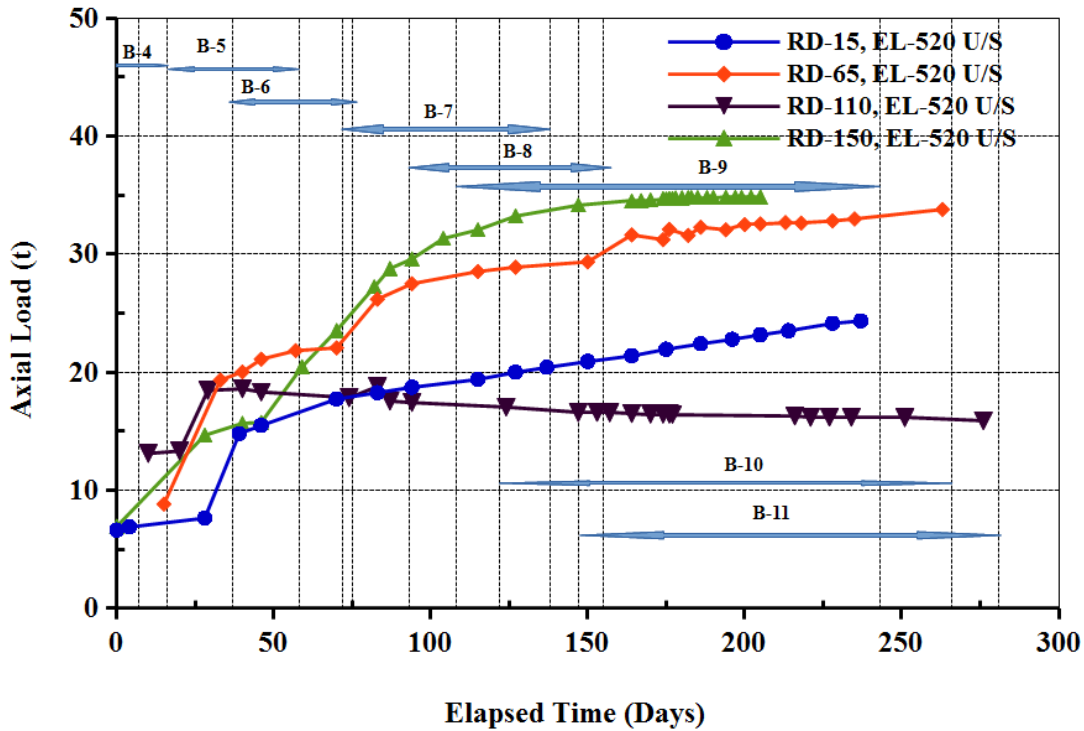


Fig. 4.36 Axial load on rock bolts at EL-520 on upstream wall of powerhouse cavern during excavation of main benches

Load cell data on rock bolts at EL-520 downstream wall and data during excavation of main benches are shown in Figs. 4.37 and 4.38, respectively.

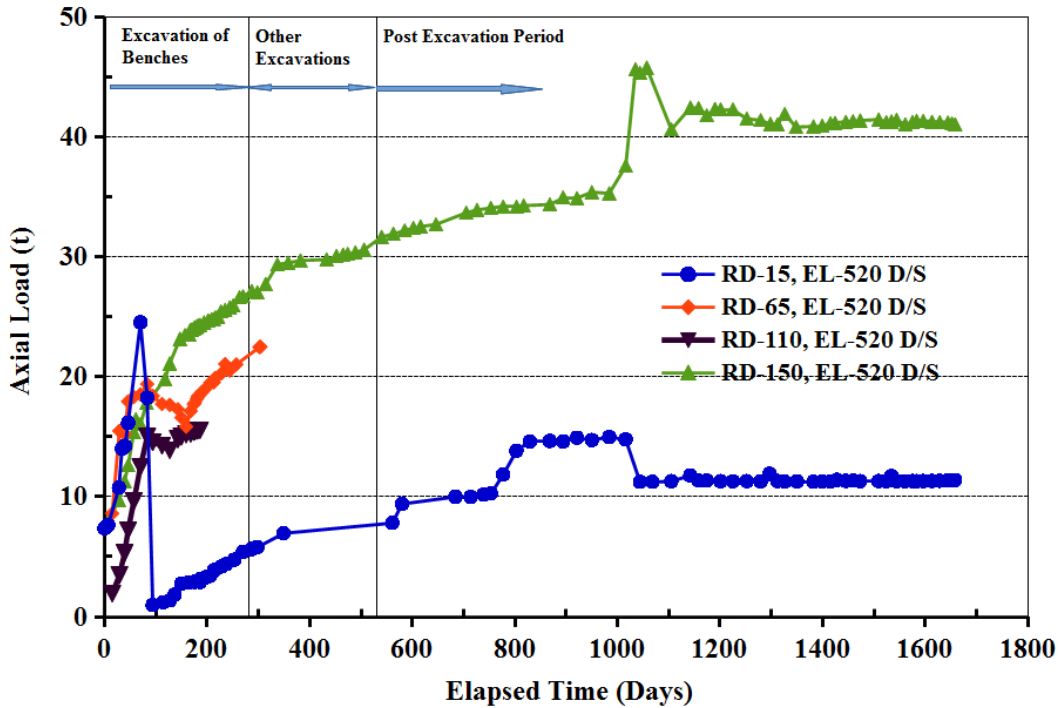


Fig. 4.37 Axial load on rock bolts at EL-520 on downstream wall of powerhouse cavern

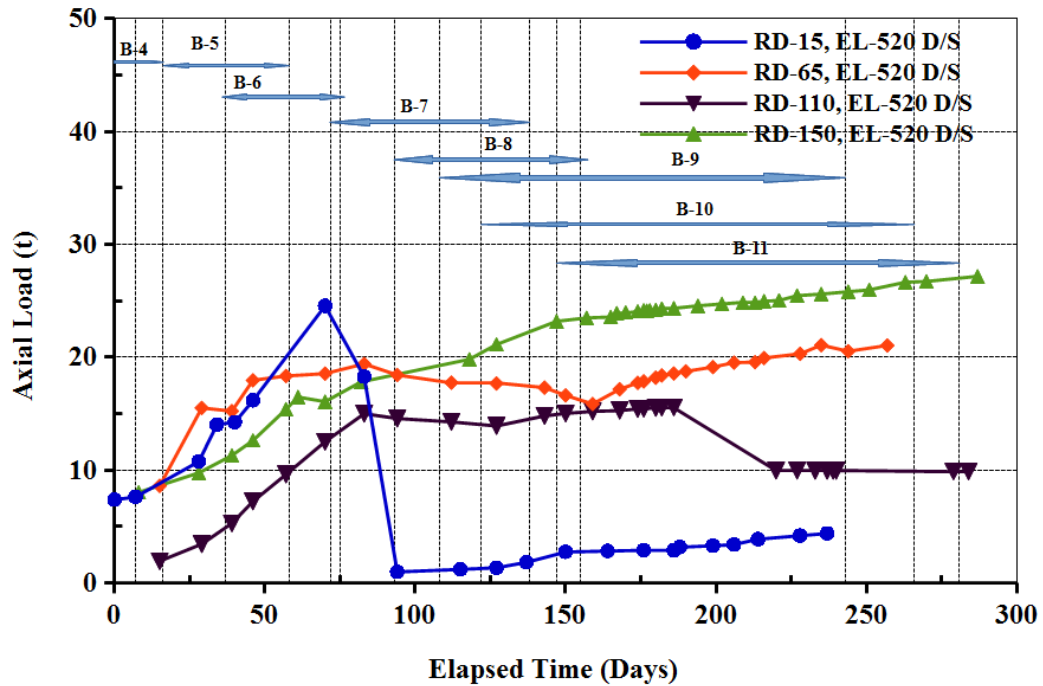


Fig. 4.38 Axial load on rock bolts at EL-520 on downstream wall of powerhouse cavern during excavation of main benches

On downstream wall, load cells at RD-15, RD-65, RD-110 and RD-150 were installed during excavation of bench-4. Excavation of bench-5 had maximum influence on rock bolts at RD-15, RD-65 and RD-150 with an increase of 12.98t, 9.49t, and 7.48t, respectively. At RD-110, bench-6 had maximum influence with an increase of 9.60t.

EL-515: Load cell data of rock bolts at EL-515 upstream wall and data during excavation of main benches are shown in Figs. 4.39 and 4.40, respectively.

Load cells at RD-65, RD-110 and RD-150 on upstream wall at EL-515 were installed during the excavation of bench-6 and 7, whereas load cells at RD-120 and RD-142 were installed later during excavation of benches 9, 10 and 11. Excavation of bench-7 had maximum influence on rock bolts at RD-110 and RD-150 with an increase of 1.28t and 7.1t, respectively. Load at RD-65 increased continuously during the excavations of bench-8 to bench-11 in the range of 2.98t to 8.66t.

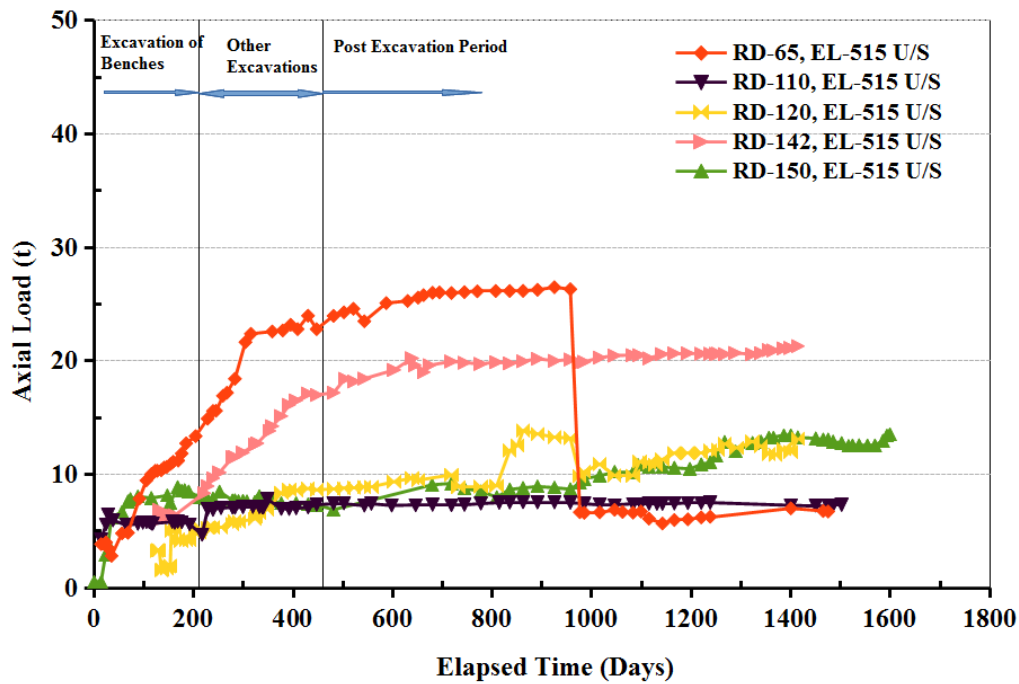


Fig. 4.39 Axial load on rock bolts at EL-515 on upstream wall of powerhouse cavern

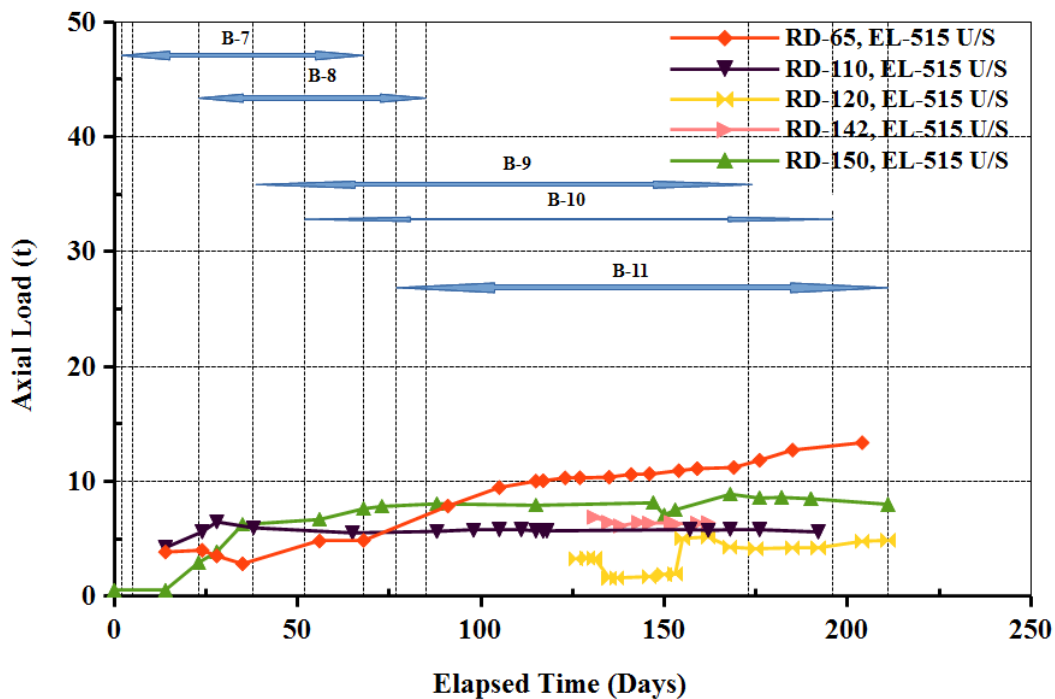


Fig. 4.40 Axial load on rock bolts at EL-515 on upstream wall of powerhouse cavern during excavation of main benches

Load cell data on rock bolts at EL-515 downstream wall and data during excavation of main benches are shown in Figs. 4.41 and 4.42, respectively.

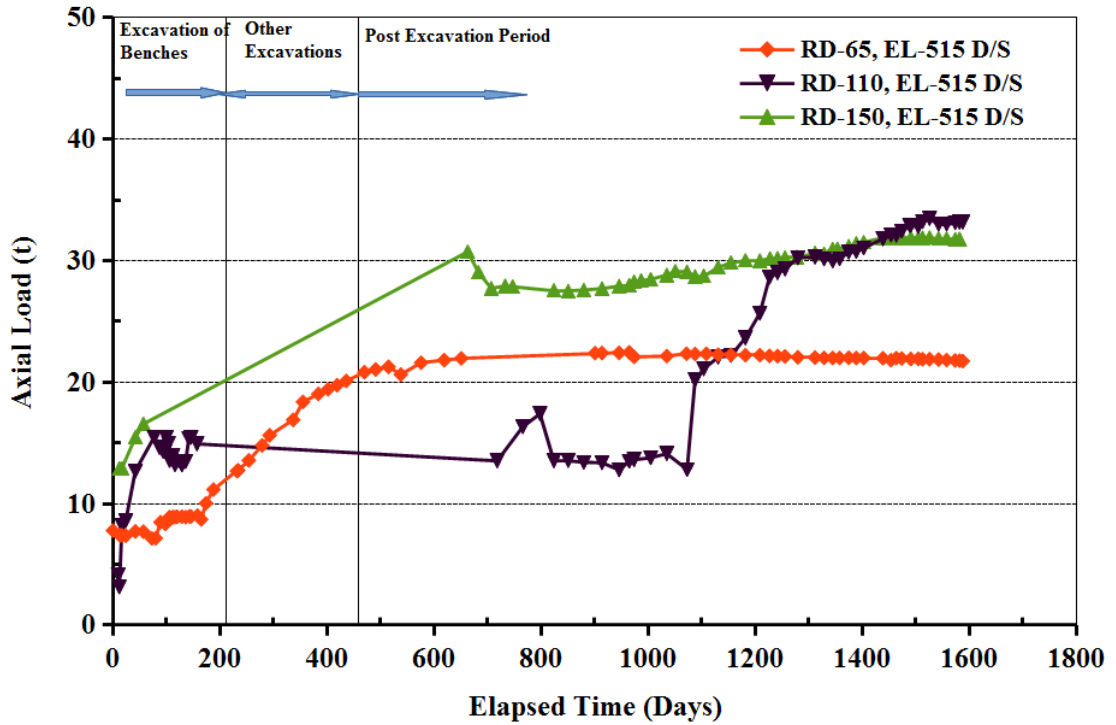


Fig. 4.41 Axial load on rock bolts at EL-515 on downstream wall of powerhouse cavern

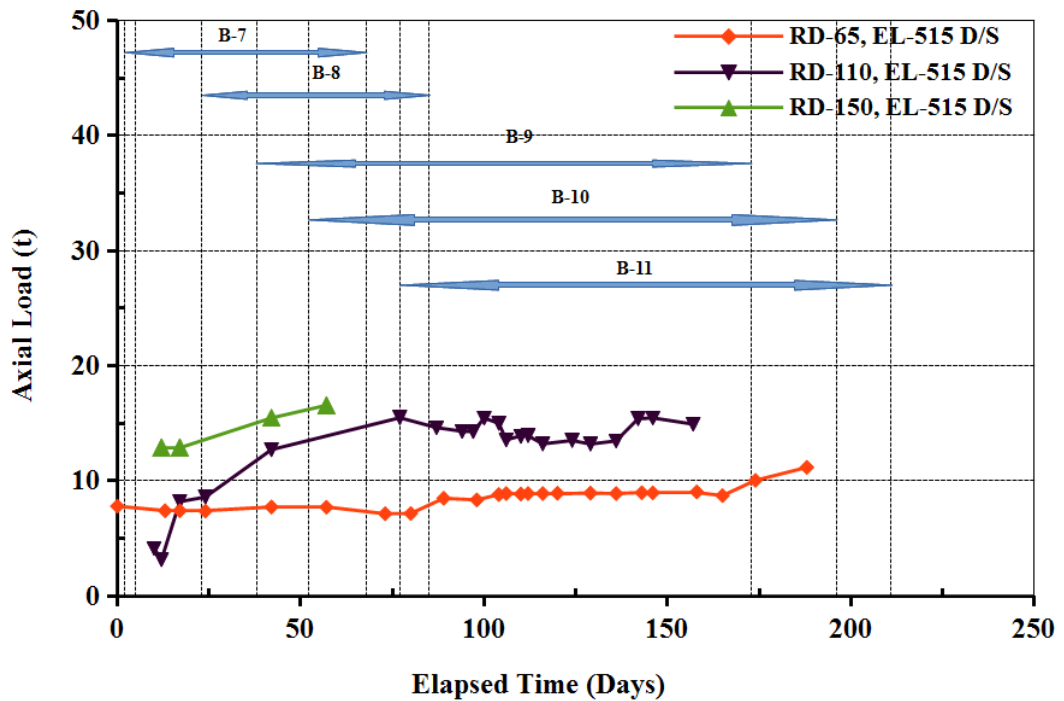


Fig. 4.42 Axial load on rock bolts at EL-515 on downstream wall of powerhouse cavern during excavation of main benches

On downstream wall, load cells at RD-65, RD-110 and RD-150 were installed during excavation of bench-6 and 7. Excavation of bench-7 had maximum influence on rock bolts at RD-110 and RD-150 with an increase of 12.57t and 3.67t, respectively. Load at RD-65 increased continuously during the excavations of bench-8 to bench-11 in the range of 0.33t to 4.03t.

EL-506: Load cell data of rock bolts at EL-506 upstream wall and data during excavation of main benches are shown in Figs. 4.43 and 4.44, respectively.

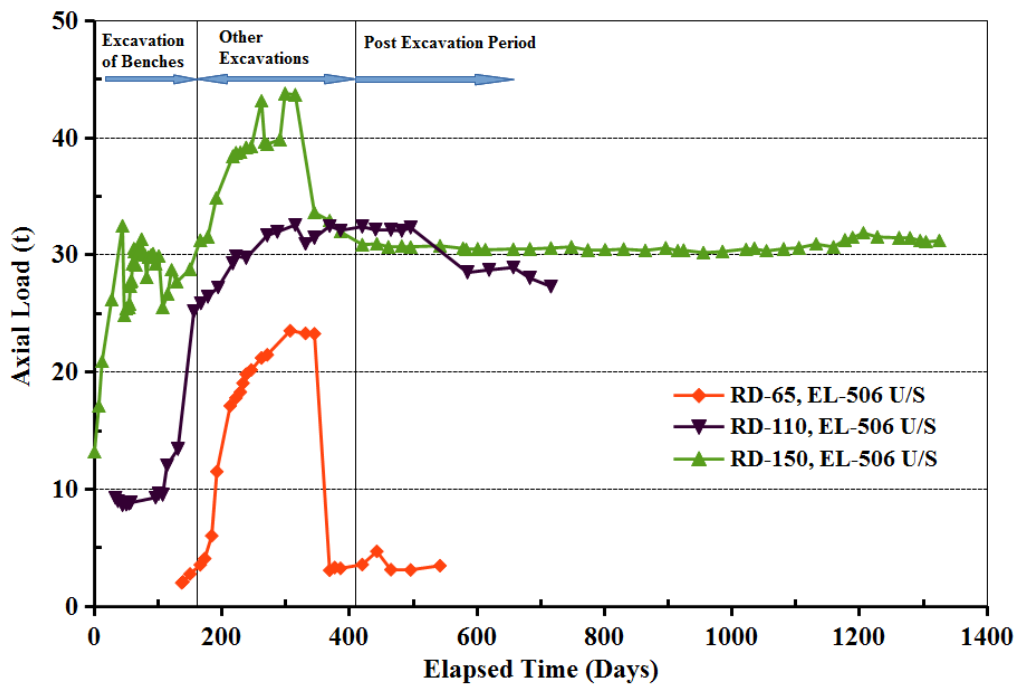


Fig. 4.43 Axial load on rock bolts at EL-506 on upstream wall of powerhouse cavern

Load cells at RD-65, RD-110 and RD-150 on upstream wall at EL-506 were installed during the excavation of bench-8 and 9. Excavation of bench-8 had maximum influence on rock bolt at RD-150 with an increase of 13.03t. Load at RD-110 increased continuously during the excavations of bench-9 to bench-11 in the range of 8.74t to 16.24t.

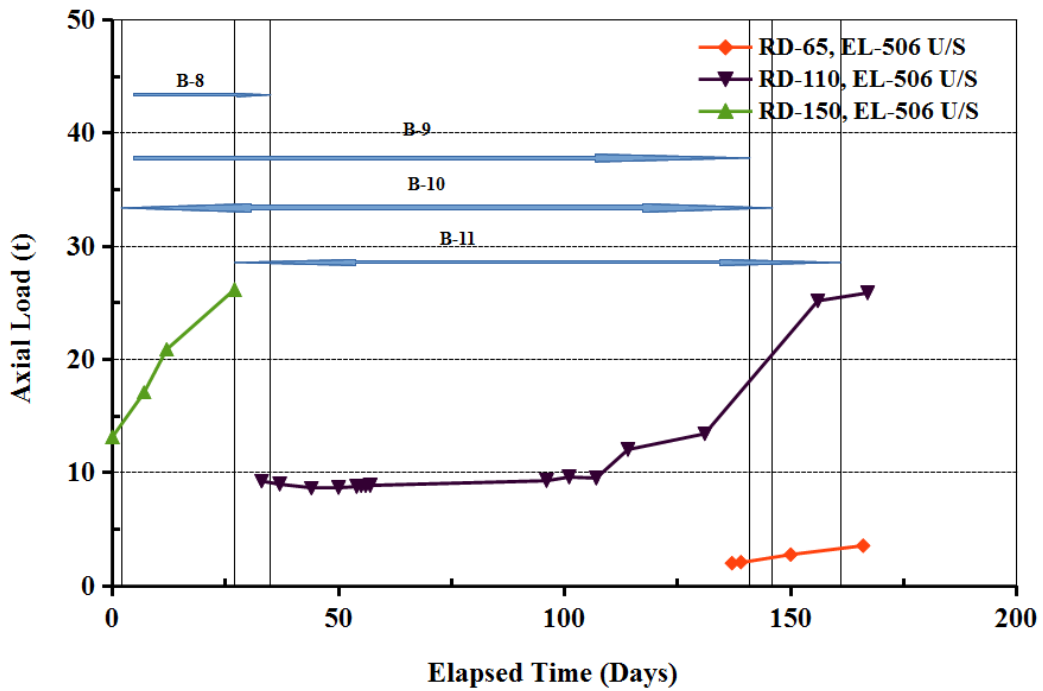


Fig. 4.44 Axial load on rock bolts at EL-506 on upstream wall of powerhouse cavern during excavation of main benches

Load cell data on rock bolts at EL-506 downstream wall and data during excavation of main benches are shown in Figs. 4.45 and 4.46, respectively.

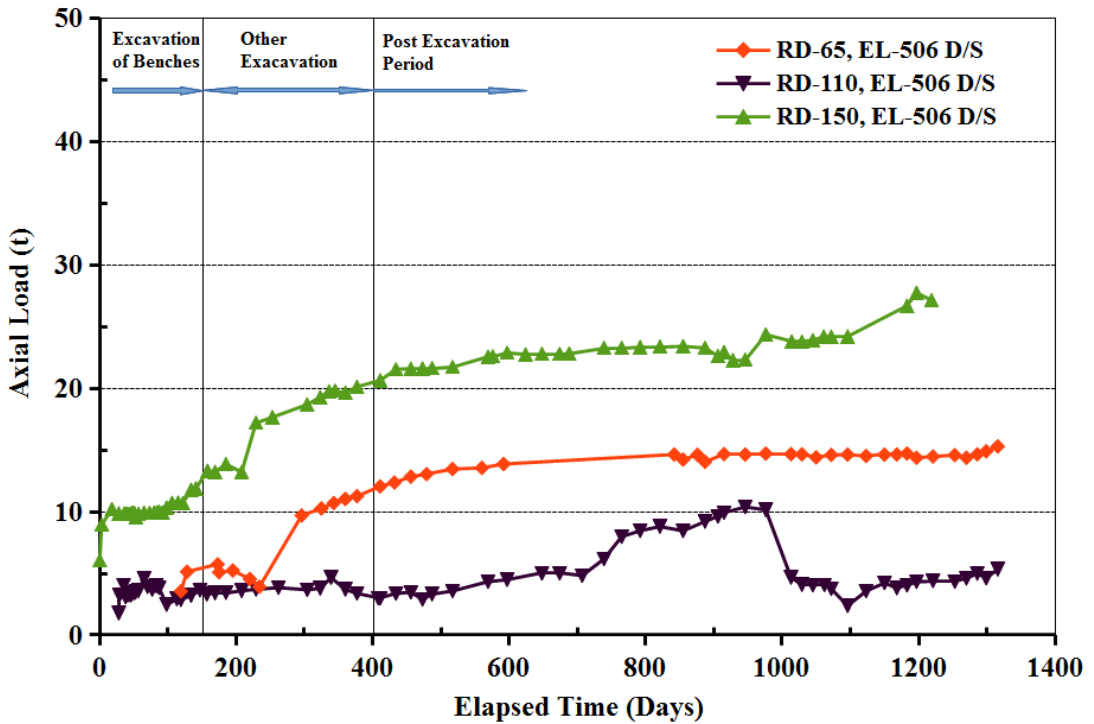


Fig. 4.45 Axial load on rock bolts at EL-506 on downstream wall of powerhouse cavern

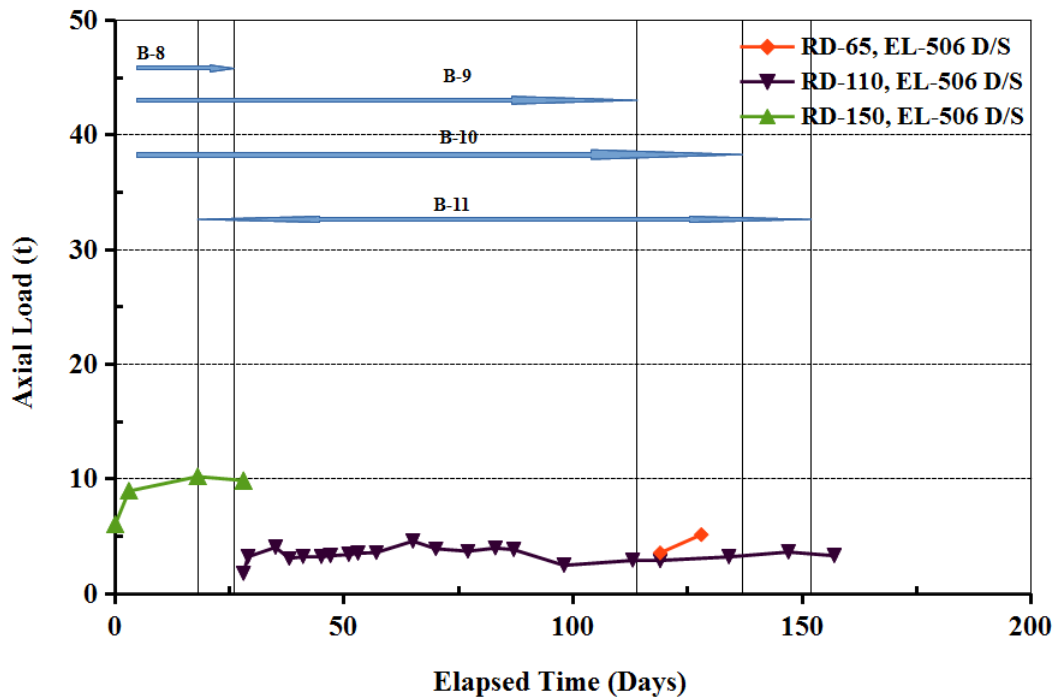


Fig. 4.46 Axial load on rock bolts at EL-506 on downstream wall of powerhouse cavern during excavation of main benches

On downstream wall, load cells at RD-65, RD-110 and RD-150 were installed during excavation of benches 8 to 10. Excavation of bench-8 had maximum influence on rock bolts at RD-150 with an increase of 3.84t, whereas, load at RD-110 increased continuously during the excavation of benches 9 to 11 in the range of 1.44t to 1.86t.

Load on 12m Dywidag rock bolts on the walls of powerhouse cavern is summarised in Table 4.21. Percentage of increase in load after benching, after complete excavation and post excavation stage were calculated with respect to the final load on the rock bolt monitored during post excavation stage. Percentage of >100% indicates that final load on that particular rock bolt at the end of monitoring period is less than the load under reference and negative percentage indicates that load under reference is less than the load in the previous stage.

Table 4.21 Summary of load on rock bolts on the walls of powerhouse cavern

	After Benching		After Complete Excavation		Post Excavation		
Location	Load (t)	% of Increase in Load	Load (t)	% of Increase in Load	Load (t)	% of Increase in Load	Final Load on Rock Bolt (t)
Downstream Side							
EL-525							
RD-15	20.3	73.0%	23.59	11.8%	27.81	15.2%	27.81
RD-16	28.6	89.4%	30.09	4.7%	31.98	5.9%	31.98
RD-69	28.6	95.5%	29.54	3.1%	29.95	1.4%	29.95
RD-110	13.93	83.5%	15.66	10.4%	16.69	6.2%	16.69
EL-520							
RD-15	5.63	49.4%	7.81	19.1%	11.39	31.4%	11.39
RD-65	21.04	-	22.52	-	-	-	-
RD-110	15.56	-	-	-	-	-	-
RD-150	27.16	66.1%	31.67	11.0%	41.06	22.9%	41.06
EL-515							
RD-65	11.17	51.4%	20.82	44.4%	21.74	4.2%	21.74
RD-110	14.92	45.0%	13.52	-4.2%	33.16	59.2%	33.16
RD-150	16.56	52.1%	25	26.6%	31.78	21.3%	31.78
EL-506							
RD-65	5.74	37.5%	12.06	41.3%	15.3	21.2%	15.3
RD-110	3.63	68.1%	2.99	-12.0%	5.33	43.9%	5.33
RD-150	13.32	49.1%	20.65	27.0%	27.15	23.9%	27.15
Upstream Side							
EL-525							
RD-16.8	24.34	-	-	-	-	-	-
RD-62	40.54	-	43.01	-	-	-	-
RD-106	9.5	105.2%	9.38	-1.3%	9.03	-3.9%	9.03
EL-522							
RD-122	9.14	33.4%	20	39.7%	27.38	27.0%	27.38
EL-520							
RD-15	24.35	72.6%	23.14	-3.6%	33.55	31.0%	33.55
RD-65	34.9	119.8%	37.43	8.7%	29.12	-28.5%	29.12
RD-110	15.89	104.6%	15.48	-2.7%	15.19	-1.9%	15.19
RD-150	34.85	76.9%	32.97	-4.1%	45.33	27.3%	45.33
EL-518							
RD-135	3.01	100.7%	3.17	5.4%	2.99	-6.0%	2.99
EL-515							
RD-65	13.38	199.7%	22.81	140.7%	6.7	-240.4%	6.7
RD-110	4.7	64.3%	7.34	36.1%	7.31	-0.4%	7.31

	After Benching		After Complete Excavation		Post Excavation		
Location	Load (t)	% of Increase in Load	Load (t)	% of Increase in Load	Load (t)	% of Increase in Load	Final Load on Rock Bolt (t)
RD-120	5.21	39.6%	8.65	26.2%	13.15	34.2%	13.15
RD-142	8.98	42.1%	17.01	37.7%	21.31	20.2%	21.31
RD-150	8.36	61.8%	7.34	-7.5%	13.53	45.8%	13.53
EL-506							
RD-65	3.55	102.6%	3.57	0.6%	3.46	-3.2%	3.46
RD-110	25.19	92.2%	32.42	26.5%	27.31	-18.7%	27.31
RD-150	31.26	100.1%	30.89	-1.2%	31.23	1.1%	31.23
EL-505							
RD-135	27.1	83.7%	30.12	9.3%	32.36	6.9%	32.36

On downstream wall at EL-525, about 73 to 95.5% of final load on the bolt (at the end of monitoring period) was recorded during the excavation of main benches and 3.1 to 11.8% was observed during excavation of other tunnels, and 1.4 to 15.2% was observed during post excavation period. At EL-520, about 49.4 to 66.1% of final measured load on the rock bolt was recorded during the excavation of main benches, 11 to 19.1% was observed during other excavations, and 22.9 to 31.4% was observed during post excavation period. At EL-515, about 45 to 52.1% of final measured load on the rock bolt was recorded during the excavation of main benches and -4.2 to 44.4% was observed during other excavations and 4.2 to 59.2% was observed during post excavation period. At EL-506, about 37.5 to 68.1% of final measured load on the rock bolt was recorded during the excavation of main benches and -12 to 41.3% was observed during other excavations, and 21.2 to 43.9% was observed during post excavation period. The data indicated that rock bolts at higher elevations have experienced higher percentage of final recorded load during excavation of main benches and bolts at lower elevations experienced higher percentage of final load during post excavation period.

On upstream wall at EL-525, rock bolt at RD-62 failed before complete excavation and maximum load recorded was 43.01t, out of which 40.54t was recorded during excavation of main benches. At EL-520, about 72 to 119.8% of final measured load on the rock bolt was recorded during the excavation of main benches, -4.1 to 8.7% was

observed during other excavations and -28.5 to 31% was observed during post excavation period. Data shows reduction in load on bolts after bench excavation and during post excavation period. At EL-515, about 39.6 to 199.7% of final measured load on the rock bolt was recorded during the excavation of main benches, -7.5 to 140.7% was observed during other excavations, and -240.4 to 45.8% was observed during post excavation period. At EL-506 also, about 92.2 to 102.6% of final measured load on the rock bolt was recorded during the excavation of main benches, -1.2 to 26.5% was observed during other excavations, and -18.7 to 1.1% was observed during post excavation period. It could be noted that on upstream wall, bolts at almost all elevations have experienced higher percentage of final recorded load during the excavation of benches and reduction of load in some cases after complete excavation and during post excavation period.

Bolts on the upstream wall experienced loads of higher magnitude compared to the bolts on downstream wall. During benching, bolts on upstream wall at almost all elevations were loaded higher (average 87.7%), whereas on downstream wall, only bolts at higher elevation (EL-525, average 85.3%) experienced higher loads. During post excavation, load on the bolts on downstream wall was greater (average 21.4%) than the load on bolts on upstream wall (average 8.7%). In many cases there was reduction in load on upstream wall.

4.1.7 Instrumented Bolt Observations

Instrumented bolts were installed at EL-506 on both upstream and downstream walls of powerhouse cavern at RD-65, RD-110 and RD-150. At RD-140, RD-150 bolts were also installed on upstream wall at EL-515. Strain measured along the rock bolt at 1m interval was analysed and presented here. Listing of all instrumented bolt observations is given in Appendix-2.

RD-65, EL-506 Downstream Wall: Change in microstrains in instrumented bolt on downstream wall at RD-65, EL-506 are shown in Fig. 4.47.

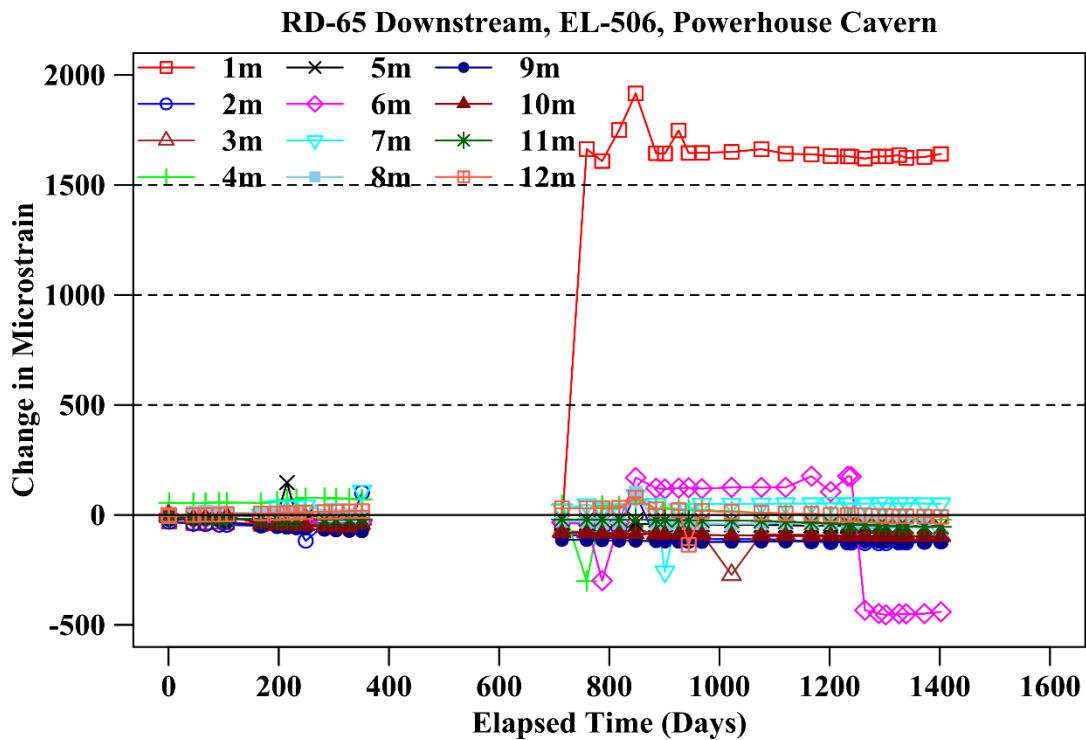


Fig. 4.47 Change in micro strain in instrumented bolt at RD 65, EL 506 at downstream wall of powerhouse cavern

At RD-65 downstream at EL-506, there was an increase in strain (maximum 1916 microstrain) at 1m depth. At 9m, 10m and 11m depths, there was decrease of strain (-5 to -17 microstrain) and at other depths, there was an increase in strain in the range of 100 to 176 microstrain (Fig. 4.47).

RD-110, EL-506 Downstream Wall: Instrumented bolt observations on downstream wall at RD-110, EL-506 are shown in Fig. 4.48.

At RD 110 downstream, increase in strains were observed at 1m, 2m, 4m and 5m depths with increase of 206.5 and 278 microstrain at 1m and 2m depths (Fig. 4.48).

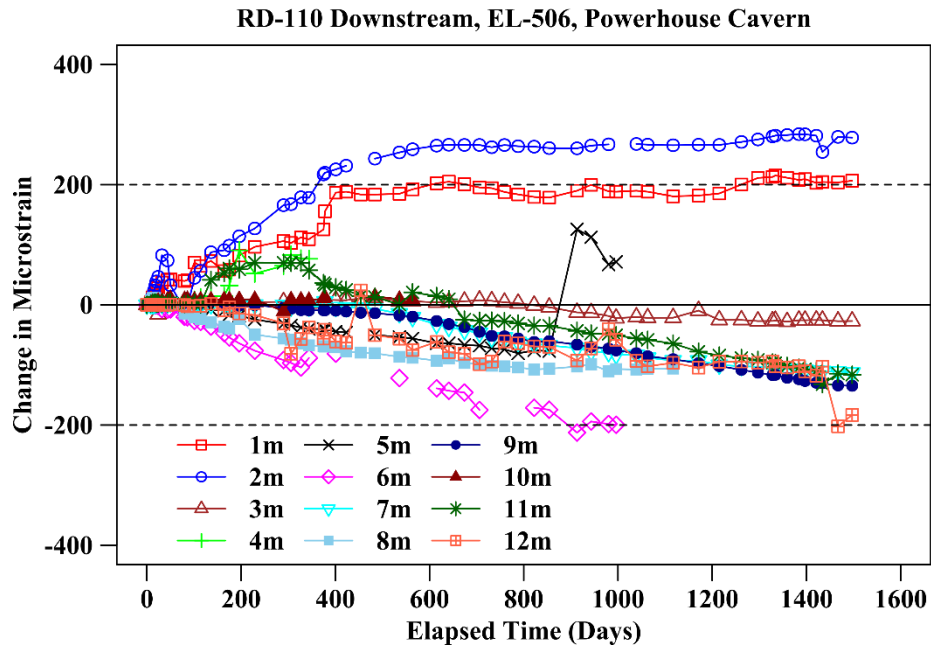


Fig. 4.48 Change in micro strain in instrumented bolt at RD 110, EL 506 at downstream wall of powerhouse cavern

RD-150, EL-506 Downstream Wall: Instrumented bolt observation on downstream wall at RD-150, EL-506 are shown in Fig. 4.49. At this location, increase in strain was observed at 1m and 2m depth with increase of 7.4 and 6.61 microstrain. There was decrease of strain at all other depths (Fig.4.49).

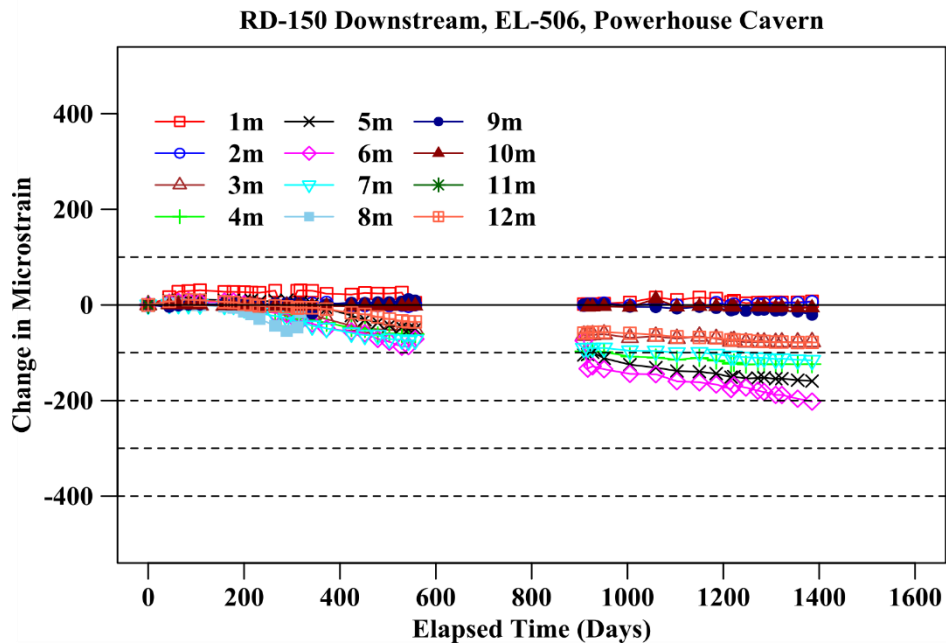


Fig. 4.49 Change in micro strain in instrumented bolt at RD 150, EL 506 at downstream wall of powerhouse cavern

RD-65, EL-506 Upstream Wall: Recordings made on upstream wall at RD-65, EL-506 are shown in Fig. 4.50. At this location, increase in strain was observed at 1m and 8m depth with an increase of 232.55 and 536.25 microstrain. At other depths, there was decrease in strain in the range of -18.34 to -105.48 microstrain (Fig. 4.50).

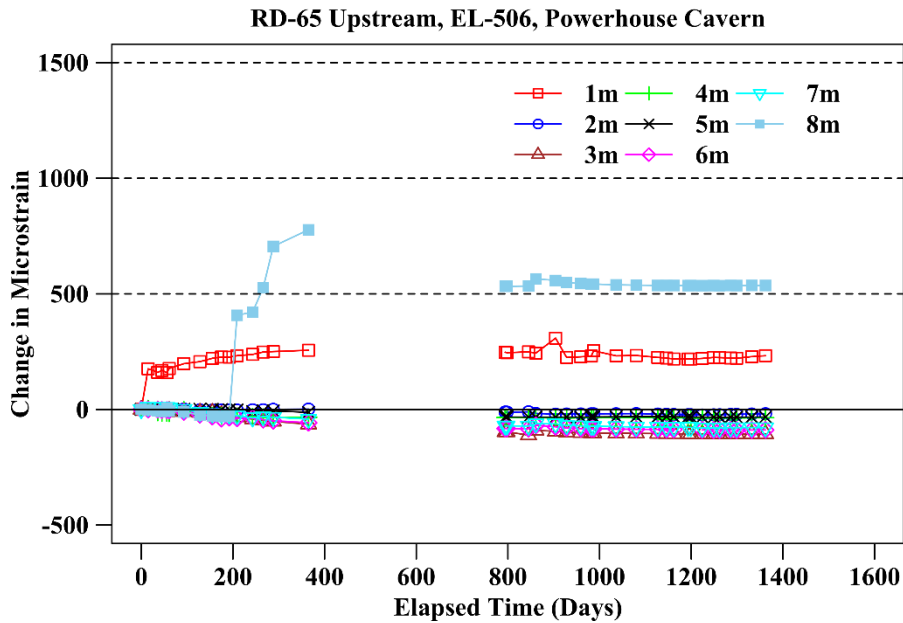


Fig. 4.50 Change in micro strain in instrumented bolt at RD 65, EL 506 at upstream wall of powerhouse cavern

RD-110, EL-506 Upstream Wall: Instrumented bolt observations on upstream wall at RD-110, EL-506 are shown in Fig. 4.51.

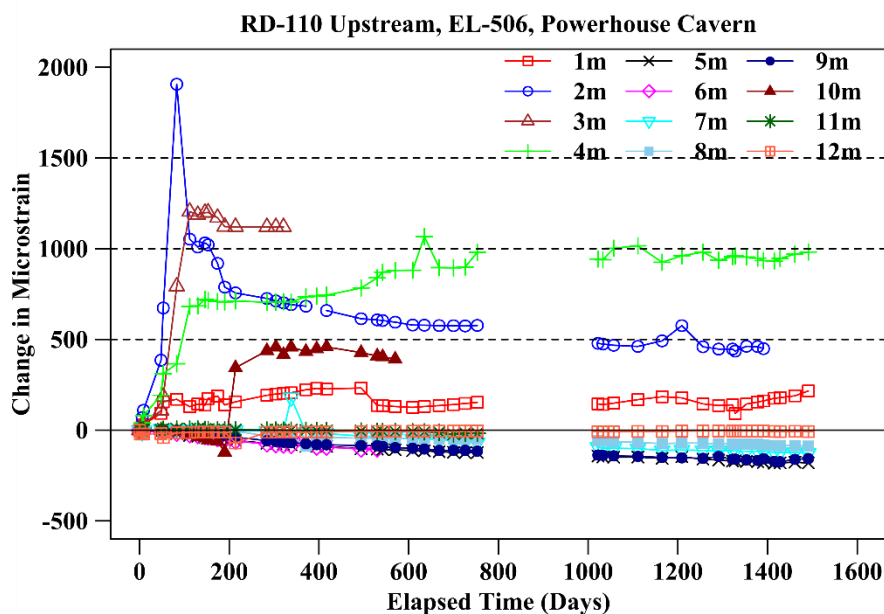


Fig. 4.51 Change in micro strain in instrumented bolt at RD 110, EL 506 at upstream wall of powerhouse cavern

At RD-110 upstream, increase in strain was observed at 1m to 4m depths with an increase in the range of 216.19 to 1119.63 microstrain. At other depths, there was decrease in strain in the range of -7.43 to -180.63 microstrain (Fig. 4.51).

RD-150, EL-506 Upstream Wall: Results of monitoring of instrumented bolts on upstream wall at RD-150, EL-506 are shown in Fig. 4.52. At RD-150 upstream, increase in strain was observed at 1m depth with an increase of 7.70 microstrain and at all other depths, there was decrease in the strain in the range of -70.35 to -342.82 microstrain (Fig. 4.52).

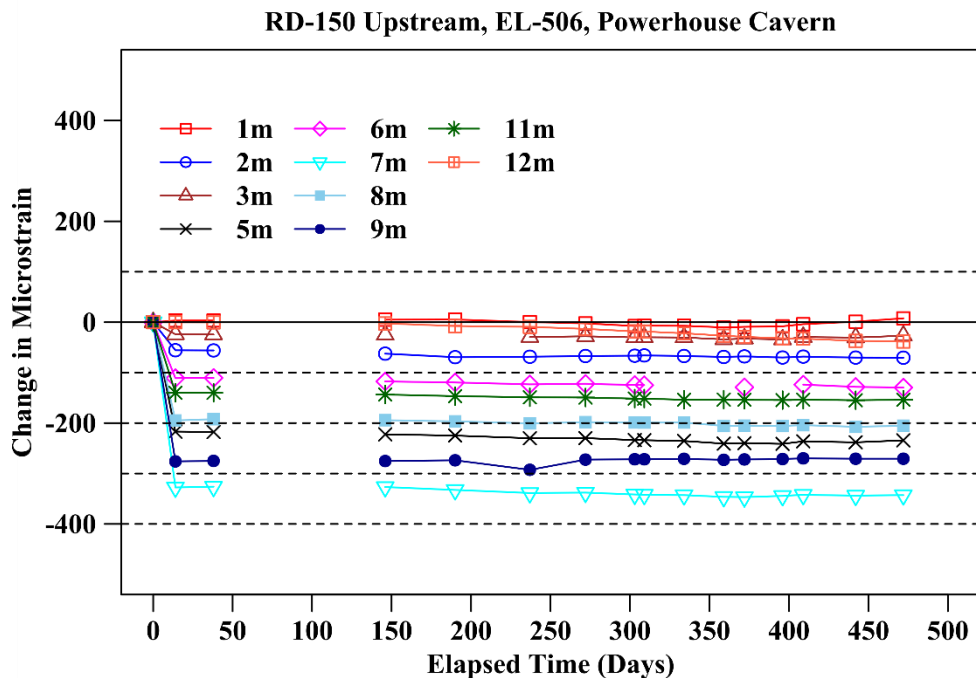


Fig. 4.52 Change in micro strain in instrumented bolt at RD 150, EL 506 at upstream wall of powerhouse cavern

RD-140, EL-515 Upstream Wall: Instrumented bolt observations on upstream wall at RD-140, EL-515 are shown in Fig. 4.53. At RD-140 upstream at EL-515, increase in strain was observed at 1m depth with an increase of 23.96 microstrain. At other depths, there was decrease in strain in the range of -3.59 to -147.86 microstrain (Fig. 4.53).

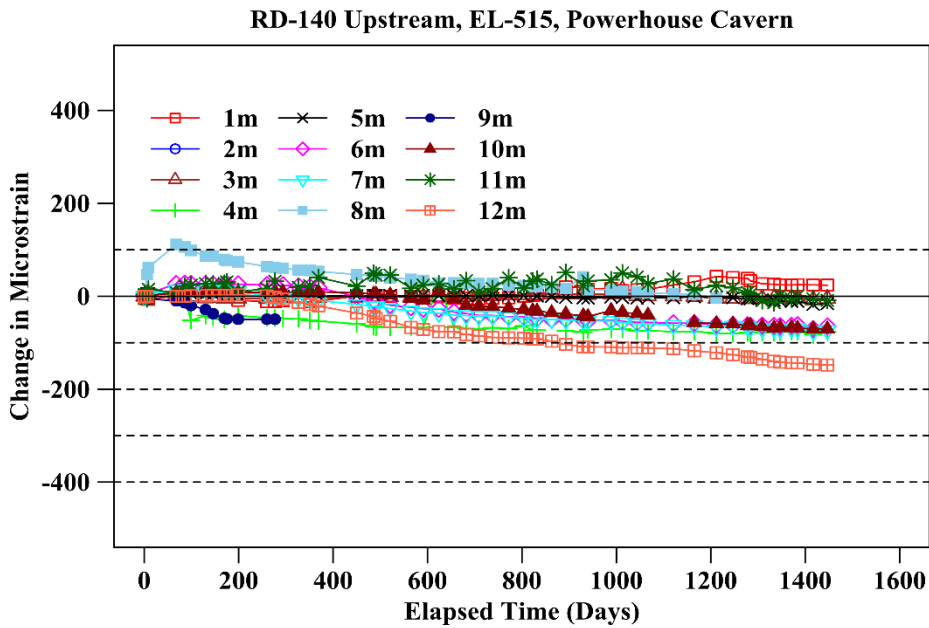


Fig. 4.53 Change in micro strain in instrumented bolt at RD 140, EL 515 at upstream wall of powerhouse cavern

RD-150, EL-515 Upstream Wall: Recordings made on upstream wall at RD-150, EL-515 are shown in Fig. 4.54. At RD-150 upstream at EL-515, increase in strain was observed at 1m, 3m and 5m depths with an increase in the range of 7.3 to 63.51 microstrain. At other depths, there was decrease in strain in the range of -3.59 to -147.86 microstrain (Fig. 4.54).

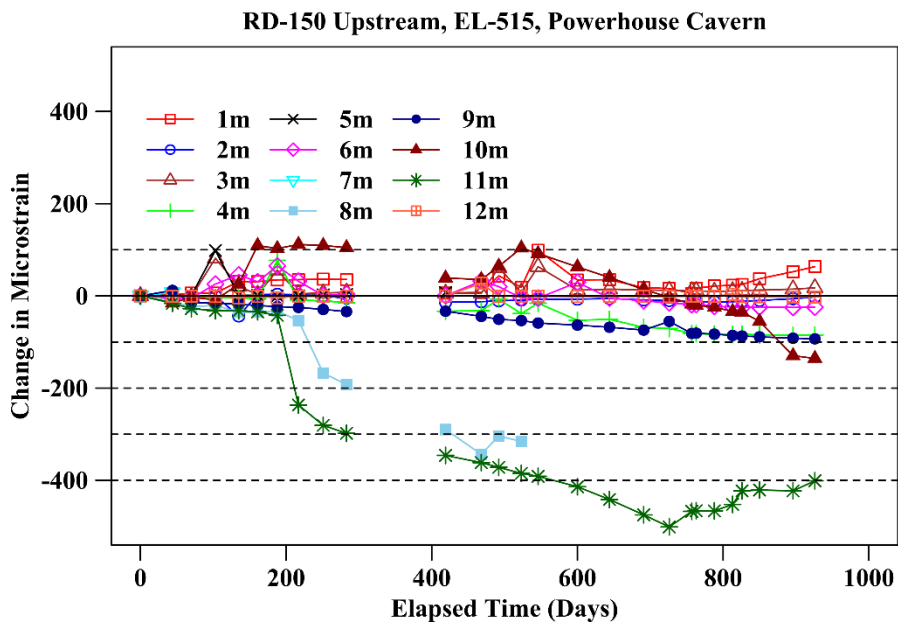


Fig. 4.54 Change in micro strain in instrumented bolt at RD 150, EL 515 at upstream wall of powerhouse cavern

Final change in strain values measured in post excavation stage at various depths in instrumented bolts are summarised in Table 4.22.

Table 4.22 Summary of strain changes in instrumented rock bolts

Depth (m)	Microstrain							
	Upstream Wall					Downstream Wall		
	RD-65 EL-506	RD-110 EL-506	RD-150 EL-506	RD-140 EL-515	RD-150 EL-515	RD-65 EL-506	RD-110 EL-506	RD-150 EL-506
1m	232.55	216.19	7.70	23.96	63.52	1640.91	206.56	7.40
2m	-18.34	449.27	-70.35		-2.37	-121.13	278.24	6.61
3m	-105.48	1119.63	-26.72	-5.13	17.50	-94.32	-26.96	-77.27
4m	-35.87	981.98		-76.74	-84.84	-21.61	453.22	-123.85
5m	-32.50	-180.63	-234.21	-15.77	7.41	-51.49	71.53	-159.42
6m	-88.58	-103.77	-129.60	-64.61	-24.54	-440.45	-199.52	-202.25
7m	-78.44	-127.32	-342.83	-73.15	7.30	51.45	-112.86	-116.02
8m	536.25	-88.19	-205.22	-3.59	-315.60	-101.14	-105.92	-15.15
9m		-156.61	-270.74	-49.33	-93.17	-124.24	-134.60	-20.56
10m		391.43		-70.07	-135.66	-98.22	8.99	-5.98
11m		-17.11	-153.80	-8.67	-401.07	-54.38	-116.30	
12m		-7.43	-38.36	-147.86	-2.43	-8.40	-183.18	-78.53

Strains in the rock bolt measured with instrumented bolt showed that there was an increase in strain at 1m depth in all cases. In some cases, there was an increase in strain upto 4 to 5m depths. At 11m and 12m depths, there was decrease in strain in all cases. Strains measured with instrumented bolts are in agreement with experimental results of Freeman (1978) on fully bonded rock bolts, where it was proved that bolt part closer to the excavation is responsible for picking up the load from rock mass (hence increase in strain) and balance part acts as anchor length, which firmly anchors the bolt to the rock mass (hence decrease in strain).

4.1.8 Pore Water Pressure Observations at Powerhouse Cavern

Piezometers were installed at EL-533, EL-525 and EL-511 in powerhouse cavern. At EL-533, the piezometers were installed at 10m depth. At EL-525, one piezometer was installed at 5m depth and one more piezometer was installed at 10m depth. During operational period, nine more piezometers were installed at EL-504 and EL-500 on powerhouse upstream wall at a depth of 3m, around pressure shaft manifold area. None of the piezometers above EL-500 recorded building up of pore water pressure in the

surrounding rock mass of the powerhouse. Maximum pore water pressure recorded above EL-500 was 0.69kg/cm^2 . It could be noted that at EL-500 there was an indication of water pressure between RD-87 and RD-167 with pore pressure in the range of 0.12 to 1.07kg/cm^2 .

4.2 TRANSFORMER HALL CAVERN

4.2.1 Load on the Steel Ribs in the Crown

While installing steel ribs in the crown of transformer hall cavern, load cells were installed on the ribs at EL-533.6 on both upstream and downstream side. Axial load on ribs on upstream side and downstream side are shown in Figs. 4.55 and 4.56, respectively. All the load cell data in the steel ribs in transformer hall cavern is given in Appendix-3.

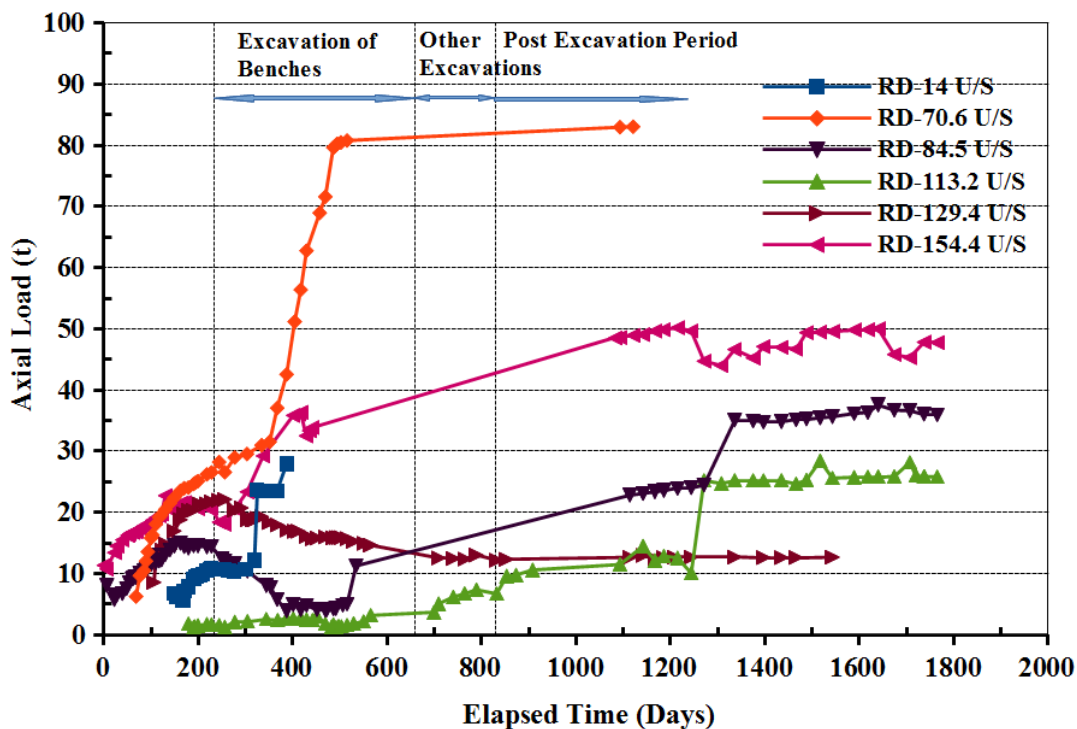


Fig. 4.55 Axial load on steel ribs on upstream side in the crown of transformer hall cavern

On upstream side, axial load on the steel ribs increased in the range of 3.4 - 52.67t during the benching and at locations, RD-84.5 and RD-129.4 there was a decrease in the load (3.19 to 9.34t). During post excavation period, load on ribs increased by 0.48 - 54.66t . At RD-70.6, load of 83.06t was measured during post excavation period.

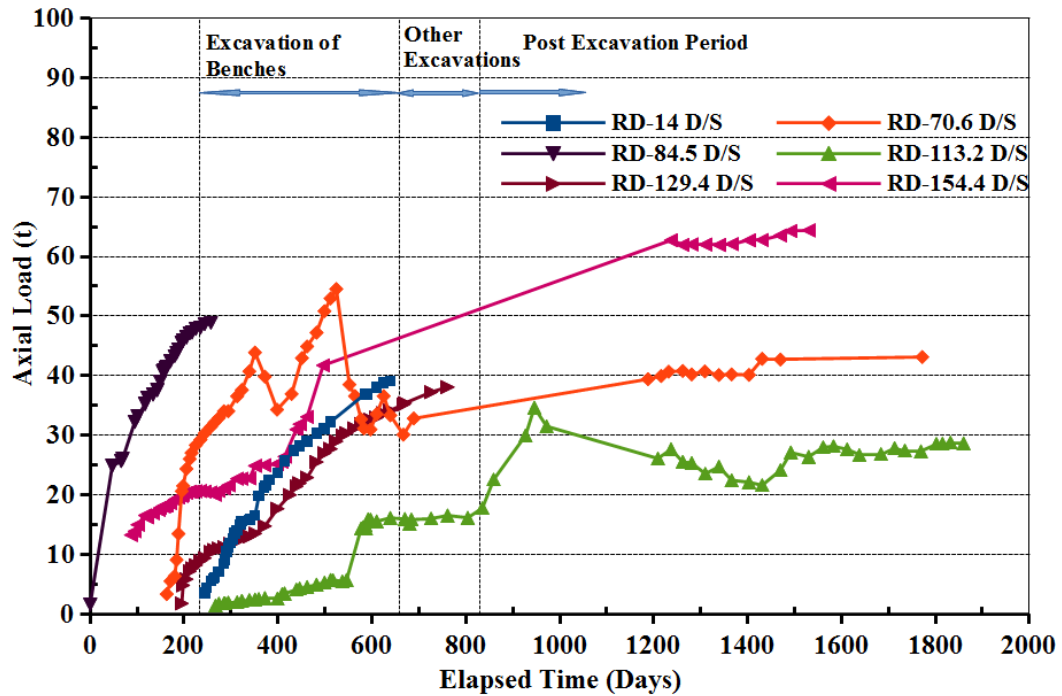


Fig. 4.56 Axial load on steel ribs on downstream side in the crown of transformer hall cavern

On downstream wall, the increase in load during the excavation of benches in transformer hall varied from 14.71t to 48.9t. During post excavation period, the load on the ribs increased in the range of 8.14-14.39t. Maximum load of 64.39t was measured at RD-154.4 on downstream side (Fig 4.56). A summary of load changes in the ribs on upstream and downstream of transformer hall is given in Table 4.23.

Table 4.23 Details of load changes in ribs in the crown of transformer hall

Details of Load on Ribs at Transformer Hall Cavern						
Upstream Side						
RD	Load Changes during Excavation of Benches (t)			Load Changes Post Excavation Period (t)		
	Load at Start of Bench Excavation (t)	Load at End of Bench Excavation (t)	Change in Load (t)	Start Load (t)	End Load (t)	Change in Load (t)
14	10.71	27.94	17.23	-	-	-
70.6	28.33	81	52.67	81	83.06	2.06
84.5	14.45	11.26	-3.19	12.56	35.97	23.41
113.2	1.68	5.08	3.4	6.69	25.8	19.11
129.4	21.9	12.56	-9.34	12.2	12.68	0.48
154.4	20.72	37	16.28	40	47.76	7.76

Details of Load on Ribs at Transformer Hall Cavern						
Downstream Side						
Load Changes during Excavation of Benches (t)				Load Changes Post Excavation Period (t)		
RD	Load at Start of Bench Excavation (t)	Load at End of Bench Excavation (t)	Change in Load (t)	Start Load (t)	End Load (t)	Change in Load (t)
14	3.57	39.11	35.54	35	43.14	8.14
70.6	30.34	54.26	23.92	-	-	0
84.5	0	48.9	48.9	-	-	0
113.2	1.43	16.14	14.71	17.78	28.65	10.87
129.4	9.42	35.4	25.98	-	-	0
154.4	20.55	45	24.45	50	64.39	14.39

Analysis of load cell data on the steel ribs on upstream side of transformer hall, indicated change in load from -9.34 to 52.67t during benching. Decrease in load was observed in the central portion of cavern (RD-84.5 to RD-129.4). During post excavation period, there was an increase in load at all locations (0.48 - 23.41t). On downstream side, there was an increase in load on steel ribs at all locations during benching (14.71-48.9t). During post excavation period, the increase in load was 8.14 - 14.39t. In the later part of post excavation period, load on the steel ribs showed a stable trend (Figs. 4.55 and 4.56).

4.2.2 Load on Rock Bolts in the Walls

Rock bolts (8m long Dywidag make) in upstream and downstream walls of transformer hall cavern were monitored with vibrating wire anchor load cells. Build-up of load in the rock bolts was monitored by regular readings with continuation of excavation of lower benches. Behaviour of rock bolts at EL-532, EL-525 and EL-520, on upstream and downstream walls during excavation and post excavation period are discussed in this section. All the load cell data on rock bolts in transformer hall cavern is given in Appendix-3.

EL-532: Axial load on rock bolts at EL-532 on the walls of transformer hall is shown in Fig. 4.57. During the excavation of benches in transformer hall, load on rock bolts at EL-532 varied from -1.43t to 11.82t. More changes in load were observed on the upstream wall. Maximum load (38.92t) was measured at RD-80 upstream. Post excavation period saw load changes in rock bolt in the range of -3.1t to 6.54t.

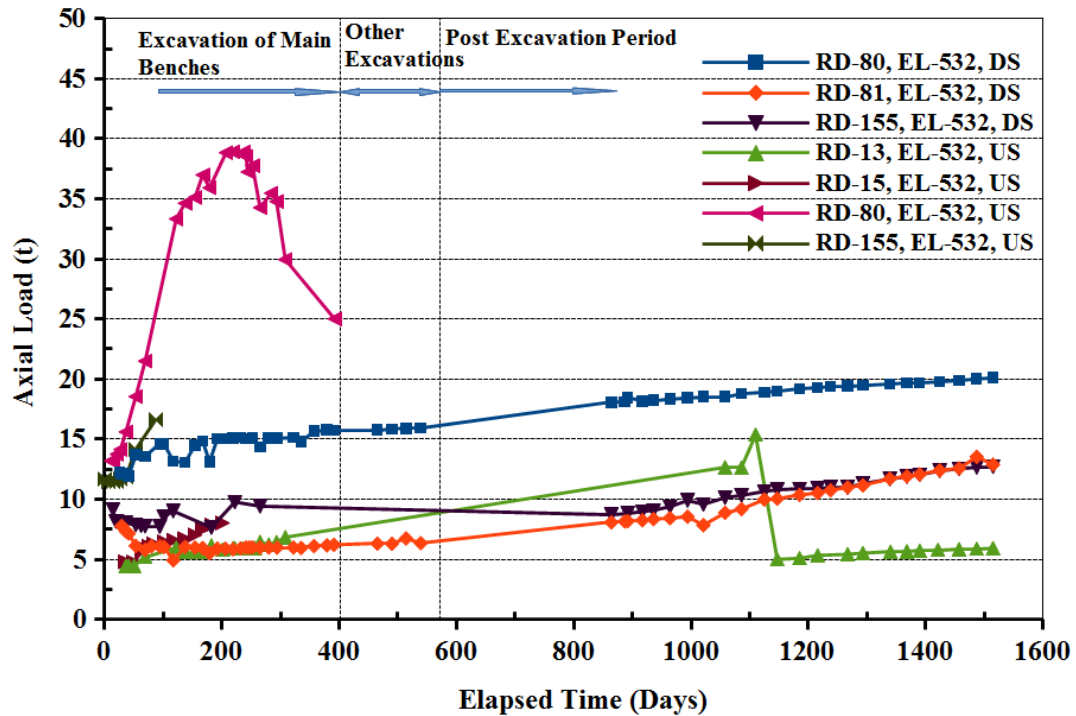


Fig. 4.57 Axial load on rock bolts at EL-532 on upstream and downstream wall of powerhouse cavern

EL-525: Axial load on rock bolts at EL-525 on the walls of transformer hall is shown in Fig. 4.58. Load changes on rock bolts at EL-525 was in the range of -5.37t to 10.71t. Maximum load (25.89t) was measured at RD-14 upstream. During post excavation load changes varied from -3.83t to 4.57t. During post excavation period, load cell at RD-60 upstream recorded maximum load of 25.92t (Fig. 4.58).

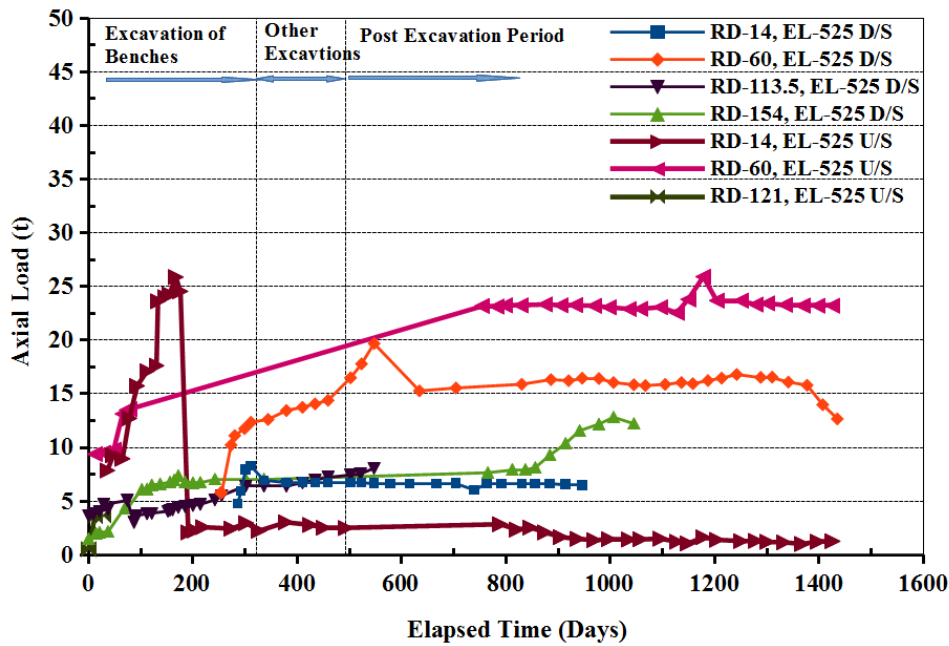


Fig. 4.58 Axial load on rock bolts at EL-525 on upstream and downstream wall of powerhouse cavern

EL-520: Axial load on rock bolts at EL-520 on the walls of transformer hall is shown in Fig. 4.59. At EL-520, change in load on rock bolts varied from -8.47t to 19.86t and maximum loads were measured at RD-58 u/s (27.84t) and at RD-162 u/s (27.54t). Here also maximum loads were recorded on upstream wall. During post excavation period, the change in load on rock bolts varied from -1.46t to 2.89t.

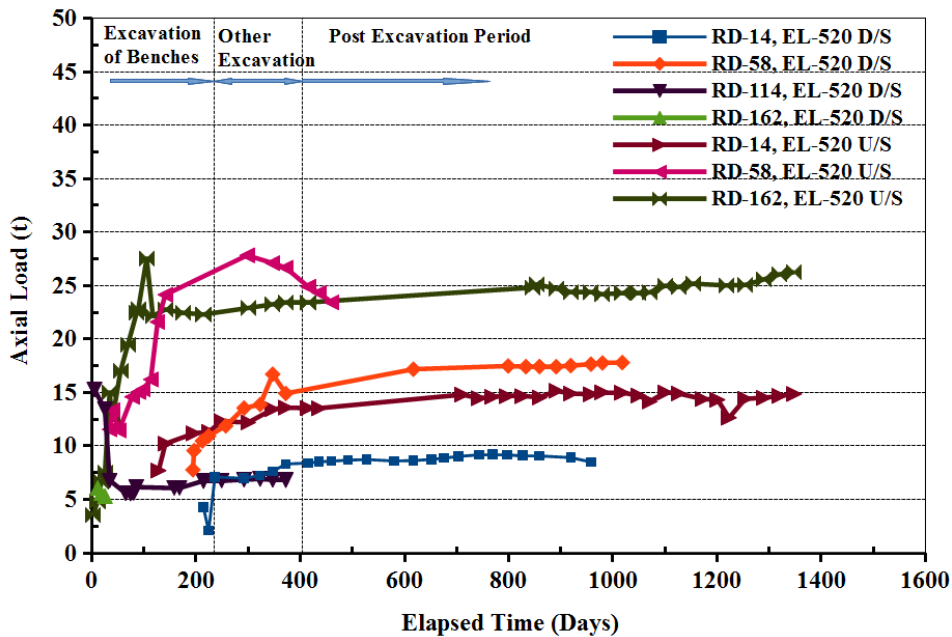


Fig. 4.59 Axial load on rock bolts at EL-520 on upstream and downstream wall of powerhouse cavern

Details of changes in load on rock bolt during excavation and post excavation period are listed in Table 4.24.

Table 4.24 Details of load changes in rock bolts in the walls of transformer hall

Location	After complete Excavation		Post Excavation Period		Final Load on Rock Bolt (t)
	Load (t)	% of Final Recorded Load (t)	Load (t)	% of Final Recorded Load (t)	
EL-532					
RD-80 D/S	15.94	79%	20.1	21%	20.1
RD-81 D/S	6.35	49%	12.89	51%	12.89
RD-155 D/S	9.01	71%	12.71	29%	12.71
RD-13 U/S	9.02	152%	5.92	-52%	5.92
RD-15 U/S	8.03	-	-	-	-
RD-80 U/S	25.01	-	-	-	-
RD-155 U/S	16.63	-	-	-	-
EL-525					
RD-14 D/S	6.74	104%	6.49	-4%	6.49
RD-60 D/S	16.5	130%	12.67	-30%	12.67
RD-113.5 D/S	7.44	92%	8.07	8%	8.07
RD-154 D/S	7.65	63%	12.22	37%	12.22
RD-14 U/S	2.49	196%	1.27	-96%	1.27
RD-60 U/S	20	86%	23.22	14%	23.22
RD-121 U/S	3.69				
EL-520					
RD-14 D/S	8.41	99%	8.51	1%	8.51
RD-58 D/S	15.02	84%	17.81	16%	17.81
RD-114 D/S	6.81	-	-	-	-
RD-162 D/S	5.36	-	-	-	-
RD-14 U/S	13.55	91%	14.87	9%	14.87
RD-58 U/S	24.9	106%	23.44	-6%	23.26
RD-162 U/S	23.41	89%	26.26	11%	26.26

Analysis of load cell data on rock bolts on walls of transformer hall cavern indicated development of load upto 38.92t during excavation period. Most of the rock bolts recorded an increase in load (49 to 196% of final load recorded during post excavation stage) during the excavation period and reduction in load during post excavation period. There was an increase of 21- 51% at EL-532 in three cases and 37% in one case at EL-525 at other locations increase was upto 16% and in five cases, there was reduction

in load during post excavation period. During post excavation period, in general stable trend was observed.

4.2.3 Movements in the Side Walls

Cumulative convergence of main walls of transformer hall cavern was monitored with reflective targets using total station. Convergence observations are depicted in the graphs and excavation periods are marked on the graphs. Listing of all cumulative convergence data in transformer hall cavern is given in Appendix-3. Convergence observation at EL-531 is shown in Fig. 4.60.

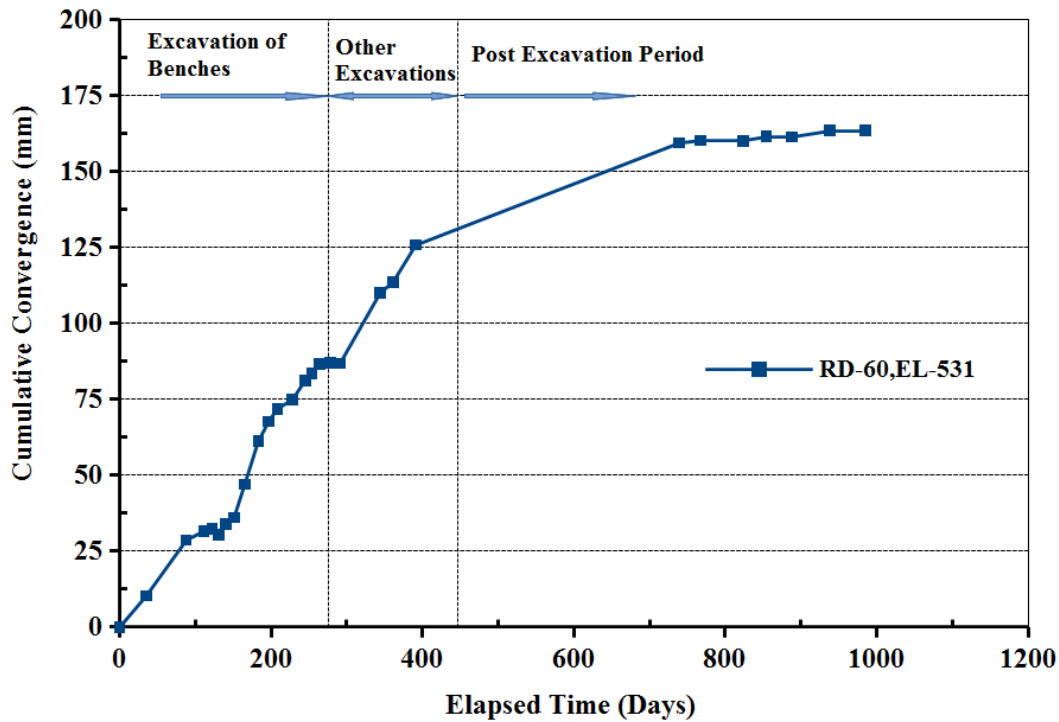


Fig. 4.60 Cumulative convergence of walls at transformer hall cavern at EL-531

At EL-531 RD-60, out of total cumulative convergence of 163.31mm, 86.92mm (53.22%) was measured during excavation of benches.

Convergence observation at EL-525 is shown in Fig. 4.61. At EL-525, cumulative convergence in the range of 32.91 to 102.91mm was measured. About 56.51% to 79.38% of total convergence was measured during the excavation of benches.

Convergence observation at EL-520 is shown in Fig. 4.62. At EL-520, cumulative convergence in the range of 19 - 82mm was measured. About 56.51% to 79.38% of total convergence was measured during the excavation of benches.

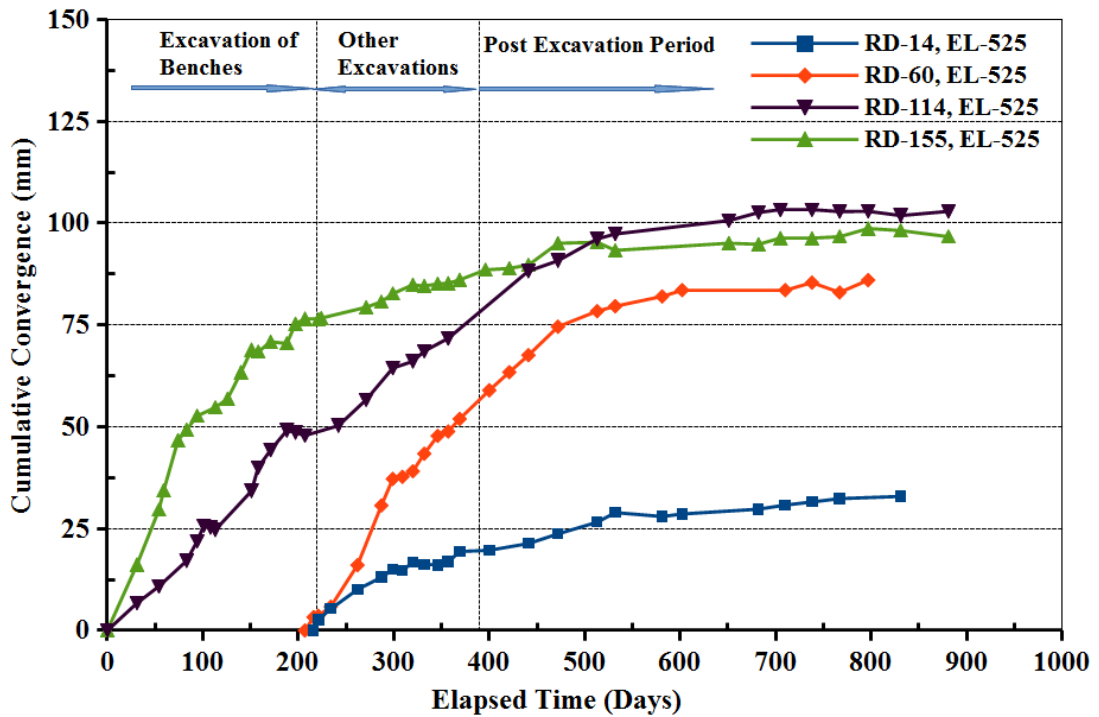


Fig. 4.61 Cumulative convergence of walls at transformer hall cavern at EL-525

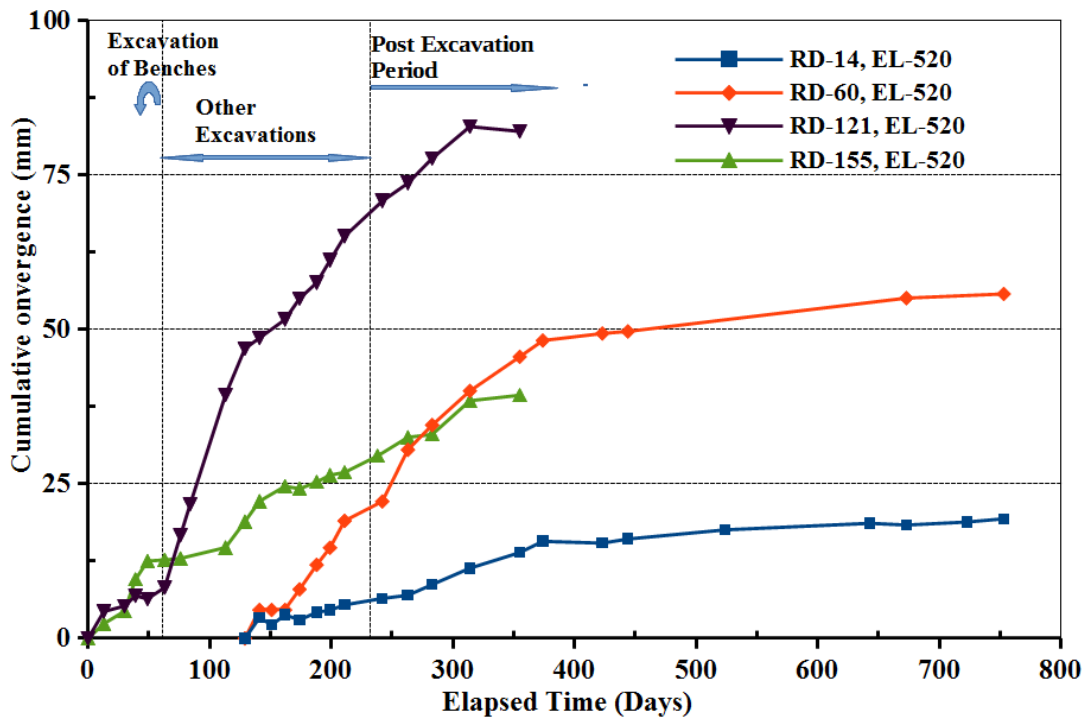


Fig. 4.62 Cumulative convergence of walls at transformer hall cavern at EL-520

Summary of convergence and the computed strain (taking the width of transformer hall cavern as 16m) is summarised in Table 4.25.

Table 4.25 Details of convergence measurements at transformer hall cavern

	Convergence during Excavation of Main Benches (mm)	Convergence after Complete Excavation (mm)	Convergence during Post Excavation Period (mm)	Total Cumulative Convergence (mm)	Per cent Strain
EL-531					
RD-60	86.92 (53.22%)	41.08 (25.15%)	35.31 (21.62%)	163.31	1.02
EL-525					
RD-14	-	19.67 (59.77%)	13.24 (40.23%)	32.91	0.21
RD-60	-	56.5 (65.67%)	29.53 (34.33%)	86.03	0.54
RD-114	47.86 (56.51%)	28.34 (27.54%)	26.71 (25.95%)	102.91	0.64
RD-155	76.69 (79.38%)	11.87 (12.28%)	8.13 (8.41%)	96.69	0.60
EL-520					
RD-14	-	6.47 (33.44%)	12.88 (66.56%)	19.35	0.12
RD-60	-	22.1	33.62	55.72	0.35
RD-121	8.24 (9.13%)	68.5 (75.9%)	13.51 (14.97%)	82.01	0.56
RD-155	12.7 (24.41%)	29.51 (56.72%)	9.82 (18.87%)	39.33	0.33

Percentage strain measured in the walls of transformer hall varied between 0.12 - 1.02%. Convergence rates of all the measurements are shown in Fig. 4.63. Convergence rates during the excavation of benches varied from 0.01 to 0.96mm/day. While excavating other tunnels, convergence rates varied from 0.01 to 0.63mm/day and during post excavation it varied from 0.01 to 0.40mm/day (Fig. 4.63).

Monitoring of cumulative convergence between upstream and downstream walls of transformer hall cavern indicated high displacement of side walls. Maximum convergence recorded at EL-531, EL-525 and EL-520 was 163.31mm, 102.9mm and 82.01mm, respectively. With width to height ratio of 0.65, transformer hall recorded

maximum strain of 1.02%. Considerable amount of convergence was recorded during post excavation period (35.31mm).

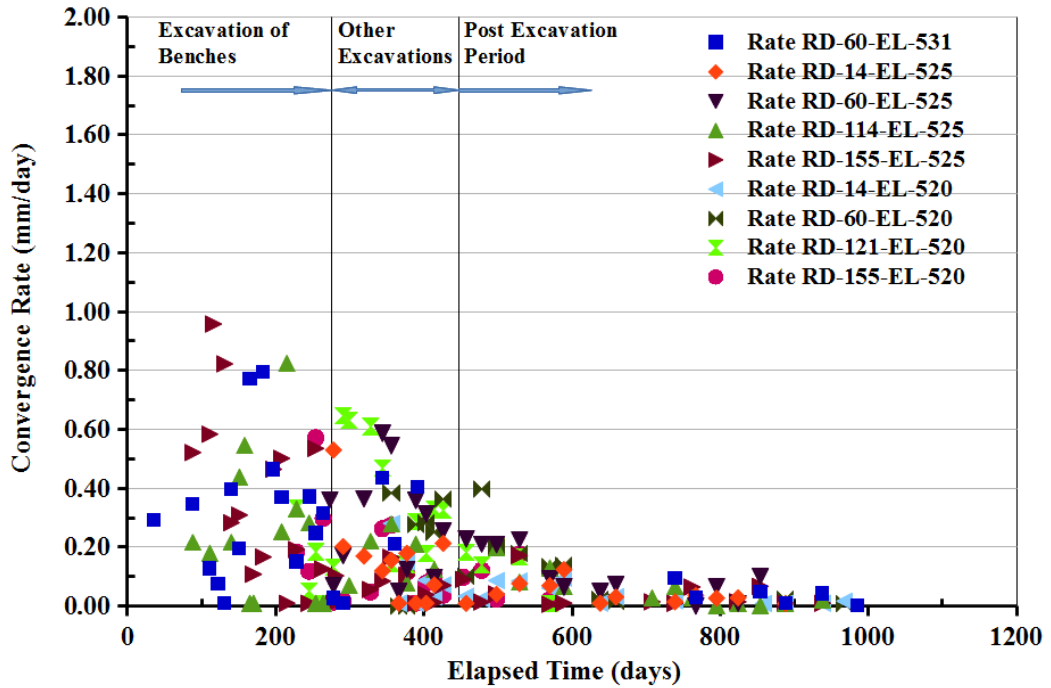


Fig. 4.63 Convergence rate of walls at transformer hall cavern

4.3 CROSS TUNNELS IN POWERHOUSE COMPLEX

The behaviour of the cross tunnels was assessed using load cell observations on rock bolts and ribs. Listing of all load cell data in the steel ribs and rock bolts in bus ducts and passage tunnel is given in Appendix-4. Load on the steel ribs in bus ducts and passage tunnels are shown in Fig. 4.64.

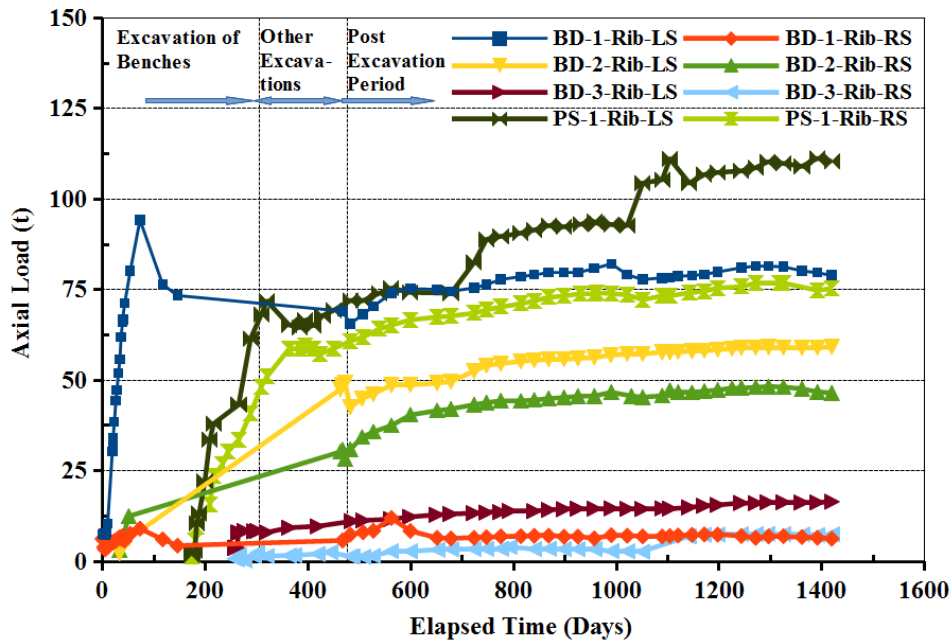


Fig. 4.64 Axial load on steel ribs in bus ducts and passage tunnels

It may be noted from Fig. 4.64 that, at bus duct No.1, the load on the left side of the ribs after the backfill was 10.51t. The load started increasing at a faster rate. The rate of loading varied from 0.50t/day to 3.3t/day between 10th day and 60th day from the date of installation and reached 94.28t during 72 days.

Considering the heavy load coming on to the ribs, eight additional bolts of 12m length were installed on the left wall of the bus duct No.1 at the mid height. It could be noted that the side walls of the bus ducts were supported with 6m long resin cum cement grouted bolts. After installation of additional bolts, the rate of loading decreased from 1.39t/day to 0.5t/day and load reached 73.42t at the end of 145 days. Subsequently, there was marginal increase in the load during the post excavation period. On the right side rib, the load was less than 12t. At bus duct No.2, the load on the ribs varied from 2.2t - 59.24t, whereas the load on the ribs at bus duct No.3 varied from 0.34t-16.49t. It could be noted from Fig. 4.64 that the load on the ribs at passage tunnel reached 111.28t on the left side and 76.81t on the right side. From the instrumentation data it was evident that, bus ducts have witnessed loads in the range of 0.03 to 94.28t (i.e. 0.003 - 0.92MN). Considering the sectional area of ISMB 300 (58.6cm²), the stresses acting on the ribs varied from 0.57 - 157.78MPa, whereas, the passage tunnel experienced load in the

range of 1.35 - 111.28t (i.e. 0.01 - 1.09MN). Considering the sectional area of ISMB 250 (47.5cm²), the stresses acting on the ribs varied from 2.26 - 229.7MPa.

Load observations on the rock bolts are shown in Fig. 4.65.

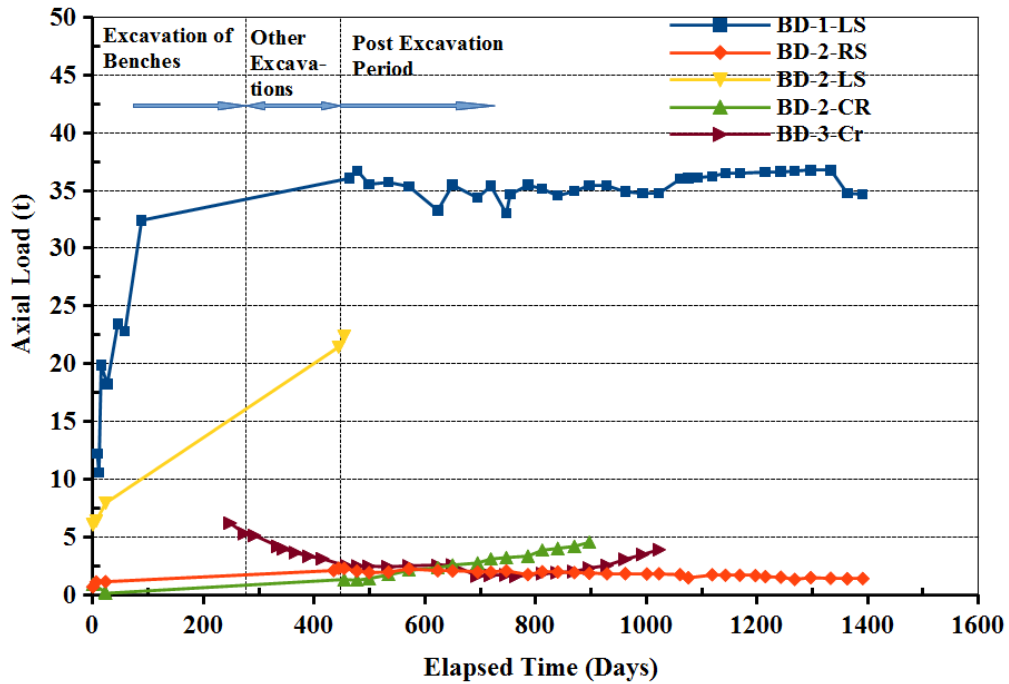


Fig. 4.65 Axial load on rock bolts in bus ducts and passage tunnels

At bus duct No.1, load cell on the rock bolt showed sharp increase in load and reached 32.4t. After installing the additional rock bolts nearby, the load stabilised as could be seen in Fig. 4.65. At bus duct No.2, the load on rock bolt increased to 22.38t and at other locations, there was no substantial increase in the load in the rock bolts.

Load cell data on the steel ribs at pressure shaft manifolds is shown in Fig. 4.66. Load cells were also installed on rock bolts in the pressure shaft manifold and the results are shown in Fig. 4.67. Listing of all load cell data in the steel ribs and on rock bolts in pressure shaft manifolds is given in Appendix-4.

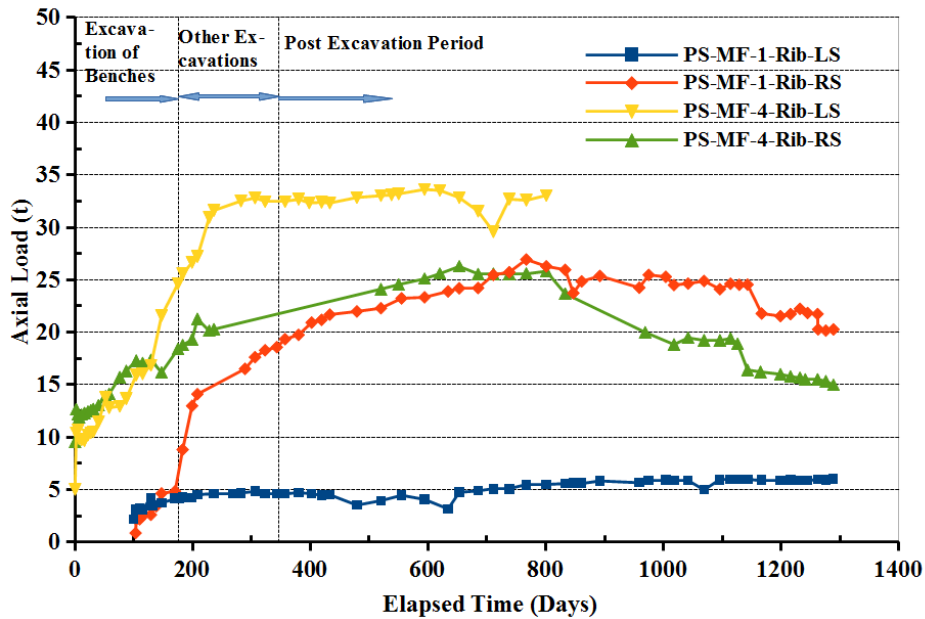


Fig. 4.66 Axial load on steel ribs in pressure shaft manifolds tunnels

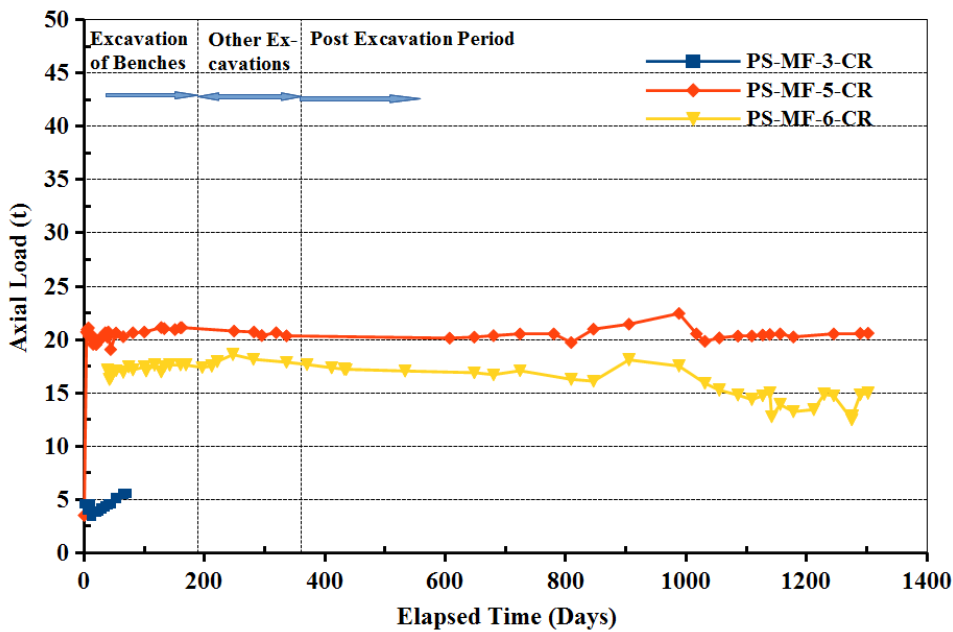


Fig. 4.67 Axial load on rock bolts in pressure shaft manifolds tunnels

At pressure shaft manifold 1, maximum load on left side was 6.01t and remained almost constant. On right side, the maximum load recorded was 26.93t. At pressure shaft manifold 4, maximum load on the left side was 33.61t during excavation period and showed stabilising trend during post excavation period. On right side, maximum load of 26.27t was recorded during post excavation period, which later decreased to about

15t. Load on the rock bolts in the manifolds did not show much variation as evident from Fig. 4.67.

During post excavation period, cracks started appearing on the walls of the bus ducts and these were vertical cracks parallel to the axis of the main caverns. These cracks could be due to the tensile stresses in the immediate vicinity of the main cavern walls. Some of the typical cracks appeared in the walls are shown in Fig. 4.68.



Fig. 4.68 Tension cracks on walls of bus ducts

Since cross tunnels were subjected to maximum principal stresses, it was expected that higher load will come on to the supports. Instrumentation results showed that steel ribs are subjected to loads in the range of 100 - 110t. Rock bolts also experienced load of more than 35t. Since rock is weak in tension, development of tensile stresses closer to the downstream wall of powerhouse cavern, resulted in tensile cracks.

4.4 NUMERICAL MODELLING

Initially, numerical modelling was done using discontinuum model using 3DEC. In this case, only major joints cutting the crown of the powerhouse cavern were chosen. However, model results did not match closely with the field observations. Analysis of the results indicated that this model could not be accepted for the following reasons:

- Rock mass around the Tala powerhouse complex is highly jointed with 5 sets of joints in addition to foliation. Average GSI value of 50 confirms this. Therefore, including few sets of joints in the model will not represent the rock mass. It is not possible to model all the joint sets in 3DEC with actual spacing.
- Presence of more than 5 sets of joints makes the 3DEC modelling not so effective.
- In the present case study, there were no specific shear zones or fractured zones, so that its effect on the cavern could be modelled using 3DEC.
- In 3DEC model, derived rock mass parameters were further reduced by the influence of joint parameters. Using laboratory tested values directly in the model could prove very conservative as all the joint sets could not be represented in the model.

Therefore, it was decided to discard the results of 3DEC modelling and consider FLAC 3D continuum modelling technique, using the rock mass parameters. Model results of FLAC-3D was further analysed and presented in this section.

4.4.1 Displacement Distribution around the Caverns

In the model, actual geometry and sequence of excavation as followed during excavation of the cavern was used. Since the excavation of the benches started after installation of the steel ribs in both the caverns, simulation studies started with excavation of crown with steel ribs as the main support (Figs. 3.30 to 3.32). To establish the validity of the model, excavation of benches was done upto bench-5 with supports and difference in convergence of walls during excavation of bench-4 and bench-5 was compared at EL-525 at RD-15, RD-65, RD-110 and RD-150 (as convergence stations at EL-525 were installed at the end of bench-4 excavation). Horizontal displacement

contours at bench-4 and bench-5 at RD-15, RD-65, RD-110 and RD-150 are given in Fig. 4.69.

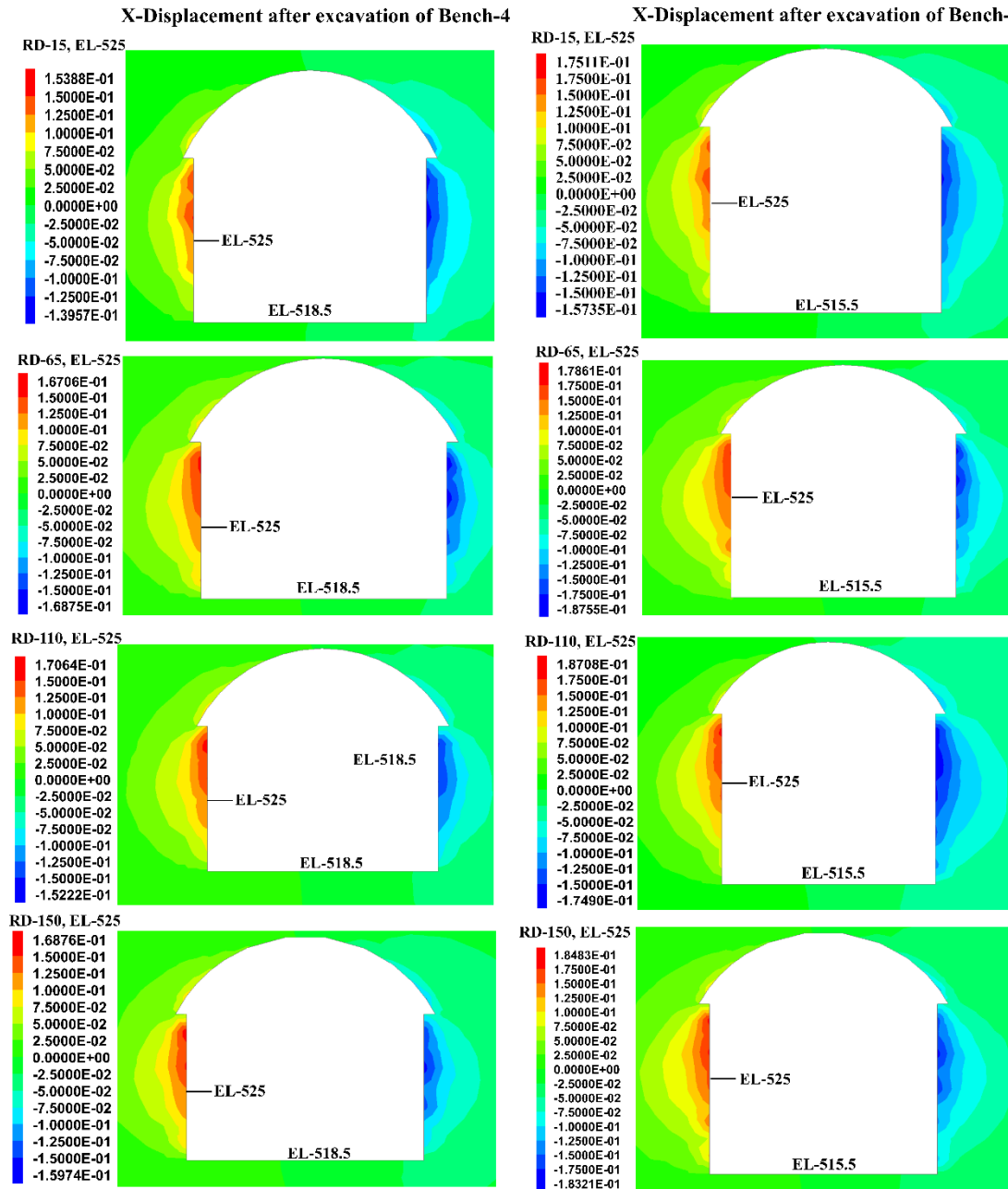


Fig. 4.69 Horizontal displacement contours after excavation of bench-4 and bench-5

Convergence from the model after bench-5 was compared with the field monitoring results and are given in Table 4.26. Measured displacement at RD-15 and RD-65 were higher by 11.33% and 3.61%, whereas at RD-110 and RD-150, model predictions were higher by 9.56% and 14.4% respectively. Since percentage difference is in the range of

-11.3 to 14.4%, validity of the model was acceptable considering the variability in geology in the cavern.

Table 4.26 Comparison of model and measured convergence between excavation of bench-4 (B-4) and bench-5 (B-5)

	Upstream Wall Disp. (mm)		Downstream Wall Disp. (mm)		Total Con. (mm)		Diff.in Con. (mm)	Measured Con. (mm)	Diff. (mm)	% Diff.
	B-4	B-5	B-4	B-5	B-4	B-5				
RD-15	112.8	134.3	116.7	141.1	229.5	275.4	45.9	51.1	-5.2	-11.33
RD-65	120.4	145	120.3	149.1	240.7	294.1	53.4	55.33	-1.93	-3.61
RD-110	122.4	149.8	121.2	150.3	243.6	300.1	56.5	51.1	5.4	9.56
RD-150	120.2	139.2	126.8	150.0	247	289.16	42.2	36.9	5.3	14.40

Same model was considered for further analysis and excavation of other benches and connecting tunnels was done and supports were installed in the same sequence, as followed during construction of the caverns.

Displacement contours at RD-15, RD-65, RD-110 and RD-150 sections after complete excavation of the caverns are shown in Figs. 4.70 to 4.74. Displacements at elevations, 525, 520 and 515 are shown in Figs. 4.75 to 4.77. Displacements at other sections are given in Appendix-5.

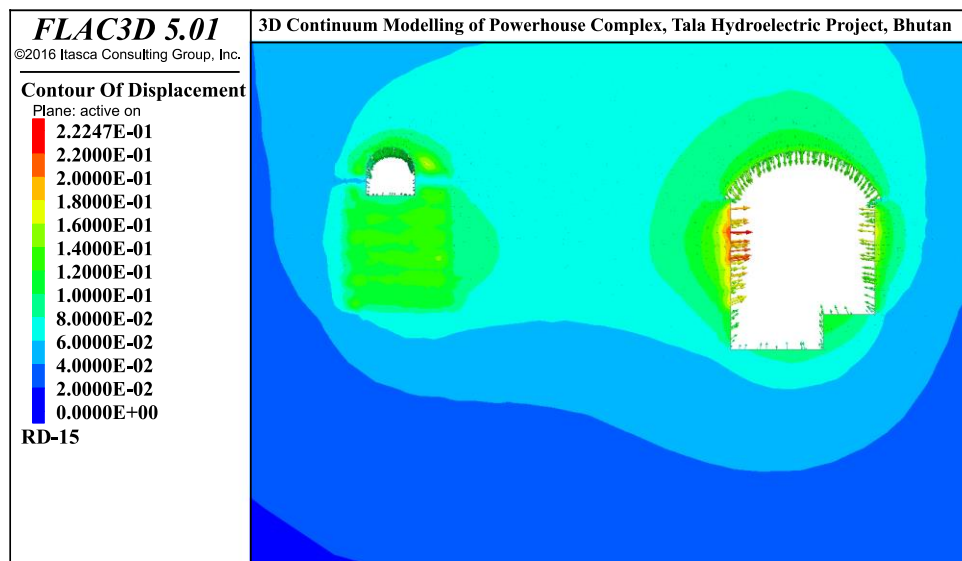


Fig. 4.70 Displacement contours at RD-15, powerhouse cavern

Maximum displacement of 222.4mm was observed at RD-15. In this section, displacements are relatively higher on downstream wall of the cavern (Fig. 4.70).

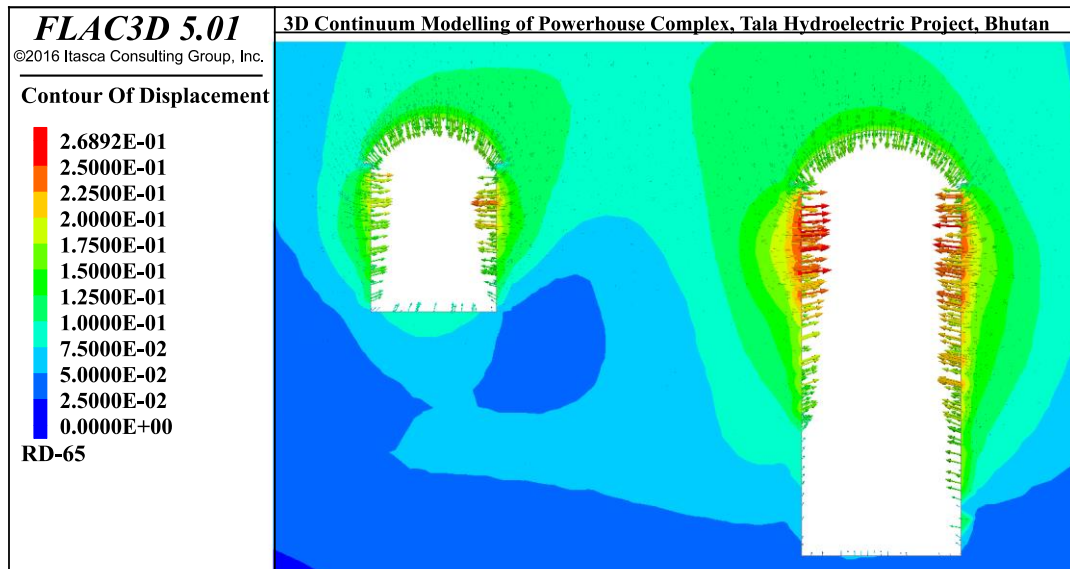


Fig. 4.71 Displacement contours at RD-65, powerhouse cavern

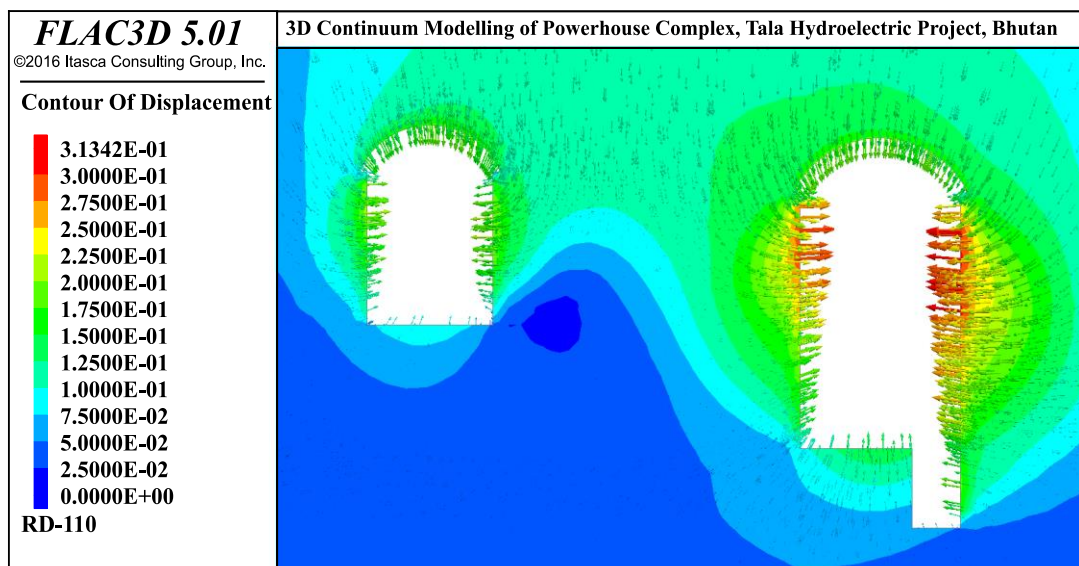


Fig. 4.72 Displacement contours at RD-110, powerhouse cavern

Maximum displacements at RD-65 and RD-110 were 268.9mm and 313.4mm respectively. In this section displacements were relatively higher on the upstream side of both powerhouse cavern and transformer hall cavern (Figs. 4.71 and 4.72). At RD-150 section, maximum displacement of 317.44mm was observed in the powerhouse cavern. In this case also, displacements were relatively higher on the upstream wall of powerhouse cavern (Fig. 4.73).

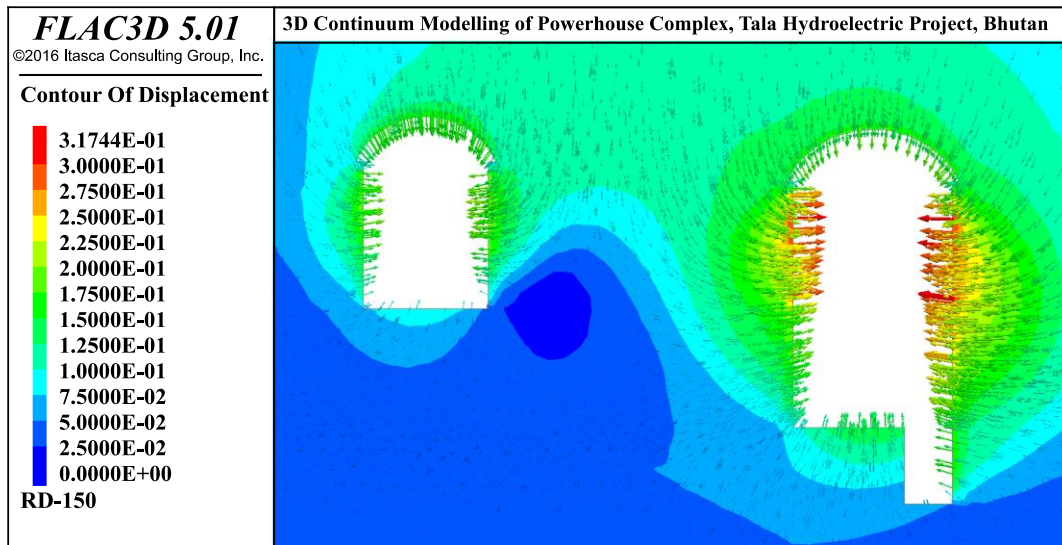


Fig. 4.73 Displacement contours at RD-150, powerhouse cavern

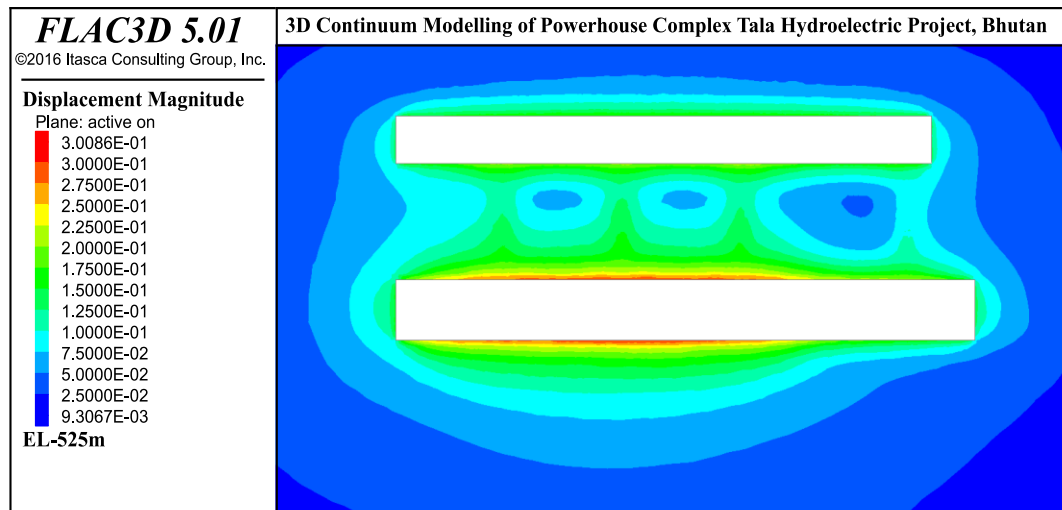


Fig. 4.74 Displacement contours at EL-525, powerhouse cavern

At EL-525, higher displacements in the range of 275-300mm were concentrated in the unit bay area on both upstream and downstream walls except at 10-15m from the end wall. Displacements in the pillar between powerhouse and transformer hall cavern were more influenced by excavation in the powerhouse cavern as the contour of smaller displacement was shifted towards transformer hall in the unit bay area. However, in the service bay area it was almost at the center of the pillar (Fig. 4.74). Similar behaviour was observed at EL-520 also (Fig. 4.75).

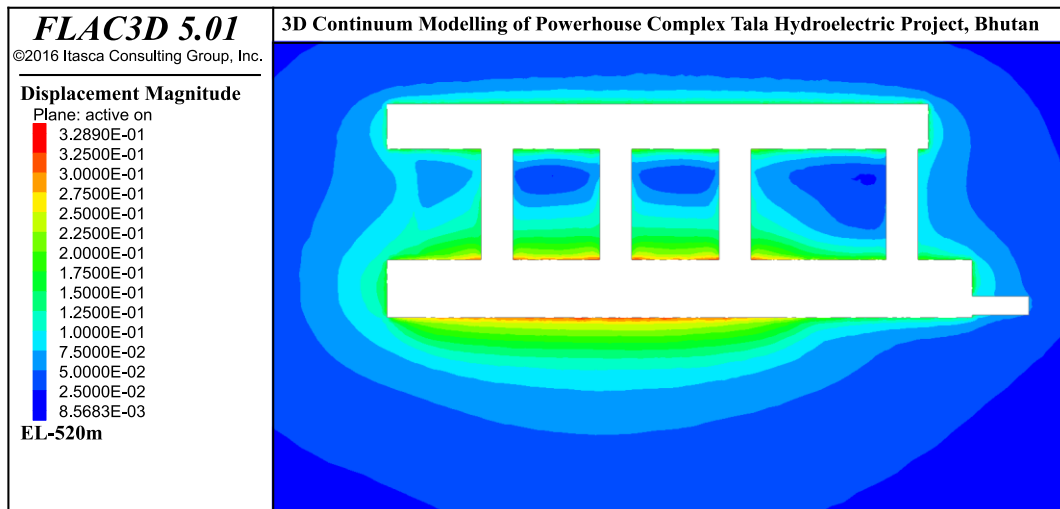


Fig. 4.75 Displacement contours at EL-520, powerhouse cavern

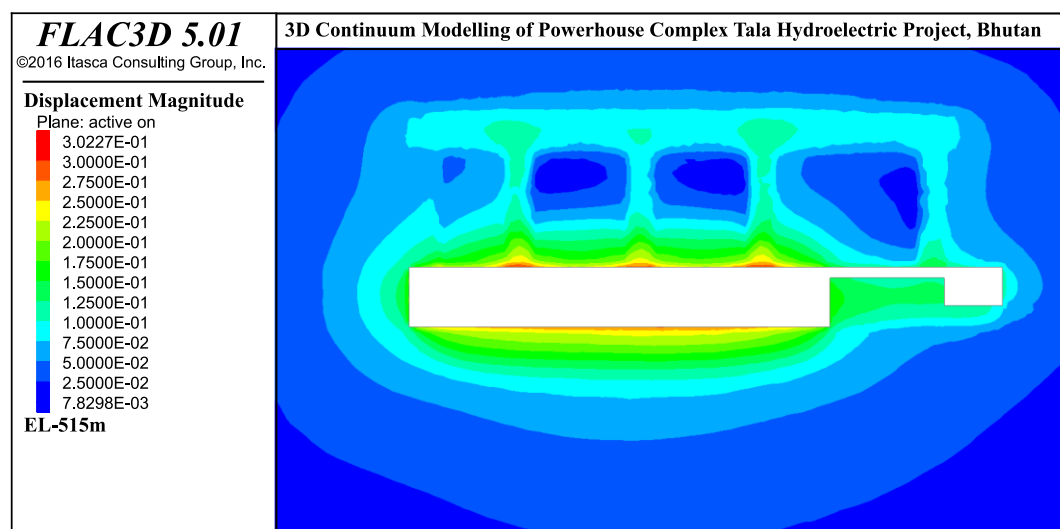


Fig. 4.76 Displacement contours at EL-515, powerhouse cavern

Displacements observed at EL-520 were greater than displacements observed at EL-525 and EL-515 by about 10%. This was due to the presence of cross tunnels like passage tunnels and bus ducts at this elevation (Fig. 4.75). EL-515 section is just below the floor of the cross tunnels. It could be observed from Fig. 4.76 that higher displacements were concentrated near the intersection of floor of the cross tunnels and downstream wall of the powerhouse cavern.

4.4.2 Comparison of Measured and Model Convergence

Cumulative convergence of the side walls of powerhouse cavern after complete excavation was compared with convergence results from the 3D model. Convergence data from the model after excavation of bench-4 was taken as the reference and convergence at each stage was compared with measured convergence at EL-525. Fig. 4.77 compares convergence at EL-525 and Table 4.27 summarises the comparison.

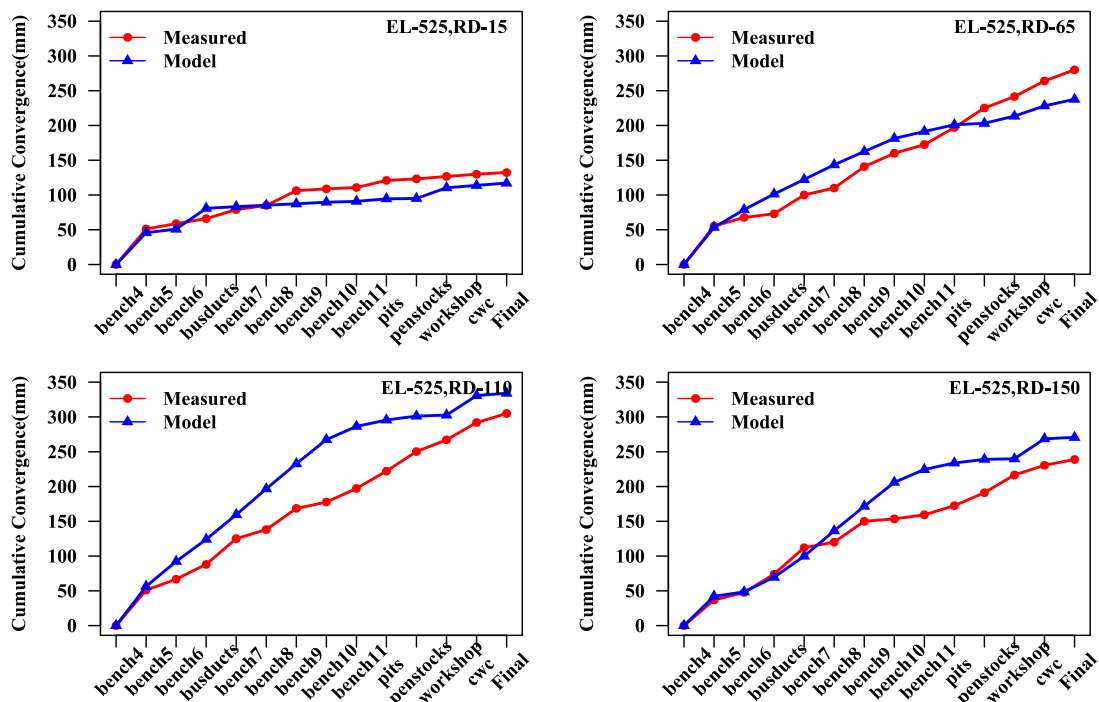


Fig. 4.77 Comparison of measured and model convergence at EL-525

Table 4.27 Comparison of convergence measurements with model results at powerhouse cavern

	Convergence (mm)											
	EL-525				EL-520				EL-515			
	Measured	Model	Difference	% age Diff	Measured	Model	Difference	% age Diff	Measured	Model	Difference	% age Diff
RD-15	132.3	117.05	15.25	11.53	133.3	127.83	5.47	4.10				
RD-65	280	237.64	42.36	15.13	181.7	196.96	-15.26	-8.40	173	183.85	-10.85	-6.27
RD-110	305	334.06	-29.06	-9.53	289.4	290.91	-1.51	-0.52	276	255.58	20.42	7.40
RD-150	238.8	270.61	-31.81	-13.32	233.7	280.76	-47.06	-20.14	270	249.78	20.22	7.49

At EL-525, measured values were higher at RD-15 and RD-65 and lower at RD-110 and RD-150. RD-15 is located in service bay area (RD-0 to RD-60) where width to height ratio is 0.85, whereas, RD-65 is in unit bay area (RD-60 to RD-206.4), where width to height ratio is 0.46. This point is just 5m away from the edge of the service bay area, where height of excavation changes from 24m to 44.5m. Measured and model values were identical at RD-15 after excavation of bench-7 and at RD-65, after excavation of pits. Measured convergence was 11.53% higher than model result at RD-15 and 15.13% higher at RD-65. Both RD-110 and RD-150 are in unit bay area and model predicted 9.53% more convergence at RD-110 and 13.32% more at RD-150. The difference between predicted and monitored values were within $\pm 15\%$, which established the reliability of the model.

Similarly, bench-6 was taken as the reference for comparing the convergence at EL-520. Fig. 4.78 depicts comparison of convergence at EL-520.

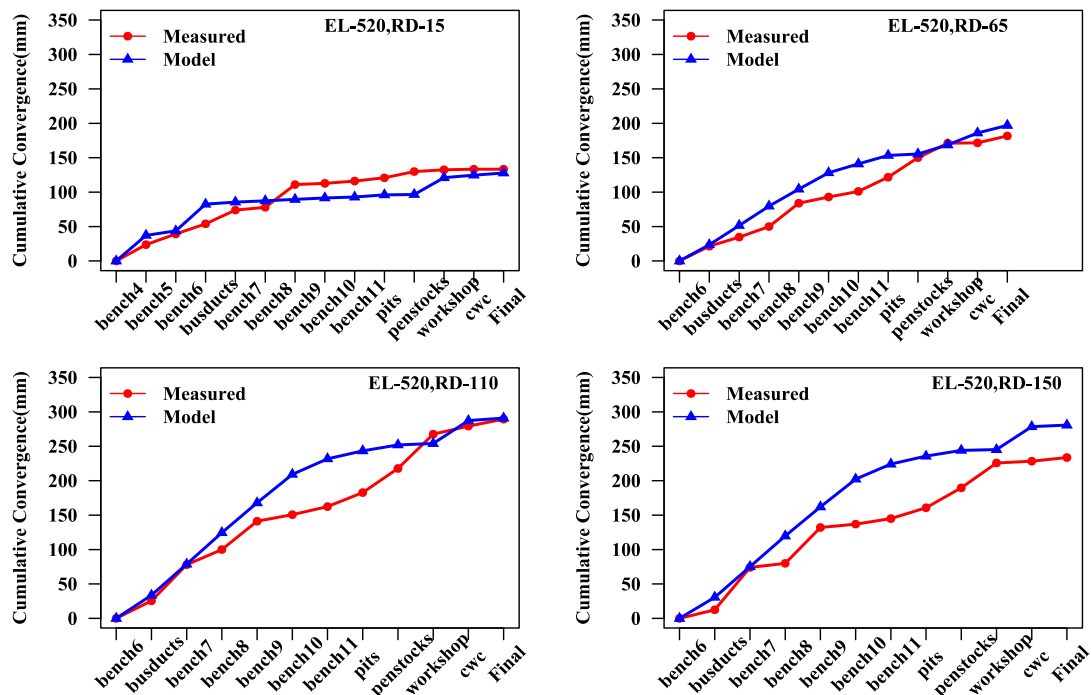


Fig. 4.78 Comparison of measured and model convergence at EL-520

At EL-520, field monitored convergence values were higher than predicted values at RD-15 and at other locations, predicted values were higher than the measured values. At RD-15, measured value was higher by 4.10% against 11.53% at EL-525. At RD-65 and RD-110, both measured and model values were very close with a difference of

8.40% and 0.52% respectively. Overall difference between predicted and monitored values at three points were -8.40% to 4.10%. At RD-150, the predicted value was higher than the measured value by 20.14% against 13.32% at EL-525 (Table 4.27).

Bench-7 was taken as the reference for comparing the convergence at EL-515. Fig. 4.79 depicts comparison of convergence at EL-515.

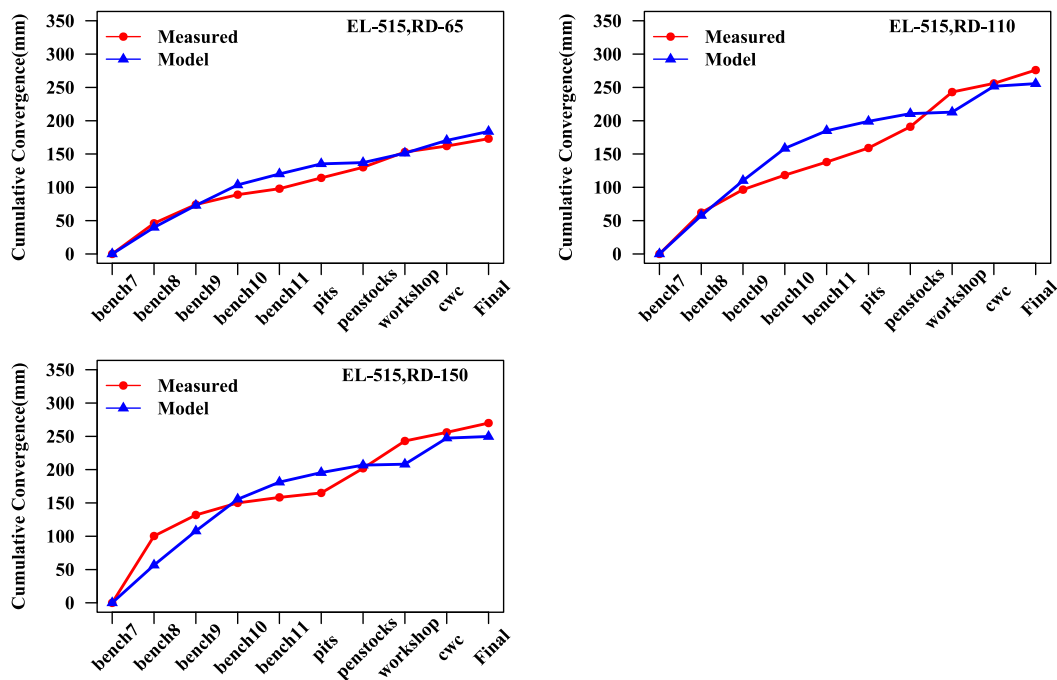


Fig. 4.79 Comparison of measured and model convergence at EL-515

At EL-515, model results were higher at RD-65 by 6.27% and at RD-110 and RD-150, measured values were higher than the model values by 7.40% and 7.49%, respectively. Measured values matched with model results very closely at six excavation stages at RD-65 and two excavation stages at RD-110 and RD-150 (Table 4.27).

Although, model and final measured convergence values match within 15% range in most cases, measured convergence values during benching stage were lower than the model predicted values. This could be due to variation in extraction rates of individual benches.

4.4.3 Stress Distribution

Principal stress contours after complete excavation at RD-15, RD-65, RD-110 and RD-150 are shown in Figs. 4.80 to 4.83.

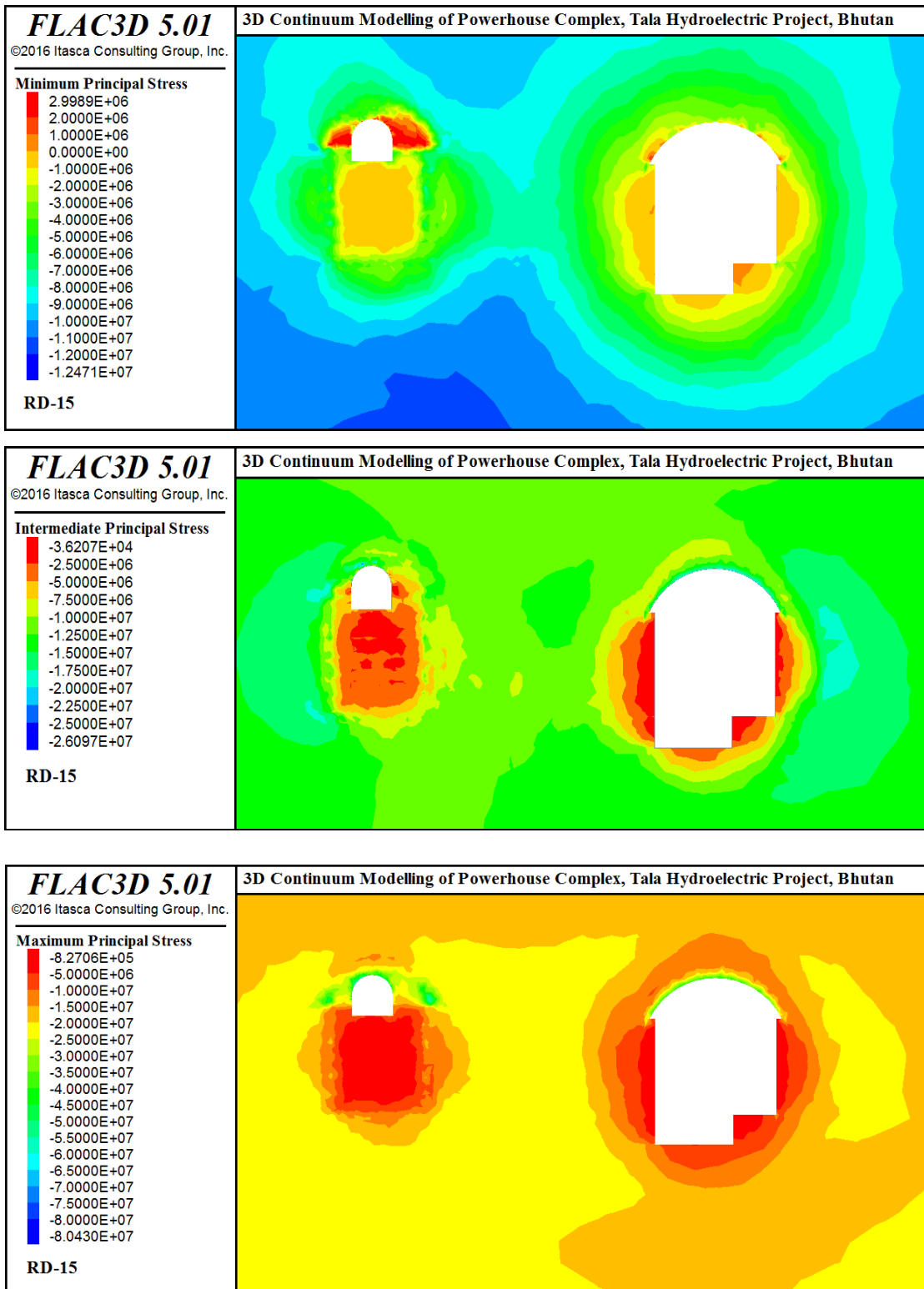


Fig. 4.80 Principal stress contours around the caverns at RD-15

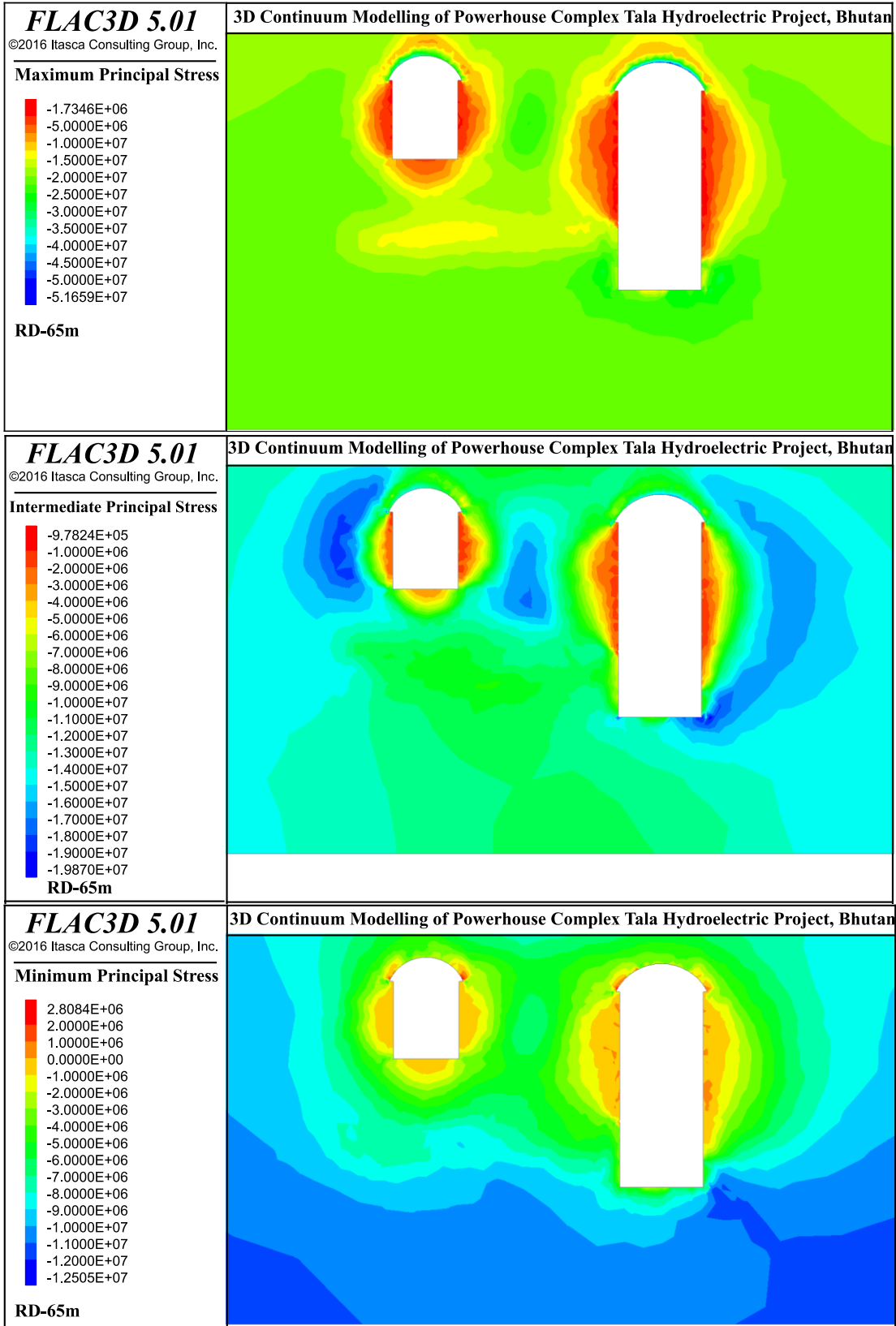


Fig. 4.81 Principal stress contours around the caverns at RD-65

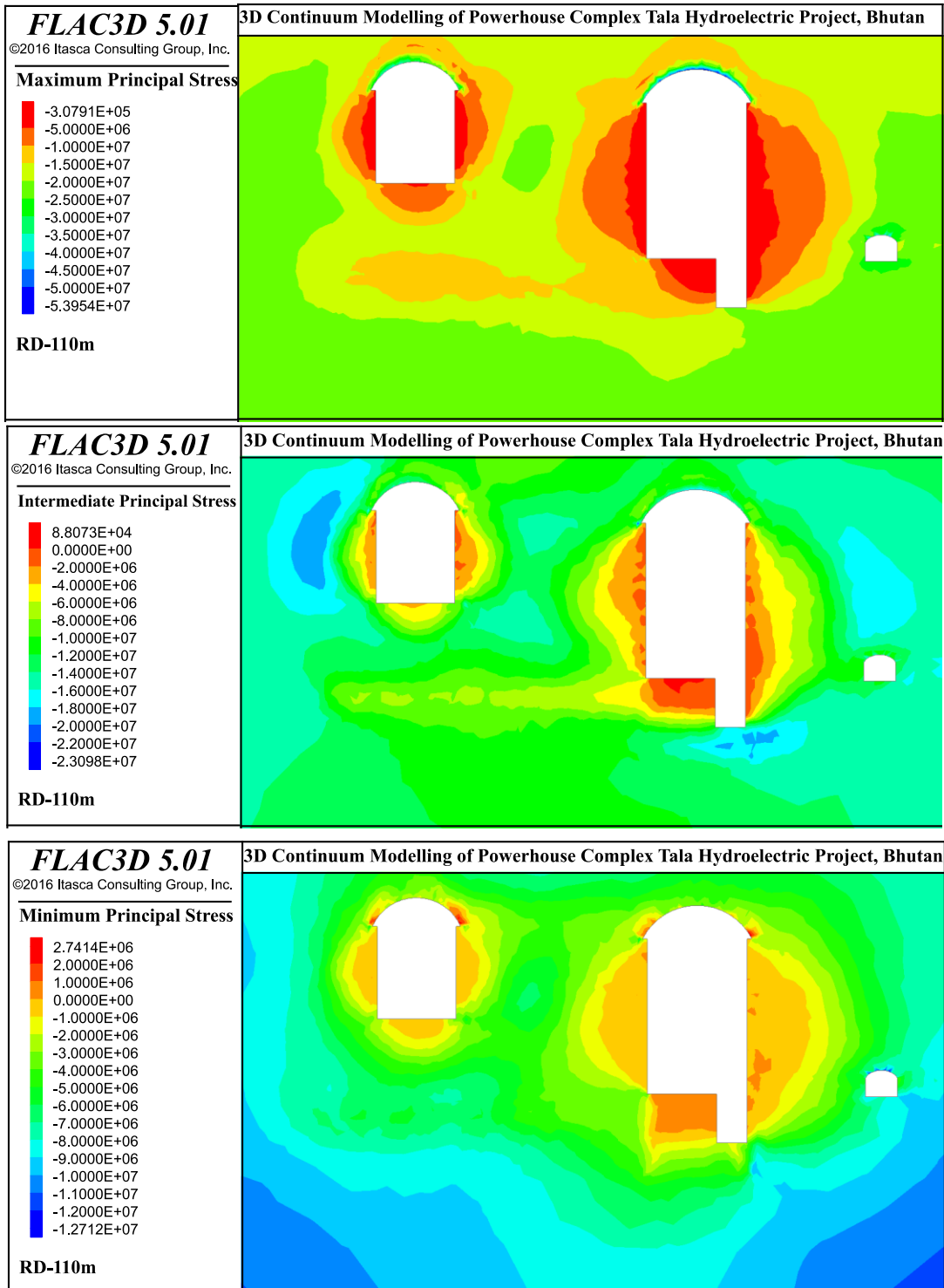


Fig. 4.82 Principal stress contours around the caverns at RD-110

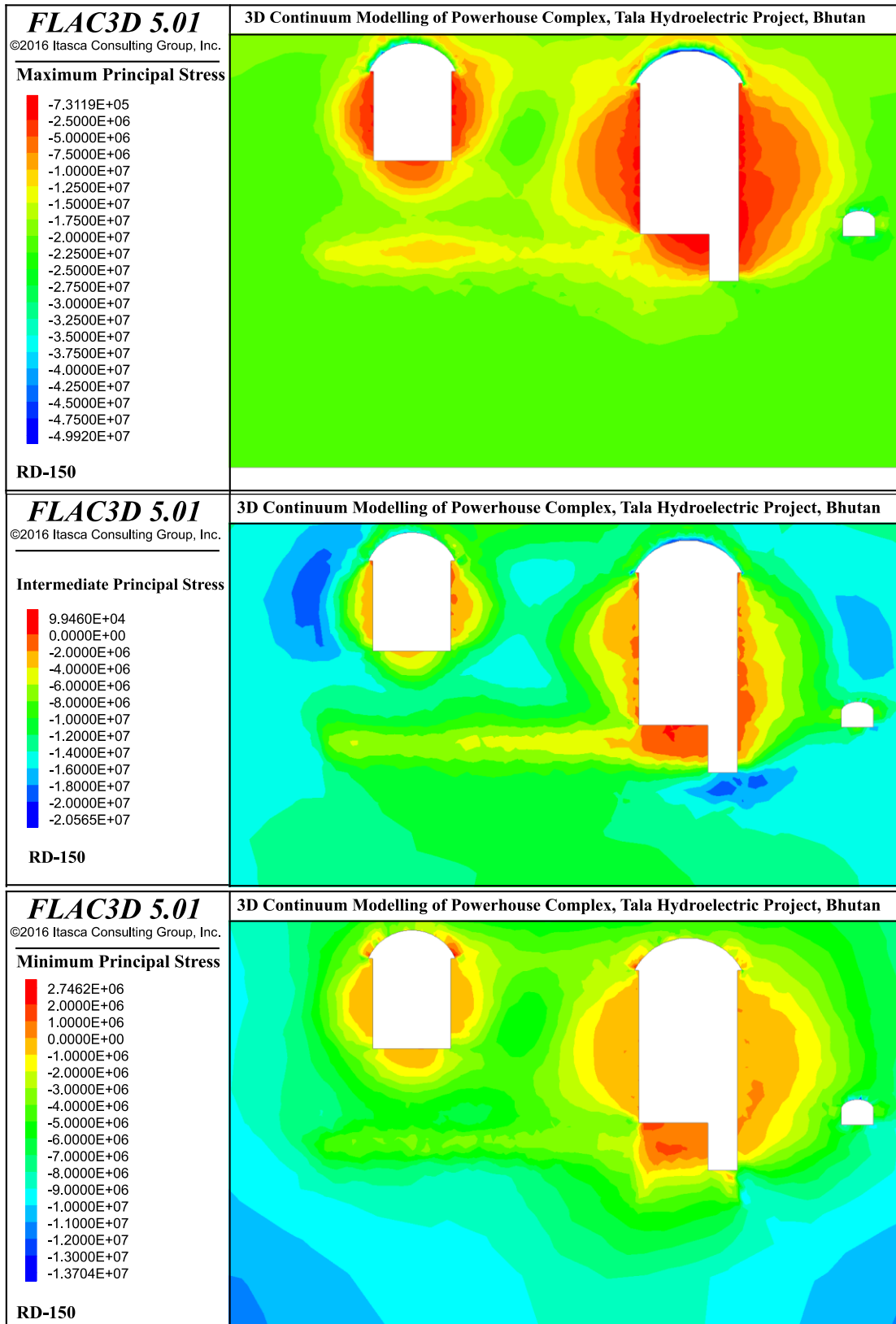


Fig. 4.83 Principal stress contours around the caverns at RD-150

It could be seen from Figs. 4.80 to 4.83 that maximum stress concentration was at the crown of powerhouse and transformer hall caverns. Maximum principal stress reached values of 59.37MPa at RD-15, 51.65MPa at RD-65, 53.95MPa at RD-110 and 49.99MPa at RD-150, an increase of 3.5 to 4.2 times the in-situ value. On the side walls, stresses were relaxed and values of maximum principal stress were 0.788MPa at RD-15, 1.73MPa at RD-65, 0.3MPa at RD-110 and 0.73MPa at RD-150, a decrease of 0.02 to 0.12 times the in-situ value. Similarly, intermediate principal stress (in this case vertical stress) reached maximum values of 20.93MPa at RD-15, 19.87MPa at RD-65, 23.09MPa at RD-110 and 20.56MPa at RD-150, an increase of 1.8 to 2.1 times the in-situ value. In the relaxation zone, it reached minimum values of 1.07MPa at RD-15, 0.97MPa at RD-65, -0.08MPa at RD-110 and -0.09MPa at RD-150, a decrease of 0.01 to 0.10 times the in-situ value. Induced tensile stresses appeared at the floor of powerhouse cavern at RD-110 and RD-150. Maximum values of minimum principal stresses were 12.47MPa at RD-15, 12.50MPa at RD-65, 12.71MPa at RD-110 and 13.70MPa at RD-150, an increase of 1.3 to 1.4 times the in-situ value. Tensile stresses were induced in the concrete above the steel ribs with maximum value of 2.8MPa. Tensile stresses were observed in the rock mass, particularly in the floor of powerhouse cavern due to floor heave. In general, there was an increase in principal stresses in the crown and reduction in principal stresses in the walls of cavern, which corroborates with high values of convergence recordings in the walls.

Ratio of principal stresses at final excavation stage and in-situ principal stresses would give stress concentration factor due to principal stresses. Similarly, ratio of normal stresses at final stage of excavation and in-situ normal stresses would give stress concentration factor due to normal stresses. Maximum, intermediate and minimum principal stresses at final stage of excavation are denoted by σ_{1f} , σ_{2f} and σ_{3f} , respectively and their in-situ values are denoted by σ_{1i} , σ_{2i} and σ_{3i} , respectively. Similarly, final normal stresses in X, Y and Z direction are denoted by σ_{xf} , σ_{yf} and σ_{zf} , respectively and their in-situ values are denoted by σ_{xi} , σ_{yi} and σ_{zi} , respectively. Ratios of stress concentration factors at EL-525, EL-520 and EL-515 for sections at RD-15, RD-65, RD-110 and RD-150 are given in Figs. 4.84 to 4.86.

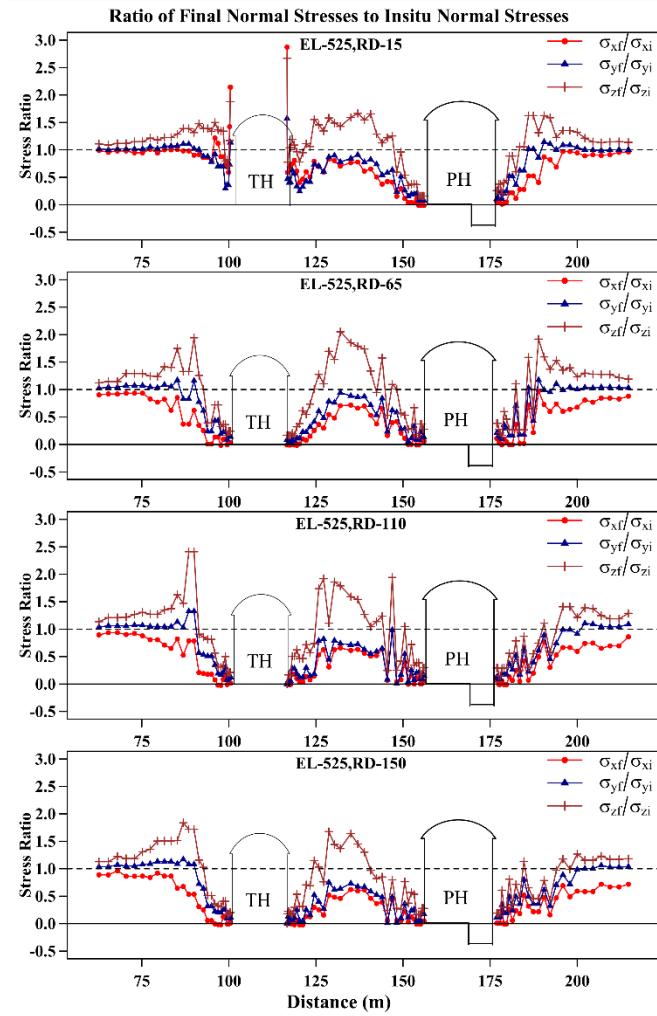
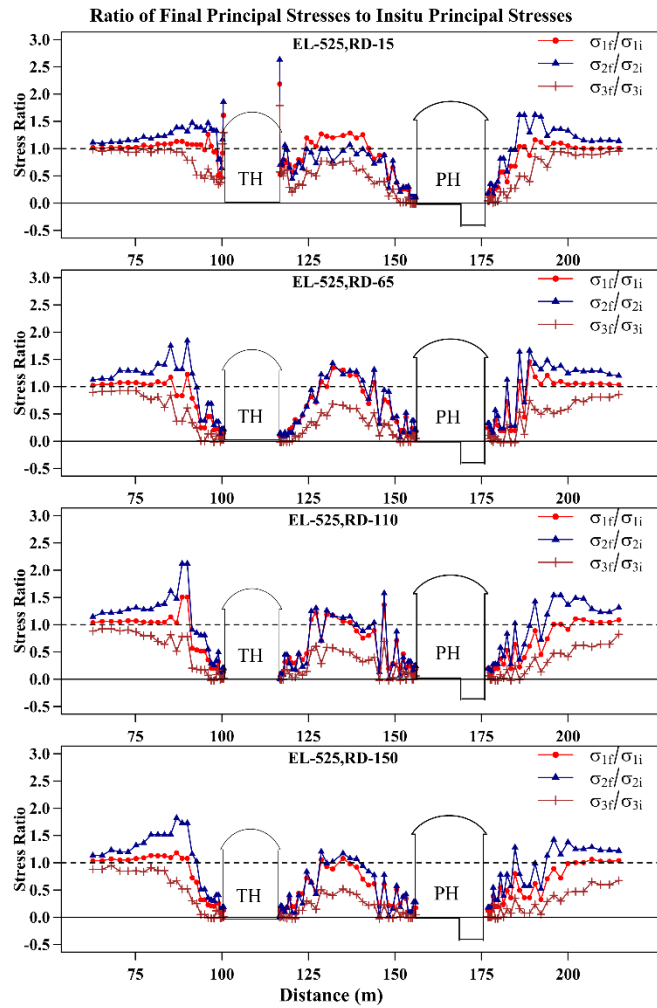


Fig. 4.84 Distribution of stress concentration factors in cross section at EL-525

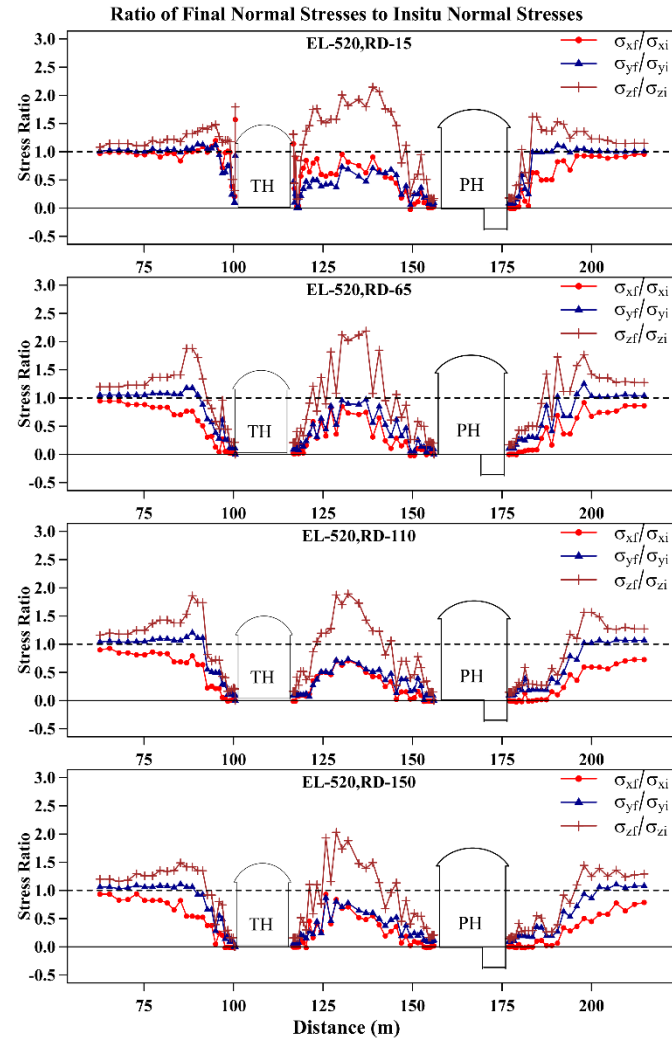
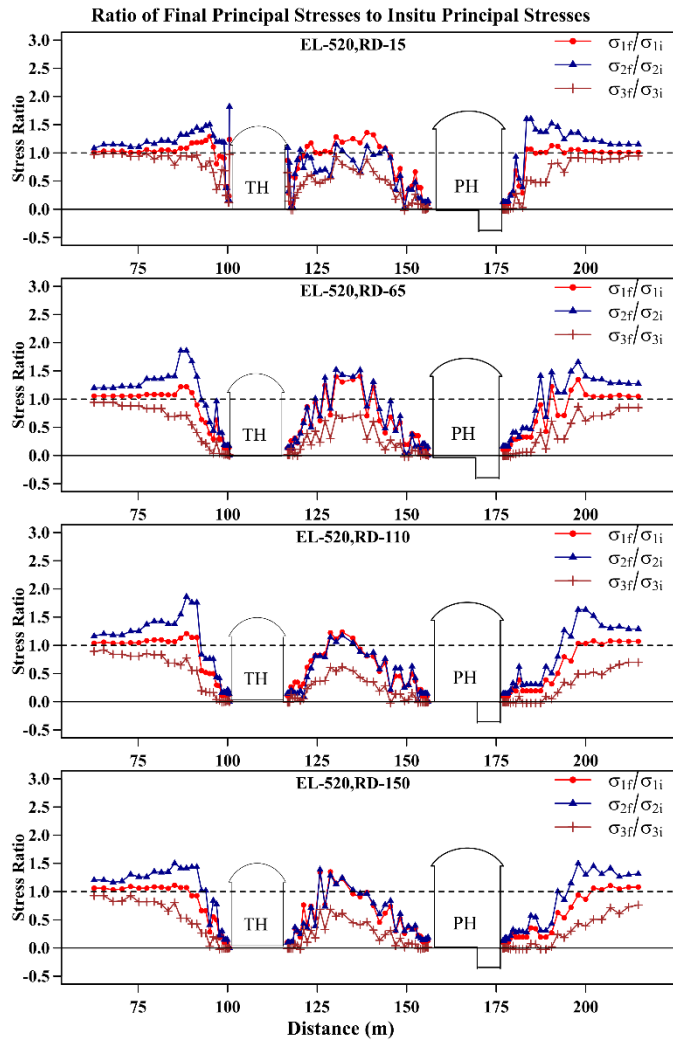


Fig. 4.85 Distribution of stress concentration factors in cross section at EL-520

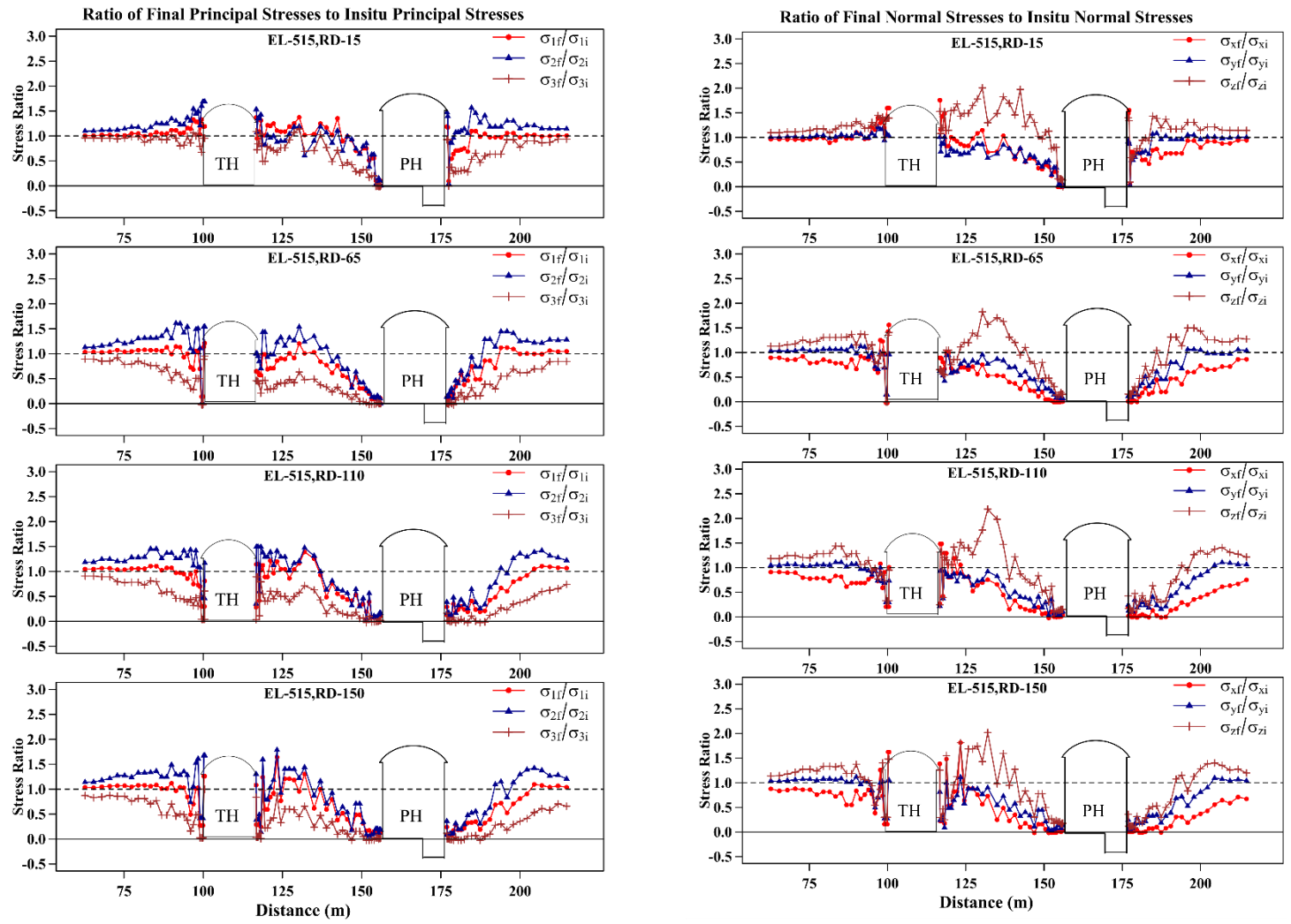


Fig. 4.86 Distribution of stress concentration factors in cross section at EL-515

Stresses in the pillar between powerhouse and transformer hall

At EL-525, stress concentration factors due to maximum and intermediate principal stresses were almost equal except at RD-15, where stress concentration factor due to maximum principal stress was higher. At RD-15, maximum stress concentration factor was 2.63, whereas at RD-65, RD-110 and RD-150 it was 1.43, 1.58 and 1.20, respectively (Fig. 4.84). Higher stress concentration was observed near the edge of transformer hall at RD-15 cross section as transformer hall is only 0.5m away from end wall at this section.

Normal stresses had higher influence on the stress concentration factors in the pillar. Vertical stress had maximum influence on the pillar and maximum stress concentration factors due to vertical stress was almost two times more than that due to two horizontal stresses. At EL-525, maximum stress concentration factor due to vertical stress was 2.67 at RD-15, 2.05 at RD-65, 1.94 at RD-110 and 1.68 at RD-150. Only at edge of transformer hall stress concentration factor due to σ_x was higher at 2.87 and at all other places it was less than 1 (Fig. 4.84).

Similar observations were observed at EL-520. Maximum stress concentration factor due to principal stresses at RD-15, RD-65, RD-110 and RD-150 were 1.36, 1.52, 1.23 and 1.39 respectively. Maximum stress concentration factor due to normal stresses at RD-15, RD-65, RD-110 and RD-150 were 2.15, 2.19, 1.89 and 2.03 respectively (Fig. 4.85).

EL-515, is just 0.5m above the floor of transformer hall and height of transformer hall is equal to height of powerhouse in service bay area. In the pillar, maximum stress concentration factors were closer to transformer hall. Maximum stress concentration factors due to principal stresses were 1.53, 1.54, 1.49 and 1.79 at RD's 15, 65, 110 and 150, respectively and that due to normal stresses were 2.01, 1.83, 2.19 and 2.02, respectively. Stress relaxation near the transformer hall floor was to a lesser extent compared to other locations (Fig. 4.86).

Stresses on upstream side of powerhouse

On upstream side of powerhouse cavern, stress concentration factors due to intermediate principal stress were higher than that due to maximum and minimum

principal stresses in all cases. At EL-525, maximum stress concentration took place at a distance of 12-19m from the upstream wall. Maximum stress concentration factors due to intermediate stress were 1.62, 1.66, 1.54 and 1.42 at RD's 15, 65, 110 and 150, respectively (Fig. 4.84).

On the upstream side of powerhouse cavern, normal stresses had higher influence than the principal stresses. Here also, stress concentration factors induced by vertical stress were higher than other two normal stresses. At EL-525, maximum stress concentration due to vertical stress took place at a distance of 12-23m from the upstream wall. Maximum stress concentration factors due to vertical stress were 1.63, 1.92, 1.41 and 1.27 at RD's 15, 65, 110 and 150, respectively (Fig. 4.84).

Similar observations were observed at EL-520. Maximum stress concentration factors due to intermediate principal stress at RD-15, RD-65, RD-110 and RD-150 were 1.60, 1.66, 1.63 and 1.50, respectively. Maximum stress concentration factor due to other two principal stresses varied from 0.70 to 1.35. Maximum stress concentration factor due to vertical stress at RD-15, RD-65, RD-110 and RD-150 were more or less same, with values of 1.62, 1.76, 1.56 and 1.44, respectively. Maximum stress concentration factor due to horizontal stresses varied from 0.73 to 1.25. At EL-520, maximum value occurred at a distance of 6.6m at RD-15 and at 21m at RD's 65, 110 and 150 (Fig. 4.85).

Maximum stress concentration factors at EL-515 due to intermediate principal stress were 1.57, 1.45, 1.42 and 1.42 at RD's 15, 65, 110 and 150 and occurred at distances of 7.8m, 17.1m, 30m and 27.6m, respectively. Similarly, maximum stress concentration factor due to vertical stress varied from 1.40 to 1.50 on the downstream wall of transformer hall (Fig. 4.86).

Stresses on downstream side of transformer hall

Similar to upstream side of powerhouse cavern, at downstream side of transformer hall also stress concentration factors induced by intermediate principal stress were higher than that due to other two principal stresses. At EL-525, maximum stress concentration factors due to intermediate stress were 1.85, 1.84, 2.12 and 1.82 at RD's 15, 65, 110 and 150 respectively (Fig. 4.84). At RD-15, maximum value occurred very close to the

wall and at other places, it occurred at 12.5-13.6m from the wall. Stress concentration factor due to other two principal stresses varied from 0.93 to 1.61.

In this case also, vertical stress had higher influence on the stress concentration factor compared to that due to other two normal stresses. Maximum stress concentration factors due to vertical stress were 1.88, 1.94, 2.41 and 1.84 at RD's 15, 65, 110 and 150, respectively. At RD-15, maximum value occurred very close to the wall and at other places, it occurred at 10.5-13.6m from the wall (Fig. 4.84).

Similar observations were observed at EL-520. Maximum stress concentration factor due to intermediate principal stress at RD-15, RD-65, RD-110 and RD-150 were 1.82, 1.86, 1.86 and 1.50, respectively. Maximum stress concentration factor due to other two principal stresses varied from 0.92 to 1.29. Maximum stress concentration factor due to vertical stress at RD-15, RD-65, RD-110 and RD-150 were 1.79, 1.88, 1.86 and 1.49, respectively (Fig. 4.85). Maximum stress concentration factor due to horizontal stresses varied from 0.93 to 1.57 (Fig. 4.85). At EL-520, maximum value occurred close to wall at RD-15 and at 13.6m, 12m, and 15.3m at RD's 65, 110 and 150, respectively.

At EL-515, maximum stress concentration factor due to intermediate principal stress were 1.69, 1.61, 1.45 and 1.68 at RD's 15, 65, 110 and 150, respectively. Maximum values were close to the downstream wall of transformer hall at RD-15 and RD-150. It was at 9.1m and 15.3m from the wall at RD-65 and RD-110. Similarly, maximum stress concentration factor due to vertical stress varied from 1.41 to 1.48 on the downstream of transformer hall (Fig. 4.86).

When the cavern is oriented along maximum principal stress direction and walls are subjected to minimum principal stress (vertical stress being intermediate principal stress), stress concentration factor induced by intermediate principal stress was higher than the other two on upstream wall of powerhouse and downstream wall of transformer hall. In the pillar between powerhouse and transformer hall, stress concentration factor induced by maximum and intermediate principal stress was almost equal and that introduced by minimum principal stress was lower.

Stress analysis of pillar between powerhouse cavern and transformer hall cavern indicated stress concentration in the center of the pillar and stress relaxation at the pillar

edges (downstream wall of powerhouse cavern and upstream wall of transformer hall cavern), resulting in considerable displacement of walls, in agreement with the convergence recordings in the field. On the upstream side of powerhouse cavern, the relaxation zones were extending upto 15m (average), indicating that large displacements were taking place upto 15m depth, with maximum displacement at the upstream wall. This aspect was proved by observation of large convergence of the walls in the field. Similar phenomenon was observed on downstream side of transformer hall also.

4.4.4 Strain on the Walls of Caverns

Strain on upstream and downstream wall was calculated considering the half width of the cavern, so that areas of relatively high strains on each wall are identified more precisely. The percentage strain calculated on upstream side and downstream side of powerhouse cavern are shown in the form of contours in Fig. 4.87 and Fig. 4.88, respectively.

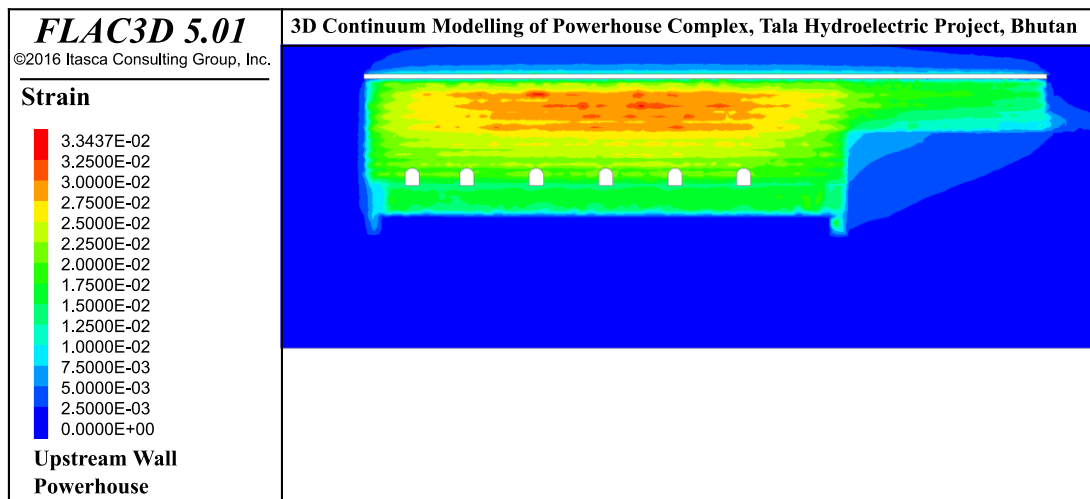


Fig. 4.87 Strain distribution on upstream wall of powerhouse cavern

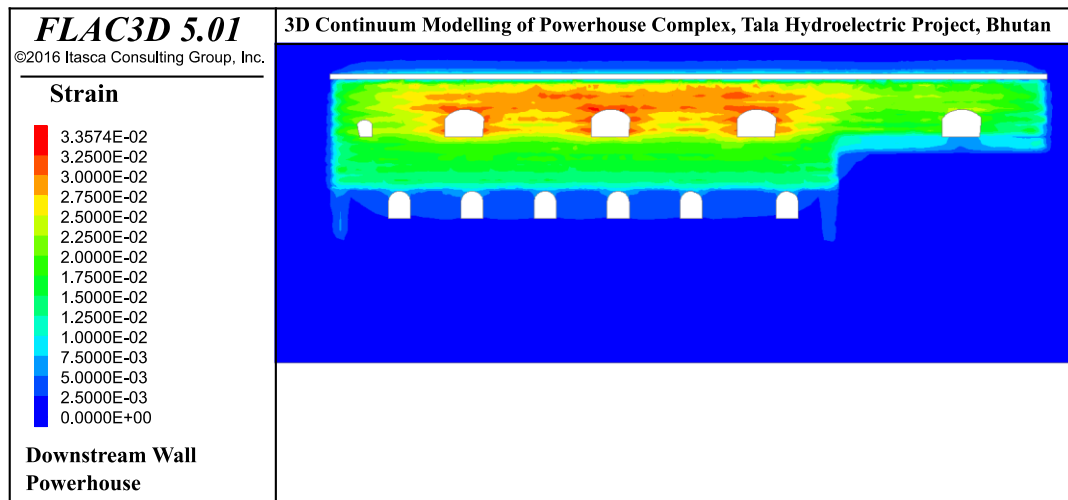


Fig. 4.88 Strain distribution on downstream wall of powerhouse cavern

A maximum strain of 3.34% was observed on the upstream wall, between elevations 527.5 and 517, inbetween RD-95 and RD-157. On the upstream wall, strains of more than 2% were observed in unit bay area from EL-531 to EL-505 (where width to height ratio is 0.46). In the service bay area, strains were restricted upto 2% (where width to height ratio is 0.85). Maximum strain observed on downstream wall was 3.35% and observed between elevations 527 and 516 inbetween RD-76 and RD-174, where bus ducts are situated. Higher strains were concentrated near the crown of bus ducts. On downstream wall, strains of less than 2% were observed in service bay area. Results clearly indicated that when the height of excavation increases (w/h ratio decreases), unit bay area experiences higher strain.

Similarly, strain on the upstream and downstream wall of transformer hall are shown in Figs. 4.89 and 4.90, respectively, indicating a similar behaviour of rock mass.

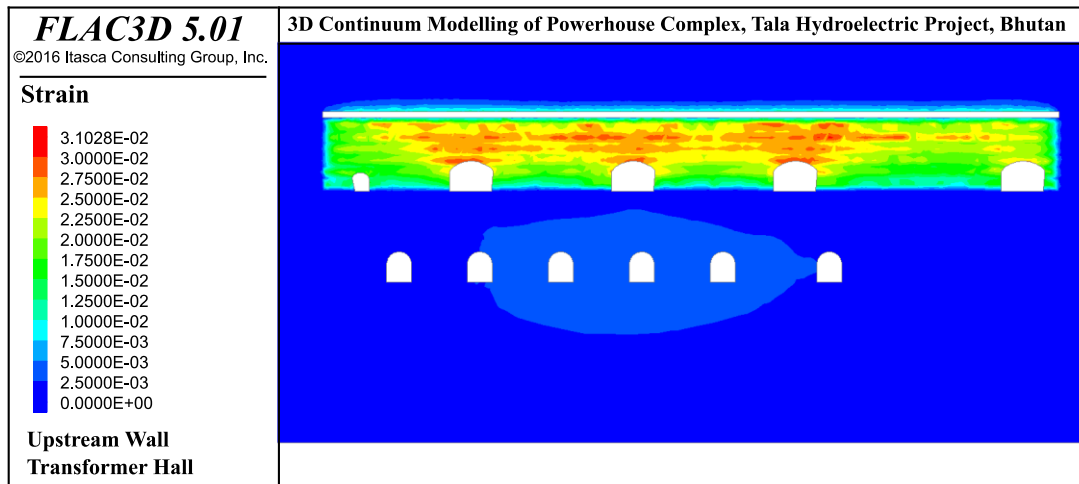


Fig. 4.89 Strain distribution on upstream wall of transformer hall cavern

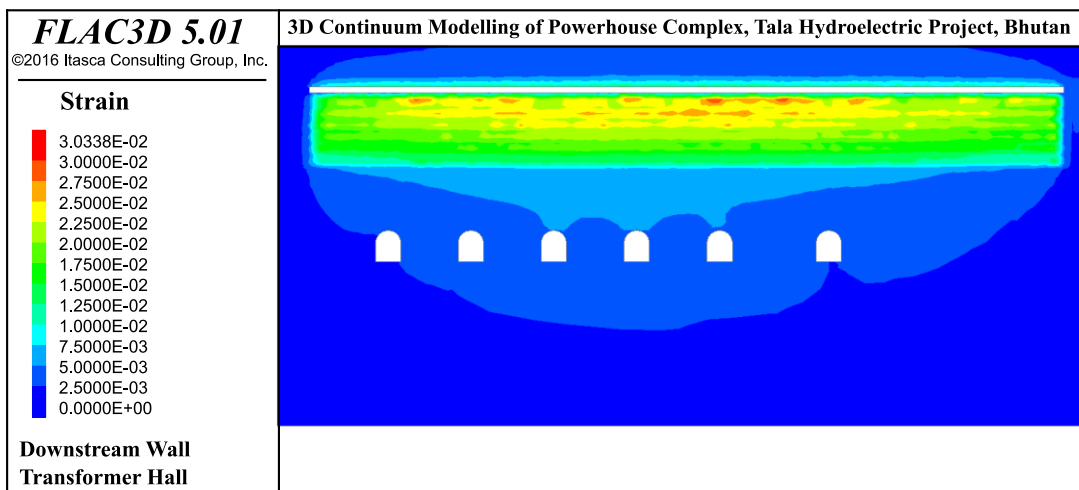


Fig. 4.90 Strain distribution on downstream wall of transformer hall cavern

4.4.5 Strength to Stress Ratio

Strength to stress ratio calculated using 3D Hoek and Brown failure criterion is shown in sections at RD-15, RD-65, RD-110 and RD-150 in Figs. 4.91 to 4.94. Tensile failures were noticed in the corners and at the floor of the powerhouse cavern (due to floor heave). Most of the surrounding rock mass had strength to stress ratio of more than two, except few isolated patches in the immediate vicinity of the walls of cavern. Overall stability of the cavern was not affected by these small patches of failed zone.

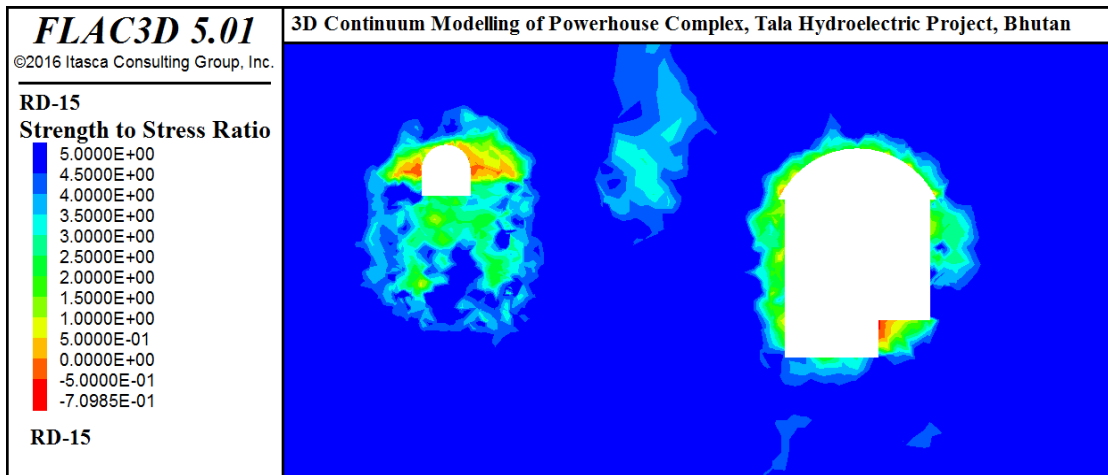


Fig. 4.91 Strength to stress ratio at RD-15, powerhouse cavern

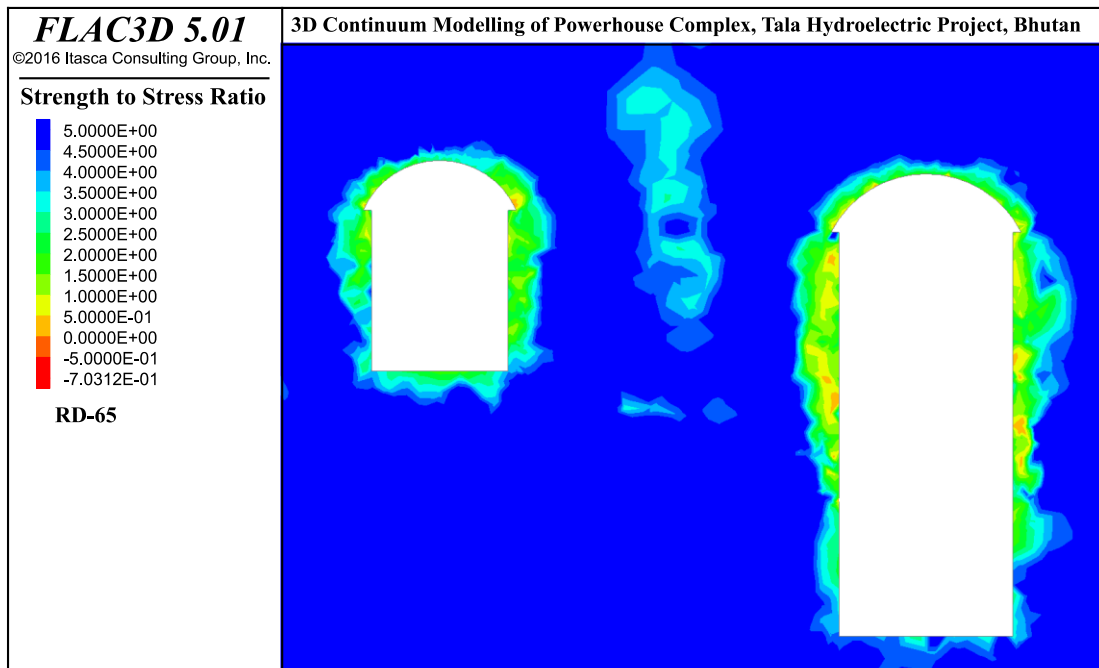


Fig. 4.92 Strength to stress ratio at RD-65, powerhouse cavern

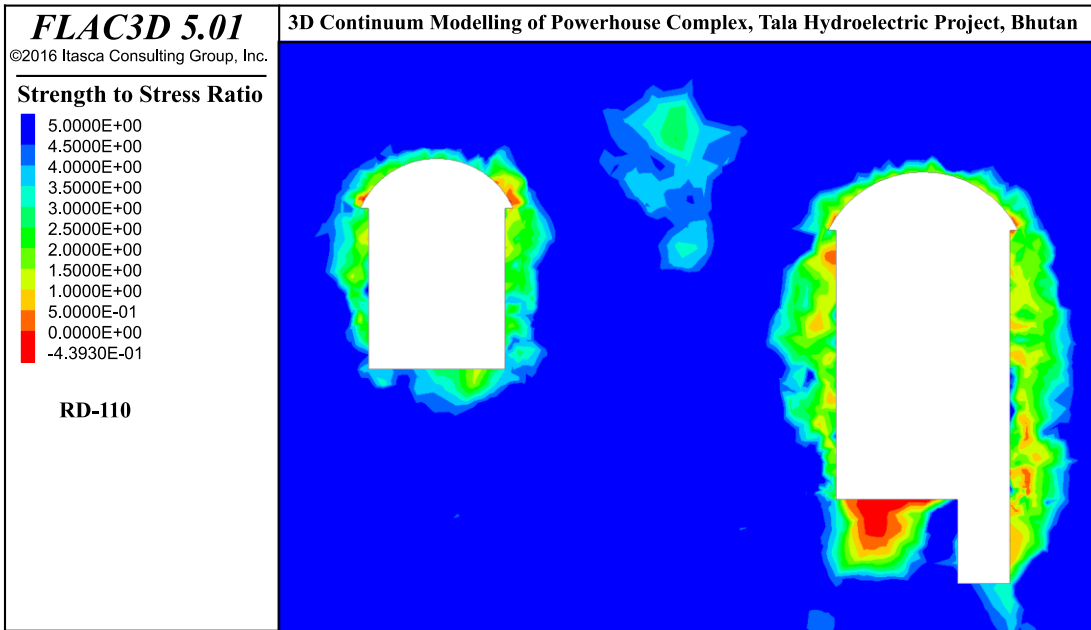


Fig. 4.93 Strength to stress ratio at RD-110, powerhouse cavern

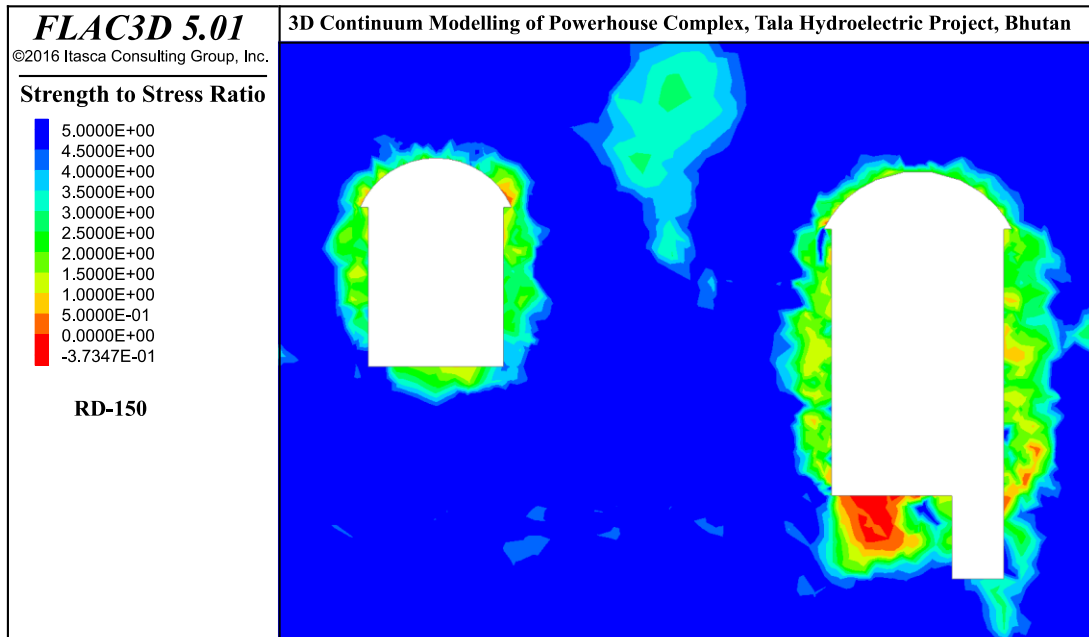


Fig. 4.94 Strength to stress ratio at RD-150, powerhouse cavern

4.4.6 Effect of Cavern Orientation on Stability

A parametric study was carried out by varying the angle (Θ) between cavern axis and direction of maximum principal stress at an interval of 15° . Variation of displacement with various configurations at EL-525, EL-520 and EL-515 are shown in Fig. 4.95.

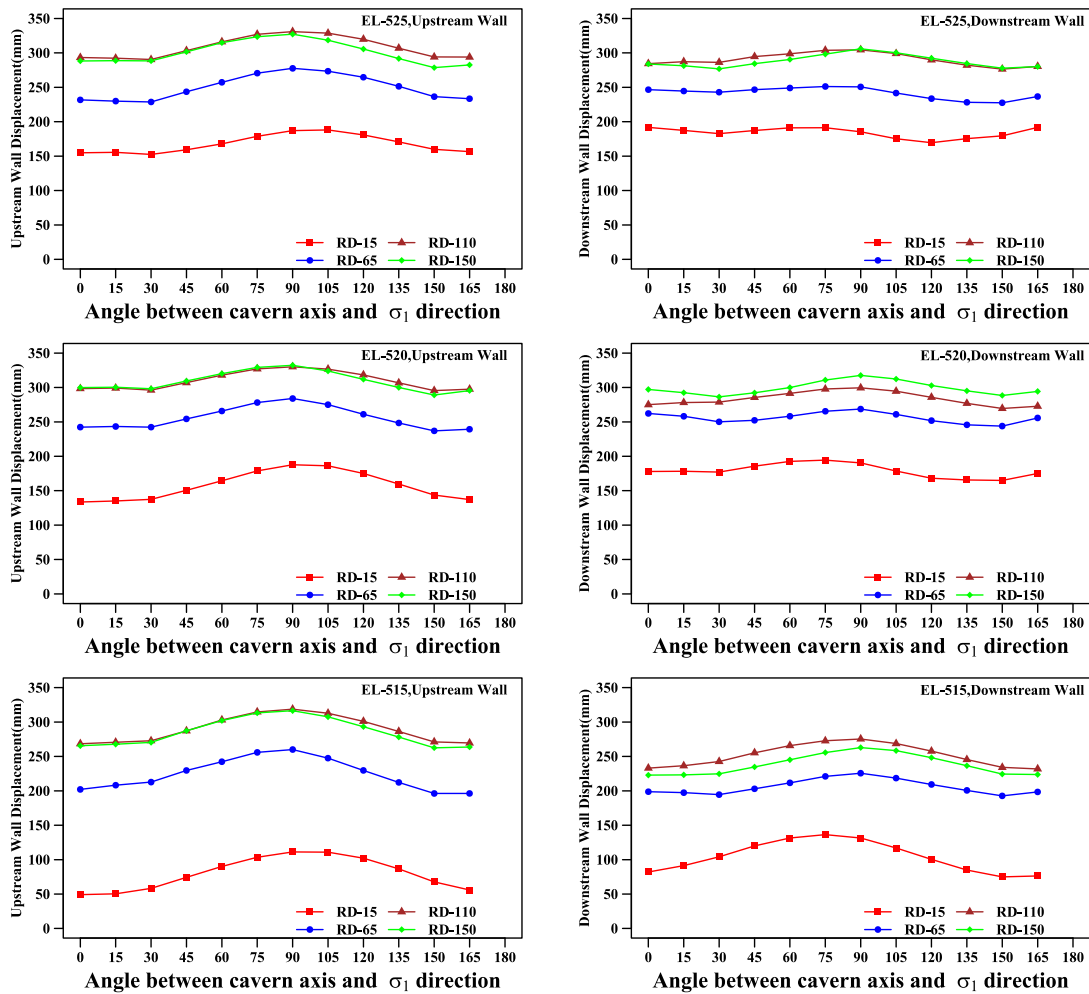


Fig. 4.95 Variation of displacement with cavern configuration

On upstream side, an increase in maximum displacement by about 28.7% was found to occur at an angle of 90° . On downstream side, increase in maximum displacement was found to be only 18.2% at an angle of 90° . Parametric study results have indicated that with an increase in angle between axis of the cavern to principal stress direction, displacements were increasing and reaching highest value at 90° orientation. Similar behaviour was observed at EL-525, EL-520 and EL-515.

Stress concentration factors at various orientations in pillar between powerhouse and transformer hall were analysed. Maximum stress concentration factors observed in the pillar with different orientations due to vertical stress and other two normal stresses are shown in Figs. 4.96 to 4.98.

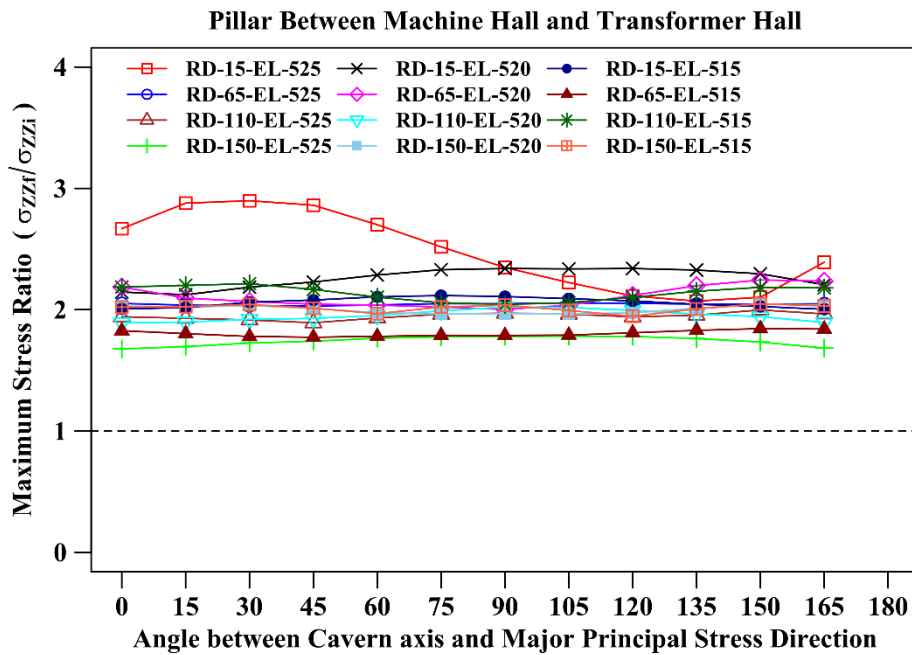


Fig. 4.96 Variation of maximum stress ratio in the pillar due to vertical stress with cavern configuration

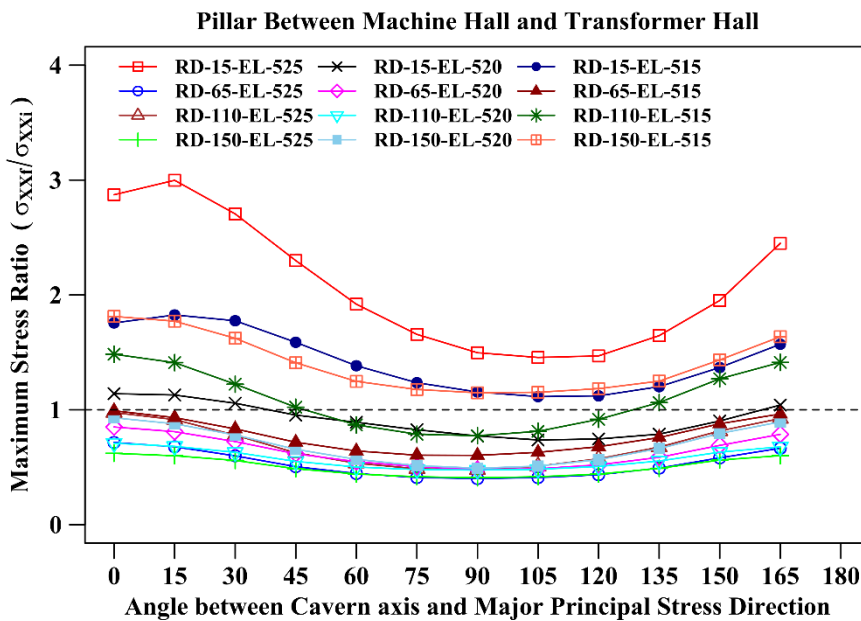


Fig. 4.97 Variation of maximum stress ratio in the pillar due to σ_{xx} with cavern configuration

Maximum stress concentration factor due to vertical stress varied in the range 1.68 to 2.25 in RD's 65,110 and 150 with maximum value at RD-65 at EL-525 at an angle of 150° and minimum at RD-150, EL-525 at an angle of zero degree. At RD-15, it varied from 2.0 to 2.90 with maximum at EL-525 at an angle of 30° and minimum at EL-515 at an angle of 165° (Fig. 4.96). Thus maximum stress concentration factor in the pillar due to vertical stress does not change significantly with cavern configuration except in the pillar near the end walls.

Maximum stress concentration factor due to σ_{xx} varied from 0.40 to 1.81 in the unit bay area and 0.74 to 3 at RD-15. That means the maximum confinement provided by σ_{xx} decreased to 0.40 times the in-situ value at an angle of 90° that may have adverse effect on the stability of the pillar (Fig. 4.97).

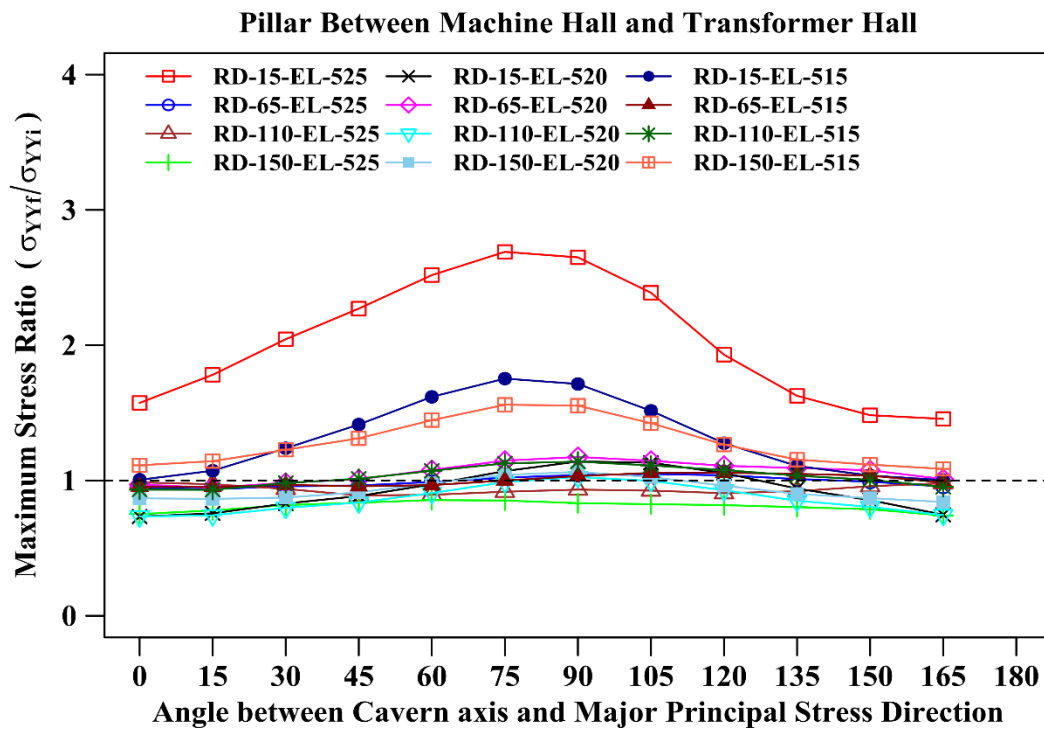


Fig. 4.98 Variation of maximum stress ratio in the pillar due to σ_{yy} with cavern configuration

Maximum stress concentration factor due to σ_{yy} varied from 0.73 to 1.56 in the unit bay area and 0.73 to 2.69 at RD-15 with maximum values at an angle of 75° and 90°. That means maximum stress concentration factor due to σ_{yy} (which already has highest magnitude) at 75° and 90° increased by 1.56 times the in-situ value (Fig. 4.98).

Maximum stress concentration factors due to vertical stress, observed in the upstream wall of powerhouse with different orientations and other two normal stresses are shown in Figs. 4.99 to 4.101.

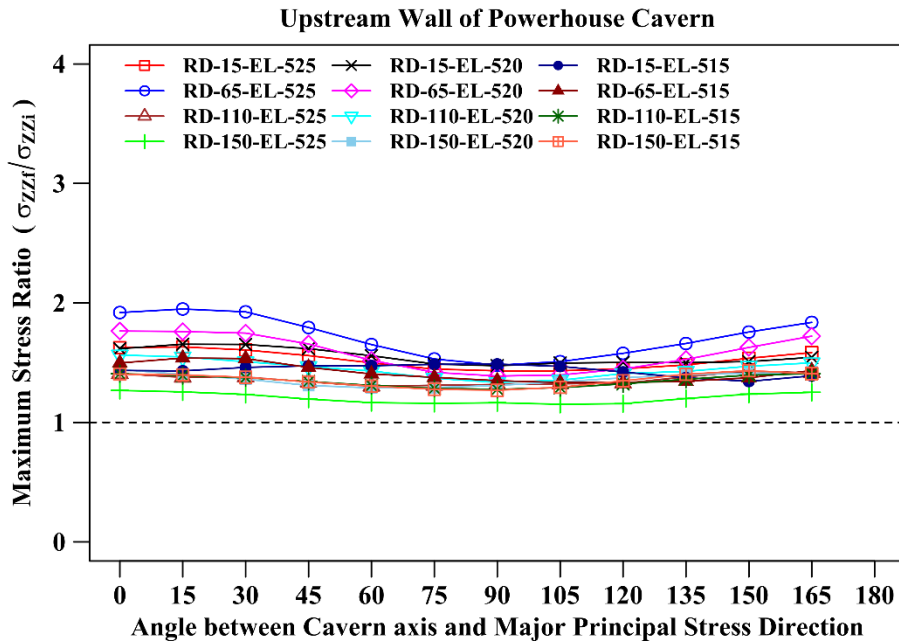


Fig. 4.99 Variation of maximum stress ratio in the upstream wall of powerhouse due to vertical stress (σ_{zz}) with cavern configuration

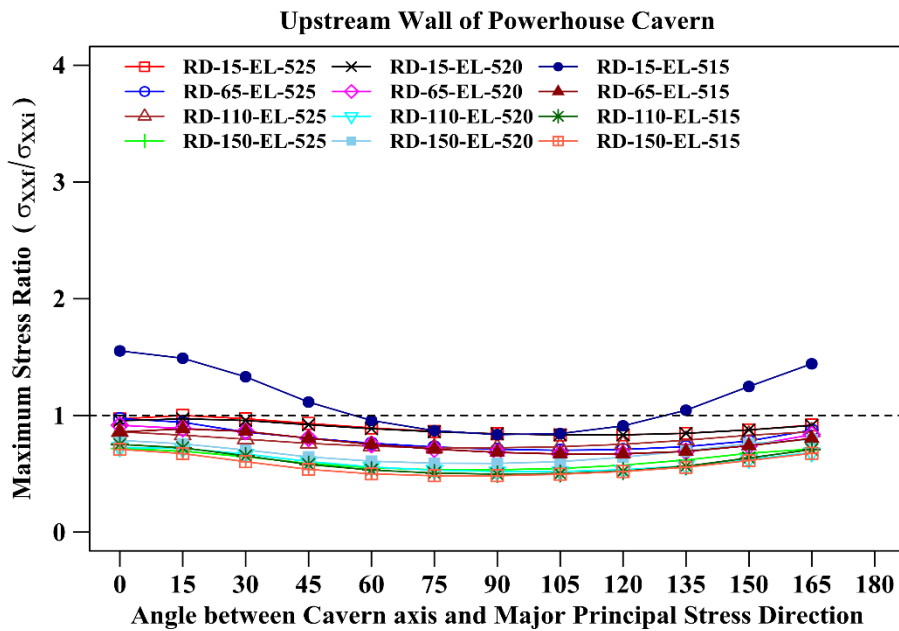


Fig. 4.100 Variation of maximum stress ratio in the upstream wall of powerhouse due to σ_{xx} stress with cavern configuration

On the upstream wall of powerhouse cavern, maximum stress concentration factor due to vertical stress varied from 1.15 to 1.95 and effect of end wall (at RD-15) was not there. Maximum values occurred at an angle of zero degree and minimum values occurred at an angle of 90° (Fig. 4.99). Maximum stress concentration factors due to σ_{xx} varied from 0.48 to 1.55 and maximum level of destressing of rock mass in the upstream wall occurred at an angle of 90°. At RD-15 at EL-515 (floor level at service bay area), destressing was minimum at an angle of zero and 165° (Fig. 4.100). Maximum stress concentration factor due to σ_{yy} varied from 0.84 to 1.26 with maximum confinement levels going below the in-situ values from angles 60° to 120° (Fig. 4.101).

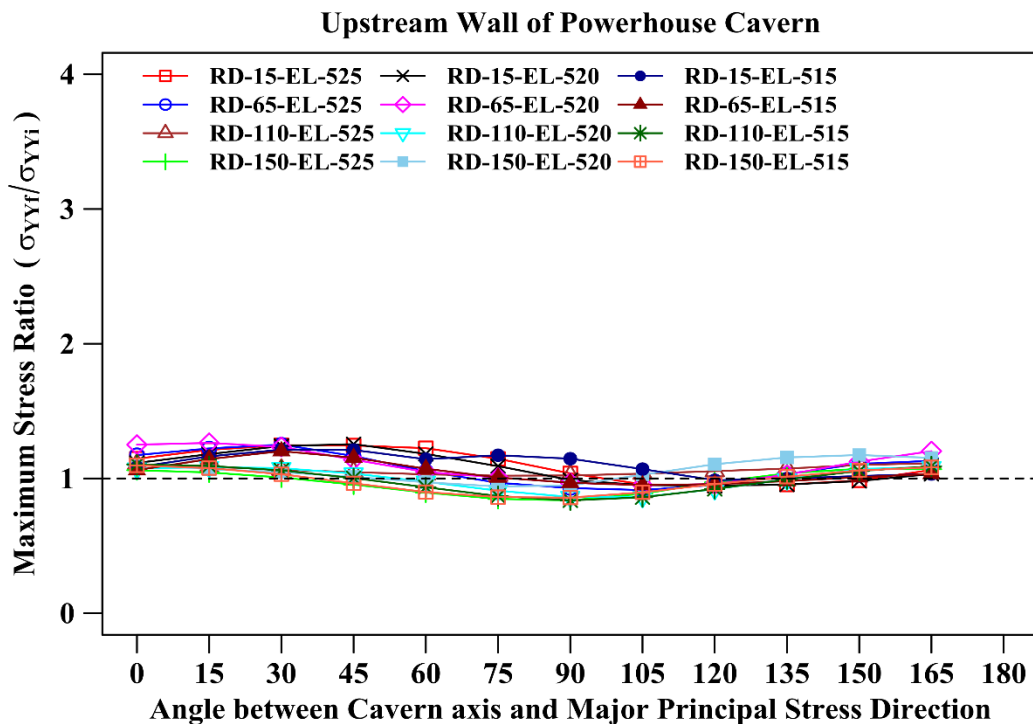


Fig. 4.101 Variation maximum stress ratio in the upstream wall of powerhouse due to σ_{yy} stress

Thus at an angle of zero degree, i.e. when the cavern was oriented parallel to maximum principal stress, maximum stress concentration factors due to vertical stress were the highest on the upstream wall of powerhouse. But at an angle of 90°, confinement provided by σ_{xx} and σ_{yy} decreased, causing instability problems in the wall.

Maximum stress concentration factors observed in the downstream wall of transformer hall cavern with different orientations due to vertical stress and other two normal stresses are shown in Figs. 4.102 to 4.104.

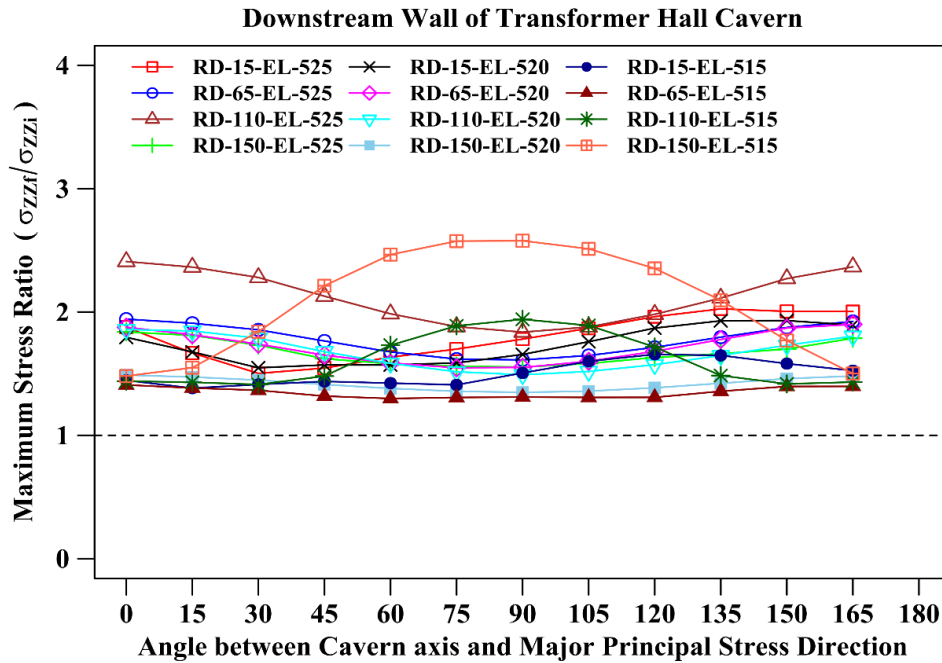


Fig. 4.102 Variation maximum stress ratio in the downstream wall of transformer hall due to vertical stress (σ_{zz})

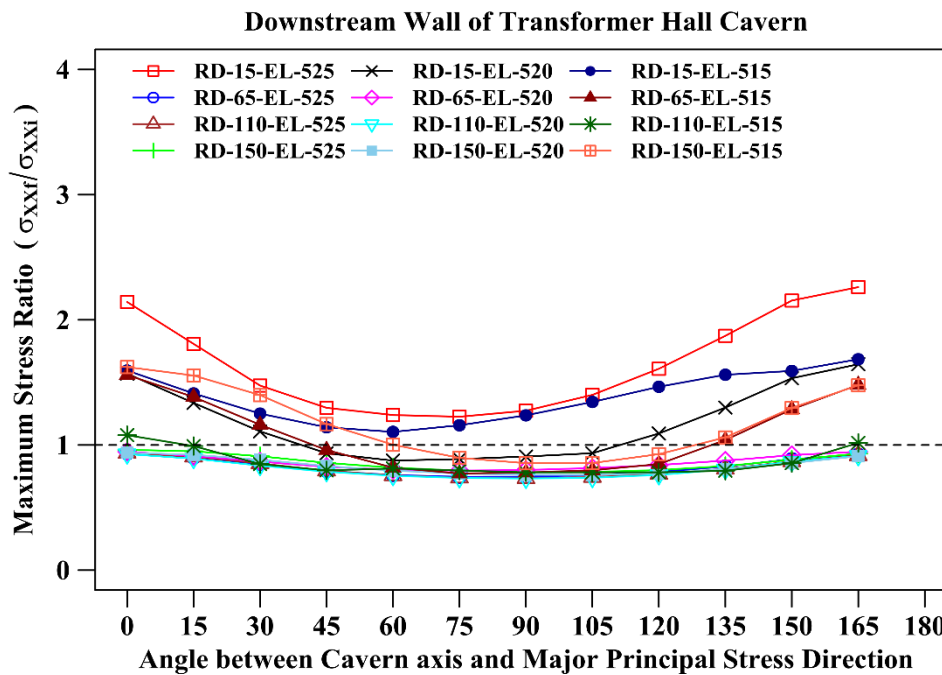


Fig. 4.103 Variation maximum stress ratio in the downstream wall of transformer hall due to σ_{xx} stress

Maximum stress concentration factor due to vertical stress in unit bay area varied from 1.3 to 2.58, maximum being at RD-150 at EL-515 when the orientation angle was 90°, whereas in service bay area at RD-15 it varied from 1.38 to 2.03 (Fig. 4.102). Maximum stress concentration factors due to σ_{xx} in unit bay area varied from 0.73 to 1.62, and in service bay area at RD-15 it varied from 0.88 to 2.26 (Fig. 4.103). Similarly, maximum stress concentration factor due to σ_{yy} in unit bay area varied from 0.96 to 1.59 and in service bay area it varied from 0.97 to 2.27 (Fig. 4.104). Confinement levels provided by σ_{xx} and σ_{yy} were greater on downstream wall of transformer hall than on the upstream wall of powerhouse cavern.

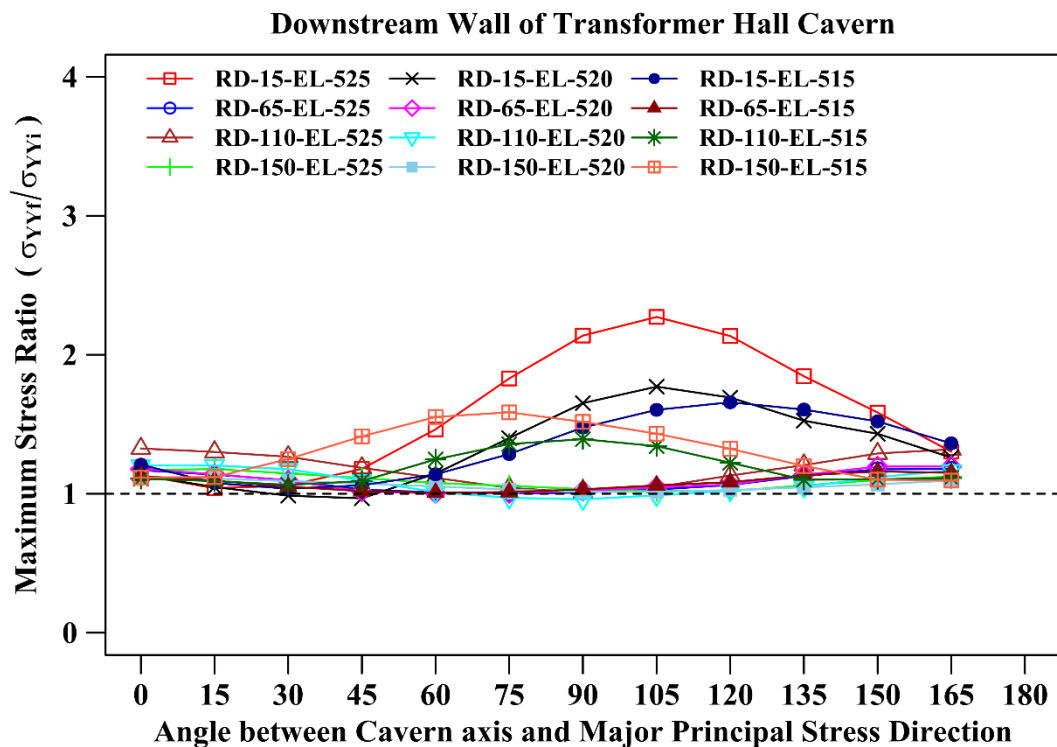


Fig. 4.104 Variation maximum stress ratio in the downstream wall of transformer hall due to σ_{yy} stress

4.4.7 Sensitivity Analysis

In this study, four independent variables - cohesion, friction angle, elastic modulus and Poisson's ratio were taken into consideration to analyse their effect on final convergence predicted from the modelling study. Independent parameters were changed from +20% to -20% at a step of 5%. Results of sensitivity analysis are listed in Table 4.28.

Table 4.28 Results of sensitivity analysis

		Predicted Convergence (mm)				Percent Change with Reference to Base Model			
RD & EL	%	C	Φ	E	ν	C	Φ	E	ν
RD-65 EL-525	80%	313.4	424.7	293.7	264.5	31.9%	78.7%	23.6%	11.3%
	85%	290.2	362.8	277.7	257.8	22.1%	52.7%	16.9%	8.5%
	90%	271.0	311.6	263.0	250.4	14.1%	31.1%	10.7%	5.4%
	95%	253.4	270.5	249.8	244.4	6.6%	13.8%	5.1%	2.9%
	100%	237.6	237.6	237.6	237.6	Base Model			
	105%	223.9	211.8	227.4	230.7	-5.8%	-10.9%	-4.3%	-2.9%
	110%	212.1	191.3	217.2	223.9	-10.8%	-19.5%	-8.6%	-5.8%
	115%	200.8	174.6	201.5	217.2	-15.5%	-26.5%	-15.2%	-8.6%
	120%	190.7	161.0	199.9	210.2	-19.8%	-32.3%	-15.9%	-11.5%
RD-110 EL-525	80%	442.6	581.9	411.8	374.3	32.5%	74.2%	23.3%	12.0%
	85%	410.9	501.4	389.3	364.2	23.0%	50.1%	16.5%	9.0%
	90%	382.1	435.1	369.1	353.7	14.4%	30.2%	10.5%	5.9%
	95%	356.8	380.5	351.0	344.7	6.8%	13.9%	5.1%	3.2%
	100%	334.1	334.1	334.1	334.1	Base Model			
	105%	314.0	297.0	319.6	324.3	-6.0%	-11.1%	-4.3%	-2.9%
	110%	295.6	265.5	306.1	314.4	-11.5%	-20.5%	-8.4%	-5.9%
	115%	278.9	239.5	284.5	305.0	-16.5%	-28.3%	-14.8%	-8.7%
	120%	263.2	218.1	282.5	295.6	-21.2%	-34.7%	-15.4%	-11.5%
RD-150 EL-525	80%	431.7	571.8	400.0	363.3	32.7%	75.8%	23.0%	11.7%
	85%	400.5	491.0	378.0	354.1	23.1%	51.0%	16.2%	8.9%
	90%	371.9	425.1	359.0	344.2	14.3%	30.7%	10.4%	5.8%
	95%	347.2	370.5	340.6	334.3	6.7%	13.9%	4.7%	2.8%
	100%	325.2	325.2	325.2	325.2	Base Model			
	105%	305.1	288.2	310.5	315.2	-6.2%	-11.4%	-4.5%	-3.1%
	110%	286.2	257.5	297.3	305.8	-12.0%	-20.8%	-8.6%	-6.0%
	115%	269.8	232.3	276.3	297.4	-17.0%	-28.6%	-15.1%	-8.6%
	120%	254.5	212.0	274.6	288.9	-21.8%	-34.8%	-15.6%	-11.2%

C – Cohesion; Φ = Friction angle; E = Elastic Modulus; ν = Poisson’s ratio

EL-525, RD-65: Results from the analysis are presented by tornado diagram at EL-525 at RD-65 as given in Fig. 105. At this location, predicted convergence was 424.7mm, when the friction angle was reduced by 20%, and 161mm when friction angle was increased by 20%. With other parameters, predicted convergence was lesser as seen in Fig. 4.105 and Table 4.28.

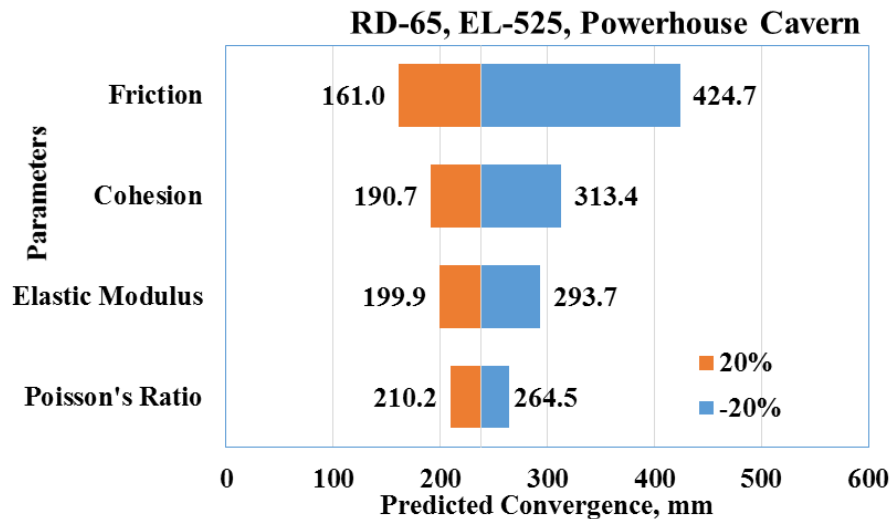


Fig. 4.105 Tornado diagram of sensitivity analysis at RD-65, EL-525

EL-525, RD-110: Tornado diagram at EL-525, RD-110 is shown in Fig. 4.106. Decreasing friction angle by 20% increased predicted convergence to 581.87mm against the base model value of 331.1mm. Increasing friction angle by 20% resulted in decrease of convergence to 218.13mm. The other parameters had relatively less influence as shown in Fig. 4.106 and Table 4.28.

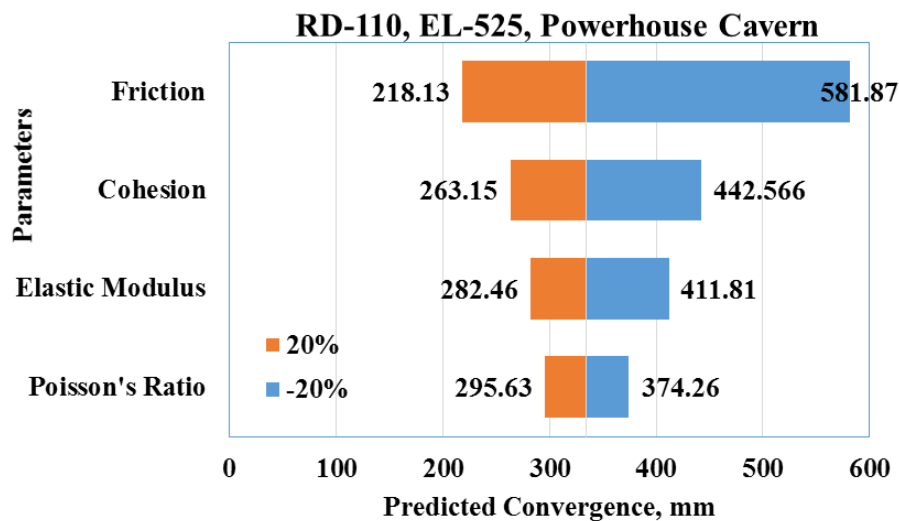


Fig. 4.106 Tornado diagram of sensitivity analysis at RD-110, EL-525

EL-525, RD-150: Tornado diagram at EL-525, RD-150 is shown in Fig. 4.107. Reduction of friction angle by 20% resulted in increased convergence to 571.8mm against the base model value of 325.2mm. The convergence decreased to 218.13mm when friction angle increased by 20%. Other parameters had less influence as shown in Fig. 4.107 and Table 4.28.

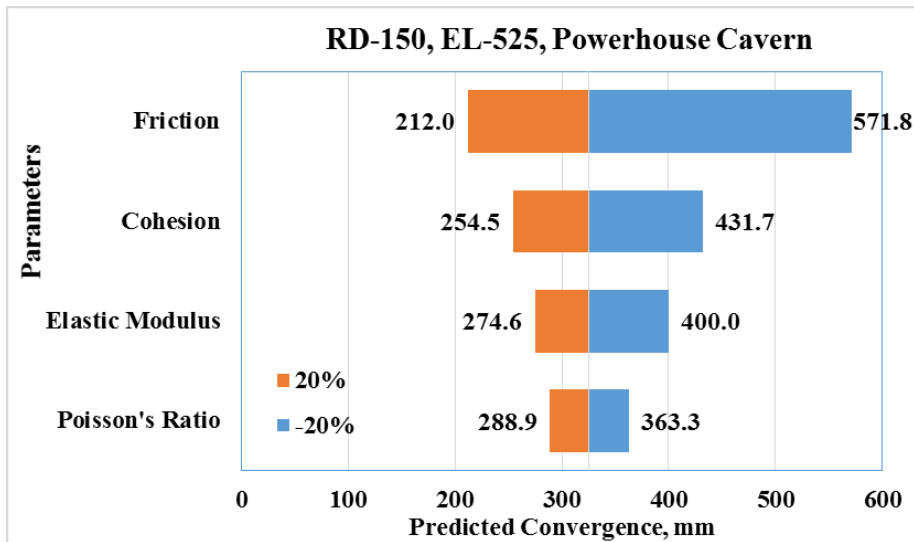


Fig. 4.107 Tornado diagram of sensitivity analysis at RD-150, EL-525

Sensitivity analysis results clearly indicated that friction angle is the most sensitive parameter among the all considered parameters. When the friction angle is reduced by 20%, predicted convergence increased by an average of 76.2%. When the cohesion is reduced by 20%, predicted convergence increased by an average 32.4%. Decreasing the elastic modulus by 20% increased the predicted convergence by an average of 23.3%. When Poisson’s ratio is reduced by 20%, there was an increase of only 11.7% in predicted convergence (Figs. 4.105 to 4.107). Similar results were obtained when the parameters were increased by 20%. Predicted convergence decreased by 33.9% (average) when friction angle was increased by 20%. It was 20.9% (average) for cohesion, 15.6% (average) for elastic modulus and 11.4% (average) for Poisson’s ratio. Thus, decreasing the friction angle has most influence on the predicted convergence in the model (Table 4.28). Cohesion, elastic modulus and Poisson’s ratio were less sensitive in that order.

CONCLUSIONS

Behaviour of large caverns in Himalayas was studied with field investigations and 3D numerical modelling. Research study provided good understanding of the response of surrounding rock mass to the construction of large caverns in typical Himalayan geological condition. Following conclusions were drawn from this study:

1. MRMPBX data indicated significant influence of side slashing in the crown (accounted for 71-88% of total displacement) on the stability of the crown and super incumbent rock mass. There was clear indication of joint separation taking place even upto 10m above the crown, indicating the requirement of long rock bolts of minimum 12m length. Strains derived from MRMPBX observations in the crown were more than 1%.
2. In the crown, load cells on rock bolts recorded upto 70% of yield load and loss of bolt loads were recorded with appearance of cracks in the roof. Complete utilisation of bolt load was not possible due to shorter length (8m) and joint separations above the bolted horizon.
3. Rate of increase in axial load in the steel ribs was influenced to maximum extent by benches within 1.05 times the width of the cavern. Time taken for excavation of each bench also had considerable influence on the rate of increase in load on the steel ribs.
4. Monitoring of cumulative convergence of upstream and downstream wall of powerhouse cavern showed convergence of about 135mm in the service bay area and 200-355mm in the unit bay area. Calculated strains were 0.92 to 1.74% in the unit bay area and upto 0.66% in the service bay area. During excavation of powerhouse cavern, about 88% of total convergence took place and about 12% was recorded during post excavation period. In transformer hall cavern, maximum strain of 1.02% was recorded with width to height ratio of 0.65.
5. Rock bolts in the walls of powerhouse cavern recorded load upto 45t. On downstream wall most of the rock bolts at higher elevations experienced about 85% of final load during benching, while most of the bolts at lower elevations experienced about 30% of final load during post excavation period. On

upstream side, bolts at almost all elevations experienced about 87% of final recorded load during the excavation of benches and reduction of load in some cases after complete excavation and during post excavation period.

6. Strains in the rock bolt measured with instrumented bolt showed that there was increase in strain at 1m depth in all cases. In some cases, there was an increase in strain upto 4 to 5m depths. At 11m and 12m depths, there was decrease in strain in all cases. This behaviour was consistent with other studies quoted in the literature.
7. Monitoring of load in the steel ribs in cross tunnels indicated development of load in the range of 100-110t (as cross tunnels were subjected to maximum principal stresses) and load on the rock bolts in cross tunnels were also very high (>35t). Vertical cracks parallel to axis of the powerhouse cavern developed in the walls of bus ducts due to tensile stresses in the downstream wall of powerhouse cavern.
8. Continuum modelling with FLAC-3D represented the behaviour of rock mass and caverns very well, compared to discontinuum modelling with 3DEC.
9. Predicted convergence from the models developed compared well with the field monitored values within 15% at most of the places. Although, there was close agreement between model and field values, measured convergence values during benching stage were lower than the model predicted values. This could be due to variation in extraction rates of individual benches.
10. Displacements observed at EL-520 were greater than displacements observed at EL-525 and EL-515 by about 10%. This was due to the presence of cross tunnels like passage tunnels and bus ducts. Higher displacements were concentrated near the intersection of floor of the cross tunnels and downstream wall of the powerhouse cavern.
11. In general, there was increase in principal stresses in the crown and reduction in principal stresses in the walls of cavern, which corroborates with high values of convergence recordings in the walls.
12. Analysis of stress concentration factors in the pillar between powerhouse and transformer hall indicated factors due to maximum and intermediate principal stresses were almost equal (varied from 1.20 to 1.58) except at end wall section

of transformer hall, where stress concentration factor due to maximum principal stress was higher (2.63). Normal stresses had higher influence on the stress concentration factors in the pillar. Vertical stress had maximum influence on the pillar and maximum stress concentration factors due to vertical stress is almost two times more than that due to two horizontal stresses.

13. Numerical modelling results indicated maximum strain of 3.34% on the upstream wall and 3.35% on downstream wall. On downstream wall maximum strain was observed near the bus ducts. Higher strains were concentrated near the crown of bus ducts. Results clearly indicated that when the height of excavation increases (w/h ratio decreases), excavation experiences higher strain.
14. Most of the surrounding rock mass had strength to stress ratio of more than two, except at few isolated patches in the immediate vicinity of the walls of cavern.
15. Parametric study conducted on orientation of cavern with respect to maximum principal stress direction showed that, maximum displacement increased by 28.7% at an angle of 90° on upstream side and 18.2% on downstream side. Maximum stress concentration factor in the pillar due to vertical stress does not change significantly with cavern orientation.
16. When the cavern is oriented parallel to maximum principal stress, maximum stress concentration factors due to vertical stress were the highest on the upstream wall of powerhouse.
17. Sensitivity analysis results clearly indicated that friction angle was the most sensitive parameter in prediction of convergence followed by cohesion, elastic modulus and Poisson's ratio in order.
18. Combined analysis of field investigations and 3D modelling results and correlation between the two could explain the behaviour of the cavern and surrounding rock mass in a comprehensive manner under a Himalayan geological setup.

Suggestions for Future Studies

1. Himalayan rock mass consisting of phyllites and phyllitic quartzite are susceptible to creep behaviour, which is evident from the continued

convergence of side walls in the cavern in this study. This aspect could not be incorporated in the current numerical model. An appropriate visco-elasto-plastic model may be developed incorporating the creep behaviour of such rock types.

2. Stresses in the pillar between the two caverns may be monitored in the field, preferably in three principal stress directions.
3. Similar field studies and numerical modelling studies may be extended to other upcoming caverns in Himalayas, so that comparison could be drawn and guidelines could be developed.
4. Such studies may be done in other geological setups for comparing the behaviour of rock mass and large caverns under various conditions.

REFERENCES

- Abolfazl, A. and Hossein, B. (2014). "Stability analysis and determination of rock pillar between two adjacent caverns in different regions of Asmari formation in Iran." *Int. J. Rock Mech. Min. Sci. and Tech.*, 24, 593-596.
- Anon. (1992). "Guide to cavern engineering." *Geoguide 4, Geotechnical engineering office*, Civil engineering department, Govt. of Hongkong.
- Anon. (2008). "India geographic map." showing *Mountains and Rivers of India*, http://en.wikipedia.org/wiki/Image:India_Geographic_Map.jpg (Jul. 8, 2016)
- Anon. (2015). India energy outlook, World energy outlook special report, International energy agency www.iea.org (Jul. 2, 2016)
- Anon. (2015a). "*Bhutan hydropower developments in 2015.*" SANDRP, South Asian network on dams, rivers and people. <https://sandrp.wordpress.com/2016/01/26/bhutan-hydropower-developments-in-2015/> (Jul. 8, 2016)
- Anon. (2015b). "*Energy in Bhutan.*" https://en.wikipedia.org/wiki/Energy_in_Bhutan (Jul. 8, 2016)
- Anon. (2016). "*Global energy statistical yearbook 2016.*" Enerdata, <https://yearbook.enerdata.net/#energy-consumption-data.html> (Jul. 6, 2016)
- Anon. (2016a). "*Electricity sector in India.*" https://en.wikipedia.org/wiki/Electricity_sector_in_India (Jul. 8, 2016)
- Anon. (2016b). "*All India installed capacity of power stations, monthly report, June 2016.*" http://www.cea.nic.in/reports/monthly/installedcapacity/2016/installed_capacity-01.pdf (Jul. 3, 2016)
- Anon. (2016c). "Nepal hydropower overview, hydroelectricity investment and development company ltd." <http://www.hidcl.org.np/index.php> (Jul. 8, 2016)
- Barton, N., Lien, R. and Lunde, J. (1974). "Engineering classification of rock masses for the design of tunnel support." *Rock Mech.*, 6(4), 189-236.

- Barton, N. and Bandis, S. C. (1990). "Review of predictive capabilities of JRC-JCS model in engineering practice." *Proc., Int. Sym. on Rock Joints*, Loen, Norway., 603-610.
- Barton, N., By, T.L., Chryssanthakis, P., Tunbridge, L., Kristiansen, J., Løset, F., Bhasin, R.K., Westerdahl, H. & Vik, G. (1994). "Predicted and measured performance of the 62m span Norwegian Olympic Ice Hockey Cavern at Gjøvik." *Int. J. Rock Mech, Min. Sci. & Geomech.*, Abstract 31:6, 617-641.
- Barton, N. (1994). A Q-system case record of cavern design in faulted rock. *5th Int. Rock Mechanics and Rock Engineering Conf., Tunnelling in difficult conditions*, Torino, Italy, 16.1-16.14.
- Barton, N. and Grimstad, E. (1994). "The Q-system following twenty years of application in NMT support selection." *43rd Geomechanic Colloquy*, Salzburg, Felsbau., 6/94, 428-436.
- Barton, N. and Grimstad, E. (2014). "40 years of Q-system lessons." *Tunnelling Journal*.
- Bhandari, T., Srivastav, A., Panwar, A., Casarus, A. and Kastner, M. (2016). "Three dimensional cavern analysis for a hydroelectric project in India using FLAC3D." *Proc., of 4th Itasca Symp. on applied numerical modelling*, March 7-9, Peru, Paper 06-07, 425-433.
- Bhasin, R.K., Barton, N., Grimstad, E., Chryssanthakis, P. and Shende, F.P. (1996). "Comparison of predicted and measured performance of a large cavern in the Himalayas." *Int. J. Rock Mech. Min. Sci. & Geomech.*, Abstract 33, 607-625.
- Bieniawski, Z.T. (1976). "Rock mass classification in rock engineering.", *proc., of the symp.*, Exploration for rock engineering, Cape Town, Balkema., 97-106.
- Bieniawski, Z.T. (1984). "Rock mechanics design in mining and tunneling." A.A. Balkema, Rotterdam, 272 pp.
- Bieniawski, Z.T. (1989). "Engineering rock mass classifications: A complete manual for engineers and geologists in mining, civil and petroleum engineering." John Wiley & Sons, New York, 251p.

- Broch, E. (2016). "Planning and utilisation of rock caverns and tunnels in Norway." *Tunnelling and Underground Space Technology*, 55, 329-338.
- Bobet, A., Fakhimi, A., Johnson, S., Morris, J., Tonon, F. and Ronald Y. M. (2009). "Numerical models in discontinuous media: Review of advances for rock mechanics applications." *Journal of geotechnical and geoenvironmental engineering*, Nov. ASCE, 1547-1561.
- Brady, B. H. G. (1987). "Boundary element and linked methods for underground excavation, analytical and computational methods in engineering rock mechanics." E. T. Brown, ed., Allen and Unwin, London, 164–204.
- Dasgupta, B. and Lorig, L.J. (1996). "Numerical modelling of underground powerhouse in India, *Journal of Rock Mech. and Tunnelling Tech.*, 2(2), 119-134.
- Dasgupta, B., Dham, R. and Lorig, L.J. (1995a). "Three dimensional discontinuum analysis of the underground power house for Sardar Sarovar project." *Proc., of the 8th Int. Congress on Rock Mech.*, Tokyo, Japan, T. Fujii, ed., Rotterdam, A.A. Balkema, Vol. II, 551-554.
- Dasgupta, B. and Lorig, L.J. (1995b). "Numerical modeling of underground power houses in India." *Proc., of the Int. workshop on observational method of construction of large underground caverns in difficult ground conditions*, 8th ISRM Congress on rock mechanics, Tokyo, Japan, Sakurai, ed., Rotterdam, A.A., Balkema, 65-74.
- Dasgupta, B., Sharma, M.K.V., Verman, M. and Sharma, V.M. (1999). "Design of underground caverns for Tehri hydro power project India by numerical modelling." *Proc., of the 9th international congress on rock mechanics*, Paris, G.Vouile and P. Berest, eds., Rotterdam, A.A. Balkema, 367-368.
- Deere, D.U. (1963). "Technical description of rock cores for engineering purposes." *Rock Mechanics and Engineering Geology*, 1 (1), 16-22.
- Desai, C.S. (1997). "Manual for DSC-SST-2D: Computer code for static and dynamic solid." *Structure and Soil-Structure Analysis*, Tucson, Arizona, U.S.A.

Dhawan, K. R., Singh, D. N. and Gupta, I. D. (2002). “2D and 3D finite element analysis of underground openings in an inhomogeneous rock mass.” *Int. J. Rock Mech. Min. Sci.*, Volume 39, Issue 2, 217–227.

Edvardsson, S. and Broch, E. (2002). “Underground powerhouses and high pressure tunnels. Hydropower development.”. *Norwegian University of Science and Technology*, Trondheim, Vol 14, 99p.

Farmer, I.W. and Shelton, P.D. (1980). “Factors that affect underground rock bolt reinforcement systems”, *Trans. Inst. Min. Metall.* 89, A68-A83.

Freeman, T.J. (1978). “The behaviour of fully bonded rock bolts in the Kielder experimental tunnel” *Tunnels and Tunnelling*, 37-40.

Ghorbani, M. and Sharifzadeh, M. (2009). “Long term stability assessment of Siah Bisheh powerhouse cavern based on displacement back analysis method.” *Tunnelling and Underground Space Technology*, 24, 574-583.

Goodman, R. E. and Shi, G. H. (1985). “*Block theory and its application to rock engineering.*” Prentice-Hall, 338p.

Grimstad, E. and Barton, N. (1993). “Updating of the Q-System for NMT.” *Proc., of Int. symp. on sprayed concrete*, Modern use of wet mix sprayed concrete for underground support, Fagernes, eds., Kompen, Opsahl and Berg., Norwegian Concrete Association, Oslo, 46-66.

Grimstad, E. (2007). “The Norwegian method of tunnelling – a challenge for support design.” *XIV European conference on soil mechanics and geotechnical engineering*, Madrid.

Grøv, E. and Lu, M. (2015). “Understanding and utilizing in-situ rock stresses in design and building large rock caverns.” *Vietrock2015 an ISRM specialized conference*, Mar. 12-13, Hanoi, Vitenam.

Hadjigeorgiou, J. (2012). “Where do the data come from? in Deep Mining 2012” Y. Potvin, ed., *Australian Centre for Geomechanics*, Perth, ISBN 978-0-9806154-8-7.

- Hibino, S. and Motojima, M. (1995). "Characteristic behavior of rock mass during excavation of large scale caverns." *Proc., of the 8th International congress on rock mechanics*, Tokyo, Japan, T. Fujii, ed., Rotterdam, A.A, Balkema, Vol. II, 583-586.
- Hoek, E. and Brown, E.T. (1980). "Underground excavations in rock." *Institution of Mining and Metallurgy*. London, 527p.
- Hoek, E. and Moy, D. (1993). "*Design of large powerhouse caverns in weak rock, in Comprehensive rock engineering, principles, practice and projects.*" Pergamon Press, Vol 5,85 – 110.
- Hoek, E. (1994). "Strength of rock and rock masses." *ISRM News Journal*, 2(2), 4-16.
- Hoek, E. (1999). "Rock engineering." *Course note*, <http://www.rocscience.com>. (May. 15, 2016).
- Hoek, E. (2000). "Practical rock engineering.", Chapter 13, Large Powerhouse caverns in weak rock, <http://home.agh.edu.pl/~cala/hoek/Chapter13.pdf> (April. 16, 2016).
- Hoek E. (2007). "Practical rock engineering.", <http://www.rocscience.com>. (May. 15, 2016).
- Hoek, E., Carter, T.G. and Diederichs, M.S. (2013). "Quantification of the geological strength index chart." *47th US Rock Mechanics/Geomechanics Symposium*, San Francisco, CA, USA Jun. 23-26.
- Holling, C.S. (1978). "*Adaptive environmental assessment and management.*" Wiley, Chichester.
- Horii, H., Yoshida, H., Uno, H., Akutagawa, S., Uchida, Y., Morikawa, S., Yambe, T., Tada, H., Kyoya, T. & Fumio, I. (1999). "Comparison of computational models for jointed rock mass through analysis of large scale cavern excavation." *Proc., of the ninth international congress on rock mechanics*, Paris, France, ISRM, Vol. 1, 389–393.
- Hudson, J. A., and Harrison, J. P. (1997). "*Engineering Rock Mechanics: an Introduction to the Principles*". Pergamon, 444p.
- Jack, C. and Parry, S. (2015). "Communicating geological uncertainty: The use of conceptual engineering geological model, engineering geology for society and territory." Vol 6, *Applied Geology for major engineering projects*, Springer, 347-350.

- Jiang, Y., Li, B. and Yamashita, Y. (2009). "Simulation of cracking near a large underground cavern in a discontinuous rock mass using the expanded distinct element method." *Int. J. Rock Mech. Min. Sci.*, 46, 97–106.
- Jing, L. (2003). "A review of techniques, advances, and outstanding issues in numerical modeling for rock mechanics and rock engineering." *Int. J. Rock Mech. Min. Sci.*, 40, 283–353.
- Jing, L. and Hudson, J. A. (2002). "Numerical methods in rock mechanics." *Int. J. Rock Mech. Min. Sci.*, 39, 409–427.
- Kao, C.Y. and Lee, H.J. (1991). "Sidewall behaviour of Mingtan power cavern during construction." *7th ISRM Congress*, Sept. 16-20, Aachen, Germany, 1139-1142.
- Lang, T. A. and Bischoff, J. A. (1984), "Stability of reinforced rock structure : Design and performance of underground excavations", British Geotechnical Society, 11-18.
- Lee, Y.N., Suh, Y.H., Kim, D.Y. and June, K.S. (1997). "Stress and deformation behaviour of oil storage caverns during excavation." *Int. J. Rock Mech. and Min. Sci.*, 305(3-4).
- Lee, Chung-In. and Song, Jae-Joon. (2003). "Rock engineering in underground energy storage in Korea." *Tunnelling and Underground Space Technology*, 18, 467 – 483.
- Li Z.K., Liu H., Dai, R. and Su, X. (2005). "Application of numerical analysis principles and key technology for high fidelity simulation to 3-D physical model tests for underground caverns." *Tunnelling and Underground Space Technology*, 20(4), 390-399.
- Li, S., Liu, Y. and Wu, F. (2009). "Numerical simulation and deformation field measurement of powerhouse cavern excavation." *ISRM Int. Symp. on Rock Mechanics - SINOROCK 2009*, May 19-22, The University of Hong Kong, China.
- Lim, H. and Kim, C. (2003). "Comparative study on the stability analysis methods for underground pumped powerhouse caverns in Korea." *10th ISRM Congress, Technology roadmap for rock mechanics*, Sandton, South Africa, Sep. 8-12, 783-786.
- Lottes, G. (1972). "The development of European pumped-storage plants. *Water Power* 24, 22-33.

- Ma, K., Tang, C.A., Wang, L. X., Tang, D.H., Zhuang, D.Y., Zhang, Q.B. and Zhao, J. (2016). “Stability analysis of underground oil storage caverns by an integrated numerical and microseismic monitoring approach.” *Tunnelling and Underground Space Technology*, 54, 81-91.
- Maejima, T., Mori, T., Iwano, K. and Aoki, K. (2003). “Estimation of joint behavior by monitoring and analysis in the rock cavern.” *10th ISRM Congress, Technology roadmap for rock mechanics*, Sandton, South Africa, Sep. 8-12, 791-794.
- Marinos, P. and Hoek, E. (2000). “GSI: a geologically friendly tool for rock mass strength estimation.” *Proc., of the GeoEng2000 International conference on geotechnical and geological engineering*, Melbourne, Technomic publishers, Lancaster, 1422–1446.
- Marinos, P. and Hoek, E. (2001). “Estimating the geotechnical properties of heterogeneous rock masses such as flysch.” *Bull Eng Geol Env.*, 60, 82–92.
- Marinos, P., Marinos, V. and Hoek, E. (2007). “Geological Strength Index (GSI) A characterization tool for assessing engineering properties for rock masses, in underground works under special conditions.” Romana, Perucho & Olalla, eds., Lisbon: Taylor and Francis. 13-21.
- Milne, D., Hadjigeorgiou, J. and Pakalnis, R. (1998). “Rock mass characterization for underground hard rock mines.” *Tunnelling and Underground Space Technology* 13 (4), 383–391.
- Moghadam, S. N., Mirzabozorg, H. and Noorzad, A. (2013). “Modeling time-dependent behavior of gas caverns in rock salt considering creep, dilatancy and failure.” *Tunnelling and Underground Space Technology*, 33, 171-185.
- Moosavi, M. and Fattahpour, V. (2009). “3D modeling of a cavern in closely spaced bedded rock mass by transversely isotropic model.” *ISRM International symposium on rock mechanics - SINOROCK 2009*, May 19-22, The University of Hong Kong, China.
- Myrvang, A. (2001). “Rock Mechanics”, Department of Geology and Mineral. Norwegian University of Science, Trondheim.

Nair, R. and Sripad, (2012). “Numerical analysis of an underground powerhouse in adverse geological conditions of upper Himalayas.” *International Conference on Tunneling and Underground Space for Global Society - WTC 2012*, Bangkok, May 18 - 23.

Nandy, S.N., Dhyani, P.P. and Samal, P.K. “Resource information database of the Indian Himalayas.” *ENVIS Monograph 3, G.B. Pant Institute of Himalayan Environment and Development*, ISSN 0972 – 1819, 123p.

Nilsen, B., Thidemann, A. (1993). “Rock Engineering. Hydropower Development”, volume 9. Norwegian Institute of Technology, Trondheim, 156p.

Panthi, K. K. (2007). “Underground space for infrastructure development and engineering geological challenges in tunneling in the Himalayas.” *Hydro Nepal: Journal of Water, Energy and Environment*, Vol 1.

Palmstrom, A. (1995). “RMi – A Rock Mass Characterization System for Rock Engineering Purposes”. Ph.D. thesis Univ. of Oslo, 400pp.

Palmstrom, A., and Stille, H. (2007). “Ground behaviour and rock engineering tools for underground excavations”, *Tunnelling and Underground Space Technology*, 22, 363-376.

Park, Y. J., You, K.H., Choi, Y.T. and Lee, H.W. (2003). “Stability of large rock caverns excavated in a highly stressed region.” *10th ISRM Congress, Technology roadmap for rock mechanics*, Sandton, South Africa, Sep. 8-12, 883-886.

Ramamurthy, T., Gupta, K.K. and Ghazvinian, A.H. (1995). “Stability of underground opening from equivalent material modelling.” *Proceedings of the 8th international conference on rock mechanics*, Tokyo, vol. 3, 1363–1366.

Ramamurthy, T. (1993). “Strength and modulus responses of anisotropic rocks.” *Comprehensive Rock Engineering*, Chapter 13, Pergamon Press, Oxford, U.K., Vol. I, 315-329.

Ramamurthy, T. (2001). “Shear strength response of some geological materials in triaxial compression.” *Int. J. Rock Mech. Min. Sci.*, 38, 683-697.

- Sakurai, S. (1997). "Lessons learned from field measurements in tunnelling", *Tunnelling and Underground Space Technology*, 12, 453-460.
- Saran, V. and Broch, E. (2008). "Three dimensional numerical analysis of underground works at Xiaolangdi multipurpose project in China." *World Tunnel Congress 2008 - Underground facilities for better Environment and Safety*, India, 637-647
- Saurer, E., Marcher, T. and John, M. (2013). "Decisive design basis and parameters for power plant caverns." *Proceedings, ITA-AITES, World Tunnel Congress*, Geneva, 1858-1864.
- Sharma, H.R. and Tiwari, A.N. (2012). "Tunnelling in the Himalayan region: geological problems and solutions." *International Water Power and Dam Construction*, 64(9), Sep. 15-19.
- Sharma, R. H. and Awal, R. (2013). "Hydropower development in Nepal." *Renewable and Sustainable Energy Reviews*, 21, 684-693.
- Sinha, R.S. (1989). "Underground structures: Design and Instrumentation", Elsevier, 480p.
- Sitharam, T.G. and Latha, G.M. (2002). Simulation of excavations in jointed rock mass using a practical equivalent continuum approach." *Int. J. Rock Mech. Min. Sci.*, 39, 517–525.
- Starfield, A.M. and Cundall, P.A. (1988). "Towards a methodology for rock mechanics modelling." *Int. J. Rock Mech. Min. Sci. & Geomechanics*, Abstracts, Vol. 25, No. 3, 99–106.
- Stille, H. and Palmstrom, A. (2003). "Rock mass classification as a tool in rock engineering." *Tunnelling and underground space technology*. 18, 331–345.
- Swarup, A. K., Goel, R. K., and Prasad, V. V. R. (2000) "Observational approach for stability of tunnels", *Tunnelling Asia 2000*, New Delhi, 38-44.
- Varadarajan, A., Sharma, K.G., Desai, C.S. and Hashemi, M. (2001). "Analysis of a powerhouse cavern in the Himalaya", *International Journal of Geomechanics*, 1(1), 109-127.

Wang, T. and Zhu, H. (2006). “The application of FLAC and FLAC3D to the support of an underground cavern.” *4th International FLAC symposium on numerical modeling in Geomechanics*, Hart, & Varona, eds., Paper 02-01.

Wu, A., Wang, J., Zhou, Z., Huang, S., Ding, X., Dong, Z. and Zhang, Y. (2016). “Engineering rock mechanics practices in the underground powerhouse at Jinping I hydropower station.” *Journal of rock mechanics and geotechnical engineering*. <http://dx.doi.org/10.1016/j.jrmge.2016.05.001>

Xiao, Y. X., Feng, X. T., Feng, G.L., Liu, H.J., Jiang, Q. and Qui, S.H. (2016). “Mechanism of evolution of stress–structure controlled collapse of surrounding rock in caverns: A case study from the Baihetan hydropower station in China.” *Tunnelling and Underground Space Technology*, 51, 56-67.

Xu, D., P., Feng, X. T., Cui, Y. J. and Jiang, Q. (2015). “Use of the equivalent continuum approach to model the behaviour of a rock mass containing an interlayer shear weakness zone in an underground cavern excavation”, *Tunnelling and Underground Space Technology*, 47, 35-51.

Yoshida, H. and Horii, H. (1995). “Micromechanics-based continuum theory for jointed rock mass and analysis”, *Proc., of the 8th international congress on rock mechanics*, Tokyo, Japan, T. Fujii, ed., Rotterdam, A.A. Balkema, Vol. II, 689-692

Yoshida, T., Ohnishi, Y., Nishiyama, S., Hirakawa, Y. and Mori, S. (2004). “Behavior of discontinuities during excavation of two large underground caverns”, *Int. J. Rock Mech. Min. Sci.*, 41, 864-869.

Yoshida, H. and Horii, H. (2004). “Micromechanics-based continuum model for a jointed rock mass and excavation analyses of a large-scale cavern”, *Int. J. Rock Mech. Min. Sci.*, 41, 119 – 145.

Zhao, B. and Ma, Z. (2009). “Influence of cavern spacing on the stability of large cavern groups in a hydraulic power station”, *Int. J. Rock Mech. Min. Sci.*, 46 506–513.

Zhang, M., Zhu, H.C. and Zhu, Y.S. (2016). “Stability analysis of blocks formed with determined joint network – A case study of Shenxu caverns with 3DEC.” *Proceedings*

of 4th *Itasca Symposium on applied numerical modelling*, Mar. 7-9, Peru. Paper 06-07, 435-443.

Zhang, Q.B., He, L. and Zhu, W. S. (2016). “Displacement measurement techniques and numerical verification in 3D geomechanical model tests of an underground cavern group”, *Tunnelling and underground space technology*, 56, 54-64.

Zhu, H. and Zhu, Y. (2013). “Crown stability analysis for the right bank cavern of the Baihetan Hydropower Station, China”, *Continuum and distinct element numerical modelling in geomechanics, Proceedings of 3rd international FLAC/DEM Symposium*, Hangzhou, Oct. 22-25.

Zhu, W. S., Sui, B., Li, X. J., Li, S. C. and Wang, W. T. (2008). “A methodology for studying the high wall displacement of large scale underground cavern complexes and its applications.” *Tunnelling and underground space technology*, vol. 23, no. 6, 651–664.

Zhu, W. S., Li, X. J., Zhang, Q.B., Zheng, W.H., Xin, X.L., Sun, A.H. and Li, S. C. (2010). A study on sidewall displacement prediction and stability evaluations for large underground power station caverns.” *Int. J. Rock Mech. Min. Sci.*, 47, 1055–1062.

Zhu, J.L. and Chen, X.T. (2009). “Study on the wall rock stability of Yantan hydrologic station’s underground caverns by using 3D numerical simulation.” *ISRM international symposium on rock mechanics - SINOROCK 2009*, 19-22 May, The University of Hong Kong, China.

APPENDIX -1

Table 1. Wedge formation at the powerhouse cavern with different sets of joints.

Intersection of Joints	Wedge No.	Plunge	Trend	Analysis of Joint (Wedges, Toppling and Sliding)		
				Upstream Wall	Downstream wall	Remark
J1 & J2	W1	23°	356°	Favorable	Favorable	Stable due to $\phi > 23^\circ$ (plunge)
F1 & J2	W2	41°	330°	Favorable	Favorable	Minute unfavourable to D/S wall
J4 & F1	W3	31°	303°	Favorable	Favorable	J4 is very unfavourable to Upstream Vertical Wall
J2 & J4	W4	53°	280°	Occasional Unfavourable	Favorable	J4 is very favourable to Downstream Vertical Wall
J2 & J5	W5	41°	235°	Highly Unfavourable	Favorable	Unstable due to $\phi < 41^\circ$ (plunge) and plunge direction perpendicular to face, toppling may possible
J2 & J3	W6	04°	198°	Favorable	Favorable	Very gentle plunge
J4 & J5	W7	54°	179°	Occasional Unfavourable	Favorable	Few chunks may topples/slide at the U/S wall
J3 & J4	W8	32°	157°	Favorable	Favorable	Minute toppling at the U/S wall
J1 & J4	W9	19°	150°	Favorable	Favorable	Very gentle plunge parallel to the U/S wall
J1 & J5, J1 & J3, and J3 & J5	W10	40°	132°	Favorable	Favorable	Minute toppling may possible at the D/SW (Sets of wedge form at the with minor variation of the trend/plunge)
J3 & F1	W11	25°	059°	Favorable	Favorable	Stable due to $\phi > 25^\circ$ (plunge)
J1 & F1	W12	44°	016°	Favorable	Favorable	Minor unstable U/S wall

J4 (65°/230°) indicates highly slide failure and intersection of J5 and J2 indicates wedge failure with plunge/trend (W5, 41° / 235°) at the upstream vertical wall. Downstream wall indicates minor toppling/slide by joint J1(60°/072°) and indicates rare wedge failure (W12, 44°/016°). Instability problems may be higher on upstream vertical wall compared to downstream vertical wall.

Table 2. Details of joints mapped and used in 3DEC model.

Joint ID	Dip Angle	Dip Direction	Joint Intersection Point in the Crown of Powerhouse		
			X	Y	Z
1	75	292	166.33	72.5	538.5
2	70	267	166.33	82.5	538.5
3	65	157	166.33	82.5	538.5
4	90	143	166.33	82.5	538.5
5	70	237	166.33	76.5	538.5
6	75	57	166.33	88.5	538.5
7	65	37	166.33	90.5	538.5
8	70	227	166.33	103.5	538.5
9	65	27	166.33	110.5	538.5
10	65	237	166.33	117.5	538.5
11	85	57	166.33	128.5	538.5
12	70	27	166.33	141.5	538.5
13	25	197	166.33	96.5	538.5
14	40	197	166.33	96.5	538.5
15	70	237	166.33	102.5	538.5
16	25	197	166.33	96.5	538.5
17	85	237	166.33	138.5	538.5
18	65	137	166.33	110.5	538.5
19	70	27	166.33	140.5	538.5
20	50	297	166.33	143.5	538.5
21	55	227	166.33	151.5	538.5
22	75	207	166.33	153.5	538.5
23	75	147	166.33	151.5	538.5
24	70	297	166.33	155.5	538.5
25	60	75	166.33	155.5	538.5
26	40	173	166.33	120.5	538.5
27	65	227	166.33	125.5	538.5
28	70	297	166.33	155.5	538.5
29	70	47	166.33	165.5	538.5
30	50	322	166.33	176.5	538.5
31	40	177	166.33	185.5	538.5
32	40	27	166.33	200.5	538.5
33	75	112	166.33	195.5	538.5
34	55	117	166.33	202.5	538.5
35	70	307	166.33	202.5	538.5
36	75	192	166.33	192.5	538.5

			Joint Intersection Point in the Crown of Powerhouse		
Joint ID	Dip Angle	Dip Direction	X	Y	Z
37	80	257	166.33	190.5	538.5
38	60	237	166.33	198.5	538.5
39	70	37	166.33	199.5	538.5
40	70	287	166.33	205.5	538.5
41	50	347	166.33	210.5	538.5
42	50	347	166.33	214.5	538.5
43	80	97	166.33	220.5	538.5
44	65	337	166.33	251.5	538.5
45	65	322	166.33	259.5	538.5
46	75	57	166.33	260.5	538.5
47	65	127	166.33	262.5	538.5
48	35	240	176.83	180	525
49	45	140	176.83	180	520
50	60	175	176.83	180	515
51	12	215	176.83	180	523
52	38	240	176.83	135	524
53	60	115	176.83	135	515.5
54	48	250	176.83	135	521.5
55	25	160	155.83	135	520
56	38	240	176.83	220	524
57	60	115	176.83	220	515.5
58	48	250	155.83	220	521.5
59	25	160	155.83	220	517
Shear Joints					
1	30	197	166.33	119.5	538.5
2	35	197	166.33	133.5	538.5
3	75	57	166.33	262.5	538.5
4	65	292	166.33	255.5	538.5
5	40	287	166.33	210.5	538.5

APPENDIX -2

Table 3. Load cell observations on rock bolts at walls of powerhouse cavern at EL-525

Load Cell Observations, Location: Powerhouse Cavern Walls, EL- 525													
Downstream Wall: Load (t)								Upstream Wall: Load (t)					
Days	RD-15	Days	RD-16	Days	RD-69	Days	RD-110	Days	RD-16.8	Days	RD-62	Days	RD-106
57	7.62	57	6.53	0	12.52	30	9.93	40	5.29	0	8.83	27	8.01
69	7.53	69	5.67	3	12.4	32	10.4	46	6.67	3	8.77	30	7.89
96	11.24	96	9.83	6	12.29	35	10.98	70	13.57	6	8.75	32	7.87
103	11.67	103	9.75	12	12.33	46	12.17	103	17.26	12	8.72	35	7.93
109	12.6	109	13.08	17	12.19	54	12.87	109	17.77	15	8.73	46	7.88
137	17.44	137	18.5	27	12.24	91	13.63	113	18.05	17	8.73	54	7.91
146	18.15	146	20.89	36	12.4	102	14.01	133	18.26	27	8.83	83	7.47
157	19.02	157	24.16	46	12.46	109	14.5	146	18.79	35	9.92	91	7.45
178	19.2	178	23.74	57	12.46	120	15.52	157	19.18	46	10.3	96	7.37
190	19.47	190	24.1	71	12.32	124	16.62	178	20.01	57	10.9	103	7.52
200	19.87	200	24.95	87	12.62	133	16.41	190	20.33	71	12.44	115	7.61
213	19.59	213	25.38	102	13.63	145	16.58	213	20.94	87	21.88	120	7.63
227	19.68	227	25.6	115	25.7	157	16.74	227	21.5	102	28.96	146	8.01
239	19.73	239	25.73	136	26.92	175	15.07	238	22.62	115	30.46	161	8.16
249	20.03	249	25.87	150	26.97	180	15.04	249	22.91	136	32.22	178	8.72
251	19.88	281	27.32	175	27.73	190	15.02	259	23.14	150	33.03	188	9.05
262	20.86	291	27.34	190	27.66	210	14.97	268	23.36	175	34.75	206	9.13
269	21.25	300	27.63	203	27.76	220	14.98	277	23.18	190	35.11	210	9.16
277	21.3	333	28.37	230	28.6	227	14.95	291	23.3	213	36.02	216	9.32
291	20.56	350	28.6	237	28.55	230	14.96	300	23.57	230	36.3	220	9.96
300	20.2	361	29.13	248	28.39	231	14.97	316	23.9	237	36.7	227	9.95
316	20.08	437	30.06	259	28.3	233	14.95	356	24.34	248	37.26	233	9.94
333	20.32	484	30.22	273	28.18	237	14.95			259	37.3	237	9.94
350	20.3	540	30.28	291	28.05	239	14.95			273	37.47	239	9.94
361	21	603	30.09	300	28.25	243	14.94			291	37.5	240	9.93
437	22.65	624	30.13	322	28.36	245	14.94			297	37.65	279	9.89
484	23.2	643	30.33	350	28.24	249	14.94			300	37.94	284	9.89
603	23.59	671	30.21	367	28.23	257	14.93			322	38.74	290	9.89
624	23.6	709	30.3	381	28.24	262	14.93			350	40.54	298	9.89
643	23.89	747	30.6	402	28.21	269	14.9			367	43.01	314	9.85

Load Cell Observations, Location: Powerhouse Cavern Walls, EL- 525													
Downstream Wall: Load (t)								Upstream Wall: Load (t)					
Days	RD-15	Days	RD-16	Days	RD-69	Days	RD-110	Days	RD-16.8	Days	RD-62	Days	RD-106
671	24.21	773	30.65	424	28.28	275	14.85			381	0.92	333	9.78
709	24.64	777	30.67	445	28.42	279	14.88			402	1.1	339	9.42
747	25.13	802	30.7	474	28.42	287	14.87			445	1.31	350	9.5
773	25.45	816	31.32	496	28.75	290	14.87			474	1.37	361	9.6
777	25.71	840	30.84	517	28.78	305	14.85			496	1.39	377	9.59
802	25.98	866	30.86	535	28.79	311	14.45			517	1.38	384	9.59
816	26.17	892	30.89	552	28.77	326	14.47			697	1.833	405	9.56
840	26.21	931	30.97	571	28.73	339	13.93			777	1.576	421	9.56
866	26.37	957	31.19	603	29.54	361	14.34					454	9.57
892	26.49	984	31.06	629	29.3	377	14.49					515	9.5
931	26.47	1013	31.06	659	29.18	400	14.51					535	9.46
957	26.41	1047	30.94	752	28.44	421	14.34					552	9.45
984	26.33	1079	30.88	777	28.86	454	14.33					569	9.42
1013	26.37	1107	31.09	816	28.86	496	14.28					603	9.38
1047	26.56	1138	31.02	872	28.83	515	14.3					626	9.36
1079	26.68	1168	31	929	28.62	531	14.32					648	9.33
1107	26.99	1205	31.01	970	29.09	552	14.19					665	9.32
1138	27.08	1221	31.02	1015	28.65	569	14.47					679	9.28
1168	27.27	1237	30.9	1047	28.62	600	15.62					725	9.29
1205	27.46	1264	31.07	1079	28.77	603	15.66					761	9.35
1221	27.35	1288	31.09	1110	29.01	626	16.01					773	9.35
1237	26.91	1315	31.16	1168	29.14	648	16.24					801	9.19
1264	27.52	1342	30.97	1206	29.2	665	16.16					809	9.38
1315	27.48	1375	31.26	1264	29.24	709	16.53					899	9.4
1342	27.54	1389	31.34	1288	29.22	761	16.85					931	9.19
1360	27.6	1413	31.43	1315	29.18	789	17.07					957	9.13
1375	27.63	1445	31.26	1361	29.1	840	17					984	9.10
1389	27.64	1462	31.55	1389	29.18	866	16.92					1205	9.07
1413	27.69	1478	31.56	1413	29.26	899	17.2					1221	9.07
1445	27.7	1491	31.03	1445	29.29	931	16.5					1237	9.03
1462	27.73	1508	31.99	1478	29.29	957	17.16					1264	9.051
1478	27.76	1522	31.74	1509	29.33	984	17.13					1288	9.03
1491	27.6	1536	31.79	1536	29.77	1013	17.09					1315	9.02
1508	27.91	1572	31.83	1572	30.1	1047	17.05					1342	9.15

Load Cell Observations, Location: Powerhouse Cavern Walls, EL- 525													
Downstream Wall: Load (t)								Upstream Wall: Load (t)					
Days	RD-15	Days	RD-16	Days	RD-69	Days	RD-110	Days	RD-16.8	Days	RD-62	Days	RD-106
1522	27.7	1587	31.92	1589	30.11	1079	17.08					1360	9.14
1536	27.75	1597	31.93	1600	30.1	1110	16.46					1375	9.13
1572	27.76	1607	31.97	1609	30.1	1138	17.11					1389	9.14
1587	27.76	1624	31.97	1624	30.08	1168	17.15					1413	9.14
1597	27.76	1638	32.02	1648	30.06	1205	17.49					1445	9.18
1607	27.76	1646	32.01	1659	30.05	1221	17.13					1462	9.19
1624	27.76	1659	32.01	1676	30.03	1237	17					1478	9.24
1638	27.92	1676	32.02	1692	30.01	1254	17.11					1491	9.25
1646	27.9	1691	32.01	1707	29.98	1264	17.1					1508	9.27
1659	27.92	1707	31.99	1722	29.95	1288	17.07					1522	9.28
1676	27.89	1715	31.99			1315	17.07					1536	9.26
1691	27.88	1721	31.98			1342	17.05					1572	9.27
1715	27.83					1375	17.01					1597	9.25
1721	27.81					1389	17					1607	9.24
						1413	16.95					1624	9.24
						1445	16.92					1638	9.19
						1478	16.91					1659	9.18
						1491	16.32					1676	9.13
						1508	16.88					1691	9.11
						1522	16.87					1707	9.11
						1536	16.82					1715	9.03
						1572	16.83					1721	9.03
						1587	16.5						
						1597	16.81						
						1607	16.82						
						1624	16.81						
						1638	16.81						
						1646	16.81						
						1659	16.51						
						1676	16.74						
						1691	16.76						
						1707	16.73						
						1715	16.69						
						1721	16.69						

Table 4. Load cell observations on rock bolts at walls of powerhouse cavern at EL-520

Load Cell Observations, Location: Powerhouse Cavern Walls, EL- 520															
Downstream Wall: Load (t)								Upstream Wall: Load (t)							
Days	RD-15	Days	RD-65	Days	RD-110	Days	RD-150	Days	RD-15	Days	RD-65	Days	RD-110	Days	RD-150
0	7.36	15	8.6	15	1.93	8	8.02	0	6.63	15	8.84	10	13.12	0	6.95
7	7.62	29	15.5	29	3.44	28	9.75	4	6.89	33	19.34	20	13.33	28	14.67
28	10.75	39	15.22	39	5.28	39	11.29	28	7.65	40	20.03	29	18.46	40	15.67
34	14.01	46	17.95	46	7.22	46	12.61	39	14.8	46	21.11	40	18.59	46	15.75
40	14.24	57	18.33	57	9.61	57	15.38	46	15.49	57	21.84	46	18.33	59	20.47
46	16.16	70	18.54	70	12.51	61	16.46	70	17.73	70	22.07	74	17.84	70	23.54
70	24.54	83	19.4	83	14.99	70	16.05	83	18.27	83	26.19	83	18.79	82	27.23
83	18.26	94	18.42	94	14.56	82	17.81	94	18.72	94	27.5	87	17.56	87	28.78
94	0.97	112	17.74	112	14.26	118	19.81	115	19.39	115	28.54	94	17.43	94	29.6
115	1.2	127	17.67	127	13.9	127	21.12	127	19.99	127	28.9	124	17.05	104	31.33
127	1.34	143	17.3	143	14.79	147	23.18	137	20.41	150	29.35	147	16.57	115	32.06
137	1.82	150	16.61	150	15.01	157	23.48	150	20.91	164	31.64	153	16.6	127	33.23
150	2.74	159	15.85	159	15.19	165	23.56	164	21.39	174	31.23	157	16.56	147	34.15
164	2.82	168	17.16	168	15.26	167	23.89	175	21.95	176	32.11	164	16.5	164	34.5
176	2.89	174	17.72	174	15.41	170	23.95	186	22.41	182	31.59	170	16.45	167	34.53
186	2.88	176	17.85	176	15.44	174	24.05	196	22.79	186	32.29	174	16.45	170	34.58
188	3.16	180	18.18	180	15.51	176	24.14	205	23.17	194	32.07	176	16.45	174	34.7
199	3.29	182	18.38	182	15.54	177	24.11	214	23.52	200	32.51	177	16.44	175	34.68
206	3.39	186	18.55	186	15.56	178	24.14	228	24.14	205	32.57	216	16.29	176	34.71
214	3.87	190	18.74			180	24.18	237	24.35	213	32.68	221	16.18	177	34.72
228	4.18	199	19.12			182	24.29	328	26.45	218	32.64	227	16.2	178	34.76
237	4.38	206	19.51			186	24.33	342	26.57	228	32.82	234	16.19	180	34.77
253	4.74	213	19.55			194	24.55	363	26.89	235	32.99	251	16.15	182	34.78
270	5.39	216	19.92			202	24.72	374	27.08	263	33.79	276	15.9	183	34.79
287	5.63	228	20.3			209	24.81	417	27.28	287	34.9	287	15.68	185	34.79
298	5.79	235	21.07			213	24.81	438	27.44	298	35.24	298	15.89	188	34.8
349	6.95	244	20.53			216	24.96	454	27.76	304	35.47	314	15.86	190	34.8
561	7.81	257	21.04			221	25.02	468	23.35	318	36.12	337	15.72	194	34.81
580	9.394	302	22.49			227	25.45	489	23.4	326	36.34	342	15.65	197	34.81
684	9.99	304	22.52			235	25.59	506	23.26	342	36.76	358	15.59	199	34.81
714	9.98					244	25.8	540	23.14	363	37.41	378	15.62	202	34.82
739	10.18					251	25.96	561	23.09	374	37.9	391	15.58	205	34.85

Load Cell Observations, Location: Powerhouse Cavern Walls, EL- 520															
Downstream Wall: Load (t)							Upstream Wall: Load (t)								
Days	RD-15	Days	RD-65	Days	RD-110	Days	RD-150	Days	RD-15	Days	RD-65	Days	RD-110	Days	RD-150
753	10.25					263	26.64	580	22.89	417	38.14	435	15.49	733	32.97
777	11.85					270	26.71	602	22.88	438	37.15	451	15.5	777	33.38
803	13.84					287	27.16	1068	33.41	454	36.07	465	15.43	803	33.15
829	14.6					298	27.04	1075	33.39	468	36.79	489	15.43	836	32.82
868	14.65					314	27.74	1105	33.38	489	36.92	506	15.5	868	33.13
894	14.61					337	29.37	1142	33.48	506	36.99	540	15.48	894	33.61
921	14.92					358	29.52	1158	33.48	540	37.43	561	15.39	921	33.77
950	14.73					382	29.71	1201	33.48	561	37.59	581	15.38	950	34.07
984	14.98					433	29.79	1225	33.46	580	37.52	602	15.39	984	34.42
1016	14.77					452	30.09	1297	33.48	602	36.74	616	15.37	1016	34.72
1044	11.24					465	30.19	1428	33.54	646	26.98	657	15.39	1035	34.9
1068	11.24					474	30.25	1459	33.55	689	26.78	705	15.47	1044	34.95
1105	11.3					489	30.39			710	26.82	738	15.48	1075	34.94
1142	11.77					506	30.61			721	26.94	777	15.53	1105	35.81
1158	11.36					540	31.67			739	26.87	803	15.47	1142	37.14
1174	11.35					563	31.93			753	27.15	836	15.55	1152	37.18
1201	11.3					585	32.21			777	27.53	873	15.25	1174	38.13
1225	11.29					602	32.41			803	27.51	894	15.2	1201	37.89
1252	11.3					616	32.54			829	27.66	921	15.16	1225	36.75
1279	11.27					646	32.72			866	27.79	950	15.16	1252	36.96
1297	11.91					705	33.69			894	27.47	984	15.14	1279	38.37
1312	11.3					726	33.93			921	27.93	1016	15.11	1297	38.34
1326	11.26					753	34.09			950	27.95	1044	15.16	1309	37.47
1350	11.27					777	34.19			984	27.79	1075	15.27	1326	38.43
1382	11.24					803	34.19			1016	27.82	1105	15.39	1348	38.3
1399	11.26					817	34.29			1035	27.88	1142	15.3	1382	38.59
1415	11.27					868	34.39			1044	27.67	1158	15.3	1399	38.74
1428	11.41					894	34.97			1075	27.78	1174	15.2	1415	39.91
1445	11.32					921	34.9			1105	28.01	1190	15.24	1424	39.96
1459	11.34					950	35.41			1121	28.06	1201	15.25	1445	39.98
1473	11.3					984	35.32			1142	27.94	1225	15.15	1459	40.05
1509	11.3					1016	37.59			1158	28.01	1252	15.2	1473	40.49
1524	11.28					1035	45.65			1174	28.13	1279	15.03	1509	40.24
1534	11.73					1044	45.35			1201	27.98	1297	15	1524	41.21

Load Cell Observations, Location: Powerhouse Cavern Walls, EL- 520															
Downstream Wall: Load (t)							Upstream Wall: Load (t)								
Days	RD-15	Days	RD-65	Days	RD-110	Days	RD-150	Days	RD-15	Days	RD-65	Days	RD-110	Days	RD-150
1544	11.3					1057	45.8			1225	27.99	1312	14.98	1534	45.48
1561	11.29					1105	40.63			1252	27.83	1326	14.98	1544	45.51
1575	11.3					1142	42.47			1279	28.41	1350	14.97	1561	45.52
1583	11.3					1158	42.41			1297	28.43	1382	15.03	1575	45.62
1596	11.3					1174	41.8			1312	28.45	1399	15.04	1583	45.62
1613	11.31					1190	42.35			1326	28.01	1415	15.17	1596	45.58
1628	11.33					1201	42.3			1350	28.43	1428	15.19	1613	45.52
1644	11.37					1225	42.3			1382	28.32	1445	15.26	1628	45.47
1652	11.37					1252	41.54			1399	28.29	1459	15.27	1644	45.37
1658	11.39					1279	41.41			1415	28.33	1473	15.24	1652	45.35
						1298	41.11			1428	28.36	1509	15.26	1658	45.33

Table 5. Load cell observations on rock bolts at walls of powerhouse cavern at EL-515

Load Cell Observations, Location: Powerhouse Cavern Walls, EL-515															
Downstream Wall: Load (t)						Upstream Wall : Load (t)									
Days	RD-65	Days	RD-110	Days	RD-150	Days	RD-65	Days	RD-110	Days	RD-120	Days	RD-142	Days	RD-150
0	7.79	10	4.13	12	12.89	14	3.87	14	4.25	126	3.28	131	6.9	0	0.53
13	7.4	12	3.15	17	12.9	24	4.02	24	5.62	129	3.35	135	6.45	14	0.53
17	7.4	17	8.19	42	15.46	28	3.52	28	6.49	131	3.32	138	6.14	23	2.94
24	7.37	24	8.59	57	16.56	35	2.84	38	5.97	135	1.58	143	6.44	28	3.88
42	7.72	42	12.7	663	30.73	56	4.82	65	5.53	137	1.61	146	6.37	35	6.25
57	7.7	77	15.48	683	29.04	68	4.87	88	5.66	146	1.72	152	6.43	56	6.7
73	7.14	87	14.62	707	27.72	91	7.87	98	5.76	150	1.9	153	6.3	68	7.63
80	7.16	94	14.3	733	27.92	105	9.48	105	5.81	153	1.96	159	6.37	73	7.83
89	8.48	97	14.28	747	27.86	115	10.03	111	5.8	155	5.05	162	6.41	88	8.06
98	8.34	100	15.45	824	27.55	117	10.07	115	5.69	162	5.18	221	8.36	115	7.93
104	8.81	104	14.99	851	27.49	123	10.32	117	5.67	168	4.29	228	8.98	147	8.15
106	8.89	106	13.55	880	27.58	127	10.33	118	5.69	175	4.15	239	9.67	150	7.07
110	8.85	110	13.86	914	27.7	135	10.38	157	5.82	185	4.23	252	10.18	153	7.53
112	8.89	112	13.93	946	27.9	141	10.61	162	5.75	192	4.23	278	11.53	168	8.89
116	8.89	116	13.21	965	27.97	146	10.67	168	5.84	204	4.8	283	11.54	176	8.56
120	8.92	124	13.5	974	28.26	154	10.94	176	5.8	211	4.89	299	11.93	182	8.62

Load Cell Observations, Location: Powerhouse Cavern Walls, EL-515															
Downstream Wall: Load (t)						Upstream Wall : Load (t)									
Days	RD-65	Days	RD-110	Days	RD-150	Days	RD-65	Days	RD-110	Days	RD-120	Days	RD-142	Days	RD-150
129	8.93	129	13.19	987	28.36	159	11.12	192	5.61	215	5.21	323	12.63	190	8.5
136	8.89	136	13.47	1005	28.46	169	11.22	217	4.7	228	5.31	328	12.75	211	8.02
143	8.96	142	15.39	1035	28.82	176	11.85	228	6.93	239	5.34	352	13.85	227	7.92
146	8.95	146	15.46	1051	29.12	185	12.74	239	6.89	255	5.35	358	14.26	239	7.88
158	9.03	157	14.92	1073	29.07	204	13.38	255	7.05	278	5.64	376	15.15	252	8.49
165	8.71	718	13.52	1088	28.69	228	14.92	278	7.1	283	5.89	392	16.14	278	7.72
174	10.04	766	16.33	1104	28.75	239	15.6	283	7.07	291	5.85	406	16.53	283	7.73
188	11.17	798	17.4	1131	29.44	245	15.62	299	7.12	323	6.09	430	17.13	290	7.65
232	12.69	824	13.53	1155	29.83	259	16.94	319	7.15	326	6.31	447	17.01	299	7.68
234	12.75	851	13.55	1182	30.01	267	17.21	332	7.12	332	6.63	481	17.21	307	7.63
254	13.57	880	13.41	1209	30	283	18.43	338	7.1	348	6.91	504	18.43	323	7.59
279	14.8	914	13.37	1228	30.17	304	21.66	340	7.08	376	8.39	522	18.2	328	7.75
293	15.63	946	12.78	1242	30.19	315	22.39	348	7.83	392	8.67	543	18.45	332	8.09
337	16.9	965	13.5	1256	30.25	358	22.6	376	6.98	406	8.6	603	19.21	352	7.84
355	18.37	974	13.62	1278	30.3	379	22.69	392	6.97	430	8.77	639	20.24	360	7.7
384	19.03	1005	13.78	1312	30.63	395	23.19	406	7.02	447	8.65	644	19.63	376	7.46
402	19.42	1035	14.11	1329	30.56	409	22.81	430	7.11	481	8.73	662	19.02	406	7.47
419	19.75	1073	12.82	1345	30.94	430	23.99	447	7.34	502	8.781	674	19.63	430	7.38
436	20.1	1088	20.18	1354	30.96	447	22.81	481	7.43	522	8.851	718	19.96	447	7.34
470	20.82	1104	21.09	1375	31.18	481	23.98	502	7.465	543	8.894	744	19.85	481	6.9
491	21.04	1131	22.05	1389	31.41	502	24.29	543	7.263	557	8.903	777	19.75	679	9.088
515	21.26	1155	22.2	1403	31.51	521	24.6	557	7.42	603	9.368	809	19.9	718	9.218
538	20.63	1182	23.64	1439	31.84	543	23.5	598	7.271	639	9.685	835	19.8	744	8.784
576	21.6	1209	25.67	1454	31.88	587	25.1	646	7.288	651	9.502	862	19.98	777	8.508
619	21.81	1227	28.63	1464	31.83	630	25.29	680	7.334	718	9.971	891	20.2	809	8.006
651	21.96	1242	28.99	1474	31.89	651	25.58	718	7.309	732	8.883	925	20.02	835	8.685
901	22.39	1256	29.3	1491	31.88	662	25.8	744	7.334	777	8.934	957	20.13	862	8.817
914	22.4	1280	30.23	1505	31.84	680	26.01	777	7.443	809	8.998	976	19.83	891	8.942
946	22.41	1312	30.29	1513	31.88	694	26.04	814	7.508	835	12.12	985	19.93	925	8.844
965	22.46	1329	30.14	1526	31.89	718	25.99	835	7.532	851	12.56	1016	20.3	957	8.706
974	22.08	1345	29.97	1543	31.82	744	26.07	862	7.57	862	13.88	1046	20.48	976	9.253
1035	22.15	1358	30.16	1558	31.82	770	26.14	891	7.547	891	13.57	1083	20.51	985	9.621
1072	22.34	1375	30.69	1574	31.76	807	26.17	925	7.549	925	13.28	1096	20.51	1016	9.894
1088	22.32	1389	30.76	1582	31.78	835	26.17	957	7.508	957	13.21	1115	20.23	1046	10.23

Load Cell Observations, Location: Powerhouse Cavern Walls, EL-515															
Downstream Wall: Load (t)						Upstream Wall : Load (t)									
Days	RD-65	Days	RD-110	Days	RD-150	Days	RD-65	Days	RD-110	Days	RD-120	Days	RD-142	Days	RD-150
1109	22.34	1403	31.05			862	26.18	985	7.423	976	9.85	1142	20.6	1083	10.18
1131	22.26	1439	31.79			891	26.27	1016	7.369	985	10.24	1166	20.67	1093	10.83
1155	22.25	1454	32.1			925	26.5	1046	7.302	1016	10.92	1193	20.68	1115	10.63
1182	22.22	1464	32.08			957	26.32	1083	7.397	1046	9.914	1220	20.64	1142	10.66
1209	22.22	1474	32.43			976	6.68	1099	7.395	1083	9.881	1238	20.64	1166	10.59
1227	22.17	1489	32.9			985	6.625	1115	7.431	1096	11.14	1250	20.63	1197	10.49
1242	22.15	1491	32.91			1016	6.668	1131	7.421	1115	11.03	1253	20.65	1220	10.89
1256	22.12	1505	32.81			1046	6.898	1142	7.416	1128	10.85	1267	20.6	1238	11.07
1280	22.05	1513	33.21			1062	6.696	1166	7.443	1142	11.32	1289	20.71	1250	11.67
1312	22.03	1526	33.46			1083	6.645	1193	7.476	1166	11.88	1323	20.59	1267	12.87
1329	22	1543	33.01			1099	6.742	1220	7.504	1193	11.88	1340	20.69	1289	12.02
1345	21.99	1558	33.01			1115	6.119	1238	7.513	1220	11.9	1356	20.96	1323	12.78
1358	21.99	1574	33.11			1142	5.685	1400	7.285	1238	12.11	1365	20.93	1340	12.9
1375	22.01	1582	33.15			1166	5.994	1450	7.261	1253	12.18	1386	21.11	1356	13.24
1389	21.99	1588	33.16			1193	6.05	1475	7.269	1267	12.7	1400	21.15	1365	13.23
1403	21.99					1220	6.228	1485	7.303	1291	12.34	1414	21.31	1386	13.44
1439	21.97					1238	6.281	1502	7.315	1323	12.91			1400	13.44
1454	21.81					1400	7.022			1340	12.5			1414	13.27
1464	21.98					1465	6.789			1356	11.81			1450	13.18
1474	21.95					1475	6.746			1369	11.73			1465	13.08
1491	21.91									1386	12.24			1475	13.08
1505	21.92									1400	11.98			1485	12.9
1513	21.89									1414	13.15			1502	12.77
1526	21.89													1516	12.51
1543	21.86													1524	12.55
1558	21.82													1537	12.58
1574	21.79													1554	12.55
1582	21.78													1569	12.55
1588	21.74													1585	12.97
														1593	13.42
														1599	13.53

Table 6. Load cell observations on rock bolts at walls of powerhouse cavern at EL-506

Load Cell Observations, Location: Powerhouse Cavern Walls, EL- 506											
Downstream Wall: Load (t)						Upstream Wall : Load (t)					
Days	RD-65	Days	RD-110	Days	RD-150	Days	RD-65	Days	RD-110	Days	RD-150
119	3.56	28	1.77	0	6.03	137	2.01	33	9.26	0	13.16
128	5.15	29	3.22	3	8.95	139	2.1	37	8.98	7	17.08
173	5.74	35	4.04	18	10.21	150	2.77	44	8.64	12	20.89
175	5.1	38	3.08	28	9.87	166	3.55	50	8.69	27	26.19
195	5.24	41	3.24	36	9.85	173	4.08	54	8.77	44	32.49
220	4.56	45	3.24	38	9.84	184	6.03	55	8.85	47	24.83
234	3.92	47	3.31	41	9.84	192	11.51	56	8.85	50	25.44
296	9.7	51	3.41	45	9.84	213	17.12	57	8.87	54	25.48
325	10.27	53	3.52	47	9.89	222	17.8	96	9.29	55	25.85
343	10.71	57	3.59	48	9.89	229	18.3	101	9.61	56	27.35
360	11.04	65	4.58	49	9.89	233	19.06	107	9.52	57	27.71
377	11.27	70	3.92	51	9.89	238	19.83	114	12.04	58	27.82
411	12.06	77	3.7	53	9.58	246	20.19	131	13.44	60	29.29
432	12.37	83	3.98	57	9.82	262	21.21	156	25.19	62	30.54
456	12.85	87	3.84	65	9.91	271	21.48	167	25.88	63	30.32
479	13.05	98	2.47	73	9.9	307	23.54	178	26.44	65	29.13
517	13.46	113	2.92	80	9.93	331	23.31	194	27.25	68	30.6
560	13.56	119	2.87	84	9.96	345	23.28	217	29.29	70	30.2
592	13.87	134	3.21	87	10	369	3.08	222	29.91	74	31.34
842	14.64	147	3.63	92	9.94	377	3.32	238	29.74	77	30.14
855	14.23	157	3.31	98	10.34	386	3.25	271	31.67	79	30.01
876	14.62	169	3.4	106	10.72	420	3.57	287	31.98	82	28.08
887	14.05	185	3.44	115	10.74	443	4.697	315	32.57	85	29.82
915	14.68	208	3.59	122	10.69	465	3.138	331	30.96	89	29.99
946	14.64	229	3.71	134	11.78	496	3.114	345	31.46	92	30.11
976	14.71	262	3.85	141	11.89	542	3.476	369	32.48	96	29.25
1013	14.67	304	3.68	158	13.32			386	32.11	101	29.91
1029	14.65	323	3.79	169	13.23			420	32.42	107	25.52
1050	14.41	339	4.66	185	13.86			441	32.17	115	26.67
1072	14.61	360	3.7	208	13.21			465	32.15	121	28.72
1096	14.63	377	3.38	229	17.2			482	32.06	129	27.69

Load Cell Observations, Location: Powerhouse Cavern Walls, EL- 506

Downstream Wall: Load (t)						Upstream Wall : Load (t)					
Days	RD-65	Days	RD-110	Days	RD-150	Days	RD-65	Days	RD-110	Days	RD-150
1123	14.52	408	3.01	253	17.66			496	32.34	150	28.8
1150	14.63	411	2.99	304	18.69			585	28.51	166	31.26
1168	14.64	434	3.379	323	19.28			619	28.73	178	31.57
1183	14.72	456	3.478	336	19.75			657	28.94	191	34.86
1197	14.38	473	2.899	345	19.8			683	28.03	217	38.44
1221	14.48	487	3.318	360	19.66			716	27.31	222	38.73
1253	14.59	517	3.58	377	20.13					229	38.76
1270	14.38	569	4.336	411	20.65					238	39.18
1286	14.65	597	4.491	434	21.54					246	39.24
1299	14.9	648	5.01	456	21.59					262	43.16
1316	15.3	674	5.011	473	21.62					267	39.61
		707	4.823	487	21.63					271	39.44
		739	6.18	517	21.72					291	39.88
		765	7.985	569	22.56					299	43.8
		792	8.46	576	22.59					315	43.69
		821	8.805	597	22.88					345	33.62
		855	8.452	624	22.75					369	32.93
		887	9.213	648	22.79					386	31.98
		906	9.63	674	22.79					420	30.89
		915	9.924	688	22.82					443	30.95
		946	10.39	739	23.28					461	30.69
		976	10.15	765	23.27					482	30.75
		1013	4.673	792	23.35					496	30.67
		1029	4.089	821	23.38					542	30.79
		1045	4.056	855	23.42					578	30.57
		1062	4.07	887	23.27					583	30.48
		1072	3.755	906	22.62					601	30.53
		1096	2.377	915	22.94					613	30.45
		1123	3.568	928	22.29					657	30.49
		1150	4.229	946	22.32					683	30.53
		1168	3.816	976	24.36					716	30.6
		1183	4.051	1014	23.81					748	30.7
		1197	4.317	1029	23.78					774	30.43
		1221	4.402	1045	23.9					801	30.44

Load Cell Observations, Location: Powerhouse Cavern Walls, EL- 506											
Downstream Wall: Load (t)						Upstream Wall : Load (t)					
Days	RD-65	Days	RD-110	Days	RD-150	Days	RD-65	Days	RD-110	Days	RD-150
		1253	4.339	1061	24.2					830	30.51
		1270	4.6	1072	24.19					864	30.39
		1286	4.992	1096	24.22					896	30.61
		1299	4.621	1183	26.7					915	30.37
		1316	5.339	1197	27.75					924	30.41
				1219	27.15					955	30.2
										985	30.29
										1022	30.47
										1035	30.56
										1054	30.35
										1081	30.53
										1105	30.62
										1132	30.93
										1159	30.69
										1177	31.29
										1189	31.49
										1206	31.88
										1228	31.54
										1262	31.48
										1279	31.46
										1295	31.22
										1304	31.12

Table 7. Instrumented bolt observations at walls of powerhouse cavern at RD-65, downstream, EL-506

Strain along Instrumented Rock Bolt (Microstrain)												
Location Powerhouse, RD-65, EL-506, Downstream Wall												
Days	12m	11m	10m	9m	8m	7m	6m	5m	4m	3m	2m	1m
0	0.00	0.00	0.00	0.00	0.00	-	0.00	0.00	0.00	0.00	0.00	0.00
1	-6.31	-14.11	-13.41	-23.78	-9.60	-	-13.19	-4.16	55.40	-8.35	-31.58	-29.58
45	-0.40	-17.15	-15.28	-19.67	11.44	-	-15.84	-1.10	54.88	-13.60	-40.72	-36.28
67	0.90	-15.99	-14.10	-17.48	16.38	-	-14.29	-1.37	55.28	-13.10	-42.13	-33.31
92	1.41	-18.02	-20.72	-26.53	12.75	-	-17.50	-3.58	56.44	-16.85	-45.10	-31.31
106	3.02	-18.45	-5.29	-33.05	11.77	-	-19.89	-2.54	55.93	-16.60	-45.45	-34.47
168	7.37	-18.89	-39.25	-50.70	6.36	0.00	-20.68	-4.04	55.28	-18.74	-49.04	-40.49
197	8.08	-19.60	-44.54	-56.07	5.37	40.06	-20.56	-4.16	60.62	-20.16	-48.68	-38.94
215	9.39	-20.32	-46.92	-58.81	4.55	39.15	-22.04	147.04	69.94	-19.74	-47.78	-40.56
232	11.23	-20.32	-48.72	-61.23	2.02	40.12	-21.92	-4.11	71.92	-20.16	-48.00	-36.03
249	12.20		-49.92	-62.92		40.88	-22.15	-4.36	77.43	-19.61	-117.51	-40.48
283	13.52	-20.89	-53.33	-67.83	-3.76	19.91	-27.11	-5.99	77.34	-20.07	-46.65	-35.01
304	15.00	-21.04	-55.31	-70.90	-4.09	24.94	-25.08	-5.60	75.48	-19.41	-48.30	-34.33
328	16.73	-19.91	-56.45	-73.01	-0.98	-	-25.86	7.37	73.47	-18.35	-53.48	-38.85
351	17.56	-20.07	-40.88	-74.62	-8.91	108.89	-27.58	-10.76	71.19	-19.61	101.28	-38.50
714	30.08	-20.46	-82.07	-113.41	-27.12	25.76	-34.94	-35.39	46.33	-74.14	-90.01	-49.86
759	30.47	-20.32	-82.67	-114.10	-31.44	47.56	-36.62	-37.07	-301.05	-76.70	-94.07	1662.93
787	31.16	-20.46	-83.71	-115.46	-37.47	27.75	-298.87	-38.36	41.81	-78.54	-61.28	1608.60
818	32.63	-20.46	-84.68	-116.84	-36.36	24.77	-34.39	-71.18	40.14	-81.64	-65.23	1750.20
848	79.70	-21.19	-85.63	-117.19	101.44	88.34	169.82	-40.70	65.34	-64.90	95.24	1916.12
885	26.74	-22.89	-87.28	-119.91	-39.70	48.67	121.48	-41.13	30.05	-85.94	-108.92	1644.34

Strain along Instrumented Rock Bolt (Microstrain)												
Location Powerhouse, RD-65, EL-506, Downstream Wall												
Days	12m	11m	10m	9m	8m	7m	6m	5m	4m	3m	2m	1m
901		-23.63	-88.23	-121.06	-40.25	-258.42	118.02	-42.56	28.77	-86.25		1642.78
926	22.07	-23.91	-89.31	-122.22	-37.64	25.47	122.07	-42.04	26.10	-84.79	-109.22	1747.97
944	-135.79	-24.77	-90.22	-123.46	-37.47	24.82	123.80	-42.96	23.95	-85.06	-110.12	1645.12
968	18.18	-24.92	-90.83	-123.34	-38.70	49.92	119.45	-42.96	21.79	-86.16	-110.30	1645.92
1022	14.08	-26.35	-92.38	-122.42	-41.60	50.19	125.10	-44.74	16.25	-272.52	-109.81	1650.20
1076	9.60	-26.93	-94.53	-121.41	-39.37	50.68	125.48	-45.23	9.10	-87.99	-110.39	1662.55
1120	7.30	-30.86	-94.95	-121.15	-37.64	51.69	125.55	-46.92	3.61	-88.41	-112.84	1642.01
1167	5.25	-35.34	-95.74	-120.83	-37.47	51.55	176.01	-48.64	-2.60	-90.63	-120.42	1639.41
1202	1.05	-38.90	-94.95	-121.31	-37.47	52.71	105.71	-49.79	-6.55	-92.37	-124.06	1631.36
1233	0.10	-42.44	-96.41	-121.43	-35.26	51.67	175.85	-49.91	-11.20	-93.58	-126.35	1629.81
1239	0.60	-43.14	-96.25	-121.18	-35.26	52.08	174.44	-49.85	-11.83	-94.24	-126.95	1629.03
1264	-2.30	-45.26	-97.11	-121.06	-34.65	51.52	-433.02	-50.95	-13.72	-95.82	-128.37	1620.00
1289	-3.82	-47.80	-97.96	-121.75	-33.98	52.84	-448.07	-50.65	-15.14	-96.95	-129.17	1629.81
1302	-4.81	-49.34	-97.96	-122.15	-32.23	52.95	-454.19	-51.37	-17.22	-97.02	-129.14	1629.29
1326	-6.61	-51.59	-98.48	-122.65	-31.70	52.08	-449.39	-51.85	-18.19	-95.82	-126.68	1635.76
1339	-6.43	-52.71	-98.39	-122.65	-31.28	52.50	-449.24	-51.60	-18.44	-95.89	-126.30	1623.04
1372	-7.21	-54.53	-98.39	-123.79	-30.32	51.58	-448.76	-50.88	-20.02	-95.74	-123.26	1627.12
1402	-8.40	-54.38	-98.22	-124.24	-101.14	51.45	-440.45	-51.49	-21.61	-94.32	-121.13	1640.91

Table 8. Instrumented bolt observations at walls of powerhouse cavern at RD-110, downstream, EL-506

Days	Strain along Instrumented Rock Bolt (Microstrain) Location Powerhouse, RD-110, EL-506, Downstream Wall											
	12m	11m	10m	9m	8m	7m	6m	5m	4m	3m	2m	1m
0	0.00	0.00	0.00	0.00	0.00	0.00	0.00	0.00	0.00	0.00	0.00	0.00
8	0.75	2.13	0.71	1.82	7.59	0.75	1.78	1.38	1.52	3.66	7.38	4.24
12	-0.26	2.87	4.27	2.45	11.38	0.59	1.78	1.29	1.08	4.80	14.77	12.61
15	-0.73	3.08	3.30	2.85	11.38	1.10	0.28	1.47	0.14	4.70	23.68	15.74
18	-0.44	3.40	3.94	2.81	10.82	1.73	-1.24	1.80	5.52	5.67	32.32	19.47
20	-0.14	2.23	3.97	3.28	10.95	2.37	-1.10	1.63	6.40	5.23	38.96	23.21
24	-0.51	1.81	6.03	3.19	8.39	3.43	-0.82	0.96	3.85	-15.69	46.62	28.16
32	0.00	2.34	6.10	3.28	3.74	1.17	-7.11	-2.10	2.61	2.00	82.54	37.23
44	-0.07	2.78	8.29	3.28	0.32	2.28	-7.93	-2.27	6.40	3.83	73.92	41.35
50	0.72	3.70	10.82	3.10	1.27	3.66	-7.51	-1.85	3.80	6.72	32.57	42.33
80	-0.28	1.28	8.91	3.22	-14.44	-5.14	-19.98	-1.08	0.90	0.61	-7.98	39.74
86	-2.32	2.46	9.16	3.82	-14.74	1.10	-20.79	-3.87	2.97	3.83	-3.84	41.45
101	-2.03	3.56	8.12	2.45	-20.73	-0.52	-26.57	-5.48	8.44	2.28	44.94	70.36
114	-1.52	0.85	8.27	2.93	-23.25	0.23	-28.32	-6.50	12.50	4.18	56.58	64.70
136	1.96	41.50	8.27	6.39	-29.21	0.33	-36.19	-7.90	14.64	4.89	87.54	73.17
164	-9.29	53.01	8.70	2.64	-36.47	0.33	-47.17	-9.86	14.64	4.45	90.89	56.16
175	-3.98	60.56	8.55	2.40	-39.49	-0.43	-54.40	-16.12	32.27	4.46	98.55	58.67
196	-14.21	59.11	9.06	-1.27	-23.70	0.42	-64.04	-17.95	90.75	6.10	114.15	82.03
229	-16.97	70.25	9.13	-0.46	-49.48	0.21	-76.32	-24.40	52.02	4.36	127.12	96.52
290	-30.71	69.95	-10.85	-4.92	-56.02	-0.18	-91.91	-31.72	65.00	5.08	165.84	106.15
306	-81.29	69.95	8.63	-6.44	-57.80	-3.40	-96.60	-34.14	83.20	4.96	167.46	102.97

	Strain along Instrumented Rock Bolt (Microstrain)											
	Location Powerhouse, RD-110, EL-506, Downstream Wall											
327	-56.54	69.95	8.05	-8.78	-63.97	-2.47	-104.26	-37.80	76.94	2.69	178.94	112.29
344	-37.46	57.54	7.61	-9.23	-67.40	-3.40	-88.34	-40.15	76.45	2.60	178.16	109.28
375	-56.20	36.20	10.53	-8.96	-68.74	-2.05		-40.07		7.44	217.00	125.56
378	-41.38	33.45	12.52	-9.05	-69.36	5.74		-41.12		8.39	219.76	155.64
401	-60.93	29.18		-9.59	-70.55	-4.08	-81.23	-44.51		7.95	225.43	186.74
423	-62.99	24.69		-11.02	-77.24	-4.50		-46.02		7.69	231.55	188.25
454	24.09	14.80		-13.16	-79.49	-4.60				10.80		183.59
484	-50.41	13.14	14.22	-13.81	-80.61	-6.68		-50.11		11.66	243.27	183.59
536	-56.37	0.43	9.43	-17.47	-86.59	-14.30	-121.89	-53.54		6.28	253.58	184.78
564	-75.14	20.81	8.99	-19.69	-88.04	-20.78		-55.87		6.02	258.88	192.24
615	-61.66	14.54		-26.93	-92.81	-32.60	-138.84	-63.86		4.01	264.89	202.18
641	-78.90	9.30		-32.05	-89.27	-37.08	-142.98	-63.79		5.03	266.32	204.90
674	-81.23	-24.63		-36.86	-96.68	-42.40	-145.87	-66.77		5.93	266.00	200.77
706	-98.66	-26.45		-44.83	-98.14	-46.98	-174.86	-67.98		7.75	266.00	195.37
732	-94.32	-26.28		-51.72	-101.27	-54.91		-72.07		6.68	262.24	194.20
759	-60.90	-27.15		-52.48	-102.30	-54.20		-74.00		4.19	265.90	187.78
788	-64.18	-30.91		-55.90	-104.12	-62.03		-80.74		2.60	263.88	183.72
822	-69.19	-34.71		-61.76	-107.50	-65.02	-171.21	-75.70		-0.70	263.21	179.48
854	-69.85	-35.03		-60.32	-106.33	-67.60	-174.51	-77.02		-4.00	260.77	178.41
913	-92.60	-43.18		-66.14	-102.66	-71.96	-212.55	125.90		-12.52	260.43	189.88
943	-72.56	-47.73		-69.92	-98.87	-77.83	-194.06	112.54		-13.22	264.99	199.71
980	-40.18	-48.14		-72.79	-110.46	-79.21	-198.37	67.02		-18.59	267.01	188.84
996	-58.13	-50.77		-75.76	-106.84	-82.97	-199.52	71.53		-22.15		188.25
1039	-93.18	-55.88		-80.41	-107.50	-83.35				-20.28	267.68	189.88

Strain along Instrumented Rock Bolt (Microstrain)												
Location Powerhouse, RD-110, EL-506, Downstream Wall												
1063	-102.29	-58.29		-85.60	-106.40	-88.15				-21.64	266.55	188.25
1117	-96.47	-64.46		-90.43	-105.92	-92.69				-21.38	265.56	180.49
1171	-104.42	-77.87		-97.05		-92.76				-9.57	266.44	181.87
1215	-94.63	-84.40		-101.87		-99.97				-25.11	266.11	185.35
1262	-94.19	-88.57		-108.12		-102.20				-25.11	271.02	200.19
1297	-96.47	-91.66		-112.74		-102.88				-27.05	275.19	211.19
1328	-94.20	-95.99		-116.79		-104.66				-26.82	280.26	212.85
1334	-101.80	-96.96		-116.32		-104.51				-26.12	281.59	215.23
1359	-104.17	-101.73		-121.28		-107.26				-27.97	282.61	211.42
1384	-102.14	-104.68		-123.63		-106.37				-25.53	284.02	207.86
1397	-110.50	-107.15		-126.60		-108.00				-25.61	283.77	209.17
1421	-117.91	-109.99		-129.56		-109.48				-25.28	281.42	202.90
1434	-102.74	-132.03		-130.33		-110.28				-25.61	254.35	204.42
1467	-202.10	-114.43		-134.06		-110.66				-27.13	279.47	203.73
1497	-183.18	-116.30		-134.60		-112.86				-26.96	278.24	206.56

Table 9. Instrumented bolt observations at walls of powerhouse cavern at RD-150, downstream, EL-506

Days	Strain along Instrumented Rock Bolt (Microstrain) Location Powerhouse, RD-150, EL-506, Downstream Wall											
	12m	11m	10m	9m	8m	7m	6m	5m	4m	3m	2m	1m
0	0.00	0.00	0.00	0.00	0.00	0.00	0.00	0.00	0.00	0.00	0.00	0.00
44	7.30		0.58	-4.21	3.13	1.39	4.76	8.61	3.05	2.33	3.47	16.30
63			0.71	-1.38	2.33	1.04	6.33	9.70	2.26	1.15	2.56	27.79
84	10.79		0.32	0.46	1.23	0.86	8.41	9.88	2.14	1.17	2.24	29.11
108	9.70		0.45	0.90	-0.58	0.26	5.85	11.45	0.00	-0.83	0.98	30.89
159	6.35		-1.22	2.21	-3.57	-0.70	6.95	9.61	-1.13	-1.46	0.98	27.57
178	5.50		-1.47	2.65	-6.10	-0.53	6.95	9.42	0.00	-1.78	0.98	27.49
200	1.55		-1.96	2.10	-13.76	-7.48	1.59	8.79	-2.94	-2.40	0.42	27.17
215	0.39		-1.34	3.41	-19.50	-10.15	-9.71	9.61	-5.07	-2.30	0.82	26.17
232	-2.26		-3.00	1.01	-29.21	-17.87	-10.15	6.76	-11.01	-5.43	-1.81	25.48
265	-2.02		-1.79	3.40	-43.69	-23.23	-16.79	8.88	-15.25	-2.09	1.89	29.92
289	-3.81		-1.66	4.17	-54.11	-27.29	-18.77	9.88	-20.13	-2.93	2.56	-32.90
311	-6.30		-3.06	4.03	-47.16	-35.70	-34.52	2.37	-29.06	-12.98	-1.56	29.92
318	-5.53		-1.54	3.96	-15.15	-34.50	-33.11	6.03	-27.96	-11.76	0.98	30.71
342	-5.95		-1.40	-18.17		-43.74	-38.97	1.42	-32.51	-20.10	3.27	29.72
372	-8.91		-2.30	1.32		-48.88	-49.35	-7.25	-37.37	-29.72	5.03	23.54
424	-16.21		-2.62	4.78		-58.52	-55.47	-22.28	-47.99	-43.75	-0.74	21.72
452	-19.74		-2.23	4.51		-63.39	-59.39	-30.74	-50.13	-48.35	-1.16	25.04
479	-25.12		-2.68	5.60		-63.25	-71.15	-36.92	-63.76	-51.03	-1.40	24.07
503	-29.53		-2.93	5.71		-71.26	-77.04	-43.05	-59.44	-52.32	-1.23	23.90
529	-33.47		-2.30	7.22		-72.70	-87.34	-46.83	-60.51	-52.52	-0.42	25.84

Strain along Instrumented Rock Bolt (Microstrain)												
Location Powerhouse, RD-150, EL-506, Downstream Wall												
543	-35.43		-3.45	12.27		-75.49	-86.26	-51.11	-63.16	-55.00	-2.80	3.89
557	-35.66		-1.72	9.23		-73.18	-71.33	-50.16	-61.12	-51.83	0.66	4.60
909	-58.79		-	1.23		-90.85	-74.90	-104.68	-97.17	-63.77	-0.33	1.72
917	-58.39		-4.26	1.89		-90.46	-133.29	-103.88	-97.36	-63.37	1.46	2.15
927	-57.38		-3.89	1.83		-90.22	-128.28	-98.98	-97.47	-62.69	1.56	2.06
951	-57.03		-3.06	2.85		-90.08	-134.55	-111.64	-98.39	-61.22	3.47	2.83
1005	-59.29		-4.40	-3.98		-95.81	-144.28	-124.98	-107.96	-68.66	-1.40	5.42
1059	-62.45		12.72	-4.64		-96.43	-144.97	-131.14	-110.29	-65.92	2.14	15.57
1103	-66.83		-3.89	-7.57		-99.84	-159.79	-138.24	-114.64	-70.41	-0.25	10.61
1150	-67.84		-2.81	-4.31		-99.39	-161.95	-139.78	-110.71	-65.65	-	15.57
1185	-69.29		-3.13	-6.58		-103.01	-166.44	-143.69	-116.44	-70.59	4.70	13.30
1216	-73.19		-4.40	-11.44		-107.22	-176.08	-151.14	-123.04	-76.24	-0.64	6.19
1222	-73.09		-3.96	-9.83		-107.45	-168.05	-150.00	-120.74	-74.66	1.73	8.97
1247	-73.97			-12.61		-109.57	-172.90	-154.00	-124.65	-78.17	-1.16	3.52
1272	-76.09		-4.14	-10.80		-110.34	-179.58	-152.96	-124.14	-77.78	1.98	4.95
1285	-76.41		-4.14	-10.26		-110.78	-182.23	-152.42	-123.85	-77.88	2.28	5.16
1309	-77.63		-5.80	-12.20		-113.45	-188.21	-154.46	-124.44	-78.65	3.22	5.68
1322	-77.53		-4.84	-11.12		-112.70	-188.31	-154.31	-123.94	-77.78	4.06	5.59
1355	-78.85		-5.73	-13.92		-114.66	-196.27	-157.32	-124.24	-77.69	4.63	5.68
1385	-78.53		-5.98	-20.56		-116.02	-202.25	-159.42	-123.85	-77.27	6.61	7.40

Table 10. Instrumented bolt observations at walls of powerhouse cavern at RD-65, upstream, EL-506

Days	Strain along Instrumented Rock Bolt (Microstrain) Location Powerhouse, RD-65, EL-506, Upstream Wall							
	8m	7m	6m	5m	4m	3m	2m	1m
0	0	0	0	0	0	0	0	0
15	-0.98	9.36	-0.28	3.51	4.24	-1.89	3.55	175.95
36	-5.66	9.22	-1.27	3.06	-13.10	-3.69	3.11	160.14
45	-8.61	9.17	-2.32	2.75	-15.57	-6.52	1.69	168.88
56	4.38	8.93	-2.87	2.59	-15.58	-10.50	3.64	159.22
61	-7.10	7.67	-3.44	2.21	-16.67	-5.86	3.21	177.17
93	-11.26	0.74	-10.47	0.85	-2.05	-9.62	1.69	197.95
128	-23.69	-12.91	-22.48	0.99	-23.18	-13.37	-1.72	206.97
155	-27.36	-17.61	-30.92	0.23	-26.80	-13.65	-2.78	221.19
175	-30.21	-20.38	-39.64	-0.46	-28.17	-23.40	-2.70	226.81
192	-30.20	-22.88	-35.05	-1.29	-28.66	-27.82	-3.04	226.05
209	407.17	-26.31	-38.19	-2.05	-30.22	-32.59	-2.53	232.55
243	421.48	-35.81	-36.91	-8.74	-31.10	-41.69	-1.60	238.02
266	525.58	-31.24	-44.27	-5.46	-33.24	-46.89	-1.51	248.46
288	705.34	-33.48	-48.87	-6.45	-36.09	-51.31	0.53	250.43
365	777.23	-41.88	-57.48	-12.17	-34.02	-63.93	1.44	256.01
794	532.62	-71.27	-82.33	-32.34	-34.99	-97.18	-11.15	247.61
798	532.62	-71.11	-82.26	-32.58	-34.51	-97.21	-11.48	245.48
845	533.75	-71.52	-83.13	-33.01	-34.90	-110.76	-10.24	249.12
861	564.80	-61.69	-68.71	-33.01	-35.57	-90.32	-17.13	243.83
904	558.02	-62.17	-74.79	-33.30	-37.12	-94.66	-20.35	308.48

928	548.72	-68.65	-79.75	-32.72	-36.73	-99.07	-19.69	225.39
959	544.69	-70.71	-82.75	-33.22	-35.76	-100.51	-19.36	227.64
982	542.67	-72.21	-83.81	-32.20	-36.15	-101.02	-18.63	231.03
987	542.53	-72.56	-84.11	-32.28	-36.27	-101.61	-18.68	254.01
1036	539.01	-73.96	-85.05	-31.92	-35.96	-102.70	-18.48	232.01
1080	537.73	-75.65	-85.52	-30.97	-36.05	-103.42	-17.91	233.42
1127	536.25	-76.45	-85.87	-31.04	-36.05	-104.14	-19.93	224.97
1146	536.31	-76.70	-86.36	-31.40	-42.39	-104.58	-20.61	222.37
1162	536.25	-76.88	-86.79	-31.77	-36.35	-104.90	-21.54	218.39
1193	535.63	-77.40		-32.46	-36.24	-105.48	-22.58	218.07
1199	536.00	-77.66		-32.79	-36.35	-105.65	-22.63	218.18
1224	535.51	-79.56	-88.52	-33.01	-36.81	-106.23	-23.72	220.76
1249	536.00	-79.07	-89.20	-33.30	-36.39	-106.45	-23.07	225.06
1262	535.38	-79.41	-89.26	-33.67	-36.73	-106.15	-22.79	224.32
1286	536.37	-78.25	-87.83	-33.52	-36.15	-105.99	-21.32	222.48
1299	535.88	-78.52	-89.40	-33.38	-36.51	-105.99	-20.95	221.51
1332	536.51	-78.25	-88.95	-33.01	-36.35	-105.67	-19.63	228.54
1362	536.25	-78.44	-88.58	-32.50	-35.87	-105.48	-18.34	232.55

Table 11. Instrumented bolt observations at walls of powerhouse cavern at RD-110, upstream, EL-506

Strain along Instrumented Rock Bolt (Microstrain)												
Location Powerhouse, RD-110, EL-506, Upstream Wall												
Days	12m	11m	10m	9m	8m	7m	6m	5m	4m	3m	2m	1m
0	0.00	0.00	0.00	0.00	0.00	0.00	0.00	0.00	0.00	0.00	0.00	0.00
2	-21.18	0.30	0.00	-0.49	-0.16	-3.09	-5.49	-5.53	-0.80	-1.04	15.72	0.81
6	-20.89	0.45	-0.77	-1.50	1.45	-10.58	-4.54	-5.95	39.71	28.78	69.49	21.09
9	-20.71	0.82	-0.77	-1.08	1.44	-0.65	-4.18	-5.21	79.49	34.56	109.45	30.91
48	-18.95	-0.36	-2.58	0.60	5.19	5.57	-6.82	-6.51	192.59	108.01	385.81	92.90
53	-40.70	5.49	-3.75	1.60	4.24	5.18	-9.46	-7.82	311.34	184.00	673.55	156.52
83	-14.72	6.32	-4.91	-1.59	-1.82	4.92	-16.87	-18.50	365.92	791.91	1906.54	170.25
112	-12.77	7.07	-26.85	-7.26	-7.42	3.74	-24.49	-28.47	682.22	1204.60	1052.68	129.47
130	-11.16	6.62	-35.27	-9.33	-10.08	5.30	-29.79	-33.50	684.84	1186.50	1009.25	144.15
174	-10.36	1.95	-61.69	-21.02	-19.33	1.55	-46.66	-47.12	708.58	1170.92	919.01	188.02
190	-10.90	2.17	-121.35	-29.06	-22.45	1.55	-52.18	-52.66	707.14	1121.87	788.44	139.16
214	-70.28	1.72	343.95	-38.55	-5.46	-0.74	-60.78	-57.70	712.52	1120.47	756.55	156.40
284	-11.53	1.13	437.84	-57.82	-31.88	-5.54	-75.38	-72.13	704.84	1119.63	725.80	192.23
304	-10.99	0.90	457.86	-61.70	-31.95	-3.60	-79.67	-74.67	705.89	1119.63	712.37	199.20
321	-10.73	0.59	415.92	-66.11	-33.14	-6.96	-82.02	-76.21	707.62	1119.63	702.03	203.34
338	-10.55	-0.15	457.72	-69.28	-33.87	179.04	-84.37	-80.33	707.00		691.72	206.11
371	-10.46	-0.97	433.59	-74.48	-86.58	-12.58	-41.05	-89.13	734.95		683.16	222.98
395	-9.75	-2.10	448.21	-79.84	-37.59	-16.80	-92.98	-88.35	738.49			230.15
417	-9.21	-2.92	458.59	-80.27	-39.25	-18.76	-93.30	-89.40	744.29		659.29	227.32
494	-7.79	-4.55	427.67	-84.86	-44.35	-32.33	-103.77	-102.25	783.79		614.23	232.51
530	-6.90	-6.26	409.00	-85.32	-44.28	-36.03	-103.77	-104.44	839.46		607.99	136.46

Strain along Instrumented Rock Bolt (Microstrain)												
Location Powerhouse, RD-110, EL-506, Upstream Wall												
542	-6.90	-6.71	404.32	-89.81	-46.13	-39.84		-106.21	870.95		604.32	135.06
570	-6.09	-7.08	391.43	-96.36	-45.33	-41.71		-108.12	880.68		595.08	130.32
609	-5.83	-8.71		-99.63	-44.35	-48.35		-112.51	881.22		579.33	125.72
635	-5.74	-9.30		-103.82	-45.27	-50.51		-113.67	1067.01		578.52	130.32
700	-5.56	-21.97		-110.69	-49.21	-61.08		-121.79	895.03		575.73	141.21
726	-5.47	-16.74		-110.80	-50.57	-64.99		-124.23	899.27		574.39	147.20
753	-4.84	-17.11		-115.70	-49.31	-68.89		-123.25	980.10		577.27	153.44
1022	-8.15			-137.32	-57.37	-94.71		-142.71	943.40		478.65	144.48
1033	-8.50			-138.67	-60.78	-98.98		-147.87	939.33		474.67	141.87
1057	-8.15			-141.17	-63.32	-99.81		-148.84	1002.29		467.91	148.83
1111	-6.81			-144.57	-67.46	-101.57		-148.14	1016.12		461.55	168.36
1165	-7.16			-150.31	-74.26	-111.51		-155.45	925.26		492.26	184.40
1209	-5.02			-152.24	-70.57	-109.21		-146.68	961.26		576.04	177.97
1256	-4.03			-155.24	-72.00	-111.42		-159.65	981.27		459.56	144.91
1291	-3.76			-145.05	-75.31	-113.71		-165.41	936.03		446.91	135.66
1322	-4.31			-160.75	-76.38	-114.35		-170.02	957.15		446.91	139.81
1328	-3.94			-160.22	-76.03	-114.70		-168.33	959.86		435.58	92.18
1353	-4.40			-163.87	-76.82	-116.33		-172.17	953.99		462.26	144.15
1378	-4.31			-166.63	-78.13	-116.22		-172.90	948.23		460.56	155.19
1391	-5.33			-157.36	-81.72	-118.41		-177.64	934.55		449.27	161.47
1415	-6.81			-172.06	-84.71	-122.01		-181.94	931.42			175.85
1428	-7.43			-174.12	-84.96	-123.18		-179.98	946.00			179.27
1461	-6.57			-161.10	-85.29	-123.48		-176.68	970.09			189.44
1491	-7.43			-156.61	-88.19	-127.32		-180.63	981.98			216.19

Table 12. Instrumented bolt observations at walls of powerhouse cavern at RD-150, upstream, EL-506

Strain along Instrumented Rock Bolt (Microstrain)												
Location Powerhouse, RD-150, EL-506, Upstream Wall												
Days	12m	11m	10m	9m	8m	7m	6m	5m	4m	3m	2m	1m
0	0.00	0.00		0.00	0.00	0.00	0.00	0.00		0.00	0.00	0.00
14	-0.11	-140.02		-275.98	-194.72	-327.57	-110.97	-216.94		-23.96	-55.57	3.31
38	-0.41	-139.85		-274.98	-192.29	-326.19	-110.41	-217.71		-24.38	-55.93	3.42
146	-2.35	-143.49		-275.26	-194.32	-326.80	-117.51	-222.24		-25.12	-62.38	4.97
190	-7.52	-146.55		-273.78	-196.55	-332.57	-119.52	-224.84			-69.33	5.33
237	-9.27	-148.88		-292.68	-200.52	-338.64	-123.19	-230.06		-29.40	-68.48	0.30
272	-13.30	-149.32		-272.46	-198.16	-337.86	-122.14	-229.86		-27.90	-67.00	-2.31
303	-18.13	-151.48		-271.73	-198.77	-341.56	-124.45	-233.59		-30.11	-66.43	-7.52
309	-18.43	-151.52		-271.78	-199.05	-342.05	-124.69	-233.88		-29.81	-65.88	-6.82
334	-22.02	-153.71		-270.88	-198.91	-342.83		-235.45		-30.22	-67.00	-7.13
359	-26.84	-153.53		-272.86	-205.62	-346.31		-240.72		-34.03	-68.87	-10.30
372	-29.09	-153.89		-272.09	-205.09	-346.80	-128.89	-239.68		-32.55	-67.78	-9.25
396	-31.85	-154.41		-271.31	-205.62	-344.37		-241.23		-34.25	-69.97	-8.09
409	-32.55	-153.53		-269.95	-204.15	-342.24	-123.75	-236.18		-29.43	-68.21	-3.95
442	-37.01	-154.76		-270.74	-207.37	-343.80	-128.17	-238.14		-30.43	-70.11	1.08
472	-38.36	-153.80		-270.74	-205.22	-342.83	-129.60	-234.21		-26.72	-70.35	7.70

Table 13. Instrumented bolt observations at walls of powerhouse cavern at RD-140, upstream, EL-515

Strain along Instrumented Rock Bolt (Microstrain)												
Location Powerhouse, RD-140, EL-515, Upstream Wall												
Days	12m	11m	10m	9m	8m	7m	6m	5m	4m	3m	2m	1m
0	0.00	0.00	0.00	0.00	0.00	0.00	0.00	0.00	0.00		0.00	0.00
1	-1.14	3.86	0.69	-1.47	1.82	-0.49	0.81	3.18	5.43		-0.12	-4.65
6	0.00	-5.37	1.59	0.37	47.02	2.88	5.94	5.73	8.17		5.17	-1.80
9		15.14	1.59	-5.55	62.17	4.31	5.94	5.85	6.55		4.54	-6.56
68	-0.09	7.68	7.52	-9.86	111.57	13.36	26.79	5.41	3.32		5.29	0.80
86	-0.12	22.14	8.14	-13.84	106.22	14.64	27.53	6.05	-0.57			0.55
99	1.12	24.12	8.01	-19.88	98.63	14.48	26.60	5.52	-51.88		-0.21	2.22
130	0.88	27.32	8.35	-28.55	86.24	13.99	26.42	5.29	-41.38		-3.79	1.64
146	2.02	26.32	8.64	-37.41	86.61	13.12	25.22	5.11	-45.67		-3.35	1.80
170	1.87	27.75	8.28	-47.40	79.23	12.57	26.51	3.29	-49.39		-4.51	4.17
175	1.90	30.96	8.71	-48.64	77.18	12.03	26.51	2.65			-4.60	-0.13
199	2.78	9.59	8.35	-49.33	74.03	9.77	25.96	1.48	-42.12		-4.55	-8.55
260	0.70	16.77	8.73	-49.33	64.23	1.55	24.29	-0.78	-46.05		-5.30	-11.71
277	-2.15	32.45	8.92	-49.33	61.94	0.12	23.65	-0.53	-46.72		-4.60	-11.15
294	-6.25		8.97		60.31	-1.04	24.10	-0.08	-48.15		-3.65	-9.30
327	-13.58	19.40	9.41		56.42	-4.33	21.55	-0.21	-48.54		-3.70	-13.20
351	-17.70	23.03	9.48		55.47	-6.68	19.88	-0.11	-52.25		-3.61	-11.80
369	-20.87	40.42	9.55		53.44	-9.09	18.41	0.53	-53.57		-2.71	-10.17
450	-36.13	22.04	7.37		46.78	-17.43	-0.83	1.17	-59.24		-1.73	0.55
486	-43.21	49.52	4.72		44.31	-21.64	-10.70	1.80	-65.07		-1.46	1.52
491	-47.88	45.47	4.80		43.52	-22.04	-12.21	1.80	-66.09		-1.64	1.64

Strain along Instrumented Rock Bolt (Microstrain)												
Location Powerhouse, RD-140, EL-515, Upstream Wall												
521	-53.77	45.81	2.91		39.84	-26.59	-19.25	2.06	-66.55		-1.46	0.38
565	-66.96	17.11	-4.43		36.40	-31.59	-23.55	0.96	-66.48		-2.18	-0.29
591	-71.12	24.12	-8.57		34.05	-34.57	-26.77	2.12	-66.28		-1.55	-0.89
624	-76.10	26.55	10.79		28.55	-36.31	-27.22	1.18	26.99		-0.83	-0.90
656	-76.45	15.69	-6.00		28.90	-39.90	-33.92	1.06	-66.38		-1.55	-4.40
682	-82.23	33.63	-19.60		28.38	-41.54	-37.14	1.59	-69.45		-0.30	-4.56
709	-85.27	9.05	-20.88		27.86	-42.80	-41.27	1.48	-69.83		0.44	-4.89
738	-88.55	16.48	-21.76		28.09	-42.58	-41.17	2.76	-67.68		1.41	-4.20
772	-89.48	39.87	-25.58		23.91	-45.33	-43.90	2.44	-69.64		2.40	-2.98
804	-90.07	17.79	-28.17		23.32	-46.88	-44.25	1.48	-63.57		3.55	0.55
823	-91.82	33.07	-31.29		21.35	-48.94	-46.46		-73.08		3.21	1.22
832	-91.82	36.96	-31.95		20.89	-49.37	-47.64	0.53	-72.80		4.02	2.90
863	-96.71	24.56	-35.28		19.74	-50.04	-50.15	-0.42			5.01	11.88
893	-103.29	51.08	-38.08		16.51	-51.00	-49.50	-2.53	-74.48		4.84	20.18
930	-108.59	22.58	-41.94		41.69	-52.77	-51.38	-3.29	-77.20		4.39	18.72
940	-108.53	33.07	-43.74		13.97	-52.54	-52.55	-3.91	-72.89		3.67	15.37
989	-109.28	35.40	-30.43		13.86	-53.20	-51.38	-1.38	-70.76		4.92	17.26
1013	-110.88	50.31	-34.59		10.52	-56.42	-53.89	-2.85	-70.76		14.24	12.13
1044	-110.53	41.87	-37.36		8.58	-59.11	-56.12	-3.70	-74.85		1.32	13.92
1067	-111.19	27.32	-40.50		7.46	-59.11	-56.09	-3.80	-74.12		0.60	15.20
1121	-112.81	37.29			5.18	-62.16	-57.93	-2.97	-75.96		0.16	24.22
1165	-117.38	14.49	-56.45		4.55	-62.95	-58.10	-1.17	-75.68		-0.47	30.99
1212	-121.57	23.21	-58.80		-3.59	-66.20	-61.53	-2.27	-79.65		-4.42	42.74
1247	-125.88	18.42	-59.49			-63.99	-61.95	-2.97	-79.86		-4.69	40.18

Strain along Instrumented Rock Bolt (Microstrain)													
Location Powerhouse, RD-140, EL-515, Upstream Wall													
1278	-130.38	8.34	-63.36				-64.55	-62.19	-5.25	-78.45		-5.39	38.55
1284	-131.22	4.53	-63.48				-68.27	-63.19	-5.50	-78.95		-5.29	33.25
1309	-135.65	-9.43	-65.44				-69.86	-63.03	-7.29	-78.08		-4.86	27.00
1334	-139.89	-13.89	-68.20				-69.50	-63.44	-8.76	-77.68		-5.13	25.96
1347	-141.83	2.12	-67.14				-70.92	-64.11	-10.43	-76.97		-4.51	24.57
1371	-143.22	-5.43	-67.59				-69.72	-63.28	-10.86	-75.13		-4.07	24.22
1384	-143.55	0.84	-68.66				-69.83	-62.03	-10.65	-75.68		-4.07	24.95
1417	-146.43	-5.58	-70.33				-75.36	-70.24	-17.44	-82.95		-7.81	24.44
1447	-147.86	-8.67	-70.07				-73.15	-64.61	-15.77	-76.74		-5.13	23.96

Table 14. Instrumented bolt observations at walls of powerhouse cavern at RD-150, upstream, EL-515

Strain along Instrumented Rock Bolt (Microstrain)												
Location Powerhouse, RD-150, EL-515, Upstream Wall												
Days	12m	11m	10m	9m	8m	7m	6m	5m	4m	3m	2m	1m
0	0.00	0.00	0.00	0.00	0.00	0.00	0.00	0.00	0.00	0.00	0.00	0.00
44	-0.98	-16.02	-15.50	11.77	-11.39	7.30	-4.48	-0.30	-4.58	4.32	-2.43	1.95
70	-0.98	-27.73	-2.52	-15.31	-24.17		-5.06	0.69	-4.15	-2.05	-2.27	6.01
103	-1.25	-31.87	-8.87	-14.74	-20.16		25.64	98.44	-4.18	81.55	-0.27	6.01
135	-4.04	-32.55	25.55	-18.61	-35.55		45.55	1.26	-4.58	20.68	-43.60	31.25
161	-1.29	-34.57	109.29	-20.61	-34.87		30.54	1.19	-5.53	3.03	2.90	30.94
188	-4.04	-42.33	102.71	-23.45	-33.11		65.14	-0.62	77.08	55.65	3.52	34.71
217	-1.05	-236.66	111.65	-25.03	-53.45		31.80	0.11	-8.64	4.48	2.67	35.25
251	-0.98	-280.82	109.29	-29.30	-167.40		0.94	2.27	-10.93	6.18	-0.28	36.31

Strain along Instrumented Rock Bolt (Microstrain)												
Location Powerhouse, RD-150, EL-515, Upstream Wall												
283	-0.49	-298.15	104.91	-34.02	-192.31		3.87	3.00	-14.69	7.59	-4.92	35.63
419	-0.08	-346.02	38.80	-33.27	-289.98		0.32	7.41	-33.33	5.26	-13.49	6.17
468	27.28	-361.73	35.43	-44.52	-343.57		32.27		-31.76	5.84	-12.64	7.52
492	-0.65	-371.92	64.12	-50.90	-304.15		20.18		-7.49	61.07	-10.67	43.43
523	-0.73	-385.05	103.88	-53.53	-315.60		-4.75		-38.24	7.79	-9.00	18.72
546	-0.98	-391.37	91.83	-58.89			-4.90		-15.83	63.48	-7.84	98.91
600	-1.45	-414.00	62.78	-63.38			29.43		-52.84	12.40	-7.07	34.32
644	-1.08	-441.74	39.92	-68.04			-4.59		-50.86	14.60	-5.65	35.25
691	-1.38	-475.02	13.96	-74.20			-10.73		-68.31	12.87	-8.79	17.80
726	-1.38	-501.16	-3.12	-55.30			-15.00		-70.80	11.83	-9.92	15.98
757	-0.81	-467.38	-17.69	-81.47			-19.09		-81.29	10.56	-12.82	5.13
763	-0.81	-466.13	-20.15	-80.95			-18.64		-82.07	11.14	-12.24	16.56
788	-1.05	-466.36	-24.76	-82.98			-22.74		-83.02	9.52	-13.01	21.46
813	3.63	-452.32	-33.63	-85.85			-24.09		-83.87	10.67	-12.66	22.99
826	-1.68	-423.01	-35.00	-87.03			-25.00		-83.23	11.37	-11.90	24.66
850	-1.87	-421.12	-55.34	-88.94			-24.09		-84.52	12.75	-9.85	37.25
896	-2.27	-422.95	-129.69	-91.79			-25.00		-85.58	14.66	-6.15	52.44
926	-2.43	-401.07	-135.66	-93.17			-24.54		-84.84	17.50	-2.37	63.52

APPENDIX -3

Table 15. Load cell readings on steel ribs on upstream side at transformer hall cavern

Axial Load on Steel Ribs on Upstream Wall (t)											
Days	RD-14 U/S	Days	RD-70.6 U/S	Days	RD-84.5 U/S	Days	RD-113.2 U/S	Days	RD-129.4 U/S	Days	RD-154.4 U/S
149	6.74	68	6.26	6	8.06	179	1.79	106	8.58	0	11.35
153	6.16	76	9.67	22	5.75	190	1.25	110	12.5	6	10.75
162	6.73	85	10.49	27	6.43	192	1.36	117	12.87	22	13.44
167	5.66	89	12.05	39	6.74	199	1.51	122	13.86	27	14.51
170	7.07	93	13.57	48	7.54	218	1.72	130	14.85	39	15.51
179	7.84	100	15.84	54	8.49	228	1.68	140	13.98	50	16.23
190	9.16	103	16.29	60	9.08	244	1.56	149	16.96	54	16.5
195	9.52	110	18.1	62	9.23	256	1.28	162	18.82	60	16.76
199	9.64	117	19.22	66	9.4	277	2.1	170	19.77	62	16.8
203	9.75	121	19.55	68	9.37	304	2.2	179	20.37	66	16.89
209	9.93	130	20.47	76	10.05	344	2.53	190	20.34	68	16.93
218	10.45	140	21.51	85	10.47	368	2.36	203	21.39	76	17.37
225	10.71	149	22.41	89	10.63	387	2.65	218	21.41	85	17.83
228	10.78	162	23.54	93	10.88	401	2.66	228	21.73	93	18.15
244	10.73	170	23.96	100	11.48	417	2.71	244	21.99	100	18.43
246	10.71	179	24.06	103	12.97	429	2.52	256	22.12	103	18.73
256	10.69	190	24.65	110	11.77	442	2.36	277	20.34	110	19.1
264	10.52	195	24.94	117	12.07	451	3.1	291	20.74	117	19.47
275	10.33	199	25.12	122	12.23	469	1.8	304	18.82	122	19.77
300	10.61	218	26.22	130	13.12	482	1.3	314	18.78	130	22.75
319	12.15	228	26.56	140	13.89	486	1.65	319	18.81	140	20.43
325	23.64	244	28.23	149	14.5	492	1.2	325	19.04	149	20.84
334	23.48	256	26.58	162	14.96	497	1.4	334	19.29	162	21.51
351	23.54	277	28.99	170	14.41	503	1.35	351	18.36	170	21.61
367	23.53	303	29.55	179	14.15	515	1.56	367	17.94	179	21.16
387	27.94	334	30.98	190	14.54	529	1.86	387	17.12	190	20.95
		351	31.54	199	14.52	550	2.14	404	16.92	199	20.61
		367	37.06	218	14.35	565	3.17	412	16.93	218	20.76
		387	42.57	228	14.45	699	3.68	429	16.09	228	20.72
		404	51.18	250	12.4	709	5.08	442	15.72	244	18.41

Axial Load on Steel Ribs on Upstream Wall (t)											
Days	RD-14 U/S	Days	RD-70.6 U/S	Days	RD-84.5 U/S	Days	RD-113.2 U/S	Days	RD-129.4 U/S	Days	RD-154.4 U/S
		417	56.39	256	12.07	740	6.17	451	15.82	256	18.04
		429	62.78	277	11.55	764	6.72	469	15.99	277	20.55
		457	68.96	304	10.39	789	7.35	486	15.84	303	23.36
		469	71.61	344	8.03	832	6.69	492	15.9	337	29.24
		486	79.65	353	7.74	853	9.62	497	15.91	401	35.86
		488	79.78	367	5.76	873	9.78	503	15.88	412	36.08
		494	80.25	387	3.9	908	10.6	515	15.72	417	36.36
		502	80.47	401	4.9	1093	11.49	529	15.27	428	32.52
		515	80.79	417	4.1	1142	14.49	551	14.95	435	33.35
		1093	82.98	429	4.81	1167	12.16	565	14.65	442	33.89
		1121	83.06	451	4.1	1186	12.86	709	12.56	1083	48.51
		1208	107.58	469	4.03	1215	12.57	740	12.47	1093	48.59
		1244	107.43	472	4.07	1244	10.06	764	12.38	1121	48.94
		1271	117.16	486	4.24	1271	25.21	789	13.04	1142	49.07
		1308	135.66	491	4.28	1308	24.73	832	12.2	1167	49.65
				506	4.83	1336	25.22	853	12.34	1186	49.87
				515	5.04	1375	25.21	1114	12.66	1215	50.19
				534	11.26	1397	25.19	1142	12.98	1244	49.66
				1114	22.81	1435	25.22	1167	12.35	1271	44.72
				1142	23.09	1466	24.66	1186	12.6	1308	44
				1167	23.37	1488	25.29	1208	12.68	1336	46.64
				1186	23.57	1517	28.43	1244	12.68	1375	45.25
				1215	23.92	1543	25.59	1336	12.69	1397	47.12
				1244	24.04	1589	25.75	1397	12.63	1435	46.98
				1271	24.46	1618	25.78	1435	12.62	1466	46.7
				1336	35.09	1640	25.84	1466	12.64	1488	49.38
				1375	34.96	1674	25.86	1543	12.68	1517	49.48
				1397	34.77	1707	28.15			1543	49.6
				1435	34.84	1720	26			1589	49.83
				1466	35.15	1737	25.84			1618	49.87
				1488	35.28	1738	25.85			1640	50.03
				1517	35.45	1765	25.8			1674	45.82
				1543	35.65					1707	45.31

Axial Load on Steel Ribs on Upstream Wall (t)											
Days	RD-14 U/S	Days	RD-70.6 U/S	Days	RD-84.5 U/S	Days	RD-113.2 U/S	Days	RD-129.4 U/S	Days	RD-154.4 U/S
				1589	36.17					1737	47.84
				1618	36.35					1765	47.76
				1640	37.55						
				1674	36.72						
				1707	36.62						
				1737	36.05						
				1765	35.97						

Table 16. Load cell readings on steel ribs on downstream side at transformer hall cavern

Axial Load on Steel Ribs on Downstream Wall (t)											
Days	RD-14 D/S	Days	RD-70.6 D/S	Days	RD-84.5 D/S	Days	RD-113.2 D/S	Days	RD-129.4 D/S	Days	RD-154.4 D/S
244	3.57	163	3.36	0	1.66	267	1.43	195	1.79	87	13.27
248	4.39	171	5.54	47	24.82	274	1.75	198	4.84	95	13.91
257	5.59	180	6.38	66	25.69	285	1.81	205	5.86	101	15.01
262	5.92	184	9.11	69	26.05	287	1.83	212	7.2	117	16.57
265	6.1	188	13.48	95	32.25	294	1.93	217	7.7	122	16.24
274	7.15	195	20.63	101	33.15	313	2	225	8.2	134	16.93
285	8.5	198	21.52	117	35.24	323	2.21	235	8.93	145	17.5
287	9.12	205	24.39	122	36.29	339	2.33	244	9.42	149	17.82
290	10.5	212	26.03	134	36.84	351	2.44	257	10.43	155	18.11
294	11.25	216	27.05	143	37.57	359	2.53	265	10.76	157	18.13
298	11.9	225	28.34	149	39.07	372	2.69	274	11	161	18.22
304	12.6	235	29.27	155	40.67	399	2.62	285	11.23	163	18.26
308	13.6	244	30.34	157	40.97	409	3.35	298	11.8	171	18.65
313	14.02	257	31.44	161	41.23	414	3.47	313	12.27	180	19.23
320	15.05	265	32.16	163	41.4	439	4.11	323	12.63	188	19.58
323	15.6	274	32.92	171	42.42	446	4.29	339	13.03	195	19.84
339	15.72	285	34.04	180	43.31	462	4.54	351	13.52	198	20.02
341	15.9	294	34.06	184	43.84	482	4.94	372	14.77	205	20.35
351	16.5	313	36.56	188	44.47	499	5.3	399	17.69	212	20.54

Axial Load on Steel Ribs on Downstream Wall (t)											
Days	RD-14 D/S	Days	RD- 70.6 D/S	Days	RD- 84.5 D/S	Days	RD- 113.2 D/S	Days	RD- 129.4 D/S	Days	RD- 154.4 D/S
359	19.8	323	37.6	195	45.5	512	5.72	425	19.99	217	20.51
370	21.2	339	40.73	198	45.85	517	5.69	439	21.44	225	20.62
374	21.58	351	43.9	205	46.41	537	5.48	446	21.96	235	20.66
381	22.51	372	39.85	212	47.11	546	5.73	462	22.92	244	20.55
399	23.65	398	34.31	217	47.24	577	14.38	482	25.54	257	20.41
414	25.68	429	36.94	225	47.87	581	14.56	499	27	265	20.04
434	27.45	451	42.96	235	48.07	586	14.89	512	27.72	274	20.68
446	28.23	462	44.91	244	48.66	587	14.38	524	28.99	285	21.1
462	28.98	482	47.23	257	48.9	592	15.92	537	29.95	294	21.63
482	30.3	499	50.84			597	15.85	546	30.38	313	22.72
499	31.07	512	52.97			610	15.57	562	31.18	323	22.72
512	32.25	524	54.56			639	16.14	577	31.92	339	22.8
586	36.9	552	38.52			670	15.96	587	32.44	351	24.89
589	36.92	564	36.58			680	15.13	589	32.49	372	24.99
610	38.04	577	32.71			684	15.85	592	32.51	398	25.19
625	38.81	583	31.16			726	16.02	597	32.61	407	25.58
639	39.11	597	30.98			761	16.56	610	32.99	414	26.43
		610	33.56			804	16.17	624	33.71	439	30.99
		625	36.58			835	17.78	639	34.18	446	31.86
		639	33.36			859	22.56	667	35.17	462	33.1
		667	30.11			927	29.97	670	35.4	496	41.74
		689	32.84			946	34.66	726	37.25	1237	62.73
		1188	39.42			972	31.52	761	38.09	1262	61.95
		1216	39.95			1209	26.11			1281	62.04
		1232	40.69			1237	27.67			1310	62.01
		1262	40.8			1262	25.55			1339	61.94
		1281	40.22			1281	25.35			1366	62.09
		1309	40.73			1310	23.54			1403	62.72
		1339	40.12			1339	24.73			1431	62.77
		1366	40.22			1366	22.46			1470	63.54
		1403	40.14			1403	22.13			1492	64.28
		1431	42.83			1431	21.63			1530	64.39
		1470	42.72			1470	24.15				

Axial Load on Steel Ribs on Downstream Wall (t)											
Days	RD-14 D/S	Days	RD-70.6 D/S	Days	RD-84.5 D/S	Days	RD-113.2 D/S	Days	RD-129.4 D/S	Days	RD-154.4 D/S
		1772	43.14			1492	27.12				
						1530	26.39				
						1561	28				
						1583	28.15				
						1612	27.65				
						1638	26.67				
						1684	26.85				
						1713	27.83				
						1735	27.42				
						1769	27.32				
						1802	28.55				
						1815	28.59				
						1832	28.78				
						1860	28.65				

Table 17. Load cell readings on rock bolts on the walls of transformer hall cavern at EL-532

Axial load on rock bolts at EL-532 (t)													
Days	RD-80, EL-532, DS	Days	RD-81, EL-532, DS	Days	RD-155, EL-532, DS	Days	RD-13, EL-532, US	Days	RD-15, EL-532, US	Days	RD-80, EL-532, US	Days	RD-155, EL-532, US
25	12.26	29	7.78	14	9.17	36	4.44	36	4.79	11	13.19	0	11.68
29	12.13	36	7.34	19	8.16	41	4.46	41	4.66	14	13.25	6	11.46
36	12.11	41	7.15	21	8.12	50	4.46	50	4.76	21	13.75	14	11.47
41	11.92	53	6.12	27	8.07	69	5.17	64	5.73	27	14.14	21	11.48
53	13.68	69	5.78	36	8.06	122	5.96	69	5.87	36	15.6	27	11.7
69	13.57	80	6.09	53	7.86	137	5.59	75	6.09	53	18.55	36	11.86
94	14.59	94	6.08	62	7.8	154	5.58	84	6.28	69	21.5	53	14.14
101	14.6	101	6.03	69	7.76	167	5.63	101	6.46	122	33.33	87	16.63
117	13.17	117	4.92	94	7.72	182	6.15	117	6.6	137	34.63		
137	13.05	137	6.02	101	8.55	201	5.78	137	6.72	154	35.12		
154	14.5	154	5.97	117	9.01	219	5.93	154	7.03	167	36.99		

Axial load on rock bolts at EL-532 (t)													
Days	RD-80, EL-532, DS	Days	RD-81, EL-532, DS	Days	RD-155, EL-532, DS	Days	RD-13, EL-532, US	Days	RD-15, EL-532, US	Days	RD-80, EL-532, US	Days	RD-155, EL-532, US
167	14.82	167	5.94	182	7.65	222	5.91	167	7.5	179	35.92		
179	13.12	179	5.52	222	9.77	236	5.89	182	7.86	207	38.85		
192	15.03	192	5.89	265	9.42	244	5.9	201	8.03	219	38.92		
206	15.04	206	5.89	864	8.71	256	5.94			236	38.9		
219	15.07	219	5.84	892	8.81	265	6.44			241	38.54		
232	15.15	232	5.91	917	8.98	280	6.23			244	37.24		
241	15.05	241	5.98	936	9.08	293	6.43			252	37.77		
247	15.05	247	5.98	964	9.38	308	6.84			265	34.27		
252	15.07	252	5.99	994	9.89	1058	12.65			284	35.47		
265	14.34	265	5.98	1021	9.58	1086	12.62			293	34.78		
280	15.09	280	5.98	1058	10.13	1110	15.35			308	29.95		
294	15.08	294	5.97	1086	10.32	1147	4.99			392	25.01		
322	15.11	322	5.98	1125	10.65	1185	5.08						
335	14.78	335	5.94	1147	10.79	1216	5.32						
357	15.66	357	6.1	1185	10.85	1267	5.42						
379	15.75	379	6.16	1216	10.89	1293	5.51						
391	15.73	391	6.21	1238	11	1340	5.62						
465	15.76	465	6.3	1267	10.97	1368	5.66						
490	15.84	490	6.29	1293	11.3	1390	5.69						
514	15.89	514	6.74	1339	11.68	1421	5.77						
539	15.94	539	6.35	1368	11.88	1457	5.83						
864	18.07	864	8.08	1390	12.05	1487	5.86						
887	18.12	887	8.16	1424	12.36	1515	5.92						
892	18.46	892	8.18	1457	12.54								
917	18.17	917	8.25	1487	12.65								
936	18.24	936	8.35	1515	12.71								

Table 18. Load cell readings on rock bolts on the walls of transformer hall cavern at EL-525

Axial Load on Rock Bolts at EL-525 (t)													
Days	RD-14, EL-525 U/S	Days	RD-60, EL-525 U/S	Days	RD-121, EL-525 U/S	Days	RD-14, EL-525 D/S	Days	RD-60, EL-525 D/S	Days	RD-113.5, EL-525 D/S	Days	RD-154, EL-525 D/S
36	7.86	12	9.39	0	0.52	286	4.75	253	5.79	0	3.62	0	1.49
47	9.28	28	9.51	12	3.62	292	5.97	255	5.81	9	3.79	14	1.99
65	8.95	48	9.8	28	3.69	301	7.96	273	10.23	21	4.06	21	2.09
78	12.72	65	13.14			311	8.28	280	11.11	37	4.24	37	2.16
93	15.74	73	13.49			336	6.95	299	11.76	29	4.69	71	4.53
112	17.12	78	13.57			379	6.73	311	12.35	74	5.06	74	4.29
130	17.63	754	23.2			410	6.77	344	12.62	87	3.02	102	6.1
133	23.63	782	23.14			434	6.75	379	13.45	92	3.66	112	6.13
147	24.01	798	23.26			459	6.7	410	13.75	112	3.83	121	6.5
155	24.28	828	23.25			502	6.74	434	14.07	121	3.87	137	6.6
167	25.89	875	23.34			523	6.72	459	14.4	152	4.07	156	6.77
176	24.56	905	23.26			547	6.67	502	16.5	156	4.16	164	6.96
191	2.09	932	23.28			578	6.61	523	17.8	161	4.19	172	7.37
204	2.27	969	23.21			615	6.63	547	19.7	172	4.42	185	6.8
219	2.58	997	23.07			667	6.65	634	15.28	185	4.49	200	6.7
274	2.44	1036	22.91			704	6.67	704	15.55	200	4.61	214	6.74
302	2.96	1058	22.93			739	6.05	830	15.9	214	4.7	242	7.04
327	2.24	1096	23.08			763	6.62	886	16.33	242	5.12	301	7.04
378	3.03	1127	22.56			791	6.64	920	16.23	255	5.53	336	7.05
425	2.79	1149	23.81			830	6.65	946	16.46	301	6.4	765	7.65
450	2.52	1178	25.92			856	6.64	978	16.43	336	6.4	812	7.95
493	2.49	1204	23.7			884	6.62	1006	16.06	379	6.39	837	7.95
789	2.85	1250	23.7			914	6.56	1045	15.85	410	6.71	856	8.13
821	2.35	1279	23.33			946	6.49	1067	15.78	434	6.98	884	9.29
847	2.54	1301	23.44					1105	15.89	459	7.22	914	10.37
875	2.09	1335	23.3					1136	16.06	502	7.44	941	11.57
905	1.65	1368	23.23					1158	15.95	521	7.54	978	12.18
937	1.49	1398	23.22					1187	16.24	547	8.07	1006	12.82
969	1.37	1426	23.22					1213	16.47			1045	12.22
997	1.46							1242	16.81				

Axial Load on Rock Bolts at EL-525 (t)													
Days	RD-14, EL-525 U/S	Days	RD-60, EL-525 U/S	Days	RD-121, EL-525 U/S	Days	RD-14, EL-525 D/S	Days	RD-60, EL-525 D/S	Days	RD-113.5, EL-525 D/S	Days	RD-154, EL-525 D/S
1036	1.43							1288	16.54				
1058	1.45							1310	16.56				
1096	1.5							1341	16.1				
1127	1.22							1377	15.81				
1149	1.06							1407	13.99				
1178	1.63							1435	12.67				
1204	1.4												
1250	1.28												
1279	1.3												
1301	1.21												
1332	1.16												
1368	1.01												
1398	1.22												
1426	1.27												

Table 19. Load cell readings on rock bolts on the walls of transformer hall cavern at EL-520

Axial Load on Rock Bolts at EL-520 (t)													
Days	RD-14, EL-520 D/S	Days	RD-58, EL-520 D/S	Days	RD-114, EL-520 D/S	Days	RD-162, EL-520 D/S	Days	RD-14, EL-520 U/S	Days	RD-58, EL-520 U/S	Days	RD-162, EL-520 U/S
214	4.28	194	7.78	5	15.28	0	6.07	128	7.71	34	11.56	2	3.55
224	2.07	196	9.57	25	13.41	11	5.54	141	10.22	40	13.37	11	4.82
236	7.11	212	10.48	34	6.79	18	5.33	196	11.19	52	11.46	18	6.66
292	6.98	224	10.94	65	5.59	25	5.36	224	11.33	77	14.61	25	7.51
323	7.25	257	11.89	74	5.56			249	12.32	89	15.06	34	15.02
347	7.63	292	13.55	80	5.62			300	12.21	98	15.31	39	12.41
372	8.32	323	13.88	85	6.16			347	13.44	113	16.23	55	17.03
415	8.41	347	16.72	158	6.1			372	13.6	126	21.61	69	19.48
436	8.52	372	14.92	168	6.11			415	13.55	141	24.15	86	22.48
460	8.59	617	17.19	214	6.72			436	13.53	298	27.84	89	22.8

Axial Load on Rock Bolts at EL-520 (t)													
Days	RD-14, EL-520 D/S	Days	RD-58, EL-520 D/S	Days	RD-114, EL-520 D/S	Days	RD-162, EL-520 D/S	Days	RD-14, EL-520 U/S	Days	RD-58, EL-520 U/S	Days	RD-162, EL-520 U/S
491	8.68	799	17.49	249	6.79			711	14.81	347	27.11	105	27.54
528	8.74	833	17.43	292	6.86			743	14.47	372	26.68	117	22.15
580	8.61	859	17.44	323	6.92			769	14.6	415	24.9	141	22.78
617	8.64	891	17.42	347	6.84			797	14.66	436	24.34	175	22.46
652	8.75	919	17.52	372	6.81			827	14.66	460	23.44	214	22.31
676	8.87	958	17.66					859	14.54			300	22.92
704	9.04	980	17.77					891	15.17			347	23.26
743	9.18	1018	17.81					919	14.91			372	23.42
769	9.21							958	14.84			415	23.41
797	9.2							980	15.03			845	24.82
827	9.12							1018	14.99			854	25.12
859	9.1							1049	14.73			891	24.72
919	8.92							1071	14.17			919	24.39
958	8.51							1100	15.02			958	24.38
								1126	14.92			980	24.2
								1172	14.4			1018	24.33
								1201	14.33			1049	24.32
								1223	12.65			1071	24.38
								1254	14.43			1100	24.99
								1290	14.51			1126	24.88
								1320	14.69			1155	25.19
								1348	14.87			1218	25.02
												1254	25.07
												1290	25.59
												1320	26.06
												1348	26.26

Table 20. Convergence observations on the walls of transformer hall cavern at EL-531 and EL-525

Cumulative Convergence of Walls of Transformer Hall at EL-531 and EL-525 (mm)									
Days	RD-60,EL-531	Days	RD-14, EL-525	Days	RD-60, EL-525	Days	RD-114, EL-525	Days	RD-155, EL-525
0	0	216	0	207	0	0	0	0	0
35	10.26	221	2.65	216	3.25	31	6.69	31	16.17
88	28.61	234	5.28	221	3.6	54	10.83	54	29.6
111	31.55	262	10.04	234	5.83	83	17.1	59	34.39
122	32.4	287	13.04	262	16.03	94	21.92	74	46.73
131	30.32	299	14.91	287	30.69	101	25.74	83	49.28
151	36.05	320	16.72	309	37.72	113	24.68	113	54.74
165	46.87	332	16.21	320	39.1	151	34.25	126	56.91
183	61.2	346	16.02	332	43.4	158	40.02	140	63.42
197	67.71	357	16.82	346	47.77	171	44.31	151	68.94
208	71.78	369	19.38	357	48.85	188	49.1	158	68.4
228	74.8	400	19.67	369	51.93	197	48.59	171	70.9
245	81.13	441	21.32	400	58.98	207	47.86	188	70.47
254	83.36	472	23.7	421	63.41	242	50.28	197	75.29
291	86.72	581	27.96	513	78.4	320	66.07	224	76.69
344	109.87	602	28.61	532	79.62	332	68.6	271	79.35
361	113.47	682	29.77	581	82.01	357	71.72	287	80.71
391	125.64	710	30.78	602	83.57	441	88.26	299	82.7
739	159.17	738	31.54	710	83.57	472	90.78	320	84.89
767	160.01	767	32.37	738	85.42	513	96.12	332	84.56
824	159.88	831	32.91	767	83.01	532	97.35	346	85.11
854	161.39			797	86.03	651	100.64	357	85.25
888	161.1					682	102.64	369	86.1
938	163.24					705	103.27	396	88.56
985	163.31					738	103.29	421	88.91
						767	102.86	441	89.74
						797	102.93	472	95.08
						831	101.87	513	95.34
						881	102.91	532	93.33
								651	95.1
								682	94.83
								705	96.32
								738	96.26
								767	96.69
								797	98.71
								831	98.19
								881	96.69

Table 21. Convergence observations on the walls of transformer hall cavern at EL-520

Cumulative Convergence of Walls of Transformer Hall Cavern at EL-520 (mm)							
Days	RD-14, EL-520	Days	RD-60, EL-520	Days	RD-121, EL-520	Days	RD-155, EL-520
129	0	129	0	0	0	0	0
141	3.37	141	4.61	13	4.35	13	2.38
151	2.17	151	4.61	30	5.24	30	4.39
162	3.82	162	4.61	39	6.9	39	9.53
174	2.99	174	7.94	49	6.39	49	12.51
188	4.22	188	11.9	63	8.24	63	12.7
199	4.56	199	14.66	76	16.65	76	12.93
211	5.43	211	19.02	84	21.7	113	14.7
242	6.47	242	22.16	113	39.38	129	18.9
263	6.97	263	30.51	129	46.88	141	22.19
283	8.71	283	34.5	141	48.6	162	24.61
314	11.36	314	40.04	162	51.57	174	24.21
355	13.89	355	45.56	174	55	188	25.29
374	15.7	374	48.19	188	57.52	199	26.42
423	15.41	423	49.33	199	61.14	211	26.86
444	16.09	444	49.66	211	65.04	238	29.51
524	17.56	673	55.05	242	70.74	263	32.53
643	18.63	753	55.72	263	73.64	283	32.99
673	18.34			283	77.66	314	38.45
723	18.83			314	82.8	355	39.33
753	19.35			355	82.01		

APPENDIX-4

Table 22. Load cell readings on steel ribs in bus ducts and passage-1

Axial Load on Steel Ribs (t)															
Days	BD-1- Rib- LS	Days	BD-1- Rib- RS	Days	BD-2- Rib- LS	Days	BD-2- Rib- RS	Days	BD-3- Rib- LS	Days	BD-3- Rib- RS	Days	PS-1- Rib-LS	Days	PS-1- Rib- RS
1	7.45	0	6.27	33	2.22	33	3.13	257	3.72	257	0.76	174	1.82	174	1.35
3	7.76	1	6.07	51	6.3	51	12.48	261	3.84	261	0.65	176	2.1	176	1.74
5	7.25	3	3.91	463	47.56	463	30.28	265	7.96	265	1.04	180	2.99	180	5.83
7	7.84	5	3.34	466	48.66	467	30.81	267	7.96	267	1.81	183	10.52	183	9.66
10	10.51	7	3.74	472	49.24	472	28.29	276	8.41	276	0.34	188	13.25	209	15.76
19	30.35	11	4.13	482	42.55	482	30.91	295	8.32	295	1.5	199	22.1	216	23.61
20	32.19	19	5.22	505	44.99	505	34.29	302	8.42	302	2.48	209	33.65	233	26.72
21	34.03	20	5.3	527	46.19	527	35.77	320	8.03	320	1.5	216	38.04	244	30.31
23	38.57	21	5.34	562	48.62	562	37.52	363	9.34	363	1.63	265	43.31	265	33.57
26	44.33	23	5.56	599	48.76	599	40.44	418	9.69	373	1.76	288	61.49	288	40.79
28	47.36	26	5.76	651	49.23	651	41.64	486	11.14	418	2.1	309	68.2	309	48.25
31	52.05	28	5.98	678	49.67	678	42.1	507	11.33	443	2.56	320	71.84	320	51.05
34	55.85	31	6.42	723	52.56	723	43.28	562	11.68	482	1.39	363	65.28	363	58.59
36	61.96	34	6.67	747	54.13	747	43.83	599	12.32	486	1.34	384	64.57	384	58.56
39	66.12	36	6.32	775	54.63	775	44.36	651	12.89	507	1.29	394	66.58	394	59.71
40	66.8	39	7.01	814	55.25	814	44.24	678	13.1	527	1.52	411	65.09	411	58.74
43	71.21	43	5.73	840	55.57	840	44.54	723	13.35	562	2.84	428	67.85	423	57.23
54	80.17	54	7.64	868	55.84	868	45	747	13.52	599	2.81	450	69.34	450	58.82
73	94.28	73	9.05	898	55.91	898	45.26	775	13.61	651	3.27	482	72.03	482	60.82
117	76.45	117	6.11	925	56.04	925	45.61	792	13.94	678	3.36	507	72	507	61.94
146	73.42	146	4.36	957	56.32	957	45.68	840	13.89	723	3.45	538	74.02	538	64.12
467	69.1	467	5.79	989	56.97	990	46.7	868	14.24	747	3.49	562	75.46	562	65.21
482	65.63	482	7.43	1021	57.35	1029	45.69	898	14.43	775	3.51	599	74.27	599	66.67
507	68.24	507	8.07	1051	57.35	1051	45.36	925	14.59	792	4.01	678	74.05	651	67.47
527	70.42	527	8.46	1089	57.68	1089	45.74	957	14.58	840	3.44	723	82.56	678	67.74
562	74.08	562	12	1104	57.72	1104	47.2	990	14.67	868	3.51	747	88.92	723	68.56
599	75.3	599	8.41	1120	57.95	1120	46.74	1021	14.51	898	3.43	775	89.73	747	69.49
651	75.12	651	6.53	1147	58.03	1147	46.57	1051	14.48	925	3.4	814	90.66	775	70.27
678	74.57	678	6.34	1171	58.23	1171	47.01	1089	14.67	957	3.41	840	91.5	814	71.15
723	75.51	723	6.53	1197	58.48	1197	47.33	1104	14.6	990	2.85	868	92.74	840	71.92
747	76.43	747	6.71	1225	58.73	1225	47.74	1142	14.92	1021	2.82	898	92.38	868	72.92
775	77.84	775	6.94	1243	58.95	1243	47.98	1171	15.37	1051	2.71	930	93.09	898	73.29
814	78.64	814	6.98	1271	59.02	1271	48.05	1197	15.62	1140	6.96	957	93.82	930	73.78
840	79.11	840	7.1	1296	59.14	1296	48.32	1243	16.14	1142	7.03	962	93.37	957	73.97
868	79.79	868	7.12	1325	59.09	1325	48.15	1271	16.09	1171	7.38	990	93.03	962	74.18
898	79.68	898	6.84	1361	58.97	1361	47.67	1294	16.35	1197	7.43	1021	92.73	990	73.98

Axial Load on Steel Ribs (t)															
Days	BD-1-Rib-LS	Days	BD-1-Rib-RS	Days	BD-2-Rib-LS	Days	BD-2-Rib-RS	Days	BD-3-Rib-LS	Days	BD-3-Rib-RS	Days	PS-1-Rib-LS	Days	PS-1-Rib-RS
925	79.84	925	6.85	1391	59.1	1391	46.83	1325	16.34	1243	7.54	1051	104.45	1021	73.58
957	80.87	957	6.38	1419	59.24	1419	46.55	1361	16.26	1271	7.54	1089	105.36	1051	72.25
990	82.18	990	7.24					1391	16.29	1294	7.66	1104	111.14	1089	73.33
1021	79.17	1021	7.11					1419	16.49	1325	7.55	1142	104.45	1104	73.38
1051	77.81	1051	6.9							1361	7.46	1171	106.82	1142	74.17
1089	78.17	1089	6.89							1391	7.31	1197	107.39	1171	74.6
1104	78.29	1104	7.03							1419	7.49	1243	107.81	1197	75.47
1120	78.72	1120	7.18									1271	108.68	1243	75.85
1147	78.97	1147	7.36									1294	110.31	1271	76.77
1171	79.25	1171	7.46									1325	109.89	1317	76.81
1197	79.94	1197	7.41									1361	109.07	1325	76.73
1243	81.08	1243	7.03									1391	111.28	1391	74.85
1271	81.47	1271	6.5									1419	110.45	1419	75.37
1296	81.55	1296	6.91												
1325	81.32	1325	6.98												
1361	80.23	1361	6.76												
1391	79.68	1391	6.52												
1419	78.99	1419	6.27												

Table 23. Load cell readings on rock bolts in bus ducts

Axial load on Rock Bolts (t)										
Days	BD-1-LS	Days	BD-2-RS	Days	BD-2-LS	Days	BD-2-CR	Days	BD-3-Cr	
8	12.2	0	0.68	0	6.06	0	0.92	248	6.2	
11	10.55	6	1.11	6	6.38	22	0.24	274	5.3	
15	19.87	23	1.13	23	7.93	23	0.13	292	5.13	
26	18.23	435	2.1	444	21.45	454	1.32	335	4.19	
45	23.44	444	2.3	454	22.38	477	1.25	345	3.98	
58	22.82	454	2.28			499	1.41	366	3.65	
88	32.42	477	2.05			534	1.72	390	3.33	
464	36.06	499	1.92			571	2.11	415	3.12	
478	36.71	534	1.96			623	2.34	458	2.51	
499	35.54	571	2.24			650	2.57	479	2.48	
534	35.7	623	2.09			695	2.75	499	2.46	
571	35.35	650	2.06			719	3.09	534	2.42	
623	33.28	695	1.96			747	3.22	571	2.5	
650	35.48	719	1.96			786	3.34	623	2.53	
695	34.36	747	2.07			812	3.85	650	2.57	
719	35.39	786	1.74			840	4.01	695	1.63	
747	33.01	812	1.99			870	4.19	719	1.69	

Axial load on Rock Bolts (t)									
Days	BD-1-LS	Days	BD-2-RS	Days	BD-2-LS	Days	BD-2-CR	Days	BD-3-Cr
754	34.65	840	1.97			897	4.54	747	1.72
786	35.47	870	1.92					764	1.6
812	35.14	897	1.85					812	1.83
840	34.54	929	1.81					840	1.91
870	34.94	962	1.83					870	2.01
897	35.42	1001	1.8					897	2.31
928	35.45	1023	1.82					929	2.54
962	34.89	1061	1.74					962	3.07
993	34.74	1076	1.47					993	3.48
1023	34.77	1119	1.73					1023	3.9
1061	35.99	1143	1.69						
1076	36.08	1169	1.68						
1092	36.12	1197	1.66						
1119	36.23	1215	1.57						
1143	36.47	1243	1.52						
1169	36.49	1268	1.33						
1215	36.58	1297	1.48						
1243	36.64	1333	1.43						
1268	36.69	1363	1.39						
1297	36.75	1391	1.4						
1333	36.75								
1363	34.75								
1391	34.69								

Table 24. Load cell readings on steel ribs in pressure shaft manifolds

Axial Load on Steel Ribs (t)							
Days	PS-MF-1-Rib-LS	Days	PS-MF-1-Rib-RS	Days	PS-MF-4-Rib-LS	Days	PS-MF-4-Rib-RS
100	2.15	100	0.86	0	5.02	0	9.55
103	3.04	103	2.16	2	10.43	2	12.65
104	3.1	104	2.18	5	10.7	5	12.2
110	3.2	110	2.48	7	9.84	7	11.83
115	3.1	115	2.6	11	9.73	11	12.13
129	4.23	129	3.43	16	9.66	16	12.29
132	3.5	132	3.41	22	10.2	22	12.43
147	3.73	138	4.63	27	10.41	27	12.55
170	4.16	147	4.83	31	10.51	31	12.67
178	4.14	170	8.81	40	11.44	40	13.02
183	4.24	183	12.98	52	13.75	52	13.89
199	4.23	199	14.09	58	12.8	58	14.11

Axial Load on Steel Ribs (t)							
Days	PS-MF-1-Rib-LS	Days	PS-MF-1-Rib-RS	Days	PS-MF-4-Rib-LS	Days	PS-MF-4-Rib-RS
208	4.52	208	16.51	76	12.94	76	15.71
236	4.58	289	17.62	87	13.65	87	16.31
268	4.62	306	18.28	104	15.91	104	17.29
282	4.67	323	18.58	115	16.03	115	17.06
306	4.83	343	19.34	129	16.85	129	17.36
323	4.61	357	19.75	147	21.57	147	16.16
343	4.59	380	20.92	175	24.62	175	18.4
357	4.58	402	21.18	183	25.55	183	18.76
380	4.7	419	21.68	199	26.65	199	19.31
402	4.61	433	21.98	208	27.2	208	21.26
419	4.44	479	22.29	228	30.93	228	20.13
433	4.5	520	23.23	236	31.61	236	20.28
479	3.51	555	23.33	282	32.51	520	24.11
520	3.94	594	23.89	306	32.8	550	24.54
555	4.45	634	24.19	323	32.46	594	25.09
594	4.06	653	24.21	357	32.46	620	25.58
634	3.16	685	25.46	380	32.67	653	26.27
653	4.74	711	25.72	398	32.33	685	25.54
685	4.87	738	26.93	419	32.38	711	25.57
711	5.06	767	26.28	433	32.32	738	25.57
738	5.06	801	25.95	479	32.84	767	25.59
767	5.45	833	23.73	520	33.02	801	25.81
801	5.5	847	24.84	538	33.09	833	23.67
833	5.58	861	25.36	550	33.19	969	19.99
847	5.62	892	24.24	594	33.61	1018	18.83
861	5.61	959	25.46	620	33.52	1042	19.46
892	5.82	975	25.28	653	32.83	1069	19.24
959	5.65	1004	24.5	685	31.54	1096	19.23
975	5.85	1018	24.64	711	29.57	1114	19.4
1004	5.89	1042	24.88	738	32.69	1126	18.89
1018	5.85	1069	24.1	767	32.58	1143	16.4
1042	5.86	1096	24.62	801	33.04	1165	16.22
1069	4.97	1114	24.52			1199	15.99
1096	5.93	1129	24.54			1216	15.78
1114	5.94	1143	21.78			1232	15.65
1129	5.97	1167	21.54			1241	15.5
1143	5.98	1199	21.73			1262	15.5
1167	5.91	1216	22.23			1276	15.33
1199	5.88	1232	21.83			1289	14.98
1216	5.9	1245	21.73				
1232	5.87	1262	20.28				

Axial Load on Steel Ribs (t)							
Days	PS-MF-1-Rib-LS	Days	PS-MF-1-Rib-RS	Days	PS-MF-4-Rib-LS	Days	PS-MF-4-Rib-RS
1245	5.87	1263	20.16				
1262	5.96	1276	20.27				
1276	5.91	1289	19.81				
1289	6.01						

Table 25. Load cell readings on rock bolts in pressure shaft manifolds

Axial load on Rock Bolts (t)					
Days	PS-MF-3-CR	Days	PS-MF-5-CR	Days	PS-MF-6-CR
0	4.59	0	3.51	39	17.14
5	4.34	4	20.71	40	16.97
6	3.98	5	20.93	42	16.26
7	4.37	6	20.56	44	16.42
10	4.6	7	21.1	46	16.64
12	3.44	8	20.32	53	17.09
18	3.81	10	20.41	65	16.93
20	3.78	12	20.42	74	17.44
24	3.92	15	19.56	81	17.16
29	4.15	18	19.7	100	17.43
35	4.32	20	19.54	103	17.06
40	4.52	24	19.99	117	17.61
44	4.6	29	20.13	128	16.97
53	5.14	35	20.64	133	17.47
65	5.49	39	20.24	142	17.61
71	5.55	40	20.71	160	17.63
		44	19.07	169	17.63
		53	20.62	196	17.39
		65	20.27	212	17.51
		81	20.64	221	17.94
		100	20.71	247	18.59
		128	21.13	281	18.15
		133	21.03	336	17.88
		151	20.94	370	17.66
		160	21.11	411	17.36
		162	21.13	432	17.22
		249	20.8	435	17.19
		282	20.71	533	17.05
		295	20.38	648	16.89
		319	20.65	680	16.71

Axial load on Rock Bolts (t)					
Days	PS-MF-3-CR	Days	PS-MF-5-CR	Days	PS-MF-6-CR
		336	20.35	724	17.08
		607	20.14	809	16.27
		648	20.23	846	16.1
		680	20.37	905	18.1
		724	20.53	988	17.52
		780	20.53	1031	15.91
		809	19.72	1055	15.25
		846	20.98	1086	14.8
		905	21.45	1109	14.37
		988	22.46	1127	14.73
		1017	20.54	1139	15.01
		1031	19.84	1142	12.76
		1055	20.16	1156	13.91
		1086	20.33	1178	13.24
		1109	20.34	1212	13.43
		1127	20.43	1229	14.85
		1139	20.48	1245	14.74
		1156	20.54	1275	12.48
		1178	20.25	1276	12.83
		1245	20.54	1289	14.82
		1289	20.58	1302	14.96
		1302	20.6		

APPENDIX-5

DISPLACEMENTS AROUND THE CAVERNS

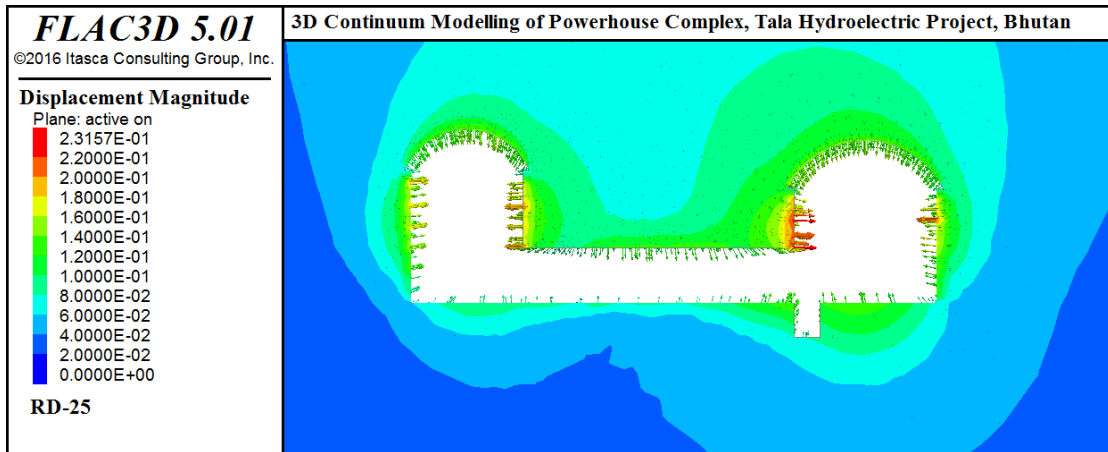


Fig. 1 Displacement contours at RD-25, powerhouse cavern

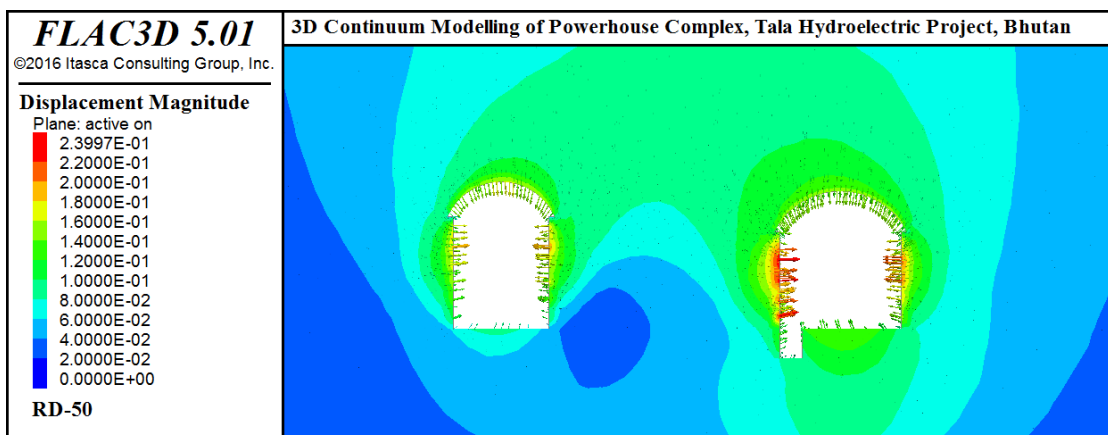


Fig. 2 Displacement contours at RD-50, powerhouse cavern

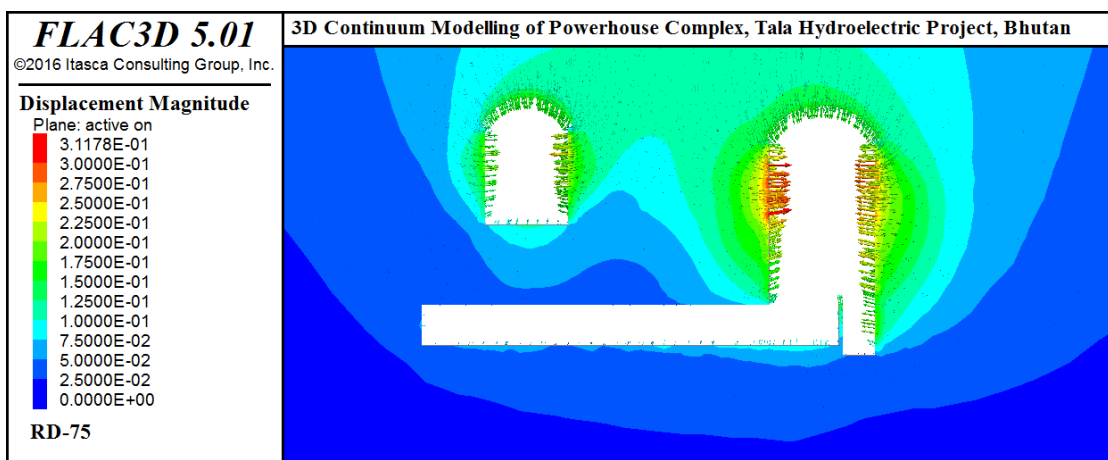


Fig. 3 Displacement contours at RD-75, powerhouse cavern

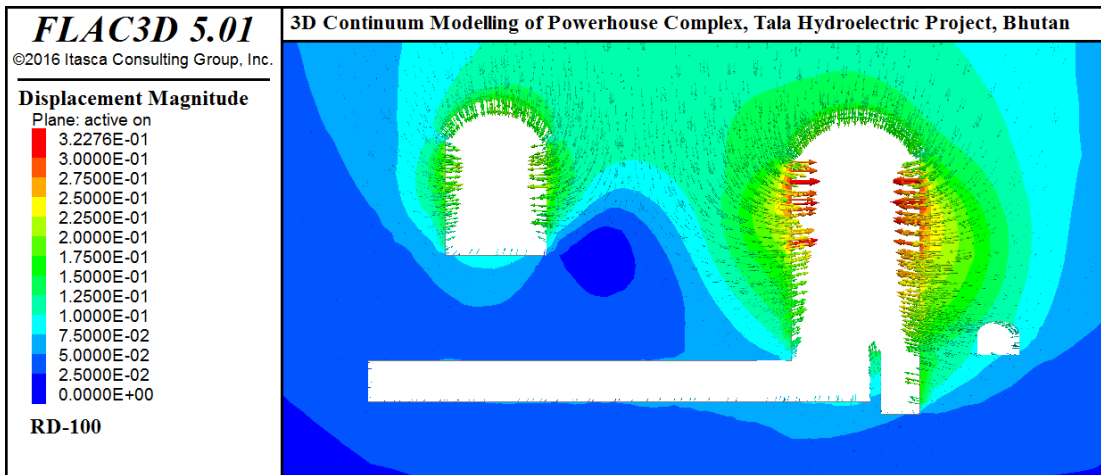


Fig. 4 Displacement contours at RD-100, powerhouse cavern

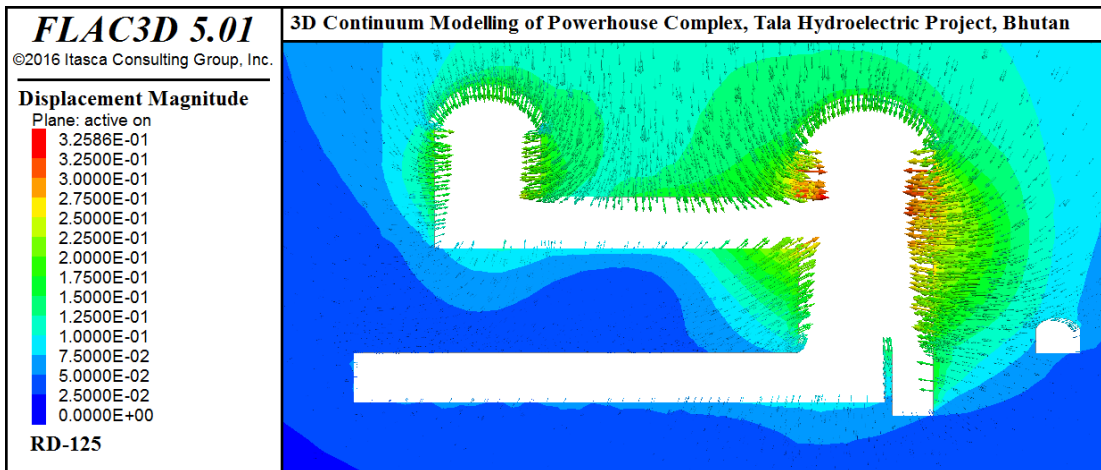


Fig. 5 Displacement contours at RD-125, powerhouse cavern

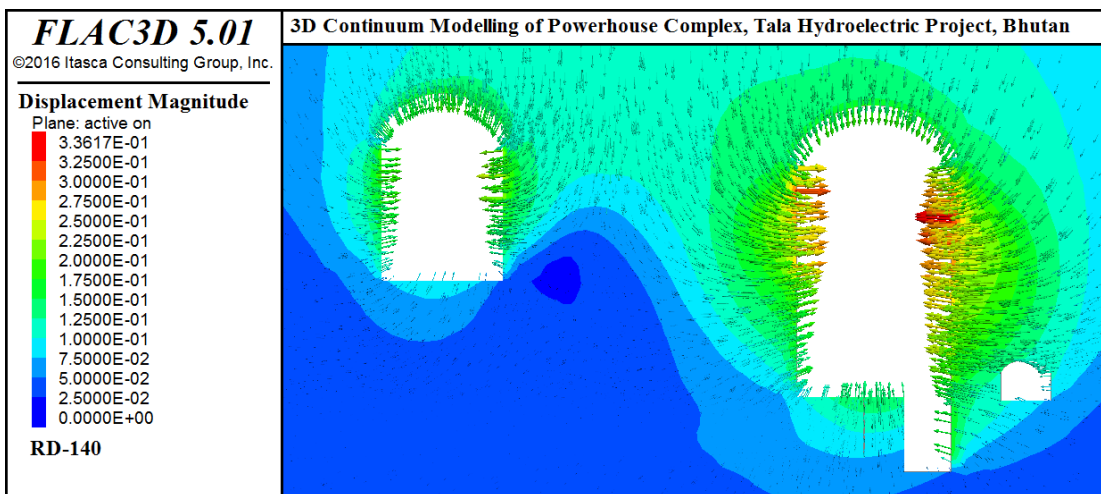


Fig. 6 Displacement contours at RD-140, powerhouse cavern

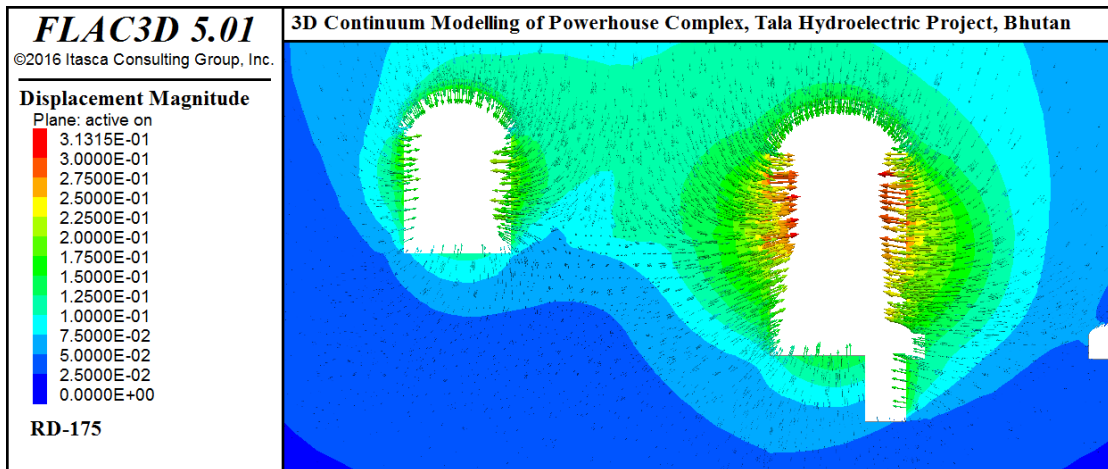


Fig. 7 Displacement contours at RD-175, powerhouse cavern

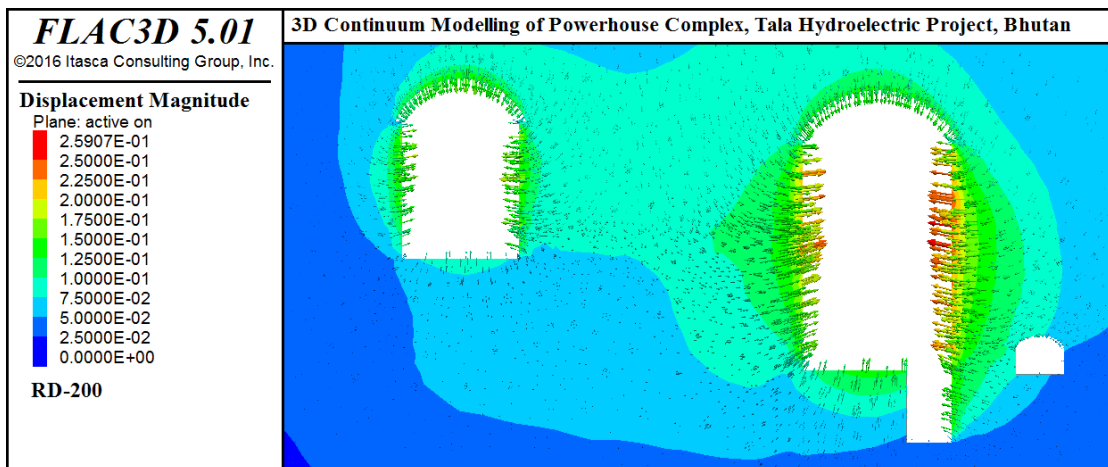


Fig. 8 Displacement contours at RD-200, powerhouse cavern

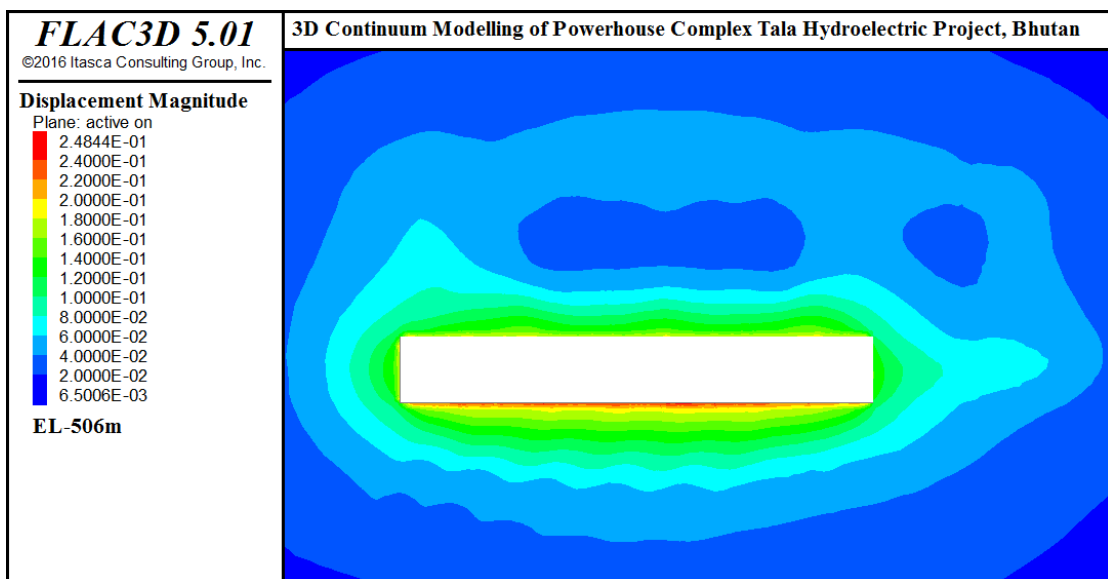


Fig. 9 Displacement contours at EL-506, powerhouse cavern

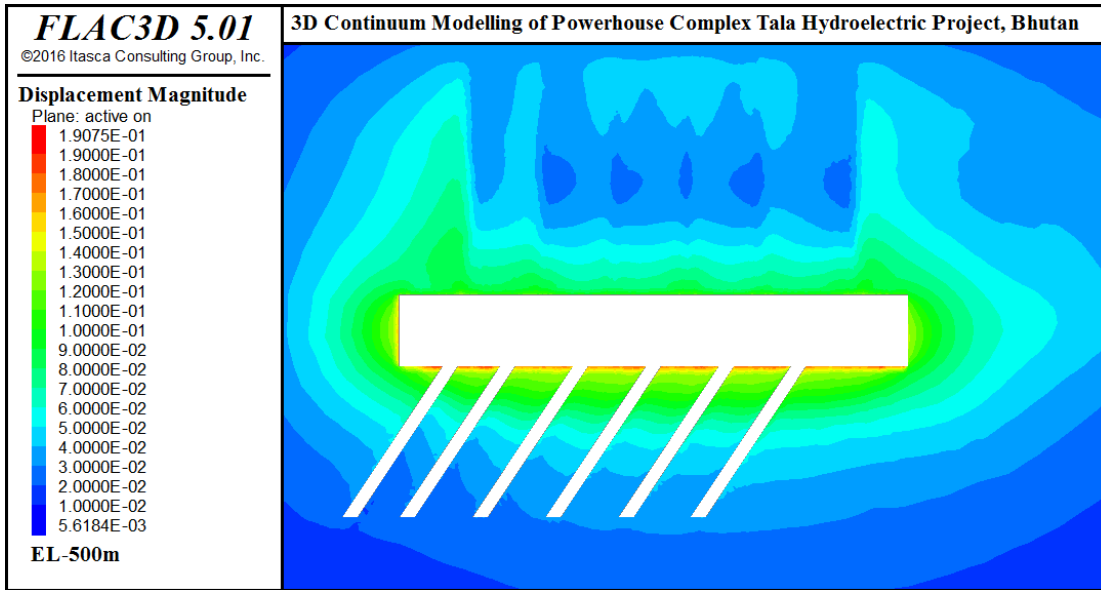


Fig. 10 Displacement contours at EL-500, powerhouse cavern

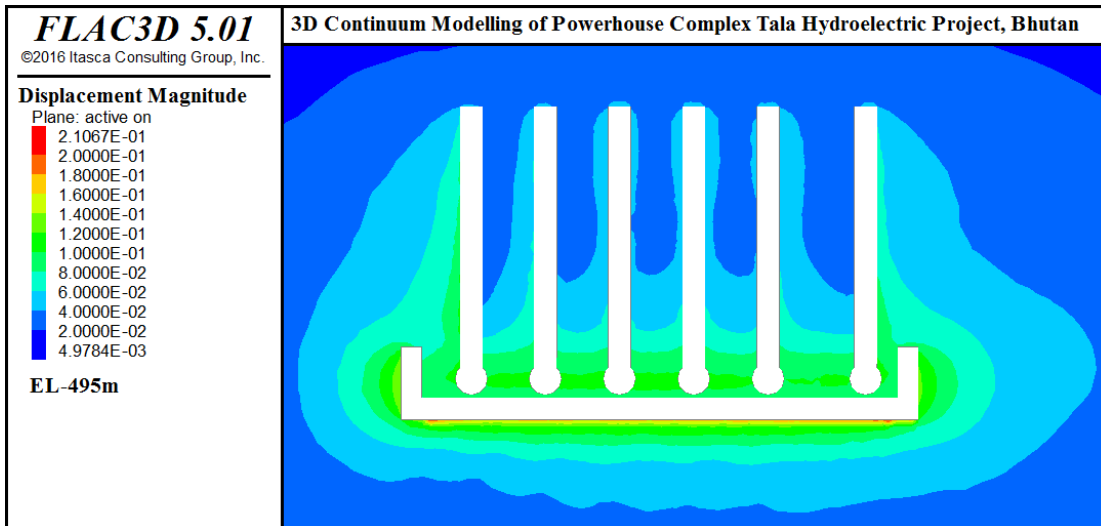


Fig. 11 Displacement contours at EL-495, powerhouse cavern

PRINCIPAL STRESS DISTRIBUTION AROUND CAVERN

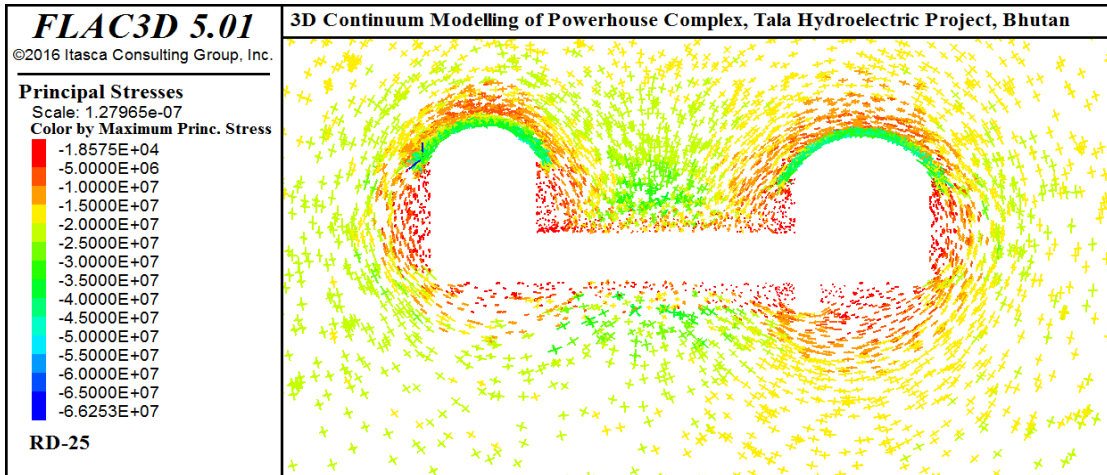


Fig. 12 Principal stress distribution at RD-25, powerhouse cavern

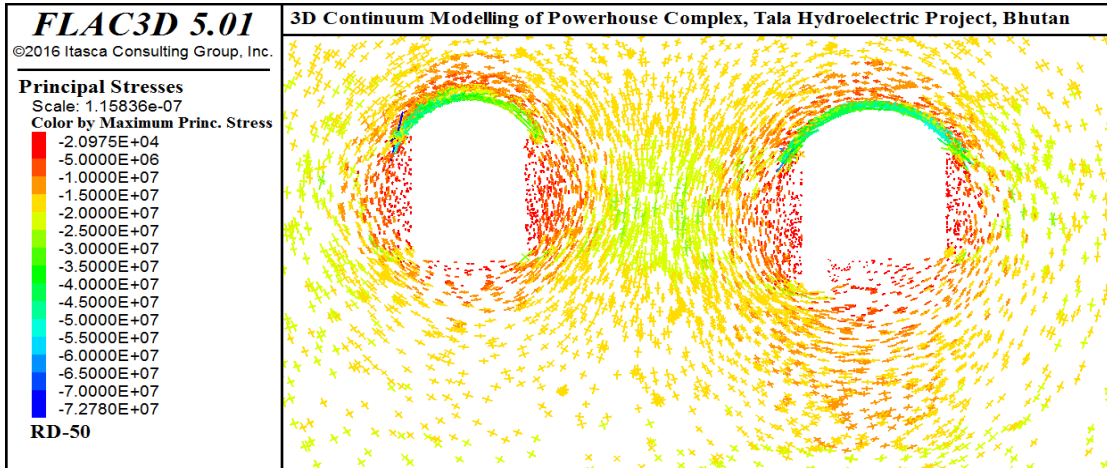


Fig. 13 Principal stress distribution at RD-50, powerhouse cavern

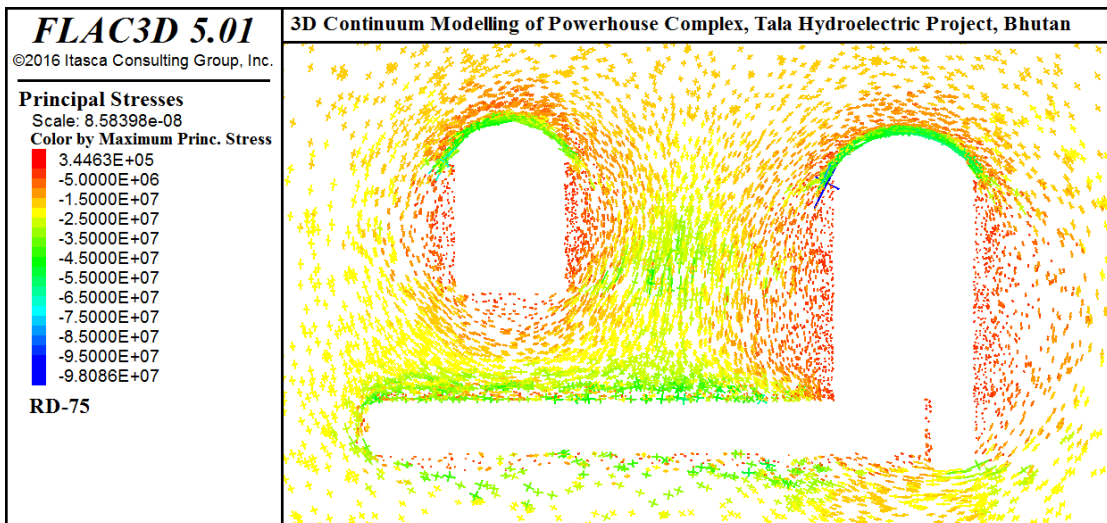


Fig. 14 Principal stress distribution at RD-75, powerhouse cavern

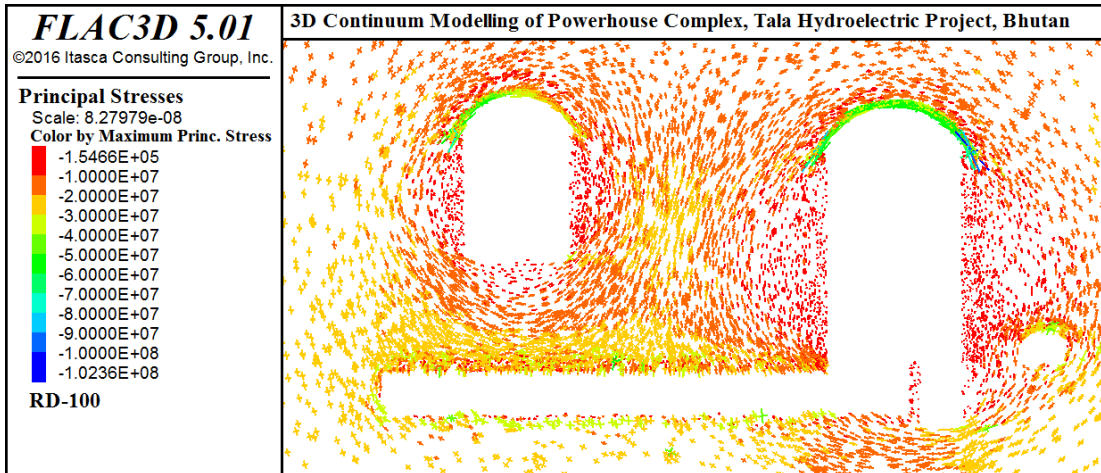


Fig. 15 Principal stress distribution at RD-100, powerhouse cavern

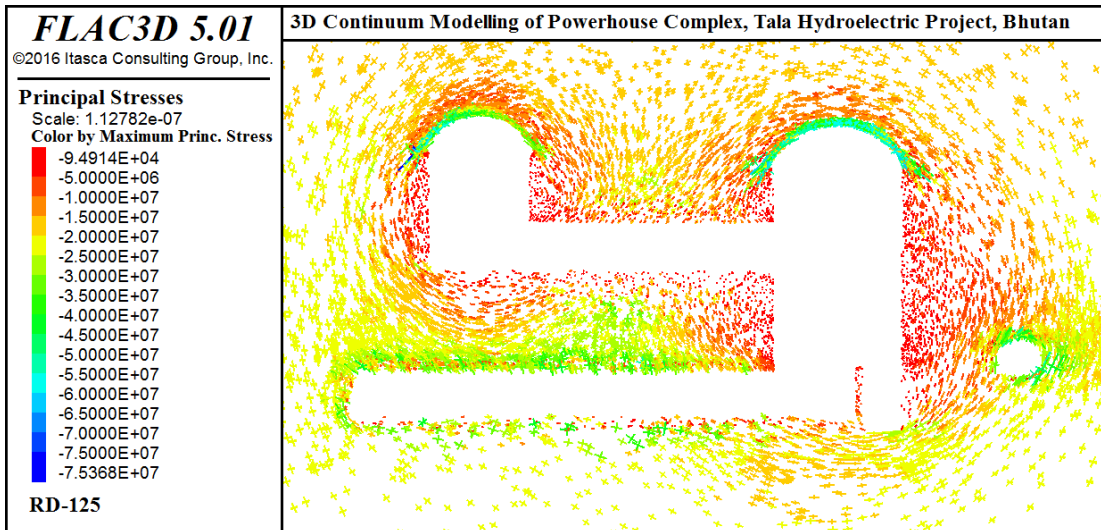


Fig. 16 Principal stress distribution at RD-125, powerhouse cavern

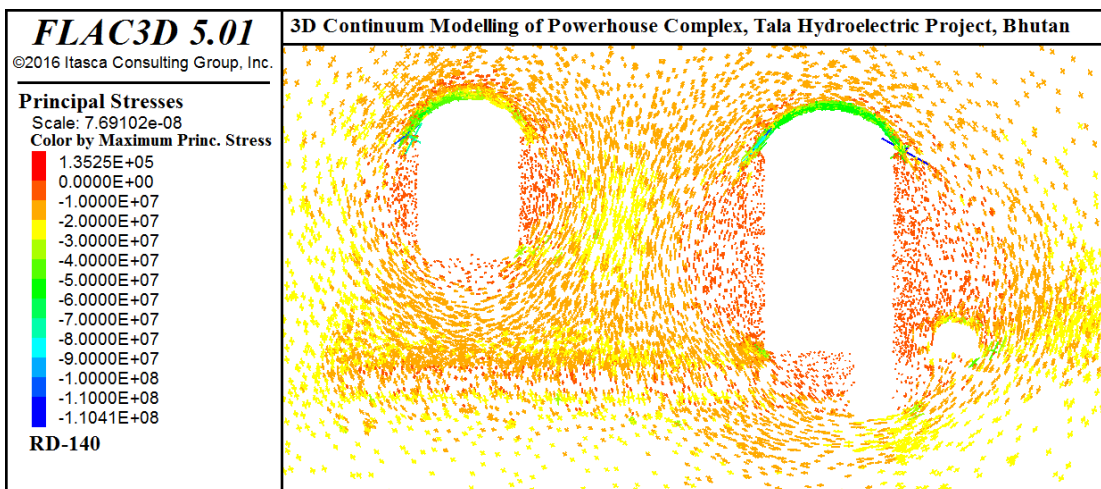


Fig. 17 Principal stress distribution at RD-140, powerhouse cavern

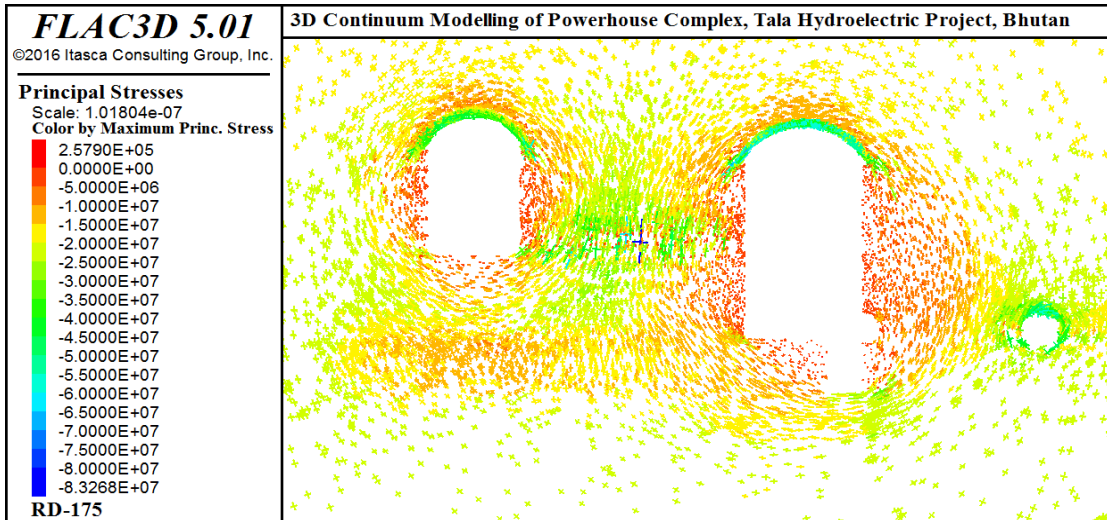


Fig. 18 Principal stress distribution at RD-175, powerhouse cavern

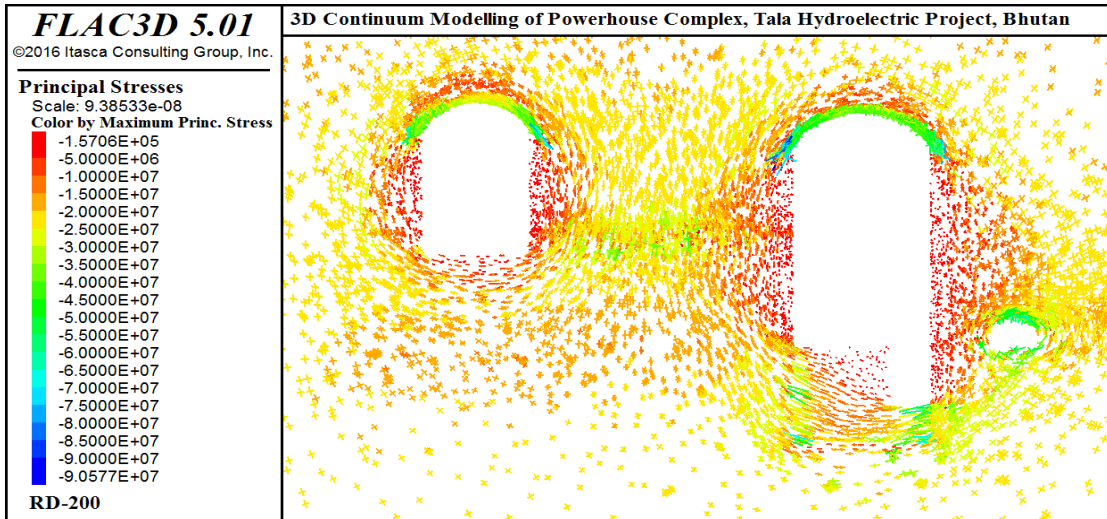


Fig. 19 Principal stress distribution at RD-200, powerhouse cavern

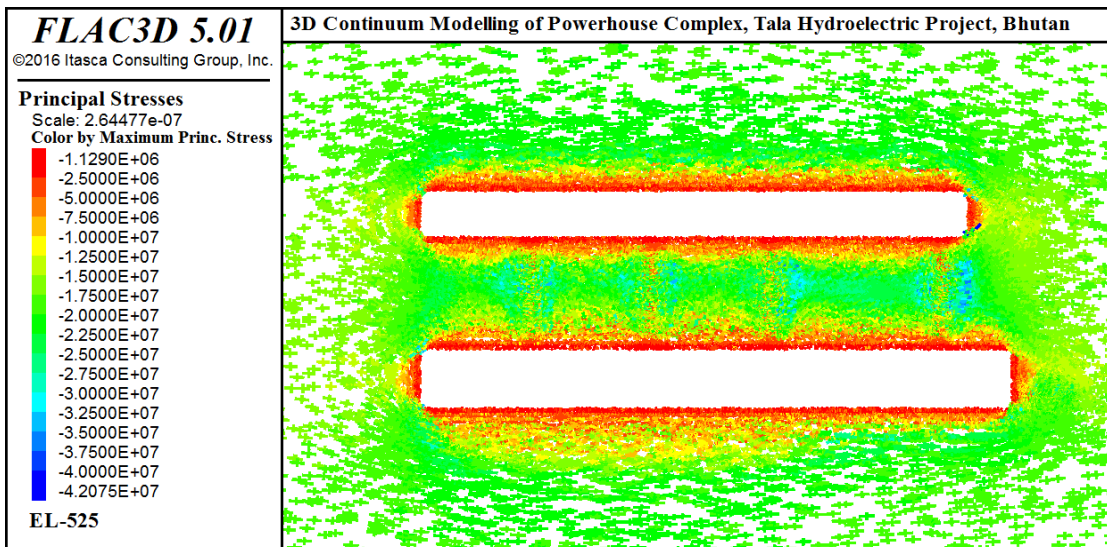


Fig. 20 Principal stress distribution at EL-525, powerhouse cavern

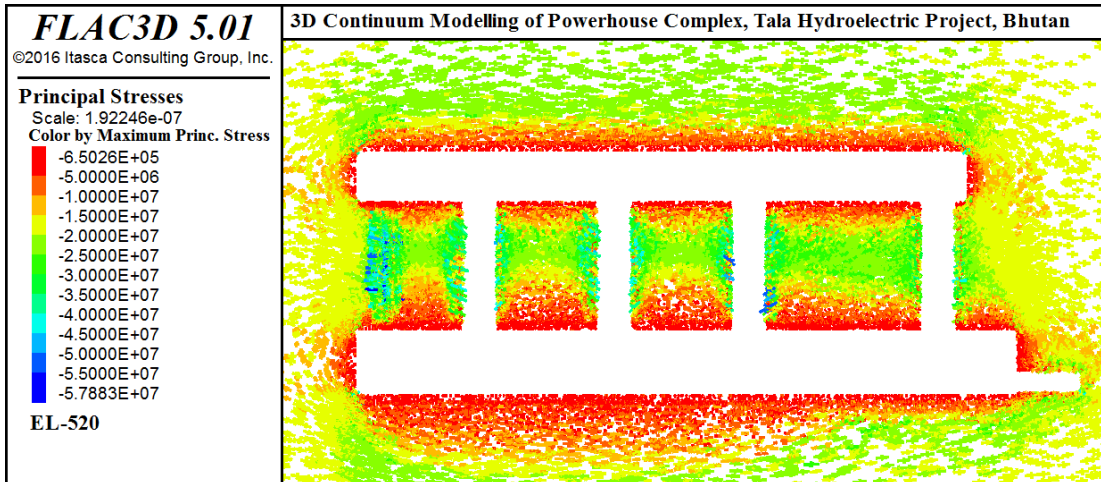


Fig. 21 Principal stress distribution at EL-520, powerhouse cavern

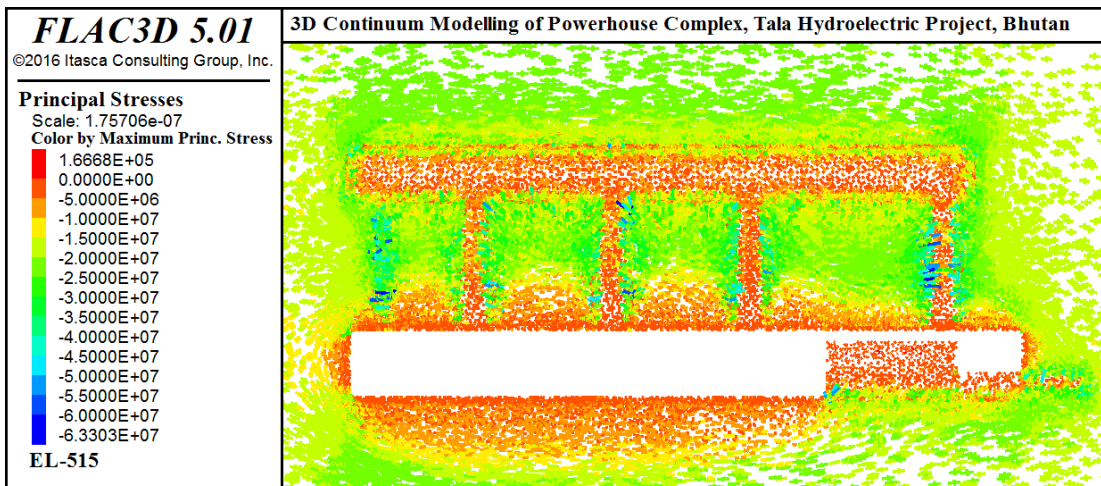


Fig. 22 Principal stress distribution at EL-515, powerhouse cavern

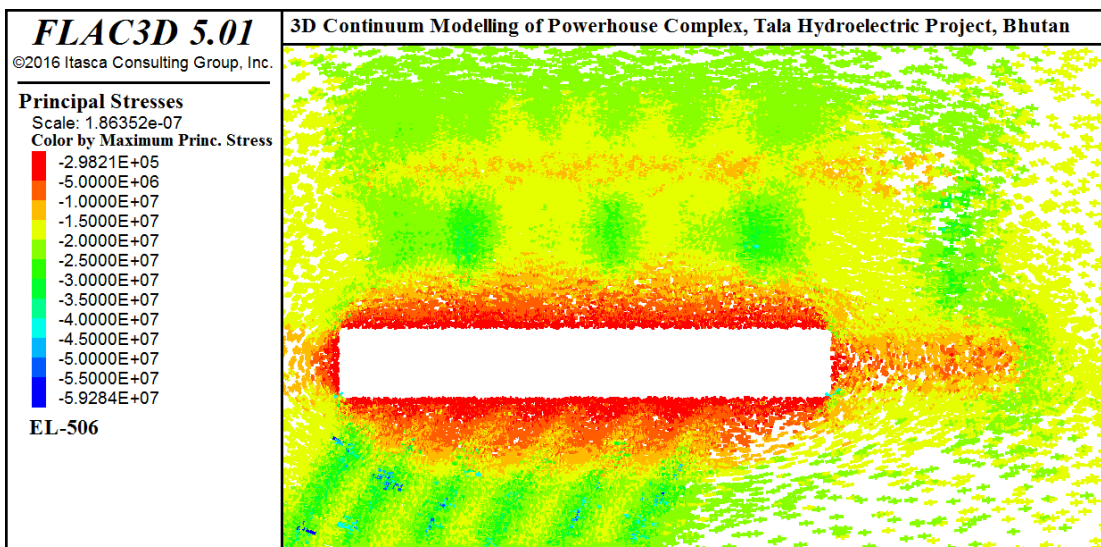


Fig. 23 Principal stress distribution at EL-506, powerhouse cavern

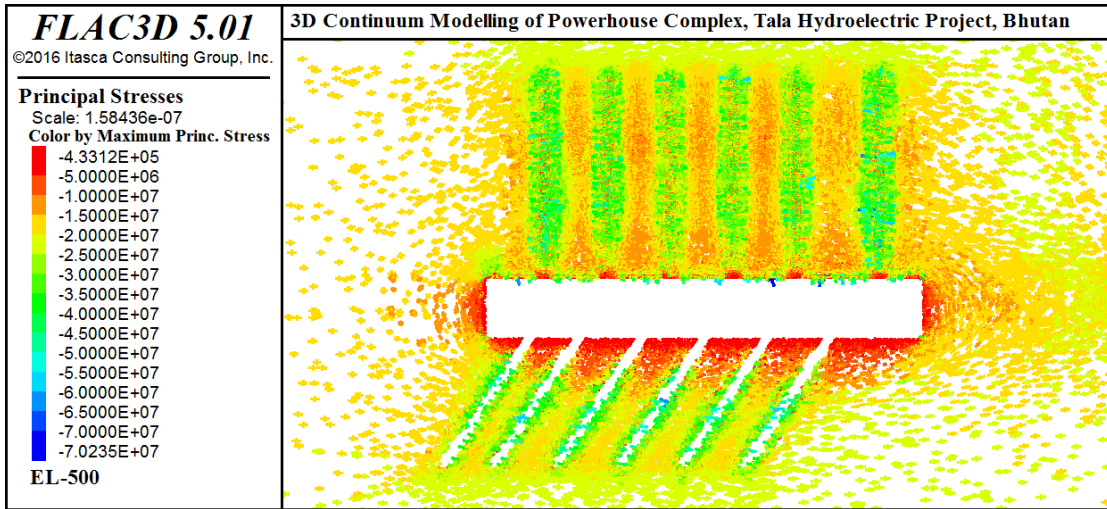


Fig. 24 Principal stress distribution at EL-500, powerhouse cavern

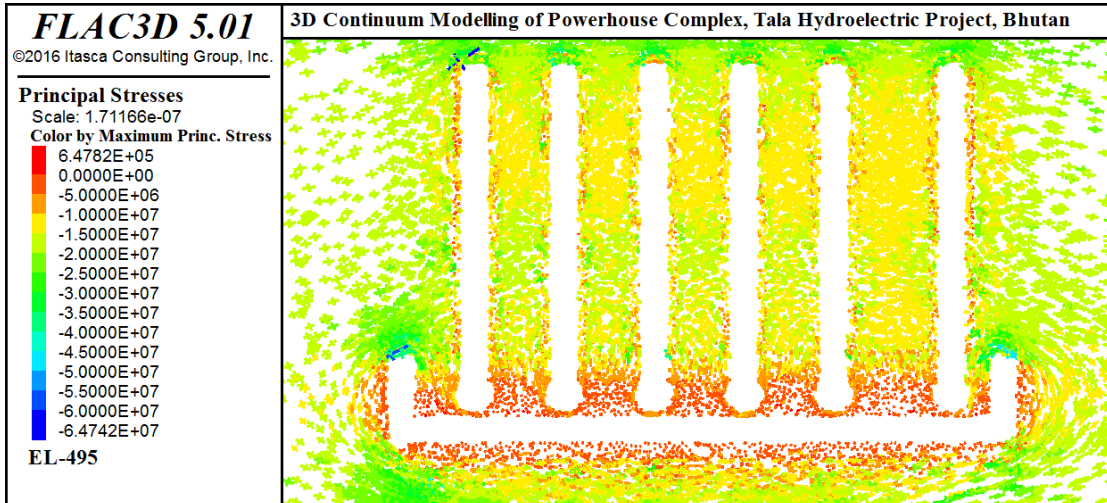


Fig. 25 Principal stress distribution at EL-495, powerhouse cavern

STRENGTH TO STRESS RATIO AROUND THE CAVERNS

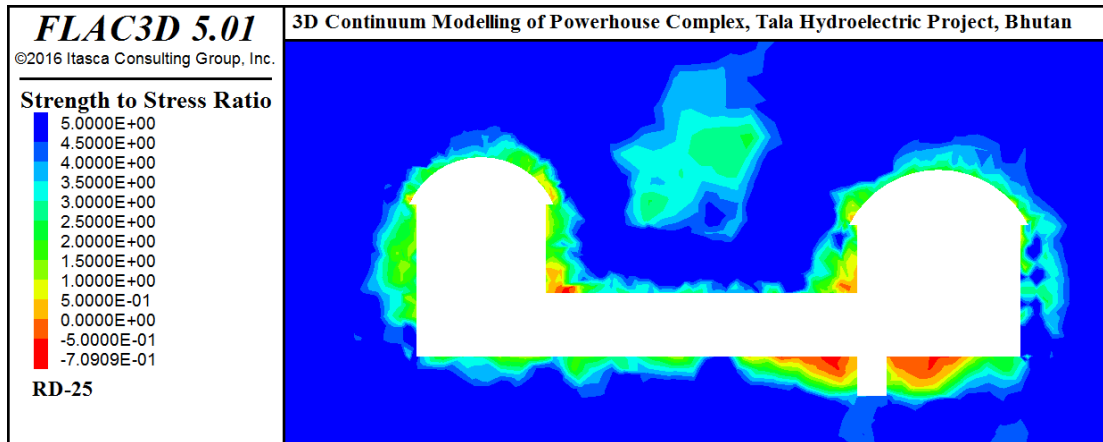


Fig. 26 Strength to stress ratio distribution at RD-25, powerhouse cavern

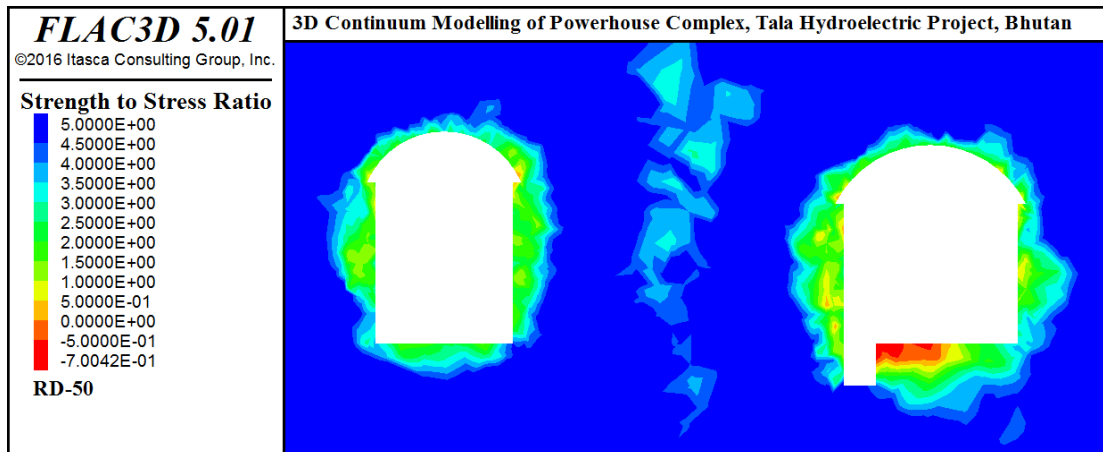


Fig. 27 Strength to stress ratio distribution at RD-50, powerhouse cavern

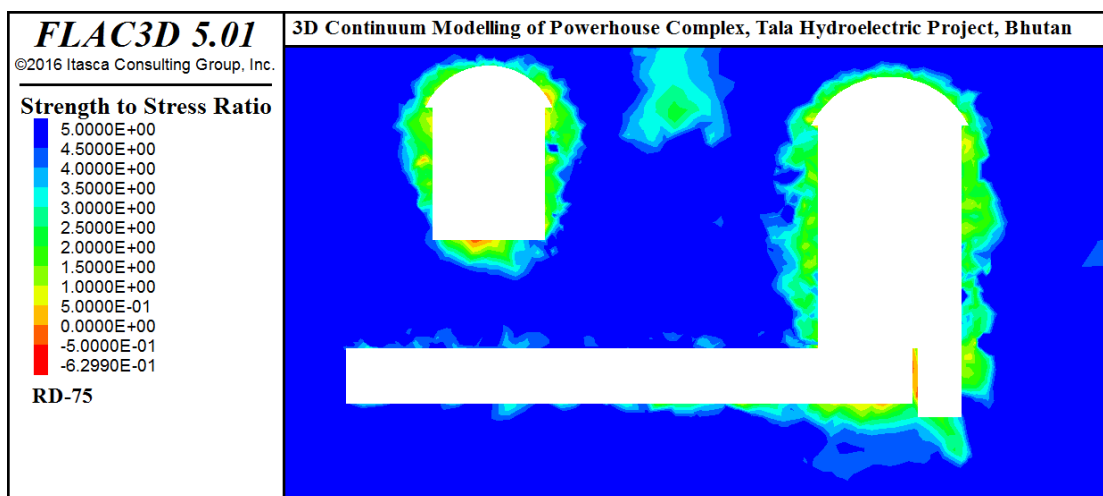


Fig. 28 Strength to stress ratio distribution at RD-75, powerhouse cavern

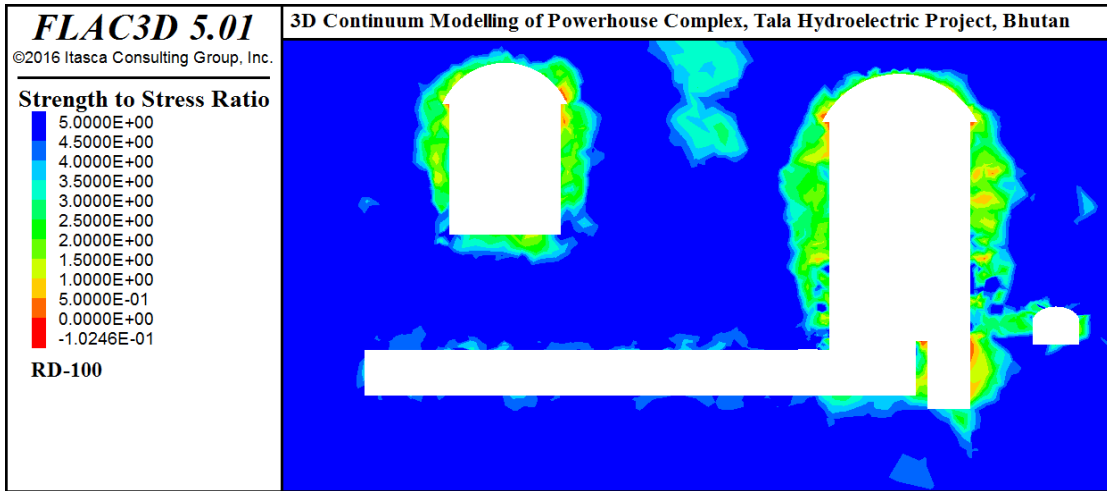


Fig. 29 Strength to stress ratio distribution at RD-100, powerhouse cavern

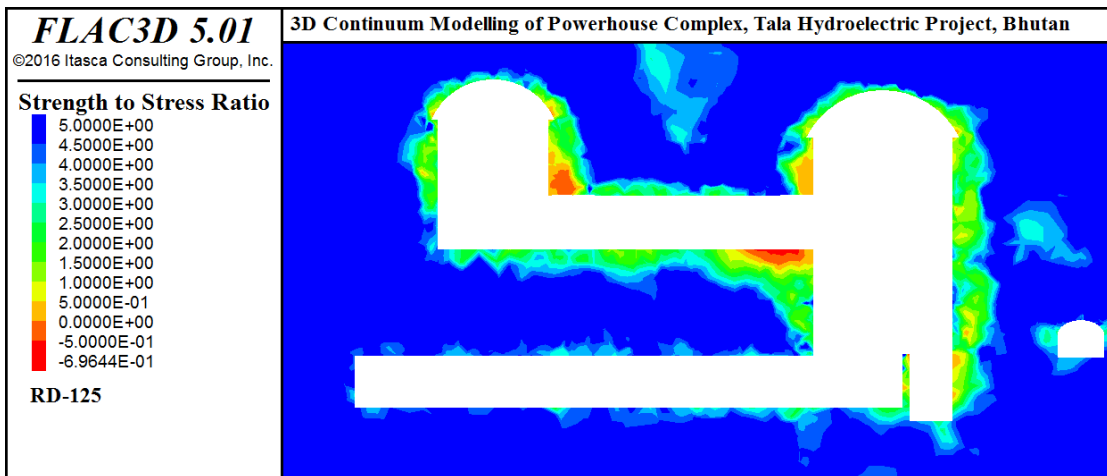


Fig. 30 Strength to stress ratio distribution at RD-125, powerhouse cavern

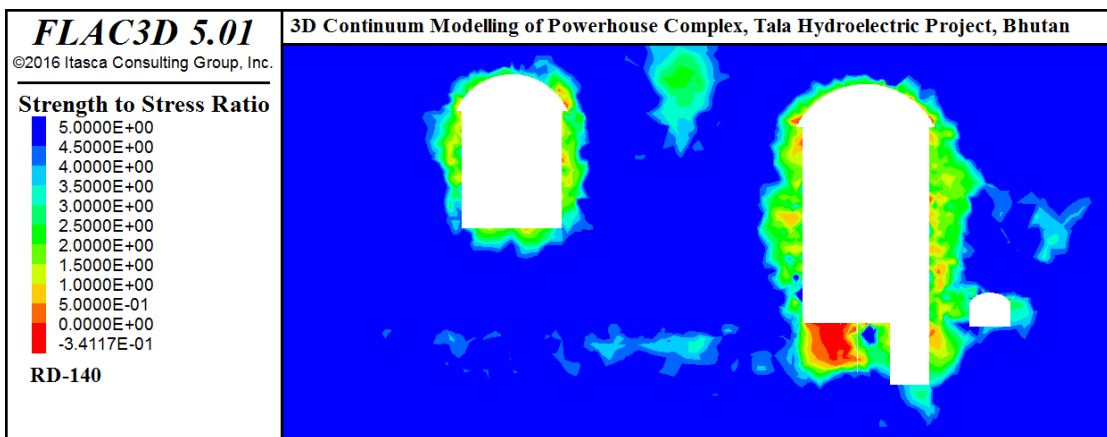


Fig. 31 Strength to stress ratio distribution at RD-140 powerhouse cavern

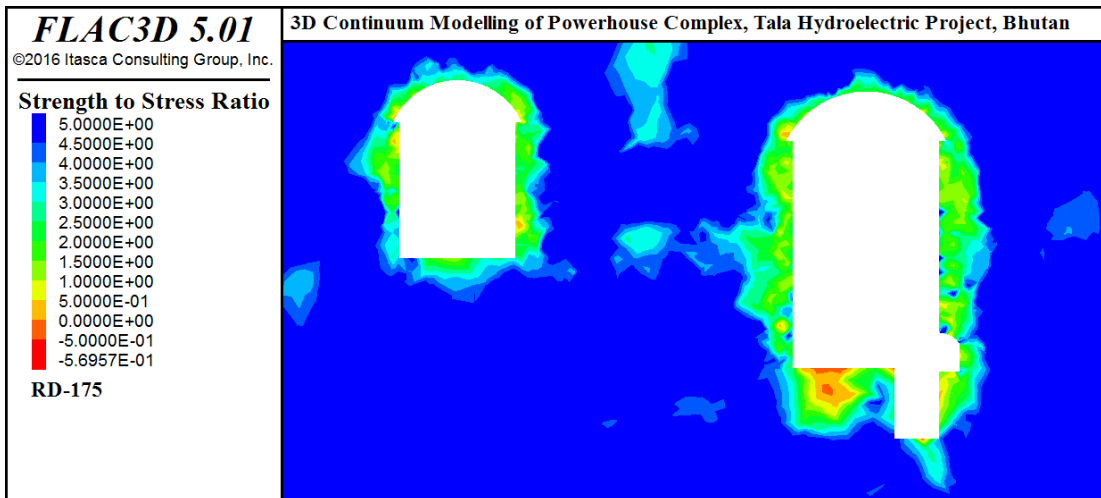


Fig. 32 Strength to stress ratio distribution at RD-175, powerhouse cavern

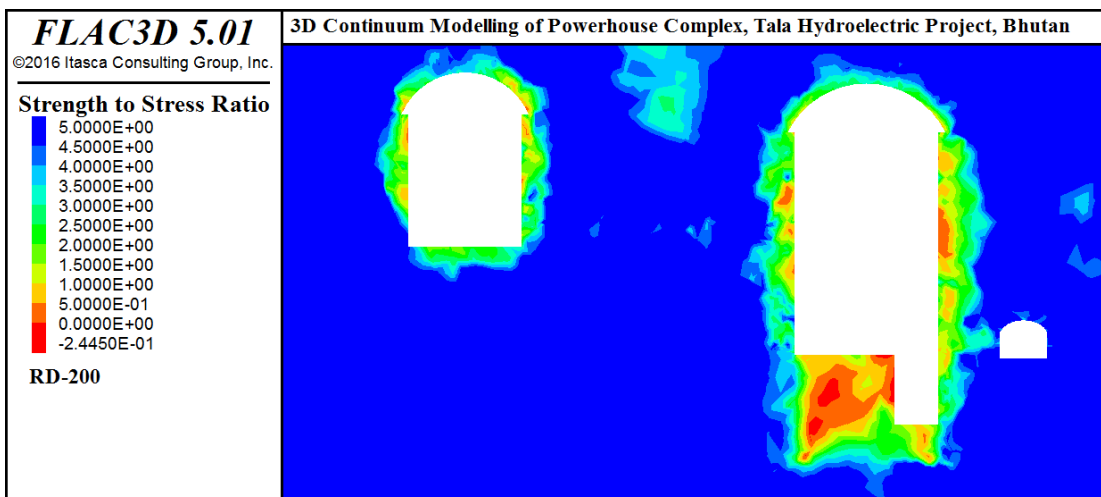


Fig. 33 Strength to stress ratio distribution at RD-200, powerhouse cavern

PUBLICATIONS

International Journals

Sripad, R. N., and Sastry, V. R., 2014. Behaviour of large underground cavern during construction in Himalayas - A case study, International journal of earth sciences and Engineering, Aug, Vol 7, No.4 pp 1601 – 1610

International Symposium

Sripad, R. N., and Sastry, V. R., 2014. Behaviour of cross tunnels in large underground cavern- A case study, International symposium ROCK MECHANICS 2014-Present Technology and Future Challenges, 20--22 August, New Delhi

Sripad, R.N., and Sastry, V.R., 2017. Assessment of stability of large caverns in Himalayas using 3D Numerical Modelling” International Conference on NexGen Technologies for Mining & Fuel Industries (NxGnMiFu-2017) February 15-17, 2017, Vigyan Bhawan, New Delhi, India.

CURRICULUM VITAE

Name : Sripad Ramachandra Naik
Contact No. : +91 9449225973
E-mail : sripad_naik@yahoo.com, sripadnaik@gmail.com
Date of Birth : 02-09-1968
Permanent Address : No. 49, Gurukrupa
1st Block, 3rd Street, 1A Cross
Prakruthi Township
Bengaluru – 560 043
Correspondence Address : Numerical Modelling Department
National Institute of Rock Mechanics
Eshwar Nagar, Outer Ring Road
Banashankari 2nd Stage
BENGALURU – 560 070

Mr. Sripad R Naik is a graduate in Mining Engineering from NIT, Surathkal in 1990 and acquired his masters from IT, BHU. Mr. Sripad joined National Institute of Rock Mechanics in the year 1992 and presently he is Head, Numerical Modelling Department. He has expertise in numerical modelling and instrumentation in the areas of mining and civil engineering. He has worked on many challenging problems in the area of hydroelectric projects, coal mine method of working and instrumentation and subsidence modelling. Substantial experience in sophisticated research techniques and technologies, particularly in the area of 3D modeling of underground structures, slopes. Expert in planning, design and execution of geotechnical instrumentation work for mining and hydroelectric projects. He has published 31 technical papers in journals and national and international conferences.

Research Publications

Journal Papers	Conference Publications	Workshops	Monographs	Total
04	21	5	1	31